Intra-Oceanic Subduction Systems

Tectonic and Magmatic Processes

Edited by

R. D. Larter and P. T. Leat

Geological Society

Special Publication 219

Intra-Oceanic Subduction Systems: Tectonic and Magmatic Processes

Special Publications reviewing procedures

The Society makes every effort to ensure that the scientific and production quality of its books matches that of its journals. Since 1997, all book proposals have been refereed by specialist reviewers as well as by the Society's Books Editorial Committee. If the referees identify weaknesses in the proposal, these must be addressed before the proposal is accepted.

Once the book is accepted, the Society has a team of Book Editors (listed above) who ensure that the volume editors follow strict guidelines on refereeing and quality control. We insist that individual papers can only be accepted after satisfactory review by two independent referees. The questions on the review forms are similar to those for *Journal of the Geological Society.* The referees' forms and comments must be available to the Society's Book Editors on request.

Although many of the books result from meetings, the editors are expected to commission papers that were not presented at the meeting to ensure that the book provides a balanced coverage of the subject. Being accepted for presentation at the meeting does not guarantee inclusion in the book.

Geological Society Special Publications are included in the ISI Index of Scientific Book Contents, but they do not have an impact factor, the latter being applicable only to journals.

More information about submitting a proposal and producing a Special Publication can be found on the Society's web site: www.geolsoc.org.uk.

It is recommended that reference to all or part of this book should be made in one of the following ways:

LARTER, R.D. & LEAT, P.T. (eds) 2003. *Intra-Oceanic Subduction Systems: Tectonic and Magmatic Processes.* Geological Society, London, Special Publications, **219**.

DESCHAMPS, A. & LALLEMAND, S. 2003. Geodynamic setting of Izu-Bonin-Mariana boninites *In*: LARTER, R.D. & LEAT, P.T. (eds) 2003. *Intra-Oceanic Subduction Systems: Tectonic and Magmatic Processes.* Geological Society, London, Special Publications, **219**, 163–185.

GEOLOGICAL SOCIETY SPECIAL PUBLICATION NO. 219

Intra-Oceanic Subduction Systems: Tectonic and Magmatic Processes

EDITED BY

R.D. LARTER & P.T. LEAT
British Antarctic Survey, UK

2003
Published by
The Geological Society
London

THE GEOLOGICAL SOCIETY

The Geological Society of London (GSL) was founded in 1807. It is the oldest national geological society in the world and the largest in Europe. It was incorporated under Royal Charter in 1825 and is Registered Charity 210161.

The Society is the UK national learned and professional society for geology with a worldwide Fellowship (FGS) of 9000. The Society has the power to confer Chartered status on suitably qualified Fellows, and about 2000 of the Fellowship carry the title (CGeol). Chartered Geologists may also obtain the equivalent European title, European Geologist (EurGeol). One fifth of the Society's fellowship resides outside the UK. To find out more about the Society, log on to www.geolsoc.org.uk.

The Geological Society Publishing House (Bath, UK) produces the Society's international journals and books, and acts as European distributor for selected publications of the American Association of Petroleum Geologists (AAPG), the American Geological Institute (AGI), the Indonesian Petroleum Association (IPA), the Geological Society of America (GSA), the Society for Sedimentary Geology (SEPM) and the Geologists' Association (GA). Joint marketing agreements ensure that GSL Fellows may purchase these societies' publications at a discount. The Society's online bookshop (accessible from www.geolsoc.org.uk) offers secure book purchasing with your credit or debit card.

To find out about joining the Society and benefiting from substantial discounts on publications of GSL and other societies worldwide, consult www.geolsoc.org.uk, or contact the Fellowship Department at: The Geological Society, Burlington House, Piccadilly, London W1J 0BG: Tel. +44 (0)20 7434 9944; Fax +44 (0)20 7439 8975; Email: enquiries@geolsoc.org.uk.

For information about the Society's meetings, consult *Events* on www.geolsoc.org.uk. To find out more about the Society's Corporate Affiliates Scheme, write to enquiries@geolsoc.org.uk.

Published by The Geological Society from:
The Geological Society Publishing House
Unit 7, Brassmill Enterprise Centre
Brassmill Lane
Bath BA1 3JN,
UK

(*Orders*: Tel. +44 (0)1225 445046
Fax +44 (0)1225 442836)
Online bookshop: http://bookshop.geolsoc.org.uk

British Library Cataloguing in Publication Data
A catalogue record for this book is available from the British Library.

ISBN 1-86239-147-5

Typeset by Type Study, Scarborough, UK
Printed by The Alden Press, Oxford, UK

Distributors

USA
AAPG Bookstore
PO Box 979
Tulsa
OK 74101-0979
USA
Orders: Tel. +1 918 584-2555
Fax +1 918 560-2652
E-mail bookstore@aapg.org

India
Affiliated East–West Press PVT Ltd
G-1/16 Ansari Road, Daryaganj,
New Delhi 110 002
India
Orders: Tel. +91 11 327-9113
Fax +91 11 326-0538
E-mail affiliat@nda.vsnl.net.in

Japan
Kanda Book Trading Co.
Cityhouse Tama 204
Tsurumaki 1-3-10
Tama-shi
Tokyo 206-0034
Japan
Orders: Tel. +81 (0)423 57-7650
Fax +81 (0)423 57-7651
E-mail geokanda@ma.kcom.ne.jp

Contents

Preface

Intra-oceanic subduction systems are generally simpler than ones at continental margins as they commonly have a shorter history of subduction and their magmas are not contaminated by ancient sialic crust. Over the past decade, there has been an enormous increase in information on these subduction systems, resulting from availability of new data types and application of improved analytical techniques. One current school of thought is that the greatest scientific advances will result from concentrating research efforts on just one or two subduction zones. There is no doubt that this approach has some advantages, but additional insights may be gained by comparing results from several different subduction zones that are subject to a range of different input parameters (e.g. convergence rate, roll-back rate, slab age, slab geometry, subducted sediment type, sediment subduction rate, sediment accretion/subduction erosion rate, thickness of arc crust, duration of subduction). Following this philosophy, we have edited this volume with the intention of providing examples of how recent research on a variety of intra-oceanic subduction systems has led to advances in understanding subduction-related tectonic, magmatic and hydrothermal processes. The volume includes papers on most of the better-known intra-oceanic subduction zones, although in a book of this size it is not possible to cover all aspects of each one.

This volume arose from a meeting with the same title held at the Geological Society, London, in September 2001. This was a joint meeting of the Marine Studies Group, the Tectonic Studies Group, and Volcanic and Magmatic Studies Group. Financial support to stage the meeting was provided by the British Antarctic Survey, the Marine Studies Group and the Volcanic and Magmatic Studies Group. We would like to thank all those who contributed to the success of the meeting, and to the production of this Special Publication. In particular, we are grateful to Clair Parks, Helen Wilson and Jennifer Last at Burlington House, and Helen Floyd-Walker and Angharad Hills at the Geological Society Publishing House. We also wish to acknowledge the people who gave their time to review manuscripts submitted to this Special Publication. These include a number of people who preferred to remain anonymous, and the following: J.F. Allan; J.H. Bédard; J.S. Collier; T. Gamo; S.A. Gibson; J.B. Gill; R. Hickey-Vargas; J. Ishibashi; S.P. Kelley; W.P. Leeman; R. Macdonald; C. Mac Niocaill; F. Martinez; T.A. Minshull; C. Müller; B.J. Murton; D.W. Peate; B. Pelletier; T. Plank; T.R. Riley; A.D. Saunders; D.W. Scholl; I.E.M. Smith; Y. Tatsumi; B. Taylor; R.N. Taylor; M.F. Thirlwall; J.P. Turner; K.L. Von Damm; G.K. Westbrook.

Robert D. Larter
Philip T. Leat

Intra-oceanic subduction systems: introduction

P.T. LEAT & R.D. LARTER

British Antarctic Survey, High Cross, Madingley Road, Cambridge CB3 0ET, UK

Abstract: Intra-oceanic arcs are the simplest type of subduction systems in that they occur where overridding plates of subduction zones consist of oceanic rocks, contrasting with arcs built on continental margins. They comprise some 40% of the subduction margins of the Earth. The better-known examples include the Izu–Bonin–Mariana arc, the Tonga–Kermadec arc, the Vanuatu arc, the Solomon arc, the New Britain arc, the western part of the Aleutian arc, the South Sandwich arc and the Lesser Antilles arc. They are thought to represent the first stage in the generation of continental crust from oceanic materials. They are generally more inaccessible than continental arcs, but, for a variety of reasons, provide insights into processes in subduction zones that are impossible or difficult to glean from the better-studied continental arcs. Intra-oceanic arcs typically have a simpler crustal structure than arcs built on continental crust, although there are significant differences between examples. Geochemically, magmas erupted in intra-oceanic arcs are not contaminated by ancient sialic crust, and their compositions more accurately record partial melting processes in the mantle wedge. They are also the sites of generation of intermediate–silicic middle crust and volcanic rocks, probably representing the earliest stage of generation of andesitic continental crust by partial melting of basaltic lower crust. They are the best locations in which to study mantle flow in the vicinity of subducting slabs using both geophysical and geochemical methods. They are the sites of significant hydrothermal activity and metallogenesis. The fact that their hydrothermal discharges typically occur shallower in the ocean than those from mid-ocean ridge vents means that they have the potential for greater environmental impact.

Volcanic arcs form above subduction zones, where oceanic plate is recycled back into the Earth's interior, and are the most visible manifestations of plate tectonics – the convection mechanism by which the Earth loses heat. The total length of margins where oceanic crust is being subducted (approximately the same as the total length of volcanic arcs) on Earth is about 43 500 km (von Huene & Scholl 1991). Most of this length of arc is situated on continental crust and is marked by spectacular, large and, often, entirely subaerial volcanoes, as typified by the Andes, Japan, the Cascades and Central America. Much research on subduction zones has concentrated on such continental arcs because of their accessibility, their clear association with metalliferous mineralization, and their manifest relationship to volcanic and seismic hazards.

Some 17 000 km, or nearly 40%, of the global length of volcanic arc is not situated on the continental margins, but is instead situated on oceanic crust. These intra-oceanic arcs are the subject of this book. Intra-oceanic arcs are significantly less well studied than continental arcs. The main reason for this is that they are typically mostly submerged below sea level, sometimes with only the tops of the largest volcanoes forming islands. They also occur in some of the most remote places on Earth and it has proved difficult to persuade funding agencies to provide time for research ships to transit to many of the key localities.

Nevertheless, intra-oceanic arcs provide vital scientific information on how subduction zones work that is very difficult, or impossible, to obtain by studying continental arcs. Because they are situated on thin, dominantly mafic crust, significant contamination of magmas by easily fusible sialic crust cannot normally occur (Wilson 1989). It is therefore significantly more straightforward to understand magma-generation processes in the mantle in intra-oceanic arcs. They are also thought to represent the first stage in the poorly understood process by which basaltic, oceanic crust is modified to form continental crust, at least in post-Archaean times (Rudnick 1995; Taylor & McLennan 1995). Intra-oceanic arcs may also have a particular environmental importance in that they are the main locations where there is significant hydrothermal discharge in shallow oceans (de Ronde *et al.* 2001).

What exactly are intra-oceanic arcs? They are magmatic arcs within ocean basins, built on crust of oceanic derivation. Such crust might be ocean crust formed at either mid-ocean ridges or back-arc spreading centres, crust forming part of an

From: LARTER, R.D. & LEAT, P.T. 2003. *Intra-Oceanic Subduction Systems: Tectonic and Magmatic Processes.* Geological Society, London, Special Publications, **219**, 1–17. 0305-8719/03/$15.00

oceanic plateau, crust formed by accretion of oceanic sediments in a subduction zone fore-arc or earlier intra-oceanic arc material. The variety of rocks that can form the basement to intra-oceanic arcs hints at the complexity that many of them show in detail. In fact, of the currently active intra-oceanic arcs only the central and western Aleutian arc overlies crust formed at a mid-ocean ridge. Perhaps it is better to define intra-oceanic arcs by what they are not – they do not overlie basement consisting of continental crust. Intra-oceanic arcs – as we define them – are equivalent to ensimatic arcs (Saunders & Tarney 1984) and are approximately equivalent to the 'oceanic island arcs' of Wilson (1989).

Over the last decade, there has been an enormous increase in knowledge of intra-oceanic arcs. New maps have become available, through the availability of Geosat and ERS 1 satellite altimetry data (Livermore *et al.* 1994; Sandwell & Smith 1997), and through greatly increased coverage by swath bathymetry mapping (Martinez *et al.* 1995; Deplus *et al.* 2001). The seismic velocity structure of arc crust has been determined in unprecedented detail using ray-tracing inversion in controlled-source seismology (Suyehiro *et al.* 1996; Holbrook *et al.* 1999). The seismic velocity structure of the upper mantle in the vicinity of arcs has been revealed using tomographic inversion in earthquake seismology (Zhao *et al.* 1992, 1997). Relocation of earthquake hypocentres using improved methods has provided better definition of Wadati–Benioff zones, showing the position of subducted slabs in the mantle (Engdahl *et al.* 1998). At the same time improvement in inductively coupled plasma-mass spectronomy (ICP-MS) techniques for high-precision determination of trace element abundances (e.g. Pearce *et al.* 1995; Eggins *et al.* 1997), and advances in radiogenic isotope analysis, have had a huge impact on the understanding of chemical fluxes in the mantle wedge and time constraints on magma ascent (Morris *et al.* 1990; Elliott *et al.* 1997; Hawkesworth *et al.* 1997).

Most previous special volumes or books on the subject have tended to deal with intra-oceanic arcs as a subset of convergent margins. Gill (1981), Thorpe (1982) and Tatsumi & Eggins (1995) provide excellent introductions to volcanic arcs, although the first two are now somewhat dated. The monograph *Subduction Top to Bottom* (Bebout *et al.* 1996) contains a wide range of recent papers on subduction zones. Other recent volumes concentrate on particular topics: *The Behaviour and Influence of Fluids in Subduction Zones* (Tarney *et al.* 1991), *Backarc Basins* (Taylor 1995) and *Active Margins and Marginal Basins of the Western Pacific* (Taylor & Natland 1995).

Characteristics of intra-oceanic arcs

The locations of the intra-oceanic arcs of the world are shown in Figure 1. All are in the western Pacific region, except three – the Aleutian arc in the north Pacific, and the Lesser Antilles and South Sandwich arcs, both in the Atlantic Ocean. The main physical characteristics of the arcs are compared in Table 1, and a schematic cross-section of an intra-oceanic subduction system is shown in Figure 2.

Convergence rates

Convergence rates vary from *c.* 20 mm a^{-1} in the Lesser Antilles arc to 240 mm a^{-1} in the northern part of the Tonga arc, the highest subduction rates on Earth (Bevis *et al.* 1995). Typical rates are in the range 50–130 mm a^{-1}. Note that intra-arc variations are almost as large as inter-arc ones. For example, in the Aleutian arc, convergence rates are about 66 mm a^{-1} beneath the eastern part of the arc where convergence is almost perpendicular to the trench (DeMets *et al.* 1990, 1994), and slightly higher in the western part of the arc, around 73 mm a^{-1}. However, because of the curvature of the arc, the convergence direction becomes increasingly oblique westwards to the point of becoming almost pure transform motion (Creager & Boyd 1991). Convergence rates vary along the Solomon arc mainly because two different plates are being subducted – the Solomon Sea and Australian plates, which are separated by an active spreading centre. Rates are significantly higher (135 mm a^{-1}) for the Solomon Sea–Pacific convergence to the north of the triple junction than for the Australian–Pacific convergence (97 mm a^{-1}) to the south (Mann *et al.* 1998). Most of the large variation in convergence rate along the Tonga–Kermadec arc is related to clockwise rotation of the arc accommodated by extension in the back-arc basin, which is spreading at a rate of 159 mm a^{-1} (full rate) at the northern end of the Lau Basin (Bevis *et al.* 1995).

In several cases, there are uncertainties about rates of convergence because of uncertainties in rates of back-arc extension, which preclude calculation of convergence rates from major plate motions (DeMets *et al.* 1990, 1994). Convergence rates at the Mariana Trench are poorly constrained, mainly for this reason. Estimates of opening rates for the central and southern parts of the Mariana Trough back-arc basin range

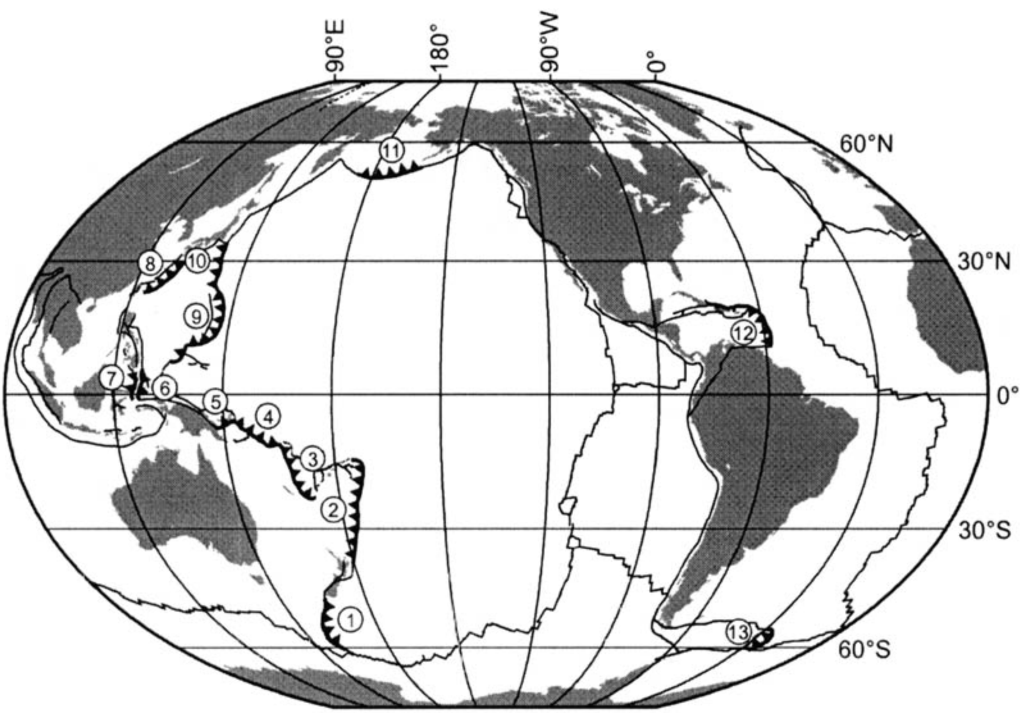

Fig. 1. Locations of modern intra-oceanic subduction systems (Mollweide projection). Trenches associated with these systems are marked by barbed lines. Other plate boundaries are shown as thin solid lines. Intra-oceanic subduction systems marked by numbers enclosed in circles are: 1, MacQuarie; 2, Tonga–Kermadec; 3, Vanuatu (New Hebrides); 4, Solomon; 5, New Britain; 6, Halmahera; 7, Sangihe; 8, Ryukyu; 9, Mariana; 10, Izu–Ogasawara (Bonin); 11, Aleutian; 12, Lesser Antilles; 13, South Sandwich. The Halmahera and Sangihe arcs are shown in their Neogene configuration; they are now in collision.

between 30 and 50 mm a^{-1} (Martinez & Taylor 2003). When combined with the plate kinematic model of Seno *et al.* (1993) these rates imply convergence rates >50 mm a^{-1} at the southern part of the Mariana Trench, increasing northward to >70 mm a^{-1} at the central part of the trench. Similar uncertainties exist for the Izu–Ogasawara arc along which convergence rates between the subducting Pacific and overriding Philippine Sea plates increase northwards from 47 to 61 mm a^{-1}, according to the plate kinematic model of Seno *et al.* (1993). The total convergence rates at the trench may be 1–3 mm a^{-1} faster than these rates as a consequence of intra-arc rifting (Taylor 1992). In several arcs accurate convergence rates have been accurately determined by geodetic Global Positioning System (GPS) measurements (Tonga–Kermadec, Bevis *et al.* 1995; Vanuatu, Taylor *et al.* 1995; Lesser Antilles, DeMets *et al.* 2000; Perez *et al.* 2001; Weber *et al.* 2001).

Ages of slabs

Ages of subducting slabs range from Late Jurassic (*c.* 152 Ma, Nakanishi *et al.* 1989) in the case of the Pacific Plate subducted beneath the Maraina arc, the oldest ocean floor currently being subducted anywhere in the world, to close to zero age along part of the Solomon arc (Mann *et al.* 1998). Along-arc variations in slab ages are not large. Of the arcs in Table 1, the age of the plate subducting beneath the Tonga–Kermadec arc is, perhaps, the most uncertain. The subducting slab is mid–Late Cretaceous in age, having formed by fast spreading at the Osbourn Trough, a fossil spreading centre that is now being subducted orthogonally to the trench. It has been suggested that the youngest crust generated at the Osbourn Trough may be as young as 70 Ma (Billen & Stock 2000), although others have argued that regional tectonic constraints preclude spreading at the Osbourn Trough more

Table 1. *Parameters of intra-oceanic subduction zones*

Arc	Convergence rate (mm a^{-1})	Age of subducting slab	Sediment thickness (m)	Sediment types	Accreting/ non-accreting	Back-arc rifting	Arc crustal thickness (km)	References
Tonga–Kermadec	60 (south) to 240 (north)	Mid–Late Cretaceous (probably >100 Ma)	70–157	Pelagic clay, chert, porcellanite, volcaniclastic deposits. Increasing terrigenous input to south	Non-accreting	Well-developed ocean spreading in Lau Basin with hydrothermal venting		Fouquet *et al.* (1991), Plank & Langmuir (1993), Bevis *et al.* (1995), Gamble *et al.* (1996), Larter *et al.* (2002)
Vanuatu	103–118	Eocene–Oligocene	650	Ash, volcaniclastic, deposits, calcareous ooze	Non-accreting	Well-developed oceanic spreading in the North Fiji Basin		Plank & Langmuir (1993), Taylor *et al.* (1995), Pelletier *et al.* (1998)
Solomon	135 (Solomon Sea–Pacific) and 97 (Australian–Pacific)	0–5 Ma		Clay, volcaniclastic, deposits, calcareous ooze	Non-accreting	None		Taylor & Exon (1987), Mann *et al.* (1998), Petterson *et al.* (1999)
New Britain	80–150	*c.* 45 Ma		Hemipelagic mud		Well-developed ocean spreading in the Manus Basin with hydrothermal venting		Binns & Scott (1993), Benes *et al.* (1994), Tregoning *et al.* (1998), Woodhead *et al.* (1998), Tregoning (2002), Sinton *et al.* (2003)
Mariana	>50 (south) to >70 (central)	*c.* 152 Ma	460	Siliceous ooze, volcaniclastic deposits, pelagic clay	Non-accreting	Complex history of rifting. Currently well-developed ocean spreading in Mariana Trough		Nakanishi *et al.* (1989), Taylor (1992), Plank & Langmuir (1993), Seno *et al.* (1993), Stern & Smoot (1998), Shipboard Scientific Party (2000), Martinez & Taylor (2003)
Izu–Ogasawara (Bonin)	>47 (south) to >61 (north)	127–144 Ma	410	Siliceous ooze, volcanic ash, calcareous ooze, pelagic clay	Non-accreting	Complex history of rifting. Recent formation of rift basins in the rear-arc	*c.* 20	Nakanishi *et al.* (1989), Taylor (1992), Seno *et al.* (1993), Suyehiro *et al.* (1996), Shipboard Scientific Party (2000)
Aleutian	66 (east) to 73 (west)	42–62 Ma	500	Siliceous ooze, clay, and tubiditic silts and sands	Accreting	None	*c.* 30	Lonsdale (1988), DeMets *et al.* (1990, 1994), Creager & Boyd (1991), Plank & Langmuir (1993), Fliedner & Klemperer (1999), Holbrook *et al.* (1999)
Lesser Antilles	*c.* 20	Jurassic–Early Cretaceous (south) to Late Cretaceous (> *c.* 75–85 Ma) (north)	Variable, from 410 m at DSDP Site 543 (north; 210 m subducted) to >6 km (south; perhaps 1 km subducted)	Subducted components: siliceous ooze, pelagic clay, carbonate ooze, turbiditic silts and sands	Accreting	The back-arc Grenada Trough is heavily sedimented and probably extinct	30–35	Boynton *et al.* (1979), Westbrook *et al.* (1984, 1988), Speed & Walker (1991), Plank & Langmuir (1993), Dixon *et al.* (1998), DeMets *et al.* (2000), McDonald *et al.* (2000), Perez *et al.* (2001), Weber *et al.* (2001)
South Sandwich	67–79	83 Ma (north) to 27 Ma (south)	<200 (south)	Siliceous mud (south)	Non-accreting	Well-developed ocean spreading along East Scotia Ridge with hydrothermal venting	<20	Ninkovich *et al.* (1964), Barker & Lawver (1988), Livermore & Woollett (1993), Vanneste & Larter (2002), Vanneste *et al.* (2002), German *et al.* (2000), Larter *et al.* (2003), Thomas *et al.* (2003)

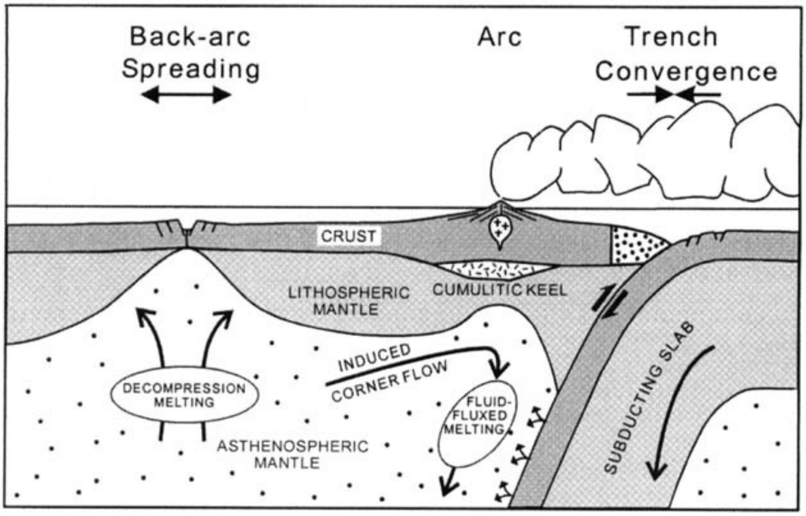

Fig. 2. Schematic cross-section of an intra-oceanic subduction zone, not to scale. The outer forearc (stippled) is the site of either sediment accretion or subduction erosion.

recently than 100 Ma (e.g. Larter *et al.* 2002), which gives a minimum age for the subducting slab. The Lesser Antilles and South Sandwich arcs show the greatest intra-arc variations in ages of subducting slabs (respectively, Jurassic or Early Cretaceous–Late Cretaceous, Westbrook *et al.* 1984, and 27–83 Ma, Barker & Lawver 1988; Livermore & Woollett 1993).

Topography of subducting plates

There are large variations in the topography of the subducting plates. Whereas some are relatively smooth, some contain ridges and seamounts that affect subduction and arc tectonics. The Jurassic ocean floor subducting at the Mariana arc is overlain by Cretaceous alkali basalts and numerous seamounts that continually collide with the trench. The Louisville Ridge hot-spot chain subducting at the Tonga–Kermadec Trench has caused indentation of the forearc. More dramatically, collision of the D'Entrecasteaux Ridge (an extinct arc) with the Vanuatu arc is causing uplift of the forearc, thrusting of the central part of the arc eastwards towards the rear-arc and development of a series of strike-slip faults approximately perpendicular to the arc (Maillet *et al.* 1995; Taylor *et al.* 1995). Similarly, recent uplift of the Solomon arc is probably a consequence of collision of the Coleman Seamount with the trench (Mann *et al.* 1998).

Sediment thickness

Sediment thicknesses are more variable than perhaps implied in Table 1, where several of the thicknesses are taken from Deep Sea Drilling Project (DSDP) or Ocean Drilling Program (ODP) cores. Sediment cover is commonly thinner over basement highs, and the resulting condensed sequences are sometimes targeted for drill sites. This tends to produce underestimates in subducted sediment thicknesses in compilations such as Table 1. Variations in thickness and composition of subducted sediments are probably greatest where arcs are close to, or cut across, ocean–continent boundaries. Thus, the sediment on the subducting plate arriving at the Lesser Antilles Trench increases dramatically southward toward the South American continental margin, where a >6 km-thick turbiditic fan is fed from the Orinoco River (Westbrook *et al.* 1984), of which 1 km is probably subducted and the rest added to an accretionary complex (Westbrook *et al.* 1988). By contrast, DSDP Site 543, near the northern part of the arc, showed just 410 m of sediment overlying basaltic basement on the subducting plate. Seismic reflection profiles here show that the upper 200 m of sediment is scrapped off and added to the accretionary complex, while the rest of the succession is subducted (Westbrook *et al.* 1984). There is a similar increase in terrigenous input derived from the New Zealand continent southward along the Tonga–Kermadec arc (Gamble *et al.* 1996).

Accretion v. non-accretion

Most modern intra-oceanic arcs are non-accreting, i.e. there is little or no net accumulation of off-scrapped sediment forming accretionary complexes. In other words, all the sediments arriving at the trenches are subducted (over a period) into the mantle. The two exceptions are the Lesser Antilles and Aleutian arcs, both of which have relatively high sediment inputs and where accretionary complexes have formed.

Back-arc spreading

Most of the arcs in Table 1 have closely associated back-arc rifts. Only the Solomon and Aleutian arcs are exceptions in having no apparent back-arc spreading. In most cases, the back-arc extension takes the form of well-organized seafloor spreading for at least part of the length of the back-arc. Such spreading appears to follow arc extension and rifting in at least some cases. The Mariana arc has had an especially complex history of arc and back-arc extension, starting with axial rifting of an Oligocene volcanic arc at about 29 Ma, beginning development of the back-arc Parece Vela Basin (Taylor 1992). A second episode of arc rifting started in Late Miocene–Pliocene times when the West Mariana Ridge rifted away from the active arc to form the Mariana Trough (Fryer 1996). The Mariana Trough is currently opening by seafloor spreading for most of its length, where mid-ocean ridge basalt (MORB)-like lavas are erupted, and by rifting of arc crust in its northern part (Martinez *et al.* 1995), where compositions are indistinguishable from those of the magmatic arc (Stolper & Newman 1994; Gribble *et al.* 1998).

The Izu–Ogasawara arc had similar early tectonic and magmatic histories to those of the Mariana arc (Taylor 1992; Macpherson & Hall 2001). An Oligocene arc rifted parallel to its length at *c.* 22 Ma to form the back-arc Shikoku Basin. However, a second episode of Late Pliocene–Recent arc-parallel rifting formed a series of rift basins in the present rear-arc that have not developed to ocean spreading centres (Taylor 1992). Ishizuka *et al.* (2003) present new Ar–Ar geochronological data to define the volcanic and extensional history of the arc and back-arc.

The East Scotia Ridge consists of nine mostly well-organized spreading segments (with a possible poorly defined tenth at the southern end of the ridge). The central segments are rift-like and erupt MORB (Livermore *et al.* 1997; Fretzdorff *et al.* 2002; Livermore 2003), but one segment in the south appears to have recently developed from arc extension to ocean spreading (Bruguier & Livermore 2001). Lavas tend to become compositionally more similar to the arc at the ends of the ridge, where it is close to the arc volcanic front (Fretzdorff *et al.* 2002). A similar relationship is observed in the Lau Basin back-arc to the Tonga arc, where water and other slab-derived chemical tracers increase as distance from the arc volcanic front decreases (Pearce *et al.* 1994; Peate *et al.* 2001). This in turn controls magma supply and crustal thickness in the back-arc (Martinez & Taylor 2002). Martinez & Taylor (2003) report similar variations related to distance from the arc volcanic front in the Manus Basin and Mariana Trough.

Arc crustal thickness and pre-arc basement

Figures for the thickness of the crust of arcs are only shown in Table 1, where high-quality wide-angle seismic and gravity data exist. Arc thicknesses depend on arc maturity, tectonic extension or shortening, and the thickness of pre-arc basement. Only approximately, therefore, is it true to say that the thin crusts of the South Sandwich (Larter *et al.* 2003) and Izu–Osgaswara (Suyehiro *et al.* 1996) arcs represent arcs in the relatively early stages of development, whereas the Lesser Antilles (Boynton *et al.* 1979) and Aleutian (Fliedner & Klemperer 1999; Holbrook *et al.* 1999) arcs with their thicker crusts are more mature.

Pre-arc basements of the arcs are very variable. The central and western parts of the Aleutian arc are built on Cretaceous oceanic plate that underlies the Bering Sea, and this is the only intra-oceanic arc built on normal ocean crust. The South Sandwich arc is a little more complex, being built on ocean plate formed since *c.* 10 Ma at the back-arc East Scotia Ridge spreading centre (Larter *et al.* 2003). Several of the arcs in Table 1 are built on earlier arc rocks. The present Izu–Ogasawara arc is built on stretched Eocene–Oligocene arc crust (Taylor 1992). The New Britain arc overlies a basement of Eocene–Miocene intra-oceanic arc rocks (Madsen & Lindley 1994; Woodhead *et al.* 1998) formed before a reversal in subduction polarity (Benes *et al.* 1994). Similarly, the Neogene Halmahera arc overlies ophiolitic basement and Early Tertiary arc volcanic rocks (Hall *et al.* 1991), and the basement to the Sangihe arc is also thought to consist of pre-Miocene ophiolitic or arc crust (Carlile *et al.* 1990).

Some of the arcs have more complex basement. The basement to the Solomon arc falls in to this category, and at present probably constitutes a zone of diffuse deformation at the edge of the Pacific Plate. It consists of several oceanic terrains, including parts of the Ontong Java Plateau, as well as MORB sequences (Petterson *et al.* 1999). The basement of the Lesser Antilles arc is poorly known. It probably consists of mid-Cretaceous–Palaeocene arc and accretionary complex crust, and possibly thick oceanic crust of the Caribbean Plateau (Macdonald *et al.* 2000). The volcanic rocks of this arc show evidence for widespread contamination by a sediment source during magma ascent. This contaminant increases to the south and is thought to be the old accretionary complex material forming basement to the arc (Davidson & Harmon 1989; Davidson 1996; van Soest *et al.* 2002). A parallel trend of southward-increasing sediment input to the mantle sources of the magmas is observed (Turner *et al.* 1996).

Exhumed intra-oceanic arcs

Structures of modern magmatic arcs inferred from geophysics and petrology can be 'ground-truthed' by studies of sections through arcs exposed by orogenic process. Slivers of arc crust are common, probably ubiquitous in collisional orogens. It is rare, however, for complete crustal sections through arcs from mantle to volcanic cover to be exposed. Well-documented examples include the Kohistan, Pakistan (Miller & Christensen 1994), Talkeetna, Alaska (DeBari & Sleep 1991) and Canyon Mountain, Oregon (Pearcy *et al.* 1990) arcs. All of these examples are thought to have been intra-oceanic. The Kohistan arc, in particular, has provided critical information on the seismic and petrological structure of arc crust (Chroston & Simmons 1989; Miller & Christensen 1994). DeBari & Sleep (1991) demonstrated that the Talkeetna arc can be used for mass-balance calculations to determine the composition of mantle-derived magma feeding the arc, and argued that it was high-Mg (and low-Al) basalt.

Current research themes

Mantle flow beneath arc and back-arc systems

Intra-oceanic arcs are the prime locations for geophysical and geochemical investigations into relationships between mantle flow and subduction. Intra-oceanic arcs lack the thick sialic crust that acts as a contaminant and density filter in continental arcs, and most magmas in them rise to the surface relatively unmodified from their original mantle-derived compositions.

It is now accepted that the majority of mafic magmas erupted in all volcanic arcs are derived by volatile-fluxed partial melting of peridotite in the mantle wedge, rather than by melting of the subducting slab (Tatsumi 1989; Pearce & Peate 1995; Tatsumi & Eggins 1995). Indeed, the characteristics of slab-melts are well known, and they form a distinctive, but relatively rare (at least in the post-Archaean record), type of subduction zone magma known as adakite (Defant & Drummond 1990).

Two-dimensional models for partial melting of mantle and the mantle 'corner' flow induced by the subducting plate in subduction zones are well developed (Davies & Stevenson 1992; Tatsumi & Eggins 1995; Winder & Peacock 2001). Extraction of a melt fraction from the mantle as it flows beneath back-arc spreading centres toward the arc is believed to cause the reduction in ratios of more incompatible, relative to less incompatible, trace elements (such as Nb/Yb and Nb/Ta) in arc basalts compared to MORBs (Woodhead *et al.* 1993, 1998; Pearce & Peate 1995). Such models of mantle flow have been adapted to explain variations in magma supply in back-arc basins by Martinez & Taylor (2002, 2003). Detailed seismic tomography images of the mantle beneath the NE Japan arc have been interpreted, together with other data, as evidence that mantle flow from back-arc to forearc is organized into 'hot fingers' (Tamura *et al.* 2002; Tamura 2003). However, measurement of seismic anisotropy beneath the Tonga arc and Lau Basin shows that mantle flow is locally parallel to the arc, and cannot be explained by coupling to the subducting slab (Smith *et al.* 2001). This is consistent with geochemical data indicating flow of mantle from the Samoan mantle plume around the north edge of the slab and into the back-arc (Turner & Hawkesworth 1998). Similar arc-parallel flow into a back-arc is thought to occur at the northern and southern ends of the slab beneath the South Sandwich arc (Livermore *et al.* 1997; Leat *et al.* 2000; Harrison *et al.* 2003; Livermore 2003). Questions remain as to what effect arc-parallel mantle flow has on magma compositions and supply in subduction zones.

Primary magmas and ultramafic keels

The major element composition of magmas feeding arcs from the mantle has been a subject of debate, particularly regarding the Mg and Al contents of primary magmas. Mafic compositions in arcs have variable MgO content, but with an abrupt cut-off at about 8 wt% MgO (less in the case of mature arcs), with very few, or zero, higher-Mg but non-cumulate compositions (Davidson 1996). One question is, therefore, whether this cut-off point represents the MgO content of the mantle-derived parental magmas, or whether the mantle-derived parental magmas are significantly more Mg-rich (>10% MgO), but are normally unable to reach the surface and erupt. Such high-Mg, primitive magmas have, in fact, been identified in many arcs, but are always volumetrically very minor. Their presence in many intra-oceanic and continental arcs indicates that they are, indeed, parental to arc magmatism (Ramsey *et al.* 1984; Heath *et al.* 1998; Macdonald *et al.* 2000). It has been argued that they have difficulty in traversing the crust because of their relatively high density (Smith *et al.* 1997) and the difficulty of traversing the crust without encountering magma chambers (Leat *et al.* 2002). Pichavant & Macdonald (2003) examine phase relationships of magnesian arc basalts and argue that only the most water-poor primitive magmas are able to traverse the crust without adiabatically freezing, explaining the rarity of primitive magmas in arcs. This raises further questions about the extent to which erupted and sampled primary magmas in arcs are typical of mantle-derived melts in arcs. There is a related debate about the origin of high-Al basalts, which have greater than *c.* 17 wt% Al_2O_3 and are characteristic of arcs. Crawford *et al.* (1987) reviewed the arguments and concluded that accumulation of plagioclase was the origin of the high Al abundances. These debates highlight the difficulty in modelling fractionation histories of arc magmas, even in intra-oceanic arcs, where primitive magmas are normally absent, and both addition and fractional removal of phenocrysts has occurred.

If the mantle-derived magmas are Mg-rich, the transition from primitive melts to low-Mg basalts by fractional crystallization must generate significant thicknesses of mafic and ultramafic cumulates. This is consistent with the presence of high-velocity (*P*-wave velocity = 6.9–7.5 km s^{-1}) layers several kilometres thick that have been seismically detected at the base of the crust in some intra-oceanic arcs (Suyehiro *et al.* 1996; Holbrook *et al.* 1999). Seismic velocity measurements on samples of exposed lower crust of the exhumed Kohistan arc strongly suggest that these high-velocity keels consist of ultramafic cumulates (Miller & Christensen 1994).

Slab-derived chemical components in intra-oceanic arcs

Subduction zones are the most important sites for fractionation of elements between different crustal and mantle reservoirs, and sites where crustal materials are returned to the mantle. They are therefore crucial for understanding the geochemical evolution of the Earth, at least since Archaean times (Hofmann & White 1982; Hart 1988; Dickin 1995; Tatsumi & Kogiso 2003). Geochemical studies of basalts from intra-oceanic arcs have been particularly important in determining how elements from different reservoirs are cycled through the mantle wedge, as contamination of magmas by ancient continental crust cannot have occurred. It has long been known that basalts of volcanic arcs are geochemically distinct from those erupted far from subduction zones. They normally have lower abundances of some incompatible trace elements (e.g. Nb, Ta, Zr, Hf, Ti and heavy rare earth elements) and higher abundances of others (e.g. K, Rb, Ba, Sr, Th, U and light rare earth elements), interpreted to be a result of addition of a 'subduction component' from the slab to the mantle wedge source of the basalts (Pearce 1983; Woodhead *et al.* 1993; Hawkesworth *et al.* 1994; Pearce & Peate 1995). Recent work has shown that the subduction component can be broken down into varying proportions of more fundamental components – the main ones are thought to be sediment and aqueous fluid. The sediment component (probably partial melt of sediment) varies in composition according to the type of sediments that are carried down the subduction zone with the slab. It is characterized by high light/heavy rare earth element, Th/Nb and Th/Tb ratios (Elliott *et al.* 1997; Woodhead *et al.* 1998). It sometimes has the continental isotopic signatures of high $^{87}Sr/^{86}Sr$ and low $^{143}Nd/^{144}Nd$ (Turner *et al.* 1996; Elliott *et al.* 1997; Class *et al.* 2000; Macpherson *et al.* 2003), and the cosmogenic signature of high ^{10}Be (Morris *et al.* 1990). The aqueous fluid component is derived by dehydration of basaltic slab and dewatering of sediments, and is characterized by high Ba/Th, Ba/Nb, B/Be and Cs/Rb ratios (Ryan *et al.* 1995; Elliott *et al.* 1997; Hawkesworth *et al.* 1997; Turner & Hawkesworth 1997; Peate & Pearce 1998). In other words, it is enriched in elements that experiments demonstrate are highly soluble in aqueous fluids at temperatures appropriate for the surface of the down-going slab (Brenan *et al.* 1995; Johnson & Plank 1999). Partial melts of the basaltic slab (adakites) may also be a minor component in some subduction zone magmas (Bédard 1999). However, much needs to be done in order to understand the nature of the element-transporting fluids, and methods of constraining the successive depletion and enrichment events in subduction environments.

The greater solubility of U than Th in aqueous fluids moving from the slab to the mantle wedge commonly results in a type of isotopic disequilibria between these elements in the erupted magmas, in which $^{238}U/^{230}Th$ is positively correlated with other tracers of the aqueous fluid component, such as Ba/Th. This type of disequilibrium is especially characteristic of intra-oceanic arcs (Elliott *et al.* 1997; Hawkesworth *et al.* 1997). The U–Th isotope disequilibria can be used to calculate the time lapse since fractionation of U from Th during slab dehydration, providing critical evidence for the timescales of melt migration (Hawkesworth *et al.* 1997). Results range from 90 ka for the Lesser Antilles (Turner *et al.* 1996) to 30–50 ka for the Tonga–Kermadec arc (Turner & Hawkesworth 1997) and *c.* 30 ka for the Mariana and Aleutian arcs (Elliott *et al.* 1997; Turner *et al.* 1998). However, the longer time for the Lesser Antilles probably includes 50 ka of magma residence in the crust, and the time for fluids and melt transport in the mantle seems to be consistently 30–50 ka. ^{226}Ra is a shorter-lived isotope (half-life of 1662 years) in the same chain as ^{230}Th. Some arc magmas have excess ^{226}Ra relative to ^{230}Th, but, because of the short half-life, these cannot result from the same slab dehydration processes as U–Th disequilibria and are assumed to reflect magma fractionation processes (Hawkesworth *et al.* 1997).

Formation of boninites

Boninites are rare, high-Mg, high-Si magmas of magmatic arcs. They dominantly occur in intra-oceanic arcs (Crawford *et al.* 1989). Their chemistry indicates that they were derived from depleted, harzburgitic sources in relatively shallow, lithospheric mantle that were subsequently enriched in incompatible elements. These incompatible elements were probably transported from subducting slabs as aqueous fluids derived from dehydration, as melts of sediment, and perhaps as partial melts of the slab crust (Crawford *et al.* 1989; Hickey-Vargas 1989; Taylor *et al.* 1994; Bédard 1999). The precise combination of circumstances that cause boninitic magmatism is debatable. Most authors appeal to processes in the evolution of subduction zones, whereas Macpherson & Hall (2001) suggested that heat convected by mantle plumes may have been critical in genesis of the Eocene Izu–Bonin–Mariana boninites. Deschamps & Lallamand (2003) describe the tectonic setting of boninites from Pacific arcs and show that intersection of a back-arc spreading centre with either an arc or a transform plate boundary are the most favourable sites for their generation.

Origin of silicic magmas

Intra-oceanic arcs dominantly erupt mafic magmas (basalt and basaltic andesite). Recently, however, there has been increasing recognition that silicic magmas form a significant proportion of their output. Tamura & Tatsumi (2002) showed that the Izu–Bonin arc is compositionally bimodal with maxima at both mafic and silicic compositions and a minimum at andesite, based on 1011 analyses from volcanic front volcanoes. This is in striking contrast to the traditional view of island arcs being dominated by andesite (e.g. Gill 1981). Analysis of ashes from cores from the Izu–Bonin and Mariana fore- and back-arcs provides further evidence for overall mafic–silicic bimodality in the arcs, or at least a high proportion of silicic magmas (Arculus *et al.* 1995; Straub 1995). Mafic–silicic bimodality is also becoming very evident in individual volcanoes of intra-oceanic arcs, and examples have been described from the Vanuatu arc (Robin *et al.* 1993; Monzier *et al.* 1994), the Tonga–Kermadec arc (Worthington *et al.* 1999; Smith *et al.* 2003) and the South Sandwich arc (Leat *et al.* 2003). Furthermore, it is becoming clear that there is a common, but possibly not ubiquitous, association of these silicic and bimodal basalt–silicic magmas with calderas. The calderas are typically 3–7 km in diameter and, because they are typically flooded, completely submerged or ice filled (in the South Sandwich Islands), many have only recently been discovered. Examples include the Raoul, Macauley and Brothers volcanoes in the Kermadec arc (Lloyd *et al.* 1996; Worthington *et al.* 1999; Wright & Gamble 1999), the Ambrym and Kuwar volcanoes, Vanuatu arc (Robin *et al.* 1993; Monzier *et al.* 1994), the South Sumisu and Myojin Knoll volcanoes, Izu–Bonin arc (Taylor *et al.* 1990; Fiske *et al.* 2001) and Southern Thule, South Sandwich arc (Smellie *et al.* 1998).

The traditional view on the origin of silicic magmas in intra-oceanic arcs is that they are generated by fractional crystallization of more mafic magmas (e.g. Ewart & Hawkesworth 1987; Woodhead 1988; Pearce *et al.* 1995). Recently, several authors have questioned this, and argued that the silicic rocks are generated by partial melting of andesitic (Tamura & Tatsumi 2002) or basaltic (Leat *et al.* 2003; Smith *et al.* 2003) igneous rocks within the crust. The debate is critical to understanding the way in which arc crust, and ultimately continental crust, is formed. The arguments are geochemical and also based on volume relationships. Suyehiro *et al.* (1996) identified a mid-crustal layer some 6 km thick in the Izu–Bonin arc that has a *P*-wave velocity of 6.0–6.3 km s^{-1}. Larter *et al.* (2001)

reported a similar, but thinner, layer in the South Sandwich arc. Suyehiro *et al.* (1996) and Larter *et al.* (2001) interpreted these layers as being intermediate–silicic plutonic rocks. The intermediate (tonalitic) to silicic Tanzawa plutonic complex, Honshu, Japan, is thought to be the lateral correlative of the 6.0–6.3 km s^{-1} layer in the Izu–Bonin arc. Geochemical and experimental results suggest that the tonalite was generated by *c.* 59% partial melting of hydrous basalt in the lower crust of the arc (Kawate & Arima 1998; Nakajima & Arima 1998), consistent with the experimental evidence for generation of silicic magmas by partial melting of amphibolites of Rapp & Watson (1995).

The role of subduction zones in the evolution of continental crust

Mechanisms for the evolution of continental crust are critical for understanding the evolution of Earth and its geochemical reservoirs. Volcanic arcs are traditionally thought to be the main sites of production of continental crust from mafic progenitors, particularly in post-Archaean times, with intra-oceanic arcs being the first stage of the process. This view has been encouraged by the fact that the dominant composition of lavas and pyroclastic deposits of many arcs (especially continental ones) is andesite (Gill 1981). Such andesite has a very similar major and trace element composition to bulk continental crust (Taylor & McLennan 1985; Rudnick 1995). However, in calculations of the composition of crust produced in volcanic arcs, the composition of volcanic products is largely irrelevant – what matters is the composition of magma added to the crust from the mantle, i.e. the composition of the magma flux across the Moho, and this is basaltic, not andesitic. Moreover, it is probably a high-Mg basalt containing some 12 wt% MgO (DeBari & Sleep 1991; Davidson 1996). If continental crust were derived from such basaltic magma generated from the mantle wedge, the crust would need to have been very significantly changed in composition. Continental crust has higher abundances of Si, alkalis and incompatible trace elements, lower abundances of Mg, and higher ratios of light rare earth elements to heavy rare earth elements than volcanic arc basalts (Pearcy *et al.* 1990; Rudnick 1995). Processes invoked to account for the change in composition from basaltic arc crust to continental crust include: (i) partial melting of basalt to generate intermediate and silicic material, which is added to the middle and upper crust as plutons and lavas; (ii) return to the mantle ('delamination') from the lower crust of mafic and ultramafic residue from such partial melting and ultramafic cumulates derived by fractional crystallization of mafic magmas; and (iii) injection of alkali- and trace-element-rich magmas into the crust after the lithosphere has been thickened to the garnet stability zone, presumably during arc–arc and arc–continent collisions (Pearcy *et al.* 1990; DeBari & Sleep 1991; Rudnick 1995; Taylor & McLennan 1995; Holbrook *et al.* 1999; Tatsumi & Kogiso 2003). Clift *et al.* (2003) describes crustal evolution of intra-oceanic arc material during arc–continent collisions in Taiwan and Ireland.

The detailed seismic velocity structure of the Izu–Bonin arc crust suggests that a 6 km-thick intermediate to silicic mid-crustal layer (*P*-wave velocity = 6.0–6.3 km s^{-1}) and 8 km-thick ultramafic lower crust (*P*-wave velocity = 7.1–7.3 km s^{-1}) are present (Suyehiro *et al.* 1996). These observations are consistent with some of the ideas about crustal modification mentioned above. However, in the central Aleutians mid-crustal material with velocities of 6.0–6.3 km s^{-1} is virtually absent, and velocities in the thick lower crust (up to 20 km) are generally slightly lower than in the Izu–Bonin arc (Holbrook *et al.* 1999). A mid-crustal layer with velocities of 6.0–6.3 km s^{-1} is present in the eastern Aleutian arc (Fliedner & Klemperer 1999) and the southern South Sandwich arc (Larter *et al.* 2001), but in both locations it is only about 2 km thick. The origin of such mid-crustal layers remains a matter of debate, and it has been suggested that the ultramafic lower crust to mantle transition is gradational in some places beneath arcs (Fliedner & Klemperer 2000). Jull & Kelemen (2001) have calculated that some arc lower crustal lithologies have densities similar to, or greater than, the underlying mantle at pressures >0.8 GPa and temperatures <800°C, possibly making lowermost arc crust prone to delamination. However, for crust comprising typical arc lithologies, 0.8 GPa is equivalent to a depth of about 28 km, which is deeper than the base of the crust in many modern intra-oceanic arcs.

Hydrothermal processes

Back-arc spreading centres of intra-oceanic arcs are well known as sites of hydrothermal activity. Hydrothermal phenomena include white and black smokers, and metallogenesis in both the Lau Basin and the Manus Basin (Fouquet *et al.* 1991; Ishibasi & Urabe 1995; Kamenetsky *et al.* 2001). Hydrothermal plumes have also been identified on the East Scotia Ridge (German *et* *al.* 2000). In these back-arc settings, the hydrothermal activity is associated with both basaltic and silicic volcanic centres (Ishibasi & Urabe 1995).

There is increasing evidence, however, that submerged volcanoes along the volcanic fronts of intra-oceanic arcs are sites of considerable hydrothermal activity. The first systematic survey of any submerged arc for hydrothermal activity revealed that seven out of the 13 submarine volcanoes in the southern Kermadec arc had hydrothermal plumes (de Ronde *et al.* 2001). Baker *et al.* (2003) present detailed observations of the distribution of these plumes and the composition of their particulate fraction. Massoth *et al.* (2003) characterize the chemistry of the gaseous and fluid components of the plumes and consider the evidence for a magmatic contribution. Projection of this frequency of hydrothermal activity to the global length of submerged arcs suggests that hydrothermal emissions from arcs may represent a significant part of the global budget. Moreover, hydrothermal vent sites of arcs are much shallower than those of mid-ocean and back-arc ridges, suggesting that hydrothermal emissions from arcs have a disproportionally high environmental impact (de Ronde *et al.* 2001). Several volcanic front volcanoes in the Mariana and Izu–Bonin arcs are also hydrothermally active and are producing metalliferous deposits (Stüben *et al.* 1992; Tsunogai *et al.* 1994; Iizasa *et al.* 1999; Fiske *et al.* 2001). Several of the hydrothermal vents in the Izu–Bonin arc (Myojin Knoll; Fiske *et al.* 2001) and the Kermadec arc (Brothers volcano; Wright & Gamble 1999; de Ronde *et al.* 2001) are within silicic calderas, and are associated with Au-rich metalliferous deposits. This raises the possibility that the calderas are formed by collapse into shallow magma chambers and that heat from the magma chambers drives the hydrothermal systems The metalliferous deposits may provide the closest analogues to Kuroko-type deposits (Iizasa *et al.* 1999).

Conclusions

- Nearly 40% of the global length of volcanic arc is situated on crust of oceanic derivation rather than continental crust, amounting to some 17 000 km of intra-oceanic arcs.
- Intra-oceanic arcs are prime locations for studies of mantle flow, elemental fluxes from subducting slabs and mantle partial melting processes in subduction systems, because such processes are not obscured by continental crust.
- There are very large variations in physical characteristics of intra-oceanic arcs, especially in convergence rates, ages, roughnesses and thicknesses of sediment cover of subducting slabs.
- Convergence rates range from *c.* 20 to 240 mm a^{-1}, and there are also large variations along the lengths of individual arcs. In the absence of geodetic GPS data, convergence rates are often poorly constrained because of uncertainties in rates of back-arc spreading.
- Only one intra-oceanic arc (the Aleutian arc) is built on normal ocean crust. The others are built on basements comprising a range of oceanic lithologies, including ocean crust formed at back-arc spreading centres, earlier intra-oceanic arcs, accretionary complexes and oceanic plateaux. It is, therefore, not possible to characterize typical intra-oceanic arc crust in terms of structure or thickness.
- It is becoming increasingly evident that silicic magmas are an important component of intra-oceanic arcs, often forming mafic–silicic bimodal series associated with calderas, and in some cases forming mid-crustal layers with *P*-wave velocities of *c.* 6.0–6.3 km s^{-1}. The silicic magmas may represent partial melts of the basaltic arc crust and, perhaps, the first stage in the development of continental crust.
- There is increasing evidence that intra-oceanic arc volcanoes are commonly sites of considerable hydrothermal venting that may form a significant part of the global hydrothermal venting budge into the oceans. Silicic calderas in intra-oceanic arcs are commonly sites of Au-rich metalliferous deposits.

We thank J. Turner and G. Westbrook for helpful reviews of the paper.

References

ARCULUS, R.J., GILL, J.B., CAMBRAY, H., CHEN, W. & STERN, R.J. 1995. Geochemical evidence of arc systems in the Western Pacific: an ash and turbidite record recovered by drilling. *In*: TAYLOR, B. & NATLAND, J. (eds) *Active Margins and Marginal Basins of the Western Pacific*. American Geophysical Union Monographs **88**, 45–65.

BAKER, E.T., FEELY, R.A., DE RONDE, C.E.J., MASSOTH, G.J. & WRIGHT, I.C. 2003. Submarine hydrothermal venting on the southern Kermadec volcanic arc front (offshore New Zealand): location and extent of particle plume signatures. *In*: LARTER, R.D. & LEAT, P.T. (eds) *Intra-oceanic Subduction Systems: Tectonic and Magmatic Processes*. Geological Society, London, Special Publications, **219**, 141–161.

BARKER, P.F. & LAWVER, L.A. 1988. South American–Antarctic plate motion over the past 50 Myr, and the evolution of the South American–Antarctic ridge. *Geophysical Journal International*, **94**, 377–386.

BEBOUT, G.E., SCHOLL, D.W., KIRBY, S.H. & PLATT, J.P. (eds). 1996. *Subduction Top to Bottom*. American Geophysical Union, Monographs, **96**.

BÉDARD, J.H. 1999. Petrogenesis of boninites from the Betts Cove ophiolite, Newfoundland, Canada: identification of subducted source components. *Journal of Petrology*, **40**, 1853–1889.

BENES, V., SCOTT, S.D. & BINNS, R.A. 1994. Tectonics of rift propagation into a continental margin: western Woodlark Basin, Papua New Guinea. *Journal of Geophysical Research*, **99**, 4439–4455.

BEVIS, M., TAYLOR, F.W., SCHUTZ, B.E., RECY, J., ISACKS, B.L., HELU, S., SINGH, R., KENDRICK, E., STOWELL, J., TAYLOR, B. & CALMANT, S. 1995. Geodetic observations of very rapid convergence and back-arc extension at the Tonga arc. *Nature*, **374**, 249–251.

BILLEN, M.I. & STOCK, J. 2000. Morphology and origin of the Osbourn Trough. *Journal of Geophysical Research*, **105**, 13 481–13 489.

BINNS, R.A. & SCOTT, S.D. 1993. Actively forming polymetallic sulphide deposits associated with felsic volcanic rocks in the eastern Manus back-arc basin, Papua New Guinea. *Economic Geology*, **88**, 2226–2236.

BOYNTON, C.H., WESTBROOK, G.K., BOTT, M.H.P. & LONG, R.E. 1979. A seismic refraction investigation of crustal structure beneath the Lesser Antilles island arc. *Geophysical Journal of the Royal Astronomical Society*, **58**, 371–393.

BRENAN, J.M., SHAW, H.F., RYERSON, F.J. & PHINNEY, D.L. 1995. Mineral–aqueous fluid partitioning of trace elements at 900°C and 2.0 GPa – constraints on the trace element chemistry of mantle and deep crustal fluids. *Geochimica et Cosmochimica Acta*, **59**, 3331–3350.

BRUGUIER, N.J. & LIVERMORE, R.A. 2001. Enhanced magma supply at the southern East Scotia ridge: evidence for mantle flow around the subducting slab? *Earth and Planetary Science Letters*, **191**, 129–144.

CARLILE, J.C., DIGDOWIROGO, S. & DARIUS, K. 1990. Geological setting, characteristics and regional exploration for gold in the volcanic arcs of North Sulawesi, Indonesia. *Journal of Geochemical Exploration*, **35**, 105–140.

CHROSTON, P.N. & SIMMONS, G. 1989. Seismic velocities from the Kohistan volcanic arc, northern Pakistan. *Journal of the Geological Society, London*, **146**, 971–979.

CLASS, C., MILLER, D.M., GOLDSTEIN, S.L. & LANGMUIR, C.H. 2000. Distinguishing melt and fluid subduction components in Umnak volcanics, Aleutian arc. *Geochemistry Geophysics Geosystems*, **1**, 1999GC000010.

CLIFT, P.D., SCHOUTEN, H. & DRAUT, A.E. 2003. A general model of arc–continent collision and subduction polarity reversal from Taiwan and the Irish Caledonides. *In*: LARTER, R.D. & LEAT, P.T. (eds) *Intra-oceanic Subduction Systems: Tectonic and Magmatic Processes*. Geological Society, London, Special Publications, **219**, 81–98.

CRAWFORD, A.J., FALLOON, T.J. & EGGINS, S. 1987. The origin of island arc high-alumina basalts. *Contributions to Mineralogy and Petrology*, **97**, 417–430.

CRAWFORD, A.J., FALLON, T.J. & GREEN, D.H. 1989. Classification, petrogenesis and tectonic setting of boninites. *In*: CRAWFORD, A.J. (ed.) *Boninites*. Unwin Hyman, London, 1–49.

CREAGER, K.C. & BOYD, T.M. 1991. The geometry of Aleutian subduction: three-dimensional kinematic flow model. *Journal of Geophysical Research*, **96**, 2293–2307.

DAVIDSON, J.P. 1996. Deciphering mantle and crustal signatures in subduction zone magmatism. *In*: BEBOUT, G.E., SCHOLL, D.W., KIRBY, S.H. & PLATT, J.P. (eds) *Subduction Top to Bottom*. American Geophysical Union Monographs, **96**, 251–262.

DAVIDSON, J.P. & HARMON, R.S. 1989. Oxygen isotope constraints on the petrogenesis of volcanic arc magmas from Martinique, Lesser Antilles. *Earth and Planetary Science Letters*, **95**, 255–270.

DAVIES, J.H. & STEVENSON, D.J. 1992. Physical model of source region of subduction zone volcanics. *Journal of Geophysical Research*, **97**, 2037–2070.

DEBARI, S.M. & SLEEP, N.H. 1991. High-Mg, low-Al bulk composition for the Talkeetna island arc, Alaska: implications for primary magmas and the nature of arc crust. *Geological Society of America Bulletin*, **103**, 37–47.

DEFANT, M.J. & DRUMMOND, M.S. 1990. Derivation of some modern arc magmas by melting of young subducted lithosphere. *Nature*, **347**, 662–665.

DEMETS, C., GORDON, R.G., ARGUS, D.F. & STEIN, S. 1990. Current plate motions. *Geophysical Journal International*, **101**, 425–478.

DEMETS, C., GORDON, R.G., ARGUS, D.F. & STEIN, S. 1994. Effects of recent revisions of the geomagnetic reversal time-scale on estimates of current plate motions. *Geophysical Research Letters*, **21**, 2191–2194.

DEMETS, C., JANSMA, P.E., MATTIOLI, G.S., DIXON, T.H., FARINA, F., BILHAM, R., CALAIS, E. & MANN, P. 2000. GPS geodetic constraints on Caribbean-North American plate motions. *Geophysical Research Letters*, **27**, 437–440.

DEPLUS, C., LE FRIANT, A., BOUDON, G., KOMOROWSKI, J.-C., VILLEMANT, B., HARFORD, C., SÉGOUFIN, J. & CHEMINÉE, J.-L. 2001. Submarine evidence for large-scale debris avalanches in the Lesser Antilles arc. *Earth and Planetary Science Letters*, **192**, 145–157.

DE RONDE, C.E.J., BAKER, E.T., MASSOTH, G.J., LUTON, J.E., WRIGHT, I.C., FEELEY, R.A. & GREENE, R.R. 2001. Intra-oceanic subduction-related hydrothermal venting, Kermadec arc, New Zealand. *Earth and Planetary Science Letters*, **193**, 359–369.

DESCHAMPS, A. & LALLEMAND, S. 2003. Geodynamic setting of Izu–Bonin–Mariana boninites. *In*: LARTER, R.D. & LEAT, P.T. (eds) *Intra-oceanic subduction Systems: Tectonic and Magmatic Processes*. Geological Society, London, Special Publications, **219**, 163–185.

DICKIN, A.P. 1995. *Radiogenic Isotope Geology*. Cambridge University Press, Cambridge.

DIXON, T.H., FARINA, F., DEMETS, C., JANSMA, P., MANN, P. & CALAIS, E. 1998. Relative motion between the Caribbean and North American plates and related boundary zone deformation from a decade of GPS observations. *Journal of Geophysical Research*, **103**, 15157–15182.

EGGINS, S.M., WOODHEAD, J.D., KINSLEY, L.P.J, MORTIMER, G.E., SYLVESTER, P. MCCULLOCH, M.T., HERGT, J.M. & HANDLER, M.R. 1997. A simple method for the precise determination of ≥40 trace elements in geological samples by ICPMS using enriched isotope international standardisation. *Chemical Geology*, **134**, 311–326.

ELLIOTT, T., PLANK, T., ZINDLER, A., WHITE, W. & BOURDON, B. 1997. Element transport from slab to volcanic front at the Mariana arc. *Journal of Geophysical Research*, **102**, 14 991–15 019.

ENGDAHL, E.R., VAN DER HILST, R. & BULAND, R. 1998. Global teleseismic earthquake relocation with improved travel times and procedures for depth determination. *Bulletin of the Seismological Society of America*, **88**, 722–743.

EWART, A. & HAWKESWORTH, C.J. 1987. The Pliocene–Recent Tonga–Kermadec arc lavas: interpretation of new isotopic and rare earth data in terms of a depleted mantle source model. *Journal of Petrology*, **28**, 495–530.

FISKE, R.S., NAKA, J., IIZASA, K., YUASA, M. & KLAUS, A. 2001. Submarine silicic caldera at the front of the Izu–Bonin arc, Japan: voluminous seafloor eruptions of rhyolite pumice. *Geological Society of America Bulletin*, **113**, 813–824.

FLIEDNER, M.M. & KLEMPERER, S.L. 1999. Structure of an island arc: wide-angle seismic studies in the eastern Aleutian Islands, Alaska. *Journal of Geophysical Research*, **104**, 10 667–10 694.

FLIEDNER, M.M. & KLEMPERER, S.L. 2000. Crustal structure transition from oceanic arc to continental arc, eastern Aleutian Islands and Alaska Peninsula. *Earth and Planetary Science Letters*, **179**, 567–579.

FOUQUET, Y., VON STACKELBERG, U., CHARLOU, J.L., DONVAL, J.P., ERZINGER, J., FOUCHER, J.P., HERZIG, P., MÜHE, R., SOAKAI, S., WIEDICKE, M. & WHITECHURCH, H. 1991. Hydrothermal activity and metallogenesis in the Lau back-arc basin. *Nature*, **349**, 778–781.

FRETZDORFF, S., LIVERMORE, R.A., DEVEY, C.W., LEAT, P.T. & STOFFERS, P. 2002. Petrogenesis of the back-arc East Scotia Ridge, South Atlantic Ocean. *Journal of Petrology*, **43**, 1435–1467.

FRYER, P. 1996. Evolution of the Mariana convergent plate margin system. *Reviews of Geophysics*, **34**, 89–125.

GAMBLE, J., WOODHEAD, J., WRIGHT, I. & SMITH, I. 1996. Basalt and sediment geochemistry and magma petrogenesis in a transect from oceanic island arc to rifted continental margin arc: the Kermadec–Hikurangi margin, SW Pacific. *Journal of Petrology*, **37**, 1523–1546.

GERMAN, C.R., LIVERMORE, R.A., BAKER, E.T., BRUGUIER, N.I., CONNELLY, D.P., CUNNINGHAM, A.P., MORRIS, P., ROUSE, I.P., STRATHAM, P.J. & TYLER, P.A. 2000. Hydrothermal plumes above the East Scotia Ridge: an isolated high-latitude back-arc spreading centre. *Earth and Planetary Science Letters*, **184**, 241–250.

GILL, J.B. 1981. *Orogenic Andesites and Plate Tectonics*. Springer, New York.

GRIBBLE, R.F., STERN, R.J., NEWMAN, S., BLOOMER, S.H. & O'HEARN, T. 1998. Chemical and isotopic composition of lavas from the northern Mariana Trough: implications for magmagenesis in back-arc basins. *Journal of Petrology*, **39**, 125–154.

HALL, R., NICHOLS, G., BALLANTYNE, P., CHARLTON, T. & ALI, J. 1991. The character and significance of basement rocks of the southern Molucca Sea region. *Journal of Southeast Asian Earth Sciences*, **6**, 249–258.

HARRISON, D., LEAT, P.T., BURNARD, P.G., TURNER, C., FRETZDORFF, S. & MILLAR, I.L. 2003. Resolving mantle components in oceanic lavas from segment E2 of the East Scotia back-arc ridge, South Sandwich Islands. *In*: LARTER, R.D. & LEAT, P.T. (eds) *Intra-oceanic Subduction Systems: Tectonic and Magmatic Processes*. Geological Society, London, Special Publications, **219**, 333–344.

HART, S.R. 1988. Heterogeneous mantle domains: signatures, genesis and mixing chronologies. *Earth and Planetary Science Letters*, **90**, 273–296.

HAWKESWORTH, C.J., GALLAGHER, K., HERGT, J.M. & MCDERMOTT, F. 1994. Destructive plate margin magmatism: geochemistry and melt generation. *Lithos*, **33**, 169–188.

HAWKESWORTH, C.J., TURNER, S.P., MCDERMOTT, F., PEATE, D.W. & VAN CALSTEREN, P. 1997. U–Th isotopes in arc magmas: implications for element transfer from the subducted crust. *Science*, **276**, 551–555.

HEATH, E., MACDONALD, R., BELKIN, H., HAWKESWORTH, C. & SIGURDSSON, H. 1998. Magmagenesis at Soufriere Volcano, St Vincent, Lesser Antilles. *Journal of Petrology*, **39**, 1721–1764.

HICKEY-VARGAS, R. 1989. Boninites and tholeiites from DSDP Site 458, Mariana forearc. *In*: CRAWFORD, A.J. (ed.) *Boninites*. Unwin Hyman, London, 339–356.

HOFMANN, A.W. & WHITE, W.M. 1982. Mantle plumes from ancient oceanic crust. *Earth and Planetary Science Letters*, **57**, 421–436.

HOLBROOK, W.S., LIZARRALDE, D., MCGEARY, S., BANGS, N. & DIEBOLD, J. 1999. Structure and composition of the Aleutian island arc and implications for continental crustal growth. *Geology*, **27**, 31–34.

IIZASA, K., FISKE, R.S., ISHIZUKA, O., YUASA, M., HASHIMOTO, J., ISHIBASHI, J., NAKA, J., HORII, Y., FUJIWARA, Y., IMAI, A. & KOYAMA, S. 1999. A Kuroko-type polymetallic sulfide deposit in a submarine caldera. *Science*, **283**, 975–977.

ISHIBASHI, J. & URABE, T. 1995. Hydrothermal activity related to arc–backarc magmatism in the Western Pacific. *In*: TAYLOR, B. (ed.) *Backarc Basins: Tectonics and Magmatism*. Plenum Press, New York, 451–495.

ISHIZUKA, O., UTO, K. & YUASA, M. 2003. Volcanic history of the back-arc region of the Izu–Bonin (Ogasawara) arc. *In*: LARTER, R.D. & LEAT, P.T. (eds) *Intra-oceanic Subduction Systems: Tectonic and Magmatic Processes*. Geological Society, London, Special Publications, **219**, 187–205.

JOHNSON, M.C. & PLANK, T. 1999. Dehydration and melting experiments constrain the fate of subducted sediments. *Geochemistry Geophysics Geosystems*, **1**, 1999GC000014.

JULL, M. & KELEMEN, P.B. 2001. On the conditions for lower crustal convective instability. *Journal of Geophysical Research*, **106**, 6423–6446.

KAMENETSKY, V.S., BINNS, R.A., GEMMELL, J.B., CRAWFORD, A.J., MERNAGH, T.P., MAAS, R. & STEELE, D. 2001. Parental basaltic melts and fluids in eastern Manus backarc basin: implications for hydrothermal mineralisation. *Earth and Planetary Science Letters*, **184**, 685–702.

KAWATE, S. & ARIMA, M. 1998. Petrogenesis of the Tanzawa plutonic complex, central Japan: exposed felsic middle crust of the Izu–Bonin–Mariana arc. *The Island Arc*, **7**, 342–358.

LARTER, R.D., CUNNINGHAM, A.P., BARKER, P.F., GOHL, K. & NITSCHE, F.O. 2002. Tectonic evolution of the Pacific margin of Antarctica 1. Late Cretaceous tectonic reconstructions. *Journal of Geophysical Research,* **107** (B12), EPMS, 1–19, 2345, 10.1029/2000JB000052.

LARTER, R.D., VANNESTE, L.E. & BRUGUIER, N.J. 2001. Structure, composition and evolution of the South Sandwich island arc: implications for rates of arc magmatic growth and subduction erosion. *Eos, Transactions, American Geophysical Union*, **82**(47), Fall Meeting Supplement, T32D-10.

LARTER, R.D., VANNESTE, L.E., MORRIS, P. & SMYTHE, D.K. 2003. Structure and tectonic evolution of the South Sandwich arc. *In*: LARTER, R.D. & LEAT, P.T. (eds) *Intra-oceanic Subduction Systems: Tectonic and Magmatic Processes*. Geological Society, London, Special Publications, **219**, 255–284.

LEAT, P.T., LIVERMORE, R.A., MILLAR, I.L. & PEARCE, J.A. 2000. Magma supply in back-arc spreading centre segment E2, East Scotia Ridge. *Journal of Petrology*, **41**, 845–866.

LEAT, P.T., RILEY, T.R., WAREHAM, C.D., MILLAR, I.L., KELLEY, S.P. & STOREY, B.C. 2002. Tectonic setting of primitive magmas in volcanic arcs: an example from the Antarctic Peninsula. *Journal of the Geological Society, London*, **159**, 31–44.

LEAT, P.T., SMELLIE, J.L., MILLAR, I.L. & LARTER, R.D. 2003. Magmatism in the South Sandwich arc. *In*: LARTER, R.D. & LEAT, P.T. (eds) *Intra-oceanic Subduction Systems: Tectonic and Magmatic Processes*. Geological Society, London, Special Publications, **219**, 285–313.

LIVERMORE, R.A. 2003. Back-arc spreading and mantle flow in the east Scotia Sea. *In*: LARTER, R.D. & LEAT, P.T. (eds) *Intra-oceanic Subduction Systems: Tectonic and Magmatic Processes*. Geological Society, London, Special Publications, **219**, 315–331.

LIVERMORE, R.A. & WOOLLETT, R.W. 1993. Seafloor spreading in the Weddell Sea and southwest Atlantic since the Late Cretaceous. *Earth and Planetary Science Letters*, **117**, 475–495.

LIVERMORE, R., CUNNINGHAM, A., VANNESTE, L. & LARTER, R. 1997. Subduction influence on magma supply at the east Scotia Ridge. *Earth and Planetary Science Letters*, **150**, 261–275.

LIVERMORE, R., MCADOO, D. & MARKS, K. 1994. Scotia Sea tectonics from high-resolution satellite gravity. *Earth and Planetary Science Letters*, **123**, 255–268.

LLOYD, E.F., NATHAN, S., SMITH, I.E.M. & STEWART, R.B. 1996. Volcanic history of Macauley Island, Kermadec Ridge, New Zealand. *New Zealand Journal of Geology and Geophysics,* **39**, 295–308.

LONSDALE, P. 1988. Paleogene history of the Kula plate – offshore evidence and onshore implications. *Geological Society of America Bulletin*, **100**, 733–754.

MACDONALD, R., HAWKESWORTH, C.J. & HEATH, E. 2000. The Lesser Antilles volcanic chain: a study in arc magmatism. *Earth Science Reviews,* **49**, 1–76.

MACPHERSON, C.G. & HALL, R. 2001. Tectonic setting of Eocene boninitic magmatism in the Izu–Bonin–Mariana forearc. *Earth and Planetary Science Letters*, **186**, 215–230.

MACPHERSON, C.G., FORDE, E.J., HALL, R. & THIRLWALL, M.F. 2003. Geochemical evolution of magmatism in an arc-arc collision: the Halmahera and Sangihe arcs, eastern Indonesia. *In*: LARTER, R.D. & LEAT, P.T. (eds) *Intra-oceanic Subduction Systems: Tectonic and Magmatic Processes*. Geological Society, London, Special Publications, **219**, 207–220.

MADSEN, J.A. & LINDLEY, I.D. 1994. Large-scale structures on Gazelle Peninsula, New Britain: implications for the evolution of the New Britain arc. *Australian Journal of Earth Sciences*, **41**, 561–569.

MAILLET, P., RUELLAN, E., GÉRARD, M., PERSON, A., BELLON, H., COTTEN, J., JORON, J.-L., NAKADA, S. & PRICE, R.C. 1995. Tectonics, magmatism, and evolution of the New Hebrides backarc troughs (Southwest Pacific). *In*: TAYLOR, B. (ed.) *Backarc Basins: Tectonics and Magmatism*. Plenum Press, New York, 177–235.

MANN, P., TAYLOR, F.W., LAGOE, M.B., QUARLES, A. & BURR, G. 1998. Accelerating late Quaternary uplift of the New Georgia island group (Solomon island arc) in response to subduction of the recently active Woodlark spreading center and Coleman Seamount. *Tectonophysics*, **295**, 259–306.

MARTINEZ, F. & TAYLOR, B. 2002. Mantle wedge control on back-arc crustal accretion *Nature*, **416**, 417–420.

MARTINEZ, F. & TAYLOR, B. 2003. Controls on back-arc crustal accretion: insights from the Lau, Manus and Mariana basins. *In*: LARTER, R.D. & LEAT, P.T. (eds) *Intra-oceanic Subduction Systems: Tectonic and Magmatic Processes*. Geological Society, London, Special Publications, **219**, 19–54.

MARTINEZ, F., FRYER, P., BAKER, N.A. & YAMAZAKI, T. 1995. Evolution of backarc rifting: Mariana Trough, 20°–24°N. *Journal of Geophysical Research*, **100**, 3807–3827.

MASSOTH, G.J., DE RONDE, C.E.J., LUPTON, J.E., FEELY, R.A., BAKER, E.T., LEBON, G.T. & MAENNER, S.M. 2003. Chemically rich and diverse submarine hydrothermal plumes of the southern Kermadec volcanic arc (New Zealand). *In*: LARTER, R.D. & LEAT, P.T. (eds) *Intra-oceanic Subduction Systems: Tectonic and Magmatic Processes*. Geological Society, London, Special Publications, **219**, 119–139.

MILLER, D.J. & CHRISTENSEN, N.I. 1994. Seismic signature and geochemistry of an island arc: a multidisciplinary study of the Kohistan accreted terrane, northern Pakistan. *Journal of Geophysical Research*, **99**, 11 623–11 642.

MONZIER, M., ROBIN, C. & EISSEN, J.-P. 1994. Kuwae (≈1425 A. D.): the forgotten caldera. *Journal of Volcanology and Geothermal Research*, **59**, 207–218.

MORRIS, J.D., LEEMAN, W.P. & TERA, F. 1990. The subducted component in island arc lavas: constraints from Be isotopes and B–Be systematics. *Nature*, **344**, 31–36.

NAKAJIMA, K & ARIMA, M. 1998. Melting experiments on hydrous low-K tholeiite: implications for the genesis of tonalitic crust in the Izu–Bonin–Mariana arc. *The Island Arc*, **7**, 359–373.

NAKANISHI, M., TAMAKI, K. & KOBAYASHI, K. 1989. Mesozoic magnetic anomaly lineations and seafloor spreading history of the northwest Pacific. *Journal of Geophysical Research*, **94**, 15 437–15 462.

NINKOVICH, D., HEEZEN, B.C., CONOLLY, J.R. & BURCKLE, L.H. 1964. South Sandwich tephra in deep-sea sediments. *Deep Sea Research*, **11**, 605–619.

PEARCE, J.A. 1983. Role of the sub-continental lithosphere in magma genesis at active continental margins. *In*: HAWKESWORTH, C.J. & NORRY, M.J. (eds) *Continental Basalts and Mantle Xenoliths*. Shiva, Nantwich, 230–249.

PEARCE, J.A. & PEATE, D.W. 1995. Tectonic implications of the composition of volcanic arc magmas. *Annual Reviews of Earth and Planetary Science*, **23**, 251–285.

PEARCE, J.A., BAKER, P.E., HARVEY, P.K. & LUFF, I.W. 1995. Geochemical evidence for subduction fluxes, mantle melting and fractional crystallization beneath the South Sandwich arc. *Journal of Petrology*, **36**, 1073–1109.

PEARCE, J.A., ERNEWEIN, M., BLOOMER, S.H., PARSON, L.M., MURTON, B.J. & JOHNSON, L.E. 1994. Geochemistry of Lau Basin volcanic rocks: influence of ridge segmentation and arc proximity. *In*: SMELLIE, J.L. (ed.) *Volcanism Associated with Extension at Consuming Plate Margins*. Geological Society, London, Special Publications, **81**, 53–75.

PEARCY, L.G., DEBARI, S.M. & SLEEP, N.H. 1990. Mass balance calculations for two sections of island arc crust and implications for the formation of continents. *Earth and Planetary Science Letters*, **96**, 427–442.

PEATE, D.W. & PEARCE, J.A. 1998. Causes of spatial compositional variations in Mariana arc lavas: trace element evidence. *The Island Arc*, **7**, 479–495.

PEATE, D.W., KOKFELT, T.F., HAWKESWORTH, C.J., VAN CALSTEREN, P.W., HERGT, J.M. & PEARCE, J.A. 2001. U-series isotope data on Lau Basin glasses: the role of subduction-related fluids during melt generation in back-arc basins. *Journal of Petrology*, **42**, 1449–1470.

PELLETIER, B., CALMANT, S. & PILLET, R. 1998. Current tectonics of the Tonga–New Hebrides region. *Earth and Planetary Science Letters*, **164**, 263–276.

PEREZ, O.J., BILHAM, R., BENDICK, R., VELANDIA, J.R., HERNANDEZ, N., MONCAYO, C., HOYER, M. & KOZUCH, M. 2001. Velocity field across the southern Caribbean plate boundary and estimates of Caribbean/South American plate motion using GPS geodesy 1994–2000. *Geophysical Research Letters*, **28**, 2987–2990.

PETTERSON, M.G., BABBS, T., NEAL, C.R., MAHONEY, J.J., SAUNDERS, A.D., DUNCAN, R.A., TOLIA, D., MAGU, R., QOPOTO, C., MAHOA, H. & NATOGGA, D. 1999. Geological–tectonic framework of Solomon Islands, SW Pacific: crustal accretion and growth within an intra-oceanic setting. *Tectonophysics*, **301**, 35–60.

PICHAVANT, & MACDONALD, R. 2003. Mantle genesis and crustal evolution of primitive calc-alkaline basaltic liquids from the Lesser Antilles arc. *In*: LARTER, R.D. & LEAT, P.T. (eds) *Intra-oceanic Subduction Systems: Tectonic and Magmatic Processes*. Geological Society, London, Special Publications, **219**, 239–254.

PLANK, T. & LANGMUIR, C.H. 1993. Tracing trace elements from sediment input to volcanic output at subduction zones. *Nature*, **362**, 739–743.

RAMSAY, W.R.H., CRAWFORD, A.J. & FODEN, J.D. 1984. Field setting, mineralogy, chemistry, and genesis of arc picrites, New Georgia, Solomon Islands. *Contributions to Mineralogy and Petrology*, **88**, 386–402.

RAPP, R.P. & WATSON, E.B. 1995. Dehydration melting of metabasalt at 8–32 kbar: implications for continental growth and crust–mantle recycling. *Journal of Petrology*, **36**, 891–931.

ROBIN, C., EISSEN, J.-P. & MONZIER, M. 1993. Giant tuff cone and 12 km-wide associated caldera at Ambrym Volcano (Vanuatu, New Hebrides arc). *Journal of Volcanology and Geothermal Research*, **55**, 225–238.

RUDNICK, R.L. 1995. Making continental crust. *Nature*, **378**, 571–578.

RYAN, J.G., MORRIS, J., TERA, F., LEEMAN, W.P. & TSVETKOV, A. 1995. Cross-arc geochemical variations in the Kurile arc as a function of slab depth. *Science*, **270**, 625–627.

SANDWELL, D.T. & SMITH, W.H.F. 1997. Marine gravity anomaly from Geosat and ERS 1 satellite altimetry. *Journal of Geophysical Research*, **102**, 10 039–10 954.

SAUNDERS, A.D. & TARNEY, J. 1984. Geochemical characteristics of basaltic volcanism within back-arc basins. *In*: KOKELAAR, B.P. & HOWELLS, M.F. (eds) *Marginal Basin Geology*. Geological Society, London, Special Publications, **16**, 59–76.

SENO, T., STEIN, S. & GRIPP, A.E. 1993. A model for the motion of the Philipine Sea plate consistent with NUVEL-1 and geological data. *Journal of Geophysical Research*, **98**, 17 941–17 948.

SHIPBOARD SCIENTIFIC PARTY 2000. Leg 185 summary: inputs to the Izu–Mariana subduction system. *In*: PLANK, T., LUDDEN, J.N., ESCUTIA, C. *et al. Proceedings of the Ocean Drilling Program, Initial Reports*, **185**, 1–63.

SINTON, J.M., FORD, L.F., CHAPPELL, B. & MCCULLOCH, M.T. 2003. Magma genesis and mantle heterogeneity in the Manus back-arc basin, Papua New Guinea. *Journal of Petrology*, **44**, 159–195.

SMELLIE, J.L., MORRIS, P., LEAT, P.T., TURNER, D.B. & HOUGHTON, D. 1998. Submarine caldera and other volcanic observations in Southern Thule, South Sandwich Islands. *Antarctic Science*, **10**, 171–172.

SMITH, G.P., WIENS, D.A., FISHER, K.M., DORMAN, L.M., WEBB, S.C. & HILDEBRAND, J.A. 2001. A complex pattern of mantle flow in the Lau backarc. *Science*, **292**, 713–716.

SMITH, I.E.M., WORTHINGTON, T.J., PRICE, R.C. & GAMBLE, J.A. 1997. Primitive magmas in arc-type volcanic associations: examples from the southwest Pacific. *The Canadian Mineralogist*, **35**, 257–273.

SMITH, I.E.M., WORTHINGTON, T.J., STEWART, R.B., PRICE, R.C. & GAMBLE, J.A. 2003. Felsic volcanism in the Kermadec arc, SW Pacific: crustal recycling in an oceanic setting. *In*: LARTER, R.D. & LEAT, P.T. (eds) *Intra-oceanic subduction Systems: Tectonic and Magmatic Processes*. Geological Society, London, Special Publications, **219**, 99–118.

SPEED, R.C. & WALKER, J.A. 1991. Oceanic crust of the Grenada Basin in the southern Lesser Antilles arc platform. *Journal of Geophysical Research*, **96**, 3835–3851.

STERN, R.J. & SMOOT, N.C. 1998. A bathymetric overview of the Mariana forearc. *The Island Arc*, **7**, 525–540.

STOLPER, E. & NEWMAN, S. 1994. The role of water in the petrogenesis of Mariana trough magmas. *Earth and Planetary Science Letters*, **121**, 293–325.

STRAUB, S.M. 1995. Contrasting compositions of Mariana Trough fallout tephra and Mariana Island arc volcanics: a fractional crystallization link. *Bulletin of Volcanology*, **57**, 403–421.

STÜBEN, D., BLOOMER, S.H., TAÏBI, N.E., NEUMANN, T., BENDEL, V., PÜSCEL, U., BARONE, A., LANGE, A., SHIYING, WU, CUIZHONG, LI & DEYU, Z. 1992. First results of study of sulphur-rich hydrothermal activity from and island-arc environment: Esmeralda Bank in the Mariana arc. *Marine Geology*, **103**, 521–528.

SUYEHIRO, K., TAKAHASHI, N., ARIIE, Y., YOKOI, Y., HINO, R., SHINOHARA, M., KANAZAWA, T., HIRATA, N., TOKUYAMA, H. & TAIRA, A. 1996. Continental crust, crustal underplating, and low-Q upper mantle beneath an ocean island arc. *Science*, **272**, 390–392.

TAMURA, Y. 2003. Some geochemical constraints on hot fingers in the mantle wedge: evidence from NE Japan. *In*: LARTER, R.D. & LEAT, P.T. (eds) *Intra-oceanic Subduction Systems: Tectonic and Magmatic Processes*. Geological Society, London, Special Publications, **219**, 221–237.

TAMURA, Y. & TATSUMI, Y. 2002. Remelting of an andesitic crust as a possible origin for rhyolitic magma in oceanic arcs: an example from the Izu–Bonin arc. *Journal of Petrology*, **43**, 1029–1047.

TAMURA, Y., TATSUMI, Y., ZHAO, D., KIDO, Y. & SHUKUNO, H. 2002. Hot fingers in the mantle wedge: new insights into magma genesis in subduction zones. *Earth and Planetary Science Letters*, **197**, 105–116.

TARNEY, J., PICKERING, K.T., KNIPE, R.J. & DEWEY, J.F. (eds). 1991. *The Behaviour and Influence of Fluids in Subduction Zones*. Royal Society, London. (*Philiosophical Transactions of the Royal Society of London, Series A*, **335**, 225–418.)

TATSUMI, Y. 1989. Migration of fluid phases and genesis of basalt magmas in subduction zones. *Journal of Geophysical Research*, **94**, 4697–4707.

TATSUMI, Y. & EGGINS, S. 1995. *Subduction Zone Magmatism*. Blackwell Science, Cambridge, MA.

TATSUMI, T. & KOGISO, T. 2003. The subduction factory: its role in the evolution of the Earth's crust and mantle. *In*: LARTER, R.D. & LEAT, P.T. (eds) *Intra-oceanic Subduction Systems: Tectonic and Magmatic Processes*. Geological Society, London, Special Publications, **219**, 55–80.

TAYLOR, B. 1992. Rifting and the volcanic-tectonic evolution of the Izu-Bonin–Mariana arc. *In*: TAYLOR, B., FUJIOKA, K. *et al. Proceedings of the Ocean Drilling Program, Scientific Results*, **126**, 627–651.

TAYLOR, B. (ed.). 1995. *Backarc Basins: Tectonics and Magmatism*. Plenum, New York.

TAYLOR, B. & EXON, N.F. 1987. An investigation of ridge subduction in the Woodlark–Solomons region: introduction and overview. *In*: TAYLOR, B. & EXON, N.F. (eds) *Marine Geology, Geophysics, and Geochemistry of the Woodlark Basin–Solomon Islands.* Circum-Pacific Council for Energy and Mineral Resources Earth Science Series, **7**, 24–235.

TAYLOR, B. & NATLAND, J. (eds). 1995. *Active Margins and Marginal Basins of the Western Pacific.* American Geophysical Union Monographs, **88**.

TAYLOR, B., BROWN, G., GILL, J.B., HOCHSTAEDTER, A.G., HOTTA, H., LANGMUIR, C.H., LEINEN, M., NISHIMURA, A. & URABE, T. 1990. ALVIN-SeaBeam studies of the Sumisu rift, Izu–Bonin arc. *Earth and Planetary Science Letters,* **100**, 127–147.

TAYLOR, F.W., BEVIS, M.G., SCHUTZ, B.E., KUANG, D., RECY, J., CALMANT, S., CHARLEY, D., REGNIER, M., PERIN, B., JACKSON, M. & REICHENFELD, C. 1995. Geodetic measurements of convergence at the New Hebrides island arc indicate arc fragmentation caused by an impinging aseismic ridge. *Geology*, **23**, 1011–1014.

TAYLOR, R.N., NESBITT, R.W., VIDAL, P., HARMON, R.S., AUVRAY, B. & CROUDACE, I.W. 1994. Mineralogy, chemistry and genesis of the boninite series volcanics, Chichijima, Bonin Islands, Japan. *Journal of Petrology*, **35**, 577–617.

TAYLOR, S.R. & MCLENNAN, S.M. 1985. *The Continental Crust: its Composition and Evolution*. Blackwell Scientific, Oxford.

TAYLOR, S.R. & MCLENNAN, S.M. 1995. The chemical evolution of the continental crust. *Reviews of Geophysics*, **33**, 241–265.

THOMAS, C., LIVERMORE, R.A. & POLLITZ, F.F. 2003. Motion of the Scotia Sea plates. *Geophysical Journal International*, in press.

THORPE, R.S. (ed.). 1982. *Andesites: Orogenic Andesites and Related Rocks*. John Wiley, Chichester.

TREGONING, P. 2002. Plate kinematics in the western Pacific derived from geodetic observations. *Journal of Geophysical Research*, **107**(B1), 2020, DOI: 10.1029/2001JB000406.

TREGONING, P., LAMBECK, K., STOLZ, A., MORGAN, P., MCCLUSKY, S.C., VAN DER BEEK, P., MCQUEEN, H., JACKSON, R.J., LITTLE, R.P., LAING, A. & MURPHY, B. 1998. Estimation of current plate motions in Papua New Guinea from Global Positioning System observations. *Journal of Geophysical Research*, **103**, 12 181–12 203.

TSUNOGAI, U., ISHIBASHI, J., WAKITA, H., GAMO, T., WATANABE, K., KAJIMURA, T., KANAYAMA, S. & SAKI, H. 1994. Peculiar features of Suiyo Seamount hydrothermal fluids, Izu-Bonin arc: differences from subaerial volcanism. *Earth and Planetary Science Letters*, **126**, 289–301.

TURNER, S. & HAWKESWORTH, C. 1997. Constraints on flux rates and mantle dynamics beneath island arcs from Tonga-Kermadec lava geochemistry. *Nature*, **389**, 568–573.

TURNER, S. & HAWKESWORTH, C. 1998. Using geochemistry to map mantle flow beneath the Lau Basin. *Geology*, **26**, 1019–1022.

TURNER, S., HAWKESWORTH, C., VAN CALSTEREN, P., HEATH, E., MACDONALD, R. & BLACK, S. 1996. U-series isotopes and destructive plate margin magma genesis in the Lesser Antilles. *Earth and Planetary Science Letters*, **142**, 191–207.

TURNER, S., MCDERMOTT, F., HAWKESWORTH, C. & KEPEZHINSKAS, P. 1998. A U-series study of lavas from Kamchatka and the Aleutians: constraints on source composition and melting process. *Contributions to Mineralogy and Petrology*, **133**, 217–234.

VAN SOEST, M.C., HILTON, D.R., MACPHERSON, C.G. & MATTEY, D.P. 2002. Resolving sediment subduction and crustal contamination in the Lesser Antilles island arc: a combined He–O–Sr isotope approach. *Journal of Petrology*, **43**, 143–170.

VANNESTE, L. & LARTER, R.D. 2002. Sediment subduction, subduction erosion and strain regime in the northern South Sandwich forearc. *Journal of Geophysical Research*, **107** (B7), EMPS, 1–24, 2149, 10.1029/2001JB000396.

VANNESTE, L.E., LARTER, R.D. & SMYTHE, D.K. 2002. A slice of intraoceanic arc: insights from the first multichannel seismic reflection profile across the South Sandwich arc. *Geology*, **30**, 819–822.

VON HUENE, R. & SCHOLL, D.W. 1991. Observations at convergent margins concerning sediment subduction, subduction erosion, and growth of the continental crust. *Reviews of Geophysics*, **29**, 279–316.

WEBER, J.C., DIXON, T.H., DEMETS, C., AMBEH, W.B., JANSMA, P., MATTIOLI, G., SALEH, J., SELLA, G., BILHAM, R. & PEREZ, O. 2001. GPS estimate of relative motion between the Caribbean and South American plates, and geologic implications for Trinidad and Venezuela. *Geology*, **29**, 75–78.

WESTBROOK, G.K., LADD, J.W., BUHL, P., BANGS, N. & TILEY, G.J. 1988. Cross section of an accretionary wedge: Barbados Ridge complex. *Geology*, **16**, 631–635.

WESTBROOK, G.K., MASCLE, A. & BIJU-DUVAL, B. 1984. Geophysics and the structure of the Lesser Antilles forearc. *In*: BIJU-DUVAL, B., MOORE, J.C. *et al. Initial Reports of the Deep Sea Drilling Project*, **78A**, 23–38.

WINDER, R.O. & PEACOCK, S.M. 2001. Viscous forces acting on subducting lithosphere. *Journal of Geophysical Research*, **106**, 21 937–21 951.

WILSON, M. 1989. *Igneous Petrogenesis*. Unwin Hyman, London.

WOODHEAD, J.D. 1988. The origin of geochemical variations in Mariana lavas: a general model for petrogenesis in intraoceanic island arcs? *Journal of Petrology*, **29**, 805–830.

WOODHEAD, J., EGGINS, S. & GAMBLE, J. 1993. High field strength and transition element systematics in island arc and back-arc basin basalts: evidence for multi-phase melt extraction and a depleted mantle wedge. *Earth and Planetary Science Letters*, **114**, 491–504.

WOODHEAD, J.D., EGGINS, S.M. & JOHNSON, R.W. 1998. Magma genesis in the New Britain island arc: further insights into melting and mass transfer processes. *Journal of Petrology*, **39**, 1641–1668.

WORTHINGTON, T.J., GREGORY, M.R. & BONDARENKO, V. 1999. The Denham caldera on Raoul Volcano: dacitic volcanism in the Tonga–Kermadec arc. *Journal of Volcanology and Geothermal Research*, **90**, 29–48.

WRIGHT, I.C. & GAMBLE, J.A. 1999. Southern Kermadec submarine caldera arc volcanoes (SW Pacific); caldera formation by effusive and pyroclastic eruption. *Marine Geology*, **161**, 207–227.

ZHAO, D., HASEGAWA, A. & HORIUCHI, S. 1992. Tomographic imaging of P and S wave velocity structure beneath northeastern Japan. *Journal of Geophysical Research*, **97**, 19 909–19 928.

ZHAO, D., XU, Y., WIENS, D.A., DORMAN, L., HILDEBRAND, J. & WEBB, S. 1997. Depth extent of the Lau back-arc spreading center and its relation to subduction processes. *Science*, **278**, 254–257.

This page intentionally left blank

Controls on back-arc crustal accretion: insights from the Lau, Manus and Mariana basins

FERNANDO MARTINEZ[1] & BRIAN TAYLOR[2]

[1]*Hawaii Institute of Geophysics and Planetology, School of Ocean and Earth Science and Technology, University of Hawaii at Manoa, 1680 East–West Road, Honolulu, HI 96822, USA (e-mail: fernando@hawaii.edu)*

[2]*Department of Geology and Geophysics, School of Ocean and Earth Science and Technology, University of Hawaii at Manoa, 1680 East–West Road, Honolulu, HI 96822, USA*

Abstract: Together, the Lau, Manus and Mariana basins encompass a broad range of conditions of back-arc basin development. Marine surveys have determined the tectonic setting and reconnaissance-scale geophysical and geochemical properties of the extension axes in these basins. We review these data to examine crustal accretion characteristics in the back-arc setting. In each basin magmatism is enhanced in spreading centres near the arc volcanic front, but decreases becoming 'deficient' in axes further from the arc. In the Lau and Manus basins the axes extend far behind the arc and develop typical mid-ocean ridge (MOR)-like characteristics. We propose that these variations are controlled by the subducting slab, which shapes composition and flow within the mantle wedge: water released from the slab lowers the mantle solidus and increases in concentration toward the volcanic arc. Spreading centres near the arc advect the hydrated mantle material, enhancing melt production. Slab-induced flow carries melt-depleted mantle material back beneath the basin where it mixes with ambient mantle. Spreading centres further from the arc advect this mantle mixture and produce thinner than normal crust. Far from the arc, spreading centres advect essentially mid-ocean ridge basalt (MORB)-source mantle and their characteristics are MOR-like. Thus, in addition to spreading-rate effects on mantle melting that predominate at MORs, in back-arc basins the subducting slab introduces additional systematic effects.

Back-arc basin formation is genetically associated with subduction zones (Weissel 1981). Despite this convergent plate-boundary setting, early geophysical and sampling surveys showed that back-arc basins form by extension and accretion of oceanic-like crust (Karig 1970, 1971; Packham & Falvey 1971; Shor *et al.* 1971; Hart *et al.* 1972; Moberly 1972; Sclater *et al.* 1972). Modern Global Positioning System (GPS) studies confirm the extensional nature of these basins on the margins of converging larger plates (Bevis *et al.* 1995; Kato *et al.* 1998, 2003; Tregoning 2002). There has been a continuing debate, however, as to how similar the extension and crustal accretion process is to seafloor spreading at mid-ocean ridges (MORs) (Weissel 1977; Karig *et al.* 1978; Lawver & Hawkins 1978; Barker & Hill 1980; Taylor & Karner 1983; Tamaki 1985; Hamburger & Isacks 1988). Detailed mapping and geophysical surveys show that, at mature stages, back-arc crustal accretion occurs in narrow neovolcanic zones and is similar in morphological, kinematic and magnetic characteristics to sea floor spreading at MORs (Parson *et al.* 1990; Ruellan *et al.* 1994; Taylor *et al.* 1996; Livermore *et al.* 1997; Zellmer & Taylor 2001). At earlier stages (analogous to continental rifting and early magmatism prior to organized seafloor spreading), however, more complex asymmetric crustal accretion occurs that may include rifting of pre-existing arc material plus juvenile arc/back-arc magmatism (Hawkins 1994; Parson & Hawkins 1994; Martinez *et al.* 1995; Wright *et al.* 1996).

Geophysical mapping has begun to achieve continuous coverage of entire spreading systems in several back-arc basins. This coverage allows assessment of the characteristics of spreading within individual basins and for comparisons to be made between basins under different opening rates, subduction rates, slab geometry, and position and development stage of the spreading systems. Geophysical data, primarily seismic, bathymetric and gravity mapping, provide direct and indirect measures of crustal thickness and therefore of variations in total crustal production in different settings. Geochemical data provide point measures of composition, which in back-arc settings can be quite heterogeneous. With sufficient sample density, however, broad

From: LARTER, R.D. & LEAT, P.T. 2003. *Intra-Oceanic Subduction Systems: Tectonic and Magmatic Processes.* Geological Society, London, Special Publications, **219**, 19–54. 0305-8719/03/$15.00

geochemical trends can be resolved, which provide information on melting conditions and the nature of the mantle sources. After a period of rifting, the seafloor spreading axis often initiates near the arc volcanic front and with time migrates away from the front by accretion of new crust and lithosphere. The melt-source regions of the back-arc spreading centres thus transect across and sample the mantle wedge. By examining the processes of active seafloor spreading, and the nature of the crust through time, important information about the mantle wedge and its effects on crustal accretion can be derived.

We examine crustal accretion characteristics using bathymetry, geophysical and geochemical observations from the Lau, Manus and Mariana back-arc basins, each of which has well-surveyed spreading/rifting regions. The Lau Basin has a large spreading-rate variation, a planar slab that dips beneath the entire basin with rapid subduction rates, and spreading centres that progressively separate from the volcanic front. The Manus Basin is a fast-opening basin with multiple rifts and spreading centres at varying distances from the volcanic front offset by transform faults. The basin is underlain by a rapidly subducting slab that nowhere underlies the extensional axes. The Mariana Trough is a slowly opening, crescent-shaped back-arc basin with intermediate subduction rates and a steeply dipping slab that only underlies the extension axis at its northern and southern ends.

Together these basins encompass a broad range of conditions and development stages of present-day intra-oceanic back-arc basins. A goal of this paper is to examine the tectonic, geophysical and geochemical features of the active extension axes in these basins, and their products comprising the basin flanks, to discern important processes and variables controlling crustal accretion in the back-arc setting.

Methods

We use several methods to assess variations in crustal thickness and infer magmatic production. Where available, direct determinations of crustal thickness by seismic techniques are used. Such determinations, however, have only been made in limited areas of the Lau Basin and central Mariana Trough. Depth variations within individual basins are another useful indication of relative crustal thickness variations, especially when combined with gravity data. The young and thin lithosphere in active basins behind the forearc is largely in local isostatic equilibrium, as indicated by Airy modelling of crustal thicknesses that yields low (<5–10 mGal) residual gravity anomalies (Martinez & Taylor 1996, 2002). Where joint gravity–topographic analyses have been carried out (Sager 1979; Sinha 1995; Peirce *et al.* 2001; Martinez & Taylor 2002) they show consistent agreement in the sense of crustal thickness variations with independent measures by seismic methods (LaTraille & Hussong 1980; Turner *et al.* 1999; Crawford *et al.* 2003). Although the mantle beneath back-arc basins can regionally differ in density (Sager 1980) and viscosity (Billen & Gurnis 2001) from mantle beneath mid-ocean settings, these differences result in broad topographic effects across the back-arc basin; local and often abrupt changes in depth within the basins are not likely to be due to sublithospheric mantle effects but rather to crustal thickness changes with a smaller contribution from crustal density changes. At spreading centre axes, however, dynamic effects related to extensional lithospheric mechanics, which are correlated with spreading rate, may systematically affect axial topography (e.g. Macdonald 1982; Chen & Morgan 1990*a*). Therefore, when assessing systematic local topographic variations within individual back-arc spreading centres, differences in spreading rate of the axes need to be considered. We find that back-arc axial topographic variations may run counter to expected spreading rate trends at MORs (e.g. transitioning from an axial valley to a high with *decreasing* spreading rate). This reinforces the interpretation that these topographic changes primarily reflect changes in crustal thickness and magmatic production, analogous to the slow-spreading Reykjanes Ridge showing fast-spreading morphology due to hot-spot influence and thick crust (Bell & Buck 1992). Although gravity and topography can provide relative measures of crustal thickness changes, additional seismic determinations are required to confirm these and to make quantitative assessments. Finally, side-scan sonar imagery shows the distribution of recent lava flows and helps assess recent magmatic activity.

To help synthesize and discuss the relevant geochemical data, we present some of the source characteristics of back-arc lavas in Tables 1–3 and Figure 1. FeO and Na_2O content fractionation corrected to 8% MgO ($Fe_{8.0}$, $Na_{8.0}$) are tabulated for comparison to global mid-ocean ridge basalt (MORB) compilations and systematics (Klein & Langmuir 1987, 1989; Langmuir *et al.* 1992; Plank & Langmuir 1992). Laboratory experiments indicate that higher pressure melts have lower SiO_2 compositions and, at higher potential temperatures, will have higher FeO (e.g. Hirose & Kushiro 1993). Na_2O is incompatible and so low $Na_{8.0}$ values reflect a high degree of partial melting. Thus, the global MORB trend is for longer melting columns and greater degrees of partial melting to be characterized by low $Na_{8.0}$ and high $Fe_{8.0}$ (Langmuir *et al.* 1992). These relations assume a uniform peridotite source and were developed for anhydrous melting, whereas basalts above subduction zones often have higher oxygen fugacity (fO_2) and water content (Carmichael 1991; Ulmer 2001). The presence of water will lower the mantle mineral solidus temperatures and promote greater degrees of melting (Hirose & Kawamoto 1995), producing trends of decreasing $Fe_{8.0}$ with decreasing $Na_{8.0}$ (Fig. 1) – trends that are similar to the 'local trend' seen in the global MORB data set (Niu *et al.* 2001). Although we characterize the lavas by their $Fe_{8.0}$, and $Na_{8.0}$, values, our interpretations of these variations *within* basins are in terms of varying source composition (as a function of previous extents of melting and water content) rather than melting column depth range and temperature (Fig. 1). We report direct measurements of the water contents, also adjusted to 8% MgO, where they have been measured by Fourier transform infrared (FTIR) spectroscopy of glass samples (Table 1–3). There are also systematic variations *between* different basins in $Fe_{8.0}$ and $Na_{8.0}$ values, however, that we do relate to regional differences in mantle temperature (Fig. 1).

As independent measures of the extent of melting, we also summarize TiO_2, Y and Yb data, fractionation corrected to 8% MgO ($Ti_{8.0}$, $Y_{8.0}$, $Yb_{8.0}$), in Tables 1–3. Each of these high-field-strength or heavy rare earth element (HFSE or HREE) concentrations decreases as the total extent of melting increases. The extent of melting reflects the combination of four effects: the depression of the mantle solidus as a function of water content (hydrous flux melting); the amount of adiabatic upwelling above the solidus (decompression melting); the original composition of the mantle (which may have experienced prior melting); and mantle temperature. HFSE and HREE depletions (relative to MORB) within arc lavas are interpreted to result from previous melt extraction. The prior melting is often attributed to current or former back-arc spreading (e.g. Ewart & Hawkesworth 1987; Woodhead *et al.* 1993, 1998; Ewart *et al.* 1998). However, the global maximum in arc depletion is sustained in the Izu–Bonin arc for >12 Ma without back-arc spreading (Hochstaedter *et al.* 2000). This argues that regular arc processes, such as magmatism behind the volcanic front (Hochstaedter *et al.* 2000, 2001) and ongoing hydrous fluxing of the arc sources (Stolper & Newman 1994), are capable of sustaining the heterogeneity of the mantle wedge (i.e. depletion of arc sources relative to back-arc and MORB sources). Thus, measures of extents of melting do not translate directly into crustal production in arc–back-arc settings, but rather reflect the history of melt extraction. Crustal production will depend on the fraction of current (not former) hydrous and decompression melting, multiplied by the (arc or back-arc) mantle melting volume, as well as other factors such as the amount of melt retained in the mantle.

Fluids progressively released from the subducting slab carry with them incompatible elements, including the large ion lithophile elements (LILE), that are enriched (relative to HFSE and HREE) in arc and some back-arc lavas (Gill 1981; Pearce & Parkinson 1993; Pearce & Peate 1995). We include Ba/Nb, Ba/La and Th/Zr (as well as H_2O) data in Tables 1–3 as measures of these enrichments by subduction components.

The Lau Basin

Tectonic setting

The Lau Basin, located between 15°–25°S and 174°–179°W, is a back-arc basin behind the Tonga subduction zone (Fig. 2). Basin depths are predominantly between 2000 and 3000 m but rise to above sea level at Niuafo'ou island. Shallow (<2000 m) 'V'-shaped, conjugate rifted arc edifices comprise the Tonga (forearc) and Lau (remnant arc) ridges that bound the basin to the east and west, respectively (Fig. 2). The basin is about 500 km wide at its northern end, and narrows southward to *c.* 200 km where it merges with the Havre Trough. The Pacific Plate subducts at rates as high as 240 mm a^{-1} at the northern end of the Tonga Trench (Bevis *et al.* 1995) and the seismically defined slab is approximately planar and extends beneath the entire Lau Basin at a dip of *c.* 45° (Isacks & Barazangi 1977; Chiu *et al.* 1991). Although the major surrounding Australian and Pacific plates are converging, the basin is opening at rates that increase northward to *c.* 160 mm a^{-1} (Bevis *et al.* 1995) as a result of trench rollback. The Tofua arc, a linear chain of predominantly submarine arc volcanoes, is located approximately above the 100 km-depth contour of the slab and just west of the Tonga Ridge. The volcanic front trends 021° and the zone of arc volcanism behind the front is only 30 km wide (Fig. 3).

Table 1. *Representative back-arc basin lava geochemistry in the Lau Basin*

Lau Basin cruise sample	CLSC SO48- 42GC	CLSC SO48- 18GA2	CLSC Keldys90- 2231-8G	CLSC CD33- 15-1-1	ILSC CD33- 41-2-1	N. ELSC CD33- 20-5-2	N. ELSC Keldys90- 2239-2G	N. ELSC CD33- 22-6-1	ELSC CD33- 23-3-2	ELSC CD33- 23-8-2	ELSC CD33- 25-1-1	S. ELSC SeapsoIV- Dr4-1C	VFR SO35- 84KD1	VFR SO48- 128KD	834-7 ODP135 Unit 7	834-8 ODP135 Unit 8	839-3 ODP135 Unit 3
Lat. (°S)	18.576	18.595	18.607	18.883	19.277	19.488	19.514	19.688	20.057	20.057	20.583	21.317	22.140	22.690	18.568	18.568	20.709
Depth	2253	2280	2248	2295	3050	2640	2750	2730	2650	2650	2620	2100	1723	1800			
SiO_2	49.72	50.23	50.83	50.53	50.5	51.23	51.98	51.4	51.5	51.8	51.1	53.2	50.36	52.8	49.99	52.48	52.94
MgO	8.19	7.1	7.57	7.3	8.11	7.93	6.91	7.06	7.45	7.9	6.57	5.4	7.31	6.13	8.23	6.37	6.70
$Na_{8.0}$	2.32	2.54	2.37	2.30	1.85	1.98	2.10	2.22	2.00	1.86	1.91	2.01	1.49	1.89	3.21	2.62	1.75
$Fe_{8.0}$	10.34	9.94	10.01	8.87	8.08	9.74	9.24	9.39	9.90	8.08	7.93	8.10	8.15	7.97	8.94	7.51	7.61
$Ti_{8.0}$	1.14	1.15	1.10	0.95	0.85	0.94	0.86	0.93	0.95	0.75	0.67	0.72	0.63	0.58	1.50	0.86	0.47
$Y_{8.0}$	32.2	30.3	29.1	23.9	21.5	27.6	19.8	24.6	23.9	17.3	15.5	15.4	12.9	14.5	30.8	16.5	8.4
$Yb_{8.0}$	3.14	2.99	2.94	2.41	2.17	2.90	1.85	2.47	2.55	1.88	1.79	1.36	1.28		2.74	1.40	0.80
Ba/Nb	7.3	6.4	10.0	6.9	11.4	8.3	20.0	7.8	10.0	25.0	13.6	38.8	130.5		3.5	37.8	142.0
Ba/La	4.4	3.4	5.2	4.5	9.5	5.1	5.4	6.2	5.5	10.6	6.0	19.3	32.0		1.55	15.64	24.3
1000Th/Zr	1.37	1.37		1.31	2.90	1.45		2.09	1.02	1.06	1.27	2.80	4.84		0.76	0.81	6.90
$(H_2O)_{8.0}$	0.18	0.22	0.27	0.22	0.46	0.37	0.61	0.50					1.08				
Reference	a, b	a, b	c, d	a, b, e	a, b, e	a, b, e	c, d	a, b, e	e	e	e	f	a, b, e	g	h	h	i

$Na_{8.0} = [Na_2O+0.115(8\text{-}MgO)]/[1+0.133(8\text{-}MgO)]$ (Plank & Langmuir 1992).
$Fe_{8.0} = [FeO^*+(8\text{-}MgO)]/[1+0.25(8\text{-}MgO)]$, where FeO^* expresses all Fe as Fe^{2+} (Taylor & Martinez 2003).
$Ti_{8.0} = [TiO_2-1/70(8\text{-}MgO)]/[1+2/7(8\text{-}MgO)]$.
$Y_{8.0} = [Y\text{-}2.5(8\text{-}MgO)]/[1+0.25(8\text{-}MgO)]$.
$Yb_{8.0} = [Yb+0.25(8\text{-}MgO)]/[1+0.25(8\text{-}MgO)]$.
$(H_2O)_{8.0} = (H_2O)(MgO^{1.7})/8^{1.7}$ (Taylor & Martinez 2003).
References: (a) Peate *et al.* (2001); (b) Kent *et al.* (2002); (c) Falloon *et al.* (1992); (d) Danyushevsky *et al.* (1993); (e) Pearce *et al.* (1995); (f) Boespflug *et al.* (1990); (g) Sunkel *et al.* (1990); (h) Hergt & Farley (1994); (i) Ewart *et al.* (1994*b*).

Table 2. *Representative back-arc basin lava geochemistry in the Manus Basin and the Sumisu Rift*

Manus Basin	ETZ-M1	ETZ-B	ETZ-M1	MSC-M1	MSC-B	MSC-B	MSC-M2	MSC-M2	SR-Bs	SR-Bs	SER-Be	SER-A2	SER-A2	SER-A2	SER-A1	Sumisu R.	Sumisu R.	Sumisu R.
cruise	MW8518	MW8518	MW8518	MW8518	MW8518	MW8518	MW8518	MW8518	MW8518	MW8518	MW8518	MW8518	MW8518	MW8518	MW8518	KK84-3	KK84-3	GSJ
sample	G32-5	G31C-8	G29A-3	G36B-1	G38C-9	G41A-3/4	G42A-3	G47-1	G21-1-3	19-12	G18B-4	G16-9/14	15-4	G15.2/4/6	14-9	12.01/1	12.06/2	962-1
Long. (°E)	149.015	149.2583	149.57	149.9633	150.0816	150.2083	150.285	150.5066	150.5016	151.1583	151.4633	151.8733	151.9833	151.9833	152.1733	30.96°N	30.96°N	31.015°N
Depth	2360	2160	2318	2160	2213	2388	2485	2535	2433	2630	2655	2023	1863	1863	1853	2020	2020	2175
SiO_2	50.3	50.3	50.8	50.7	52.6	52	50.9	51.1	51.6	52.75	53.9	54.8	52.73	53.3	52.92	49.9	50	48.09
MgO	7.89	8.25	8.16	6.79	5.52	6.25	6.55	5.47	6.39	5.84	5.7	5.5	7.18	5.03	5.47	6.3	8	7.35
$Na_{8.0}$	2.21	1.50	2.20	1.96	2.27	2.24	2.14	2.32	1.95	2.25	1.96	2.26	1.86	1.73	2.48	2.39	2.6	1.67
$Fe_{8.0}$	10.42	7.27	10.88	10.30	9.68	7.97	10.09	10.98	8.28	7.75	7.17	6.34	8.20	7.43	7.42	7.70	9.19	8.46
$Ti_{8.0}$	1.01	0.43	1.07	0.95	0.80	0.62	0.87	1.04	0.47	0.52	0.36	0.32	0.30	0.23	0.33	0.75	1.04	0.6
$Y_{8.0}$	25.6	11.3	22.3	20.7	14.7	10.9	18.6	20.6	8.5	13.4	3.3	3.5	4.9	0.9	4.3	13.9	22	9.8
$Yb_{8.0}$	2.50					1.43	2.05	2.74	1.04	1.33	0.63		0.65		0.45			0.89
Ba/Nb	5.9	30	4.4	20.0	33.3	19.0	15.0	11.0	51.4	47.7	113.3	150.0	170.0	288.3	257.8			
Ba/La	3.6					9.0	9.0	6.5	21.2	15.8	34.0	36.5	40.5		42.3			
1000Th/Zr	1.39									2.95					8.66			
$(H_2O)_{8.0}$		1.21	0.19		0.66	0.88	0.57	0.27	0.82	0.88		0.86						
Reference	a	a	a	a	a	a	a	a	a	a	a	a	a	a	a	b	b	c

See the footnotes to Table 1 for the definitions of $Na_{8.0}$, $Fe_{8.0}$, $Ti_{8.0}$, $Y_{8.0}$, $Yb_{8.0}$ and $(H_2O)_{8.0}$.
References: (a) Sinton *et al.* (2003); (b) Hochstaedter *et al.* (1990*a*, *b*); (c) Fryer *et al.* (1990).

Table 3. *Representative back-arc basin lava geochemistry in the Mariana Trough*

Mariana Trough													Arc-like			C. Graben	VTZ	VTZ
cruise	Sonne69	Sonne69	Sonne69	Sonne69	Sonne69	Sonne69	Sonne69	Atlantis II	Atlantis II	Atlantis II	Atlantis II	Atlantis II	Atlantis II	TWtunes7	TWtunes7	TWtunes7	TWtunes7	TWtunes7
sample	S84: 2-1	S88: 1-2	S88: 2-1	S79: 2-2	S74: 2-3	S74: 3-1	S71: 1-7	WOK27-1	A1849-9	WOK2-8	A1833-11	A1846-12	A1846-9	T75: 1-2	T76: 1-1	T46: 1-6	T68: 1-2	T54: 1-1
Lat. (°N)	15.01	15.3	15.3	16.08	16.53	16.53	16.99	17.71	17.75	17.83	18.08	18.35	18.35	19.44	19.45	20.82	21.35	22.79
Depth	4159	4475	4475	3686	3655	3655	3400	3950	3910	4080	3650	3500	3500	4415	3923	3700	3850	3445
SiO_2	51.29	50.77	50.71	50.43	50.78	51.64	49.36	50.3	50.56	50.68	51.13	50.75	49.67	52.3	52.79	51.46	52.48	50.6
MgO	7.22	6.18	6.72	7.39	6.29	7.13	7.74	8.07	7.36	6.98	7.55	7	6.95	7.33	7.23	7.07	6.26	6.53
$Na_{8.0}$	3.00	3.03	2.80	2.95	2.35	2.55	2.43	2.96	2.92	2.82	2.75	2.53	1.92	3.07	3.24	2.50	2.49	2.49
$Fe_{8.0}$	8.54	7.34	7.42	7.51	6.77	7.25	7.42	8.70	8.23	7.73	7.19	6.85	6.40	7.75	8.60	7.09	6.45	6.70
$Ti_{8.0}$	1.20	1.09	0.98	0.98	0.69	0.97	0.83	1.42	1.15	1.07	0.92	0.85	0.43	1.34	1.32	0.87	0.66	0.68
$Y_{8.0}$								33.8	22	27.5		18.0	9.8					
$Yb_{8.0}$	2.48	2.12	1.98	2.07	1.29	1.98	1.71							2.60	2.88	1.97	1.12	1.15
Ba/Nb								8	6.8	48		11	49					
Ba/La	2.6	6.5	8.1	9.5	10.3	11.8	11.8		7.0		7.0	5.4	6.0	5.5	5.1	12.1	12.4	12.3
1000Th/Zr									2.78		3.29	3.45	12.05					
$(H_2O)_{8.0}$	0.18	0.84	0.77	0.85	1.44	0.97	1.27				1.06	1.26	1.52	0.62	0.61	1.14	1.23	1.20
Reference	a	a	a	a	a	a	a	b	b	b	b, c	b, c	b, c	d	d	d	d	d

See the footnotes to Table 1 for the definitions of $Na_{8.0}$, $Fe_{8.0}$, $Ti_{8.0}$, $Y_{8.0}$, $Yb_{8.0}$ and $(H_2O)_{8.0}$.
References: (a) Gribble *et al.* (1996); (b) Hawkins *et al.* (1990); (c) Stolper & Newman (1994); (d) Gribble *et al.* (1998).

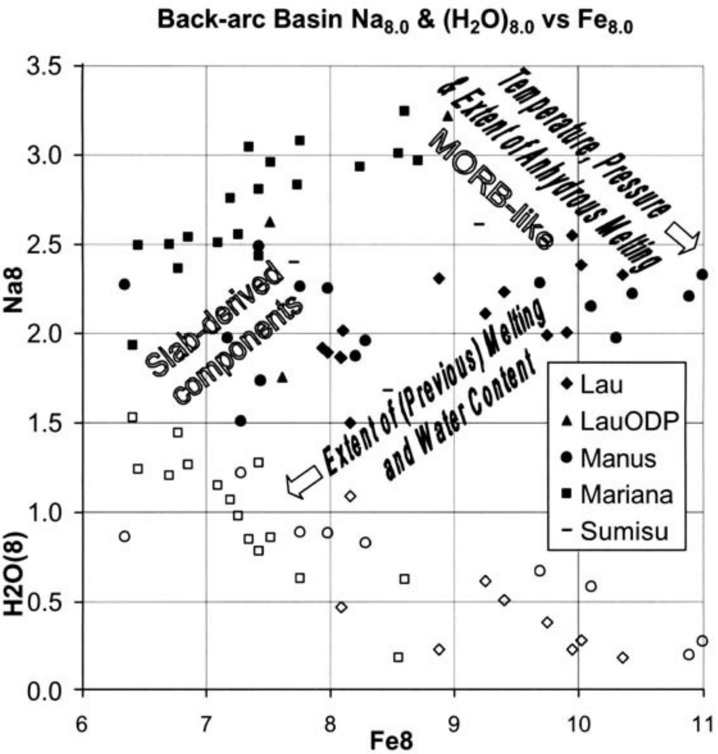

Fig. 1. Plot of Na_2O (solid symbols) and H_2O (open symbols) v. total FeO, both fractionation corrected to 8% MgO, for back-arc basin lavas (Tables 1–3). This is a representative subset of the more complete data presented in Taylor & Martinez (2003). MORB-like samples from the Mariana Trough (S84), Manus Basin (M1) and Lau Basin (CLSC), with low water contents (0.2–0.3%, Tables 1–3), follow global MORB trends that reflect their extent of melting under almost anhydrous conditions (Langmuir *et al.* 1992). Strongly slab-influenced samples from shallow segments of the Mariana Trough (VTZ), Manus Basin (A2, A1) and Lau Basin (S. ELSC, VFR) have high extents of previous melting and high water contents (1.2–1.7%, Tables 1–3). The back-arc basin basalts in each basin lie along trends of decreasing $Na_{8.0}$ with decreasing $Fe_{8.0}$ that reflect varying extents of previous melting and water addition between these end-member compositions. The offset of the $Na_{8.0}$–$Fe_{8.0}$ trend for the Mariana Trough from those of the Lau and Manus basins reflects lower mantle temperatures beneath the Mariana Trough associated with its slow spreading and subduction rates. Note that rift (Sumisu) and early basin (Lau ODP) lavas can be BABB or MORB-like (Tables 1–3).

The initial rifting that formed the Lau Basin was on the forearc side of the then-active (now remnant) volcanic arc (the Lau Ridge), whose arc volcanism represented by the Korobasaga Group continued until 2.4 Ma (Cole *et al.* 1985, 1990; Whelan *et al.* 1985). The modern Tofua arc did not start to develop on the eastern edge of the Lau Basin until 3.5 Ma (Tappin *et al.* 1994). Spreading propagation was not symmetric down the middle of the basin, but rather was along the eastern part of the basin near the location of the modern volcanic front (Parson *et al.* 1990; Parson & Hawkins 1994). Physiographically, the basin interior can be divided into a western part referred to as the 'western extensional basins' (WEB) (Hawkins 1995) and an eastern area formed by organized seafloor spreading (Parson & Hawkins 1994). The two regions are separated by a structural lineation that is the southward propagation boundary of organized seafloor spreading (Parson & Hawkins 1994; Taylor *et al.* 1996). An inferred eastern conjugate to this propagation boundary is not evident as its expected position would lie near the arc volcanic front and be obscured by arc volcanism. Although the geophysical and morphological evidence for the organized spreading phase is clear (Parson *et al.* 1990; Taylor *et al.* 1996), the nature of the WEB terrain remains less understood. It has been interpreted as rifted remnants of the predecessor arc system with intrusions and volcanism that accompanied the early

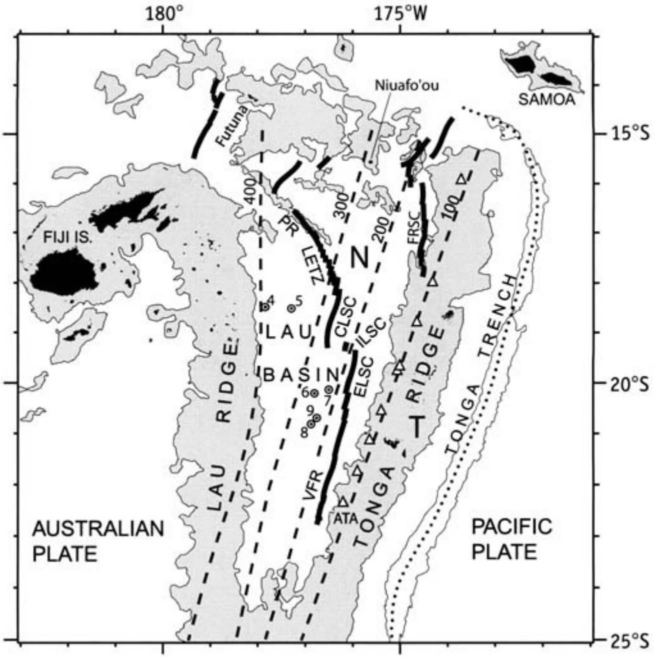

Fig. 2. Tectonic setting of the Lau Basin. The areas shallower than 2000 m are shaded grey and highlight the Lau and Tonga ridges that surround the Lau Basin. The Pacific Plate subducts at the Tonga Trench (dotted line and 7000 m-depth contour) and the slab is nearly planar, dipping at *c.* 45° beneath the back-arc basin. Dashed contours show slab depth in km following Isacks & Barazangi (1977) and Chiu *et al.* (1991). Arc volcanoes (triangles) form a linear chain approximately above the 100 km-slab contour. Spreading centres are shown as heavy lines. The Valu Fa Ridge (VFR), East Lau Spreading Centre (ELSC), Intermediate Lau Spreading Centre (ILSC), Central Lau Spreading Centre (CLSC), Peggy Ridge (PR) and Lau Extensional Transform Zone (LETZ) are indicated. The Niuafo'ou Plate (N) lies between the Tonga (T) and Australian plates. ODP drill sites 834–839 are indicated by circled points labelled with the last digit of corresponding the site number.

(pre-organized seafloor spreading) opening of the basin (Parson & Hawkins 1994; Hawkins 1995). However, drilling and dredging have failed to uncover material older than the opening age of the basin (Hawkins 1994, 1995).

Spreading centres and rifts are well identified within the basin between *c.* 17° and 23°S from nearly full-coverage swath mapping (bathymetry and backscatter). Compilations include: (i) across-basin HAWAII MR1 data between *c.* 17° and 18°45′S; and (ii) southward Hydrosweep, GLORIA and Sea Beam data primarily surrounding the spreading segments along the eastern part of the basin to *c.* 23°S (Parson *et al.* 1990; Wiedicke & Collier 1993; Harding *et al.* 2000; Zellmer & Taylor 2001). Much of the basin north of *c.* 17°S and the western basin south of 18°45′S have only scattered single beam and isolated swath coverage (Wright *et al.* 2000; Zellmer & Taylor 2001). However, merging of these data with a satellite-derived bathymetric prediction (Smith & Sandwell 1994) and sea surface and aeromagnetic data allows a preliminary identification of the location of the spreading systems within the entire basin (Zellmer & Taylor 2001). Recent surveys in the NW part of the basin have identified additional new spreading segments south and west of Futuna (Pelletier *et al.* 2001). Together, these data show that spreading in the Lau Basin is presently well organized within narrow neovolcanic zones that produce distinct magnetic lineations, like those of MORs (Parson *et al.* 1990; Taylor *et al.* 1996; Pelletier *et al.* 2001; Zellmer & Taylor 2001) and is not diffusely distributed as previously proposed (Lawver & Hawkins 1978; Hamburger & Isacks 1988).

The principal spreading centres of interest here are the Central and East Lau Spreading Centres (CLSC and ELSC, respectively) (Parson *et al.* 1990) including the southern segments of the latter termed the Valu Fa Ridge (VFR) (Chase 1985; Morton & Sleep 1985) (Fig. 3). The southern end of the VFR is the limit of organized seafloor spreading. To the south the Havre Trough is interpreted as being in a rift

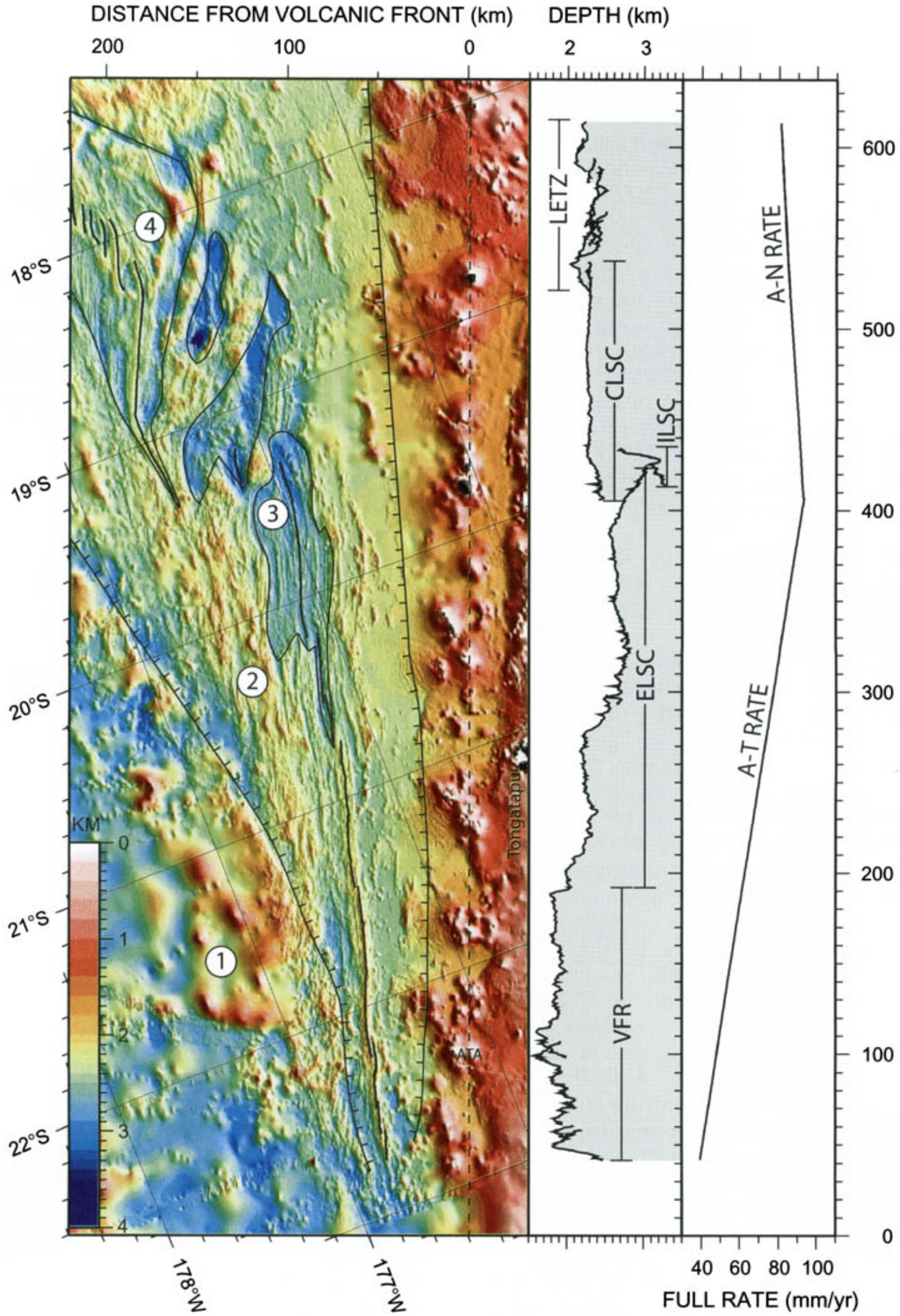

Fig. 3. Bathymetry, axial depths and opening rates of the Lau Basin spreading centres south of *c.* 18°S. The left panel shows the bathymetry of the Lau Basin surrounding the spreading centres in an oblique Mercator projection with the volcanic front (dashed line) aligned vertically. The various crustal domains discussed in the text are labelled 1–4. Also shown is the tectonic boundary (ticked line) formed by the southward propagation of organized spreading. The middle panel shows the axial bathymetric profile projected perpendicular to the volcanic front with segments labelled as in Fig. 2. The right panel shows spreading rates at the axis calculated using the Euler poles of Zellmer & Taylor (2001) for Australia–Tonga (A–T) opening and Australia–Niuafo'ou (A–N) opening.

stage (Parson & Wright 1996; Wright *et al.* 1996; Fujiwara *et al.* 2001; Delteil *et al.* 2002). Modelling of basin opening poles (Zellmer & Taylor 2001), as well as mapped sea-floor fabric trends (Caress 1991; Delteil *et al.* 2002), however, indicate that the Havre Trough and Lau Basin are opening under different kinematic constraints. To the north the CLSC and ELSC are offset across a *c.* 65 km non-transform discontinuity that encompasses a short (<20 km-long) spreading segment termed the Intermediate Lau Spreading Centre (ILSC) (Parson *et al.* 1990). The CLSC is actively propagating southward replacing the ELSC (Parson *et al.* 1990; Wiedicke & Habler 1993). Further north, the CLSC breaks up into a series of short overlapping spreading segments referred to as the Lau Extensional Transform Zone (LETZ) (Taylor *et al.* 1994) that obliquely merges with the Peggy Ridge, the only identified transform fault in the basin.

To the east of the Peggy Ridge–LETZ–northern CLSC, the Fonualei Rift and Spreading Centre (FRSC) (Zellmer & Taylor 2001) is propagating southward into the volcanic arc. The southernmost part of this system is a tectonic rift rather than a true seafloor spreading centre. The FRSC passes northward through the Mangatolu triple junction to the northern termination of the Tonga Trench (Wright *et al.* 2000). The FRSC forms the eastern boundary of a microplate referred to as the Niuafo'ou microplate (Zellmer & Taylor 2001). The southwestern boundary of this microplate is the CLSC–LETZ–Peggy Ridge system. The existence of this microplate has important implications for the kinematics of the basin – although overall Lau Basin opening rates increase northward, north of the ELSC they become partitioned between the CLSC–LETZ–Peggy Ridge system and the FRSC. According to Zellmer & Taylor (2001), spreading rates decrease northwards on the CLSC to rates less than those on the northernmost ELSC, whereas rates increase northward on the FRSC. An unresolved issue, however, is the nature of the southern boundary of the Niuafo'ou Plate. There is no distinct plate boundary observed in bathymetry and backscatter data. Scattered seismicity (Eguchi *et al.* 1989; Pelletier *et al.* 1998) suggests diffuse deformation between the CLSC and FRSC.

Geophysical characteristics

The main Lau spreading centres (VFR, ELSC, CLSC) and their flanking crust display large contrasts in morphology and geophysical characteristics (Martinez & Taylor 2002) (Fig. 3). We describe each ridge in turn from south to north following their progressive separation from the volcanic front (near Ata). The basin floor flanking the axes forms distinct terrains corresponding to different tectonic environments and magmatic production at the time it was formed. We refer to these terrains as zones 1–4 and they are delineated in Figure 3.

The VFR is the present-day southernmost tip of organized spreading propagation. It extends from 22°45'S to 21°25'S and is the ridge system closest (*c.* 40–60 km) to the arc volcanic front. The VFR is the shallowest part of the Lau spreading axes (1500–1900 m; Fig. 3). The ridge crest has a peaked triangular shape in cross-section that has been attributed (Wiedicke & Collier 1993) to the viscous and porous nature of its andesitic lavas (Jenner *et al.* 1987; Vallier *et al.* 1991). A small non-transform offset at 21°25'S, where the ridge crest abruptly deepens by >200 m to the north, separates the VFR from the rest of the ELSC. An overlapping spreading centre (OSC) at 22°13'S is magmatically robust (Collier & Sinha 1990) and has been a focus of several geophysical surveys (Sinha 1995; Turner *et al.* 1999; Peirce *et al.* 2001). The VFR exhibits low mantle Bouguer anomalies with minimum values centred in the area of the OSC (Sinha 1995) and increasing southward to the rift tip and northward to the northern end of the ELSC (Martinez & Taylor 2002). An axial magma lens reflector was first imaged beneath the VFR (Morton & Sleep 1985; Collier & Sinha 1990, 1992) and recently has been almost continuously imaged south of 20°30'S (Harding *et al.* 2000). Active hydrothermal vent fields occur south of 21°50'S (von Stackelberg 1988, 1990; von Stackelberg & Von Rad 1990; Fouquet *et al.* 1991*a*, *b*, 1993; Herzig *et al.* 1990, 1993, 1998; Lécuyer *et al.* 1999). Seismic refraction data show that in terrain zone 2 (Fig. 3) crustal thicknesses are 7.5–9 km near the VFR axis at 22°–22°30'S and west of the CLSC at 18°25'S (Turner *et al.* 1999; Crawford *et al.* 2003). Martinez & Taylor (2002) inferred that terrain zone 2 crust was generated when the spreading centre was near the volcanic front and in a magmatically robust stage, analogous to the present-day VFR. Terrain zone 2 seafloor typically displays a hummocky texture with numerous crescent-shaped highs that are concave toward the axis in plan view. This landform is characteristic of enhanced ridge volcanism forming small split volcanoes (Kappel & Ryan 1986) and its prevalence here implies that terrain zone 2 upper crust is dominated by volcanic extrusion. Away from the propagation boundary with terrain zone 1, zone 2 seafloor maintains shallow depths off-axis (Fig. 3) and has 7.5–9 km-thick crust (Turner *et al.* 1999; Crawford *et al.* 2003). Although these features indicate robust magmatism along the VFR and within terrain zone 2, the VFR has the lowest spreading rates (*c.* 40–60 mm a^{-1}) of the Lau spreading centres (Fig. 3) (Zellmer & Taylor 2001).

North of the VFR, the ELSC spreading axis deepens from 2 to 3 km and develops an axial depression (deeper than off-axis areas), even as spreading rates progressively increase from 60 to 95 mm a^{-1} (Fig. 3). Separation from the volcanic front concomitantly increases from 65 to 110 km. The greatest depth, broadest valley and highest axial mantle Bouguer anomalies are located along the northern segment of the ELSC, where it is spreading fastest (80–95 mm a^{-1}) (Martinez & Taylor 2002). Despite these fast rates, no axial magma lens reflector has been imaged north of 20°30′S (Harding *et al.* 2000). The northern ELSC seafloor morphology is dominated by low relief linear abyssal hills in marked contrast to the more volcanic morphology of terrain zone 2. The low tectonic relief is likely to be a result of the fast spreading producing hot and weak lithosphere incapable of supporting high relief blocks despite low magma production. The deep seafloor (relative to zone 2) is referred to as terrain zone 3. We infer that the valley morphology that it imparts to the northern ELSC thus has a different origin than that of slow-spreading MORs: it is due to thinner crust, as discussed below, rather than dynamic effects.

There is a short spreading segment (ILSC; Fig. 3) in the overlap zone between the CLSC and the ELSC (Parson *et al.* 1990). This and spreading segments further north that failed as the CLSC propagated southward have the deep-water characteristics of the northern ELSC. A refraction profile across the extinct segments at 18°33′S reveals crust that is 5.5 km thick (Crawford *et al.* 2003). Thus, terrain zone 3 crust, which flanks the northern ELSC and its failed segments, is characterized by high mantle Bouguer anomalies, seafloor that is more than 1 km deeper and crust 2–3.5 km thinner than in terrain zone 2 (Martinez & Taylor 2002). Together, with the lack of imaged axial magma lens reflectors on the ELSC north of 20°30′S, these geophysical parameters indicate a decreased magma supply on the northern ELSC relative to the VFR (and CLSC), despite higher spreading rates.

The CLSC is located 65 km west of the northern ELSC and 160–190 km from the volcanic front. Spreading rates on the CLSC decrease slightly northward (92–84 mm a^{-1}; Fig. 3) as a result of a three-plate configuration and sharing the total basin opening rate with the Fonualei rift and spreading centre to the NE (see Fig. 2) (Zellmer & Taylor 2001). The CLSC maintains a nearly constant and shallow axial depth (*c.* 2300 m, north of the propagating rift tip) characteristic of fast-spreading centres with axial magma lenses (Scheirer & Macdonald 1993). An axial magma lens reflector has been imaged beneath the CLSC from 18°21′S to 19°05′S (Harding *et al.* 2000), and hydrothermal vents occur at the segment summit at 18°36′S (Lisitsyn *et al.* 1992; Bortnikov *et al.* 1993). The southward propagation of the CLSC (Wiedicke & Habler 1993) left wakes of slightly deeper crust along its bounding pseudofaults (Fig. 3). Otherwise, the depths and flank subsidence with age of the CLSC are consistent with normal thickness (6–7 km) oceanic crust. Seismic refraction data at 18°30′S confirm that crust formed at the CLSC is 7 km thick (Crawford *et al.* 2003). Thus, the CLSC and terrain zone 4 crust has geophysical characteristics similar to fast-spreading mid-ocean ridges.

Geochemical characteristics

The presence of young volcanic rocks in the Lau Basin and their first-order similarity to MORB provided some of the early evidence for extension in back-arc basins (Sclater *et al.* 1972). In detail, it was recognized that the lavas differed from MORB in volatile content, Fe oxidation ratio, and abundances of LILE and HFSE, related to variable source depletion and metasomatism in a supra-subduction zone setting (Hawkins 1974; Hawkins & Melchior 1985). The axes of extension were only locally known until regional swath bathymetry–side-scan surveys and magnetization inversions were conducted (Parson *et al.* 1990; Taylor *et al.* 1996). This allowed existing rock samples to be located, and new samples to be collected, in tectonic context (Pearce *et al.* 1995).

Drilling on ODP Leg 135 provided basement samples from beneath sediments in the older parts of the basin (Hawkins 1994). Some of the basement samples from the oldest ODP sites (834 and 835) have MORB-like characteristics (Hawkins & Allan 1994; Hawkins 1995). Lava Unit 7 from ODP Site 834, for example, is light rare earth element (LREE)-depleted and has low Ba/La, Ba/Nb and Th/Zr, and high $Na_{8.0}$ and $Ti_{8.0}$ (Table 1), similar to MORB. Even so, Rb and Sr values are slightly higher, and Ta and Nb values are slightly lower, than typical MORB, reflecting minor slab influence (Hawkins 1995). Other samples from the same sites (e.g. Unit 8, Site 834, Table 1) (Hergt & Farley 1994) reveal evidence of significant subduction components. Indeed, all other samples from zone 1 have transitional to arc-like characteristics (Hawkins 1995). Unit 3 from ODP Site 839, for example, has flat REE, high Ba/La, Ba/Nb and Th/Zr, and low $Na_{8.0}$ and $Ti_{8.0}$, similar to the Tofua arc and VFR (Table 1) (Ewart *et al.* 1994*a*, *b*; Hawkins & Allan 1994).

The sampled portions of the VFR and southernmost ELSC (S. ELSC) show strong arc affinities (Jenner *et al.* 1987; Boespflug *et al.* 1990; Davis *et al.* 1990; Frenzel *et al.* 1990; Sunkel 1990; Vallier *et al.* 1991; Peate *et al.* 2001). Most of the analysed lavas are basaltic andesites and andesites, with only a few basalts (and those, most commonly, off-axis) and dacites. Although LREE-depleted, they are markedly enriched in LILE and so have high Ba/La, Ba/Nb and Th/Zr ratios (Table 1). They have low $Fe_{8.0}$, $Na_{8.0}$, $Ti_{8.0}$, $Y_{8.0}$ and $Yb_{8.0}$, and a high water content (Kent *et al.* 2002), indicating high total extents of melting (Fig. 1; Table 1). Off-axis within zone 2, ODP drilling in a small basin (Site 836) and dredging of a nearby high (RND-2) revealed both MORB-like and arc-like compositions in close proximity (Hawkins 1995). This scale of source heterogeneity is characteristic of this and other back-arc basins (e.g. Hawkins & Melchior 1985; Volpe *et al.* 1988).

The geochemistry of rocks sampled from the northern ELSC (N. ELSC in Table 1) indicate a decreased subduction geochemical signature relative to the southern ELSC including the VFR (Falloon *et al.* 1992; Hawkins 1995; Pearce *et al.* 1995; Peate *et al.* 2001). Ba/La, Ba/Nb and Th/Zr ratios are all lower (Table 1). The majority of this segment (as represented between 19°29′ and 19°53′S by samples from MIR dive 2239 and CD33 dredges 20 and 22) has higher extents of melting than along the CLSC (e.g. $Na_{8.0}$, $Ti_{8.0}$ and $Y_{8.0}$ are each 10% lower), concomitant with higher water contents (0.4–0.7% v. <0.3%) and oxygen fugacities (represented by lower $Fe_{8.0}$, Table 1) (Falloon *et al.* 1992; Danyushevsky *et al.* 1993; Hawkins 1995; Pearce *et al.* 1995; Dril *et al.* 1997; Peate *et al.* 2001; Kent *et al.* 2002). In contrast, samples from one dredge haul of the ELSC (CD33–23, 20°03′S) show higher Ba/La, as well as lower $Na_{8.0}$, $Fe_{8.0}$, and $Y_{8.0}$ (Table 1) (Pearce *et al.* 1995). These values indicate Ba enrichment and greater extents of melting, characteristics transitional to those of the southern ELSC and VFR. Therefore, this could represent a gradient in mantle source characteristics. However, one dredge of the ILSC (CD33-41) recovered samples with somewhat similar characteristics to CD33-23 (Table 1). Thus, these individual dredge hauls may reflect the geochemical heterogeneity of the mantle source regions rather than the average composition of segment lavas. As many have recognized previously (Volpe *et al.* 1987, 1988; Sinton *et al.* 2003), this scale of mantle heterogeneity is expressed in all the back-arc basins studied. It may not be representative, however, of the first-order variations in crustal production that we seek to explain as characteristic of whole spreading segments and crustal zones. In the case of zone 3 and the axial deeps of the northern ELSC, we take the samples from M2239, CD33-20 and -22 as representative of the crustal extrusives.

Lavas from the CLSC are LREE-depleted and have normal MORB-like geochemistry, with the only trace of a minor subduction component being slightly enriched Rb and Ba, and reduced Ta and Nb (Table 1; Falloon *et al.* 1992; Danyushevsky *et al.* 1993; Hawkins 1995; Pearce *et al.* 1995; Peate *et al.* 2001). These CLSC lavas all have low $(H_2O)_{8.0}$ contents (<0.3%), although some CLSC source heterogeneity is reflected in sample CD33–15–1-1 whose geochemistry is otherwise similar to samples from the northern ELSC (Table 1; Fig. 1). Note that the representative rock samples included in Tables 1–3 exclude the (often highly) fractionated lavas from the propagating rift tip. Thus, the current first-order progression spatially away from the arc, and the temporal trend since all but the earliest back-arc lavas, is from greater to lesser subduction influence (i.e. from arc-like to MORB-like compositions) but with significant local heterogeneity.

The Manus Basin

Tectonic setting

The Manus Basin is located in the eastern Bismarck Sea (3°–4°S, 149°–152°E) surrounded by the islands of New Britain, New Ireland and Manus, and is a back-arc basin associated with subduction of the Solomon Sea Plate at the New Britain Trench (Fig. 4). GPS studies define a North Bismarck Plate (distinct from the Pacific Plate), which is separating from a South Bismarck Plate with a rotation vector of 10°12′N, 33°30′W, 8.75° Ma^{-1} (Tregoning 2002). This vector predicts opening in the eastern basin at rates of between 115 and 145 mm a^{-1}, making the Manus Basin one of the fastest-opening basins in the world. The axis of extension was first delineated from a band of shallow seismicity and termed the Bismarck Sea Seismic Lineation (BSSL) (Denham 1969), displaying primarily

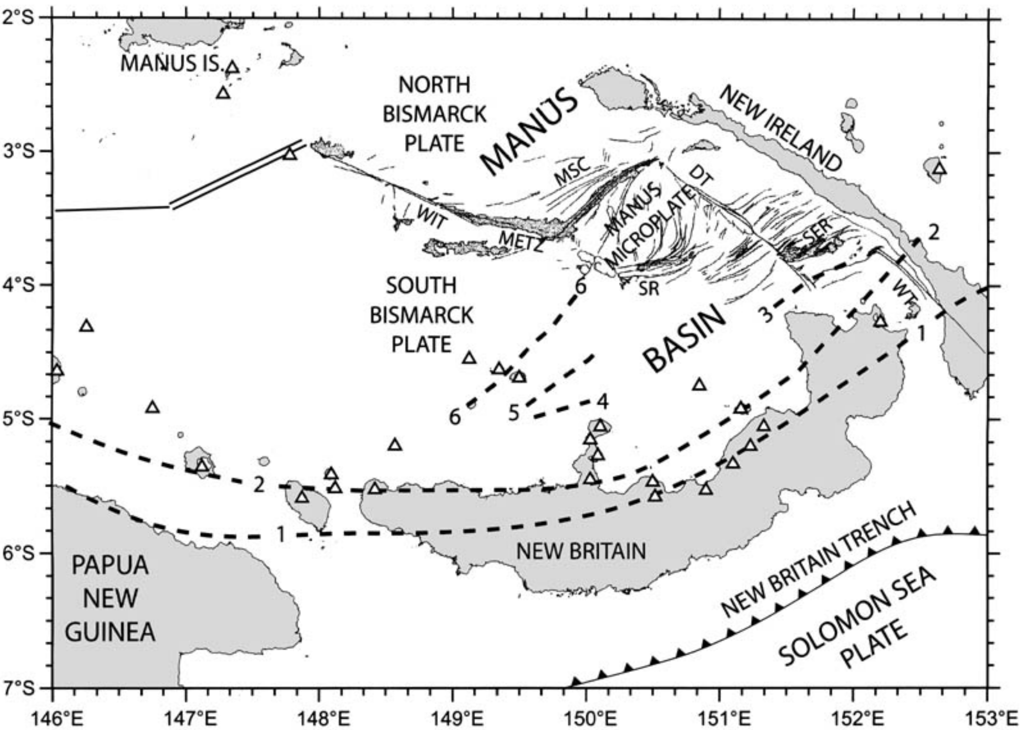

Fig. 4. Tectonic setting of the Manus Basin. Tectonic features are shown on an interpretation of SeaMARC II data (Martinez & Taylor 1996), where fine lines are structural lineations and stippled areas are high backscatter lava flows. The Solomon Sea Plate subducts beneath the basin at the New Britain Trench (line with triangles) and the slab contours are shown as dashed lines labelled in hundreds of km that follow the interpretation of Cooper & Taylor (1987, 1989). Indicated are the Weitin Transform (WT), Southeast Ridges (SER), Djaul Transform (DT), the Southern Rifts (SR), the Manus Spreading Centre (MSC), the Manus Extensional Transform Zone (METZ) and the Willaumez Transform (WIT). Triangles show volcanic edifices.

left-lateral strike-slip mechanisms (Johnson & Molnar 1972; Ripper 1975, 1977, 1982). Taylor (1979) identified a distinct spreading segment between two transform faults and a leaky transform segment. Later, complete SeaMARC II side-scan sonar coverage of the eastern Manus Basin (Taylor *et al.* 1991*b*, 1994) identified the currently known tectonic boundaries (Fig. 4). From east to west the survey mapped: the Weitin Transform (WT), the Southeast Ridges (SER), the Djaul Transform (DT), the Southern Rifts (SR) the Manus Spreading Centre (MSC), the Manus Microplate (MM), the Manus Extensional Transform Zone (METZ) and the Willaumez Transform (WIT). The WT at the eastern limit of the basin intersects southern New Ireland. The SER are a series of en echelon volcanic ridges that are bounded by the WT on the east and the DT on the west. West of the DT a complex terrain includes the MM. The MM is bounded to the northeast by the DT, to the south by the deep rifts of the SR, to the west by a compressional zone, and to the north and NW by the MSC (Martinez & Taylor 1996). The MSC merges at its SW end with the METZ that links it to the WIT further to the west (Taylor *et al.* 1994).

Because of the existence of a microplate between the DT and WIT, extension rates are partitioned between the overlapping axes of the MSC and SR (Martinez & Taylor 1996). Individual rates are poorly constrained from independent magnetics data, however. Spreading rates on the MSC are based on the assumption that positively magnetized crust marks the beginning of the Brunhes chron following a tectonic reconfiguration of the plate boundaries in the basin (Martinez & Taylor 1996). Other extensional boundaries do not have identified magnetic isochrons. Nevertheless, applying these conservative assumptions leads to general agreement with GPS results that indicate fast

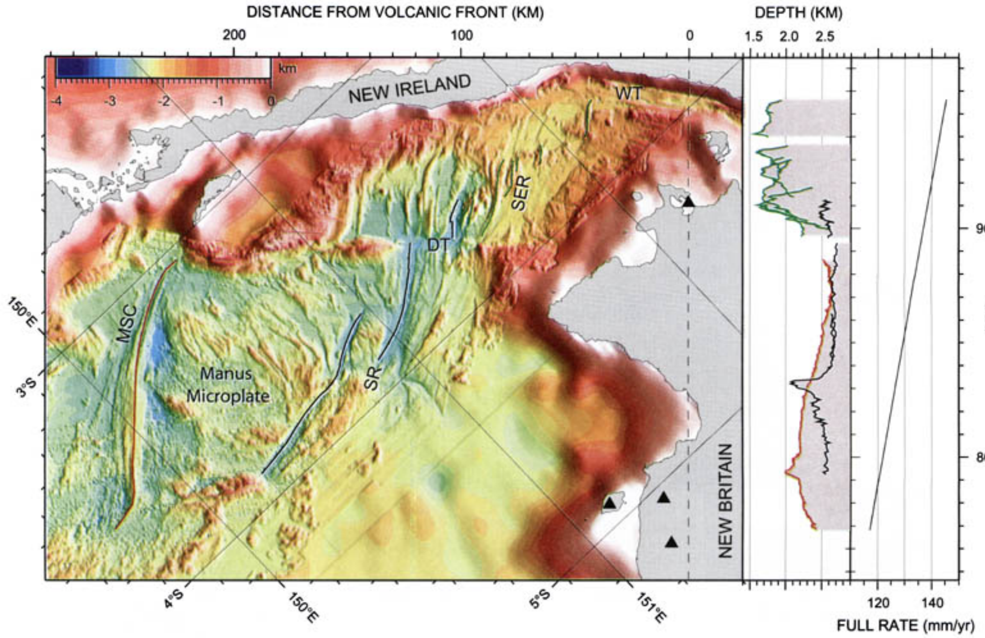

Fig. 5. Manus Basin spreading centres, axial depths and opening rate. The left panel shows the bathymetry of the Manus Basin surrounding the spreading centres in an oblique Mercator projection with the volcanic front (dashed line) aligned vertically. The bathymetry map combines SeaMARC II side-scan (Martinez & Taylor 1996) and R/V *Yokosuka* multibeam data (Auzende *et al.* 1996). Volcanoes are shown as black triangles. Tectonic elements are labelled as in Figure 4. The central panel shows axial depth profiles projected perpendicular to volcanic front with colours corresponding to axes shown in map view in the left panel. The right panel shows overall basin opening rates from the Euler pole of Tregoning (2002).

overall basin opening. The kinematic model of Martinez & Taylor (1996) proposes that the MM is pivoting about a pole located at the NE tip of the MSC, so that spreading rates on the MSC vary from an estimated 92 mm a^{-1} at its SW end to zero at the NE tip. Extension rates on the SR are expected to vary in a complementary way (fast to the east and slow to the west) to sum to the overall GPS-determined basin opening rates.

The subducted Solomon slab is discontinuously mapped from seismicity but is shown to extend to at least 600 km depth, and approaches the SR and SER but does not extend beneath the MSC (Cooper & Taylor 1987, 1989) (Fig. 4). There is no direct measurement of subduction rate of the Solomon Sea Plate at the New Britain Trench. Subduction is probably very fast, however, and at least as rapid as opening of the Manus Basin, as it must take up this opening plus most the opening of the Woodlark Basin to the south and the oblique convergence between the surrounding Pacific and Australia plates (as other intervening trenches are inactive or slowly subducting). The active arc volcanic front within New Britain lies above the *c.* 100–200 km-slab contours and curves gently, concave to the NNW (Fig. 4) but can be approximated as a straight line in the area opposite the Manus extensional axes (Fig. 5).

Geophysical characteristics

The modes of extension in the Manus Basin include the single continuous axis of the MSC, grabens on the SR, and multiple short en echelon volcanic ridges on the SER. These differences in spreading style have been attributed to differences in the nature of the crust (back-arc v. arc) in which the extensional axes formed following a plate boundary reconfiguration event within the Brunhes chron (Martinez & Taylor 1996). Although the distinction in crustal types remains valid, the variation in magmatic robustness, style of accretion and magmatic compositions may be understood in terms of tectonic position of the extensional centres over the mantle wedge and proximity to the arc volcanic front. The geophysical characteristics presented below are largely summarized from Martinez & Taylor (1996), and are described from east to west across the basin.

Southeast Ridges. The Southeast Ridges (SER) are the easternmost extensional boundaries separating the North and South Bismarck plates, and were classified as a group based on their tectonic position between the WT and DT. However, a distinction can be made between a set closest to the volcanic front and one axis furthest from the front. The group closest to the volcanic front forms a series of en echelon ridges that step from the DT to the WT as they approach from 100 to 43 km from the arc volcanic front. Depths on these ridges vary mostly between *c.* 1500 and 2000 m, making them the shallowest extensional axes in the basin (Fig. 5). Side-scan backscatter data show high-reflectivity lava flows surrounding these ridges, indicating that they are magmatically robust (Taylor *et al.* 1991*a*; Martinez & Taylor 1996). The northwesternmost extensional axis of the SER lies at a distance of 100–105 km from the volcanic front and also displays evidence of recent lava flows, however, it forms a narrow ridge with depths of *c.* 2500–2700 m within a graben (Fig. 5). Geochemical data also show that this ridge is distinct (see Geochemistry below). The GPS-determined overall opening rates (Tregoning 2002) in the area of the SER are the fastest in the basin, and vary between 137 and 145 mm a^{-1}, although, owing to the overlapping geometry of individual ridges and poorly developed magnetic lineations (Martinez & Taylor 1996), the partitioning of opening rates between the ridges is not constrained. Given the lack of a Brunhes magnetic anomaly, Martinez & Taylor (1996) interpreted the area of the SER as being in a rift stage (and correspondingly referred to them as the Southeast Rifts) with dyke-fed volcanic ridges – that is, primarily stretching pre-existing arc crust. Side-scan data and submersible observations, however, indicate significant volcanism in the area (Auzende *et al.* 2000*a–c*). The shallow depth of the SER area and of the volcanic ridges (excluding the northwesternmost ridge), despite fast opening rates, also indicate that magmatic accretion is largely accommodating the fast extension and preventing deep tectonic graben from forming.

Southern Rifts. The Southern Rifts (SR) are located between the WIT and DT, at a distance of *c.* 120–190 km from the volcanic front, and form the southern boundary of the MM (Fig. 5). Side-scan backscatter data indicate that the extensional axes lie within two partly overlapping grabens and exhibit much more restricted recent volcanism than the SER. The axes of the SR lie mostly at depths of 2500–2700 m, but a small volcanic edifice within the western graben shallows to *c.* 2100 m. GPS-determined opening rates in this part of the basin vary between 136 and121 mm a^{-1}, but are partitioned between the grabens and the MSC. Because spreading rate on the MSC decreases essentially to zero at its NE tip (see below), Martinez & Taylor (1996) infer that the eastern end of the SR is opening faster than the western end. Despite inferred faster eastern opening rates, the eastern SR are *c.* 200 m deeper than the western part.

Manus Spreading Centre. The Manus Spreading Centre (MSC) is *c.* 100 km long and lies 220–250 km from the arc volcanic front (Fig. 5). The spreading centre bisects a wedge of positively magnetized crust and conformably fanning seafloor spreading fabric. Prominent faults imaged in seismic reflection profiles delineate the boundaries of this wedge (Martinez & Taylor 1996). These features indicate that spreading on the MSC initiated as a rift jump at the beginning of, or within, the Brunhes chron. Assuming that the rift jump occurred at the start of the Brunhes chron (0.78 Ma) implies that spreading rates on the MSC vary from 92 mm a^{-1} to zero from SW to NE, respectively. The axis of the MSC varies from a high at the SW end to a narrow valley at the NE end, qualitatively consistent with the sense of topographic spreading rate variations at MORs.

Manus Extensional Transform Zone. The Manus Extensional Transform Zone (METZ) obliquely links the SW end of the MSC to the WT. It represents a highly oblique extensional zone composed of a series of short en echelon volcanic segments that individually are nearly orthogonal to the opening direction but together constitute the oblique plate boundary (Taylor *et al.* 1994).

Geochemical characteristics

The first closely spaced sampling of all the neovolcanic zones of a back-arc basin sited using full side-scan coverage was completed in the Manus Basin in January 1986 (Taylor *et al.* 1991*b*). The R/V *Moana Wave* cruise (MW8518) (Table 2) also located some of the first back-arc hydrothermal chimneys and distinctive western Pacific vent fauna (Both *et al.* 1986). It presaged extensive international investigations of the widespread hydrothermal activity in the Manus

Basin (Craig *et al.* 1987; Tufar 1990; Binns & Scott 1993; Gamo *et al.* 1993, 1997; Lisitsyn *et al.* 1993; Shadlum *et al.* 1993; Scott & Binns 1995; Sinton 1997; Auzende *et al.* 2000*c*; Kamenetsky *et al.* 2001; Binns *et al.* 2002).

A comprehensive geochemical study of the MW8518 and some Mir dive samples has recently been completed by Sinton *et al.* (2003). Our discussion of Manus Basin geochemistry is based entirely on their results. Sinton *et al.* (2003) grouped the analysed lavas based on their geochemistry. They found that the lava groups so defined are systematically disposed with respect to the back-arc extensional zones and their distance from the volcanic front. Some other analyses of Manus Basin lavas have been published (Davies & Price 1987; Binns & Scott 1993; Dril *et al.* 1997; Macpherson *et al.* 1998, 2000; Kamenetsky *et al.* 2001; Marty *et al.* 2001), but they are either on just a few samples or elements (e.g. He or volatiles). All the available rock samples are from neovolcanic or recently volcanic zones; there have been no off-axis investigations of the evolution of lava geochemistry with basin opening.

A calc-alkaline suite of basalts–andesites–rhyodacites has been erupted from the en echelon ridges and individual volcanoes of the SER (Fig. 4) (Binns & Scott 1993; Kamenetsky *et al.* 2001; Sinton *et al.* 2003). The two representative lava groups (A1 and A2) are LREE-enriched, show a high water content ($\geq$ 1%), high Ba/Nb, Ba/La and Th/Zr ratios, and low $Fe_{8.0}$, $Na_{8.0}$, $Ti_{8.0}$, $Y_{8.0}$, $Yb_{8.0}$ (Table 2), indicating significant enrichments in slab-derived components (water and LILE) to a depleted mantle source that has undergone large extents of total melting (Sinton *et al.* 2003). These characteristics also typify the adjacent New Britain arc lavas (Woodhead *et al.* 1998).

Sinton *et al.* (2003) recognized three groups of slightly LREE-depleted back-arc basin basalts (BABB) that systematically vary in composition away from the arc. Group Be is from the small SER ridge in the axial deep just east of the DT fault, group Bs is from the SR and group B lavas occur from the central MSC to the METZ (Fig. 5). $Fe_{8.0}$, $Ti_{8.0}$, $Y_{8.0}$, $Yb_{8.0}$ contents sequentially increase, and Ba/Nb, Ba/La, Th/Zr and water contents progressively decrease, in the order Be, Bs, B, corresponding to increasing distance to, and decreasing source contributions from, the arc/slab (Table 2). Note the sharp transition in morphology between the volcanic features that have erupted group A2 and Be lavas, which occurs at a distance from the arc volcanic front of 100 km (Fig. 5; Table 2).

The two tholeiitic basalt groups (M1 and M2) least influenced by slab contributions occur along the MSC and METZ (Sinton *et al.* 2003). Both are LREE-depleted and similar to MORB, but the M2 lavas from the northeast MSC are more differentiated, show higher water contents (0.4–0.7%), and Ba/Nb, Ba/La, Th/Zr ratios, and lower $Fe_{8.0}$, $Na_{8.0}$, $Ti_{8.0}$, $Y_{8.0}$, $Yb_{8.0}$ (Table 2). This is consistent with their slightly closer distance to the volcanic front, but may also be related to the decreasing spreading rate and increasing rift-tip proximity NE along the MSC. Note that even the most MORB-like lavas in the Manus Basin (group M1) retain slight enrichments in Cs, Rb, Ba, U, Pb, and depletions in Ta, Nb, relative to MORB that are like the CLSC lavas and characteristic of some minor slab contribution to their mantle sources (Sinton *et al.* 2003).

Sinton *et al.* (2003), using Nb–, Zr– and TiO_2–Y systematics, modelled progressive (accumulated fractional) melting of the Manus parental lava groups. Assuming that the MORB–type M1 magmas were produced by 10% total melting, they model 16, 20, 30 and 40% melting for magma types B, Bs, Be and A2, respectively. They argue that these extents of melting are so high as to be unrealistic, exceeding the expected increases in melting due to the addition of water and far exceeding the expected thermal barriers to melting above the exhaustion of mantle phases such as clinopyroxene (at *c.* 20–25%). Instead, they suggest that the strong depletions in Ti, Y and Yb require mantle sources that were already depleted by prior (melting) events. They also note that the greatest LILE enrichments (e.g. Ba/Nb ratios) occur in the most depleted lavas (and that, in the Manus system, Na_2O is enriched like these lithophile elements; Fig. 1). They infer from the Manus data that greater extents of melting of originally more depleted mantle occur as slab-derived components progressively enrich the mantle sources arcwards (Sinton *et al.* 2003). Note that this enrichment appears to be tightly zoned spatially for the BABB and calc-alkaline suites of the SR and SER, respectively, but that the BABB and MORB-like suites erupted on the MSC and METZ are spatially intermixed.

The Mariana Trough

Tectonic setting

The Mariana Trough is a back-arc basin at the eastern edge of the Philippine Sea Plate (12°–24°N, 142°–146°E) associated with subduction of the Pacific Plate at the Mariana Trench (Fig. 6). Formation of the basin is estimated to

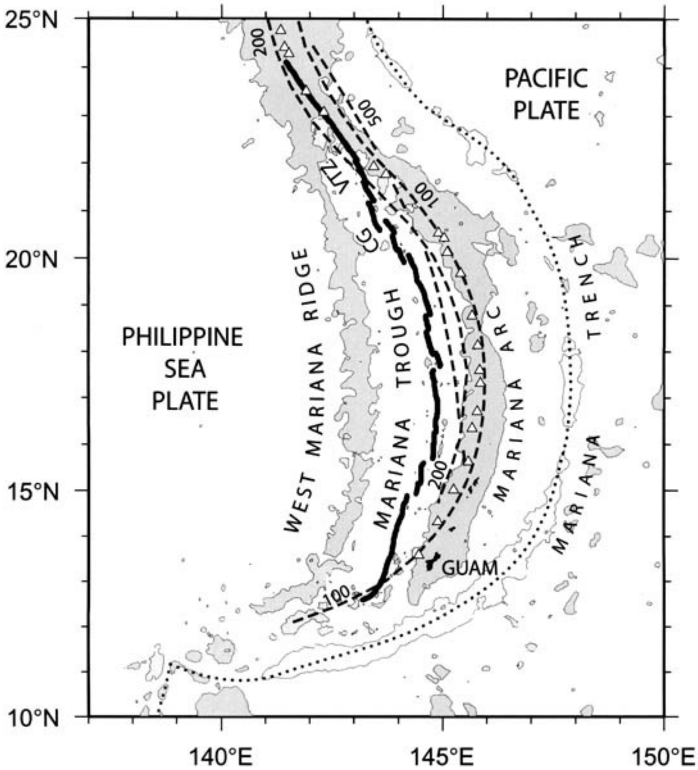

Fig. 6. Tectonic setting of the Mariana Trough. Spreading centre and active rifts are shown as heavy lines. The Pacific Plate subducts beneath the Mariana arc at the Mariana Trench (dotted line) where the 6000 m-contour is shown. The 100, 200 and 500 km-contours of the subducted slab are shown as labelled dashed lines following Isacks & Barazangi (1977). Note the overturned nature of the slab in places. The Mariana Trough is opening between the remnant West Mariana Ridge and active Mariana arc, with depths above 3000 m shaded grey. Arc volcanoes are shown as triangles. CG indicates the Central Graben and VTZ the volcano-tectonic zone discussed in the text.

have begun about 5 Ma ago, following rifting of the progenitor arc (Hussong & Uyeda 1981). Geological and geophysical data indicate that the Mariana Trough is opening at a slow rate. Various measures of current opening rates from GPS studies have now been made (Kato *et al.* 1998, 2003; Kotake 2000). The solution of Kato *et al.* (2003) indicates that, with reference to the Philippine Plate (Kotake & Kato 2002), the basin is opening at *c.* 45 mm a^{-1} at Guam, slowing to about 16 mm a^{-1} at Agrihan (18°45′N). The stations along the Mariana islands indicate a component of trench-parallel strain. Solutions for a best-fit rigid-plate opening (Kotake 2000; Kato *et al.* 2003), however, determine a pole position well south of the basin physiographic apex, also implying non-rigid behaviour of the arc/forearc. This appears especially so for the southernmost Mariana forearc, where seafloor mapping provides structural evidence of significant trench-parallel, as well as trench-normal, faulting (Martinez *et al.* 2000). Significant active tectonic deformation is also indicated by a 7.7 Mw (moment magnitude) earthquake near Guam in 1993 (Beavan *et al.* 1994; Campos *et al.* 1996).

Magnetic anomalies in the basin are complex and poorly correlated along the trough, but provide a measure of its long-term opening history. Estimates of total opening rates of about 30 mm a^{-1} near 18°N have been proposed (Bibee *et al.* 1980). Honsho *et al.* (1997) derived a full opening rate of 38 mm a^{-1} at 15°30′–16°45′N from a magnetization inversion. A 4.7–5.0 Ma palaeontological age and a 5.0±0.2 Ma palaeomagnetic age from basal sediments recovered by Deep Sea Drilling Project (DSDP) Leg 60 drilling at Site 453 near the western boundary of the basin at *c.* 18°N also yield a slow overall basin opening rate of *c.* 43 mm a^{-1} (Hussong & Uyeda 1981). In the northern trough magnetization

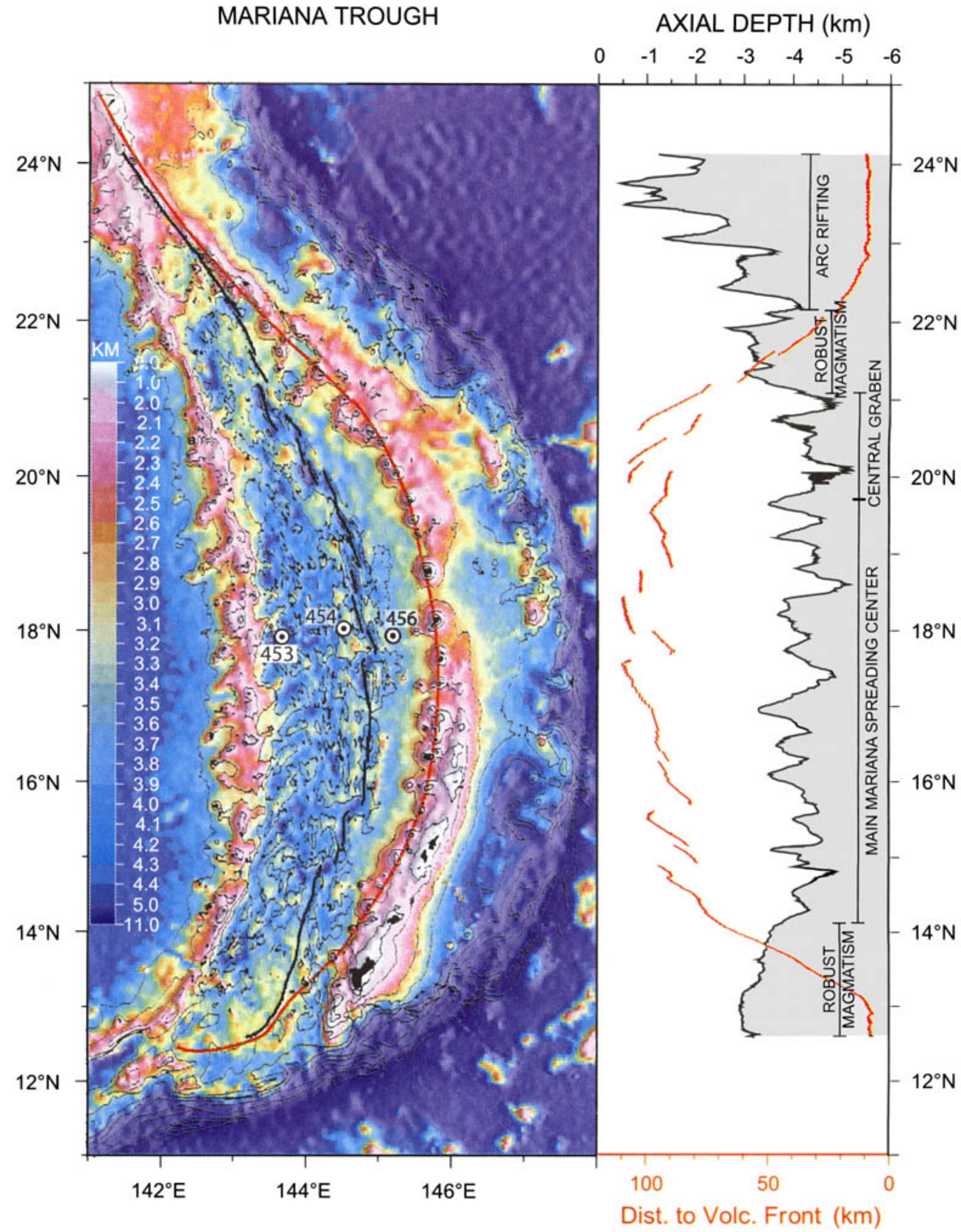

Fig. 7. Mariana Trough bathymetry and axial depth profile. The left panel shows a map of the Mariana Trough with the extension axis indicated with a heavy black line and the volcanic front with a red line. Coloured shaded relief surface is from a 2′ × 2′ gridded database (Smith & Sandwell 1997) with 500 fathom-contours from Smoot (1990) superimposed to show the structural fabric. The right panel shows the axial depth profile measured from swath surveys of the axis projected N–S. The separation between the extension axis and volcanic front is shown as red lines. Also shown are the various tectonic/magmatic domains discussed in the text and DSDP drill sites 453, 454 and 456.

lineations resulting from intrusions and volcanism have been identified (Martinez *et al.* 1995). Together with the northward closing shape of the basin and the lack of large-scale extensional faulting north of the trough apex, these observations imply that opening propagated northward and decreases to near zero just south of the Volcano Islands (Stern *et al.* 1984; Martinez *et al.* 1995). The Izu–Bonin arc and trench further to the north forms the northward continuation of Pacific–Philippine convergent system. The Izu–Bonin arc shows extensional faulting (Karig & Moore 1975; Honza & Tamaki 1985; Taylor 1992) but is in a rift stage without organized spreading. Opening rates are estimated to be very slow (2–5 km of extension in the last 2 Ma; Taylor 1992). The Mariana Trough opening kinematics are complex, as the basin is widest in the central trough (*c.* 18°N) but is opening fastest in the southern trough (12°–13°N), although basin widths are smaller there. This may be reconciled if opening developed earlier in the central trough (Karig *et al.* 1978) and propagated north and south from there, increasing in rate to the south as it did so. Such a model implies non-rigid plate separation and deformation of the region between the extension axis and the trench. It is supported by the higher curvature of the present-day volcanic arc and forearc relative to its conjugate remnant, the West Mariana Ridge (Fig. 6) (Karig *et al.* 1978), by faulting at high angles to the trench observed throughout the Mariana forearc (Wessel *et al.* 1994; Stern & Smoot 1998; Martinez *et al.* 2000), and by GPS measurement of trench-parallel strain between the islands of the arc and forearc (Kato *et al.* 2003).

Benioff zone seismicity shows that the Pacific slab is steeply dipping beneath the Mariana Trough (Isacks & Barazangi 1977; Chiu *et al.* 1991). Plate kinematic solutions (Seno *et al.* 1993) indicate that the Pacific Plate at the Mariana Trench is converging towards the Philippine Plate at rates that vary from *c.* 21 mm a^{-1} at the southern trench to *c.* 45 mm a^{-1} at the northern trench in a WNW direction. These relative motion directions are generally oblique to the plate boundary and do not include the component from Mariana Trough opening so that convergence rates calculated normal to the trench are generally different from Pacific–Philippine vectors. The Pacific slab underlies the extension axis at the northern and southern ends of the basin, but elsewhere lies entirely to the east of the axis (Fig. 6). Arc volcanoes form islands in the central part of the arc and become smaller submarine edifices to the north and south.

Geophysical characteristics

A 500 fathom (1 fathom ≈ 1.83 m) contour interval map of the Mariana Trough has been published (Smoot 1990) from US Navy multibeam data. We combined these contours with a digital 2-arc-minute bathymetry grid (Smith & Sandwell 1997) to broadly delineate seafloor depth, fabric and structural trends throughout the basin (Fig. 7). Other areas, primarily along the length of the extension axis, have higher resolution published maps made using swath systems (Kong *et al.* 1992; Fryer 1995; Martinez *et al.* 1995, 2000; Baker *et al.* 1996; Stuben *et al.* 1998). Our axial depth profile (Fig. 7) is made primarily using high-resolution swath data.

The nature of extension along the northern axis remains under debate. One issue is the extent of organized seafloor spreading v. rifting. Yamazaki *et al.* (1993) proposed that organized seafloor spreading does not extend north of *c.* 22°N, Martinez *et al.* (1995) proposed that organized spreading does not occur north of 20°N, and Fryer (1995) proposed that organized spreading occurs south of a northward-propagating spreading centre at 19°45′N. The nature of the southern trough (south of *c.* 14°N) has also been variably interpreted (Bracey & Ogden 1972; Karig & Ranken 1983; Masuda *et al.* 1994; Fryer *et al.* 1998; Martinez *et al.* 2000). These divergent interpretations result, in part, from the large changes in morphology of the extension axis north of 19°45′N and south of 14°N from the better-surveyed central trough that closely resembles slow-spreading MORs (Kong *et al.* 1992). We describe the characteristics of the extension axis starting with the central trough and proceed to the northern and southern ends of the basin.

Central Mariana Trough. The central Mariana Trough near 18°N is approximately 250 km wide. The spreading centre forms an axial valley with depths generally between 4000 and 4500 m, but ranging between *c.* 5000 m and less than 3500 m. Across-axis relief is high and can exceed 1000 m. Inside corner highs are sometimes developed at segment discontinuities, giving the axis an asymmetric appearance. The spreading centre is divided into variable length segments generally approximately 30–60 km long, which are offset by non-transform discontinuities, except at 17°40′N at the Pagan transform fault (Sinton & Hussong 1983). The spreading centre valleys may contain axial volcanic ridges (Kong 1993). Magnetic lineations (Seama & Fujiwara 1993) have been identified that correlate with the structural segmentation. Various determinations of crustal thickness have been made using different techniques in the central Mariana Trough near 18°N. Bibee *et al.* (1980) reported an average thickness of approximately 7 km measured by two-ship refraction techniques, LaTraille & Hussong (1980) found an average crustal thickness of 5 km using sonobuoys and explosive sources, and Ambos & Hussong (1982) found 4 and 6 km thicknesses using ocean bottom seismometers and explosive charges. The reason for the different crustal thickness determinations is not clear, but rough and heterogeneous crustal structure, as well as the unreversed acquisition of some of the profiles, have been cited as possible causes (Ambos & Hussong 1982). Sager (1980) was able to model the free-air gravity variation across the Mariana Trough using the LaTraille & Hussong (1980) crustal thickness, but this required low densities in the mantle beneath the back-arc basin. Park *et al.* (1990) analysed the basement depth and subsidence characteristics of the Mariana Trough and Philippine Sea, and concluded that subsidence with age is similar to that of MORs but that depth is systematically greater by about 800 m. Taken together, the data suggest thin to normal crustal thickness in the central Mariana Trough relative to MORs.

Volcano-tectonic zone (VTZ). 19°45′N marks the northern tip of what may be a northward-propagating spreading centre with spreading characteristics similar to those of the central trough (Fryer 1995). Northward, deep grabens referred to as the Central Graben (Martinez *et al.* 1995) are located between 19°50′N and 21°10′N. These grabens reach depths of 5500 m, are asymmetric in cross-section, and tectonically expose lower crust and mantle with back-arc geochemical characteristics (Stern *et al.* 1996). A hornblende $^{40}Ar/^{39}Ar$ age of 1.8±0.6 Ma was determined from a rock dredge of the graben walls (Stern *et al.* 1996). To the north of the Central Graben, the extension axis undergoes significant changes and is referred to as a 'volcano-tectonic zone' (VTZ) (Martinez *et al.* 1995; Baker *et al.* 1996) to distinguish it from the central Mariana spreading centre. The VTZ approaches the volcanic front, and shallows to 3000–3500 m (Fig. 7). SeaMARC II side-scan data show high backscatter lava flows associated with the volcanic ridge that characterizes this area (Baker *et al.* 1996). North of *c.* 22°N the VTZ lies along the volcanic front and is the locus of rifting. SeaMARC II data show that it consists of small graben often having high-backscatter lava flows between rifted arc volcanic edifices (Baker *et al.* 1996). A seafloor magnetization solution shows a discontinuous series of positive magnetizations tracking the VTZ from the northern Central Graben toward the arc and along the northern volcanic front (Martinez *et al.* 1995).

The 1.8 Ma age samples recovered from the Central Graben, the back-arc geochemical characteristics, and magnetic and side-scan sonar evidence of intrusions and volcanism indicate that significant back-arc crustal accretion (rather than primarily tectonic rifting of a pre-existing arc massif) has occurred in the VTZ, but in a manner different from that in the central trough.

Southern Spreading Centre. South of *c.* 14°N, another transition occurs along the axis of extension. The axial valley of the central trough shallows and becomes an axial high by 13°N (Fig. 7) (Martinez *et al.* 2000). Tectonic deformation in this area, however, involves significant trench-parallel extension of the back-arc area between the spreading centre and the trench axis, with the development of complex faulting at high angles to the spreading centre. Significantly, the spreading centre appears to decouple these stresses so that high-angle faulting does not continue west of the spreading centre to the Philippine Plate proper (Martinez *et al.* 2000). South of Tracey Seamount (Dixon & Stern 1983) arc volcanoes had not been previously identified, but based on recent mapping and sampling it has been suggested that a series of small seamounts located just east of the spreading centre form the continuation of the arc volcanic front (Fryer *et al.* 1998). These volcanoes, however, have geochemical differences from and are smaller than the arc volcanoes to the north (Masuda *et al.* 1994; Yamatani *et al.* 1994; Fryer *et al.* 1998).

Geochemical characteristics

The essential major, trace and isotopic characteristics of Mariana Trough basalts (MTB), that they are intermediate in composition between MORB and island arc tholeiites (IAT) and variably enriched in water, were recognized from early dredge hauls and DSDP Leg 60 drilling (Hart *et al.* 1972; Meijer 1976; Garcia *et al.* 1979; Fryer *et al.* 1981; Wood *et al.* 1981). Fryer *et al.* (1981) showed that MTB glasses have lower total iron and TiO_2, and higher Al_2O_3 at a given MgO content, with chondritic REE patterns and approximately 1% water (Garcia *et al.* 1979), and coined the term BABB (back-arc basin basalt) to distinguish them from MORB. From the only two DSDP holes to penetrate MTB (sites 454 and 456), Wood *et al.* (1981) reported a BABB series with end-member MORB-like and arc-like compositions interlayered. Subsequent papers, plus additional dredge and Deep Sea Research Vessel ALVIN samples, confirmed these essentials, including the proximal eruption of end-member compositions (Hawkins & Melchior 1985; Sinton & Fryer 1987; Volpe *et al.* 1987, 1990; Hawkins *et al.* 1990; Stern *et al.* 1990).

Improvements in analytical techniques, such as inductively coupled plasma-mass spectroscopy (ICP-MS) and FTIR spectroscopy, together with systematic sampling of the spreading axes as they became better known and surveyed, allowed more detailed characterization of the MTB geochemistry and its spatial variations. Stolper & Newman (1994) showed that melting mixtures of a MORB-type mantle source with, and in direct proportion to the amount of, a H_2O-rich component can produce the range of MTB observed and its arc-like end-member (A1846–9, Table 3). Gribble *et al.* (1996, 1998) extended the collection of studied lavas to the spreading segments north and south of the previous focus area at 18°N, as well as to the arc rifting segments in the north. We use their analyses, together with those of Hawkins *et al.* (1990) and Stolper & Newman (1994), to characterize the lava types of the Mariana Trough axis from 15° to 23°N (Table 3). To date, the only published analyses south of 15°N are of off-axis samples (e.g. Masuda *et al.* 1994; Yamatani *et al.* 1994).

The first-order segment-scale depth and geochemical differences are between lavas from the VTZ and those from the spreading axes at 15°–21°N (including the 'Central Graben'). The VTZ lavas are transitional in major, trace and isotope compositions between the MTB and nearby island arc lavas (Stern *et al.* 1990; Gribble *et al.* 1998). The MTB from the spreading axes at 15°–21°N show evidence of hydrous flux melting in addition to decompression melting (Hawkins *et al.* 1990; Stolper & Newman 1994; Gribble *et al.* 1996, 1998). They are characterized by mantle sources variably enriched in water and other incompatible elements derived from subduction (e.g. high Ba/La and Th/Zr, Table 3). Estimates of the total degree of melting from Ti–Yb systematics range from 7 to 16% for MTB, and 12–36% for VTZ and A1846-9 lavas (Gribble *et al.* 1998). Like the Manus data, this extent of total melting requires prior melting of the mantle sources.

MTB compositions are between end members (locally erupted at the spreading centre) of Sonne S84: 2–1 (15°N, normal MORB) and A1846–9 (18°21′N, IAT) (Table 3; Fig. 1). Note that MORB, BABB and IAT lava types all occur in close/overlapping proximity in the most densely studied/sampled region at 17°42′–18°24′N (Table 3; Hawkins *et al.* 1990; Volpe *et al.* 1990). With this level of eruptive heterogeneity, segment-scale systematics may be difficult to identify or may not exist. Nevertheless, comparing data from spreading segments at 15°–16°N v. 16°–17°N, Gribble *et al.* (1996) proposed that variations in magma supply along the spreading axes correlate with the abundance of highly incompatible elements and water in the lavas (i.e. that shallower segments have compositions consistent with higher degrees of mantle melting). Certainly the shallowest, hour-glass-shaped neovolcanic zone occurs at 17°N and sheet-flow samples dredged from there have some of the lowest $Na_{8.0}$, $Ti_{8.0}$, $Yb_{8.0}$ values, and highest Ba/La and $(H_2O)_{8.0}$ contents of the MTB (Table 3). Other segments, however, may be more like those at 18°N, and therefore difficult to characterize with a few samples.

Taken as a whole, the Mariana Trough samples have systematically lower $Fe_{8.0}$ and higher $Na_{8.0}$ contents than comparable Lau and Manus basin samples (Tables 1–3; Fig. 1). We interpret this to reflect lower overall extents of melting in the Mariana Trough than the other basins, associated with slower spreading and cooler mantle temperatures (the global trend) – on top of which is superimposed the local trend (e.g. decreasing $Na_{8.0}$ and $Fe_{8.0}$) associated with higher extents of prior melting plus flux melting proportional to water content. This is consistent with data from one of the rare exposures of peridotites and gabbros within active back-arc basins that occur in the Central Graben of the Mariana Trough at *c.* 20°03′N (Stern *et al.* 1996; Ohara *et al.* 2002). Open-system melting models indicate that these peridotites correspond to residual compositions after approximately 7% near-fractional melting of a depleted MORB-type upper mantle, consistent with a low magma budget resulting in ultramafic exposure (Ohara *et al.* 2002). This is lower than globally reported extents of melting for abyssal peridotites (8–25%; Elthon 1992; Johnson & Dick 1992).

Model

In order to evaluate controls on back-arc crustal accretion, we assess proposed physical processes in the mantle wedge and how these may affect and lead to differences from the better understood process of crustal accretion at MORs. At MORs conditions generally assumed include a uniform composition mantle, mantle advection driven by plate separation and a thermal structure controlled by cooling to the surface. Crustal accretion results from adiabatic decompression melting of mantle material within a volume referred to as a 'melting regime', melt extraction from the mantle and its delivery to or near the seafloor, and the flow of residual (less fertile) mantle out of the melting regime (e.g. Langmuir *et al.* 1992) (Fig. 8A). Other effects, such as melt buoyancy, may add dynamic components to this process (e.g. Su & Buck 1993), but the passive plate-separation model provides a simple first-order explanation of the crustal-accretion process at MORs. At MORs, systematic changes in morphology and geophysical characteristics that vary with spreading rate have been identified (Macdonald 1982). These variations are thought to be due to spreading-rate control on the shallow thermal structure of the ridge. At fast-spreading rates the lithosphere is hotter and long-lived magma lenses can exist, buffering the thermal structure and allowing along-axis flow

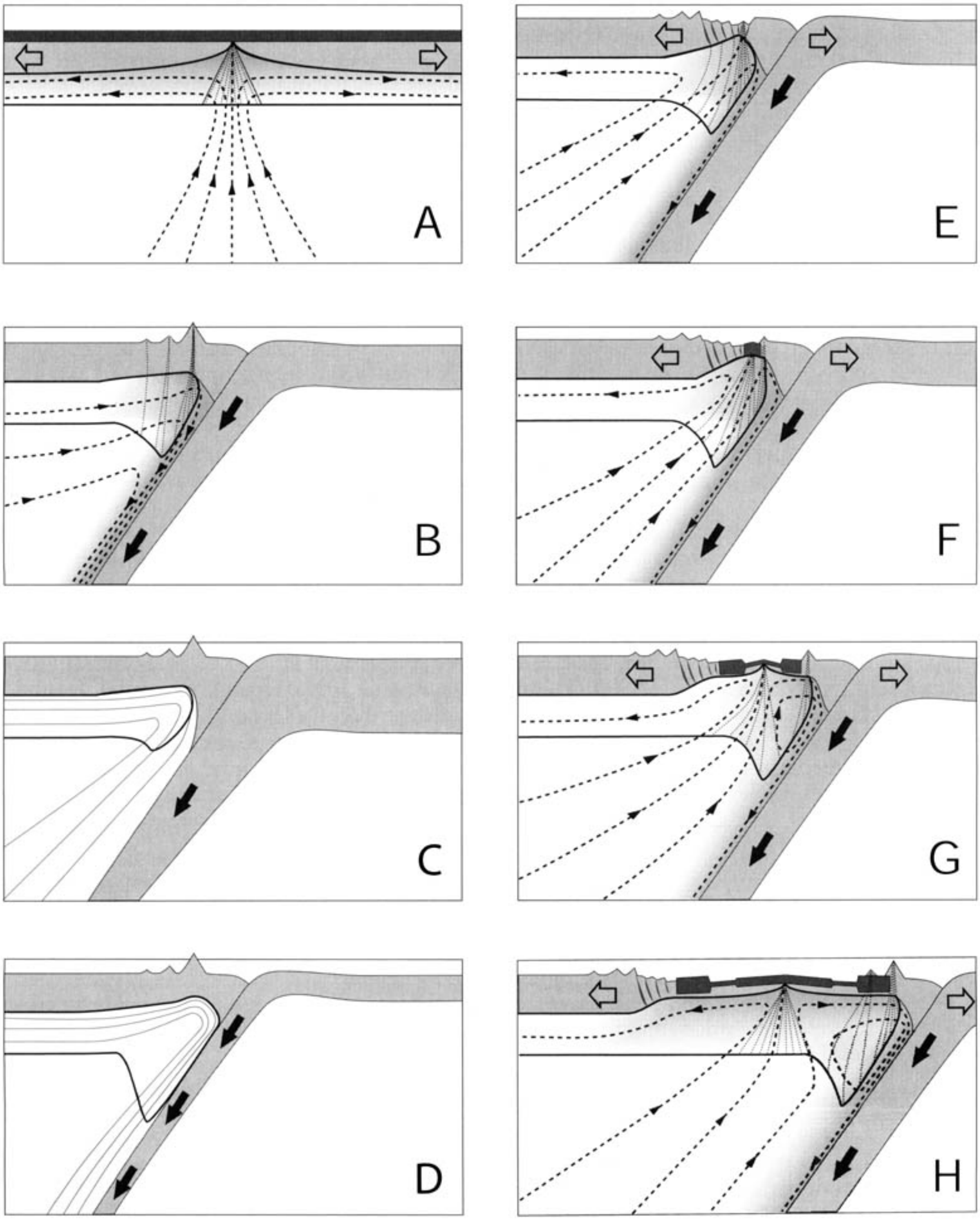

of melt. At slow rates cooler lithosphere does not permit long-lived magma lenses to exist and there is limited along-axis transport of melt. Lithospheric mechanical effects related to these different thermal structures and the presence or absence of magma lenses create axial valleys or axial highs, although a variety of differing processes have been proposed (Chen & Morgan 1990*b*; Chen & Phipps Morgan 1996; Shah & Buck 2001).

Similarly, back-arc crustal accretion should be tied to processes that affect mantle melting, extraction and delivery. In back-arc settings, however, the subducting slab affects the composition, flow field and thermal structure of the mantle wedge (Fig. 8B–D).

- The slab is a source of water and other volatiles that lower the solidus; geochemical studies show that volatile contents are elevated for the arc and back-arc lavas close to the volcanic front (Garcia *et al.* 1979; Stolper & Newman 1994; Ewart *et al.* 1998; Gribble *et al.* 1998). Melt can therefore be produced in subduction settings without surface plate separation inducing upward mantle advection and decompression melting.
- Mechanical models predict corner flow in the wedge driven by slab subduction (Fig. 8B) (McKenzie 1969; Sleep & Toksöz 1971; Ribe 1989; Davies & Stevenson 1992; Winder & Peacock 2001). Some models also predict a component of vertical advection induced by slab motion that contributes to mantle wedge melting (Conder *et al.* 2002). Geochemical observations show increasing source depletion from the back-arc toward the volcanic front and also argue for an inward flux of fertile mantle, variable melt extraction and removal of depleted mantle by slab-induced flow (Woodhead *et al.* 1993, 1998; Hochstaedter *et al.* 1996, 2000, 2001) (Fig. 8B). Mantle wedge flow models also predict the advection of slab-influenced mantle material into the melting regimes of back-arc spreading centres (Ribe 1989).
- Numerical models predict that the thermal structure of the mantle wedge is controlled by the rate of subduction in addition to the age of the slab: fast subduction induces rapid mantle advection toward the slab and downward with the slab so that cooling within the mantle wedge is minimized, whereas slow subduction allows significant growth of a

Fig. 8. Schematic model of controls on back-arc crustal accretion. (**A**) At MORs surface lithospheric plates (grey areas) separate (open arrows) and drive advection in the mantle (dashed stream lines). On rising above the solidus (heavy solid line) pressure-release melting occurs. Melt is transported to the spreading axis (fine dotted lines) accreting the crust (dark grey area), and melt-depleted mantle flows horizontally away with the separating lithospheric plates. Grey shading in the mantle above the solidus indicates increasing depletion of the residual mantle toward the surface. (**A**) follows Langmuir *et al.* (1992). (**B**) In subduction settings the motion of the slab (black arrows) drives corner-flow advection in the mantle wedge (indicated by dashed stream lines with small arrows). Water released by the slab increases in concentration toward the volcanic front and correspondingly lowers the mantle solidus (indicated by a heavy solid line that deepens beneath volcanic front). As mantle material is advected into the zone of hydration partial melting occurs. Melt rises (fine dotted lines) and may form back-arc seamount chains (indicated by surface triangular shapes). Mantle is progressively depleted (indicated by darker grey shading) of a melt component toward the volcanic front (large surface triangular shape) and is advected toward the wedge corner and downward with the slab. (**B**) follows Hochstaedter *et al.* (1996, 2001). (**C**) Slow subduction causes slow mantle wedge advection allowing significant cooling of the mantle wedge (indicated by widely spaced isotherms). The cooling is enhanced if the subducting plate is old (indicated by thick slab). (**D**) Fast subduction induces rapid mantle advection towards and downward with, the slab and leads to a hotter mantle wedge corner with isotherms tightly compressed against the slab (closely spaced lines), especially if the subducting plate is young (indicated by thin slab). (**C**) and (**D**) follow Davies & Stevenson (1992) and Peacock (1996). In (**C**) and (**D**) effects on the solidus are indicated by the thick solid line. (**E**) When back-arc extension commences it tends to initiate surface lithospheric plate separation near the rheologically weak volcanic front. Hydrated mantle material in this region is advected upward into the stretching and thinning lithosphere, leading to high degrees of melting in the rift phase, unless slow subduction (**C**) leads to significant mantle wedge cooling. (**F**) With increasing extension a seafloor spreading centre is established near the volcanic front advecting highly hydrated mantle. As a consequence, an enhanced magmatic stage and thick crust (indicated by a dark grey layer) result. (**G**) With continued spreading the extension axis separates from the volcanic front. Mantle hydration from the slab decreases and strongly melt-depleted mantle is mixed with ambient mantle as a result of corner flow and advection by the spreading centre (indicated by closed streamline loop). These conditions result in diminished magmatism and thinner crust (indicated by thinner dark grey crustal layer). (**H**) Eventually, the back-arc spreading system separates sufficiently from the volcanic front that it is not significantly affected by hydration, re-circulated melt-depleted mantle and slab-derived geochemical components. Spreading centres now advect ambient MORB-source mantle and their crustal accretion characteristics are like MORs, largely controlled by spreading rate.

thermal boundary layer outward from the slab into the mantle wedge (Fig. 8C and D) (e.g. Davies & Stevenson 1992; Peacock 1996). Mantle wedge cooling is most pronounced in the area beneath the volcanic front for slow subduction of old cold lithosphere.

Following Martinez & Taylor (2002), these observations and theories indicate a mantle wedge partitioned into various thermal/compositional zones that control back-arc crustal accretion: (i) far behind the volcanic front normal (fertile) MORB-source mantle is advected into the mantle wedge due to viscous coupling with the subducting slab; (ii) close to the volcanic front, fluids released from the slab hydrate a zone of the mantle wedge and cause melting. These slab-derived components (including those from sediments, crust and mantle lithosphere) give mantle wedge melts in this region a distinctive geochemical signature. This melt is extracted from the mantle to form arc volcanoes or is underplated or intruded into the crust. Depending on subduction rate and slab age, a zone of cooled mantle grows outward from the slab into the mantle wedge; and (iii) residual mantle (which is less fertile because it has had a melt component removed) is entrained within the corner flow induced by the subducting slab, which continues to release additional fluids. Its greater buoyancy relative to fertile mantle and low viscosity due to continued water addition from the slab may facilitate mixing with fertile mantle within the mantle wedge. The mixing process does not result in uniform compositions or even uniform gradients, but rather produces highly heterogeneous volumes on a variety of scales that retain distinctive compositions (as shown by sample heterogeneity). Overall, however, mantle compositions vary between highly subduction-influenced and depleted near the arc volcanic front to MORB-source like far from the volcanic front. Despite the large chemical heterogeneity, geophysical features such as crustal thickness, seafloor depth and gravity variations integrate these effects and provide a measure of systematic changes in total melt production.

When back-arc spreading develops (Fig. 8E–H) an advective system similar to that of MORs is superimposed on this mantle wedge environment. When arc systems rift to form back-arc basins the initial rift may occur along, seaward of, or behind the volcanic front (±50 km; Taylor & Karner 1983). The initial position of the spreading centre that follows the rifting phase may thus vary with respect to the underlying compositional zones in the mantle wedge. Spreading will cause migration of the ridge axis with time in a direction away from the trench axis. The extraction of melt by the spreading centre itself will also significantly modify the composition of the mantle wedge. Melt-depleted residual mantle created by seafloor spreading plus that from arc melt extraction may become entrained in the mantle wedge corner flow and be re-introduced beneath the back-arc basin, variably mixing with ambient fertile mantle. As the melting regimes of the back-arc spreading centres intersect the various mantle wedge compositional zones, corresponding changes in melt production may be expected: (i) enhanced melt production near the volcanic front when the spreading centre advects highly hydrated mantle. This effect may be countered, however, in slow-subduction environments where low rates of slab-derived volatile input and appreciable cooling of the mantle wedge near the volcanic front are predicted; (ii) low melt production when back-arc melting regimes intersect residual depleted (low fertility) mantle that has been swept back beneath the basin by the subducting slab; and (iii) normal (MOR-like) melting when intersecting normal (MORB-source) mantle far from slab-derived input and thermal effects. As at MORs, shallow melting effects will be modulated by spreading rate, which controls the shallow thermal and hence mechanical structure of the spreading centre. An addition characteristic feature of subduction systems is the spaced nature of the arc volcanic edifices and presumably of the melt generation and/or transport processes that feed them (Marsh 1979; Tamura *et al.* 2002). This may impart additional chemical heterogeneity and morphological variability to the early stages of back-arc spreading systems when they are in close proximity to the volcanic front.

Despite multiple controlling parameters proposed for back-arc melt generation and crustal accretion, systematic effects can be observed in back-arc basins spanning a broad range of subduction and opening conditions. We summarize and discuss these variations in crustal accretion with respect to the extension axes of the Lau, Manus and Mariana basins.

Discussion

Enhanced magmatism near the volcanic front

Consistently, the Lau, Manus and Mariana extension axes are magmatically robust when near the volcanic front. Despite slow-spreading rates (*c.* 40–60 mm a^{-1}), the VFR forms the shallowest and thickest crust of the Lau Basin spreading system (Fig. 3), and has high inflation, axial magma lens reflectors and active hydrothermal systems (Martinez & Taylor 2002). The SER in the Manus Basin form a series of high-standing neovolcanic ridges that are the shallowest extensional axes in the basin (Fig. 5). The SER are predicted to have the fastest opening rates in the basin (Tregoning 2002) so that, although they may not yet constitute long-lived or well-organized seafloor spreading centres, magmatism is accommodating much of the fast opening preventing the development of deep tectonic grabens that would otherwise form. The northern and southern Mariana Trough spreading axes approach the volcanic front and become shallow and ridge-like, in contrast to the central part of the basin where the axis forms a valley typical of slow-spreading centres (Fig. 7). Side-scan imagery also shows that both arc-proximal areas have high neovolcanic activity (Baker *et al.* 1996; Becker *et al.* 2001), despite the northward decreasing opening rate.

Together with the morphological and geophysical evidence for robust magmatism, the subduction geochemical signature becomes stronger near the volcanic front at the VFR, SER and VTZ extension axes (Tables 1–3, Fig. 1) (Gribble *et al.* 1998; Peate *et al.* 2001; Sinton *et al.* 2003). In accord with these findings and following Martinez & Taylor (2002), we infer that increased melting due to slab-derived hydration of the mantle wedge near the volcanic front is a primary cause of the present-day enhanced magmatism, consistent with the high water contents measured in these lavas. Enhanced magmatism is also observed at the northern (segment E2; Leat *et al.* 2000) and southern (segment E9; Bruguier & Livermore 2001) ends of the East Scotia Ridge, the back-arc spreading centre west of the South Sandwich arc, in the South Atlantic Ocean. These segments also have the most pronounced subduction influence. Thus, although the influence of the Bouvet mantle plume has been suggested as a cause of the enhanced magmatism (Livermore *et al.* 1997; Leat *et al.* 2000; Bruguier & Livermore 2001), hydrous fluxing by the slab near the volcanic front is likely to be a contributing factor (also see Livermore, 2003).

Several examples, however, show that these geophysical and geochemical characteristics are not always present but rather depend on additional factors, including subduction rate and the spaced nature of arc volcanism. In the case of the Mariana Trough, similar early spreading enhanced magmatism does not appear to characterize the entire length of the basin. In most of the central and southern Mariana Trough, the early opening of the basin is apparently characterized by normal to diminished magmatism, as indicated by deep seafloor bordering the West Mariana Ridge. This may be explained by a cooler mantle wedge due to slow subduction rates at that time. Back-arc basin opening adds to the subduction rate predicted by the convergence of the surrounding major plates. Assuming that former Pacific–Philippine convergence was similar to the current motion predicted by Seno *et al.* (1993), then slow subduction is predicted along the Mariana Trench prior to basin formation (*c.* 20 mm a^{-1} for the southern Mariana arc increasing to *c.* 40 mm a^{-1} near the northern Mariana arc, but becoming more oblique). Even slower subduction rates are predicted for the period before basin opening adopting current GPS-determined Pacific–Philippine vectors (Kato *et al.* 2003). Numerical models indicate that slow subduction significantly lowers the temperature of the mantle wedge in the region beneath the volcanic front (Davies & Stevenson 1992; Peacock 1996). As seafloor spreading in the Mariana Trough initiated through rifting of the arc, the thermal models suggest that cool mantle in this area (depressed by hundreds of °C) may suppress even hydrous melting, leading to decreased magmatism during early seafloor spreading. Once back-arc extension commences, however, the basin opening rate adds to the Pacific–Philippine convergence rate, subduction rate increases, slab-derived volatile flux rate increases and the mantle wedge apex gets hotter.

Two other examples illustrate additional controls on back-arc accretion related to the spaced locus of arc volcanism. In the case of the Sumisu and other active rifts of the Izu–Bonin arc, the rift lavas are distinct from the volcanic front and cross-chain lavas. Some of them have characteristics of BABB, not of the proximal island arc tholeiites (Table 2) (Fryer *et al.* 1990; Hochstaedter *et al.* 1990*a*, *b*). This reflects the vertically separate and horizontally spaced nature of the rift and arc sources (Taylor 1992). Secondly, some of the early basalts in the Lau Basin (e.g. ODP Site 834, Table 1; Fig. 1) have MORB-like characteristics and low extents of melting (Hawkins & Allan 1994; Hergt & Hawkesworth 1994). In this case, rifting split the forearc side of the (now-remnant) Lau arc, whose continued arc volcanism did not dominate the early Lau Basin lavas (prior to *c.* 3.5 Ma ago when the Tofua arc started to form) (Hawkins 1995).

Diminished magmatic phase

In the fast-opening Lau and Manus basins an abrupt deepening of the extension axis occurs with increasing distance from the volcanic front (Figs 3 and 5). In the Lau Basin, the ELSC north of the VFR becomes deeper and north of 20°30′S looses robust magmatic characteristics, such as axial magma chamber reflectors and axial high morphology. The northern ELSC crust is also deeper and thinner than the CLSC crust (Crawford *et al.* 2003). In the Manus Basin, the SR, as well as the northwesternmost ridge of the SER, become abruptly deeper than the rest of the SER, form grabens and are less magmatic (as indicated by fewer lava flows on side-scan imagery). The SR axes are likewise deeper than the MSC axis. These observations indicate lower magmatic production on the northern ELSC and SR relative to other axes in the Lau and Manus basins. Coincident with these geophysical indications of low magmatic production, however, there are apparently contradictory geochemical indications of higher extents of melting relative to normal MORB and the lavas of the CLSC and MSC (e.g. lower $Na_{8.0}$, $Ti_{8.0}$ and $Y_{8.0}$ contents). These observations may be reconciled by our model of corner flow re-fluxed mantle. Thus, the mantle sources of the northern ELSC and SR have, in fact, experienced high extents of melting, but not all beneath the present axes. Corner-flow circulation implies that at least some of the mantle material now beneath the ELSC and SR was previously closer to the volcanic front where it would be subject to hydrous melting and melt extraction by earlier spreading/rifting (analogous to the VFR and SER) and arc volcanic front magmatism. A consequence of this melting would be the significant removal of incompatible elements. As this depleted and less fertile mantle moves away from the volcanic front it receives additional slab-derived water and varyingly mixes with ambient MORB-source mantle. This will tend to increase source fertility and partly replenish incompatible elements, so that significant melting can still occur beneath the ELSC and SR (without extreme depletion characteristics), but not to the extent of the MORB-source end member. The end result is a thinner crust yet having a geochemical signature of high extents of melting. We note that there are a few samples on the northern ELSC and ILSC (especially CD33–23, Table 1; Pearce *et al.* 1995) that do show extreme depletion characteristics (as or more depleted than the volcanic arc itself) that probably represent a poorly mixed depleted end-member composition. The existence of these extreme sample compositions is particularly difficult to explain without corner flow re-circulation of previously melted mantle material.

The Mariana Trough axis is slow spreading and, between 14°N and 21°N, generally has morphology typical of slow-spreading MORs. A decreased magmatic stage may therefore not be easily distinguished morphologically from typical slow-spreading characteristics, which often include areas of thin or no crust exposing gabbros and peridotites at the seafloor (Cannat 1993; Cannat *et al.* 1995; Cann *et al.* 1997). Thus, in the case of slow-spreading back-arc basins, a reduction in melt production would not necessarily produce a morphologically distinct axial deepening relative to typical crustal variations. Gribble *et al.* (1996) have noted, however, the systematically deeper axis of the Mariana Trough compared to MORs, and the majority (LaTraille & Hussong 1980; Ambos & Hussong 1982) but not all (Bibee *et al.* 1980) of seismic determinations indicate thinner crust in the Mariana Trough than MOR average values. It could be argued that as the slab in the Mariana system dips steeply and does not underlie most of the spreading axis (Fig. 6), previously melt-depleted mantle may not be re-introduced in significant amounts beneath the back-arc melting regime. This is difficult to reconcile, however, with the geochemical evidence for high water contents and degrees of melting of the majority of Trough lavas that are BABB (Table 3) (Hawkins *et al.* 1990; Stolper & Newman 1994; Gribble *et al.* 1996, 1998). Thus, we conclude, based largely on geochemical data, that most of the Mariana Tough spreading axis (*c.* 14°–21°N) is in a diminished magmatic phase, due to advection of mantle that has previously undergone melt extraction. We note that the location of this part of the Mariana Trough spreading axis is comparable to that of the diminished melting parts of the Lau and Manus basins. This suggests that despite near-vertical slab subduction, mantle convection loops or 'eddies' extend out from the slab and are able to re-circulate depleted mantle material at least as far as the central Mariana Trough axis. Variable mixing of ambient (fertile) mantle and melt-depleted mantle with slab-derived additions in this convective process may explain the extreme heterogeneity of Mariana Trough axial lavas. The slow-spreading cool shallow thermal regime minimizes melt homogenization by not sustaining long-lived axial magma chambers, contributing to sample heterogeneity. The exposure of gabbros and peridotites directly exhibiting *low* extents of melting in the Mariana Trough Central Graben (Stern *et al.* 1996; Ohara *et al.*

2002) may be an extreme expression of a poorly mixed fertile mantle end-member component. The Central Graben forms offset and overlapping extension axes (Yamazaki *et al.* 1993), which partition spreading rates between them and, like large transform offsets at slow-spreading MORs, possibly represent tectonic 'cool spots' where mantle exhibiting low degrees of melting is often found (e.g. Ghose *et al.* 1996).

Normal magmatic phase

In the Lau and Manus basins, the CLSC and MSC show typical MOR-like morphology (Figs 3 and 5). At *c.* 180 and 240 km, respectively, from the volcanic front, these spreading axes are least influenced by slab effects. The CLSC and M1 lava compositions are very similar, LREE-depleted and MORB-like (Tables 1 and 2), with low water contents (0.17–0.3%) and only slight enrichments in Rb, Ba and depletions in Ta, Nb (Peate *et al.* 2001; Sinton *et al.* 2003). With average ridge depths of approximately 2300 m, their $Fe_{8.0}$ and $Na_{8.0}$ values fall on the global trend for MORB systematics (Klein & Langmuir 1987; Langmuir *et al.* 1992). Note, however, the additional presence of BABB (group B) lavas interspersed along the MSC and the METZ (even further from the New Britain arc) that indicate additional source heterogeneity (Sinton *et al.* 2003), possibly related to prior subduction events (Woodhead *et al.* 1998). Our prediction from these observed relationships is that back-arc spreading far behind the volcanic front should be MOR-like in all aspects, although some slab-derived geochemical heterogeneity in the mantle may be far-reaching. At approximately 300–550 km behind the New Hebrides arc, the central spreading ridge of the North Fiji Basin is a modern example whose characteristics fully satisfy this prediction (Auzende *et al.* 1995). In the Mariana Trough, the axis between the northern and southern melt-enhanced areas is only approximately 100 km from the volcanic front and, as described above, is accreting BABB crust. Continued spreading should eventually cause the spreading axis to migrate further from the volcanic front and eventually accrete MOR-like crust.

Conclusion

Systematic variations in depth, morphology, geophysical characteristics and geochemistry along the active extensional axes of the Lau, Manus and Mariana back-arc basins are interpreted to reflect changes in melt production within the underling mantle wedge, which are largely controlled by the subducting slab. The slab introduces water into the mantle wedge causing increasing hydration and lowering of the solidus toward the volcanic front. The slab motion interacts viscously with mantle wedge material, inducing corner flow. Corner flow can re-introduce previously melted mantle material into the melting regimes of back-arc spreading centres, thereby lowering their crustal production. Slab subduction controls the temperature structure of the mantle wedge. Fast subduction is expected to compress mantle wedge isotherms against the slab, whereas slow subduction allows for the significant growth of a cold thermal boundary layer away from the slab at shallow mantle levels where melt production occurs.

Enhanced melt production (with strongly subduction-influenced compositions), indicated by shallow axes (and thick crust where measured in the Lau Basin), occurs in each of the basins studied where the spreading centres are near the arc volcanic front and their melting regimes advect hydrated mantle. Early rifting/spreading in the Mariana Trough, however, appears to show a magma-starved phase, as indicated by deeps bordering the West Mariana Ridge. This phase may have been induced by predicted slow subduction and resultant cool mantle wedge temperatures near the volcanic front during early basin evolution. The early Lau Basin and Sumisu Rift provide examples of MORB-like and BABB magmas, respectively, sourced between the loci of contemporaneous arc magmatism.

Further from the arc volcanic front, a decreased melting phase is indicated in each of the basins by axial deepening (and thinner crust where measured in the Lau Basin). The geochemistry of samples in this stage typically show greater extents of melting than normal MORB, in contrast to the geophysical indications of decreased melt production. We reconcile these observations by proposing that mantle corner flow re-introduces a melt-depleted mantle component back beneath the melting regimes of the spreading centres, melt extraction having occurred closer to the volcanic front.

As back-arc spreading centres with time increasingly separate from the arc volcanic front through crustal accretion, they eventually are underlain by ambient MORB-source mantle with little subduction influence. Normal magmatic production, as indicated by normal depth (and thickness crust where measured), results as mantle mixing with a depleted component is eliminated. This stage has been largely achieved in the Lau (CLSC, *c.* 180 km from volcanic front) and Manus (MSC, *c.* 240 km from the volcanic front) basins, but not yet in the central Mariana Trough axis (*c.* 100 km from volcanic front), which is primarily erupting BABB. Once this stage is achieved and thereafter (e.g. the North Fiji Basin), crustal accretion and morphological characteristics become MOR-like – largely controlled by parameters, such as spreading rate, that determine the thermo-mechanical behaviour of the lithosphere and shallow mantle, rather than by slab controls on the composition, flow field and temperature within the mantle wedge.

We thank J.-M. Auzende for providing R/V *Yokosuka* multibeam data from the ManusFlux cruise in the Manus Basin, and J.M. Sinton for providing a prepublication manuscript and for discussions of Manus Basin geochemistry. We also thank Jenny Collier and David Peate for constructive reviews, and editor Rob Larter for comments that improved the manuscript. SOEST contribution 6100, HIGP contribution 1265.

References

AMBOS, E.L. & HUSSONG, D.M. 1982. Crustal structure of the Mariana Trough. *Journal of Geophysical Research*, **87**, 4003–4018.

AUZENDE, J.-M., ISHIBASHI, J., BEAUDOIN, Y., CHARLOU, J.L., DELTEIL, J., DONVAL, J.P., FOUQUET, Y., GOUILLOU, J.P., ILDEFONSE, B., KIMURA, H., NISHIO, Y., RADFORD-KNOERY, J. & RUELLAN, E. 2000*a*. Les Extrémités orientale et occidentale du bassin de Manus, Papouasie-Nouvelle-Guinée, explorées par submersible: la campagne Manaute. *Comptes Rendus de l'Academie des Sciences, Serie II. Sciences de la Terre et des Planètes*, **331**, 119–126.

AUZENDE, J.-M., ISHIBASHI, J., BEAUDOIN, Y., CHARLOU, J.-L., DELTEIL, J., DONVAL, J.-P., FOUQUET, Y., GOUILLOU, J.-P., ILDEFONSE, B., KIMURA, H., NISHIO, Y., RADFORD-KNOERY, J. & RUELLAN, E. 2000*b*. Rift propagation and extensive off-axis volcanic and hydrothermal activity in the Manus Basin (Papua New Guinea): MANAUTE Cruise. *InterRidge News*, **9**(2), 21–25.

AUZENDE, J.-M., ISHIBASHI, J.-I., BEAUDOIN, Y., CHARLOU, J.-L., DELTEIL, J., DONVAL, J.-P., FOUQUET, Y., ILDEFONSE, B., KIMURA, H., NISHIO, Y., RADFORD-KNOERY, J. & RUÉLLAN, E. 2000*c*. Extensive magmatic and hydrothermal activity documented in Manus Basin. *Eos, Transactions, American Geophysical Union*, **81**, 449–453.

AUZENDE, J.-M., PELLETIER, B. & EISSEN, J.-P. 1995. The North Fiji Basin: geology, structure and geodynamic evolution. *In*: TAYLOR, B. (ed.) *Backarc Basins: Tectonics and Magmatism*. Plenum, New York, 139–175.

AUZENDE, J.-M., URABE, T. & SCIENTIFIC PARTY. 1996. Cruise explores hydrothermal vents of the Manus Basin. *Eos, Transactions, American Geophysical Union*, **77**, 244.

BAKER, N.A., FRYER, P., MARTINEZ, F. & YAMAZAKI, T. 1996. Rifting history of the northern Mariana Trough: SeaMARC II and seismic reflection surveys. *Journal of Geophysical Research*, **101**, 11 427–11 455.

BARKER, P.F. & HILL, I.A. 1980. Asymmetric spreading in back-arc basins. *Nature*, **285**, 652–654.

BEAVAN, J., MURATA, I., NAKAO, S., KATO, T., HIRAHARA, K., TANAKA, T., ABAD, R., SCHOLZ, C., ROECKER, S. & DAVIS, D. 1994. Determination of the Philippine Sea Plate velocity from Global Positioning System observations, and effects of the 1993 Guam earthquake. *Eos, Transactions, American Geophysical Union*, **75**, Western Pacific Meeting Supplement, 59.

BECKER, N.C., FRYER, P., MARTINEZ, F., STERN, R.J. & BLOOMER, S.H. 2001. Magma piracy in the Southern Mariana backarc. *Eos, Transactions, American Geophysical Union*, **82**(47), Fall Meeting Supplement, T52A-0921.

BELL, R.E. & BUCK, W.R. 1992. Crustal control of ridge segmentation inferred from observations of the Reykjanes Ridge. *Nature*, **357**, 583–586.

BEVIS, M., TAYLOR, F.W., SCHUTZ, B.E., RECY, J., ISACKS, B.L., HELU, S., SINGH, R., KENDRICK, E., STOWELL, J., TAYLOR, B. & CALMANT, S. 1995. Geodetic observations of very rapid convergence and back-arc extension at the Tonga arc. *Nature*, **374**, 249–251.

BIBEE, L.D., SHOR, G.G. & LU, R.S. 1980. Inter-arc spreading in the Mariana Trough. *Marine Geology*, **35**, 183–197.

BILLEN, M.I. & GURNIS, M. 2001. A low viscosity wedge in subduction zones. *Earth and Planetary Science Letters*, **193**, 227–236.

BINNS, R.A. & SCOTT, S.D. 1993. Actively forming polymetallic deposits associated with felsic volcanic rocks in the eastern Manus backarc basin, Papua New Guinea. *Economic Geology*, **88**, 2226–2236.

BINNS, R.A., BARRIGA, F.J.A.S., MILLER, D.J. ET AL. 2002. Leg 193 summary. *In*: BINNS, R.A., BARRIGA, F.J.A.S., MILLER, D.J. *et al. Proceedings of the Ocean Drilling Program, Initial Reports*, **193**, 1–84.

BOESPFLUG, X., DOSSO, L., BOUGAULT, H., PEGRAM, W.J. & JORON, J.L. 1990. Arc and back-arc geochemical features of the Lau Basin; trace element and isotopic (Sr, Nd, Pb) data. *Eos, Transactions, American Geophysical Union*, **71**, 1019.

BORTNIKOV, N.S., FEDOROV, D.T. & MURAV'EV, K.G. 1993. Mineral composition and conditions of the formation of sulfide edifices in the Lau Basin (southwestern sector of the Pacific Ocean). *Geology of Ore Deposits*, **35**, 476–488.

BOTH, R., CROOK, K., TAYLOR, B., BROGAN, S., CHAPPELL, B., FRANKEL, E., LIU, L., SINTON, J. & TIFFIN, D. 1986. Hydrothermal chimneys and associated fauna in the Manus back-arc basin, Papua New Guinea. *Eos, Transactions, American Geophysical Union*, **67**, 489–490.

BRACEY, D.R. & OGDEN, T.A. 1972. Southern Mariana Arc: geophysical observations and hypothesis of evolution. *Geological Society of America Bulletin*, **83**, 1509–1522.

BRUGUIER, N.J. & LIVERMORE, R.A. 2001. Enhanced magma supply at the southern East Scotia Ridge: evidence for mantle flow around the subducting slab? *Earth and Planetary Science Letters*, **191**, 129–144.

CAMPOS, J., MADARIAGA, R. & SCHOLZ, C. 1996. Faulting process of the August 8, 1993, Guam earthquake: a thrust event in an otherwise weakly coupled subduction zone. *Journal of Geophysical Research*, **101**, 17 581–17 596.

CANN, J.R., BLACKMAN, D.K., SMITH, K.D., MCALLISTER, E., JANSSEN, B., MELLO, S., AVGERINOS, E., PASCOE, A.R. & ESCARTIN, J. 1997. Corrugated slip surfaces formed at ridge–transform intersections on the Mid-Atlantic Ridge. *Nature*, **385**, 329–332.

CANNAT, M. 1993. Emplacement of mantle rocks in the seafloor at mid-ocean ridges. *Journal of Geophysical Research*, **98**, 4163–4172.

CANNAT, M., MEVEL, C., MAIA, M., DEPLUS, C., DURAND, C., GENTE, P., AGRINIER, P., BELAROUCHI, A., DUBUISSON, G., HUMLER, E. & REYNOLDS, J. 1995. Thin crust, ultramafic exposures, and rugged faulting patterns at the Mid-Atlantic Ridge (22°–24°N). *Geology*, **23**, 49–52.

CARESS, D.W. 1991. Structural trends and back-arc extension in the Havre Trough. *Geophysical Research Letters*, **18**, 853–856.

CARMICHAEL, I.S.E. 1991. The redox states of basic and silicic magmas: a reflection of their source regions? *Contributions to Mineralogy and Petrology*, **106**, 129–141.

CHASE, T.E. 1985. Submarine topography of the Tonga–Fiji region and the southern Tonga platform area. *In*: SCHOLL, D.W. & VALLIER, T.L. (eds) *Geology and Offshore Resources of Pacific Island Arcs – Tonga Region*. Circum Pacific Council for Energy and Mineral Resources, Houston, TX, Earth Science Series, **2**, 21–23.

CHEN, Y. & MORGAN, W.J. 1990*a*. Rift valley/no rift valley transition at mid-ocean ridges. *Journal of Geophysical Research*, **95**, 17 571–17 581.

CHEN, Y. & MORGAN, W.J. 1990*b*. A nonlinear rheology model for mid-ocean ridge axis topography. *Journal of Geophysical Research*, **95**, 17 583–17 604.

CHEN, Y.J. & PHIPPS MORGAN, J. 1996. The effects of spreading rate, the magma budget, and the geometry of magma emplacement on the axial heat flux at mid-ocean ridges. *Journal of Geophysical Research*, **101**, 11 475–11 482.

CHIU, J.-M., ISACKS, B.L. & CARDWELL, R.K. 1991. 3-D configuration of subducted lithosphere in the western Pacific. *Geophysical Journal International*, **106**, 99–111.

COLE, J.W., GILL, J.B. & WOODHALL, D. 1985. Petrologic history of the Lau Ridge. *In*: SCHOLL, D.W. & VALLIER, T.L. (eds) *Geology and Offshore Resources of Pacific Island Arcs – Tonga Region*. Circum Pacific Council for Energy and Mineral Resources, Houston, TX, Earth Science Series, **2**, 379–414.

COLE, J.W., GRAHAM, I.J. & GIBSON, I.L. 1990. Magmatic evolution of late Cenozoic volcanic rocks of the Lau Ridge, Fiji. *Contributions to Mineralogy and Petrology*, **104**, 540–554.

COLLIER, J. & SINHA, M. 1990. Seismic images of a magma chamber beneath the Lau Basin back-arc spreading centre. *Nature*, **346**, 646–648.

COLLIER, J.S. & SINHA, M.C. 1992. Seismic mapping of a magma chamber beneath the Valu Fa Ridge, Lau Basin. *Journal of Geophysical Research*, **97**, 14 031–14 053.

CONDER, J.A., WIENS, D.A. & MORRIS, J. 2002. On the decompression melting structure at volcanic arcs and back-arc spreading centers. *Geophysical Research Letters*, **29**(15), 20, 1–4, 1727, 10.1029/2002GL015390.

COOPER, P. & TAYLOR, B. 1987. Seismotectonics of New Guinea: A model for arc reversal following arc–continent collision. *Tectonics*, **6**, 53–67.

COOPER, P. & TAYLOR, B. 1989. Seismicity and focal mechanisms at the New Britain Trench related to deformation of the lithosphere. *Tectonophysics*, **164**, 25–40.

CRAIG, H., CRAIG, V.K. & KIM, K.R. 1987. PAPATUA Expedition 1: hydrothermal vent surveys in back-arc basins: the Lau, N. Fiji, Woodlark, and Manus basins and Havre Trough. *Eos, Transactions, American Geophysical Union*, **68**, 1531.

CRAWFORD, W.C., HILDEBRAND, J.A., DORMAN, L.M., WEBB, S.C. & WIENS, D.A. 2003. Tonga Ridge and Lau Basin crustal structure from seismic refraction data. *Journal of Geophysical Research*, **108**(B4), EPM, 6, 1–17, 2195, 10.1029/2001JB001435.

DANYUSHEVSKY, L.V., FALLOON, T.J., SOBOLEV, A.V., CRAWFORD, A.J., CARROLL, M. & PRICE, R.C. 1993. The H_2O content of basalt glasses from Southwest Pacific back-arc basins. *Earth and Planetary Science Letters*, **117**, 347–362.

DAVIES, H.L. & PRICE, R.C. 1987. Basalts from the Solomon and Bismarck seas. *Geo-Marine Letters*, **6**, 193–202.

DAVIES, J.H. & STEVENSON, D.J. 1992. Physical model of source region of subduction zone volcanics. *Journal of Geophysical Research*, **97**, 2037–2070.

DAVIS, A.S., CLAGUE, D.A. & MORTON, J.L. 1990. Volcanic glass compositions from two spreading centers in Lau Basin, southwest Pacific Ocean. *Geologische Jahrbuch*, **92**, 481–501.

DELTEIL, J., RUELLAN, E., WRIGHT, I. & MATSUMOTO, T. 2002. Structure and structural development of the Havre Trough. *Journal of Geophysical Research*, **107**(B7), ETG, 7, 1–17, 2143, 10.1029/2001JB000494.

DENHAM, D. 1969. Distribution of earthquakes in the New Guinea–Solomon Islands region. *Journal of Geophysical Research*, **74**, 4290–4299.

DIXON, T.H. & STERN, R.J. 1983. Petrology, chemistry, and isotopic composition of submarine volcanoes in the southern Mariana arc. *Geological Society of America Bulletin*, **94**, 1159–1172.

DRIL, S.I., KUZMIN, M.I., TSIPUKOVA, S.S. & ZONENSHAIN, L.P. 1997. Geochemistry of basalts from the western Woodlark, Lau and Manus basins: implications for their petrogenesis and source rock compositions. *Marine Geology*, **142**, 57–83.

EGUCHI, T., FUJINAWA, Y. & UKAWA, M. 1989. Microearthquakes and tectonics in an active back-arc basin: the Lau Basin. *Physics of the Earth and Planetary Interiors*, **56**, 210–229.

ELTHON, D. 1992. Chemical trends in abyssal peridotites: refertilization of depleted suboceanic mantle. *Journal of Geophysical Research*, **97**, 9015–9025.

EWART, A. & HAWKESWORTH, C.J. 1987. The Pleistocene–Recent Tonga–Kermadec arc lavas: Interpretation of new isotopic and rare earth data in terms of a depleted mantle source model. *Journal of Petrology*, **28**, 495–530.

EWART, A., BRYAN, W.B., CHAPPELL, B.W. & RUDNICK, R.L. 1994*a*. Regional geochemistry of the Lau-Tonga arc and back-arc systems. *In*: HAWKINS, J.W., PARSON, L.M., ALLAN, J.F. *et al. Proceedings of the Ocean Drilling Program, Scientific Results*, **135**, 385–426.

EWART, A., COLLERSON, K.D., REGELOUS, M., WENDT, J.I. & NIU, Y. 1998. Geochemical evolution within the Tonga–Kermadec–Lau Arc–Back-arc system: the role of varying mantle wedge composition in space and time. *Journal of Petrology*, **39**, 331–368.

EWART, A., HERGT, J. & HAWKINS, J.W. 1994*b*. Major, trace element and Pb, Sr, and Nd isotope geochemistry of Site 839 basalts and basaltic andesites: implications for arc volcanism. *In*: HAWKINS, J.W., PARSON, L.M., ALLAN, J.F. *et al. Proceedings of the Ocean Drilling Program, Scientific Results*, **135**, 519–532.

FALLOON, T.J., MALAHOFF, A., ZONENSHAIN, L.P. & BOGDANOV, Y. 1992. Petrology and geochemistry of backarc basin basalts from Lau Basin spreading ridges at 15°, 18°, and 19°S. *Mineralogy and Petrology*, **47**, 1–35.

FOUQUET, Y., VON STACKELBERG, U. & CHARLOU, J. 1991*a*. Hydrothermal activity in the Lau back arc basin: Sulfides and water chemistry. *Geology*, **19**, 303–306.

FOUQUET, Y., VON STACKELBERG, U., CHARLOU, J.L., DONVAL, J.P., ERZINGER, J., FOUCHER, J.P., HERZIG, P., MUHE, R., SOAKAI, S., WIEDICKE, M. & WHITECHURCH, H. 1991*b*. Hydrothermal activity and metallogenesis in the Lau back-arc basin. *Nature*, **349**, 778–781.

FOUQUET, Y., VON STACKELBERG, U., CHARLOU, J.L., ERZINGER, J., HERZIG, P., MUHE, R. & WIEDICKE, M. 1993. Metallogenesis in back-arc environments: The Lau Basin example. *Economic Geology*, **88**, 2154–2181.

FRENZEL, G., MUHE, R. & STOFFERS, P. 1990. Petrology of the volcanic rocks from the Lau Basin, southwest Pacific. *Geologische Jahrbuch*, **92**, 395–479.

FRYER, P. 1995. Geology of the Mariana Trough. *In*: TAYLOR, B. (ed.) *Backarc Basins: Tectonics and Magmatism*. Plenum, New York, 237–279.

FRYER, P., FUJIMOTO, H., SEKINE, M., JOHNSON, L.E., KASAHARA, J., MASUDA, H., GAMO, T., ISHII, T., ARIYOSHI, M. & FUJIOKA, K. 1998. Volcanoes of the southwestern extension of the active Mariana island arc: New swath-mapping and geochemical studies. *The Island Arc*, **7**, 596–607.

FRYER, P., SINTON, J.M. & PHILPOTTS, J.A. 1981. Basaltic glasses from the Mariana Trough. *In*: HUSSONG, D.M. & UYEDA, S. *et al. Initial Reports of the Deep Sea Drilling Project*, **60**, 601–609.

FRYER, P., TAYLOR, B., LANGMUIR, C.H. & HOCHSTAEDTER, A.G. 1990. Petrology and geochemistry of lavas from the Sumisu and Torishima backarc rifts. *Earth and Planetary Science Letters*, **100**, 161–178.

FUJIWARA, T., YAMAZAKI, T. & JOSHIMA, M. 2001. Bathymetry and magnetic anomalies in the Havre Trough and southern Lau Basin: from rifting to spreading in back-arc basins. *Earth and Planetary Science Letters*, **185**, 253–264.

GAMO, T., OKAMURA, K., CHARLOU, J.-L., URABE, T. & AUZENDE, J.-M. 1997. Acidic and sulfate-rich hydrothermal fluids from the Manus Back Arc Basin, Papua New Guinea. *Geology*, **25**, 139–142.

GAMO, T., SAKAI, H., ISHIBASHI, J., NAKAYAMA, E., ISSHIKI, K., MATSUURA, H., SHITATSHIMA, K., TAKEUCHI, K. & OHTA, S. 1993. Hydrothermal plumes in the eastern Manus Basin, Bismarck Sea: CH_4, Mn, Al, and pH anomalies. *Deep-Sea Research*, **40**, 2335–2349.

GARCIA, M.O., LIU, N.W.K. & MUENOW, D. 1979. Volatiles in submarine volcanic rocks from the Mariana Island arc and trough. *Geochimica et Cosmochimica Acta*, **43**, 305–312.

GHOSE, I., CANNAT, M. & SEYLER, M. 1996. Transform fault effect on mantle melting in the MARK area (Mid-Atlantic Ridge south of the Kane transform). *Geology*, **24**, 1139–1142.

GILL, J. 1981. *Orogenic Andesites and Plate Tectonics*. Springer, New York.

GRIBBLE, R.F., STERN, R.J., BLOOMER, S.H., STUBEN, D., O'HEARN, T. & NEWMAN, S. 1996. MORB mantle and subduction components interact to generate basalts in the southern Mariana Trough back-arc basin. *Geochimica et Cosmochimica Acta*, **60**, 2153–2166.

GRIBBLE, R.F., STERN, R.J., NEWMAN, S., BLOOMER, S.H. & O'HEARN, T. 1998. Chemical and isotopic composition of lavas from the northern Mariana Trough: implications for magmagenesis in back-arc basins. *Journal of Petrology*, **39**, 125–154.

HAMBURGER, M.W. & ISACKS, B.L. 1988. Diffuse back-arc deformation in the southwestern Pacific. *Nature*, **332**, 599–604.

HARDING, A.J., KENT, G.M. & COLLINS, J.A. 2000. Initial results from a multichannel seismic survey of the Lau back-arc basin. *Eos, Transactions, American Geophysical Union*, **81**(48), Fall Meeting Supplement, T61C-16.

HART, S.R., GLASSLEY, W.E. & KARIG, D.E. 1972. Basalts and sea floor spreading behind the Mariana island arc. *Earth and Planetary Science Letters*, **15**, 12–18.

HAWKINS, J.W. 1974. Geology of the Lau Basin, a marginal sea behind the Tonga Arc. *In*: BURK, C.A. & DRAKE, C.L. (eds) *The Geology of Continental Margins*. Springer, New York, 505–520.

HAWKINS, J.W. 1994. Petrologic synthesis: Lau Basin transect (Leg 135). *In*: HAWKINS, J.W., PARSON, L.M., ALLAN, J.F. *et al. Proceedings of the Ocean Drilling Program, Scientific Results*, **135**, 879–905.

HAWKINS, J.W. 1995. The geology of the Lau Basin. *In*: TAYLOR, B. (ed.) *Backarc Basins: Tectonics and Magmatism*. Plenum, New York, 63–138.

HAWKINS, J.W. & ALLAN, J.F. 1994. Petrologic evolution of the Lau Basin, Sites 834–839. *In*: HAWKINS, J.W., PARSON, L.M., ALLAN, J.F. *et al. Proceedings of the Ocean Drilling Program, Scientific Results*, **135**, 427–470.

HAWKINS, J.W. & MELCHIOR, J.T. 1985. Petrology of Mariana Trough and Lau Basin basalts. *Journal of Geophysical Research*, **90**, 431–468.

HAWKINS, J.W., LONSDALE, P.F., MACDOUGALL, J.D. & VOLPE, A.M. 1990. Petrology of the axial ridge of the Mariana Trough backarc spreading center. *Earth and Planetary Science Letters*, **100**, 226–250.

HERGT, J.M. & FARLEY, K.N. 1994. Major element, trace element, and isotope variations in Site 834 basalts: Implications for the initiation of backarc opening. *In*: HAWKINS, J.W., PARSON, L.M., ALLAN, J.F. *et al. Proceedings of the Ocean Drilling Program, Scientific Results*, **135**, 471–489.

HERGT, J.M. & HAWKESWORTH, C.J. 1994. Pb-, Sr-, and Nd-isotopic evolution of the Lau Basin: Implications for mantle dynamics during backarc opening. *In*: HAWKINS, J.W., PARSON, L.M., ALLAN, J.F. *et al. Proceedings of the Ocean Drilling Program, Scientific Results*, **135**, 505–517.

HERZIG, P., HANNINGTON, D.M., FOUQUET, Y., VON STACKELBERG, U. & PETERSEN, S. 1993. Gold-rich polymetallic sulfides from the Lau back arc and implications for the geochemistry of gold in seafloor hydrothermal systems of the Southwest Pacific. *Economic Geology*, **88**, 2182–2209.

HERZIG, P.M., HANNINGTON, M.D. & ARRIBAS, A., JR. 1998. Sulfur isotopic composition of hydrothermal precipitates from the Lau back-arc: implications for magmatic contributions to seafloor hydrothermal systems. *Mineralium Deposita*, **33**, 226–237.

HERZIG, P.M., VON STACKELBERG, U. & PETERSEN, S. 1990. Hydrothermal mineralization from the Valu Fa Ridge, Lau Back-arc Basin (SW Pacific). *Marine Mining*, **9**, 271–301.

HIROSE, K. & KAWAMOTO, T. 1995. Hydrous partial melting of lherzolite at 1 GPa: the effect of H_2O on the genesis of basaltic magma. *Earth and Planetary Science Letters*, **133**, 463–473.

HIROSE, K. & KUSHIRO, I. 1993. Partial melting of dry peridotites at high pressures: determination of compositions of melts segregated from peridotite using aggregates of diamond. *Earth and Planetary Science Letters*, **90**, 477–489.

HOCHSTAEDTER, A.G., GILL, J., PETERS, R., BROUGHTON, P., HOLDEN, P. & TAYLOR, B. 2001. Across-arc geochemical trends in the Izu–Bonin arc: Contributions from the subducting slab. *Geochemistry, Geophysics, Geosystems*, **2**, 2000GC000105.

HOCHSTAEDTER, A.G., GILL, J.B., KUSAKABE, M., NEWMAN, S., PRINGLE, M., TAYLOR, B. & FRYER, P. 1990*a*. Volcanism in the Sumisu Rift, I. Major element, volatile, and stable isotope geochemistry. *Earth and Planetary Science Letters*, **100**, 179–194.

HOCHSTAEDTER, A.G., GILL, J.B. & MORRIS, J.D. 1990*b*. Volcanism in the Sumisu Rift, II. Subduction and non-subduction related components. *Earth and Planetary Science Letters*, **100**, 195–209.

HOCHSTAEDTER, A.G., GILL, J.B., TAYLOR, B., ISHIZUKA, O., YUASA, M. & MORITA, S. 2000. Across-arc geochemical trends in the Izu–Bonin arc: Constraints on source composition and mantle melting. *Journal of Geophysical Research*, **105**, 495–512.

HOCHSTAEDTER, A.G., KEPEZHINSKAS, P., DEFANT, M., DRUMMOND, M. & KOLOSKOV, A. 1996. Insights into the volcanic arc mantle wedge from magnesian lavas from the Kamchatka arc. *Journal of Geophysical Research*, **101**, 697–712.

HONSHO, C., TAMAKI, K. & FUJIMOTO, H. 1997. Bathymetric and geomagnetic survey of the Mariana Trough 16°N. *JAMSTEC Journal of Deep Sea Research*, **13**, 21–29.

HONZA, E. & TAMAKI, K. 1985. The Bonin Arc. *In*: NAIRN, A.E.M. & UYEDA, S. (eds) *The Ocean Basins and Margins Vol. 7, The Pacific Ocean*. Plenum, New York, 459–502.

HUSSONG, D.M. & UYEDA, S. 1981. Tectonic processes and the history of the Mariana arc: a synthesis of the results of Deep Sea Drilling Project Leg 60. *In*: HUSSONG, D.M. & UYEDA, S. *et al. Initial Reports of the Deep Sea Drilling Project*, **60**, 909–929.

ISACKS, B.L. & BARAZANGI, M. 1977. Geometry of Benioff Zones: lateral segmentation and downwards bending of the subducted lithosphere. *In*: TALWANI, M. & PITMAN, W.C. (eds) *Island Arcs, Deep Sea Trenches, and Back-arc Basins*. Maurice Ewing Series, American Geophysical Union, **1**, 99–114.

JENNER, G.A., CAWOOD, P.A., RAUTENSCHLEIN, M. & WHITE, W.M. 1987. Composition of back-arc basin volcanics, Valu Fa ridge, Lau Basin: Evidence for a slab-derived component in their mantle source. *Journal of Volcanology and Geothermal Research*, **32**, 209–222.

JOHNSON, K.T.M. & DICK, H.J.B. 1992. Open system melting and temporal and spatial variation of peridotite and basalt at the Atlantis II Fracture Zone. *Journal of Geophysical Research*, **97**, 9219–9241.

JOHNSON, T. & MOLNAR, P. 1972. Focal mechanisms and plate tectonics of the southwest Pacific. *Journal of Geophysical Research*, **77**, 5000–5032.

KAMENETSKY, V.S., BINNS, R.A., GEMMELL, J.B., CRAWFORD, A.J., MERNAGH, T.P., MAAS, R. & STEELE, D. 2001. Parental basaltic melts and fluids in eastern Manus backarc Basin: implications for hydrothermal mineralization. *Earth and Planetary Science Letters*, **184**, 685–702.

KAPPEL, E.S. & RYAN, W.B.F. 1986. Volcanic episodicity and a non-steady state rift valley along northeast Pacific spreading centers: evidence from SeaMARC I. *Journal of Geophysical Research*, **91**, 13 925–13 940.

KARIG, D.E. 1970. Ridges and basins of the Tonga–Kermadec island arc system. *Journal of Geophysical Research*, **75**, 239–254.

KARIG, D.E. 1971. Origin and development of marginal basins in the western Pacific. *Journal of Geophysical Research*, **76**, 2542–2561.

KARIG, D.E. & MOORE, G.F. 1975. Tectonic complexities in the Bonin arc system. *Tectonophysics*, **27**, 97–118.

KARIG, D.E. & RANKEN, B. 1983. Marine geology of the forearc region, southern Mariana island arc. *In*: HAYES, D.E. (ed.) *The Tectonic and Geologic Evolution of the Southeast Asian Seas and Islands: Part 2*. American Geophysical Union, Geophysical Monographs, **27**, 266–280.

KARIG, D.E., ANDERSON, R.N. & BIBEE, L.D. 1978. Characteristics of back arc spreading in the Mariana trough. *Journal of Geophysical Research*, **83**, 1213–1226.

KATO, T., BEAVAN, J., MATSUSHIMA, T., KOTAKE, Y., CAMACHO, J.T. & NAKAO, S. 2003. Geodetic evidence of back arc spreading in the Mariana Trough as derived from GPS observations. *Geophysical Research Letters*, **30**(12), 27, 1–4.

KATO, T., KOTAKE, Y., NAKAO, S., BEAVAN, J., HIRAHARA, K., OKADA, M., HOSHIBA, M., KAMIGAICHI, O., FEIR, R.B., PARK, P.H., GERASIMENKO, M.D. & KASAHARA, M. 1998. Initial results from WING, continuous GPS network in the western Pacific area. *Geophysical Research Letters*, **25**, 369–372.

KENT, A.J.R., PEATE, D.W., NEWMAN, S., STOLPER, E.M. & PEARCE, J.A. 2002. Chlorine in submarine glasses from the Lau Basin: seawater contamination and constraints on the composition of slab-derived fluids. *Earth and Planetary Science Letters*, **202**, 361–377.

KLEIN, E.M. & LANGMUIR, C.H. 1987. Global correlations of ocean ridge basalt chemistry with axial depth and crustal thickness. *Journal of Geophysical Research*, **92**, 8089–8115.

KLEIN, E.M. & LANGMUIR, C.H. 1989. Local versus global variations in ocean ridge basalt composition: A reply. *Journal of Geophysical Research*, **94**, 4241–4252.

KONG, L.S.L. 1993. Seafloor spreading in the Mariana Trough. *In*: SEGAWA, J. (ed.) *Preliminary Report of the Hakuho-Maru Cruise KH92-1*. Ocean Research Institute, University of Tokyo, Tokyo, 5–16.

KONG, L.S.L., SEAMA, N., FUJIMOTO, H., KASAHARA, J. & KH92-1 SHIPBOARD SCIENTIFIC PARTY. 1992. Segmentation of the Mariana Trough Back-Arc Spreading Center at 18°N. *InterRidge News*, **1**(1), 2–5.

KOTAKE, Y. 2000. Study of the tectonics of western Pacific region derived from GPS data analysis. *Bulletin Earthquake Research Institute, University of Tokyo*, **75**, 229–334.

KOTAKE, Y. & KATO, T. 2002. Re-estimation of the relative motion of Philippine Sea plate derived from GPS observations. *Eos, Transactions, American Geophysical Union*, **83**(22), Western Pacific Geophysics Meeting Supplement, SE31A-19.

LANGMUIR, C.H., KLEIN, E.M. & PLANK, T. 1992. Petrological systematics of mid-ocean ridge basalts: constraints on melt generation beneath ocean ridges. *In*: PHIPPS MORGAN, J., BLACKMAN, D.K. & SINTON, J.M. (eds) *Mantle Flow and Melt Generation at Mid-ocean Ridges*. American Geophysical Union, Geophysical Monographs, **71**, 183–280.

LATRAILLE, S.L. & HUSSONG, D.M. 1980. Crustal structure across the Mariana island arc. *In*: HAYES, D.E. (ed.) *The Tectonic and Geologic Evolution of Southeast Asian Seas and Islands*. American Geophysical Union, Geophysical Monographs, **23**, 209–221.

LAWVER, L.A. & HAWKINS, J.W. 1978. Diffuse magnetic anomalies in marginal basins: their possible tectonic and petrologic significance. *Tectonophysics*, **45**, 323–339.

LEAT, P.T., LIVERMORE, R.A., MILLAR, I.L. & PEARCE, J.A. 2000. Magma supply in back-arc spreading centre segment E2, East Scotia Ridge. *Journal of Petrology*, **41**, 845–866.

LÉCUYER, C., DUBOIS, M., MARIGNAC, C., GRUAU, G., FOUQUET, Y. & RANBOZ, C. 1999. Phase separation and fluid mixing in subseafloor back arc hydrothermal systems: A microthermometric and oxygen isotope study of fluid inclusions in the barite-sulfide chimneys of the Lau basin. *Journal of Geophysical Research*, **104**, 17 911–17 927.

LISITSYN, A.P., CROOK, K.A.W., BOGDANOV, Y.A., ZONENSHAYN, L.P., MURAV'YEV, K.G., TUFAR, W., GURVICH, Y.G., GORDEYEV, V.V. & IVANOV, G.V. 1993. A hydrothermal field in the rift zone of the Manus basin, Bismarck Sea. *International Geology Review*, **35**, 105–126.

LISITSYN, A.P., MALAHOFF, A.R., BOGDANOV, Y.A., SOAKIA, S., ZONENSHAYN, L.P., GURVICH, Y.G., MURAV'YEV, K.G. & IVANOV, G.V. 1992. Hydrothermal formations in the northern part of the Lau Basin, Pacific Ocean. *International Geology Review*, **34**, 828–847.

LIVERMORE, R. 2003. Back-arc spreading and mantle flow in the East Scotia Sea. *In*: LARTER, R.D. & LEAT, P.T. (eds) *Intra-oceanic Subduction Systems: Tectonic and Magmatic Processes*. Geological Society, London, Special Publications, **219**, 315–331.

LIVERMORE, R., CUNNINGHAM, A., VANNESTE, L. & LARTER, R. 1997. Subduction influence on magma supply at the East Scotia Ridge. *Earth and Planetary Science Letters*, **150**, 261–275.

MACDONALD, K.C. 1982. Mid-ocean ridges: Fine scale tectonic, volcanic and hydrothermal processes within the plate boundary zone. *Annual Review of Earth and Planetary Sciences*, **10**, 155–190.

MACPHERSON, C.G., HILTON, D.R., MATTEY, D.P. & SINTON, J.M. 2000. Evidence for an ^{18}O-depleted mantle plume from contrasting $^{18}O/^{16}O$ ratios of back-arc lavas from the Manus Basin and Mariana Trough. *Earth and Planetary Science Letters*, **176**, 171–183.

MACPHERSON, C.G., HILTON, D.R., SINTON, J.M., POREDA, R.J. & CRAIG, H. 1998. High $^{3}He/^{4}He$ ratios in the Manus backarc basin: Implications for mantle mixing and origin of plumes in the western Pacific Ocean. *Geology*, **26**, 1007–1010.

MARSH, B.D. 1979. Island arc development: some observations, experiments, and speculations. *Journal of Geology*, **87**, 687–714.

MARTINEZ, F. & TAYLOR, B. 1996. Backarc spreading, rifting, and microplate rotation between transform faults in the Manus Basin. *Marine Geophysical Researches*, **18**, 203–224.

MARTINEZ, F. & TAYLOR, B. 2002. Mantle wedge control on back-arc crustal accretion. *Nature*, **416**, 417–420.

MARTINEZ, F., FRYER, P., BAKER, N.A. & YAMAZAKI, T. 1995. Evolution of backarc rifting: Mariana Trough, 20°–24°N. *Journal of Geophysical Research*, **100**, 3807–3827.

MARTINEZ, F., FRYER, P. & BECKER, N. 2000. Geophysical characteristics of the Southern Mariana Trough, 11°50'N–13°40'N. *Journal of Geophysical Research*, **105**, 16 591–16 608.

MARTY, B., SANO, Y. & FRANCE-LANORD, C. 2001. Water-saturated oceanic lavas from the Manus Basin: volatile behaviour during assimilation–fractional crystalization–degassing (AFCD). *Journal of Volcanology and Geothermal Research*, **109**, 1–10.

MASUDA, H., LUTZ, R.A., MATSUMOTO, S., MASUMOTO, S. & FUJIOKA, K. 1994. Topography and geochemical aspects on the most recent volcanism around the spreading axis of the southern Mariana Trough at 13°N. *JAMSTEC Journal of Deep Sea Research*, **10**, 176–185.

MCKENZIE, D.P. 1969. Speculations on the consequences and causes of plate motion. *Geophysical Journal of the Royal Astronomical Society*, **18**, 1–32.

MEIJER, A. 1976. Pb and Sr isotope data bearing on the origin of volcanic rocks from the Mariana island arc system. *Geological Society of America Bulletin*, **87**, 1359–1369.

MOBERLY, R. 1972. Origin of lithosphere behind island arcs, with reference to the western Pacific. *In*: SHAGAM, R., HARGRAVES, R.B., MORGAN, W.J., HOUTEN, F.B.V., BURK, C.A., HOLLAND, H.D. & HOLLISTER, L.C. (eds) *Studies in Earth and Space Sciences, A Memoir in Honor of Harry H. Hess*. Geological Society of America, Memoirs, **132**, 35–55.

MORTON, J.L. & SLEEP, N.H. 1985. Seismic reflections from a Lau Basin magma chamber. *In*: SCHOLL, D.W. & VALLIER, T.L. (eds) *Geology and Offshore Resources of Pacific Island Arcs – Tonga Region*. Circum Pacific Council for Energy and Mineral Resources, Houston, TX, Earth Science Series, **2**, 441–453.

NIU, Y., BIDEAU, D., HEKINIAN, R. & BATIZA, R. 2001. Mantle compositional control on the extent of mantle melting, crust production, gravity anomaly, ridge morphology, and ridge segmentation: a case study at the Mid-Atlantic Ridge 33–35°N. *Earth and Planetary Science Letters*, **186**, 383–399.

OHARA, Y., STERN, R.J., ISHII, T., YURIMOTO, H. & YAMAZAKI, T. 2002. Peridotites from the Mariana Trough: first look at the mantle beneath an active back-arc basin. *Contributions to Mineralogy and Petrology*, **143**, 1–18.

PACKHAM, G.H. & FALVEY, D.A. 1971. An hypothesis for the formation of marginal seas in the western Pacific. *Tectonophysics*, **11**, 79–109.

PARK, C.-H., TAMAKI, K. & KOBAYASHI, K. 1990. Age-depth correlation of the Philippine Sea back-arc basins and other marginal basins in the world. *Tectonophysics*, **181**, 351–371.

PARSON, L.M. & HAWKINS, J.W. 1994. Two-stage ridge propagation and the geological history of the Lau backarc basin. *In*: HAWKINS, J.W., PARSON, L.M., ALLAN, J.F. *et al. Proceedings of the Ocean Drilling Program, Scientific Results*, **135**, 819–828.

PARSON, L.M. & WRIGHT, I.C. 1996. The Lau–Havre–Taupo back-arc basin: A southward-propagating, multi-stage evolution from rifting to spreading. *Tectonophysics*, **263**, 1–22.

PARSON, L.M., PEARCE, J.A., MURTON, B.J., HODKINSON, R.A. & RRS CHARLES DARWIN SCIENTIFIC PARTY. 1990. Role of ridge jumps and ridge propagation in the tectonic evolution of the Lau backarc basin, southwest Pacific. *Geology*, **18**, 470–473.

PEACOCK, S.M. 1996. Thermal and petrological structure of subduction zones. *In*: BEBOUT, G.E., SCHOLL, D.W., KIRBY, S.H. & PLATT, J.P. (eds) *Subduction: Top to Bottom*. American Geophysical Union, Geophysical Monographs, **96**, 119–133.

PEARCE, J. & PEATE, D. 1995. Tectonic implications of the composition of volcanic arc magmas. *Annual Reviews of Earth and Planetary Science*, **23**, 251–285.

PEARCE, J.A. & PARKINSON, I.J. 1993. Trace element models for mantle melting: application to volcanic arc petrogenesis. *In*: PITCHARD, H.M., ALABASTER, T., HARRIS, N.B.W. & NEARY, C.R. (eds) *Magmatic Processes and Plate Tectonics*. Geological Society, London, Special Publications, **76**, 373–403.

PEARCE, J.A., ERNEWEIN, M., BLOOMER, S.H., PARSON, L.M., MURTON, B.J. & JOHNSON, L.E. 1995. Geochemistry of Lau Basin volcanic rocks: influence of ridge segmentation and arc proximity. *In*: SMELLIE, J.L. (ed.) *Volcanism Associated with Extension at Consuming Plate Margins*. Geological Society, London, Special Publications, **81**, 53–75.

PEATE, D.W., KOKFELT, T.F., HAWKESWORTH, C.J., CALSTEREN, P.W.V., HERGT, J.M. & PEARCE, J.A. 2001. U-series isotope data on Lau Basin glasses: the role of subduction-related fluids during melt generation in back-arc basins. *Journal of Petrology*, **42**, 1449–1470.

PEIRCE, C., TURNER, I.M. & SINHA, M.C. 2001. Crustal structure, accretionary processes and rift propagation: a gravity study of the intermediate-spreading Valu Fa Ridge, Lau Basin. *Geophysical Journal International*, **146**, 53–73.

PELLETIER, B., CALMANT, S. & PILLET, R. 1998. Current tectonics of the Tonga–New Hebrides region. *Earth and Planetary Science Letters*, **164**, 263–276.

PELLETIER, B., LAGABRIELLE, Y., BENOIT, M., CABIOCH, G., CALMANT, S., GAREL, E. & GUIVEL, C. 2001. Newly identified segments of the Pacific–Australia plate boundary along the North Fiji transform zone. *Earth and Planetary Science Letters*, **193**, 347–358.

PLANK, T. & LANGMUIR, C.H. 1992. Effects of the melting regime on the composition of the oceanic crust. *Journal of Geophysical Research*, **97**, 19 749–19 770.

RIBE, N.M. 1989. Mantle flow induced by back arc spreading. *Geophysical Journal International*, **98**, 85–91.

RIPPER, I.D. 1975. *Earthquake focal mechanism solutions in the New Guinea Solomon Islands region, 1963–1968*. Australian Bureau of Mineral Resources Reports, **178**.

RIPPER, I.D. 1977. *Some earthquake focal mechanisms in the New Guinea/Solomon Islands region, 1969–1971*. Australian Bureau of Mineral Resources Reports, **192**.

RIPPER, I.D. 1982. Seismicity of the Indo-Australian/Solomon Sea plate boundary in the southeast Papua region. *Tectonophysics*, **87**, 355–369.

RUELLAN, E., HUCHON, P., AUZENDE, J.-M. & GRÀCIA, E. 1994. Propagating rift and overlapping spreading center in the North Fiji Basin. *Marine Geology*, **116**, 37–56.

SAGER, W.W. 1979. *The structure of the Mariana arc as inferred from gravity and seismic data*. M.S. thesis, University of Hawaii.

SAGER, W.W. 1980. Structure of the Mariana Arc inferred from gravity and seismic data. *Journal of Geophysical Research*, **85**, 5382–5388.

SCHEIRER, D. & MACDONALD, K.C. 1993. Variation in cross-sectional area of the axial ridge along the East Pacific Rise: Evidence for the magmatic budget of a fast spreading center. *Journal of Geophysical Research*, **98**, 7871–7885.

SCLATER, J.G., HAWKINS, J.W., MAMMERICKX, J. & CHASE, C.B. 1972. Crustal extension between the Tonga and Lau ridges: petrologic and geophysical evidence. *Geological Society of America Bulletin*, **83**, 505–518.

SCOTT, S.D. & BINNS, R.A. 1995. Hydrothermal processes and contrasting styles of mineralization in the western Woodlark and eastern Manus basins of the western Pacific. *In*: PARSON, L.M., WALKER, C.L. & DIXON, D.R. (eds) *Hydrothermal Vents and Processes*. Geological Society, London, Special Publications, **87**, 191–205.

SEAMA, N. & FUJIWARA, T. 1993. Geomagnetic anomalies in the Mariana Trough, 18°N. *In*: SEGAWA, J. (ed.) *Preliminary Report of the Hakuho-Maru Cruise KH92-1*. Ocean Research Institute, University of Tokyo, Tokyo, 70–73.

SENO, T., STEIN, S. & GRIPP, A.E. 1993. A model for the motion of the Philippine Sea Plate consistent with NUVEL-1 and geological data. *Journal of Geophysical Research*, **98**, 17 941–17 948.

SHADLUM, T.N., BORTNIKOV, N.S., BOGDANOV, Y.A., TUFAR, W., MURAV'YEV, K.G., GURVICH, Y.G., MURAVITSKAYA, G.N., KORINA, Y.A. & TOPA, T. 1993. Mineralogy, textures, and formation conditions of modern sulfide ores, Manus Basin rift zone. *International Geology Review*, **35**, 127–145.

SHAH, A.K. & BUCK, W.R. 2001. Causes for axial high topography at mid-ocean ridges and the role of crustal thermal structure. *Journal of Geophysical Research*, **106**, 30 865–30 879.

SHOR, G.G., KIRK, H.K. & MENARD, H.W. 1971. Crustal structure of the Melanesian area. *Journal of Geophysical Research*, **76**, 2562–2586.

SINHA, M.C. 1995. Segmentation and rift propagation at the Valu Fa ridge, Lau Basin: Evidence from gravity data. *Journal of Geophysical Research*, **100**, 15 025–15 043.

SINTON, J.B. & HUSSONG, D.M. 1983. Crustal structure of a short length transform fault in the central Mariana Trough. *In*: HAYES, D.E. (ed.) *The Tectonic and Geologic Evolution of the Southeast Asian Seas and Islands: Part 2*. American Geophysical Union, Geophysical Monographs, **27**, 236–254.

SINTON, J.M. 1997. The Manus Spreading Center near 3°22'S and the Worm Garden hydrothermal site: results of Mir2 submersible dive 15. *Marine Geology*, **142**, 207–209.

SINTON, J.M. & FRYER, P. 1987. Mariana Trough lavas from 18°N: Implications for the origin of backarc basin basalts. *Journal of Geophysical Research*, **92**, 12 782–12 802.

SINTON, J.M., FORD, L.L., CHAPPELL, B. & MCCULLOCH, M. 2003. Magma genesis and mantle heterogeneity in the Manus back-arc basin, Papua New Guinea. *Journal of Petrology*, **44**, 159–195.

SLEEP, N.H. & TOKSÖZ, M.N. 1971. Evolution of marginal basins. *Nature*, **233**, 548–550.

SMITH, W.H.F. & SANDWELL, D.T. 1994. Bathymetric prediction from dense satellite altimetry and sparse shipboard bathymetry. *Journal of Geophysical Research*, **99**, 21 803–21 824.

SMITH, W.H.F. & SANDWELL, D.T. 1997. Global sea floor topography from satellite altimetry and ship depth soundings. *Science*, **277**, 1956–1962.

SMOOT, N.C. 1990. Mariana trough by multi-beam sonar. *Geo-Marine Letters*, **10**, 137–144.

STERN, R.J. & SMOOT, N.C. 1998. A bathymetric overview of the Mariana forearc. *The Island Arc*, **7**, 525–540.

STERN, R.J., BLOOMER, S.H., MARTINEZ, F., YAMAZAKI, T. & HARRISON, T.M. 1996. The composition of back-arc lower crust and upper mantle in the Mariana Trough: A first report. *The Island Arc*, **5**, 354–372.

STERN, R.J., LIN, P.-N., MORRIS, J.D., JACKSON, M.C., FRYER, P., BLOOMER, S.H. & ITO, E. 1990. Enriched back-arc basin basalts from the northern Mariana Trough: implications for the magmatic evolution of back-arc basins. *Earth and Planetary Science Letters*, **100**, 210–225.

STERN, R.J., SMOOT, N.C. & RUBIN, M. 1984. Unzipping of the Volcano Arc, Japan. *Tectonophysics*, **102**, 153–174.

STOLPER, E. & NEWMAN, S. 1994. The role of water in the petrogenesis of Mariana trough magmas. *Earth and Planetary Science Letters*, **121**, 293–325.

STUBEN, D., NEUMANN, T., TAIBI, N.E. & GLASBY, G.P. 1998. Segmentation of the southern Mariana back-arc spreading center. *The Island Arc*, **7**, 513–524.

SU, W. & BUCK, W.R. 1993. Buoyancy effects on mantle flow under mid-ocean ridges. *Journal of Geophysical Research*, **98**, 12 191–12 207.

SUNKEL, G. 1990. Origin of petrological and geochemical variations of Lau Basin lavas (SW Pacific). *Marine Mining*, **9**, 205–234.

TAMAKI, K. 1985. Two modes of back-arc spreading. *Geology*, **13**, 475–478.

TAMURA, Y., TATSUMI, Y., ZHAO, D., KIDO, Y. & SHUKUNO, H. 2002. Hot fingers in the mantle wedge: new insights into magma genesis in subduction zones. *Earth and Planetary Science Letters*, **197**, 105–116.

TAPPIN, D.R., BRUNS, T.R. & GEIST, E.L. 1994. Rifting of the Tonga/Lau Ridge and formation of the Lau backarc basin: evidence from Site 840 on the Tonga Ridge. *Proceedings of the Ocean Drilling Program, Scientific Results*, **135**, 367–371.

TAYLOR, B. 1979. Bismarck Sea: Evolution of a back-arc basin. *Geology*, **7**, 171–174.

TAYLOR, B. 1992. Rifting and the volcanic–tectonic evolution of the Izu–Bonin–Mariana arc. *In*: TAYLOR, B., FUJIOKA, K. *et al. Proceedings of the Ocean Drilling Program, Scientific Results*, **126**, 627–651.

TAYLOR, B. & KARNER, G.D. 1983. On the evolution of marginal basins. *Reviews of Geophysics and Space Physics*, **21**, 1727–1741.

TAYLOR, B. & MARTINEZ, F. 2003. Back-arc basin basalt systematics. *Earth and Planetary Science Letters*, **210**, 481–497.

TAYLOR, B., CROOK, K.A.W. & SINTON, J.M. 1994. Extensional transform zones and oblique spreading centers. *Journal of Geophysical Research*, **99**, 19 707–19 718.

TAYLOR, B., CROOK, K.A.W., SINTON, J.M. & PETERSON, L. 1991*a*. Manus Basin, Papua New Guinea, Sea MARC II sidescan sonar imagery, 1:250 000. *In*: *Pacific Seafloor Atlas*. Hawaii Institute of Geophysics, Honolulu, sheets 1–3.

TAYLOR, B., CROOK, K.A.W., SINTON, J.M., PETERSEN, L., MALLONEE, R., KELLOGG, J.N. & MARTINEZ, F. 1991*b*. Manus Basin, Papua New Guinea: SeaMARC II sidescan sonar imagery, bathymetry, magnetic anomalies, and free-air gravity anomalies, 1:1 000 000. *In*: *Pacific Seafloor Atlas*. Hawaii Institute of Geophysics, Honolulu, Sheet 7.

TAYLOR, B., ZELLMER, K., MARTINEZ, F. & GOODLIFFE, A. 1996. Sea-floor spreading in the Lau back-arc basin. *Earth and Planetary Science Letters*, **144**, 35–40.

TREGONING, P. 2002. Plate kinematics in the western Pacific derived from geodetic observations. *Journal of Geophysical Research*, **107**(B1), ECV 7, 1–8, 2020, 10.1029/2001JB000406.

TUFAR, W. 1990. Modern hydrothermal activity, formation of complex massive sulfide deposits and associated vent communities in the Manus back-arc basin (Bismarck Sea, Papua New Guinea). *Mitteilungen der Osterreichischen Geologischen Gesellschaft*, **82**, 183–210.

TURNER, I.M., PEIRCE, C. & SINHA, M.C. 1999. Seismic imaging of the axial region of the Valu Fa Ridge, Lau Basin: the accretionary processes of an intermediate back-arc spreading ridge. *Geophysical Journal International*, **138**, 495–519.

ULMER, P. 2001. Partial melting in the mantle wedge: the role of H_2O in the genesis of mantle-derived 'arc related' magmas. *Physics of the Earth and Planetary Interiors*, **127**, 215–232.

VALLIER, T.L., JENNER, G.A., FREY, F.A., GILL, J.B., DAVIS, A.S., VOLPE, A.M., HAWKINS, J.W., MORRIS, J.D., CARWOOD, P.A., MORTON, J.L., SCHOLL, D.W., RAUTENSCHLEIN, M., WHITE, W.M., WILLIAMS, R.W., STEVENSON, A.J. & WHITE, L.D. 1991. Subalkaline andesite from Valu Fa Ridge, a back-arc spreading center in southern Lau Basin: petrogenesis, comparative chemistry, and tectonic implications. *Chemical Geology*, **91**, 227–256.

VOLPE, A.M., MACDOUGALL, J.D. & HAWKINS, J.W. 1987. Mariana Trough basalts (MTB): trace element and Sr–Nd isotopic evidence for mixing between MORB-like and arc-like melts. *Earth and Planetary Science Letters*, **82**, 241–254.

VOLPE, A.M., MACDOUGALL, J.D. & HAWKINS, J.W. 1988. Lau Basin basalts (LBB): trace element and Sr–Nd isotopic evidence for heterogeneity in backarc basin mantle. *Earth and Planetary Science Letters*, **90**, 174–186.

VOLPE, A.M., MACDOUGALL, J.D., LUGMAIR, G.W., HAWKINS, J.W. & LONSDALE, P. 1990. Fine-scale isotopic variation in Mariana Trough basalts: evidence for heterogeneity and a recycled component in backarc basin mantle. *Earth and Planetary Science Letters*, **100**, 251–264.

VON STACKELBERG, U. 1988. Active hydrothermalism in the Lau back-arc basin (SW-Pacific): First results from the SONNE 48 Cruise (1987). *Marine Mining*, **7**, 431–442.

VON STACKELBERG, U. 1990. R.V. *Sonne* Cruise SO48: summary of results testing a model of mineralization. *Marine Mining*, **9**, 135–144.

VON STACKELBERG, U. & VON RAD, U. 1990. Geological evolution and hydrothermal activity in the Lau and North Fiji basins. *Geologisches Jahrbuch*, **92**, 629–660.

WEISSEL, J.K. 1977. Evolution of the Lau Basin by the growth of small plates. *In*: TALWANI, M. & PITMAN, W.C. (eds) *Island Arcs, Deep Sea Trenches and Back-arc Basins*. Maurice Ewing Series, American Geophysical Union, **1**, 429–436.

WEISSEL, J.K. 1981. Magnetic lineations in marginal basins of the west Pacific. *Philosophical Transactions of the Royal Society of London, Series A*, **300**, 223–247.

WESSEL, J.K., FRYER, P., WESSEL, P. & TAYLOR, B. 1994. Extension in the northern Mariana inner forearc. *Journal of Geophysical Research*, **99**, 15 181–15 203.

WHELAN, P.M., GILL, J.B., KOLLMAN, E., DUNCAN, R.A. & DRAKE, R.E. 1985. Radiometric dating of magmatic stages in Fiji. *In*: SCHOLL, D.W. & VALLIER, T.L. (eds) *Geology and Offshore Resources of Pacific Island Arcs – Tonga Region*. Circum Pacific Council for Energy and Mineral Resources, Houston, TX, Earth Science Series, **2**, 415–440.

WIEDICKE, M. & COLLIER, J. 1993. Morphology of the Valu Fa Spreading Ridge in the Southern Lau Basin. *Journal of Geophysical Research*, **98**, 11 769–11 782.

WIEDICKE, M. & HABLER, W. 1993. Morphotectonic characteristics of a propagating spreading system in the northern Lau Basin. *Journal of Geophysical Research*, **98**, 11 783–11 797.

WINDER, R.O. & PEACOCK, S.M. 2001. Viscous forces acting on subducting lithosphere. *Journal of Geophysical Research*, **106**, 21 937–21 951.

WOOD, D.A., MARSH, N.G., TARNEY, J., JORON, J.L., FRYER, P. & TREUIL, M. 1981. Geochemistry of igneous rocks recovered from a transect across the Mariana Trough, arc and trench, Sites 453–461. *In*: HUSSONG, D.M. & UYEDA, S. *et al.* *Initial Reports of the Deep Sea Drilling Project*, **60**, 611–646.

WOODHEAD, J., EGGINS, S. & GAMBLE, J. 1993. High field strength and transition element systematics in island arc and backarc basin basalts: Evidence for multiphase melt extraction and a depleted mantle wedge. *Earth and Planetary Science Letters*, **114**, 491–504.

WOODHEAD, J.D., EGGINS, S.M. & JOHNSON, R.W. 1998. Magma genesis in the New Britain island arc: further insights into melting and mass transfer processes. *Journal of Petrology*, **39**, 1641–1668.

WRIGHT, D.J., BLOOMER, S.H., MACLEOD, C.J., TAYLOR, B. & GOODLIFFE, A.M. 2000. Bathymetry of the Tonga trench and forearc: a map series. *Marine Geophysical Researches*, **21**, 489–511.

WRIGHT, I.C., PARSON, L.M. & GAMBLE, J.A. 1996. Evolution and interaction of migrating cross arc volcanism and back-arc rifting: An example from the southern Havre Trough (35°20′–37°S). *Journal of Geophysical Research*, **101**, 22 071–22 086.

YAMATANI, Y., MASUDA, H., AMAKAWA, H., NOZAKI, Y. & GAMO, T. 1994. Rare earth element chemistry of submarine volcanic rocks from a spreading axis, the Southern Mariana Trough. *JAMSTEC Journal of Deep Sea Research*, **10**, 187–193.

YAMAZAKI, T., MURAKAMI, F. & SAITO, E. 1993. Mode of seafloor spreading in the northern Mariana Trough. *Tectonophysics*, **221**, 207–222.

ZELLMER, K.E. & TAYLOR, B. 2001. A three-plate kinematic model for Lau Basin opening. *Geochemistry, Geophysics, Geosystems*, **2**, 2000GC000106.

The subduction factory: its role in the evolution of the Earth's crust and mantle

YOSHIYUKI TATSUMI & TETSU KOGISO

Institute for Frontier Research on Earth Evolution (IFREE), Japan Marine Science and Technology Center (JAMSTEC), Yokosuka 237–0061, Japan

(e-mail: tatsumi@jamstec. go.jp)

Abstract: Subduction zones are major sites of magmatism on the Earth. Dehydration processes and associated element transport, which take place in both the subducting lithosphere and the down-dragged hydrated peridotite layer at the base of the mantle wedge, are largely responsible for the following characteristics common to most subduction zones: (1) the presence of dual volcanic chains within a single volcanic arc; (2) the negative correlation between the volcanic arc width and the subduction angle; (3) selective enrichment of particular incompatible trace elements; and (4) systematic across-arc variations in incompatible trace element concentrations. The occurrence of two types of andesites, calc-alkalic and tholeiitic, typifies magmatism in subduction zones. Examination of geochemical characteristics of those andesites in the NE Japan arc and bulk continental crust reveals marked compositional similarity between calc-alkalic andesites and continental crust. One of the principal mechanisms of generation of calc-alkalic andesites, at least those on the NE Japan arc, is the mixing of two magmas, having basaltic and felsic compositions and being derived from partial melting of the mantle and the overriding basaltic crust, respectively. It may be thus suggested that this process would also have contributed greatly to continental crust formation. If this is the case, then the melting residue after extraction of felsic melts should be removed and delaminated from the initial crust into the mantle in order to form 'andesitic' crust compositions. These processes cause accumulation in the deep mantle of residual materials, such as delaminated crust materials and dehydrated, compositionally modified subducted oceanic crusts and sediments. Geochemical modelling suggests that such residual components have evolved to form enriched mantle reservoirs.

Subduction zones, where the oceanic lithosphere is foundering into the Earth's interior, have been working as factories and have contributed significantly to the evolution of the solid Earth. Raw materials, such as pelagic/terrigenous sediments, oceanic crust and mantle lithosphere, are supplied to the factory (Fig. 1). In the process of transportation and processing of these raw materials, the factory causes vibrations as earthquakes. The major products of the factory are arc magmas, their solidified products and, ultimately, continental crust. Subduction zones are creating >20% of the current, terrestrial magmatic products and have formed 7.35×10^9 km^3 of andesitic crust throughout Earth's history (Taylor & McLennan 1995). Although the continental crust occupies less than 1% of the total mass of the solid Earth, the origin of such a 'differentiated' component should provide a clue to understanding the evolution of the Earth. Furthermore, formation of andesitic crust is probably one of the greatest dilemmas facing those who are interested in the origin of continental crust, because basaltic magmas dominate the magmatism on the modern Earth.

The waste materials processed in the subduction factory, such as chemically modified slab materials and probably delaminated lower continental crust, sink into the mantle (Fig. 1). Basaltic oceanic crust, with an average thickness of 7 km, has constantly been accumulating somewhere in the deep mantle. Assuming that such basaltic materials could be stored at the base of the mantle for the last 3 billion (10^9) years, the volume of such a layer, with a composition different from both the overlying peridotitic mantle and the underlying metallic core, would be *c.* 4.2×10^9 km^3, occupying *c.* 4% of the total mass of the solid Earth. Such voluminous basaltic materials may thus be regarded as the 'anti-crust' at the base of the mantle. Water should have been transported from the surface to the interior of the Earth with the sinking oceanic lithosphere. Although H_2O bound in altered oceanic crusts and subducting sediments is largely recycled to the surface, through fluid migration in accretionary prisms and arc

From: LARTER, R.D. & LEAT, P.T. 2003. *Intra-Oceanic Subduction Systems: Tectonic and Magmatic Processes.* Geological Society, London, Special Publications, **219**, 55–80. 0305-8719/03/$15.00

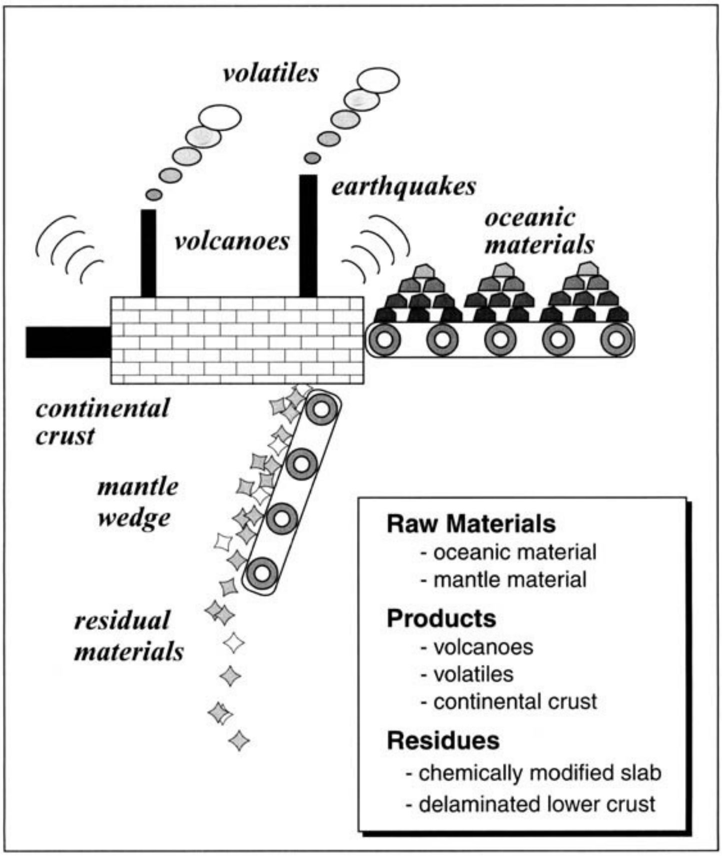

Fig. 1. Processes occurring in the subduction factory. Raw materials, such as oceanic sediments, oceanic crust and mantle lithosphere, are fed into the factory and are manufactured into arc magmas and continental crust. The waste materials processed in this factory, such as chemically modified oceanic crust/sediments and delaminated lower continental crust, sink into the deep mantle and are likely to have greatly contributed to mantle evolution.

magmatism, the sinking oceanic crust could carry *c.* 1 wt% of H_2O to depths of >200 km (e.g. Poli & Schmidt 1995). This indicates that *c.* 3×10^{20} kg of H_2O, about a quarter of the present hydrosphere, has been injected into the mantle. The presence of such H_2O should have profound effects on the rheological property of the mantle and would govern the dynamic processes in the Earth's interior.

This paper will provide an overview of the general characteristics of subduction-zone magmatism and discuss the role of subduction factories in the formation of some geochemical reservoirs in the solid Earth, such as continental crust and enriched mantle end-member components, based on examination of the process of continental crust formation and chemical differentiation through dehydration of the subducting oceanic lithosphere.

Arc magmatism: general characteristics and possible origins

The interaction of physical and chemical processes in subduction zones is complex. In essence, there is no generalized model for arc magma generation that can account for magmatism in all subduction zones on the Earth. Faced with this, one of the practical approaches may be to identify general characteristics in arc magmatism common to most subduction zones and to provide possible explanations for such characteristics. Subsequently, we can try to understand the origin of unusual phenomena. Although several such general characteristics have been documented (e.g. Tatsumi & Eggins 1995), our interest in this paper will focus on volcano distribution and incompatible element compositions of arc lavas. Such an approach is valid as these

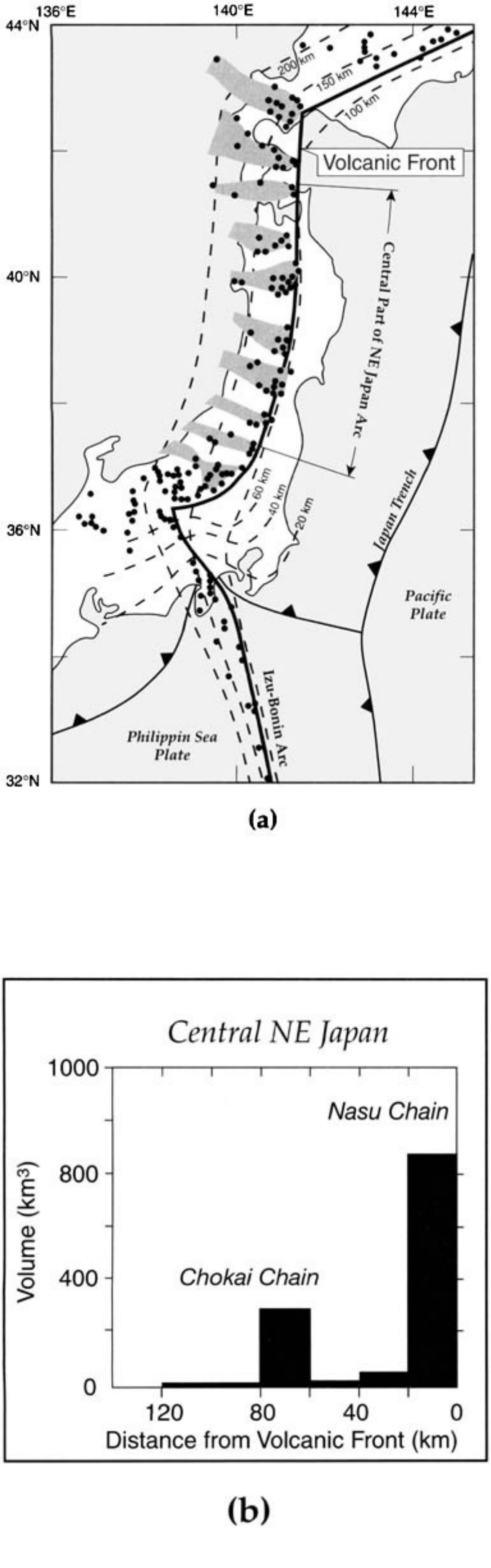

characteristics may be closely related to the origin of andesites and continental crust, which are the major products of the subduction factory.

Volcano distribution

One of the striking features in volcano distribution at convergent plate margins is the presence of an abrupt trenchward limit of volcanoes (Fig. 2), defined as the volcanic front (Sugimura 1960). The presence of such a volcanic front intuitively suggests that partial melting in the mantle wedge or in the subducting oceanic lithosphere occurs solely beneath the volcanic arc. Although the number of volcanoes and the amount of material discharged from volcanoes are greatest along the volcanic front (Sugimura 1960), they do not tend to decrease uniformly away from it. In subduction zones with relatively wide arcs, a second volcano concentration is located in the back-arc side of the volcanic arc (Fig. 2). The occurrence of such dual volcanic chains, within a single volcanic arc, was first emphasized by Marsh (1979) and discussed for current subduction zones by Tatsumi & Eggins (1995). Furthermore, Tamura *et al.* (2002) have demonstrated the along-arc distribution of two topographic highs, which correspond to the dual volcanic chains in the NE Japan arc.

As always, there are some exceptions to the rule. For example, arcs such as the Mariana and Tonga arcs are composed of a single volcanic chain, while others such as the Kamchatka and Sunda arcs contain three chains (Tatsumi & Eggins 1995). Interestingly, however, volcanic arcs comprising a single volcanic chain tend to form above high-angle subduction zones. This is clearly demonstrated in the Izu–Bonin–Mariana arc, where the width of the volcanic arc decreases southwards as the subduction angle varies from *c.* 30°, beneath the northern tip of

Fig. 2.(**a**) Distribution of Quaternary volcanoes in the NE Japan arc. The volcanic front, which is defined as the boundary between forearcs and volcanic arcs (solid lines), is located *c.* 100 km above the surface of the subducting Pacific Plate in the central part of this arc are illustrated by broken lines, with numbers representing depth to slab. The bimodal distribution of volcanic materials in the across-arc direction provides evidence for the formation of dual volcanic chain. Quaternary volcanoes on this arc can be grouped into 10 volcanic clusters striking transverse to the arc (hatched regions), which may suggest the location of hot fingers in the mantle wedge beneath such clusters. (**b**) Volume of volcanic rocks in the NE Japan arc plotted against distance from the volcanic front.

this arc, to nearly vertical in the southern part. This phenomenon is widely observed in modern arc–trench systems, with a concurrent decrease in the width of the forearc (Tatsumi & Eggins 1995). The negative correlation between the volcanic arc width and the subduction angle provides compelling evidence to suggest that pressure variations control magma production in subduction zones, which is further demonstrated by the relationship between a constant plate depth and the position of a volcanic arc (Gill 1981; Tatsumi & Eggins 1995). The majority of volcanic fronts occur 108 ± 18 km (1σ) above the slab surface and the volcanic–back-arc boundaries form 173 ± 12 km above the top of the subducting plate (Tatsumi & Eggins 1995). These values are obtained by the compilation of seismic data beneath the central part of volcanic arcs. It should thus be stressed that the observation is not necessarily applicable for the margins of volcanic arcs (Fig. 2). Although there certainly exist arc–trench systems that do not follow the above general characteristics, they appear to be special cases. One of the possible mechanisms responsible for these characteristic volcano distributions at convergent margins would be the pressure-dependent breakdown of chlorite and phlogopite in the down-dragged hydrous layer at the base of the mantle wedge, and not in the subducting oceanic crust, beneath the trench- and back-arc-side volcanic chains, respectively (Tatsumi 1989, 2003; Tatsumi & Eggins 1995).

Arc volcanoes or subduction-zone-related volcanoes are generally considered as being regularly spaced (Marsh & Carmichael 1974; Vogt 1974; Marsh 1979; Shimozuru & Kubo 1983). Shimozuru & Kubo (1983) provided an average volcano spacing value of 58 ± 24 km for current subduction zones. However, de Bremond d'Ars *et al.* (1995) concluded that volcanoes are randomly distributed at convergent plate margins, based on examination of volcano distribution in 16 arcs, consisting of 479 volcanic systems. Tamura *et al.* (2002) documented that Quaternary volcanoes in the NE Japan arc can be grouped into 10 volcanic clusters striking transverse to the arc; these possess an average width of 50 km and are separated by gaps 30–75 km wide (Fig. 2). This clustering of volcanoes is closely correlated with low-velocity regions within the mantle wedge and local negative Bouguer gravity anomalies, This led Tamura *et al.* (2002) to speculate that hot regions, in the form of inclined 50 km-wide fingers, are locally developed within the mantle wedge beneath the arc (Fig. 2). Although irregular spacing of volcanoes may be the case at subduction zones, the presence of such clustering of volcanic centres must be re-examined.

Incompatible element chemistry

Lavas emplaced in subduction zones are noted for their distinct chemistry compared with those in other tectonic settings. In particular, they are distinct in over-abundance of the large ion lithophile elements (e.g. Cs, Rb, K, Ba, Pb, Sr) and depletion in the high-field-strength elements (e.g. Ta, Nb, Zr, Ti) (Fig. 3). Such characteristic compositions of arc magmas are broadly consistent with selective transport of elements by aqueous fluids from both subducting sediments and oceanic crust.

In order to understand the origin of the above incompatible trace element characteristics in arc lavas more quantitatively, several experiments have been conducted on the distribution of elements between aqueous fluids and solid minerals (Ryabchikov & Boettcher 1980; Tatsumi *et al.* 1986; Tatsumi & Nakamura 1986; Tatsumi & Isoyama 1988; Brenan *et al.* 1994, 1995*a*, *b*; Keppler 1996; Adams *et al.* 1997; Ayers *et al.* 1997; Kogiso *et al.* 1997; Stalder *et al.* 1998; Aizawa *et al.* 1999; Johnson & Plank 1999). Here we shall examine whether such element transport can explain the geochemical characteristics of arc magmas based on simple modelling of dehydration, partial melting and fluid–solid reactions.

The steps taken and assumptions made in the present modelling are shown in Table 1 and numerated as follows:

1 Hydrothermally altered mid-ocean ridge basalt (MORB) and sediments in the subducting lithosphere are widely accepted as the primary source of subduction zone fluid phases. We have used amphibolite and sediment compositions reported by Plank & Langmuir (1993) and Kogiso *et al.* (1997) as representative of subducting oceanic materials (Table 1). Such compositions are well within the range of altered MORB and oceanic sediments.
2 The trace element compositions of slab-derived fluids are calculated by using the element mobility data of Kogiso *et al.* (1997) for amphibolite (altered oceanic crust) and Aizawa *et al.* (1999) for sediments (Table 1). The reasons for this are twofold. First, the starting materials used in their experiments are natural amphibolite and sediment with compositions similar to the oceanic crust and subducting sediments, respectively. Secondly, element transport during open-system

Table 1. *Geochemical modelling for arc magma compositions*

	K	Rb	Sr	Pb	Ba	Yb	Y	Sm	Nd	La	Zr	U	Th	Nb
Amphibolite	11 050	24	495	3.6	388	3.1	28	5	11	5.1	74	1.7	5	2.3
Mobility	0.55	0.63	0.41	0.85	0.53	0.05	0	0.14	0.3	0.56	0	0.29	0.38	0
Sediments	30 000	57	327	19.9	776	2.76	29.8	5.78	27	28.8	130	1.68	6.91	8.94
Mobility	0.15	0.02	0.12	0.65	0.08	0.03	0	0.03	0.03	0.03	0	0.03	0.03	0
Fluid composition	384 133	822	11 347	336	11 795	9.4	0	40	187	164	0	27	104	0
N-MORB	600	0.56	90	0.3	6.3	3.05	28	2.63	7.3	2.5	74	0.047	0.12	2.33
Partition coefficient														
olivine	0.00001	0.000001	0.0001	0.00008	0.00001	0.009	0.008	0.003	0.002	0.001	0.0005	0.0005	0.0004	0.0001
opx	0.0001	0.00001	0.001	0.0008	0.0001	0.1	0.06	0.02	0.009	0.005	0.01	0.001	0.0008	0.003
cpx	0.007	0.0001	0.1	0.05	0.001	0.4	0.45	0.29	0.19	0.05	0.53	0.1	0.08	0.1
MORB mantle	90	0.084	14	0.045	0.95	0.60	5.5	0.43	1.1	0.38	14	0.0071	0.018	0.35
IAB Source	858	1.7	36	0.72	25	0.62	5.5	0.51	1.5	0.70	14	0.061	0.23	0.35
IAB Magma	5721	12	241	4.8	164	3.1	28	3.1	9.7	4.7	74	0.41	1.5	2.3

Abbreviations: opx, orthpyroxene; cpx, clinopyroxene; IAB, island arc basalt.
Mobility of an element is defined as the fraction of an element removed by fluids during dehydration.
Element concentrations are in ppm.

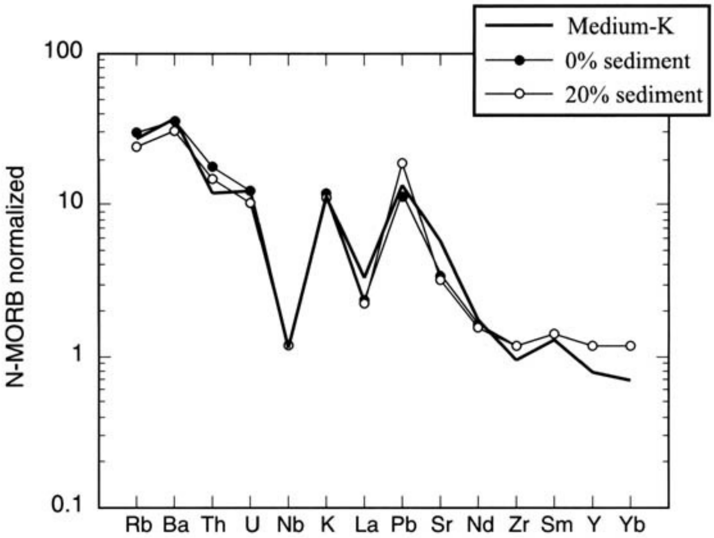

Fig. 3. N-MORB normalized incompatible element characteristics of an average medium-K oceanic arc basalt and inferred basalt magma with different sediment contributions. The diagnostic geochemical characteristics of arc basalt magmas can be well reproduced by dehydration of subducting oceanic crust/sediments, associated selective overprint of elements onto the mantle wedge, and partial melting of such metasomatized mantle materials. Normalizing factors are from Sun & McDonough (1989).

dehydration operating in the sinking slab may be better reproduced in such dehydration experiments than in equilibrium partitioning experiments. A value of 1.5 wt% H_2O both in amphibolite and sediment is assumed. It has been well documented that the subducting sediments play a significant role in controlling the geochemical signature of arc magmas (e.g. Kay *et al.* 1978; Tera *et al.* 1986; Plank & Langmuir 1993). The degree of contribution of sediment to produce slab-derived fluids is thus varied in the present calculation.

3 The process of adding slab-derived fluids to the subarc mantle wedge is probably complicated. Such fluids may interact with the mantle wedge to form hydrous peridotites that are subsequently dragged downward on the slab releasing secondary fluids immediately beneath the volcanic arc (Tatsumi 1989; Tatsumi & Eggins 1995). Such multistep processes were geochemically examined by Tatsumi & Kogiso (1997). However, this approach is too complex and relies on unconstrained parameters such as the Na content in slab-derived fluids and the amount of phlogopite and amphibole, both crystallizing in the down-dragged hydrous peridotites at the base of the mantle wedge. In the present assessment, therefore, the net effect of fluid fluxing is deduced by using a single-step metasomatic process in which slab-derived fluids interact directly with the original mantle wedge.

4 The pre-flux, original subarc mantle is assumed to possess compositions identical to those of the normal MORB (N-MORB) source mantle, which can be calculated based on N-MORB compositions (Sun & McDonough 1989) by assuming 15% fractional melting of a peridotite composed of 50% olivine, 30% orthopyroxene and 20% clinopyroxene (Table 1). The crystal–liquid partition coefficients used in the present calculation are listed in Table 1 (after Tatsumi 2000*a*).

5 Assuming that the fraction of slab-derived fluids in the arc magma source is 0.2 wt%, the trace element concentrations in a primary arc basalt magma can be calculated (Table 1). This amount of fluid is largely equivalent to 1.5 wt% H_2O in the primary magma produced by 15% fractional partial melting, an acceptable value for H_2O content in arc magmas (Sakuyama 1979; Sisson & Layne 1993).

The trace element composition of an inferred arc basalt magma, with different contributions of subducting sediments, is plotted on a multi-element diagram (Fig. 3), together with those of an average oceanic arc medium-K basalt (Tatsumi & Eggins 1995). It is clearly demonstrated in Fig. 3 that the distinctive incompatible element characteristics of subduction zone basalt magmas are well reproduced by the present modelling, including element fluxing from subducting oceanic crust and sediments by fluid overprint into the mantle wedge and subsequent partial melting of such metasomatized subarc mantle.

Across-arc variation in incompatible element concentrations

It has been repeatedly documented that concentrations of incompatible trace elements tend to increase with distance from the volcanic front, termed the K–*h* (potash–depth) relationship (Dickinson 1975). Although at least two exceptions, the Vanuatu and the Miocene NE Japan arcs, exist, a compilation by Tatsumi & Eggins (1995) confirms that this geochemical feature is common to most arc–trench systems. Across-arc variation in incompatible trace element abundances has also been associated with the across-arc change in major element magma compositions (e.g. Kuno 1966; Jakes & White 1969; Jakes & Gill 1970; Gill 1981). For example, basalts in the NE Japan arc, which have undergone similar degrees of differentiation and have FeO*/MgO ratios of *c.* 1.5, show a higher normative quartz component in the trench-side volcanic chain than in the back-arc-side chain (Tatsumi & Eggins 1995).

A diversity of mechanisms has been proposed to cause these across-arc incompatible element concentration and normative composition variations, such as the difference in crustal thickness (e.g. Condie & Potts 1969; Miyashiro 1974; Meen 1987), source compositions (e.g. Jakes & White 1970) and degrees of partial melting (e.g. Gill 1981; Sakuyama & Nesbitt 1986). However, the mechanism most consistent with results of melting experiments on Mg-rich basalt compositions (Tatsumi *et al.* 1983) is variation in the degree of partial melting of a uniform source material across the arc with decreasing partial melting towards the back-arc. Deep-seated separation of magmas from the mantle is likely to be caused by the presence of a thicker lithosphere beneath the back-arc side of the volcanic arc (Tatsumi *et al.* 1983). This is clearly demonstrated by both seismic tomography data (e.g. Zhao *et al.* 1997) and numerical simulation of the mantle wedge (e.g. Furukawa 1993).

Andesite problem

Over 80% of arc volcanoes contain andesitic lavas and clastics (Gill 1981). However, melts generated in the mantle at subduction zones, as in other tectonic settings, are mostly basaltic. Andesite genesis has thus been one of the central topics in magma genesis at subduction zones. Furthermore, continental crust, which is a geochemical reservoir characterized by concentration of light elements, is andesitic in composition (Taylor & McLennan 1985; Rudnick & Fountain 1995). The origin of such 'differentiated' andesitic crust thus provides a clue to understanding of the evolution of the solid Earth.

Andesites can be defined megascopically as grey-coloured, porphyritic volcanic rocks containing plagioclase, but not quartz, alkali feldspar or felspathoid as phenocryst phases. Chemically, andesites are hypersthene-normative, with SiO_2 content from 53 to 63 wt% (e.g. Gill 1981). Although, in a broad sense, the definition of andesite is rather simple, considerable confusion exists with regard to the meaning of nomenclature such as calc-alkalic v. tholeiitic, hypersthenic v. pigeonitic series, high-Mg andesites and adakites. The reasons for these numerous classification schemes are the compositional diversity of arc magmas and the contribution of plural mechanisms to their generation. The use of such classification schemes has often been plagued by inconsistencies, leading those interested in andesite genesis to further confusion and misunderstanding. Calc-alkalic andesites, unfortunately, provide an excellent example of this problem.

Here we present a brief review of calc-alkalic andesite magma genesis. The compositional similarity between calc-alkalic andesites and bulk continental crust, as discussed later, provides evidence to suggest an intimate genetic linkage between the two. The present discussion will focus mainly on andesites within the NE Japan arc, because: (1) this is undoubtedly one of the most thoroughly studied volcanic arcs on Earth; (2) its general magmatic characteristics are common to most other volcanic arcs; and (3) two types of andesite magmas, tholeiitic and calc-alkalic, are present within a single volcano, providing a rare opportunity for examining the origin of such magma types.

Calc-alkalic andesite definition revisited

Calc-alkalic andesites typify magmatism at convergent plate boundaries, where various types of volcanic rocks with intermediate compositions also occur. In order to reveal the geochemical characteristics of calc-alkalic andesites and discuss their origin, the definition of such rock types needs to be summarized.

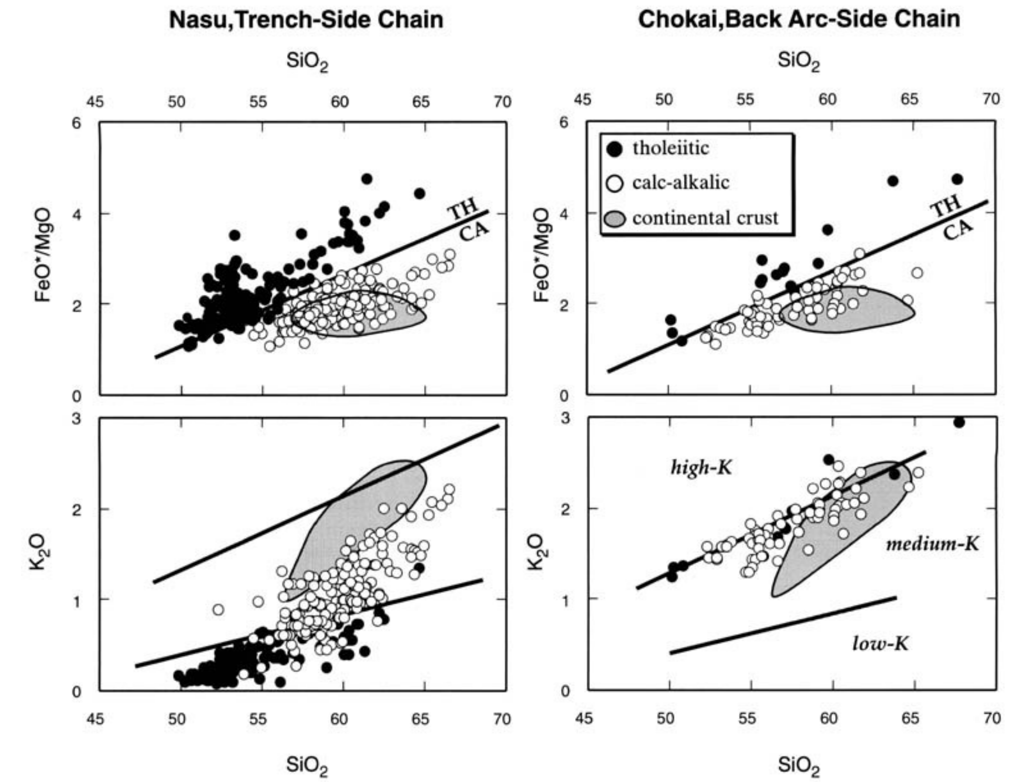

Fig. 4. FeO*/MgO and K_2O v. SiO_2 relations for Quaternary volcanic rocks in the Nasu trench- and Chokai back-arc-side volcanic chains on the NE Japan arc. The across-arc variation in K_2O content is observed both for calc-alkalic (CA) and tholeiitic (TH) rocks. Compositions of continental crust are from Taylor & McLennan (1985), Christensen & Mooney (1995) and Rudnick & Fountain (1995).

The division of igneous rocks into alkalic and non-alkalic series serves as a fundamental distinction of magma suites that consist of consanguineous magmas. The significant characteristics of the alkalic series are their peralkalic or silica-undersaturated compositions or both. Therefore, alkalic and non-alkalic magma series are defined on the basis of normative (Yoder & Tilley 1962) or groundmass (Tilley 1950; Kuno 1959) mineralogy. As alkalic rocks generally exhibit higher concentrations of total alkalies (Na_2O+K_2O) at a given SiO_2 content than non-alkalic rocks, these two magma series are commonly distinguished from each other by a total alkalis v. SiO_2 diagram (e.g. MacDonald & Katsura 1964). The combination of K_2O and SiO_2 has also been adopted as a practical and simple criterion for the two series and subdivision of the non-alkalic series (e.g. Gill 1981). In this diagram, non-alkalic series generally consist of low-, medium- and, in part, high-K magmas.

Two distinctive differentiation trends, tholeiitic and calc-alkalic, are recognized in the non-alkalic igneous rock series, representing the presence or absence of iron-enrichment during magmatic differentiation, respectively (Wager & Deer 1939; Nockolds & Allen 1953), as can be illustrated in an 'AFM' diagram. In order to further quantitatively distinguish the two magma series, FeO*/MgO v. SiO_2 variation plots (FeO*, total iron as FeO) (Miyashiro 1974) are commonly used (Fig. 4). In this diagram, calc-alkalic and tholeiitic series display steeper and gentler slopes, respectively, than the straight line:

$$SiO_2\ (\mathrm{wt\%}) = 6.4 \times \mathrm{FeO^*/MgO} + 42.8.$$

It should be stressed here that the calc-alkalic v. tholeiitic definition is based exclusively on the difference in degree of iron-enrichment or in the rate of change of FeO*/MgO ratios with increasing degrees of magmatic differentiation, and not on other parameters such as K_2O contents.

Although the term calc-alkalic series should be used for lavas displaying little iron-enrichment during magmatic differentiation, frequent

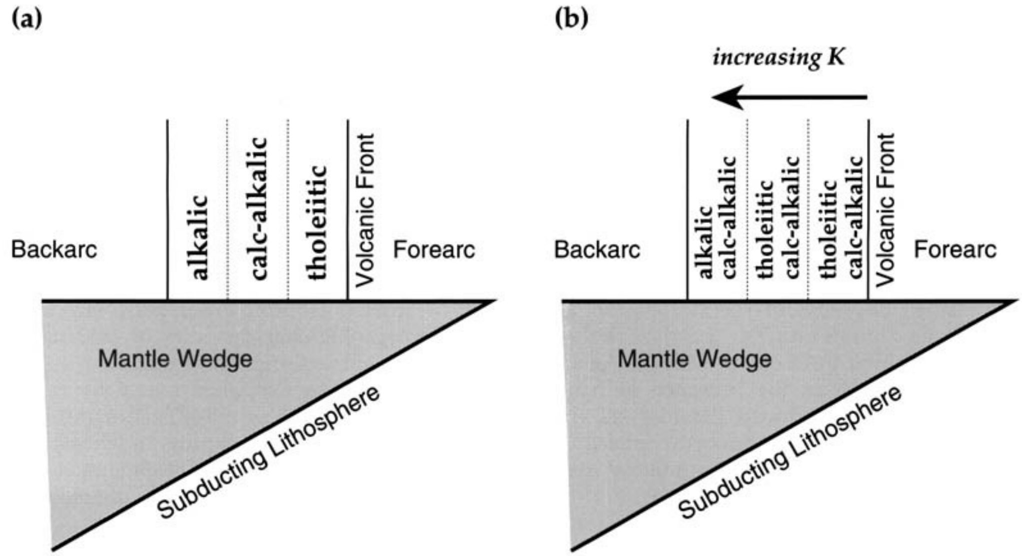

Fig. 5. Schematic diagrams showing spatial variations in the magma types of subduction zone magmas. (**a**) is an inadequate, but often cited, idea for the spatial variation in magma compositions, and (**b**) may demonstrate spatial variation more reasonably.

inconsistent application of this term has distorted the real nature of this magma series. One such example is the usage of calc-alkalic magmas as a general term for all subduction-zone magmas (e.g. Basaltic Volcanism Study Project 1981), even though tholeiitic rocks *do* exist in subduction zones. Another, and more common, problem is the interchangeable use of the terms medium-K and calc-alkalic series (e.g. Hess 1989; Wilson 1989). Such misusage may be due to poor understanding of the following two observations. First, when comparing these rocks from a single volcano or within an along-arc volcanic chain calc-alkalic andesites tend to be more enriched in K_2O than tholeiitic andesites (Fig. 4). Secondly, concentrations of incompatible elements such as potassium in andesites tend to increase with distance from the volcanic front or the distance between the slab surface and a volcano (Fig. 4), namely the K–*h* relationship (Dickinson 1975).

The schematic illustration showing the spatial, across-arc variation in the compositions of arc magmas (Fig. 5a) is regularly cited (e.g. Wilson 1989). However, this diagram is misleading as it denotes the absence of calc-alkalic and tholeiitic andesites in the frontal and rear sides of a volcanic arc, respectively. As previously mentioned, calc-alkalic rocks should be defined by the absence of iron-enrichment not by concentration of K_2O. Both calc-alkalic and tholeiitic rocks defined as low-K and medium-K series occur within the NE Japan arc (Fig. 4). Therefore, the spatial distribution of magma types in a volcanic arc should be summarized as shown in Figure 5b.

Kuno (1960) demonstrated that basalts occurring in the NE Japan and Izu–Bonin arcs are classified into three types: tholeiites with low Al_2O_3 and total alkalis; high-alumina basalts with higher Al_2O_3 and intermediate alkalis; and alkali basalts with variable Al_2O_3 and higher alkalis. Kuno (1960) further suggested that high-alumina basalts form a zone extending between tholeiitic and alkali basalts, which occur at the trench- and back-arc-side of the volcanic arc, respectively. This, together with the inadequate interchangeable use of calc-alkalic series and medium-K series, has led some petrologists to suggest that calc-alkalic andesites are derived from high-alumina basalt magmas. This is clearly incorrect as calc-alkalic andesites occur both in tholeiitic and alkali basalt zones, as well as in the high-alumina basalt zone (e.g. Yoshida & Aoki 1984).

Magma mixing: a possible mechanism for calc-alkalic andesite formation

It is well established that tholeiitic andesites, including those in the NE Japan arc, are formed primarily by crystallization differentiation of mantle-derived, tholeiitic basalt magmas (e.g. Masuda & Aoki 1979; Sakuyama 1981; Wada 1981; Grove & Baker 1984; Helz 1987; Fujinawa 1988, 1990). The reasons for believing so are threefold. First, smooth major and trace element composition trends, which typify the tholeiitic series, are successfully modelled by simple fractional crystallization of phenocryst phases (Fig. 6). Secondly, composition of the phenocryst phases change systematically with increasing degrees of crystallization and decreasing temperatures. Lastly, tholeiitic andesites exhibit little or no evidence for disequilibration, such as the presence of banded structures, reversely zoned phenocrysts, dusty zones within single phenocryst phase and thermodynamic disequilibrium mineral assemblages. On the other hand, the genesis of calc-alkalic andesites has been a considerable question for debate. At present, there are many hypotheses to account for calc-alkalic magma generation, some of which will be further explored here.

One possible explanation for the characteristic compositional trends observed for the calc-alkalic series is the removal of magnetite, in addition to other phenocryst phases such as plagioclase, orthopyroxene, clinopyroxene and olivine, resulting in increasing silica content while preventing iron-enrichment (e.g. Osborn 1959; Gill 1981). Sisson & Grove (1993) demonstrated experimentally that a high magmatic H_2O content reduces the stability of silicate minerals and has less effect on Fe–Ti oxide stability, with the result that magnetite crystallizes early in H_2O-rich basalt magmas. It is thus suggested that crystallization differentiation of parental H_2O-rich basalt magma can produce calc-alkalic andesite daughter liquids. Analyses of volatiles in melt inclusions in phenocryst phases further indicate that calc-alkalic andesites are generally H_2O-rich, and that arc tholeiitic magmas are relatively poor in H_2O (Sisson & Layne 1993; Roggensack *et al.* 1996; Sisson & Bronto 1998). These observations provide a compelling reason to favour differentiation of H_2O-rich basalt magmas in the production of calc-alkalic andesitic magmas.

Experimental results both on simple and natural systems indicate that melts produced by partial melting of basaltic rocks at rather low pressures possess andesitic compositions (e.g. Kushiro 1969; Holloway & Burnham 1972; Rapp & Watson 1995). It is thus likely that anatexis of the lower crust may contribute to the formation of andesite magmas. Takahashi (1986) documented the following observations for calc-alkalic andesites in the Ichinome–Gata volcano of the NE Japan arc: (1) hornblende-bearing hydrous gabbros occur as xenoliths; (2) partial melting of these xenoliths has been recognized; and (3) calc-alkalic andesites possess Sr isotopic compositions identical to those of the gabbroic xenoliths. As the presence of hornblende in the melting residue could account for enrichment of the liquid in silica but not in iron, the above observations may be consistent with generation of calc-alkalic andesite by anatexis of hornblende-bearing gabbroic lower crust. However, the petrographic characteristics of calc-alkalic andesites, such as disequilibrium mineral assemblages, cannot be explained solely by rather simple processes such as crystallization differentiation and lower crustal melting, and thus it may be safe to say that, at this present stage, such processes are not likely to account for the majority of calc-alkalic andesites.

Experimental results indicate that andesitic melts can be generated by partial melting of peridotites under hydrous conditions (e.g. Kushiro 1969; Mysen & Boettcher 1975; Hirose 1997). Particular andesites with high MgO content and high Mg/(Mg+Fe) ratios (= Mg#), which have been referred to as high-Mg# andesites (HMAs; Kelemen 1995), may represent such unfractionated, mantle-derived melts (e.g. Kuroda *et al.* 1978; Jenner 1981; Tatsumi & Ishizaka 1981, 1982; Crawford *et al.* 1989). Melting-phase relations for primitive HMAs indicate equilibration of such magmas with mantle peridotites at upper mantle pressures under hydrous, but not necessarily H_2O-saturated, conditions (e.g. Kushiro & Sato 1978; Tatsumi 1981, 1982; Van der Laan *et al.* 1989; Umino & Kushiro 1989). Primitive HMAs and 'normal' calc-alkalic andesites may form a single compositional trend, implying that mantle-derived andesitic magmas could differentiate to produce calc-alkalic andesites. Tamura (1994) documented that phenocryst compositions and magmatic temperatures, inferred from the two-pyroxene geothermometer, show a systematic difference between tholeiitic and calc-alkalic series from the Mio-Pliocene Shirahama Group in the Izu–Bonin arc, both of which exhibit little evidence for magma mixing. These observations may suggest that the two chemically distinct magmas were produced at different temperatures within the upper mantle. Thus, it has been speculated that tholeiitic and calc-alkalic andesites are derived through fractional crystallization of mantle-derived basaltic and andesitic magmas, respectively (Tamura 1994; Tamura & Nakamura 1996). However, the majority of researchers do not favour this mechanism, as

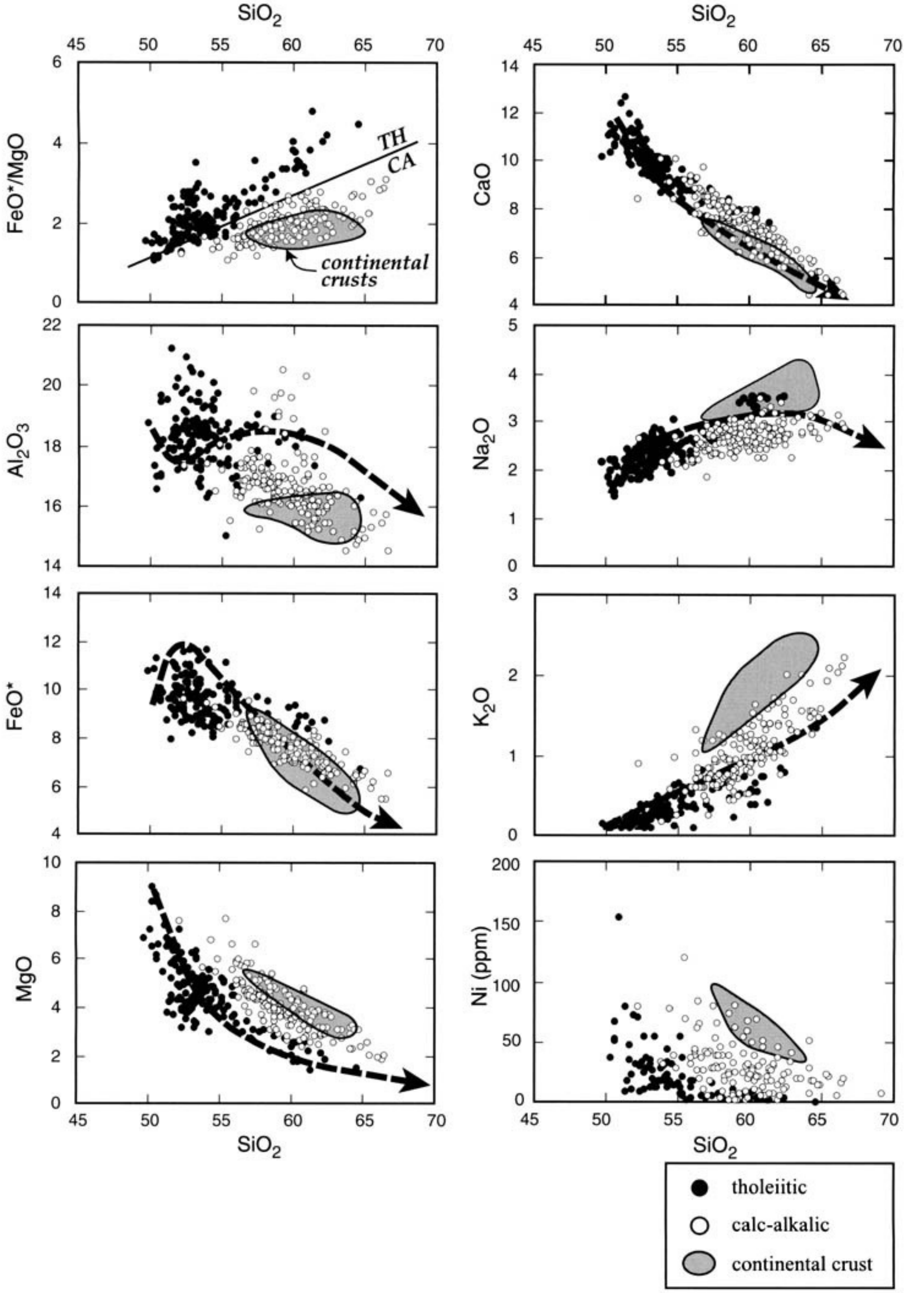

Fig. 6. Major and trace element characteristics of calc-alkalic (CA) and tholeiitic (TH) rocks in the NE Japan arc. The former is more enriched in MgO, K_2O and Ni than the latter. The tholeiitic trend can be explained by crystallization differentiation of a basaltic parental magma that was modelled by the computer program MELTS (Ghiorso & Sack 1995) (broken lines). On the other hand, rather linear trends for calc-alkalic rocks may not be explained by such differentiation processes. It should be stressed that continental crust possesses compositions close to those of calc-alkalic andesite in the NE Japan arcs. Compositions of continental crust are from Taylor & McLennan (1985), Christensen & Mooney (1995) and Rudnick & Fountain (1995).

primitive HMAs rarely occur in subduction zones. Furthermore, the consanguinity between HMAs and calc-alkalic andesites, occurring within a single volcano, has not yet been proven petrographically or geochemically. Tatsumi *et al.* (2002) present petrographical and geochemical characteristics of calc-alkalic andesites on Shodo–Shima Island, SW Japan, which occur in a close time–spatial relation to mantle-derived HMAs and basalts (Tatsumi 1982; Tatsumi & Ishizaka 1982). It was concluded that the calc-alkalic andesites were produced by mixing of at least five end-member magmas, including two types of primitive HMAs, basalt, differentiated andesite and felsic magmas, and were not simply the result of fractional crystallization of HMA or basalt magmas.

Calc-alkalic andesites often exhibit the following disequilibrium petrographic characteristics: (1) the presence of plagioclase phenocryst with a dusty zone containing fine melt inclusions and with wide range of compositions; (2) the presence of reversely zoned pyroxene phenocrysts with rounded cores mantled by rims of higher Mg/Fe ratios; (3) the presence of subhedral to rounded olivine phenocrysts rimmed by pyroxene; and (4) the occurrence of disequilibrium mineral assemblages such as Mg-rich olivine and quartz. These petrographic observations suggest the role of magma-mixing processes in the formation of the magmas (Eichelberger 1975; Sakuyama 1979; Bloomfield & Arculus 1989; Kawamoto 1992; Clynne 1999). It should be stressed that calc-alkalic andesites form rather linear trends on variation diagrams (Fig. 6), suggesting the role of mixing of two end-member components.

Couch *et al.* (2001) demonstrated that the above disequilibrium features observed in andesite lava at the Soufrière Hills Volcano could also be produced by convection within a magma body, of a single composition, that is heated from below and cooled from above. Although this newly developed mechanism may be valid for magmatic evolution in other arc volcanoes, the systematic difference in isotopic composition between calc-alkalic andesites and tholeiitic basalts, as discussed later, may suggest the generalized minor role of such processes in the production of calc-alkalic andesite magmas.

The range of disequilibrium petrographic features suggest the involvement of at least two magmas, one with a higher temperature and more mafic composition, and the other with a lower temperature and more felsic composition. The origin of a mafic end-member magma could be rather simple, and would be produced essentially by crystallization differentiation of a mantle-derived basalt magma; i.e. one of the end-member magmas for calc-alkalic andesites would be a tholeiitic basalt. However, the origin of a felsic end-member magma is controversial. Some workers favour an internal mixing process for the production of mixed calc-alkalic andesites (e.g. Sakuyama 1981); such a felsic magma could be derived from a tholeiitic basalt magma through crystallization differentiation, and hence would belong to the tholeiitic series. On the other hand, a felsic magma could be produced by anatexis of mafic–intermediate crust (e.g. Hildreth 1981), and would thus be 'external' in origin.

In order to investigate internal or external mixing models for calc-alkalic andesite genesis, isotopic compositions of tholeiitic and calc-alkalic rocks that occur in a single volcano in the NE Japan arc are re-examined. Figure 7 shows data from the Adatara and Towada volcanoes (Kurasawa *et al.* 1985; Fujinawa 1988) and demonstrates that calc-alkalic lavas possess Sr isotopic compositions that are systematically different from the tholeiitic lavas, suggesting that the two types of magma are not derived from a single mantle-derived source. More importantly, the isotopic characteristics suggest that calc-alkalic andesites cannot be produced by internal mixing processes, i.e. mixing between tholeiitic mafic and felsic magmas. If the mafic end-member magma for a mixed calc-alkalic andesite is a differentiated tholeiitic basalt, it would need to mix with a felsic magma that is derived from a source isotopically distinct from the upper mantle. One such source could be the arc crust, which would undergo partial melting to form a felsic magma.

Hunter & Blake (1995) presented Sr and Nd isotopic compositions for tholeiitic and calc-alkalic andesite lavas from the Towada Volcano and suggested that they did not possess systematically different isotopic ratios. This result does not agree with the data of Kurasawa *et al.* (1985) shown in Figure 7. This contradiction is derived from the definition of the two magma series; Hunter & Blake (1995) defined the calc-alkalic and tholeiitic series as having compositions lying above and below the discrimination line on a FeO*/MgO v. SiO_2 diagram (Miyashiro 1974), whereas Kurasawa *et al.* (1985) defined them based both on petrographic observations and compositional trends. As stated by Miyashiro (1974), the latter definition is preferable.

It may be intuitive to expect that crust-derived magmas would generally possess more enriched isotopic compositions than mantle-derived magmas; however, this is not always the case. For

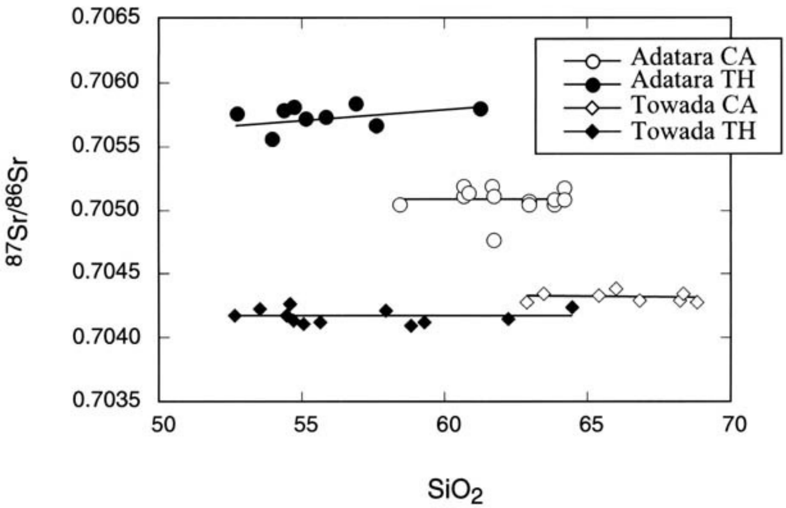

Fig. 7. Sr isotopic compositions of lavas from Adatara and Towada volcanoes in the NE Japan arc after Kurasawa *et al.* (1985) and Fujinawa (1988). Calc-alkalic (CA) and tholeiitic (TH) rocks possess systematically different isotopic compositions. If magma-mixing processes are a possible mechanism for calc-alkalic magmas, then a felsic end-member magma may be 'external' in origin, and not a differentiation product of a tholeiitic basaltic magma.

example, in the NE Japan arc tholeiitic, hence probably mantle-derived basalts, show remarkable along-arc variations in $^{87}Sr/^{86}Sr$ isotopic compositions, increasing from 0.7038 in the northern part to 0.7065 in the southern part (e.g. Notsu 1983). This, together with the isotopic characteristics of tholeiitic and calc-alkalic lavas, suggests that the Sr isotopic compositions of calc-alkalic andesites, at least in the NE Japan arc, can be explained by the mixing of tholeiitic mafic magmas, reflecting isotopically variable upper mantle, with felsic magmas produced by anatexis of an isotopically homogeneous arc crust.

Continental crust formation

The continental crust has an average composition equivalent to andesites (Taylor & McLennan 1985; Rudnick & Fountain 1995); however, modern-day mantle-derived magmatism is dominated by basalt. This is probably one of the greatest dilemmas concerning the origin and evolution of the solid Earth. The geochemical characteristics of the bulk andesitic continental crust, such as incompatible trace element signatures, are broadly identical to those of current subduction zone lavas; this has led several researchers to speculate that continental crust was created at convergent plate margins (e.g. Kelemen 1995; Rudnick 1995; Taylor & McLennan 1995). In order to explain the characteristic andesitic composition of the bulk continental crust, several mechanisms have been proposed, including: (1) differentiation of HMA magmas produced by partial melting of a hydrous mantle (Shirey & Hanson 1984; Stern & Hanson 1991); (2) partial melting of the subducting oceanic crust (Martin 1987; Drummond & Defant 1990); (3) reaction of mantle- or slab-derived melts with the mantle wedge peridotites (Kelemen 1995; Rapp *et al.* 1999); and (4) basaltic underplating, anatexis of such initial crust and subsequent delamination of residual, mafic lower crust (Turcotte 1989; Kay & Kay 1993). Among these, the last two hypotheses are widely accepted as the major mechanisms for continental crust formation (Kelemen 1995; Rudnick 1995). Tatsumi (2000*b*) demonstrated, based on geochemical formulation, that the residual compositions after slab melting cannot explain the isotopic signature of deep-seated mantle geochemical reservoirs. On the other hand, a mechanism that includes delamination of the residual crusts can comprehensively account for andesitic crust formation. It can also account for the complementary accumulation of the enriched mantle I component (EMI) geochemical reservoir in the deep mantle (Tatsumi 2000*a*), suggesting that such a mechanism is likely to have operated in Archean subduction zones.

It should be stressed, however, that at least two types of andesites (tholeiitic and calc-alkalic) are produced in modern-day subduction

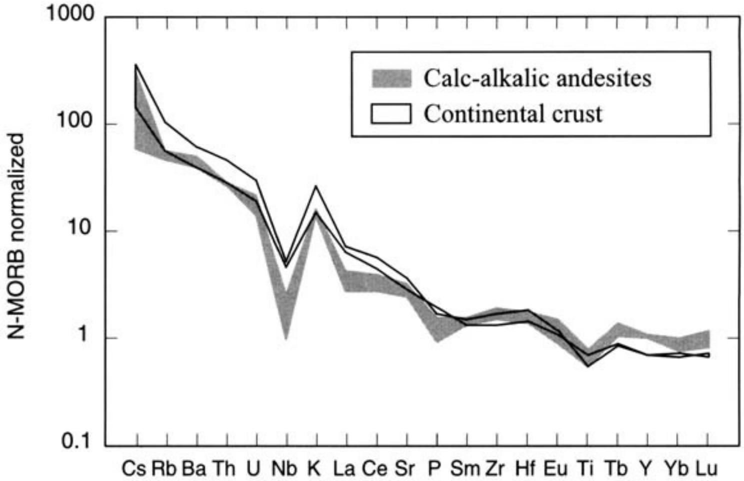

Fig. 8. Incompatible trace element characteristics of calc-alkalic andesites and the bulk continental crust (Taylor & McLennan 1985; Rudnick & Fountain 1995). N-MORB values are from Sun & McDonough (1989).

zones by different mechanisms. In order to discuss the origin of the andesitic continental crust, we therefore need to compare crustal compositions with those of calc-alkalic and tholeiitic andesites.

Calc-alkalic andesites v. continental crust

Estimates of bulk continental crust composition are based on observations of the rock types distributed in the upper continental crust and on models of lower crustal composition. As the latter estimates are rather uncertain, current estimates of the bulk continental crust composition are variable. These uncertainties aside, Figure 6 demonstrates that: (1) the bulk continental crust possesses major element signatures close to those of calc-alkalic, rather than tholeiitic andesites; (2) on Miyashiro's diagram continental crust estimates plot well within the region of the calc-alkalic series, although they do *not necessarily* form a calc-alkalic 'trend'; and (3) they exhibit MgO concentrations higher than lavas of the tholeiitic series for a given SiO_2 content. On the other hand, bulk continental crust tends to have higher concentrations of the alkali elements, especially K, than calc-alkalic andesites of the NE Japan arc (Fig. 6). The reasons for this discrepancy are twofold. First, there is a variation by a factor of more than 2 in the estimate of concentrations of incompatible elements, such as K, in the bulk continental crust (Rudnick 1995). Secondly, Figure 6 is derived from the composition of lavas along the volcanic front, suggesting that calc-alkalic andesites occurring in the back-arc-side of the volcanic arc may have a K content identical to those of bulk continental crust (cf. Fig. 4). The compositional similarity between calc-alkalic andesites and andesitic continental crust is further shown by their incompatible trace element patterns (Fig. 8). Both display a rather monotonous decrease in incompatible element concentrations with decreasing incompatibility, and have a remarkable 'Nb-trough'.

Rudnick (1995) compared the composition of the bulk continental crust with orogenic andesites and suggested that the former is characterized by its higher Ni and Cr concentrations. This is certainly true, as illustrated in Figure 6. This apparent discrepancy could be explained if we accept higher mantle temperatures for the Archean, which may have produced more magnesian and Cr- and Ni-rich basalt magmas than the modern-day mantle. Another counter-argument is higher light rare earth element (LREE)/Nb ratios in arc andesites compared to bulk andesitic crust (Rudnick 1995). However, calc-alkalic andesites on the trench-side volcanic chain of the NE Japan arc exhibit Ce/Nb ratios (4.0 ± 0.8; data from Yoshida & Aoki 1984) close to those of inferred bulk continental crust (3.0–3.5; Rudnick & Fountain 1995; Taylor & McLennan 1995). This small, but probably significant, difference would suggest the contribution of intraplate magmatism to the growth of the continental crust (Rudnick 1995).

Although the compositional similarity between andesitic continental crust and calc-alkalic andesites do not necessarily mean that they were produced by an identical mechanism, it is still interesting to discuss the origin of the andesitic continental crust in comparison with the genesis of calc-alkalic andesites. As the majority of current calc-alkalic andesites are unlikely to have been produced from the simple anatexis of basaltic crust, it is equally unlikely that continental crust formed by this process. Furthermore, although such a process may also account for the formation of the isotopically distinct EMI geochemical reservoir in the deep mantle (Tatsumi 2000*a*), unrealistically high degrees of partial melting (*c*. 60%) of the initial basaltic crust are required for simultaneously producing andesitic magmas and pyroxenitic restites, i.e. the continental crust and the EMI reservoir, respectively. On the other hand, a plausible mechanism of calc-alkalic andesite magma genesis, and hence probably of the bulk continental crust, is mixing of mantle-derived basalt and crust-derived felsic magmas. In this scenario, felsic magmas could be derived by reasonable degrees of partial melting from an initial basaltic crust. It is thus interesting to examine how such a process may account for the geochemical characteristics of both the continental crust and a certain geochemical end-member component in the deep mantle.

Geochemical examination of magma mixing–delamination model

The aforementioned possible mechanism of continental crust formation, via magma mixing, is here examined by geochemical modelling. The method for the calculation of trace element compositions of andesitic melts is identical to that of Tatsumi (2000*a*), except that the present modelling takes into account the mixing of mantle-derived basalt and crust-derived felsic magmas instead of simple remelting of the initial basaltic crust (Fig. 9). The steps taken and assumptions made in the modelling are numerated as follows:

1 The composition of the present arc magma source in the mantle wedge is calculated based on compositions of modern arc basalts by assuming a medium-K basalt as the best candidate to use and 15% fractional melting of a peridotite composed of 50% olivine, 30% orthopyroxene and 20% clinopyroxene.
2 The slab flux is calculated by comparing the inferred mantle wedge and the normal MORB (N-MORB) source as the preflux, original mantle wedge, which is calculated from N-MORB compositions and inferred melting conditions.
3 Trace element compositions of slab-derived fluids are calculated by assuming 0.2 wt% slab fluid in the magma source. Such an amount of aqueous fluid yields *c*. 1.3 wt% H_2O in a primary magma, which may be an acceptable value as H_2O content in arc magmas (e.g. Sisson & Layne 1993).
4 Trace element compositions of subducting altered oceanic crust (amphibolite) are estimated based on element mobility data (Kogiso *et al.* 1997) by assuming a single-step overprinting process onto the original mantle wedge.
5 The element mobilization during amphibolization at spreading ridges is estimated by comparing compositions of the inferred amphibolitic oceanic crust with the fresh N-MORB compositions.
6 Ancient altered oceanic crust (amphibolite) compositions are calculated by applying the above effect of overprinting during amphibolization onto an ancient MORB produced by 15% fractional melting of primitive mantle.
7 Compositions of the ancient arc basalt magma or the initial arc crust (Table 2) are obtained by the inverse steps of the above formulation.
8 Partial melting of the initial basaltic crust can be formulated based on experimental results by Beard & Lofgren (1991), which demonstrate that a felsic melt with *c*. 74% SiO_2 is generated at 0.3 GPa and 900°C from a basaltic material leaving 55% plagioclase, 22% clinopyroxene, 10% orthopyroxene, 12% magnetite and 1% ilmenite.
9 A 1:1 mixture of this felsic melt and the primitive basalt (Table 2) provides major element compositions close to the bulk continental crust.

The incompatible trace element compositions of an inferred mixed andesitic melt (Table 2) are shown in an N-MORB normalized (Sun & McDonough 1989) spidergram (Fig. 10), together with those of the continental crust. A good overall agreement (e.g. in the relative enrichment of large ion lithophile elements and the relative depletion of Nb) is evident. Small, but probably significant, discrepancies are observed between these two for Y and Yb (Fig. 10). Although the present modelling assumes a pyroxenitic restite for crustal anatexis, it is likely that garnet, into which such trace elements are strongly partitioned, would be present as one of the residual minerals.

A critical problem that needs to be addressed for the above process is the density of the pyroxenitic restite. Delamination of the lower crust takes place due to its greater density than that of

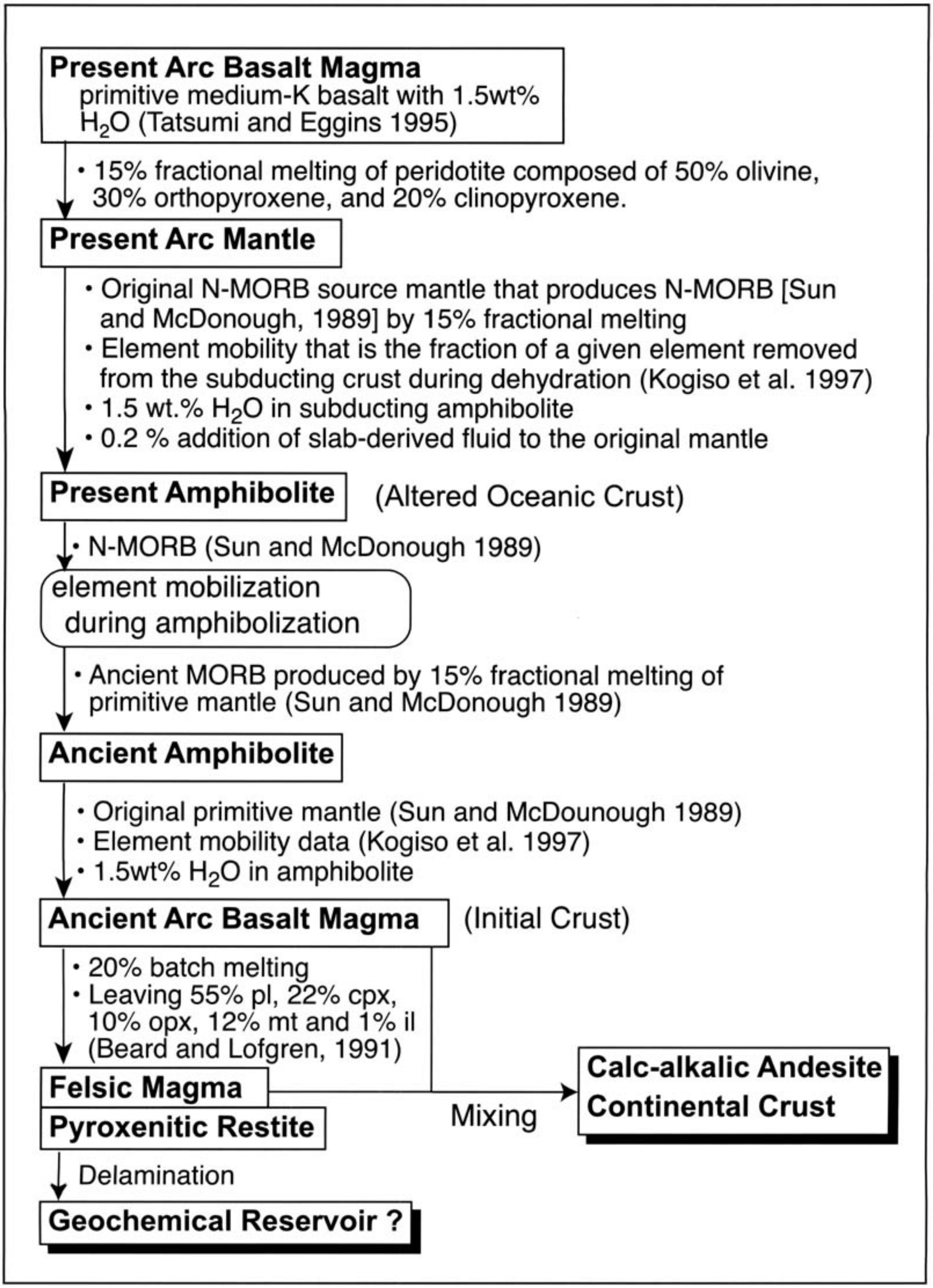

Fig. 9. Scheme of geochemical modelling for continental crust formation.

Table 2. *Geochemical modelling for continental crust formation*

	K	Rb	Sr	Pb	Ba	Yb	Y	Sm	Nd	La	Zr	U	Th	Nb
Partition coefficient														
opx	0.0001	0.00001	0.001	0.0008	0.0001	0.1	0.06	0.02	0.009	0.005	0.01	0.001	0.0008	0.003
cpx	0.007	0.0001	0.1	0.05	0.001	0.4	0.45	0.29	0.19	0.05	0.53	0.08	0.07	0.1
pl	0.3	0.01	3	1.5	0.3	0.008	0.01	0.04	0.05	0.1	0.001	0.001	0.002	0.001
spinel	0.000006	0.000001	0.000001	0.000001	0.000001	0.045	0.015	0.006	0.005	0.004	0.006	0.006	0.005	0.01
Initial crust	7587	20	339	4.7	248	2.5	23	3.3	12	8.1	58	0.49	1.9	1.6
Crust melt	22 767	96	221	5.4	747	8.7	80	12	47	32	195	2.3	8.9	7.5
Restite (pyroxenite)	3792	0.53	369	4.5	123	0.95	9.0	1.1	3.3	2.2	23	0.044	0.15	0.18
Mixed andesite	15 177	58	280	5	498	6	52	8	30	20	127	1	5	5

Abbreviations: opx, orthopyroxene; cpx, clinopyroxene; pl, plagioclase.
Element concentrations are in ppm.

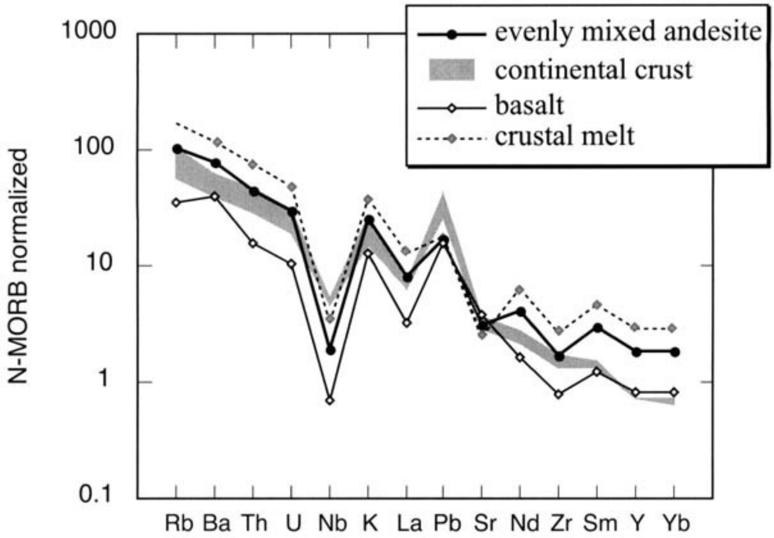

Fig. 10. N-MORB normalized (Sun & McDonough 1989) multi-element diagram comparing continental crust (Taylor & McLennan 1985; Rudnick & Fountain 1995), inferred mantle-derived basalt, crust-derived felsic magmas and an andesite magma produced by an even mixture of basalt and felsic magmas.

upper mantle. However, the density of the inferred pyroxenite is *c.* 3.2, a value less than that of the normal upper mantle density (*c.* 3.3). This model therefore requires some additional mechanisms, such as crustal thickening and the transition of pyroxenitic to eclogitic assemblages presumably associated with arc–arc collision.

Evolution of geochemical reservoirs in the deep mantle

The subduction factory may also have played a key role in the evolution of the mantle through injection of surface materials such as crust and sediments into the deep mantle, imparting a significant heterogeneity. The presence of variable components within the mantle is well established from geochemical studies on MORBs and ocean island basalts (OIBs); the isotopic compositions of such lavas are suggestive of the presence of at least four end-member components or geochemical reservoirs (DMM, EMI, EMII, and HIMU; Zindler & Hart 1986), in addition to primitive mantle (Fig. 11). Among these, depleted MORB-source mantle (DMM) is distinct in its isotopically depleted signature. The origin of enriched mantle components is essential for understanding the dynamic processes and evolution of the deep mantle, as such components typify magmas rising from deep-seated hot spots. It has been repeatedly suggested that subducted crustal materials significantly contribute to these enriched end-member components (e.g. Chase 1981; Hofmann & White 1982; Chauvel *et al.* 1992; Kogiso *et al.* 1997), although some authors argued against such scenarios (Kamber & Collerson 2000; Rudnick *et al.* 2000). Here we review the chemical differentiation processes in subduction zones relevant to the isotopic evolution of sinking materials and discuss the role of the subduction factory in the evolution of the deep mantle.

Oceanic crusts and sediments: origin of high-μ (HIMU) and enriched mantle II component (EMII) reservoirs

The upper-crustal portion of subducting oceanic lithosphere mainly consists of MORB-like basalts. The upper portion of the basaltic oceanic crust is hydrated and altered by hydrothermal processes and through mechanical fracturing before subduction. However, the rest of the crust remains anhydrous and may keep its original composition until it reaches the subduction zone. As the solidus temperature of anhydrous basalt is higher than estimated temperature distributions along the foundering lithosphere (Yasuda *et al.* 1994; Pertermann & Hirschmann 1999), the fresh (anhydrous) part of

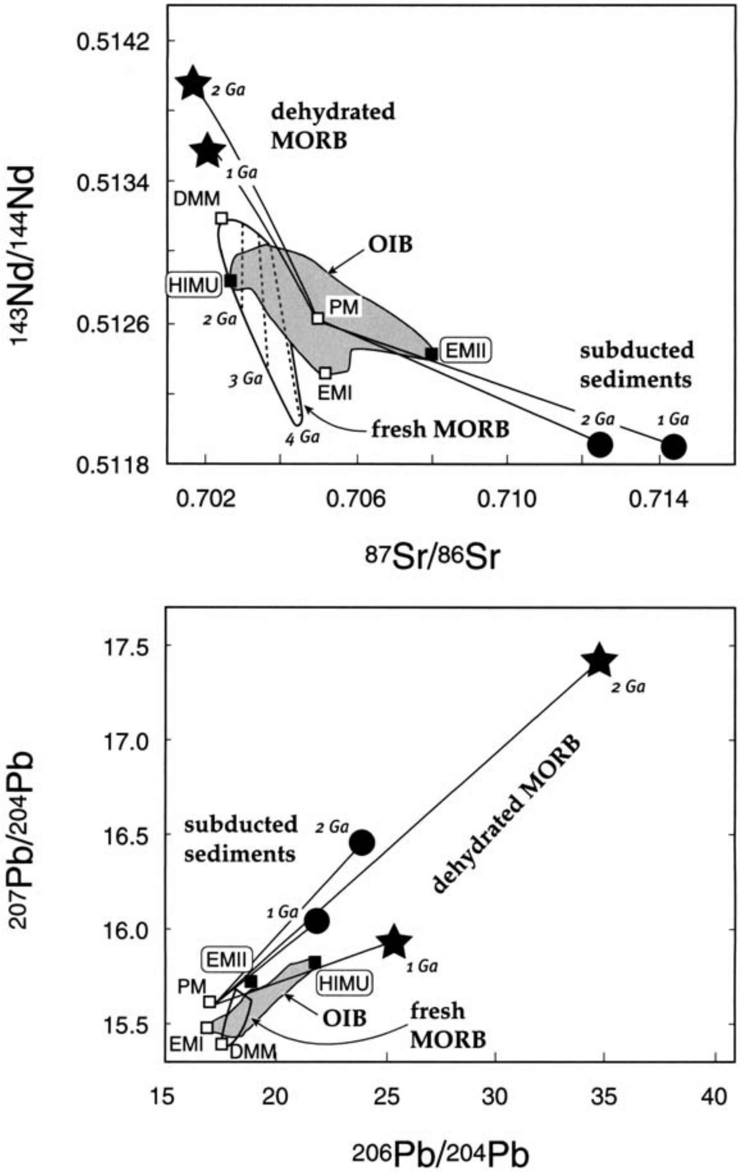

Fig. 11. Variation of isotopic compositions of subducted fresh MORB, dehydrated residue of hydrous MORB and sediments. Ages of subduction are shown with symbols and lines. Compositions of the fresh MORB are calculated with Rb/Sr and Nd/Sm ratios 1% (upper curve) to 10% (lower curve) higher than the MORB source. U/Pb ratios of the fresh MORB are assumed to be same as the source. The MORB source is assumed to be derived from the primitive mantle at 4.0 Ga with parent/daughter ratios that changed continuously from 4 Ga to present. Present isotopic composition of the MORB source is: $^{87}Sr/^{86}Sr = 0.7026$, $^{143}Nd/^{144}Nd = 0.5131$, $^{206}Pb/^{204}Pb = 17.5$, $^{207}Pb/^{204}Pb = 15.4$. Compositions of dehydrated MORB residue and sediments are taken from Kogiso *et al.* (1997) and Aizawa *et al.* (1999), respectively.

basaltic oceanic crust does not melt upon subduction and thus sinks into the deep mantle without changing its composition. In contrast, the hydrated part of basaltic crust dehydrates to release fluids with increasing pressures and temperatures until all hydrous minerals in the crust break down (Schmidt & Poli 1998). Also, hydrated basaltic crust may partially melt if the slab temperature is high enough to cross the solidus of hydrous basalt (Peacock 1993; Rapp & Watson 1995). Therefore, at least three compositionally different materials should be regarded as basaltic components that are transported, by plate subduction, into the deep mantle: fresh MORB and melting and dehydration residues of hydrous MORB.

As basaltic oceanic crust is normally generated by partial melting of depleted MORB-source mantle (DMM) at mid-ocean ridges, the trace element signatures of the subducting fresh MORB crust can be estimated from those of DMM. MORB crust has higher Rb/Sr and lower Sm/Nd ratios than its source DMM peridotites, because the order of compatibility in mantle peridotites (spinel lherzolites) is Rb < Sr < Nd < Sm (Green 1994; Hauri *et al.* 1994; Blundy *et al.* 1998). Although the partition coefficient of U between melt and mantle minerals, especially garnet and clinopyroxene, is highly variable (Watson *et al.* 1987; Hauri *et al.* 1994), it is smaller than 0.1 (Pertermann & Hirschmann 1999) and largely identical to that of Pb (Hauri *et al.* 1994). Consequently, the U/Pb ratio of MORB crust is likely to be close to that of the DMM source. It may be thus concluded that long-term residence of fresh MORB crust in the mantle results in higher $^{87}Sr/^{86}Sr$, lower $^{143}Nd/^{144}Nd$ and similar $^{206}Pb/^{204}Pb$ values compared with DMM (Fig. 11), suggesting that accumulated MORB crust may contribute to the isotopic diversity of the mantle. However, characteristic high $^{206}Pb/^{204}Pb$ ratios for the HIMU reservoir cannot be explained solely by the involvement of the MORB crust.

Several lines of evidence compel a significant majority of researchers to believe that the subducting oceanic crust does not melt in most 'normal' subduction zones in the modern Earth (Tatsumi & Eggins 1995). However, in subduction zones with unusually high-temperature conditions, partial melting of the sinking hydrous basaltic crust may take place. This might develop where a young and hot lithosphere subducts (Drummond & Defant 1990; Peacock 1990; Furukawa & Tatsumi 1999) and thus may have existed more widely during the Earth's early history (Martin 1986). Furthermore, slab melting and subsequent melt–mantle interactions may produce andesitic magmas with major and trace element compositions largely similar to those of the bulk continental crust (Kelemen 1995; Tatsumi 2000*b*). It is therefore interesting to assess the complementary formation of the continental crust and the mantle geochemical reservoirs. Tatsumi (2000*b*) examined this process, based on geochemical formulation of partial melting and melt–solid reactions, and demonstrated that the Sr–Nd–Pb isotopic compositions of melting residues in the subducting slab, which may have foundered and been stored in the deep mantle, do not match those of any proposed geochemical reservoir.

Dehydration reactions within subducting hydrated basaltic crust occur continuously from very shallow levels to over 300 km depth (e.g. Schmidt & Poli 1998), but experimental studies on trace element behaviour during dehydration are almost limited to those related to the amphibolite–eclogite transformation (Kogiso *et al.* 1997) and element partitioning between aqueous fluids and garnet–clinopyroxene (Brenan *et al.* 1995*a*, *b*; Keppler 1996; Ayers *et al.* 1997; Stalder *et al.* 1998). A notable feature demonstrated by these experiments is that Pb is more preferentially partitioned into H_2O fluids than U and Th, leaving the residue, after dehydration, to have higher U/Pb and Th/Pb ratios than its original compositions. It is also demonstrated that Rb and Nd are released from the subducting crust more readily than Sr and Sm (Brenan *et al.* 1995*b*; Keppler 1996; Ayers *et al.* 1997; Kogiso *et al.* 1997). Thus, residual basaltic crust post the amphibolite–eclogite transformation will have lower $^{87}Sr/^{86}Sr$, higher $^{143}Nd/^{144}Nd$, and higher $^{206}Pb/^{204}Pb$ ratios than hydrated basaltic crust (Fig. 11). $^{206}Pb/^{204}Pb$ ratios of the dehydrated residue are likely to be significantly greater than that of the HIMU component, implying that subducted dehydrated basaltic crust may contribute to the genesis of this mantle component (Brenan *et al.* 1995*b*; Kogiso *et al.* 1997). The Sr and Nd isotopic evolution of the dehydrated crust is dependent on Rb/Sr and Sm/Nd ratio changes during partial melting at mid-oceanic ridges and dehydration reactions in subduction zones. Although it is difficult to estimate quantitatively, suitable parent/daughter ratios to produce HIMU-like Sr and Nd isotopic ratios could be explained through the above two processes including accumulation of both fresh and dehydrated MORB crusts (Fig. 11).

The role of subducting sediments in the formation of EMII, one of the enriched geochemical reservoirs in the mantle, has been emphasized by several authors because oceanic sediments generally have high $^{87}Sr/^{86}Sr$ and relatively low $^{143}Nd/^{144}Nd$ ratios (e.g. Devey *et al.* 1990; Weaver 1991). However, oceanic sediments that are subducted into the mantle contain significant amounts of hydrous phases, all of which will decompose to release fluids, causing significant fractionation of trace elements through fluid migration (Aizawa *et al.*

1999; Johnson & Plank 1999). Experiments on sediment dehydration by Aizawa *et al.* (1999) have demonstrated that ancient subducted oceanic sediments, while experiencing compositional modification in the subduction factory, may evolve to an enriched component having high $^{87}Sr/^{86}Sr$ and $^{206}Pb/^{204}Pb$ ratios. They further indicated that the isotopic signature of the EMII component can be achieved by the addition of small amounts (*c.* 1 wt%) of dehydrated sediments to DMM-like mantle or primitive mantle (Fig. 11).

Delaminated pyroxenite: origin of enriched mantle component I (EMI)

Trace-element modelling in the previous section suggests that the geochemical characteristics of bulk continental crust can be reasonably explained by mixing of mantle-derived basaltic and crust-derived felsic magmas. In order to make an andesitic continental crust, the melting residue after extraction of felsic melts should be removed and delaminated from the initial crust. It is thus interesting to examine the isotopic evolution of a delaminated 'anti-crust' component, based on inferred parent–daughter element concentrations (Table 2), and to compare such signatures with those of the mantle reservoirs.

Seawater is characterized by an extremely high present-day $^{87}Sr/^{86}Sr$ ratio of 0.7092 and a rather high abundance of Sr (8 ppm). Its incorporation into the amphibolitic oceanic crust through alteration processes at oceanic ridges strongly affects the Sr isotope composition of the subducting oceanic crust. Furthermore, it is well known that seawater Sr isotope ratios have changed through time, with values generally decreasing with increase in age (e.g. Veizer & Compston 1976). We have evaluated the effect of amphibolization at ridges on the Sr isotope compositions of an oceanic crust by the method proposed by Tatsumi (2000*a*). The temporal variation in seawater compositions is formulated for the last 2.5 billion years using the following equation, which is based on the data by Veizer & Compston (1976): $(^{87}Sr/^{86}Sr)_t = 0.70927 - 2.6944 \times 10^{-3} \times t$ (Ga). For $t > 2.5$ Ga, the ratio is assumed to be constant at 0.70250. The Nd and Pb isotope ratios of oceanic crust were assumed to be unchanged during the alteration processes at ridges and those ratios of an ancient subducting amphibolite were calculated based on both the estimates of primitive mantle compositions (Sun & McDonough 1989) and the isotopic ratios in the present bulk mantle. The isotopic compositions of primary arc basalt magma can be obtained from those of the subducting amphibolite, of the original mantle (primitive mantle) and the aforementioned formulation.

An important factor for the evaluation of the isotopic evolution of melting residues in the initial basaltic crust is the degree of segregation of felsic melts from partially molten crust. The viscosity of a partial melt is one of the most critical parameters governing the velocity of melt migration. A felsic melt may have a viscosity of about 2 orders of magnitude higher than a basaltic melt under the same hydrous conditions. It is thus suggested that perfect separation of such viscous melts from the solid restite are unlikely. Although quantitative estimation of the degree of melt separation is difficult, the present modelling assumes that the slab restites contain 0–15% of the trapped melt component that possesses a composition identical to an extracted felsic melt.

The results of the calculation are shown in Figure 12, together with the isotope compositions of the geochemical reservoirs in the mantle. Quite distinct evolutionary curves with large variations in isotope ratio are obtained, due to differences in the degrees of involvement of the felsic partial melt with the residuum, i.e. the delaminated component. However, a pyroxenite with a 10–15% felsic melt component can reasonably explain the EMI isotopic signature. Simple mixing of the bulk silicate Earth component, which is likely to occupy the deep mantle, and a 3–4 billion-year-old delaminated component could form the EMI component.

Conclusions

The subduction factory is the major site of injection of surface materials into the Earth's interior. The raw materials are processed into magmas, which cause characteristic arc volcanism and makes continental crust through complex processes including remelting of an initial basaltic crust and magma mixing. The waste materials, such as chemically modified subducting sediments/crusts and melting residues delaminated from the crust, have accumulated in the mantle and are likely to have evolved into enriched geochemical reservoirs in the deep mantle. Magmas, which tap such mantle components, are erupting where mantle plumes are rising from the deep mantle. Recycling of surface materials through subduction factories and mantle plumes may have played the central role in the evolution of the solid Earth.

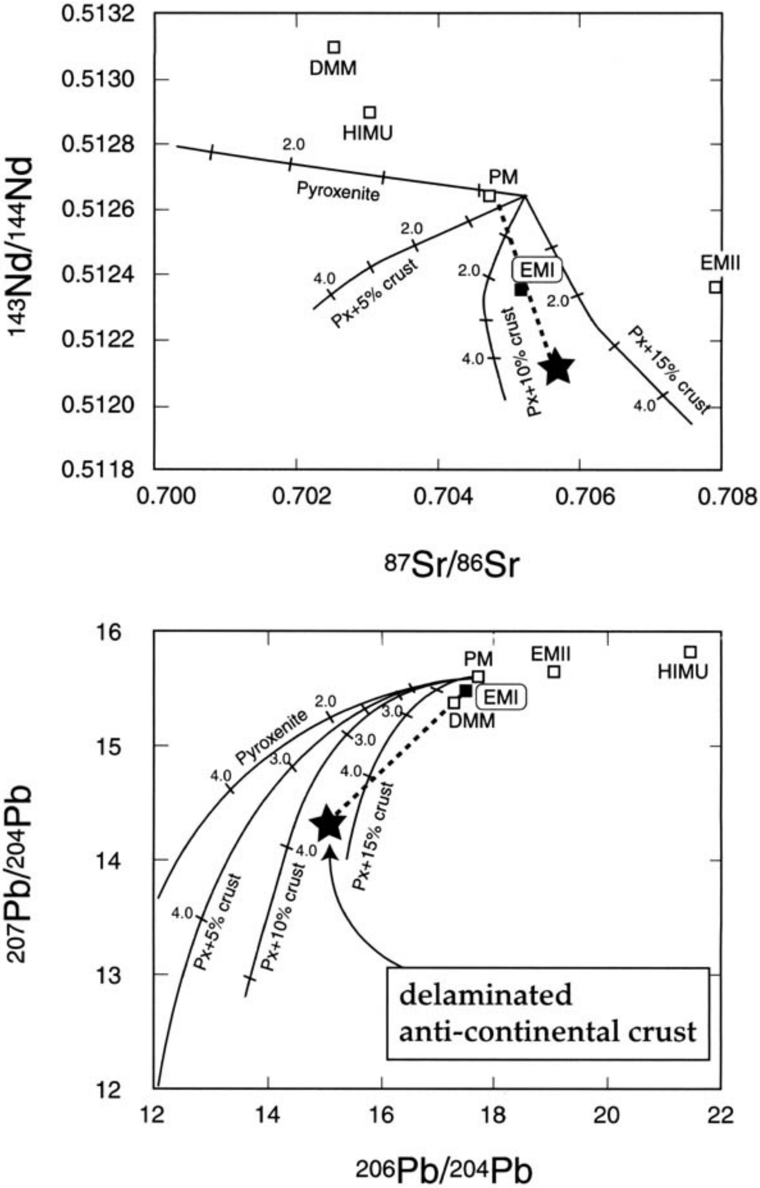

Fig. 12. Isotopic evolution of an inferred pyroxenitic restite with 0–15% contribution of felsic magmas. The ages of formation of such delaminated, anti-continental components are shown in Ga. The pyroxenitic restite was produced by partial melting of an initial basaltic crust, delaminated from the crust and stored in the deep mantle. The isotopic signature of the EMI reservoir may be explained by mixing of the primitive mantle, which represents normal mantle compositions, and delaminated/accumulated pyroxenite with a 10–15% felsic magma component (stars). Isotopic compositions of other mantle components such as the depleted MORB source mantle (DMM), high-μ (HIMU) and enriched mantle component II (EMII) are also shown.

Constructive suggestions and comments from Philip Leat, Sally Gibson, Simon Johnson and an anonymous reviewer are gratefully acknowledged. Thanks also go to Miki Fukuda for preparing the manuscript and figures.

References

ADAMS, J., GREEN, T.H., SIE, S.H. & RYAN, C.G. 1997. Trace element partitioning between aqueous fluids, silicate melts and minerals. *European Journal of Mineralogy*, **9**, 569–584.

AIZAWA, Y., TATSUMI, Y. & YAMADA, H. 1999. Element transport during dehydration of subducting sediments: implication for arc and ocean island magmatism. *The Island Arc*, **8**, 38–46.

AYERS, J.C., DITTMER, S.K. & LAYNE, G.D. 1997. Partitioning of elements between peridotite and H_2O at 2.0–3.0 GPa and 900–1100°C, and application to models of subduction zone processes. *Earth and Planetary Science Letters*, **150**, 381–398.

BASALTIC VOLCANISM STUDY PROJECT. 1981. *Basaltic Volcanism on the Terrestrial Planets*. Pergamon Press, New York.

BEARD, J.S. & LOFGREN, G.E. 1991. Dehydration melting and water-saturated melting of basaltic and andesitic greenstones and amphibolites at 1, 3 and 6.9 kb. *Journal of Petrology*, **32**, 365–401.

BLOOMFIELD, A.L. & ARCULUS, R.J. 1989. Magma mixing in the San Francisco volcanic field, AZ; petrogenesis of the O'Leary Peak and Strawberry Crater volcanics. *Contributions to Mineralogy and Petrology*, **102**, 429–453.

BLUNDY, J.D., ROBINSON, J.A.C. & WOOD, B.J. 1998. Heavy REE are compatible in clinopyroxene on the spinel lherzolite solidus. *Earth and Planetary Science Letters*, **160**, 493–504.

BRENAN, J.M., SHAW, H.F., PHINNEY, D.L. & RYERSON, F.J. 1994. Rutile–aqueous fluid partitioning of Nb, Ta, Hf, Zr, U and Th; implications for high field strength element depletions in island-arc basalts. *Earth and Planetary Science Letters*, **128**, 327–339.

BRENAN, J.M., SHAW, H.F. & RYERSON, F.J. 1995*a*. Experimental evidence for the origin of lead enrichment in convergent-margin magmas. *Nature*, **378**, 54–56.

BRENAN, J.M., SHAW, H.F., RYERSON, F.J. & PHINNEY, D.L. 1995*b*. Mineral–aqueous fluid partitioning of trace elements at 900 degrees C and 2.0 GPa; constraints on the trace element chemistry of mantle and deep crustal fluids. *Geochimica et Cosmochimica Acta*, **59**, 3331–3350.

CHASE, C.G. 1981. Oceanic island Pb; two-stage histories and mantle evolution. *Earth and Planetary Science Letters*, **52**, 277–284.

CHAUVEL, C., HOFMANN, A.W. & VIDAL, P. 1992. HIMU-EM; the French Polynesian connection. *Earth and Planetary Science Letters*, **110**, 99–119.

CLYNNE, M.A. 1999. A complex magma mixing origin for rocks erupted in 1915, Lassen Peak, California. *Journal of Petrology*, **40**, 105–132.

CONDIE, K.C. & POTTS, M.J. 1969. Calcalkaline volcanism and the thickness of the early Precambrian crust in North America. *Canadian Journal of Earth Sciences*, **6**, 1179–1184.

COUCH, S., SPARKS, R.S.J. & CARROLL, M.R. 2001. Mineral disequilibrium in lavas explained by convective self-mixing in open magma chambers. *Nature*, **411**, 1037–1039.

CRAWFORD, A.J., FALLOON, T.J. & GREEN, D.H. 1989. Classification, petrogenesis and tectonic setting of boninites. *In*: CRAWFORD, A.J. (ed.) *Boninites and Related Rocks*. Unwin Hyman, London, 1–49.

CHRISTENSEN, N.I. & MOONEY, W.D. 1995. Seismic velocity structure and composition of the continental crust: a global view. *Journal of Geophysical Research*, **100**, 9761–9788.

DE BREMOND D'ARS, J., JAUPART, C. & SPARKS, R.S.J. 1995. The distribution of volcanoes in active margins. *Journal of Geophysical Research*, **100**, 20 421–20 432.

DEVEY, C.W., ALBAREDE, F., CHEMINEE, J.L., MICHARD, A., MUEHE, R. & STOFFERS, P. 1990. Active submarine volcanism on the Society hotspot swell (West Pacific); a geochemical study. *Journal of Geophysical Research*, **95**, 5049–5066.

DICKINSON, W.R. 1975. Potash–depth (K–*h*) relations in continental margin and intra-oceanic magmatic arcs. *Geology*, **3**, 53–56.

DRUMMOND, M.S. & DEFANT, M.J. 1990. A model for trondhjemite-tonalite-dacite genesis and crustal growth via slab melting; Archean to modern comparisons. *Journal of Geophysical Research*, **95**, 21 503–21 521.

EICHELBERGER, J.C. 1975. Origin of andesite and dacite; evidence of mixing at Glass Mountain in California and at other circum-Pacific volcanoes. *Geological Society of America Bulletin*, **86**, 1381–1391.

FUJINAWA, A. 1988. Tholeiitic and calc-alkaline magma series at Adatara Volcano, northeast Japan: 1. Geochemical constraints on their origin. *Lithos*, **22**, 135–158.

FUJINAWA, A. 1990. Tholeiitic and calc-alkaline magma series at Adatara Volcano, northeast Japan: 2. Mineralogy and phase relations. *Lithos*, **24**, 217–236.

FURUKAWA, Y. 1993. Magmatic processes under arcs and formation of the volcanic front. *Journal of Geophysical Research*, **98**, 8309–8319.

FURUKAWA, Y. & TATSUMI, Y. 1999. Melting of a subducting slab and production of high-Mg andesite magmas; unusual magmatism in SW Japan at 13–15 Ma. *Geophysical Research Letters*, **26**, 2271–2274.

GHIORSO, M.S. & SACKS, R.O. 1995. Chemical mass transfer in magmatic processes; IV, a revised and internally consistent thermodynamic model for the interpolation and extrapolation of liquid–solid equilibria in magmatic systems at elevated temperatures and pressures. *Contributions to Mineralogy and Petrology*, **119**, 197–212.

GILL, J.B. 1981. *Orogenic Andesites and Plate Tectonics*. Springer, Berlin.

GREEN, T.H. 1994. Experimental studies of trace-element partitioning applicable to igneous petrogenesis – Sedona 16 years later. *Chemical Geology*, **117**, 1–36.

GROVE, T.L. & BAKER, M.B. 1984. Phase equilibrium controls on the tholeiitic versus calc-alkaline differentiation trends. *Journal of Geophysical Research*, **89**, 3253–3274.

HAURI, E.H., WAGNER, T.P. & GROVE, T.L. 1994. Experimental and natural partitioning of Th, U, Pb and other trace elements between garnet, clinopyroxene and basaltic melts: trace-element partitioning with application to magmatic processes. *Chemical Geology*, **117**, 149–166.

HELZ, R.T. 1987. Differentiation behavior of Kilauea Iki lava lake, Kilauea volcano, Hawaii: an overview of past and current work. *In*: MYSEN, B.O. (ed.) *Magmatic Processes: Physiochemical*

Principles. Special Publications, Geochemical Society, University Park, PA, **1**, 241–258.

HESS, P.C. 1989. *Origins of Igneous Rocks*. Harvard University Press, Cambridge, MA.

HILDRETH, W. 1981. Gradients in silicic magma chambers: implications for lithospheric magmatism. *Journal of Geophysical Research*, **86**, 10 153–10 192.

HIROSE, K. 1997. Melting experiments on lherzolite KLB-1 under hydrous conditions and generation of high-magnesian andesitic melts. *Geology*, **25**, 42–44.

HOFMANN, A.W. & WHITE, W.M. 1982. Mantle plumes from ancient oceanic crust. *Earth and Planetary Science Letters*, **57**, 421–436.

HOLLOWAY, J.R. & BURNHAM, C.W. 1972. Melting relations of basalt with equilibrium water pressure less than total pressure. *Journal of Petrology*, **13**, 1–29.

HUNTER, A.G. & BLAKE, S. 1995. Petrogenetic evolution of a transitional tholeiitic–calc-alkaline series: Towada volcano, Japan. *Journal of Petrology*, **36**, 1579–1605.

JAKES, P. & GILL, J. 1970. Rare earth elements and the island arc tholeiitic series. *Earth and Planetary Science Letters*, **9**, 17–28.

JAKES, P. & WHITE, A.J.R. 1969. Structure of the Melanesian arcs and correlation with distribution of magma types. *Tectonophysics*, **8**, 223–236.

JAKES, P. & WHITE, A.J.R. 1970. K/Rb ratios of rocks from island arcs. *Geochimica et Cosmochimica Acta*, **34**, 849–856.

JENNER, G.A. 1981. Geochemistry of high-Mg andesites from Cape Vogel, Papua New Guinea. *Chemical Geology*, **33**, 307–332.

JOHNSON, M.C. & PLANK, T. 1999. Dehydration and melting experiments constrain the fate of subducted sediments. *Geochemistry Geophysics Geosystems*, **1**, 1999GC000014.

KAMBER, B.S. & COLLERSON, K.D. 2000. Zr/Nb systematics of ocean island basalts reassessed; the case for binary mixing. *Journal of Petrology*, **41**, 1007–1021.

KAWAMOTO, T. 1992. Dusty and honeycomb plagioclase; indicators of processes in the Uchino stratified magma chamber, Izu Peninsula, Japan. *Journal of Volcanology and Geothermal Research*, **49**, 191–208.

KAY, R.W. & KAY, S.M. 1993. Delamination and delamination magmatism. *Tectonophysics*, **219**, 177–189.

KAY, R.W., SUN, S.S. & LEE-HU, C.N. 1978. Pb and Sr isotopes in volcanic rocks from the Aleutian Islands and Probilof Islands, Alaska. *Geochimica et Cosmochimica Acta*, **42**, 263–273.

KELEMEN, P.B. 1995. Genesis of high Mg-andesites and the continental crust. *Contributions to Mineralogy and Petrology*, **120**, 1–19.

KEPPLER, H. 1996. Constraints from partitioning experiments on the composition of subduction-zone fluids. *Nature*, **380**, 237–240.

KOGISO, T., TATSUMI, Y. & NAKANO, S. 1997. Trace element transport during dehydration processes in the subducted oceanic crust; 1, experiments and implications for the origin of ocean island basalts. *Earth and Planetary Science Letters*, **148**, 193–205.

KUNO, H. 1959. Origin of Cenozoic petrographic provinces of Japan and surrounding areas. *Bulletin Volcanologique*, **20**, 37–76.

KUNO, H. 1960. High-alumina basalt. *Journal of Petrology*, **1**, 121–145.

KUNO, H. 1966. Lateral variation of basalt magma type across continental margins and island arcs. *Bulletin Volcanologique*, **29**, 195–222.

KURASAWA, H., FUJINAWA, A. & LEEMAN, W.P. 1985. Calc-alkaline and tholeiitic rock series magmas coexisting within volcanoes in Japanese island arcs. Strontium isotopic study. *Journal of the Geological Society of Japan*, **92**, 255–268.

KURODA, N., SHIRAKI, K. & URANO, H. 1978. Boninite as a possible calc-alkalic primary magma. *Bulletin Volcanologique*, **41**, 563–575.

KUSHIRO, I. 1969. The system forsterite–diopside–silica with and without water at high pressures. *American Journal of Science*, **267A**, 269–294.

KUSHIRO, I. & SATO, H. 1978. Origin of some calc-alkalic andesites in Japanese islands. *Bulletin Volcanologique*, **41**, 576–585.

MACDONALD, G.A. & KATSURA, T. 1964. Chemical composition of Hawaiian lavas. *Journal of Petrology*, **5**, 82–133.

MARSH, B.D. 1979. Island arc development; some observations, experiments, and speculations. *Journal of Geology*, **87**, 687–713.

MARSH, B.D. & CARMICHAEL, I.S.E. 1974. Benioff Zone magmatism. *Journal of Geophysical Research*, **79**, 1196–1206.

MARTIN, H. 1986. Effect of steeper Archean geothermal gradient on geochemistry of subduction-zone magmas. *Geology*, **14**, 753–756.

MARTIN, H. 1987. Petrogenesis of Archaean trondhjemites, tonalites and granodiorites from eastern Finland; major and trace element geochemistry. *Journal of Petrology*, **28**, 921–953.

MASUDA, Y. & AOKI, K. 1979. Trace element variations in the volcanic rocks from the Nasu Zone, Northeast Japan. *Earth and Planetary Science Letters*, **44**, 139–149.

MEEN, J.K. 1987. Formation of shoshonites from calcalkaline basalt magmas; geochemical and experimental constraints from the type locality. *Contributions to Mineralogy and Petrology*, **97**, 333–351.

MIYASHIRO, A. 1974. Volcanic rock series in island arcs and active continental margins. *American Journal of Science*, **274**, 321–355.

MYSEN, B.O. & BOETTCHER, A.L. 1975. Melting of a hydrous mantle; I, phase relations of natural peridotite at high pressures and temperatures with controlled activities of water, carbon dioxide, and hydrogen. *Journal of Petrology*, **16**, 520–548.

NOCKOLDS, S.R. & ALLEN, R. 1953. The geochemistry of some igneous rock series [Part 1]. *Geochimica et Cosmochimica Acta*, **4**, 105–142.

NOTSU, K. 1983. Strontium isotope composition in volcanic rocks from the northeast Japan Arc. *Journal of Volcanology and Geothermal Research*, **18**, 531–548.

OSBORN, E.F. 1959. Role of oxygen pressure in the crystallization and differentiation of basaltic magma. *American Journal of Science*, **257**, 609–647.

PEACOCK, S.M. 1990. Numerical simulation of metamorphic pressure-temperature–time paths and fluid production in subducting slabs. *Tectonics*, **9**, 1197–1211.

PEACOCK, S.M. 1993. The importance of blueschist: eclogite dehydration reactions in subducting oceanic crust. *Geological Society of America Bulletin*, **105**, 684–694.

PERTERMANN, M. & HIRSCHMANN, M.M. 1999. Partial melting experiments on a MORB-like pyroxenite at 3.0 GPa and 1300–1500°C. *Eos, Transactions, American Geophysical Union*, **80**, 1112.

PLANK, T. & LANGMUIR, C.H. 1993. Tracing trace elements from sediment input to volcanic output at subduction zones. *Nature*, **362**, 739–743.

POLI, S. & SCHMIDT, M.W. 1995. H_2O transport and release in subduction zones: experimental constraints on basaltic and andesitic systems. *Journal of Geophysical Research*, **100**, 22 299–22 314.

RAPP, R.P. & WATSON, E.B. 1995. Dehydration melting of metabasalt at 8–32 kbar: implications for continental growth and crust–mantle recycling. *Journal of Petrology*, **36**, 891–931.

RAPP, R.P., SHIMIZU, N., NORMAN, M.D. & APPLEGATE, G.S. 1999. Reaction between slab-derived melts and peridotite in the mantle wedge: experimental constraints at 3.8 GPa. *Chemical Geology*, **160**, 335–356.

ROGGENSACK, K., WILLIAMS, S.N., SCHAEFER, S.J. & PARNELL, R.A.J. 1996. Volatiles from the 1994 eruptions of Rabaul; understanding large caldera systems. *Science*, **273**, 490–493.

RUDNICK, R.L. 1995. Making continental crust. *Nature*, **378**, 571–578.

RUDNICK, R.L. & FOUNTAIN, D.M. 1995. Nature and composition of the continental crust: a lower crustal perspective. *Reviews of Geophysics*, **33**, 267–309.

RUDNICK, R.L., BARTH, M., HORN, I. & MCDONOUGH, W.F. 2000. Rutile-bearing refractory eclogites; missing link between continents and depleted mantle. *Science*, **287**, 278–281.

RYABCHIKOV, I.D. & BOETTCHER, A.L. 1980. Experimental evidence at high pressure for potassic metasomatism in the mantle of the Earth. *American Mineralogist*, **65**, 915–919.

SAKUYAMA, M. 1979. Evidence of magma mixing; petrological study of Shirouma–Oike calc-alkaline andesite volcano, Japan. *Journal of Volcanology and Geothermal Research*, **5**, 179–208.

SAKUYAMA, M. 1981. Petrological study of the Myoko and Kurohime volcanoes, Japan; crystallization sequence and evidence for magma mixing. *Journal of Petrology*, **22**, 553–583.

SAKUYAMA, M. & NESBITT, R.W. 1986. Geochemistry of the Quaternary volcanic rocks of the northeast Japan arc. *Journal of Volcanology and Geothermal Research*, **29**, 413–450.

SCHMIDT, M.W. & POLI, S. 1998. Experimentally based water budgets for dehydrating slabs and consequences for arc magma generation. *Earth and Planetary Science Letters*, **163**, 361–379.

SHIMOZURU, D. & KUBO, N. 1983. Volcano spacing and subduction. *In*: SHIMOZURU, D. & YOKOYAMA, I. (eds) *Arc Volcanism: Physics and Tectonics*. Terra Publications, Tokyo, 141–151.

SHIREY, S.B. & HANSON, G.N. 1984. Mantle-derived Archaean monzodiorites and trachyandesites. *Nature*, **310**, 222–224.

SISSON, T.W. & BRONTO, S. 1998. Evidence for pressure-release melting beneath magmatic arcs from basalt at Galunggung, Indonesia. *Nature*, **391**, 833–886.

SISSON, T.W. & GROVE, T.L. 1993. Experimental investigations of the role of H_2O in calc-alkaline differentiation and subduction zone magmatism. *Contributions to Mineralogy and Petrology*, **113**, 143–166.

SISSON, T.W. & LAYNE, G.D. 1993. H_2O in basalt and basaltic andesite glass inclusions from four subduction-related volcanoes. *Earth and Planetary Science Letters*, **117**, 619–635.

STALDER, R., FOLEY, S.F., BREY, G.P. & HORN, I. 1998. Mineral–aqueous fluid partitioning of trace elements at 900–1200°C and 3.0–5.7 GPa: new experimental data for garnet, clinopyroxene, and implications for mantle metasomatism. *Geochimica et Cosmochimica Acta*, **62**, 1781–1801.

STERN, R.A. & HANSON, G.N. 1991. Archean high-Mg granodiorite; a derivative of light rare earth element-enriched monzodiorite of mantle origin. *Journal of Petrology*, **32**, 201–238.

SUGIMURA, A. 1960. Zonal arrangement of some geophysical and petrological features in Japan and its environs. *Journal of the Faculty of Science, University of Tokyo, Section 2: Geology, Mineralogy, Geography, Geophysics*, **12**, 133–153.

SUN, S.S. & MCDONOUGH, W.F. 1989. Chemical and isotopic systematics of oceanic basalts; implications for mantle composition and processes *In*: SAUNDERS, A.D. & NORRY, M.J. (eds) *Magmatism in the Ocean Basins*. Geological Society, London, Special Publications, **42**, 313–345.

TAKAHASHI, E. 1986. Genesis of calc-alkali andesite magma in a hydrous mantle–crust boundary; petrology of lherzolite xenoliths from the Ichinomegata Crater, Oga Peninsula, Northeast Japan; Part II. *Journal of Volcanology and Geothermal Research*, **29**, 355–395.

TAMURA, Y. 1994. Genesis of island arc magmas by mantle-derived bimodal magmatism: evidence from the Shirahama Group, Japan. *Journal of Petrology*, **35**, 619–645.

TAMURA, Y. & NAKAMURA, E. 1996. The arc lavas of the Shirahama Group, Japan: Sr and Nd isotopic data indicate mantle-derived bimodal magmatism. *Journal of Petrology*, **37**, 1307–1319.

TAMURA, Y., TATSUMI, Y., ZHAO, D., KIDO, Y. & SHUKUNO, H. 2002. Hot fingers in the mantle wedge: new insights into magma genesis in subduction zones. *Earth and Planetary Science Letters*, **197**, 107–118.

TATSUMI, Y. 1981. Melting experiments on a high-magnesian andesite. *Earth and Planetary Science Letters*, **54**, 357–365.

TATSUMI, Y. 1982. Origin of high-magnesian andesites in the Setouchi volcanic belt, southwest Japan; II, melting phase relations at high pressures. *Earth and Planetary Science Letters*, **60**, 305–317.

TATSUMI, Y. 1989. Migration of fluid phases and genesis of basalt magmas in subduction zones. *Journal of Geophysical Research*, **94**, 4697–4707.

TATSUMI, Y. 2000*a*. Continental crust formation by crustal delamination in subduction zones and complementary accumulation of the enriched mantle I component in the mantle. *Geochemistry Geophysics Geosystems*, **1**, 2000GC000094.

TATSUMI, Y. 2000*b*. Slab melting: its role in continental crust formation and mantle evolution. *Geophysical Research Letters*, **27**, 3941–3944.

TATSUMI, Y. 2003. Some constraints on arc magma genesis. *In*: EILER, J. (ed.) *The Subduction Factory*. American Geophysical Union Monographs, in press.

TATSUMI, Y. & EGGINS, S. 1995. *Subduction Zone Magmatism*. Blackwell, Cambridge, MA.

TATSUMI, Y. & ISHIZAKA, K. 1981. Existence of andesitic primary magma; an example from southwest Japan. *Earth and Planetary Science Letters*, **53**, 124–130.

TATSUMI, Y. & ISHIZAKA, K. 1982. Magnesian andesite and basalt from Shodo-Shima Island, southwest Japan, and their bearing on the genesis of calc-alkaline andesites. *Lithos*, **15**, 161–172.

TATSUMI, Y. & ISOYAMA, H. 1988. Transportation of beryllium with H_2O at high pressures; implication for magma genesis in subduction zones. *Geophysical Research Letters*, **15**, 180–183.

TATSUMI, Y. & KOGISO, T. 1997. Trace element transport during dehydration processes in the subducted oceanic crust; 2, Origin of chemical and physical characteristics in arc magmatism. *Earth and Planetary Science Letters*, **148**, 207–221.

TATSUMI, Y. & NAKAMURA, N. 1986. Composition of aqueous fluid from serpentinite in the subducted lithosphere. *Geochemical Journal*, **20**, 191–196.

TATSUMI, Y., HAMILTON, D.L. & NESBITT, R.W. 1986. Chemical characteristics of fluid phase released from a subducted lithosphere and origin of arc magmas; evidence from high-pressure experiments and natural rocks. *Journal of Volcanology and Geothermal Research*, **29**, 293–309.

TATSUMI, Y., SAKUYAMA, M., FUKUYAMA, H. & KUSHIRO, I. 1983. Generation of arc basalt magmas and thermal structure of the mantle wedge in subduction zones. *Journal of Geophysical Research*, **88**, 5815–5825.

TATSUMI, Y., TAMURA, Y. & NAKASHIMA, T. 2002. The petrology and geochemistry of calc-alkaline andesites on Shodo-Shima Island, SW Japan. *Journal of Petrology*, **43**, 3–16.

TAYLOR, S.R. & MCLENNAN, S.M. 1985. *The Continental Crust: its Composition and Evolution*. Blackwell, Oxford.

TAYLOR, S.R. & MCLENNAN, S.M. 1995. The geochemical evolution of the continental crust. *Reviews of Geophysics*, **33**, 241–265.

TERA, F., BROWN, L., MORRIS, J., SACKS, I.S., KLEIN, J. & MIDDLETON, R. 1986. Sediment incorporation in island-arc magmas; inferences from ^{10}Be. *Geochimica et Cosmochimica Acta*, **50**, 535–550.

TILLEY, C.E. 1950. Some aspects of magmatic evolution. *Quarterly Journal of the Geological Society of London*, **106**, 37–61.

TURCOTTE, D.L. 1989. Geophysical processes influencing the lower continental crust. *In*: MEREU, R.F., MUELLER, S. & FOUNTAIN, D.M. (eds) *Properties and Processes of Earth's Lower Crust*. American Geophysical Union Monographs, **51**, 321–329.

UMINO, S. & KUSHIRO, I. 1989. Experimental studies on boninite petrogenesis. *In*: CRAWFORD, A.J. (ed.) *Boninites and Related Rocks*. Unwin Hyman, London, 89–111.

VAN DER LAAN, S.R., FLOWER, M.F.J. & VAN GROOS, A.F.K. 1989. Experimental evidence for the origin of boninites: near-liquidus phase relations to 7.5 kbar. *In*: CRAWFORD, A.J. (ed.) *Boninites and Related Rocks*. Unwin Hyman, London. 112–147.

VEIZER, J. & COMPSTON, W. 1976. $^{87}Sr/^{86}Sr$ in Precambrian carbonates as an index of crustal evolution. *Geochimica et Cosmochimica Acta*, **40**, 905–914.

VOGT, P.R. 1974. Volcanic spacing, fractures, and thickness of the lithosphere. *Earth and Planetary Science Letters*, **21**, 235–252.

WADA, K. 1981. Contrasted petrological relations between tholeiitic and calc-alkalic series from Funagata volcano, northeast Japan. *Journal of the Japanese Association of Mineralogists, Petrologists and Economic Geologists*, **76**, 215–231.

WAGER, L.R. & DEER, W.A. 1939. Geological investigations in East Greenland. Part III. The petrology of the Skaergaard intrusion, Kangerdlugssuaq, East Greenland. *Meddelelser om Gronland*, **105**, 4, 335.

WATSON, E.B., BEN, O.D., LUCK, J.M. & HOFMANN, A.W. 1987. Partitioning of U, Pb, Cs, Yb, Hf, Re and Os between chromian diopsidic pyroxene and haplobasaltic liquid. *Chemical Geology*, **62**, 191.

WEAVER, B.L. 1991. The origin of ocean island basalt end-member compositions; trace element and isotopic constraints. *Earth and Planetary Science Letters*, **104**, 381–397.

WILSON, M. 1989. *Igneous Petrogenesis*. Unwin Hyman, London.

YASUDA, A., FUJII, T. & KURITA, K. 1994. Melting phase relations of an anhydrous mid-ocean ridge basalt from 3 to 20 GPa; implications for the behavior of subducted oceanic crust in the mantle. *Journal of Geophysical Research*, **99**, 9401–9414.

YODER, H.S.J. & TILLEY, C.E. 1962. Origin of basalt magmas; an experimental study of natural and synthetic rock systems. *Journal of Petrology*, **3**, 342–532.

YOSHIDA, T. & AOKI, K.-I. 1984. Geochemistry of major and trace elements in the Quaternary volcanic rocks from northeast Honshu, Japan. *Science Reports, Tohoku University, Series 3: Mineralogy, Petrology, Economic Geology*, **16**, 1–34.

ZHAO, D., XU, Y., WIENS, D.A., DORMAN, L.M., HILDEBRAND, J. & WEBB, S.C. 1997. Depth extent of the Lau back-arc spreading center and its relation to subduction processes. *Science*, **278**, 254–257.

ZINDLER, A. & HART, S. 1986. Chemical geodynamics. *Annual Review of Earth and Planetary Sciences*, **14**, 493–571.

A general model of arc–continent collision and subduction polarity reversal from Taiwan and the Irish Caledonides

PETER D. CLIFT [1], HANS SCHOUTEN[1] & AMY E. DRAUT[2]

[1]*Department of Geology and Geophysics, Woods Hole Oceanographic Institution, Woods Hole, MA 02543, USA (e-mail: pclift@whoi.edu)*

[2]*Woods Hole Oceanographic Institution–Massachusetts Institute of Technology Joint Program in Oceanography, Woods Hole, MA 02543, USA*

Abstract: The collision of the Luzon Arc with southern China represents the best example of arc–continent collision in the modern oceans, and compares closely with the Early Ordovician accretion of the Lough Nafooey arc of Connemara, Ireland, to the passive margin of Laurentia. We propose a general model for steady-state arc–continent collision in which arc crust is progressively added to a passive margin during a process of compression, metamorphism and magmatism lasting 3–10 Ma at any one location on the margin. Depending on the obliquity of the angle of collision, the timing of active collision may be diachronous and long-lived along the margin. Magmatism accompanying accretion can be more enriched in incompatible trace elements than average continental crust, contrasting with more depleted magmatism prior to collision. Accretion of a mixture of depleted and enriched arc lithologies to the continental margin allows the continental crust to grow through time by arc–passive margin collision events. During the collision the upper and middle arc crust are detached from the depleted ultramafic lower crust, which is subducted along with the mantle lithosphere on which the arc was founded. Rapid (2–3 Ma) exhumation and gravitational collapse of the collisional orogen forms the Okinawa and South Mayo Troughs in Taiwan and western Ireland, respectively. These basins are filled by detritus eroded from the adjacent collision zone. During subsequent subduction polarity reversal, continuous tearing and retreat of the oceanic lithosphere along the former continent–ocean transition provides space for the new subducting oceanic plate to descend without need for breaking of the original slab.

Arc–continent collision is an important part of the Wilson cycle by which intra-oceanic arc crust is added to the margins of continents, and is probably the principle method by which the continental crust is built, at least during the Phanerozoic (e.g. Taylor & McLennan 1985; Rudnick & Fountain 1995). The recognition in average continental crust of a depletion in Nb relative to other trace elements, a feature long associated with subduction magmatism (Pearce 1982), represents compelling evidence to suggest a subduction-related origin to the continental crust. However, the link between arc and continental crustal genesis is not a simple one, because intra-oceanic arc crust is too mafic and too light rare earth element (LREE)-depleted to be a direct analogue for continental crust (e.g. Kay 1985; Ellam & Hawkesworth 1988). Although some oceanic arcs do seem to produce melts with more LREE-enriched chemistries (e.g. Yogodzinski & Kelemen 1998), these are typically geographically restricted and are often in areas of unusual tectonics, such as the oblique convergence in the western Aleutians.

Active continental margins

The role of active continental, rather than oceanic, margins in generating new continental crust is presently unclear. Although isotopic and geochemical evidence from such arcs does suggest that much of the output involves reworking existing continental crust (e.g. Rogers & Hawkesworth 1989), there must be some component of new melt extraction from the mantle. However, high rates of tectonic erosion limit the amount of new material added to the continent by magmatism at many active margins. Subduction accretion is limited to regions where there is major influx of clastic sediments from the continents. Reymer & Schubert (1984) estimated that globally only 23–33 km^3 of new melt were added every Ma per km of active margin during the Phanerozoic, but Holbrook *et al.* (1999) estimated higher rates of 55–82 km^3 Ma^{-1} km^{-1} for the Aleutians. Similarly, Suyehiro *et al.* (1996) indicated long-term, average accretion rates of 66 km^3 Ma^{-1} km^{-1} in the Izu arc. In comparison, estimated long-term rates of crustal erosion

From: LARTER, R.D. & LEAT, P.T. 2003. *Intra-Oceanic Subduction Systems: Tectonic and Magmatic Processes.* Geological Society, London, Special Publications, **219**, 81–98. 0305-8719/03/$15.00

reach 70 km^3 Ma^{-1} km^{-1} in Tonga (Clift & MacLeod 1999), 96 km^3 Ma^{-1} km^{-1} in Costa Rica (Vannucchi *et al.* 2001), 96 km^3 Ma^{-1} km^{-1} in Honshu (von Huene & Lallemand 1990), 37–54 km^3 Ma^{-1} km^{-1} in northern Chile (von Huene *et al.* 1999) and 109 km^3 Ma^{-1} km^{-1} along the Peruvian margin (Clift *et al.* 2003*b*). These rates imply net loss of continental crust in such settings. In contrast, the accretion of an oceanic arc to a continental margin represents a clear net gain in crust, and may be the most efficient mechanism for producing new continental crust, at least since the Precambrian.

Arc crustal composition

If oceanic arcs are, in fact, the building blocks of the continental crust then our inability to relate the compositions of the two might reflect a misunderstanding of the bulk composition of one or the other. One possible solution is that the bulk crust of oceanic arcs is actually much more silicic and LREE-enriched than is apparent from the volcanic cover. This hypothesis was supported by the identification of lower seismic velocity, high silica, middle crust in the Izu arc (Suyehiro *et al.* 1996). However, subsequent seismic refraction experiments in other oceanic arcs have failed to identify similar siliceous crustal units (e.g. Aleutians; Holbrook *et al.* 1999). Accreted island arc crustal sections in orogenic belts also argue against significant volumes of siliceous mid crust in oceanic arcs (e.g. Kohistan: Miller & Christensen 1994; Talkeetna, Alaska: Pearcy *et al.* 1990). Although the volcaniclastic apron surrounding the arc volcanic front may be up to 6 km thick and dominated by silica-rich tephra (e.g. Tonga: Tappin *et al.* 1994), these sediments do not show LREE enrichment (Clift 1995) and cannot shift the bulk composition of the accreted crust in the manner required to transform it into LREE-enriched continental crust.

The significance of arc–continent collision

If oceanic arc crust does not have the same composition as the continental crust then it is possible that the process of its accretion to the continent is instrumental in effecting a transformation. Draut & Clift (2001) showed that during collision of the oceanic Lough Nafooey arc, now exposed in the Caledonides of western Ireland, to the passive margin of Laurentia during the early Ordovician (*c.* 480–470 Ma), volcanism underwent a transition from mafic and LREE-depleted to siliceous and LREE-enriched. This syncollisional volcanism (represented by the Tourmakeady Group in South Mayo, Ireland) is more

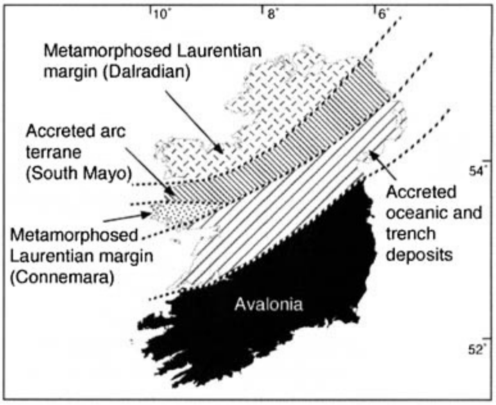

Fig. 1. Large-scale terrane map of Ireland, showing the major units discussed in this study.

enriched than both average continental crust and the local Dalradian continental basement of the adjacent Connemara region (Leake 1989; Draut *et al.* 2002), and could thus form crust with a chemistry close to normal continental values when mixed with the older oceanic arc crust, which is similar to modern western Pacific oceanic arcs in being mafic and LREE-depleted (Clift & Ryan 1994).

In this paper we investigate the tectonics of arc–continent collision, a process which would allow the enriched upper and middle crust to be detached from the ultramafic, probably depleted, lower crust (Draut *et al.* 2002), and transferred from the oceanic plate to the continental margin. To do this we draw on evidence from the Caledonides in western Ireland (Figs 1 and 2), but also from the active arc–continent collision zone in Taiwan (Fig. 3).

Birth of active continental margins

Regions of arc–passive margin collision are not only areas where new crust is being added to the continents, but are also the birth places of active continental margins. The mechanical difficulties of breaking cold, stiff oceanic lithosphere imply that transforming a rifted passive margin into an active margin would be difficult unless initiated by arc–continent collision (e.g. Casey & Dewey 1984). Collision of an oceanic arc with a passive margin, followed by a subduction polarity reversal, represents a simple method for initiating active margins. In contrast, even when a passive margin is placed in regional compression a new subduction zone does not seem to form readily. The passive margins of southern India have probably been in compression since the start of

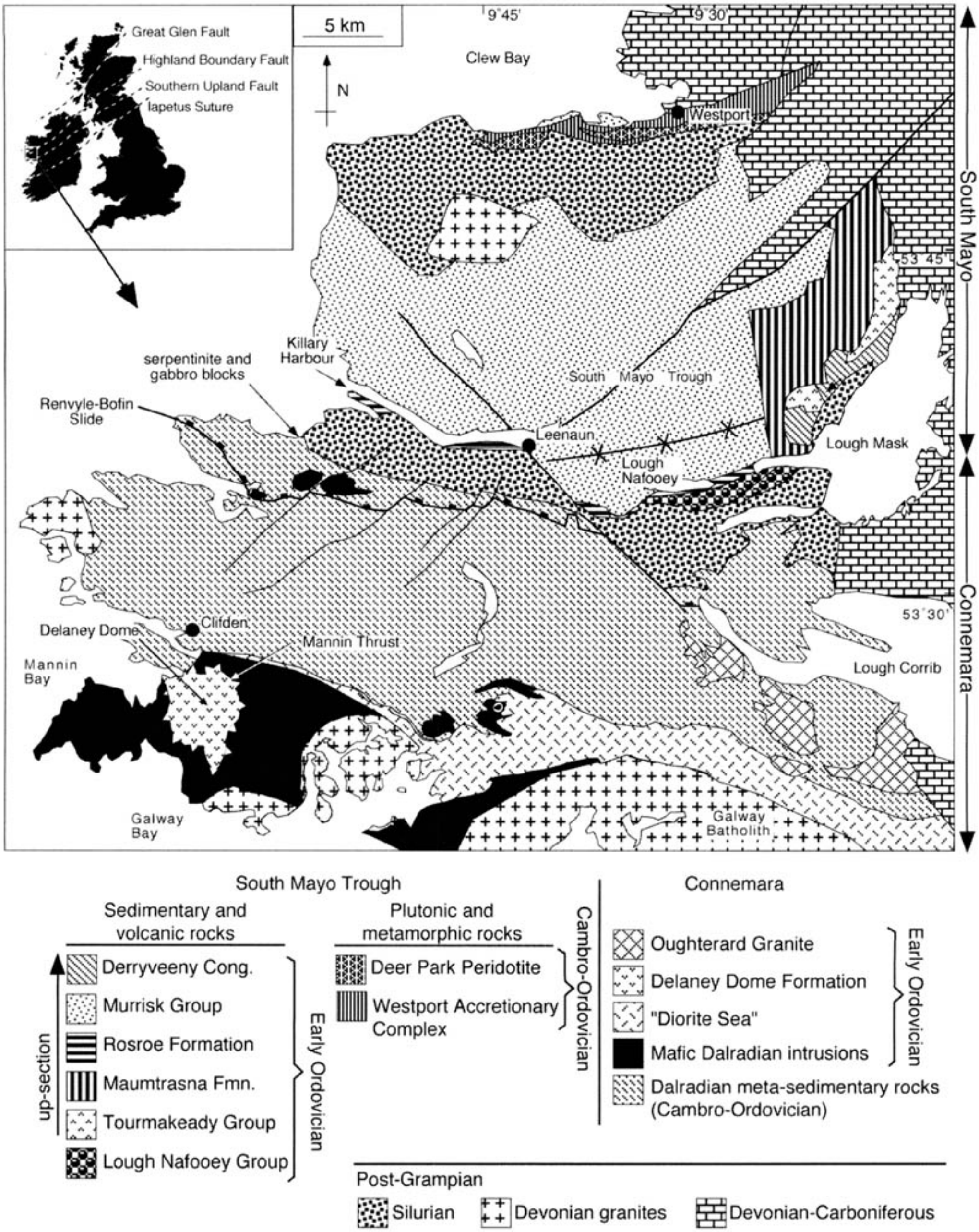

Fig. 2. Geological map of South Mayo Trough and Connemara, Ireland (after Draut & Clift 2001), showing the thick successions of clastic sedimentary rocks, largely deposited during exhumation of the high-grade Connemara terrane after collision of the Lough Nafooey arc with the Laurentian passive margin.

the India-Asia collision (i.e. >45 Ma; Rowley 1996), but still show no tendency to form a new subduction zone. Instead compression has caused long-wavelength buckling of the Indian Ocean crust south of India (Cochran 1990).

Taiwan and Connemara as examples of arc accretion

Despite its importance to large-scale tectonic and geochemical issues, the nature of

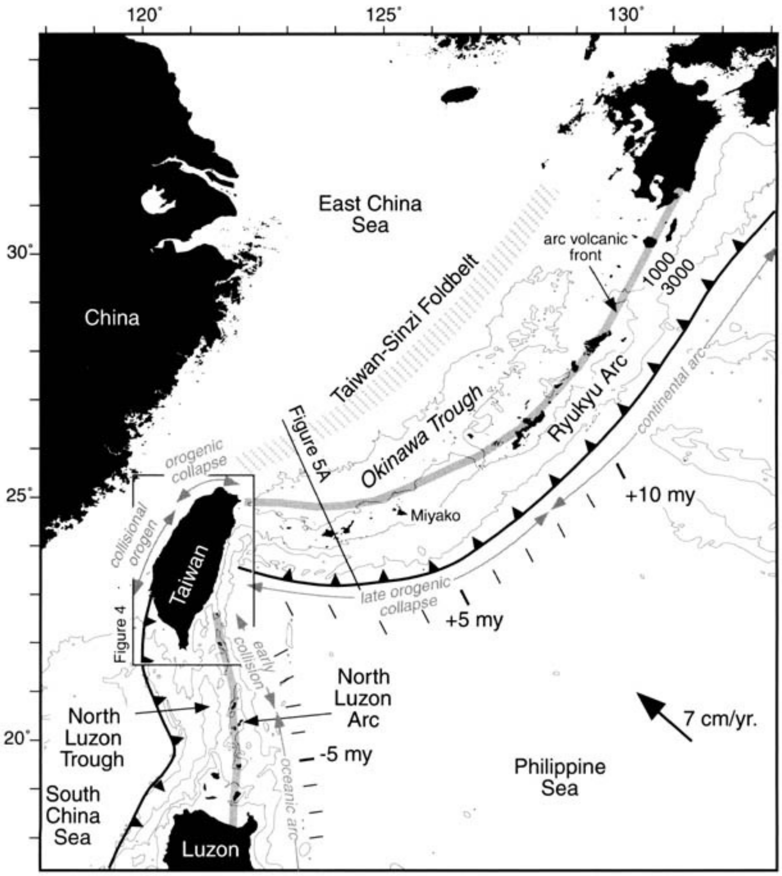

Fig. 3. Bathymetric map of the Taiwan region showing the collisional orogen, the opposing subduction polarities and the Okinawa Trough opening in the wake of orogenic collapse. Bathymetry in metres.

arc–continent collision remains poorly understood. The collision of the Luzon Arc with the South China margin is probably the simplest example of this phenomenon in the modern oceans (Fig. 3). There, the N-trending Luzon arc, located above an E-dipping South China slab, has been in oblique collision with the continental margin of China since the mid-Miocene (Teng 1990; Sibuet *et al.* 2002). Taiwan straddles the active collision zone; in the eastern (post-collisional) part of this region, subduction polarity reversal has resulted in the northward subduction of the Philippine Sea Plate under the Ryukyu Arc, on the active Eurasian margin (Fig. 3).

The seismicity and strain involved in arc–continent collision may be assessed from the active Taiwan example. However, many deep-level processes are not exposed there and the influence of along-strike variations is difficult to assess. As a result, we also consider a deeply exhumed example from the Irish Caledonides, where an orogenic core of metamorphosed passive margin sediments (called the Dalradian) and associated mid-crustal arc intrusions is exposed in Connemara (Harris 1993; Harris *et al.* 1994). Associated arc lavas and forearc sedimentary rocks are exposed across a strike-slip boundary in the adjacent South Mayo terrane, deformed into a broad syncline known as the South Mayo Trough (Dewey & Shackleton 1984; Dewey & Ryan 1990) (Fig. 2). Plate tectonic reconstructions based on faunal and palaeomagnetic evidence (e.g. McKerrow *et al.* 1991), as well as the identification of a late Ordovician–Silurian accretionary complex south of the accreted arc terrane (Leggett *et al.* 1983), demonstrate that, although the accretion of the Lough Nafooey arc to Laurentia did produce significant orogeny, there is clear evidence for continued subduction and a long-lived oceanic tract offshore Laurentia for *c.* 50 Ma after collision. This therefore implies that Early Ordovician arc–continent collision was followed by a subduction polarity reversal, after which a N-dipping slab descended below the newly active Laurentian margin.

Connemara provides a record of collision between a short section of the oceanic Lough Nafooey arc and the Laurentian margin during the Early Ordovician Grampian Orogeny (475–462 Ma ago; Soper *et al.* 1999). The sediment and tuff record in the adjacent South Mayo Trough is well preserved, with little post-orogenic deformation or metamorphism. The temporal evolution of an intra-oceanic arc can thus be traced through the full collisional process, with ages constrained by high-resolution radiometric dating of plutons (Cliff *et al.* 1996; Tanner *et al.* 1997; Friedrich *et al.* 1999*a*, *b*) and graptolite biostratigraphy of sediments and volcanic rocks (Graham *et al.* 1989). In both the modern Taiwan example and the ancient Irish example, arc–continent collision was followed by subduction polarity reversal and the development of a continental arc and back-arc trough at a newly active continental margin.

Orogenic exhumation

In the arc–continent collision zones of Taiwan and western Ireland, the latter stages of collision involve uplift and exhumation of the new orogenic belt. In both Taiwan and Connemara proximity of the passive margin to the trench resulted in development of an accretionary complex composed of the passive margin sediments, which subsequently underwent regional high-grade metamorphism during arc–continent collision and orogeny. Because of continued convergence, subduction magmatism intruded the metamorphic sequences associated with the arc crust. Not surprisingly, the geochemistry of intrusions and volcanic rocks emplaced during collision shows significant reworking of the continental crust (Leake 1989; Defant *et al.* 1990; Draut & Clift 2001). In Connemara *c.* 10 Ma of such magmatism and peak metamorphism was followed by a rapid transition to uplift, extension and associated cooling (Friedrich *et al.* 1999*a*, *b*), probably linked to low-angle detachment faulting (e.g. Williams & Rice 1989). The N-dipping Renvyle–Bofin Slide in northern Connemara (Fig. 2) has been proposed as one of the major structures that allow the metamorphosed passive margin sediments to be rapidly exhumed (Wellings 1998). Extension on the Renvyle–Bofin Slide appears to be synchronous with low-angle thrusting of the Dalradian metamorphosed sediments over the syncollisional arc volcanic units (Draut & Clift 2002). Such exhumation is similar to that proposed for the High Himalaya in the India–Asia collision zone through synchronous motion on the South Tibetan Detachment and Main Central Thrust (Burchfiel *et al.* 1992).

The location of the extensional detachment faults in Connemara is not well defined. Williams & Rice (1989) proposed S-dipping detachment faulting in southern Connemara. In both proposed models of faulting in Connemara the metamorphic contrast across the structures is not high, despite strong evidence of shearing, implying that while they may be conjugate to the major detachment these are not the major controlling structures. In Connemara it is possible that the major detachment surfaces have been largely eroded or buried by post-orogenic sedimentation. They may be further obscured by strike-slip faulting that has transferred the Connemara terrane south of the suture zone (Hutton 1987), thus truncating the original outcrop. North of Clew Bay where the Dalradian is repeated in North Mayo, a major structure, the Achillbeg Fault, running E–W along the north coast of Clew Bay, separates low-grade rocks of the South Mayo Trough from the higher-grade rocks of the North Mayo Dalradian. Although this structure was reactivated during the later Palaeozoic (D. Chew pers. comm. 2002), it is of the correct magnitude and sense of motion to be a major orogenic exhumation structure. Comparison with the exposed detachment surfaces in the Basin and Range Province of western North America with the situation in Connemara raises the possibility that the unconformity on which Silurian marine sediments overlie Dalradian metamorphic rocks represents an eroded detachment surface. It is of note that blocks of serpentinite are mapped along and close to the unconformity, but nowhere else in the Connemara Dalradian. We have also found sheared gabbro blocks immediately below the unconformity, southwest of Killary Harbour (Fig. 2). A possible explanation for these relationships is that lower crustal and mantle lithologies were entrained along a deep-rooted detachment fault, which brought them to the surface, where they were subsequently transgressed during the Silurian.

In northern Taiwan, the zone of active collision between Luzon and southern China, there is rapid uplift and exhumation of high-grade metamorphic rocks associated with major detachment faults, such as the Lishan Fault (Fig. 4) (Teng 1990, 1996; Lee *et al.* 1997). Most

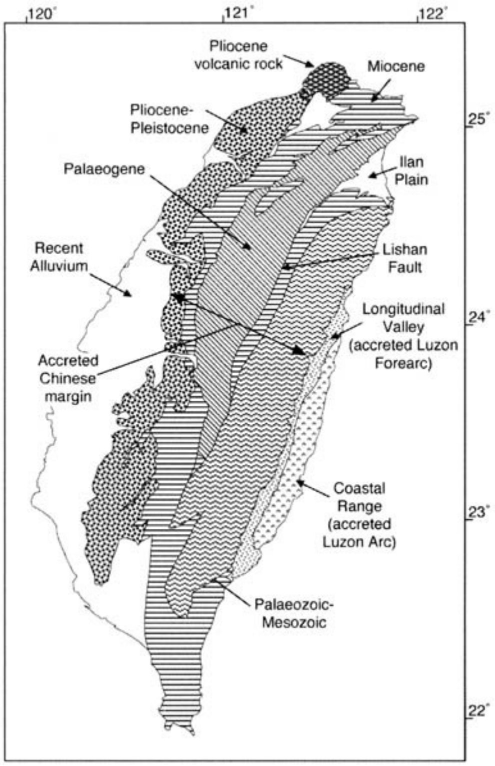

Fig. 4. Schematic geological map of Taiwan showing the major tectonic units discussed in the text.

of the Taiwan Orogen appears to represent deformed and metamorphosed sediments from the south China passive margin, and thus represents equivalents of the Connemara Dalradian metasedimentary rocks, the deformed passive margin of Laurentia. East of the Longitudinal Valley Fault in Taiwan, the Luzon arc is represented as a tectonically shortened section in the Coastal Range (Dorsey 1992). Lundberg *et al.* (1997) have shown that the northern equivalents of the North Luzon Trough, the principal basin in the Luzon forearc, are overthrust by eastward (arcward)-directed thrusting of the accretionary complex south of Taiwan, so that the old Luzon forearc is buried under syncollisional basins, represented onshore by the Longitudinal Valley (Lundberg & Dorsey 1990) (Fig. 4).

Sedimentary response to arc collision

The sedimentary response to uplift, extension and exhumation of the Connemara Dalradian collisional orogen is preserved in the South Mayo Trough directly north of Connemara, where much of the total sedimentary thickness (4.4 km out of 6.8 km) is synchronous with, or post-dates, the tectonic exhumation (Fig. 5). It is a crucial observation that, although the South Mayo Trough represents the pre-collisional forearc to the Lough Nafooey arc (Dewey & Shackleton 1984; Dewey & Ryan 1990), the sediment does appear to span the collision and metamorphism of the Laurentian margin (Dalradian passive margin sediments). In that context, the lack of a recognized unconformity between pre- and syncollisional sedimentary and volcaniclastic sequences in the northern limb of the syncline that forms the South Mayo Trough is curious. The completeness of the section in South Mayo Trough requires that the collision did not cause strong deformation to the point of uplift above sea level in this area. The forearc basin to the Lough Nafooey arc persisted as an active depositional environment throughout the time of collision and orogeny.

On the south limb of the South Mayo Trough post-collisional sediments (Rosroe and Maumtrasna formations) are in unconformable contact with underlying syncollisional volcanic units (Tourmakeady Formation). Their sandstone and conglomeratic facies testify to rapid erosion of a metamorphosed Laurentian (Dalradian) source (Dewey & Mange 1999; Clift *et al.* 2003*a*). Proximal sedimentation in the Rosroe and Maumtrasna units occurs in the form of submarine and alluvial fans, which pass upward into similar facies of the Murrisk Group (Archer 1984; Pudsey 1984).

The actively extending Okinawa Trough, located north of the southward-facing Ryukyu arc and adjacent to the Taiwan collision zone, is analogous to the South Mayo Trough of western Ireland in containing tuffs and proximal volcaniclastic deposits that succeed arc–continent collision. Depositional environments similar to those of the Rosroe and Maumtrasna formations are noted in northern Taiwan, where alluvial fans derive material from the Coastal Ranges that is then transported onto the Ilan Plain and subsequently offshore into the Okinawa Trough. Lundberg & Dorsey (1990) demonstrate that rapid Quaternary uplift of the Coastal Range has resulted in proximal sedimentation in the Longitudinal Valley overlying the accreted arc and forearc. Although erosion rates in the Coastal Range are high, those in the higher and more extensive Central Range of the Taiwan Orogen are greater and contribute the bulk of the sediment reaching the Okinawa Trough (Lundberg & Dorsey 1990). Although the Longitudinal Valley Basin is rather narrower

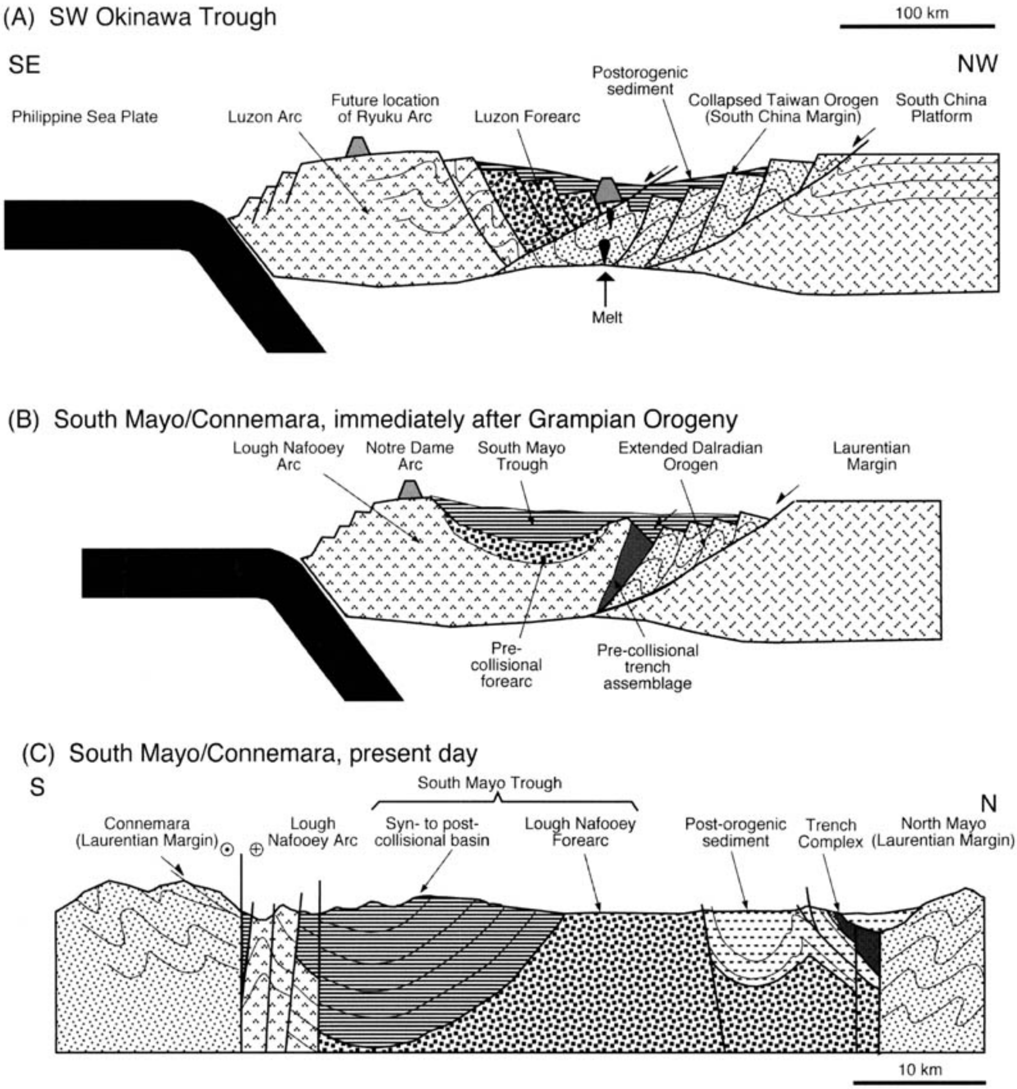

Fig. 5. (**a**) Schematic cross-section across the southern Okinawa Trough, compared to (**b**) across South Mayo Trough immediately after the Grampian Orogeny, and (**c**) in the present day, showing the similar units

than South Mayo Trough (5–10 km v. 20–25 km), the same progression of pre-collisional forearc basin overlain by syncollisional basin is recognized in both examples. The provenance of both South Mayo Trough and Okinawa Trough sediment deposited in the wake of collision thus reflects substantial reworking of the deformed continental passive margin (Clift *et al.* 2003). In the Okinawa Trough, like the South Mayo Trough, sedimentation rates are initially very high, exceeding 325 cm ka^{-1} in Ocean Drilling Program (ODP) Site 1202 in the southern Okinawa Trough (Salisbury *et al.* 2002). In comparison, Graham *et al.* (1989) estimate 1350 m of Rosroe sediment deposited during the lower Artus graptolite zone, 464–467 Ma, according to the time scale of Tucker & McKerrow (1995); a mean rate of 45 cm ka^{-1}.

Magmatic evolution

The development of volcanic chemistry during arc–continent collision in South Mayo was highlighted by Draut & Clift (2001) and used to demonstrate that the bulk chemical character of the arc crust could be changed by the collision from mafic and LREE-depleted material into a composition close to the continental crustal average. These authors noted that there was a strong temporal correlation between changes in volcanic chemistry and the tectonic evolution of the arc. In particular, a change was noted in the trace element chemistry of tuffs in the post-collisional Rosroe Formation compared to the underlying syncollisional Tourmakeady Volcanic Formation, i.e. during the extensional collapse of the Grampian Orogeny. The wide range in high-field-strength element (HFSE) enrichment of the Rosroe Formation and its temporal equivalents suggested the presence of a heterogeneous mantle source region, while differences in the Nd isotopic character of the Tourmakeady and Rosroe Formation (ε_{Nd} rises from –14.1 to –8.3) are consistent with the advection of fresh mantle material under the arc and a reduced contribution from continental crust compared to the magmatism during the compressional deformation that accompanied Tourmakeady Group development. Although the eruptive centres of the tuffs found in the Rosroe Formation and Murrisk Group are not now exposed, they must have been close to the South Mayo Trough in view of the great thickness of the tuffs (2–3 m) and their commonly welded texture.

In central Taiwan, where Chinese continental margin lithosphere continues to subduct eastward under the deformed Luzon arc, the collision orogen grows to its maximum height. However, neither arc volcanism nor deep earthquakes have been observed and, hence, the plate interaction remains obscure beneath the orogen. However, in northern Taiwan, subduction polarity has reversed, and the Philippine Sea Plate is underthrusting the arc. Here magmatism is controlled by lithospheric stretching and by melting associated with the new Ryukyu subduction zone (Teng *et al.* 2000) (Pliocene volcanic province, Fig. 4). As extension has advanced in the southern Okinawa Trough the volcanism has become focused in the centre of the basin near the active extension. In this area it is of note that there is no separate development of a Ryukyu arc. In practice, the Okinawa Trough volcanism represents the new arc volcanic front, which only comes to lie over the non-volcanic forearc ridge in the central and northern Ryukyu arc where active extension has ceased (Fig. 3).

In northern Taiwan and the southern Okinawa Trough magmatism during orogenic collapse is marked by LREE-enriched chemistries (Chen *et al.* 1995). Figure 6 shows that in terms of high-field-strength (HFSE) and

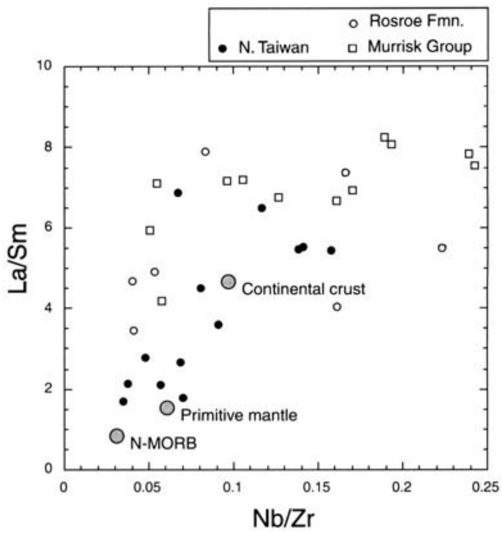

Fig. 6. Volcanic rocks emplaced during the orogenic extension that follows peak metamorphism in both Taiwan and South Mayo have compositions more enriched in HFSEs and LREEs than MORB and in some cases than the continental crust (values from Rudnick & Fountain 1995).

rare earth elements the Taiwan and Irish volcanic rocks are very enriched and several exceed the bulk continental crustal values (Wang *et al.* 1999; Chung *et al.* 2000). This requires fractional crystallization in addition to crustal assimilation in order to explain the range of REE compositions (Draut & Clift 2001). The same is true of the syncollisional mafic intrusions that penetrate the Connemara mid-crust (Draut *et al.* 2002), and implies that the depleted cumulate residue that would have been produced during the fractionation must have been located in the lower crust. Nd isotope data were employed by Draut *et al.* (2002) to quantify the amount of crustal recycling in the collisional magmatism, with no more than 35% of the Connemara mid-crustal plutons being generated by crustal melting. The syncollisional Tourmakeady Volcanic Formation showed *c.* 80–90% of crustal recycling, but still required an enriched liquid that must originally have derived from the mantle, to explain the high LREE enrichment and the Nd isotope character of the volcanism.

Lower crustal–mantle tectonics

The chemical change in the magmatism seen in Taiwan and Mayo, coincident with the start of orogenic extension and exhumation (represented by the Okinawa Trough and Rosroe

Formation and Murrisk Group tuffs, respectively), implies a link between these processes. We suggest that detachment of the upper and middle arc crust from the lower crust and mantle root may be part of this process. Orogenic extension is caused by the topographic load and weakness of the orogenic belt. Once the compressive forces that form the mountains are released from the thrust belt, due to renewed subduction following polarity reversal, there will be a tendency for the stack to collapse and extend under its own weight. In the case of Taiwan, the motion of the Philippine Sea Plate towards the northwest will keep the Taiwan Orogen under compression until the generation of the new SE-facing subduction zone in the Ryukyu Arc immediately north of the present Taiwan Orogen. Once the new Ryukyu Trench has been lengthened, as the new subduction zone migrates to the southwest, then the southern edge of the orogenic stack is unconstrained by compression. The trench thus forms a free space into which the orogen can collapse, triggering extension of the deformed arc and passive margin sequences (Teng 1996). The load of the Taiwan Orogen causes flexure of the underlying Chinese continental crust (Wang 2001; Yu & Chou 2001). Where the load slides southward away from the margin's edge in northern Taiwan, the continental crust quickly rebounds and regains much of its normal thickness (Rau &Wu 1995) as a result of the extensional collapse of the orogen (Teng 1996).

Lower crustal delamination?

An additional cause of uplift and extension may be the loss of a dense, ultramafic arc lower crustal root. The relative densities of arc lower crust and the upper mantle are strongly dependent on composition, temperature and pressure. However, the cumulate lithologies that comprise the lower crustal residue of crystal fractionation are sometimes denser than the upper mantle (cf. Bird 1979; Houseman *et al.* 1981; Kay & Kay 1993; Jull & Kelemen 2001) and might be susceptible to detachment from the shallower crust and re-incorporation back into the mantle. Jull & Kelemen (2001) considered this loss to be a convective instability of a viscous fluid and suggested that delamination is most likely to occur on geological timescales <10 Ma where geothermal gradients are high and where the lower crustal lithologies are gabbronorites or cumulate ultramafics. Given the arc-collisional setting and high orogenic heat flow it is possible that the conditions predicted by Jull & Kelemen (2001) to favour delamination may be met in Connemara and Taiwan. However, because neither the Connemara nor the Taiwan arc lower crusts are now exposed we cannot prove that these lithologies were present during collision. Instead, we can only argue that the chemical evidence for fractional crystallization (Draut & Clift 2001; Draut *et al.* 2002) is consistent with the generation of cumulates, while the chemical similarity of the South Mayo arc volcanic rocks to those in modern western Pacific arcs does argue that gabbronorites or ultramafic cumulates were probably developed.

The density of lower crustal cumulates exceeds that of typical mantle by 50–250 kg m^{-3} (Jull & Kelemen 2001), and implies a surface uplift of 90–360 m for a hypothetical lower crustal loss of 6 km. This uplift represents <10% of the total topography in the Taiwan Orogen and consequently uplift following lower crustal loss cannot be expected to trigger extensional collapse by itself.

Lower crustal subduction?

Consideration of the strength profile of synorogenic arc crust suggests that the dense lower crust might be susceptible to detachment from the shallower levels during collision. Figure 7 shows a hypothetical strength profile based on the observed lithologies in the Connemara–Mayo arc (after Kohlstedt *et al.* 1995). Crustal strength might be expected to increase with depth in the upper crust, in the manner normally attributed to Byerlee's law. Once the temperatures have reached a threshold of *c.* 200°C, at *c.* 12 km depth, the quartz-bearing lithologies that make up much of the Connemara middle crust will be ductile and weak (Carter 1976), as shown by the common ductile folding seen in the Dalradian. In contrast, ultramafic rocks of the lower crust and mantle lithosphere are stronger because of their olivine-dominated plasticity (Kohlstedt & Goetze 1974; Kirby & Kronenberg 1987; Kohlstedt *et al.* 1995). The weak zone in the middle crust could form a detachment surface, allowing the dense, strong lower layers to be removed and subducted along with the upper mantle when subduction is renewed following polarity reversal. The presence of trace amounts of water in arc lithospheric mantle will reduce the thickness of the strong lower layer compared to anhydrous mantle (Hirth & Kohlstedt 1996), but will not eliminate the strength contrast between upper and lower crust in the orogen.

Although unequivocal demonstration of Ordovician delamination is impossible, seismic reflection evidence from across the Iapetus

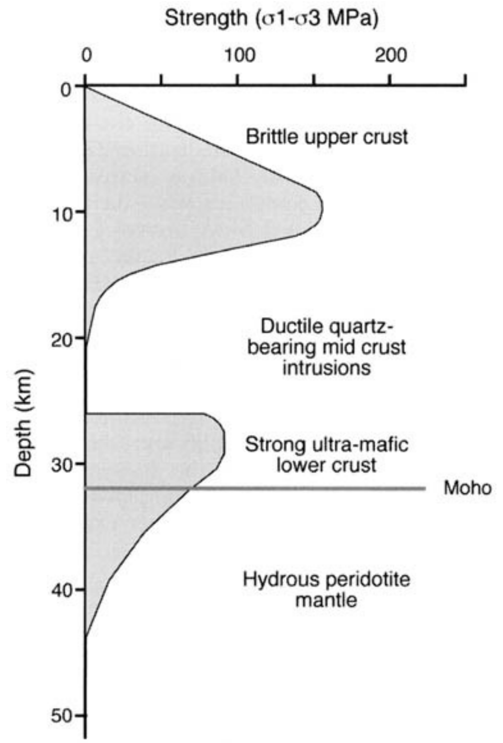

Fig. 7. Schematic diagram showing the strength of the collisional arc lithosphere. The upper part of the plate is cool and brittle, getting stronger with depth in accordance with Byerlee's law. The middle crust is hot and weak due to the quartz-dominated lithologies and forms a natural décollement surface within the plate. In contrast, ultramafic cumulates are likely to be strong in the lower crust, with no mechanical break between them and the mantle tectonite rocks below.

suture in Ireland does not show the presence of fast, reflective lower crust (Klemperer 1991), such as might be expected from the seismic character of modern oceanic island arcs (e.g. Holbrook *et al.* 1999). In addition, Klemperer (1991) noted that the Connemara block appeared to have shallow roots and lie above a low-angle thrust fault, implying that the Dalradian had been removed from its lower crustal roots at some stage in the past.

There has been no previous suggestion of lower crustal delamination in Taiwan, but the rapid change to extension and exhumation just prior to gravitational collapse of the orogen in northern Taiwan, culminating in active basin extension and volcanism forming the Okinawa Trough, suggests that this process may be active here too. Volcanism during extensional collapse follows the pattern of South Mayo in being very enriched in LREEs and with widely scattered HFSE ratios (Wang *et al.* 1999; Chung *et al.* 2000), although not quite reaching the highest values measured in Ireland. Focal mechanism solutions of earthquakes associated with the North Luzon arc indicate slip partitioning with thrusting perpendicular to the trench between the arc and the South China Sea Plate to the west, while strike-slip motion occurs between the arc and the Philippine Sea Plate to the east. This implies that the upper part of the North Luzon arc is already decoupled from the Philippine Sea Plate long before the arc collides with the Chinese margin. Consequently, when collision occurs the Philippine Sea Plate is incapable of dragging the upper arc crust down with it beneath the Chinese margin, and detachment of the lower crust and upper mantle from the middle and upper arc crust will occur.

Formation of post-orogenic basins

Letouzey & Kimura (1985) suggested that the Okinawa Trough opened due to shearing generated by the extrusion of crust east from the Taiwan collision zone. However, most earlier studies favour the Okinawa Trough opening as a back-arc basin to the Ryukyu arc (Sibuet *et al.* 1987), with extension driven by trench suction and slab roll-back. In the back-arc model the volcanism now located in the southern Okinawa Trough represents a northward-propagating spreading centre, while most of the northern trough is still rifting. Volcanism is focused at the Ryukyu arc until drawn to the back-arc spreading axis by the active extension.

In contrast, in our revised model we follow the suggestion of Teng (1996) that the Okinawa Trough is created by extensional collapse of the Taiwan Orogen, after which time it remains relatively inactive. There is no activity in the Ryukyu arc near Taiwan because subduction of the Philippine Sea slab has only just begun in that area. Shinjo (1999) notes that mid-Miocene volcanic rocks from the southern Ryukyu arc are not subduction related, but instead similar to intra-plate volcanism seen in China. Such an observation implies propagation of the subduction-related Ryukyu volcanic front into the area since that time, a hypothesis supported by recent geochemical evidence from the southernmost Okinawa Trough (Chung *et al.* 2000). In our model the Okinawa Trough becomes increasingly younger to the south, the opposite of the roll-back model, in which the Okinawa Trough spreading centres are propagating into the basin away from Taiwan. Importantly, mid–late

Miocene (6–9 Ma; Letouzey & Kimura 1985) extension ages are recorded in the northern Okinawa Trough, while recent faulting in the trough adjacent to Taiwan cuts the thick sedimentary sequences right to the seafloor, observations consistent with a collapse origin of the trough. The basement to the Okinawa Trough is inferred to be the extended remnants of the Taiwan Orogen and the accreted Luzon arc (Fig. 5).

Although the South Mayo Trough includes large volumes of post-collisional sediment, similar to the Okinawa Trough, there is a real difference between the two basins in that South Mayo does not preserve evidence for intrabasinal magmatism or continued normal faulting. The large thicknesses of sediment preserved do require significant tectonic subsidence of the basin. The South Mayo area may represent a special area in the Caledonian Orogen because the pre-collisional forearc is not deformed and overthrust in the fashion seen for the North Luzon Trough. The reason for this might be related to irregularities in the trend of the Laurentian margin, with the South Mayo Trough having been located opposite an embayment in the continental margin.

Subduction polarity reversal

Evidence for a subduction polarity flip is clear in the Irish Caledonides, where the S-dipping slab beneath the Lough Nafooey arc (Dewey & Ryan 1990; Clift & Ryan 1994) became a N-dipping subduction zone after the Grampian Orogeny. After arc–continent collision there is regional evidence for N-dipping subduction under a Laurentian margin that was previously passive, forming the Bronson Hill arc in the northern Appalachians and the subduction accretionary complex in Northern Ireland and the Scottish Southern Uplands (Leggett *et al.* 1983; Karabinos *et al.* 1998; Van Staal *et al.* 1998) (Fig. 1).

The difference in subduction polarity on either side of Taiwan is clear from the location of the volcanic arcs and active seismicity (Teng *et al.* 2000). A space problem arises when trying to accommodate two oceanic slabs that dip in opposite directions in close proximity to one another. Teng *et al.* (2000) suggested that subduction polarity reversal under Taiwan can be achieved through the break-off of the subducting South China slab at depth, in the manner suggested by Davies & von Blanckenburg (1995). Although a possibility, there is little evidence for this process. If this model is correct this might represent a non-steady-state condition that followed the initial, very oblique collision between the Luzon Arc and the South China margin. Alternatively, the snapping slab model implies that the collision process operates in a series of discontinuous steps.

We here suggest a mechanism by which subduction polarity is reversed by a gradual tearing and roll-back of the South China oceanic slab towards the west, thereby opening a gap through which the newly subducting Philippine Sea Plate can descend (Fig. 8). A progressive tearing of the lithosphere, approximately along the old rifted continent–ocean transition, allows the collision zone and accompanying polarity reversal to migrate continuously westward along the continental margin. In this way, space is made for the new subducting slab with no need for episodic slab break-off. Sibuet *et al.* (2002) present seismic reflection data from across the South Chinese passive margin west of Taiwan showing a sharp tectonic discontinuity between an old accretionary complex and an arc–forearc complex. This lineament and its northeast extension beneath Taiwan limits to the northwest the deep earthquakes associated with the subduction of the South China Sea beneath the Philippine Sea Plate. This discontinuity represents a pre-existing weakness in the crust, facilitating the westward tearing we envisage.

Evidence for a tearing of the Chinese margin crust at the point of collision was first proposed by Lallemand *et al.* (1997). More recently, Lallemand *et al.* (2001) postulated that a tear along the ocean–continent boundary accommodated the subduction of the northwestward progressing Philippine Sea Plate beneath the Chinese margin. Lallemand *et al.* (2001) highlighted the importance of a relatively short NW-trending tear into the continental margin crust across northern Taiwan that would explain the northward termination of mountain building and a number of other geological and geophysical observations. According to Lallemand *et al.* (2001), this tear fault forms the northeastern edge of a piece of Chinese continental margin subducting southeastward beneath Taiwan and the Philippine Sea Plate. Using seismic tomographic data, Lallemand *et al.* (2001) inferred that the piece of subducted Chinese continental plate reaches the 650 km upper-mantle velocity discontinuity.

In this study we emphasize the dynamic nature of the Taiwan collision zone and rifting Okinawa Trough as a westward-migrating zone of collision and active lithospheric tearing. The rate of westward migration of the lithospheric tear is determined by the rate of oblique collision between the Philippine Sea Plate on which the Luzon arc is located and South China.

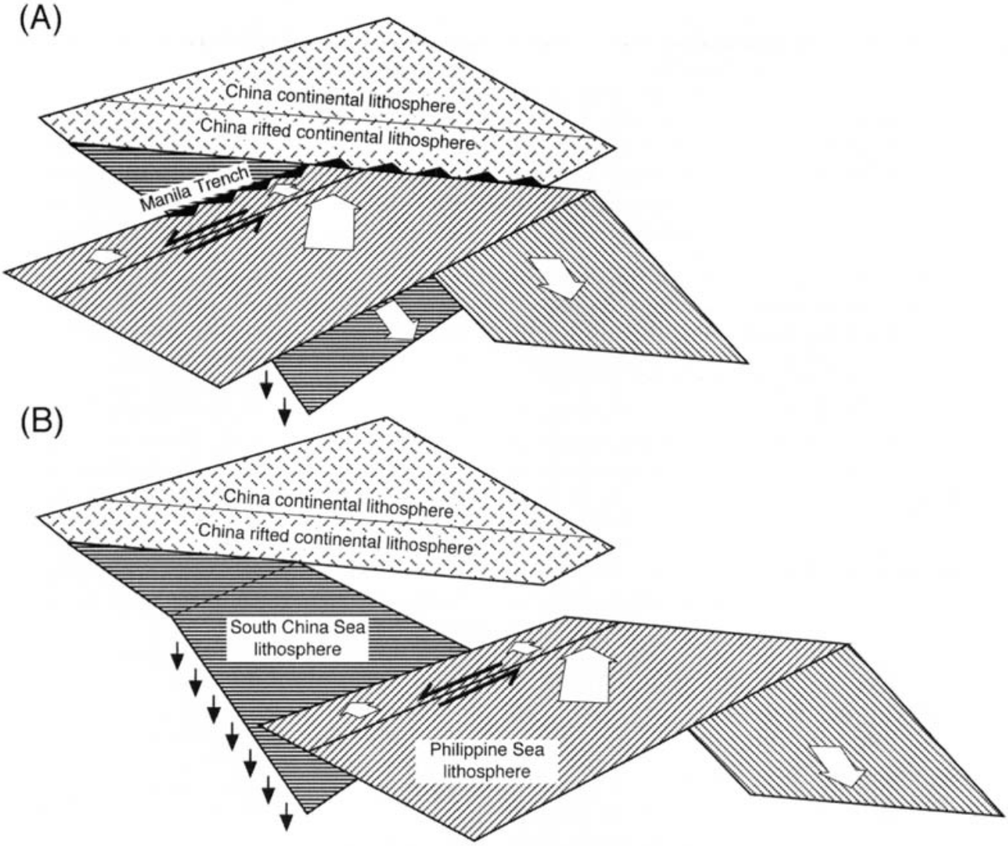

Fig. 8. Tectonic cartoon of (**A**) the modern plate tectonic setting around Taiwan with the Luzon arc free to move semi-independently of the oceanic Philippine Sea Plate as a result of slip-partitioning along large strike-slip faults. (**B**) Shows the behaviour of the Chinese Plate by schematically removing the Philippine Sea Plate. The progressive tearing of the original South China passive margin and the westward retreat of the Manila Trench provides a space into which the newly subducting Philippine slab can descend. This model removes the need to snap the old Chinese slab to allow subduction polarity reversal to occur.

We recognize that gravitational instability of a dense slab would eventually cause failure of the slab at depth (e.g. Shemenda 1994), but a break in the slab is not required in our model to make space for the new slab to descend, as has been required by previous models of subduction polarity reversal (e.g. Shemenda 1994; Konstantinovskaya 1999). Teng *et al.* (2000), like Lallemand *et al.* (1997), recognized the lithospheric tearing along the ocean–continent boundary, but instead emphasized the importance of slab break-off in facilitating subduction polarity reversal.

The progressive tearing of the Eurasian lithosphere implies that polarity reversal may happen more quickly than previously thought, because the time needed for the lowest part of the slab to break off and sink far enough through the mantle to make space for a new slab is no longer a rate-limiting step. As a result collision, orogeny and subduction polarity flip may now be understood to occur within 10 Ma (Table 1). In Connemara rapid orogeny was documented by the radiometric work of Friedrich *et al.* (1999*a*, *b*) to peak at 475–463 Ma, consistent with a rapid reversal of subduction polarity. Friedrich *et al.* (1999*a*) also noted that the age of the Grampian–Taconic Orogeny is similar along strike in Canada and New England (Cawood *et al.* 1995; Swinden *et al.* 1997; Karabinos *et al.* 1998), implying that the arc was oriented in a less oblique fashion to the continental margin than the Luzon arc is relative to China and/or that the plates were moving at higher relative speeds.

An important consequence of our new model is that the Philippine Sea Plate slides laterally

Table 1. *Comparison of the Taiwan and Connemara collisional orogenies showing the equivalent units and phases of activity during each accretion event. Duration of orogeny may be variable and dependent on the plate velocity and obliquity of collision*

Time ↑	Taiwan	Mayo–Connemara	Duration (Ma)
Continental arc	Volcanic front stabilizes on the Ryukyu Arc. End of extension in Okinawa Trough	Formation of Southern Uplands Accretionary Complex and eruption of Notre Dame Arc	
Late orogenic collapse	Submarine volcanism, rapid sedimentation and active extension in Okinawa Trough	Eruption of Mweelrea Tuffs; deposition of Glennumera and Mweelrea formations	3–5
Orogenic collapse	Rapid cooling of Taiwan Orogen, motion on Lishan Fault, sedimentation on Ilan Plain. Volcanism in N Taiwan	Rapid cooling of Connemara Dalradian, motion on Renvyle–Bofin Slide, intrusion of Oughterard Granite, deposition of Rosroe and Derrylea formations	2–3
Collisional orogen	Metamorphism of South China margin sediments in Taiwan Mountains	Metamorphism of Dalradian metasediments, eruption of Tourmakeady Formation rhyolites and intrusion of Connemara gabbros and quartz diorites	3–10
Early collision	Formation of submarine accretionary complex	Westport Complex formation, sedimentation of Letterbrock–Sheefry formations, and eruption of Derry Bay Formation	2–4
Oceanic arc	Andesitic–basaltic Luzon arc volcanism	Basaltic Lough Nafooey Group arc volcanism	

westward under the southern Okinawa Trough, so that an oceanic slab is present instantaneously as the subduction zone propagates. If this lateral sliding into the gap were not occurring then it would take >3 Ma for the tip of the new slab to migrate from the trench to a location under the Okinawa Trough (Fig. 9).

Continuous arc accretion

Neither Teng *et al.* (2000) nor Lallemand *et al.* (2001) describe the Taiwan Orogeny as migrating southwestward along the Chinese continental margin, although they do describe the arc–continent intersection migrating that way. Most authors seem to suggest that Taiwan has been an orogeny that started at that particular location, rather than as a migrating collision point. Prior to Luzon–China collision Lallemand *et al.* (2001) propose a transform fault connecting the Manila and Ryukyu trenches that was consumed *c.* 8 Ma ago when the North Luzon arc hit the Chinese passive margin. It is following this collision, close to the location of modern Taiwan, that the tear fault propagates westward along the continent–ocean transition. According to Lallemand *et al.* (2001), major mountain building in Taiwan started at 3–5 Ma ago following the detachment of the Philippine Sea Plate slab beneath the central and northern Ryukyu arc and the northwestward propagation of a tear fault into the Chinese passive margin. These events allowed the continental Chinese margin plate to subduct beneath the Luzon Arc. Rifting of the southern Okinawa Trough started at *c.* 3 Ma north of Miyako and propagated westward during the Quaternary, as a consequence of slab pull exerted by the Philippine Sea Plate slab.

Sibuet *et al.* (2002) propose that the Luzon Arc started to form progressively after 15 Ma ago, since which time the Luzon Arc subducted beneath Eurasia as part of the Philippine Sea Plate. In this model it is only from 6 to 9 Ma ago that the Luzon arc resisted subduction and collided with the Chinese margin, composed of the extinct portion of a proto-Ryukyu forearc, arc and back-arc system (Sibuet & Hsu 1997). It is this collision that is considered to have uplifted the ancestral mountain belt located at the present-day position of the southwestern Okinawa Trough (Sibuet *et al.* 1998; Hsiao *et al.* 1999). Sibuet *et al.* (2002) note a structural kink in southern Taiwan between the N–S trend of the Luzon Arc and the more SW–NE trend of Taiwan. These authors suggest that this boundary has existed since 15 Ma and was located at the base of the Chinese margin. The kink

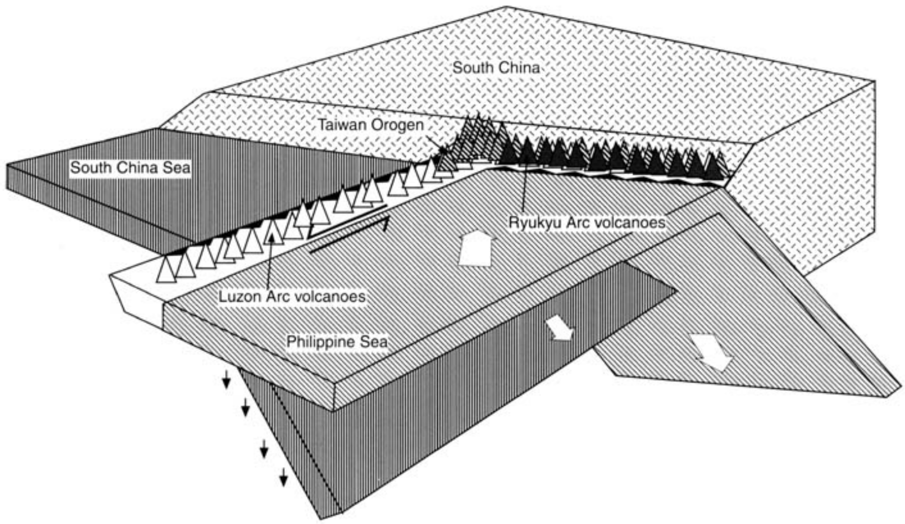

Fig. 9. Model of continuous arc accretion to a passive continental margin, in which the igneous edifice of the Luzon arc is accreted to the margin, deformed in the Taiwan Orogen and then overlain by sediments of the Okinawa Trough or volcanic rocks of the new Ryukyu Arc as the thrust stack collapses.

presently divides the Luzon Arc into two segments. South of the kink the subduction of the South China Sea is still active and the Luzon Arc is still growing as attested by the emplacement of present-day intra-oceanic rocks on the islands (Yang *et al.* 1996; Maury *et al.* 1998). North of the kink collision between the Luzon Arc and the Chinese margin is active.

In our revised model (Fig. 9) the modern Taiwan Orogen is not the product of a collisional, tearing or slab detachment event, but represents the modern point of an ongoing and continuous collision of the Luzon Arc and the Chinese margin. The recognition of a continuous Taiwan–Sinzi folded zone under the southeast edge of the East China Sea (Hsiao *et al.* 1999) would suggest a continuous migration of the orogen from Sinzi *c.* 12 Ma ago to the present Taiwan.

Conclusions

The oblique collision of the Luzon and Lough Nafooey arcs with the South China and Laurentian passive margins, respectively, resulted in a similar sequence of tectonic and magmatic events initially involving compressional orogeny and highly enriched magmatism lasting <10 Ma. Collision is followed by extensional collapse of the orogen and variably enriched magmatism. Collapse is the result of the generation of a new trench and the release of the compressive forces of the collision zone. Possible loss of the arc ultramafic lower crust would enhance uplift and exhumation, and facilitate subsequent orogenic collapse. The upper arc crust is accreted to the continental margin, a process that may be accomplished through detachment in the ductile middle crust from the ultramafic lower crust and mantle lithosphere that forms the western edge of the subducting Philippine Sea Plate. This mechanism appears to be the principal mode of continental crustal growth in the modern oceans.

Orogenic extensional collapse culminates in the formation of a basin (the Okinawa and South Mayo Troughs) located above the deformed passive margin and forearc of the accreted oceanic arc. This basin is rapidly infilled by several kilometres of coarse clastic material eroded from the adjacent collisional orogen and by minor tuff and lava units. Each basin is located adjacent to a new continental volcanic arc formed by subduction polarity reversal. Magmatism associated with this new system can become focused into the basin during active extension, but subsequently occurs in a stable trenchward setting above the subducting slab. Unlike other back-arc basins these basins are not formed by trench forces. As the collision point migrates along the margin, the oceanic lithosphere that adjoins the original passive margin tears to form a gap through which the newly subducting oceanic lithosphere can descend. Arc–continent collision can thus be viewed as a continuous and migrating process that does not require breaking or catastrophic loss of the subducting slab in order to accommodate the plate motions. This in turn allows collision, orogeny and polarity reversal to be completed within 10 Ma.

David Chew, Nobu Shimizu, Matthew Jull, Greg Hirth, Anke Friedrich and Peter Kelemen provided stimulating discussion on this work, which was supported by Woods Hole Oceanographic Institution. We wish to thanks Tony Lee and Tim Byrne for help and advice in the preparation of this paper. The work benefited from careful reviews by Yoshi Tatsumi, Conall MacNiocaill and Rob Larter. This is WHOI contribution # 10772.

References

ARCHER, J.B. 1984. Clastic intrusions in deep-sea fan deposits of the Rosroe Formation, Lower Ordovician, western Ireland. *Journal of Sedimentary Petrology*, **54**, 1197–1205.

BIRD, P. 1979. Continental delamination and the Colorado plateau. *Journal of Geophysical Research*, **84**, 7561–7571.

BURCHFIEL, B.C., CHEN, Z., HODGES, K.V., LIU, Y., ROYDEN, L.H., DENG, C. & XU, J. 1992. *The South Tibetan Detachment System, Himalayan Orogen: Extension Contemporaneous With and Parallel to Shortening in a Collisional Mountain Belt*. Geological Society of America, Special Papers, **269**.

CARTER, N.L. 1976. Steady state flow of rocks. *Reviews of Geophysics and Space Physics*, **14**, 301–360.

CASEY, J.F. & DEWEY, J.F. 1984. Initiation of subduction zones along transform and accreting plate boundaries, triple-junction evolution, and forearc spreading centres – implications for ophiolitic geology and obduction. *In*: GASS, I.G., LIPPARD, S.J. & SHELTON, A.W. (eds) *Ophiolites and Oceanic Lithosphere*. Geological Society, London, Special Publications, **13**, 269–290.

CAWOOD, P.A., VAN GOOL, J.A.M. & DUNNING, G.R. 1995. Collisional tectonics along the Laurentian margin of the Newfoundland Appalachians. *In*: HIBBARD, J.P., VAN STAAL, C.R. & CAWOOD, P.A. (eds) *Current Perspectives in the Appalachian–Caledonian Orogen*. Geological Association of Canada, St. John's, Newfoundland, Special Papers, **41**, 283–301.

CHEN, C.-H., LEE, T., SHIEH, Y.N., CHEN, C.H. & HSU, W.Y. 1995. Magmatism at the onset of back arc basin spreading in Okinawa Trench. *Journal of Volcanology and Geothermal Research*, **69**, 313–322.

CHUNG, S.L., WANG, S.L., SHINJO, R., LEE, C.S. & CHEN, C.H. 2000. Initiation of arc magmatism in an embryonic continental rifting zone of the southernmost part of Okinawa Trough. *Terra Nova*, **12**, 225–230.

CLIFF, R.A., YARDLEY, B.W.D. & BUSSY, F.R. 1996. U–Pb and Rb–Sr geochronology of magmatism and metamorphism in the Dalradian of Connemara, western Ireland. *Journal of the Geological Society, London*, **153**, 109–120.

CLIFT, P.D. 1995. Volcaniclastic sedimentation and volcanism during the rifting of Western Pacific backarc basins. *In*: TAYLOR, B. & NATLAND, J. (eds) *Active Margins and Marginal Basins of the Western Pacific*. American Geophysical Union Monographs, **88**, 67–96.

CLIFT, P.D. & MACLEOD, C.J. 1999. Slow rates of tectonic erosion estimated from the subsidence and tilting of the Tonga Forearc Basin. *Geology*, **27**, 411–414.

CLIFT, P.D. & RYAN, P.D. 1994. Geochemical evolution of an Ordovician island arc, South Mayo, Ireland. *Journal of the Geological Society, London*, **151**, 329–342.

CLIFT, P.D., DRAUT, A.E., HANNIGAN, R., LAYNE, G. & BLUSZTAJN, J. 2003*a*. Trace element and Pb isotopic constraints on the provenance of the Rosroe Formation, South Mayo, Ireland. *Transactions of the Royal Society of Edinburgh, Earth Science*, **93** (2), 101–110.

CLIFT, P.D., PECHER, I., KUKOWSKI, N. & HAMPEL, A. 2003*b*. Tectonic erosion of the Peruvian forearc, Lima Basin, by steady-state subduction and Nazca Ridge collision. *Tectonics*, **22** (3), 1023, 10.1029/2002 TC001386.

COCHRAN, J.R. 1990. Himalayan uplift, sea level, and the record of Bengal Fan sedimentation at the ODP Leg 116 sites. *In*: COCHRAN, J.R., STOW, D.A.V. *et al.*, *Proceedings of the Ocean Drilling Program, Scientific Results*, **116**, 397–414.

DAVIES, J.H. & VON BLANCKENBURG, F. 1995. Slab breakoff; a model of lithosphere detachment and its test in the magmatism and deformation of collisional orogens. *Earth and Planetary Science Letters*, **129**, 85–102.

DEFANT, M.J., MAURY, R.C., JORON, J.-L., FEIGENSON, M.D., LETERRIER, J., BELLON, H., JACQUES, D. & RICHARD, M. 1990. The geochemistry and tectonic setting of the northern section of the Luzon arc (the Philippines and Taiwan). *Tectonophysics*, **183**, 187–205.

DEWEY, J.F. & MANGE, M. 1999. Petrology of Ordovician and Silurian sediments in the western Irish Caledonides: tracers of short-lived Ordovician continent–arc collision orogeny and the evolution of the Laurentian Appalachian–Caledonian margin. *In*: MACNIOCAILL, C. & RYAN, P.D. (eds) *Continental Tectonics*. Geological Society, London, Special Publications, **164**, 55–108.

DEWEY, J.F. & RYAN, P.D. 1990. The Ordovician evolution of the South Mayo Trough, western Ireland. *Tectonics*, **9**, 887–901.

DEWEY, J.F. & SHACKLETON, R.M. 1984. A model for the evolution of the Grampian tract in the early Caledonides and Appalachians. *Nature*, **312**, 115–121.

DORSEY, R.J. 1992. Collapse of the Luzon volcanic arc during onset of arc–continent collision; evidence from a Miocene–Pliocene unconformity, eastern Taiwan. *Tectonics*, **11**, 177–191.

DRAUT, A.E. & CLIFT, P.D. 2001. Geochemical evolution

of arc magmatism during arc–continent collision, South Mayo, Ireland. *Geology*, **29**, 543–546.
DRAUT, A.E. & CLIFT, P.D. 2002. The origin and significance of the Delaney Dome Formation, Connemara, Ireland. *Journal of the Geological Society, London*, **159**, 95–103.
DRAUT, A.E., CLIFT, P.D., HANNIGAN, R.E., LAYNE, G. & SHIMIZU, N. 2002. A model for continental crust genesis by arc accretion: rare earth element evidence from the Irish Caledonides. *Earth and Planetary Science Letters*, **203**, 861–877.
ELLAM, R.M. & HAWKESWORTH, C.J. 1988. Is average continental crust generated at subduction zones? *Geology*, **16**, 314–317.
FRIEDRICH, A.M., BOWRING, S.A., MARTIN, M.W. & HODGES, K.V. 1999*a*. Short-lived continental magmatic arc at Connemara, western Irish Caledonides. Implications for the age of the Grampian Orogeny. *Geology*, **27**, 27–30.
FRIEDRICH, A.M., HODGES, K.V., BOWRING, S.A. & MARTIN, M.W. 1999*b*. Geochronological constraints on the magmatic, metamorphic, and thermal evolution of the Connemara Caledonides, western Ireland. *Journal of the Geological Society, London*, **156**, 1217–1230.
GRAHAM, J.R., LEAKE, B.E. & RYAN, P.D. 1989. *The Geology of South Mayo, Western Ireland.* Scottish Academic Press, Glasgow.
HARRIS, A.L., HASELOCK, P.J., KENNEDY, M.J., MENDUM, J.R., LONG, C.B., WINCHESTER, J.A. & TANNER, P.W.G. 1994. The Dalradian Supergroup in Scotland, Shetland and Ireland. *In*: GIBBONS, W. & HARRIS, A.L. (eds) *A Revised Correlation of Precambrian Rocks in the British Isles*. Geological Society, London, Special Reports, **22**, 33–53.
HARRIS, D.H.M. 1993. The Caledonian evolution of the Laurentian margin in western Ireland. *Journal of the Geological Society, London*, **150**, 669–672.
HIRTH, G. & KOHLSTEDT, D.L. 1996. Water in the oceanic upper mantle; implications for rheology, melt extraction and the evolution of the lithosphere. *Earth and Planetary Science Letters*, **144**, 93–108.
HOLBROOK, W.S., LIZARRALDE, D., MCGEARY, S., BANGS, N. & DIEBOLD, J. 1999. Structure and composition of the Aleutian island arc and implications for continental crustal growth. *Geology*, **27**, 31–34.
HOUSEMAN, G.A., MCKENZIE, D.P. & MOLNAR, P. 1981. Convective instability of a thickened boundary layer and its relevance for the thermal evolution of continental convergent belts. *Journal of Geophysical Research*, **86**, 6115–6132.
HSIAO, L.-Y., LIN, K.-A., HUNAG, S.T. & TENG, L.S. 1999. Structural characteristics of the southern Taiwan–Sinzi folded zone. *Petroleum Geology of Taiwan*, **32**, 133–153.
HUTTON, D.H.W. 1987. Strike-slip terranes and a model for the evolution of the British and Irish Caledonides. *Geological Magazine*, **124**, 405–425.
JULL, M. & KELEMEN, P.B. 2001. On the conditions for lower crustal convective instability. *Journal of Geophysical Research*, **106**, 6423–6446.
KARABINOS, P., SAMSON, S.D., HEPBURN, J.C. & STOLL, H.M. 1998. Taconian orogeny in the New England Appalachians: collision between Laurentia and the Shelburne Falls arc. *Geology*, **26**, 215–218.
KAY, R.W. 1985. Island arc processes relevant to crustal and mantle evolution. *Tectonophysics*, **112**, 1–15.
KAY, R.W. & KAY, S.M. 1993. Delamination and delamination magmatism. *Tectonophysics*, **219**, 177–189.
KIRBY, S.H. & KRONENBERG, A.K. 1987. Rheology of the lithosphere: selected topics. *Reviews of Geophysics*, **25**, 1219–1244.
KLEMPERER, S.L. 1991. A deep seismic reflection transect across the Irish Caledonides. *Journal of the Geological Society, London*, **148**, 149–164.
KOHLSTEDT, D.L. & GOETZE, C. 1974. Low-stress high-temperature creep in olivine single crystals. *Journal of Geophysical Research*, **79**, 2045–2051.
KOHLSTEDT, D.L., EVANS, B. & MACKWELL, S.J. 1995. Strength of the lithosphere; constraints imposed by laboratory experiments. *Journal of Geophysical Research*, **100**, 17 587–17 602.
KONSTANTINOVSKAYA, E.A. 1999. Geodynamics of island arc–continent collision in the western Pacific margin. *Geotectonics*, **33**, 15–34.
LALLEMAND, S.E., LIU, C.-S. & FONT, Y. 1997. A tear fault boundary between the Taiwan Orogen and the Ryukyu subduction zone. *Tectonophysics*, **274**, 171–190.
LALLEMAND, S.E., FONT, Y., BIJWAARD, H. & KAO, H. 2001. New insights on 3-D plates interaction near Taiwan from tomography and tectonic implications. *Tectonophysics*, **335**, 229–253.
LEAKE, B.E. 1989. The metagabbros, orthogneisses and paragneisses of the Connemara Complex, western Ireland. *Journal of the Geological Society, London*, **146**, 575–596.
LEE, J.-C., ANGELIER, J. & CHU, H.-T. 1997. Polyphase history and kinematics of a complex major fault zone in the northern Taiwan mountain belt: the Lishan Fault. *Tectonophysics*, **274**, 97–115.
LEGGETT, J.K., MCKERROW, W.S. & SOPER, N.J. 1983. A model for the crustal evolution of southern Scotland. *Tectonics*, **2**, 187–210.
LETOUZEY, J. & KIMURA, M. 1985. Okinawa Trough genesis: structure and evolution of a backarc basin developed in a continent. *Marine and Petroleum Geology*, **2**, 111–130.
LUNDBERG, N. & DORSEY, R.J. 1990. Rapid Quaternary emergence, uplift, and denudation of the Coastal Range, eastern Taiwan. *Geology*, **18**, 638–641.
LUNDBERG, N., REED, D.L., LIU, C.-S. & LIESKE, J. 1997. Forearc-basin closure and arc accretion in the submarine suture zone south of Taiwan. *Tectonophysics*, **274**, 5–23.
MAURY, R.C., DEFANT, M.J., BELLON, H., JACQUES, D., JORON, J.-L., MCDERMOTT, F. & VIDAL, P. 1998. Temporal geochemical trends in northern Luzon arc lavas (Philippines): implications on metasomatic processes in the island arc mantle. *Bulletin de la Societé Geologique de France*, **169**, 69–80.
MCKERROW, W.S., DEWEY, J.F. & SCOTESE, C.R. 1991. The Ordovician and Silurian development of the

Iapetus Ocean. *Special Papers in Palaeontology*, **44**, 165–178.

MILLER, D.J. & CHRISTENSEN, N.I. 1994. Seismic signature and geochemistry of an island arc; a multidisciplinary study of the Kohistan accreted terrane, northern Pakistan. *Journal of Geophysical Research*, **99**, 11 623–11 642.

PEARCE, J.A. 1982. Trace element characteristics of lavas from destructive plate boundaries. *In*: THORPE, R.S. (ed.) *Andesites: Orogenic Andesites and Related Rocks*. John Wiley, Chichester.

PEARCY, L.G., DEBARI, S.M. & SLEEP, N.H. 1990. Mass balance calculations for two sections of island arc and implications for the formation of continents. *Earth and Planetary Science Letters*, **96**, 427–442.

PUDSEY, C.J. 1984. Fluvial to marine transition in the Ordovician of Ireland: a humid-region fan-delta? *Geological Journal*, **19**, 143–172.

RAU, R.-J. & WU, F.T. 1995. Tomographic imaging of lithospheric structures under Taiwan. *Earth and Planetary Science Letters*, **133**, 517–532.

REYMER, A. & SCHUBERT, G. 1984. Phanerozoic addition rates to the continental crust and crustal growth. *Tectonics*, **3**, 63–77.

ROGERS, G. & HAWKESWORTH, C.J. 1989. A geochemical traverse across the North Chilean Andes; evidence for crust generation from the mantle wedge. *Earth and Planetary Science Letters*, **91**, 271–285.

ROWLEY, D.B. 1996. Age of initiation of collision between India and Asia: a review of stratigraphic data. *Earth and Planetary Science Letters*, **145**, 1–13.

RUDNICK, R.L. & FOUNTAIN, D.M. 1995. Nature and composition of the continental crust: a lower crustal perspective. *Reviews of Geophysics*, **33**, 267–309.

SALISBURY, M.H., SHINOHARA, M., RICHTER, C. *et al.* 2002. *Proceedings of the Ocean Drilling Program, Initial Reports*, **195** (CD-ROM).

SHEMENDA, A.I. 1994. *Subduction: Insights from Physical Modeling*. Kluwer Academic, New York.

SHINJO, R. 1999. Geochemistry of high Mg andesites and the tectonic evolution of the Okinawa Trough–Ryukyu Arc system. *Chemical Geology*, **157**, 69–88.

SIBUET, J.-C. & HSU, S.-K. 1997. Geodynamics of the Taiwan arc–arc collision. *Tectonophysics*, **274**, 221–251.

SIBUET, J.-C., DEFFONTAINES, B., HSU, S.-K., THAREAU, N., LE FORMAL, J.-P., LIU, C.-S. & ACT PARTY 1998. Okinawa Trough backarc basin: early tectonic and magmatic evolution. *Journal of Geophysical Research*, **103**, 30 245–30 267,

SIBUET, J.-C., HSU, S.-K., LE PICHON, X., LE FORMAL, J.-P., REED, D., MOORE, G. & LIU, C.-S. 2002. East Asia plate tectonics since 15 Ma: constraints from the Taiwan region. *Tectonophysics*, **344**, 103–134.

SIBUET, J.-C., LETOUZEY, J., BARBIER, F., CHARVET, J., FOUCHER, J.-P., HILDE, T.W.C., KIMURA, M., LING-YUN, C., MARSSET, B., MULLER, C. & STEPHAN, J.-F. 1987. Backarc extension in the Okinawa Trough. *Journal of Geophysical Research*, **92**, 14 041–14 063.

SOPER, N.J., RYAN, P.D. & DEWEY, J.F. 1999. Age of the Grampian Orogeny in Scotland and Ireland. *Journal of the Geological Society, London*, **156**, 1231–1236.

SUYEHIRO, K., TAKAHASHI, N., ARIIE, Y., YOKOI, Y., HINO, R., SHINOHARA, M., KANAZAWA, T., HIRATA, N., TOKUYAMA, H. & TAIRA, A. 1996. Continental crust, crustal underplating, and low-Q upper mantle beneath an oceanic island arc. *Science*, **272**, 390–392.

SWINDEN, H.S., JENNER, G.A. & SZYBINSKI, Z.A. 1997. Magmatic and tectonic evolution of the Cambrian–Ordovician Laurentian margin of Iapetus; geochemical and isotopic constraints from the Notre Dame Subzone, Newfoundland. *In*: SINHA, A.K., WHALEN, J.B. & HOGAN, J.P. (eds) *The Nature of Magmatism in the Appalachian Orogen*. Geological Society of America, Memoirs, **191**, 337–365.

TANNER, P.W.G., DEMPSTER, T.J. & ROGERS, G. 1997. New constraints upon the structural and isotopic age of the Oughterard Granite, and on the timing of events in the Dalradian rocks of Connemara, western Ireland. *Geological Journal*, **32**, 247–263.

TAPPIN, D.R., HERZER, R.H. & STEVENSON, A.J. 1994. Structure and history of an oceanic forearc – the Tonga Ridge 22° to 26° South. *In*: STEVENSON, A.J., HERZER, R.H. & BALLANCE, P.F. (eds) *Geology and Submarine Resources of the Tonga–Lau–Fiji Region*. SOPAC, Suva, Technical Bulletins, **8**, 81–100.

TAYLOR, S.R. & MCLENNAN, S.M. 1985. *The Continental Crust: its Composition and Evolution*. Blackwell Scientific, Oxford.

TENG, L.S. 1990. Geotectonic evolution of late Cenozoic arc–continent collision in Taiwan. *Tectonophysics*, **183**, 57–76.

TENG, L.S. 1996. Extensional collapse of the northern Taiwan mountain belt. *Geology*, **24**, 949–952.

TENG, L.S., LEE, C.T., TSAI, Y.B. & HSIAO, L.Y. 2000. Slab break-off as a mechanism for flipping of subduction polarity in Taiwan. *Geology*, **28**, 155–158.

TUCKER, R.D. & MCKERROW, W.S. 1995. Early Paleozoic chronology: a review in light of new U–Pb zircon ages from Newfoundland and Britain. *Canadian Journal of Earth Sciences*, **32**, 368–379.

VAN STAAL, C.R., DEWEY, J.F., MACNIOCAILL, C. & MCKERROW, W.S. 1998. The Cambrian–Silurian tectonic evolution of the northern Appalachians and British Caledonides: history of a complex, west and southwest Pacific-type segment of Iapetus. *In*: BLUNDELL, D.J. & SCOTT, A.C. (eds) *Lyell: the Past is the Key to the Present*. Geological Society, London, Special Publications, **143**, 199–242.

VANNUCCHI, P., SCHOLL, D.W., MESCHEDE, M. & MCDOUGALL-REID, K. 2001. Tectonic erosion and consequent collapse of the Pacific margin of Costa Rica: combined implications from ODP Leg 170, seismic offshore data, and regional geology of the Nicoya Peninsula. *Tectonics*, **20**, 649–668.

VON HUENE, R. & LALLEMAND, S. 1990, Tectonic erosion along the Japan and Peru convergent margin. *Geological Society of America Bulletin*, **102**, 704–720.

VON HUENE, R., WEINREBE, W. & HEEREN, F. 1999. Subduction erosion along the North Chile margin. *Journal of Geodynamics*, **27**, 345–358.

WANG, K.L., CHUNG, S.L., CHEN, C.-H., SHINJO, R., YANG, T.F. & CHEN, C.H. 1999. Post-collisional magmatism around northern Taiwan and its relation with opening of the Okinawa Trough. *Tectonophysics*, **308**, 363–376.

WANG, W.-H. 2001. Lithospheric flexure under a critically tapered mountain belt; a new technique to study the evolution of the Tertiary Taiwan orogeny. *Earth and Planetary Science Letters*, **192**, 571–581.

WELLINGS, S.A. 1998. Timing of deformation associated with the syn-tectonic Dawros–Currywongaun–Doughruagh Complex, NW Connemara, western Ireland. *Journal of the Geological Society, London*, **155**, 25–37.

WILLIAMS, D.M. & RICE, A.H.N. 1989. Low-angle extensional faulting and the emplacement of the Connemara Dalradian, Ireland. *Tectonics*, **8**, 427–428.

YANG, T.F., LEE, T., CHEN, C.-H., CHENG, S.-N., KNITTEL, U., PUNONGBAYAN, R.S. & RASDAS, A.R. 1996. A double island arc between Taiwan and Luzon: consequence of ridge subduction. *Tectonophysics*, **258**, 85–101.

YOGODZINSKI, G.M. & KELEMEN, P.B. 1998. Slab melting in the Aleutians; implications of an ion probe study of clinopyroxene in primitive adakite and basalt. *Earth and Planetary Science Letters*, **158**, 53–65.

YU, H.-S. & CHOU, Y.-W. 2001. Characteristics and development of the flexural forebulge and basal unconformity of western Taiwan foreland basin. *Tectonophysics*, **333**, 277–291.

Felsic volcanism in the Kermadec arc, SW Pacific: crustal recycling in an oceanic setting

IAN E.M. SMITH[1], TIMOTHY J. WORTHINGTON[1,2], ROBERT B. STEWART[3], RICHARD C. PRICE[4] & JOHN A. GAMBLE[5]

[1]*Department of Geology, University of Auckland, PB 92019, Auckland, New Zealand (e-mail ie.smith@auckland.ac.nz)*

[2]*Present address: University of Kiel, Olshausenstrasse 40, 24118 Kiel, Germany*

[3]*Soil and Earth Sciences, INR, Massey University, PB 11–222, Palmerston North, New Zealand*

[4]*School of Science and Technology, University of Waikato, PB 3105, Hamilton, New Zealand*

[5]*Department of Geology, National University of Ireland, University College Cork, Cork, Ireland*

Abstract: Large-scale felsic volcanic systems are a common, but not ubiquitous, feature of volcanic arc systems in continental settings. However, in oceanic volcanic arcs the erupted materials are dominated by basalts and basaltic andesites, whereas intermediate compositions are rare and dacites and rhyolites relatively uncommon. The Kermadec arc is an intra-oceanic convergent system in the SW Pacific. Volcanoes occur as a continuous arc that is mainly submarine. Despite its simple tectonic setting, felsic magmatism is widespread. In the Kermadec Islands, Macauley Volcano is a basaltic volcano that produced a large felsic eruption about 6000 years ago. A comparable pattern of magmatic evolution is seen on adjacent Raoul Volcano, where basaltic activity built the main edifice of the volcano and where activity during the last 3000 years has been characterized by felsic eruptions of varying size. Elsewhere in the Kermadec arc and in its northward extension, the Tonga arc, felsic eruptions are recorded from 11 of the 30 volcanoes for which petrographic information is available, and in many cases these are the most recent eruptions. Felsic eruptions are a widespread recent feature of the arc, and the scale and extent of this magmatism appears to be unusual for a tectonically simple oceanic subduction system. One explanation of the origin of the felsic magmatism is prolonged fractional crystallization from a parental basalt composition, but modelling of the chemical compositions of the felsic rocks does not support this. A second explanation, albeit apparently at odds with the oceanic setting, is crustal anatexis. An important feature of the felsic eruptives from the Kermadec arc is that each tephra sequence or occurrence has a unique chemical composition, although all show the same generalized characteristics. We suggest that this feature supports a model of crustal anatexis rather than fractionation of a range of parental magmas. We also suggest that in the thermal evolution of an oceanic arc system the processes of underplating, together with the continuous magmatic (and thermal) flux, can generate a crustal thickness in which dehydration melting of underplated arc material generates felsic magmas. Further, this condition can represent a unique 'adolescent' stage in a developing oceanic arc, as once the felsic melts are extracted the lower crust becomes an infertile residue.

The presence of high-silica (>70 wt% SiO_2) volcanic rocks in caldera complexes is a conspicuous feature of many continental arc systems. In contrast rocks with >63 wt% SiO_2 are generally considered to be only a minor component of intra-oceanic volcanic arcs. However, recent work on the Izu–Bonin and Scotia arcs (Tamura & Tatsumi 2002; Leat *et al.* 2003) has shown that silicic caldera-forming eruptions can be a significant component of oceanic subduction systems. Recent volcanic activity in the Tonga–Kermadec arc in the SW Pacific has also involved widespread production of felsic magmas and at least some of these eruptions have been associated with formation of calderas. The occurrence of widespread and relatively large-scale felsic volcanism is unexpected in a simple oceanic setting and its explanation requires an assessment of both tectonic and petrogenetic factors. Felsic rocks have been described from Raoul Island

From: LARTER, R.D. & LEAT, P.T. 2003. *Intra-Oceanic Subduction Systems: Tectonic and Magmatic Processes.* Geological Society, London, Special Publications, **219**, 99–118. 0305-8719/03/$15.00

(Worthington 1998), Macauley Island (Lloyd *et al.* 1996; Smith *et al.* 2003) and Curtis Island (Smith *et al.* 1988) in the Kermadec Group, and dredged from several submarine volcanoes in the southern part of the arc (Gamble *et al.* 1997; Wright & Gamble 1999). In this paper we review these occurrences and discuss the origin of felsic magmas in the Kermadec arc.

Among oceanic subduction settings globally, the principal occurrences of felsic volcanism are associated with young calderas in the central New Hebrides arc (Crawford *et al.* 1988; Robin *et al.* 1993; Monzier *et al.* 1994), calderas of late Pleistocene–Recent age in the western Aleutian arc (Miller 1995) and young submarine calderas in the northern Izu arc (Gill *et al.* 1992). These arc segments all share crustal extension and tectonic complexity. Specifically, the central segment of the New Hebrides arc is associated with subduction of an extinct arc, the D'Entrecasteaux Zone (Greene *et al.* 1988), the west Aleutian forearc consists of structural blocks that are rotating relative to each other (Geist *et al.* 1988) and the northern Izu arc is actively rifting (Taylor *et al.* 1991). Eruptions of felsic magma have also been recorded from the Bonin, Mariana and South Sandwich oceanic arcs (Bloomer *et al.* 1989; Pearce *et al.* 1995; Tamura & Tatsumi 2002; Leat *et al.* 2003). Although the Tonga–Kermadec arc is tectonically simple, felsic volcanism has occurred at 11 of 30 volcanoes for which information is available, and this includes large-scale caldera-forming eruptions of a style more characteristic of continental settings.

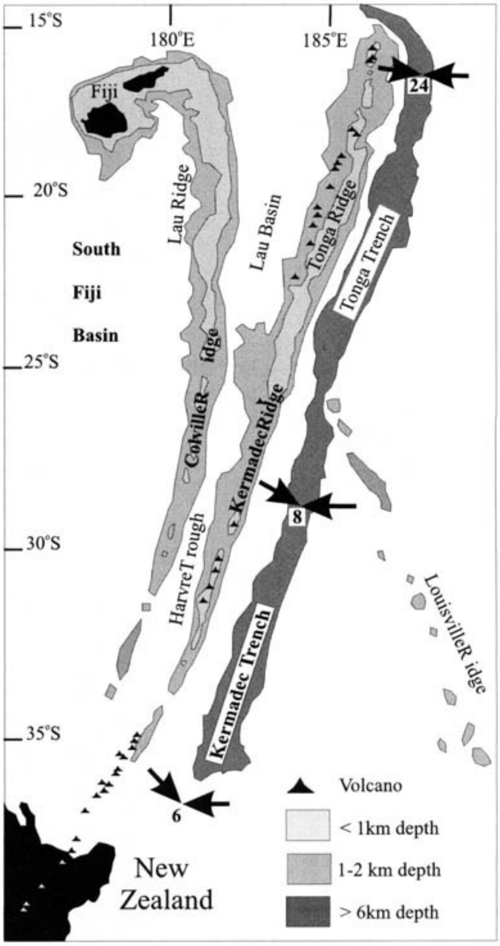

Fig. 1. Map of the Tonga–Kermadec arcs with principle topographic features. Bathymetry after NGDC (1996). Arrows are a schematic representation of plate motions at the trench with subduction rates given in cm year^{-1}.

The Kermadec subduction system

The Tonga–Kermadec subduction system (Fig. 1) is an intra-oceanic convergent plate margin that extends for 2550 km between Tonga and New Zealand in the SW Pacific Basin. The Louisville seamount chain intersects the arc at 25.6°S, dividing it into the Tonga arc to the north and the Kermadec arc to the south. The principal features of the system are subduction of the Pacific Plate and its sedimentary veneer at the Tonga–Kermadec Trench, subduction-related magmatism along the Tonga–Kermadec Ridge and crustal extension behind the arc that is expressed as the Lau Basin and Harvre Trough. Southward these features extend into the Hikurangi Trench and Taupo Volcanic Zone as the arc impinges on the continental crust of New Zealand. Along the length of the arc there is a systematic change in tectonic parameters. Subduction rates decrease southward from 24 to 6 cm a^{-1} (Bevis *et al.* 1995; Parson & Wright 1996). For the Tonga arc this reflects a reduction in the extension rate across the Lau Basin, whereas for the Kermadec arc the decrease is primarily a function of distance from the Pacific–Australian pole of rotation at 60.1°S, 181.7°E (DeMets *et al.* 1994). In both sectors the convergence vectors become increasingly oblique toward the south. The Wadati–Benioff seismic zone dips westward beneath the arc at a shallow angle to a depth of approximately 50 km and then increases to 70° by 200 km depth. The volcanoes of the arc are consistently located 100 km above the zone. A lateral inflection of the slab surface coincides with the boundary between the Tonga and Kermadec arcs, and the

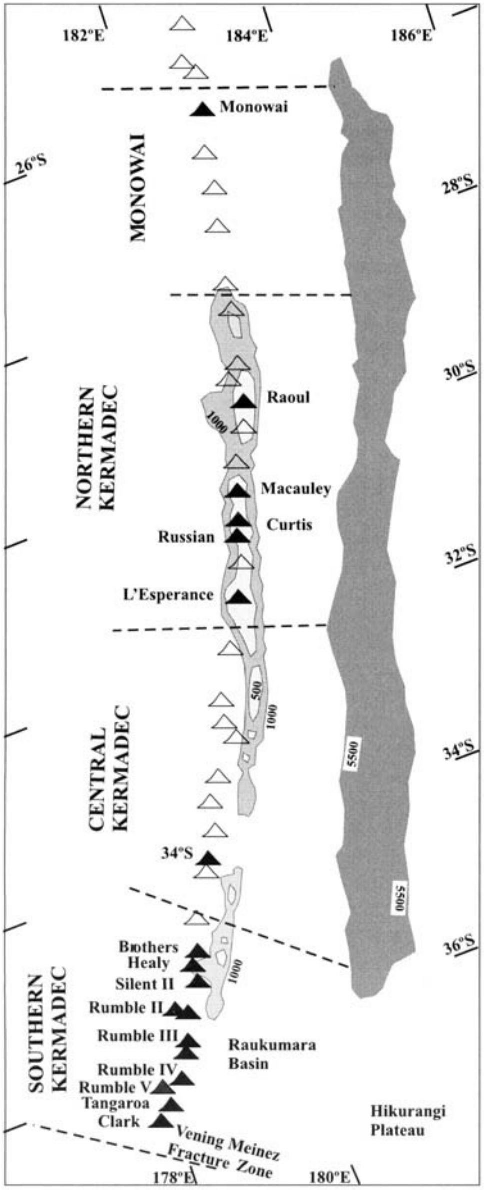

Fig. 2. The Kermadec arc. Major topographic features are defined by bathymetric contours (after NGDC 1996). Confirmed volcanoes are shown as solid symbols and inferred volcanoes as open symbols. Dashed lines separate the subdivisions of the arc.

behaviour of the slab at depth differs for each segment. To the west of the Tonga arc it flattens below 300 km, although it continues to 670 km depth. To the west of the Kermadec arc, seismic activity terminates at shallower depths and cannot be traced below 350 km depth south of 32.5°S, although tomographic images of P-wave velocity variations in the mantle have been interpreted to show the slab subducting to depths greater than 800 km throughout the length of the Tonga–Kermadec system (Van der Hilst 1995).

Volcanoes of the Kermadec arc are confined to a 40 km-wide zone, defining an arc that is curvilinear in form and convex toward the Kermadec Trench. The arc can be subdivided according to changes in arc–ridge and arc–trench separation, primarily reflecting changes in width and structure of the fore arc. These divisions are the Monowai, northern Kermadec, central Kermadec and southern Kermadec segments (Fig. 2).

In the Monowai segment both the volcanic arc and the trench are offset eastward relative to an extrapolation of the Tonga arc–trench system, and the arc–ridge separation progressively decreases to the south. In the northern Kermadec segment the ridge continues as a narrow feature that is shallower in the north. The only subaerial volcanoes of the Kermadec system rise from the ridge in the central and southern parts of this segment. Each of these, as well as several submarine edifices, are large low-aspect ratio volcanoes that extend across most of the arc. Raoul consists of a series of coalescing stratocones with two known summit calderas. Similarly, Macauley is dominated by a large centrally located submarine volcano formed in part during a voluminous eruption at 6.3 ka. Curtis Island is the eroded remnant of an extensive pyroclastic sheet. L'Esperance has two widely separated summit peaks whose relative ages are unknown; L'Esperance rock is located on the eastern summit and east of the crest of the arc, whereas Havre Rock, lying to the west and emergent only at low tide during rough sea conditions, is centrally located relative to the arc. In the central Kermadec domain both the ridge and trench are offset 30 km to the east, and the ridge summit becomes progressively deeper towards the south. A series of conical submarine edifices surmounts the ridge but these are not known in any detail. The boundary of the central and southern Kermadec segments coincides with the northern limit of the fore arc Raukumara Basin and with an increase in the arc–trench separation. The ridge continues to deepen and eventually disappears beneath the sediments of the Raukumara Basin at water depths of 2–4 km. A series of large volcanic edifices are located 20–30 km west of the ridge and evidence of recent volcanic activity is found on the eastern, but not the western, of two E–W paired

Table 1. *The occurrence of felsic rocks in the Kermadec arc*

Volcano	Details	SiO_2 of felsic samples (wt%)
Raoul	Eight separate felsic eruptions during last 3.7 ka	63–70
Macauley	Large felsic eruption at 6 ka, chemical evidence of an earlier felsic eruption	63–72
Curtis	Dacitic pyroclastic flow deposits	63–71
Russian Seamount	Dacite pumice fragment dredged	70
34°S	Dredged dacite pumice	67
Brothers	Abundant felsic pumice in dredge collections	64–67
Healy	Abundant dredged felsic pumice	67–71
Rumble II	Dacite pumice dredged	64
Rumble IV	Dredged pumice	65–67
Tangaroa	Abundant dredged pumice	63–68
Clark	Pumice dredged	65

volcanoes (Wright *et al.* 1996). The only confirmed eruption in historic times was that of Rumble III in 1986 (Wright 1994). Rumble III is an unpaired eastern volcano and has the largest volume of any of the Tonga–Kermadec volcanoes. The southern boundary of this segment is the Vening Meinesz Fracture Zone marking the transition of the arc from intra-oceanic to continental.

Felsic rocks of the Kermadec arc

Kermadec arc volcanoes that have subaerial exposure or have been surveyed in detail form widely separated groups in the northern and southern parts of the arc. Recent high-quality bathymetric maps show a series of topographic highs along the trace of the arc (Chase 1985; CANZ 1997; Smith & Sandwell 1997). Those that have more than 500 m of relief and a conical form are inferred to be previously unrecognized volcanoes (Fig. 2) and in some cases their existence is corroborated by geophysical transects (Tagudin & Scholl 1994).

Felsic rocks have been described from the Raoul, Macauley and Curtis islands, and dredged from Russian Seamount in the Kermadec Group. They have also been dredged from 34°S, Brothers, Healey, Rumble II, Rumble IV, Tangaroa and Clark submarine volcanoes in the southern part of the arc. Thus, of the 18 Kermadec volcanoes for which lithological information is available, 11 are known to have erupted felsic magma. There is presently no lithological information for a further 19 inferred volcanoes, mainly from the central Kermadec and Monowai segments of the arc.

The record of felsic volcanism in the Kermadec arc is extremely variable. The most detailed is that of the last 3.7 ka from Raoul Volcano, where the physical characterization and petrological nature of eight felsic units have been described in detail (Worthington 1998). Macauley Island, immediately to the south of Raoul, also provides good exposures of deposits from a large felsic eruption about 6300 years ago, as well as evidence for earlier felsic eruptions. Elsewhere in the arc felsic rocks are known only from dredged samples and the ages and volumes of the eruptions they represent are problematic, although the association of felsic material with caldera structures suggests eruption on a medium to large scale.

Although the record of volcanism in the Kermadec arc is limited by the submarine nature of most of its volcanoes, the available data do suggest that felsic eruptions have been a significant aspect of this subduction system in recent times. Details of the records from individual volcanoes are given below and summarized in Table 1.

The Kermadec islands

Raoul Island is the emergent summit of a large submarine volcanic massif that rises 900 m from the crest of the Kermadec Ridge and is 28 × 20 km at its base. Assuming a simple cone rising from a plateau, Raoul Volcano has a volume of 214 km^2 of which the island represents 4 km^3 (2%). Physiographically the island is dominated by two adjacent collapse structures. Raoul Caldera is approximately 3 × 3 km across and occupies the central part of the island. Denham Caldera forms the western margin of Raoul Island and is mostly submarine (Worthington *et al.* 1999).

The stratigraphy of Raoul Island has been described in papers by Brothers & Searle (1970) and Lloyd & Nathan (1981). The oldest exposed rocks are pillow lavas, hyaloclastite and interbedded calcareous sediments. Unconformably overlying this basement are the deposits of three successive strata cone-building episodes, each consisting of subaerial lava and volcaniclastic deposits that range from basalt to andesite. An abrupt change to explosive eruptions of felsic magma occurred at 3.7 ka, together with a reduction in the frequency of basalt and andesite eruptions. Raoul Caldera formed as the youngest basaltic cone collapsed early during this period and Denham Caldera either formed or was reactivated during a large-scale felsic eruption about 2.2 ka BP. Tephra formations record 16 eruptions since 3.7 ka; dacite was erupted in eight of these eruptions, andesite in two and the remaining six were phreatic (Lloyd & Nathan 1981).

Macauley Island is the small emergent fragment (*c.* 3km^2) of a large submarine volcano, Macauley Volcano, which has an area of about 380 km^2 at the 900 m isobath. Immediately to the north of the island there is a roughly circular submarine depression, about 12 km in diameter and up to 1.1 km deep, that is interpreted as a young caldera (Lloyd *et al.* 1996). Despite the small size of the island, excellent coastal exposures provide a record of the most recent volcanic episodes from the volcano. The oldest deposits are the products of phreatomagmatic and effusive eruptions, and they provide a record of the submarine–subaerial development of a basaltic volcano. A series of basalt lava flows exposed on the shore platform around most of the island represents a subaerial basaltic shield about 4 km in diameter and 150 m above sea level. A large felsic eruption at 6310±190 years BP (Lloyd *et al.* 1996) from a vent area just north of Macauley Island produced the Sandy Bay Tephra and caused the collapse of the summit area, thus creating Macauley Caldera. More recently, renewal of basaltic volcanism built a composite tephra and lava cone at the western end of the island.

The Sandy Bay Tephra was produced by a medium-scale felsic eruption in an oceanic arc setting. Because of very limited subaerial exposure and only limited knowledge of the submarine distribution of tephra, the size of the eruption can only be estimated within wide limits. Deposits of the Sandy Bay Tephra on Macauley Island have a total volume of between 0.1 and 0.2 km^3, but this only represents a portion of one sector of the dispersal area of erupted material and there would undoubtedly have been a large, widely distributed, tephra fall component. Bearing this in mind, Lloyd *et al.* (1996) estimated that a minimum size for the eruption would be in the range 1–5 km^3. Lithic fragments of pitchstone and obsidian with a distinct composition occur within the Sandy Bay Tephra and provide evidence for an earlier felsic eruption from Macauley Volcano.

Curtis Island is a steep-sided, flat-topped island with an elevation of about 100 m above sea level. A crater enclosed by steep walls and breached on its northern side dominates the interior of the island. This crater is interpreted as a collapse feature. The island is composed of subaerial pyroclastic material cut in places by thin (<1 m) dacite dykes. The pyroclastic rocks consist of pumice and dense lithic clasts in a poorly sorted tuffaceous matrix. The pumices are dacitic, and the rock fragments are dacite with subordinate andesite and rare basalt. Curtis Island is the subaerial summit of a shallow (<100 m water depth) submarine plateau. The nature of its constituent rocks together with its geomorphology indicates that it is part of an extensive felsic pyroclastic unit, possibly a pyroclastic flow, but its eruption source is not known.

South of Curtis Island at 30.41°S, submarine mapping has defined a volcano (referred to as Russian Seamount) with a diameter of 12–15 km rising to at least 800–1000 m from the sea floor, with a broad plateau-like summit on which there are active hydrothermal plumes (Stoffers *et al.* 1999). Little is known of the petrography of this volcano apart from dredged pumice and volcaniclastic breccia (Smith *et al.* 1988; Stoffers *et al.* 1999).

Southern Kermadec arc

In recent years a programme of systematic bathymetric mapping and dredge sampling has revealed the presence of large, young submarine volcanoes in the southern part of the Kermadec arc (Wright, 1994; Wright *et al.* 1996; Stoffers *et al.* 1999). Further mapping has recently been completed in the central segment.

In the north of the south Kermadec arc segment, the volcanic edifice on the arc lineament, but behind the Kermadec Ridge, at 34°S has not been mapped in detail and is known only from dredged samples (Stoffers *et al.* 1999). These samples include basalt and a significant proportion of dark grey aphyric pumice.

In the southern Kermadec segment of the arc there is a well-defined, linearly distributed group of 12 submarine volcanoes lying immediately behind the ridge crest (Fig. 2). They have been well described by Wright (1994), Wright *et al.* (1996), Gamble *et al.* (1997), Stoffers *et al.* (1999) and Wright & Gamble (1999). Felsic rocks have been dredged from six of these volcanoes and make up a significant proportion of collections from the Brothers and Healy volcanoes. Brothers, Healy and Rumble II all have calderas that were associated with the eruption of felsic magmas.

Petrography of felsic rocks in the Kermadec arc

The predominant lava types in the Kermadec arc are basalts and basaltic andesites containing abundant phenocrysts of plagioclase with subordinate and typically smaller phenocrysts of clinopyroxene, olivine and orthopyroxene (Ewart *et al.* 1977). Aphyric to sparsely porphyritic basaltic and intermediate rocks are a minor component of Kermadec sample collections. These rocks are typical of those found in oceanic arcs worldwide.

Felsic rocks occur as pumiceous clasts in pyroclastic flow and fall deposits on Raoul, Macauley and Curtis islands, and as dredged material from the southern volcanoes of the arc. They range in colour from cream through shades of grey to dark reddish or brownish grey and may show pink–pale grey interiors. Less common in pyroclastic deposits of the subaerial volcanoes and in the dredged material are dense dark grey–black pitchstone and obsidian lithic fragments.

Most pumiceous pyroclasts are similar in appearance. In general, they are strongly vesiculated, averaging 80% vesicles, although the total range of vesicularity is 10–90%. They contain sparse, subhedral–anhedral, plagioclase phenocrysts <1.4 mm across, together with smaller augite and hypersthene, and accessory magnetite and ilmenite. Plagioclase phenocrysts commonly occur as clusters, with or without smaller pyroxene crystals. The groundmass is typically colourless or rarely pale brown glass. Flow banding is defined by elongation of vesicles, layers with different vesicle sizes or by degree of vesicularity or microlite orientation.

Pitchstone and obsidian lithic fragments are dense, lack vesicles and are therefore more phyric (3–10% total crystals), although their modal characteristics are essentially the same as those of the pumices. Devitrification banding is common. The groundmass of obsidian is colourless–pale brown glass, devoid of significant crystalline phases; that of the pitchstones is variably microcrystalline, grading to textures in which glass is a minor interstitial phase.

A consistently observed feature of the felsic rocks is the presence of a bimodal phenocryst assemblage consisting of: (A) sodic plagioclase (andesine–labradorite) together with hypersthene and magnetite ± ilmenite; and (B) relatively calcic plagioclase (bytownite–anorthite) together with one or more of augite, orthopyroxene and olivine with molecular 100 × Mg/Mg+Fe ratios >50. Small rounded globules of basaltic glass containing assemblage (B) have been reported within pumice clasts from Macauley Island. Assemblage (A) has been interpreted as the equilibrium product of crystallization of felsic magma and assemblage (B) as a basaltic contaminant (Smith *et al.* 2003); these petrographic features appear to be common in Kermadec felsic rocks

Geochemistry

The sample suite from the Kermadec arc comprises an extensive set of samples collected from subaerial exposures in the Kermadec Islands and dredged samples from submarine volcanoes in the southern part of the arc. It should be emphasized that there is considerable variation in the numbers of samples from different volcanoes and that in all cases they represent only a small part of the volcanic history of their respective edifice. The data set (NZAP–Kermadec) is available at www2.Auckland.ac.nz/glg/geoweb/research.htm and representative analyses of felsic rocks are presented in Table 2. The predominant magma compositions represented in the data set are relatively high-Al (typically > 16 wt% Al_2O_3) basalts and basaltic andesite with low Mg-numbers, but there is compositional diversity at any given SiO_2 content, including some relatively primitive compositions (i.e. Mg numbers > 65) (Smith *et al.* 1997). Intermediate compositions are a minor component of the suite, but felsic rocks (SiO_2 > 65 wt%) are locally abundant.

The sample suite is essentially bimodal in terms of SiO_2 content with mafic–intermediate rocks defining a roughly normal distribution between 47 and 64 wt% SiO_2 with a peak at 50–55 wt%, and felsic rock compositions ranging from 65 to 73 wt% SiO_2 with a peak at 67–69 wt% (Fig. 3). The felsic rocks thus range continuously from dacite to rhyolite. There are no clear petrographic criteria on which to distinguish dacitic pumice and pitchstone from rhyolitic pumice and obsidian, and on the basis of this SiO_2 distribution we have used the term felsic for compositions covering the spectrum with SiO_2>65 wt%.

Figures 4–7 serve to illustrate the spectrum of compositions in the Kermadec arc. For the most part the arc is low-K verging on medium-K in terms of Gill's (1981) classification of arc–type rocks (Fig. 4a). There is no discernible grouping

Table 2. *Representative chemical analyses of felsic rocks from the Kermadec arc*

Sample	46333	23392	23404	46309	46386	46381	45623	45637b	45644	45634d	Br 58/6	Br 67/1
	Raoul Volcano						**Macauley Volcano**				**Brothers Volcano**	
Eruption	Rangitahua		Green Lake		Fleetwood		Sandy Bay Tuff		Felsic lithics			
wt%												
SiO_2	65.53	66.63	65.09	69.49	63.80	67.94	67.17	71.18	65.30	68.65	63.92	63.82
TiO_2	0.66	0.66	0.59	0.59	0.58	0.63	0.57	0.57	0.88	0.83	1.01	0.95
Al_2O_3	14.60	14.58	14.03	14.08	13.70	14.43	12.26	12.91	13.53	13.41	15.26	14.09
Fe_2O_3	6.23	6.28	5.91	5.15	5.79	6.00	4.67	4.56	7.35	6.12	6.45	5.52
MnO	0.21	0.21	0.17	0.18	0.21	0.18	0.15	0.14	0.21	0.17	0.12	0.13
MgO	1.69	1.68	1.92	1.12	1.73	1.43	1.13	0.72	1.63	0.85	1.79	1.29
CaO	5.65	5.59	4.19	4.53	5.24	5.08	2.95	2.82	5.01	3.81	4.62	3.70
Na_2O	3.24	3.29	3.31	3.52	3.66	3.39	5.46	4.64	3.20	3.49	4.37	4.63
K_2O	0.51	0.50	0.63	0.61	0.68	0.63	1.49	1.64	1.09	1.16	1.85	2.16
P_2O_5	0.13	0.14	0.14	0.15	0.15	0.16	0.11	0.12	0.29	0.26	0.293	0.260
H_2O^-	0.06	0.10	1.02	0.04	0.98	0.02	1.60	0.08	0.33	0.31	0.19	1.19
LOI	1.00	0.14	2.77	0.29	3.07	−0.02	2.29	1.15	0.93	1.09	−0.03	2.12
Total	99.51	99.80	99.77	99.75	99.59	99.87	99.85	100.53	99.77	100.15	99.86	99.86
ppm												
Ba	182	196	227	212	204	210	392	428	323	336	988	987
Rb	7	8	10	9	9	10	25	28	18	15	43	41
Sr	173	174	150	170	167	165	142	141	185	186	257	203
Pb	5	7	8	4	5	5	7	7	4	6	6	9
Zr	72	73	77	80	75	80	146	163	107	112	173	182
Nb	2	2	2	2	2	2	1	1	<1	1	4	4
Y	39	39	38	41	38	41	42	48	47	47	43	44
La	5	3	6	5	6	3	11	12	11	11	15	14
Ce	14	6	14	13	16	12	20	24	15	17	37	35
Sc	22	27	24	24	21	21	14	13	24	20	15	11
V	60	63	71	23	49	45	9	7	66	20	133	85
Cr	6	5	11	5	10	4	2	<1	5	3	7	12
Ni	4	3	6	2	4	2	<1	<1	1	<1	6	3
Cu	8	7	27	5	11	10	15	14	24	13	12	32
Zn	109	107	104	83	88	90	82	85	114	92	67	81
Ga	16	16	15	15	15	16	12	14	15	16	18	17

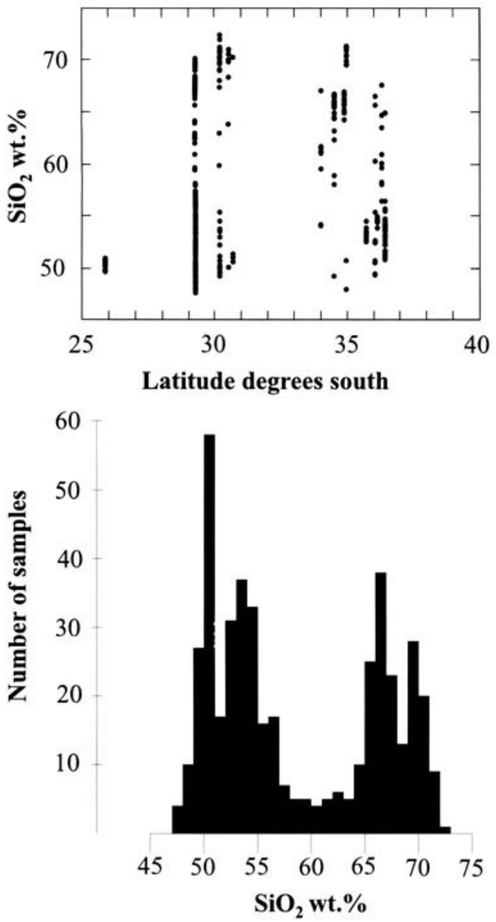

Fig. 3. Distribution of SiO_2 content in the Kermadec arc sample suite (total number of samples 480). The upper part of the diagram shows the range of SiO_2 content with respect to latitude southward along the arc. The lower part of the diagram shows the number of samples in 1% increments through the compositional spectrum.

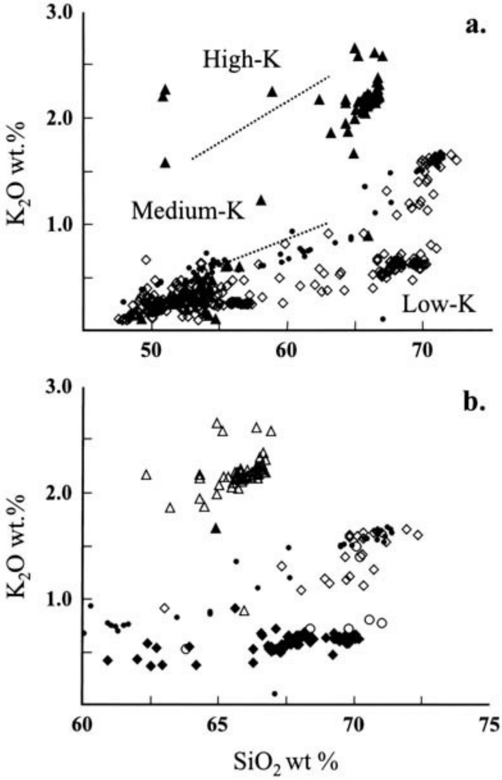

Fig. 4. K_2O variation with respect to SiO_2 in Kermadec arc rocks. The lines indicating low-K, medium-K and high-K arc type compositions are from Gill (1981). (**a**) The total compositional spectrum. Northern Kermadec and Monowai segments shown as open diamonds, southern Kermadec segment shown as dots except for the Brothers and Clark volcanoes, which are represented as solid triangles. (**b**) Rocks with SiO_2 >60 wt%. Symbols are: solid diamonds, Raoul; open diamonds, Macauley; open circles, Curtis Island and Russian Seamount; dots, southern arc segment; solid triangle, Clark; open triangles, Brothers.

within this compositional spectrum with respect to position in the arc. Brothers Volcano near the northern end of the southern Kermadec segment and Clark Volcano at the southern end adjacent to the New Zealand continental margin are distinguished by unusually high K_2O contents. The sample suite from both of these volcanoes includes mafic and felsic compositions that are typical of the Kermadec arc generally, as well as the high-K rocks. The presence of high-K magmas from Clark Volcano was noted by Gamble *et al.* (1997), who interpreted them as a rare example of near-slab small-volume melts of a mantle wedge source enriched by sediment and fluid transfer from the descending lithospheric slab. The high-K suite from Clark includes one high-K dacite. Mafic samples from Brothers are typical Kermadec basalts and basaltic andesites. Felsic samples from Brothers are almost entirely high-K.

Figure 4b illustrates K_2O–SiO_2 variation among the felsic rocks of the Kermadec Arc. Raoul and Curtis Island felsic rocks define a low-K trend, Macauley Island, Russian Seamount and most southern Kermadec volcanoes (including one sample from Brothers) define a medium-K trend and most of the sample collection from Brothers, together with one from Clark, define a

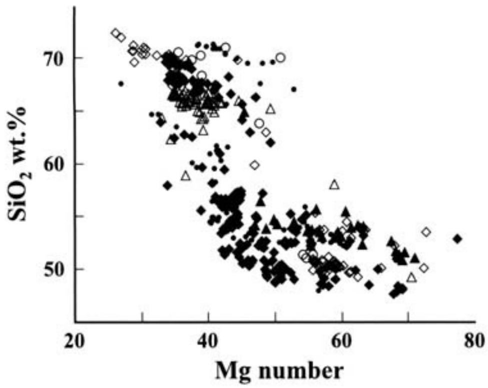

Fig. 5. SiO_2 variation with respect to Mg-number (mol.% MgO/(MgO+FeO); Fe_2O_3/FeO ratio = 0.2). Symbols as for Figure 4b.

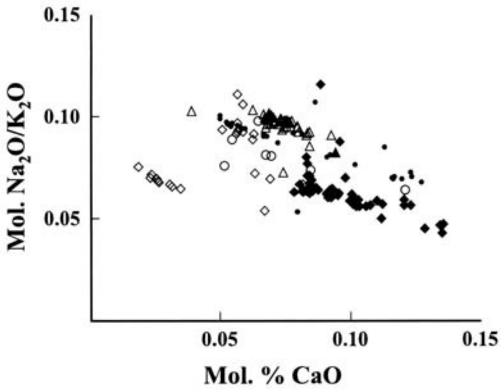

Fig. 6. Molecular alkalies v. CaO for Kermadec rocks >60 wt% SiO_2. Symbols as for Figure 4b.

high-K group. An important observation is that there is considerable compositional diversity amongst the felsic rocks erupted from Kermadec arc volcanoes.

The spectrum includes compositions that are relatively Mg-rich (up to 10 wt% MgO) as well as probable cumulates and low-Mg basalts and basaltic andesites. Felsic compositions show a considerable range of Mg-numbers (Fig. 5) and we argue below that this suggests complex and variable processes of magma generation. Similarly, the variation in alkali ratio and CaO content (Fig. 6) shows Kermadec felsic compositions defining multiple trends and groups rather than the simple variation pattern that could be expected of a simple petrogenetic process involving one type of parental basalt. Further chemical plots (Fig. 7) also serve to support our central point that the composition of Kermadec felsic rocks define fields that are distinct both between volcanoes and, as far as can be determined, within the petrological evolution of single volcanoes, even within short time spans. This is particularly evident for Raoul Volcano, where closely spaced felsic eruptions of different sizes have produced batches of magma that are quite distinct and which do not fall along a single liquid line of descent.

Rare earth element (REE) abundances are available for a representative suite of samples from Raoul (Worthington 1998), for a limited group from Macauley (Smith *et al.* 2003) and for some of the southern Kermadec segment volcanoes (Gamble *et al.* 1997) (Fig. 8). From this limited data set there appear to be two types of REE abundance pattern among Kermadec felsic rocks. A light REE-depleted pattern is correlated with the low-K trend (e.g. Raoul, Tangaroa) and a slightly light REE-enriched pattern correlates with the medium-K trend (Macauley, Rumble IV), and is also found in a high-K sample from Clark Volcano. A small negative Eu anomaly is a feature of both types of pattern.

Isotopic data for a limited range of Kermadec felsic rocks are illustrated in Fig. 9. As noted by previous authors (Gamble *et al.* 1996; Turner *et al.* 1997), there is a correlation between isotopic composition and latitude that defines a Kermadec trend. The available data for felsic rocks indicate that they follow the trend defined by mafic rocks, but for individual volcanoes compositional fields are typically slightly displaced relative to the trend for mafic rocks from the same volcano.

In summary, the chemical compositions of felsic rocks from the Kermadec arc show a pattern of distinct compositional groups, with no consistent trends either between volcanoes or within individual volcanoes. Clearly, because of the submarine nature of most of the volcanoes, samples representing all stages of their petrological evolution are unlikely to ever be available. Because of this, emphasis is placed on the Raoul data set in developing a petrogenetic model.

The origin of intra-oceanic felsic magmatism

One of the most difficult aspects of studying felsic rocks in oceanic settings is the fragmentary nature of the subaerial record and the limitations of sampling in the submarine environment. In the Kermadec arc, felsic rocks have been sampled from the subaerial fragments of

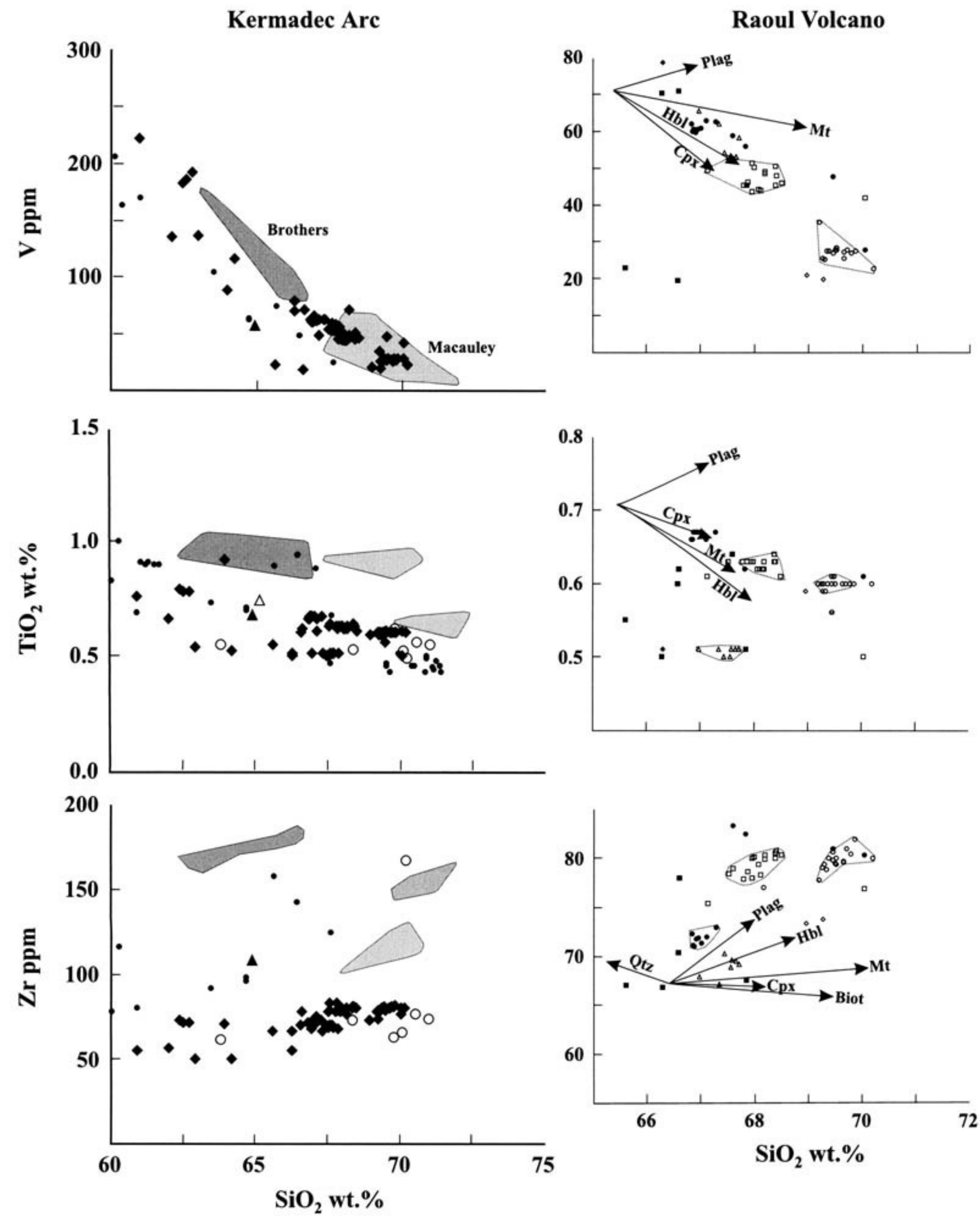

Fig. 7. Chemical variation in Kermadec arc felsic rocks. Symbols for the plots on the left-hand side of the diagram are as for Figure 4b. The right-hand side of the diagram illustrates variation in Raoul felsic batches. Samples from some of the larger individual eruption units are encircled to emphasize their distinct compositions.

major submarine volcanoes in the northern segment and from submarine exposures of large volcanoes in the southern segment. Although it is clear that these volcanoes have been built mainly of basalt and basaltic andesite, the extent to which felsic materials have been produced during their lifetimes is a major uncertainty. In Recent times an abrupt change from early

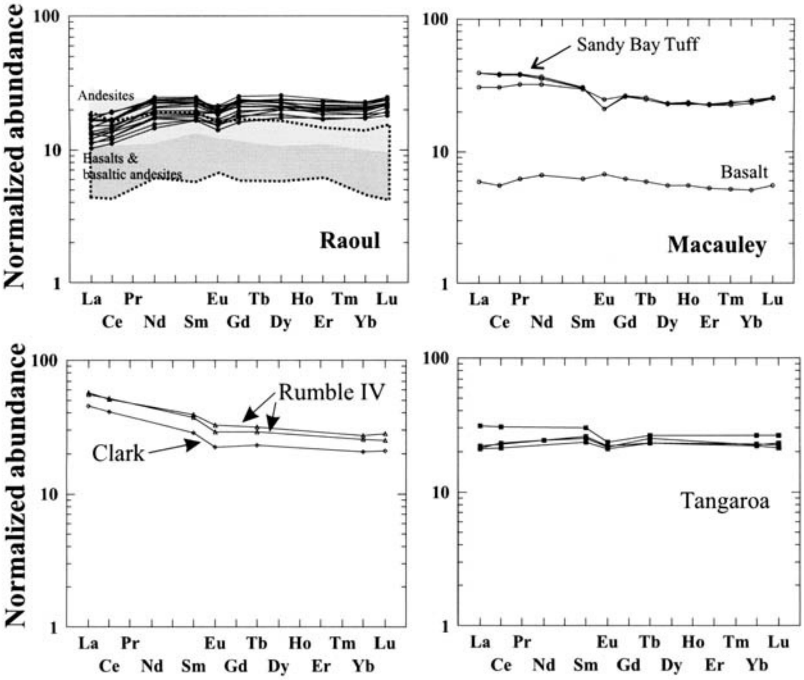

Fig. 8. Chondrite-normalized (values from Wasson & Kallemeyn 1988) rare earth element abundances for Kermadec felsic rocks. Data sources are Raoul (Worthington 1998), Macauley (Smith *et al.* 2003) and Southern Kermadec arc (Gamble *et al.* 1997).

cone-building eruptions of basalt and basaltic andesite to pyroclastic eruptions of dacite occurred on Raoul and Macauley islands. No evidence of earlier felsic volcanism has been found in the more extensive stratigraphic record of Raoul Island. On Macauley the most recent felsic eruption has been followed by a return to basaltic eruptions.

Felsic magmas in intra-oceanic settings could be generated by either fractional crystallization of basaltic parents or by crustal anatexis. Fractional crystallization models require relatively high degrees of crystallization of the parent magma and would be expected to generate small volume melts containing complex phenocryst assemblages that show evidence of a long crystallization history. Derivative melts originating in this way should be erupted intermittently throughout the life of the volcano. A further prediction arising from this type of model is that different batches of felsic magma should be broadly similar in their geochemical characteristics as their evolution should be governed by phenocryst–melt equilibria involving only five phases – plagioclase, olivine, clinopyroxene, orthopyroxene and magnetite. Because no evolved crustal material exists beneath the Kermadec arc an external component cannot be appealed to as a source of compositional variation.

In fact, none of the predictions expected of a fractional crystallization model are met in the suites of samples available from the Kermadec arc. There is a wide diversity within eruption sequences from individual volcanoes and between different volcanoes of the arc. Perhaps the most compelling example is that of Raoul Volcano, where more than 15 km^3 of sparsely porphyritic magma has been erupted during the last 3.7 ka, mostly in the large-scale Fleetwood eruption but also in smaller eruptions that preceded and followed it. Each eruption produced geochemically homogeneous felsic magma, yet each batch is geochemically distinct. The trends defined by this sequence of eruptions from a single volcano cannot be modelled by fractional crystallization if either the parent magma or the fractionating assemblage is held constant. This implies a model in which every magma batch is generated by a unique fractionating assemblage or from a unique parent magma; this appears to us to be unnaturally complicated. On a broader scale, these observations can be applied to the whole Kermadec arc where each volcano has

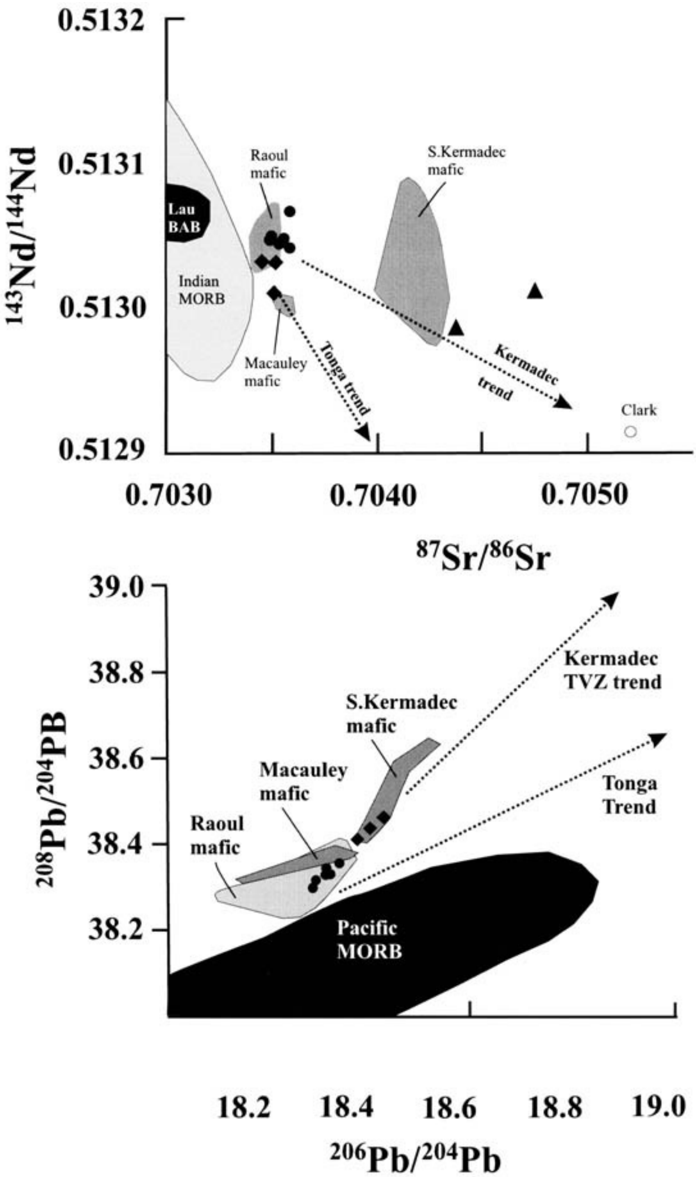

Fig. 9. Plots of isotope ratios for Kermadec felsic samples. Fields after Hergt & Hawkesworth (1994), Turner *et al.* (1997) and references therein, data on felsic rocks from Gamble *et al.* (1997), Worthington (1998) and Smith *et al.* (2003).

produced felsic magma that is distinct, despite the fact that potential parental magmas are essentially similar.

Crustal anatexis

Models that invoke crustal anatexis can explain compositionally diverse magma batches by the generation of near-liquidus melts from a lower crust that in detail is of heterogeneous composition. Many of the petrological characteristics of Kermadec arc dacites that are obstacles to fractional crystallization models are not problems for models based on crustal anatexis. The sparsely porphyritic character of the dacites and their almost complete lack of groundmass crystals are suggestive of near-liquidus primary magmas unmodified prior to eruption.

The critical factors of an anatectic model in oceanic environments are the thermal structure of the crust and the mineralogical and chemical makeup of the lower arc crust. Knowledge of the subarc Kermadec crust can be deduced from information available for the basement of the Tonga segment of the arc (Duncan *et al.* 1985; Bloomer *et al.* 1994; McDougall 1994) and from dredge sampling of basement exposed along the inner trench wall near 20°S, where sediment and lava outcrop from 5 to 7 km water depth, arc lava and gabbro from 7 to 8.5 km, and harzburgite and dunite from 8.9 to 9 km (Bloomer & Fisher 1987). P-wave velocities increase to >6 km s^{-1} at 9–10 km depth below the Tonga–Kermadec Ridge, coinciding with the appearance of arc-type peridotite in the inner trench wall, and the crust-mantle boundary is at 16–19 km depth (Shor *et al.* 1971; Dupont 1988).

The Eocene inception of both the Tonga–Kermadec and Izu–Bonin–Mariana subduction systems was marked by volcanism over a zone >65 to several hundred kilometres wide (Falloon & Crawford 1991; Stern & Bloomer 1992; Bloomer *et al.* 1994). Models constructed to explain these observations envisage that subduction systems are initiated when old oceanic crust founders along a transform fault, inducing extension and subsidence on both sides of the crustal break (Stern & Bloomer 1992). These models predict a progressive change from initial mid-ocean ridge basalts (MORB)-like magmatism across a belt up to several hundred kilometres wide, to boninitic- and supra-subduction-type magmas and eventually to typical subduction-related magmas focused along a narrow volcanic front.

If subduction systems develop along the lines described above, the lower crust of the Tonga–Kermadec Ridge will be a collage of foundered and metamorphosed Mid-Eocene MORB, boninite and subduction-related lava, together with plutonic equivalents of these extrusive rock types, pelagic and deep-sea sediment, and pre-Eocene oceanic crust. The extrusive rocks in this assemblage will have been erupted in a submarine environment and it is reasonable to assume that they will have been hydrothermally altered. Although the bulk composition of the crust would be basaltic, two important implications of this model are, first, that the subarc crust may be heterogeneous in composition over small horizontal and vertical distances and, secondly, that parts will be hydrated and in appropriate pressure–temperature (*P–T*) conditions will be metamorphosed to greenschist- and amphibolite-facies rocks (Peacock *et al.* 1994).

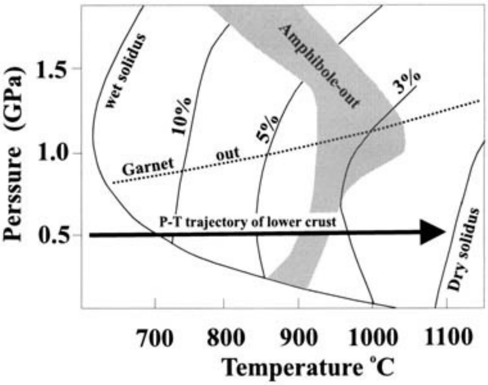

Fig. 10. *P–T* conditions at the base of Kermadec arc crust and the trajectory that would be followed with thermal evolution as the arc crust thickens and matures. Wet and dry solidi after Green (1982) and amphibole-out after Peacock *et al.* (1994). Contours indicate wt% in the melt fraction (Peacock *et al.* 1994).

A major interface in oceanic arc systems is the base of the crust where ascending magma encounters a density change and becomes neutrally buoyant and where ambient temperatures in crustal lithologies are highest. Rock densities near the base of the crust should be between 3.0 (basalt) and 3.3 g cm^{-3} (peridotite), giving a lithostatic pressure range of 0.44–0.61GPa (15–19 km of overlying basalt–peridotite). The temperature near the base of the crust can be estimated from average and maximum geothermal gradients in oceanic crust of 35 and 40°C km^{-1} (calculated from heat flow data in Spear 1993) and a possible range is 525–760°C. Thus, a reasonable estimate of the ambient *P–T* conditions near the base of the crust is 0.5 GPa and 600°C.

In water-undersaturated conditions, fluid-absent (dehydration) melting of amphibole-bearing metabasalt commences at some temperature between the wet and dry solidi (Beard & Lofgren 1991; Rushmer 1991; Peacock *et al.* 1994; Rapp 1995; Rapp & Watson 1995; Nakajima & Arima 1998), and produces melt and an anhydrous residue. The temperature at which amphibole decomposes, the melt composition and the actual make-up of the residual solid assemblage are all sensitive to the bulk composition of the system (Beard & Lofgren 1991; Rushmer 1991; Rapp 1995).

A plausible *P–T* trajectory for Kermadec arc crust starting from ambient conditions of *c.* 0.5 GPa and 600°C is illustrated in Figure 10. Assuming that the crust is not water-saturated, heat derived from the flux of magma through the system will drive the conditions in the crust along an isobaric path toward higher temperatures. When sufficient heat is transferred, melting will begin at a temperature below the amphibole-out phase boundary that depends on bulk composition and water content. Amphibole will be totally consumed at the amphibole-out boundary between 900 and 950°C, generating magma and an anhydrous granulitic residue. Further heat transfer would take the restite assemblage towards the dry solidus located at a temperature above 1100°C. However, extraction of melt, and therefore removal of heat from the system, makes it unlikely that such temperatures will actually be reached.

The geochemistry of the melt generated by heating metabasalt is a complex function of *P*, *T*, water content and bulk composition of the system (Bloomer *et al.* 1994; Winther 1996; Springer & Seck 1997). To a first approximation the effect of water content on the ratio of plagioclase to amphibole entering the melt phase is dominant below the garnet-in boundary. Water-saturated experiments consistently generate peraluminous alkali-rich melts that reflect the melting of plagioclase and quartz, but these are unlike the compositions that are actually observed among the materials that have been erupted from Kermadec arc volcanoes. Dry experiments produce metaluminous melts with relatively low alkali and silica contents, and these do resemble most of the dacites and rhyolites erupted from Kermadec volcanoes

One of the major issues in crustal anatectic models is the origin of the thermal energy needed to raise potential source materials above the ambient *P–T* conditions that can be reasonably assumed for the base of the crust. In continental environments, models involving tectonic shear heating (Hochstein *et al.* 1993) or high heat flux resulting from herniation of the mantle into the lower crust have been suggested. In the relatively simple oceanic setting of the Kermadec arc, evidence for such processes is lacking and we propose an alternative in which the controlling factors are time and the flux of mafic magma from the mantle.

A thermal budget for generating crustal melts in an oceanic arc is given in Table 3. The aim of the model is to assess whether the amount of heat required to melt the crust (Q_M) is of the same order of magnitude as the amount of heat that could reasonably be added to the crust by the flux of magma from below. An important point here is that it is only magma that remains at or near the base of the crust that will have an effect on potential source areas.

Estimates of the volumes of magma involved in individual felsic eruptions from Kermadec volcanoes range up to 15 km^3 for the Fleetwood Tephra eruption from Raoul Volcano. Experimental work (Beard & Lofgren 1991; Rapp 1995; Nakajima & Arima 1998) has shown that dehydration melting of metabasalt typically yields a melt fraction of 15–25% at the amphibole-out boundary. Assuming a melt fraction of 20% and a magma volume of 10 km^3, a reasonable estimate for the volume of crust involved in a melting episode (V_C) is 50 km^3. A value of 3.1 g cm^{-3} is a reasonable estimate for the density of crust (ρ_C) composed of basalt with an ultramafic component. Assuming an ambient lower crustal temperature (T_A) of 600°C and a melt temperature (T_M) of 950°C, the crustal heat content (H_A, H_{MC}) at T_A and T_M can be calculated for average oceanic crust by interpolating from thermodynamic data listed in Robie *et al.* (1979). The latent heat of fusion of Kermadec dacite (ΔH_F) can be estimated from thermodynamic data listed in Lange & Carmichael (1990) and the density (ρ_M) can be calculated using the method of Bottinga & Weill (1970). The magnitude of Q_M is most sensitive to errors in V_C, V_M and T_M and relatively insensitive to possible errors in ρ or to assumptions used in calculating H and ΔH_F.

For a first-order model the heat added to the subarc crust (Q_M) is provided by the latent heat of crystallization of underplated magma cooling from an initial temperature (T_B) to the solidus temperature (T_X), and of the resulting crystalline accumulation to the temperature at which dehydration melting occurs in the adjacent crust T_M. The major uncertainties in this calculation are the volume of magma that underplates the crust, the estimated volume of crystals formed and the assumptions made regarding the ratio of intruded to erupted magma. A reasonable estimate for the volume of magma that underplates the crust is 300 km^3 (V_B) and this crystallizes 50 km^3 of cumulates. The complementary fractionated magma rises through the crust, building a volcanic edifice of approximately 200 km^3 that is the approximate size of many Kermadec volcanoes. Magma generated in the mantle has a temperature of about 1250°C and the density of primitive melts is about 2.8g cm^{-3} (Stolper *et al.* 1981). A reasonable estimate for T_X is 1100°C. A crystal cumulate composition based on 50% fractionation at the olivine–clinopyroxene cotectic and 50% fractionation within the plagioclase-dominated interval is 15% olivine, 50% pyroxene, 30% plagioclase, 5% oxide. Cumulate heat content, latent heat of crystallization and density of the cumulate pile can be estimated using data from Deer *et al.* (1966),

Table 3. *A thermal budget for generating felsic magmas in intra-oceanic arcs by crustal anatexis (values for variables given are assumed or (estimated)*

(a) Heat required to generate a crustal melt (Q_M)

$$Q_M = [V_C \times (H_{MC} - H_A) \times \rho_C] + [V_M \times \Delta H_F \times \rho_M]$$
$$= [(1.0 \times 10^{16}) \times (990 - 580) \times 3.1] + [(1.0 \times 10^{16}) \times 313 \times 2.52]$$
$$= 2.06 \times 10^{19}$$

V_C	Total volume of crustal source	$1.0 \times 10^{16} cm^3$
H_{MC}	Heat content of crust at melting temperature T_M ($J\ g^{-1}$)	$990\ J\ g^{-1}$
H_A	Heat content of crust at ambient temperature T_A ($J\ g^{-1}$)	$580\ J\ g^{-1}$
ρ_C	Density of the crust ($g\ cm^{-3}$)	$3.1\ g\ cm^{-3}$
V_M	Volume of melt produced (cm^3)	1.0×10^{16}
ΔH_F	Latent heat of fusion ($J\ g^{-1}$)	$313\ J\ g^{-1}$
ρ_M	Density of the melt ($g\ cm^{-3}$)	$2.52\ g\ cm^{-3}$

(b) Heat available to heat the crust by underplating magma (Q_B)

$$Q_B = [V_B \times (T_B - T_X) \times C_B \times \rho_B] + [V_X \times \Delta H_X \times \rho_X] + [V_X \times (H_X - H_{MX}) \times \rho_X]$$
$$= [(3.0 \times 10^{17}) \times (1525 - 1370) \times 1.23 \times 2.8] + [(5.0 \times 10^{16}) \times 580 \times 3.27]$$
$$+ [(5.0 \times 10^{16}) \times (1160 - 980) \times 3.27]$$
$$= 28.44 \times 10^{19}$$

V_B	Volume of magma underplating crust (cm^3)	$3.0 \times 10^{17} cm^3$
T_B	Temperature of magma reaching the lower crust (K)	1525 K
T_X	Temperature at which last crystals form (K)	1370 K
C_B	Specific heat capacity of the magma ($J\ g^{-1}\ K^{-1}$)	$1.23\ J\ g^{-1}\ K^{-1}$
ρ_B	Density of the magma ($g\ cm^{-3}$)	$2.8\ g\ cm^{-3}$
V_X	Volume of the crystal cumulate (cm^3)	$5.0 \times 10^{16} cm^3$
ΔH_X	Latent heat of crystallization ($J\ g^{-1}$)	$580\ J\ g^{-1}$
ρ_X	Density of the crystal cumulate ($g\ cm^{-3}$)	$3.27 g\ cm^{-3}$
H_X	Heat content of crystal cumulate at T_X ($J\ g^{-1}$)	$1160\ J\ g^{-1}$
H_{MX}	Heat content of crystal cumulate at T_M ($J\ g^{-1}$)	$980\ J\ g^{-1}$

Robie *et al.* (1979) and Lange & Carmichael (1990). Substantial variations in the composition of the crystal assemblage cause small changes in these parameters. The specific heat capacity of basalt magma is taken as $1.23\ J\ g^{-1}\ K^{-1}$ (Guffanti *et al.* 1996). The magnitude of Q_B is most sensitive to V_B, V_X and T_X. Approximately 55% of Q_B is released during cooling of the magma, 35% during crystallization and 10% by cooling of the crystal pile.

The calculations presented in Table 3 show that to a first approximation there is enough heat contributed by the process of underplating and deep crustal intrusion to drive the physical conditions in the lower crust into the *P–T* window where dehydration melting is feasible. Approximately 90% of Q_M is required to heat the crust prior to melting. In reality, the problem of heat transmission is significant but difficult to quantify. However, once a fluid is present even within a small volume of source material, heat transmission becomes more efficient and melting can propagate through a volume of pre-conditioned material. In this way, once melting is triggered, relatively large volumes of felsic magma can be generated rapidly.

A time-span of the order of 1 Ma is required for convective heating of the subarc crust to the point of anatexis; this timescale is consistent with recent modelling of the thermal effects of deep magma intrusion (Annen & Sparks 2002) and also with the suggestion that the Kermadec arc has entered into a felsic phase in Recent times. An implication of the proposal that time is the controlling factor in determining the process of anatexis in oceanic arcs is that it is a unique and irreversible process. Once the crust has dehydrated no more melting can occur unless the crust is rehydrated or the temperature raised to unrealistic levels, in which case partial melts will not resemble Kermadec dacites. However, it must be recognized that this conclusion is based on a record that is far from complete.

Structural setting of felsic volcanism

Both Denham Caldera on Raoul (Worthington *et al.* 1999) and the larger and more complex Macauley Caldera 110 km to the south (Lloyd *et al.* 1996; Smith *et al.* 2003) are elongate with their long axes trending 065°, suggesting control by a regional fracture system. However, the margins of Denham Caldera are not coincident with preferred fault directions on Raoul Island, which are either parallel (015°) or orthogonal (105°) to the Tonga–Kermadec arc and reflect a stress field dominated by extension orthogonal to the arc (Apperson 1991; Lloyd & Nathan 1981). Instead, the long axes of both Denham Caldera and Macauley Caldera are subparallel to the tectonic fabric of the active back arc Harvre Trough (045°–060°) (Caress 1991; Worthington *et al.* 1999).

Crustal extension across the Lau–Colville Ridge (a Miocene arc) commenced at about 6 Ma culminating with the separation of the Tonga–Kermadec Ridge and inception of the back-arc Lau Basin–Havre Trough (Hawkins 1995). Volcaniclastic sediments record a period of voluminous felsic eruptions during the arc rifting phase analogous to that of the presently rifting northern Izu arc. At both arcs voluminous felsic volcanism has been attributed to a strongly extensional stress regime (Gill *et al.* 1992; Clift 1995). Subsequently, the Tonga–Kermadec arc has developed since 3 Ma and mafic volcanism has predominated (Clift 1995). In the back-arc basin, new crust is generated at spreading centres in the Lau Basin north of 23°S, whereas crustal extension continues throughout the Havre Trough (Wright 1993; Parson & Wright 1996).

The northern Harvre Trough is now 120–130 km wide and the period of felsic volcanism associated with rifting of the Lau–Colville arc is long gone. It is suggested that the recent voluminous reoccurrence of felsic eruptions at Raoul and Macauley reflects the geometry of the Havre Trough, in which extension takes place within a series of en echelon rifts that are oblique to the arc (Caress 1991; Wright 1993). This model envisages that these 045°–060°-trending rifts propagate to the volcanic front, where they transfer a significant component of extension to the magmatic system and overlying crust. This facilitates both the ascent of relatively viscous felsic magmas and caldera formation. A series of 060°-trending bathymetric depressions can be seen crossing the northern Havre Trough and heading towards the volcanic front near Raoul, Macauley and elsewhere on high-resolution maps compiled from satellite altimetry (Smith & Sandwell 1997). These depressions are inferred to be rifts.

Conclusions

A significant feature of the petrology of felsic rocks in the Kermadec arc is their variability within and between volcanoes despite the fact that the predominant basaltic–andesitic rocks are essentially the same along the length of the arc. This leads us to the conclusion that an anatectic model provides a more likely explanation for the origin of the felsic magmas than fractionation in this particular arc setting. First-order quantification of the thermal structure and evolution of the Kermadec arc indicates that sufficient heat is available to drive crustal anatexis provided that there was sufficient time for transfer of heat from underplating and intruding magma. We suggest that by extrapolating the thermal models for cooling of single plutons (e.g. Norton & Knight 1977) that the time involved in attaining anatectic conditions in the subarc crust is of the order of 0.1–1.0 Ma. This timescale of <1 Ma for convective cooling of magma and convective heating of adjacent lower crust is one of the keys to understanding the origin of large-scale felsic magmatism in oceanic arcs.

The widespread felsic magmatism observed in the recent record of the Kermadec arc is anomalous. Dehydration melting of lower arc crust best explains the observed diverse chemistry of felsic magmas, and the timescale of heat transfer by means of the flux of primitive magma from the underlying subduction system is comparable with the age of the arc. An important question is whether the crustal anatexis in oceanic arc settings is a singular event in the evolution of an intra-oceanic arc or whether, once initiated, it accompanies basaltic–andesitic subduction-related magmatism through the subsequent life of the system.

Observations from the Kermadec arc show that felsic magmatism has become a feature of the system in Recent times but the record is limited. Observations from other oceanic arcs shows that felsic magmatism is relatively rare in this type of tectonic environment. These observations can be reconciled if, once the lower crust has dehydrated, no more crustal melting can occur in the anhydrous lower crustal residue.

Following from this argument, oceanic arcs can be seen as evolving through four stages (Fig. 11).

1 Generation of subduction-related basaltic magmas initiates a volcanic system on oceanic crust. Primitive magmas underplate and intrude the subarc crust across a (typically) 40 km-wide zone. Underplating magmas cool and crystallize, and hydrothermal convection

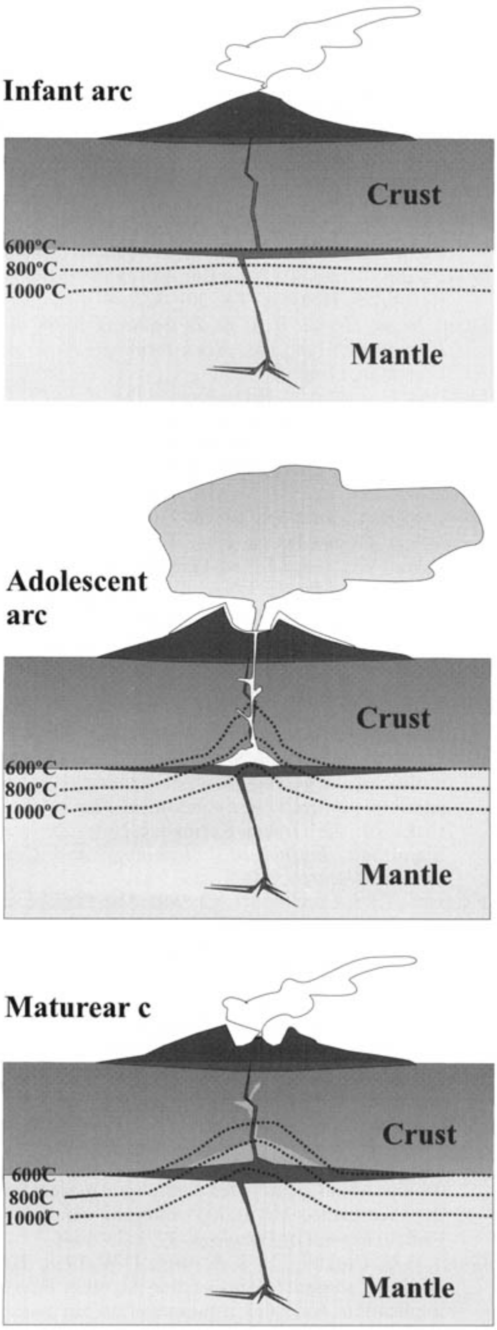

Fig. 11. Schematic model for the evolution of intra-oceanic volcanic arcs (see text for explanation).

develops through the lower crust. Isotopic constraints suggest that the source of water is the underplating subduction-related magma (e.g. Borg & Clynne 1998). Subduction-related magmas do contain significant water, there is experimental evidence for up to 4 wt% water in arc–type basalts (Sisson & Grove 1993). However, if this is the only source of water there is a finite limit on the extent to which hydrothermal systems can modify the deep subarc crust. At the top of the system relatively fractionated (but still essentially basaltic) magmas begin to build a volcanic edifice.

2 During arc infancy (0.5–1.0 Ma) heat is transferred by convection to the lower arc crust. Hydration of crust through reaction of pyroxene±olivine-bearing lithologies with hydrous fluids produces amphibole and this is an exothermic reaction (Spear 1993) that further raises crustal isotherms. Surficial eruption continues with eruption of basalt–andesite magmas.

3 A stage of arc adolescence (1–2 Ma) commences as the temperature of a significant volume of lower crust approaches the amphibole-saturated solidus at 850–950°C. Initiation of dehydration melting fluxes the crust and melt volumes of a few km^3 to tens of km^3 are rapidly generated. A 20–30% melt fraction segregates from a granulitic residue and ascends to upper levels in the system. Triggering mechanisms include episodic transfer of extensional strain into the crust or a pulse of magma associated with a major recharge event. Felsic magmatic eruptive activity may be interspersed with continuing basaltic–andesitic activity.

4 Arc maturity (>3 Ma) sees a continuation of basaltic to andesitic activity. The lower crust having undergone dehydration melting is now anhydrous granulite significantly below its solidus temperature and it acts as a thermal insulator preventing convection of hydrothermal fluids. Further anatexis can only occur if appropriate source materials remain to participate in the hydration–dehydration cycle.

This model predicts that felsic magmatism in intra-oceanic systems will be a feature of those arcs passing through adolescence. This fits the observation from the Kermadec arc of widespread Recent felsic volcanism and the relative scarcity of felsic rocks in other intra-oceanic arcs.

We would like to acknowledge the New Zealand Lottery Grants Board who supported field work on Macauley Island (Lottery Science Grant SR022590) and John Young of the yacht *Blackadder* who provided unrivalled logistic support in the Kermadec Islands. We also acknowledge the University of Auckland Research Committee for providing a grant to support participation in SONNE 135 research cruise, and P. Stoffers and I. Wright who led the cruise. Thoughtful reviews were provided by R. Macdonald and T. Riley.

References

ANNEN, C. & SPARKS, R.S.J. 2002. Effects of repetitive emplacement of basaltic intrusions on thermal evolution and melt generation in the crust. *Earth and Planetary Science Letters*, **203**, 937–955.

APPERSON, K.D. 1991. Stress fields of the overriding plate at convergent margins and beneath active volcanic arcs. *Science*, **254**, 670–678.

BEARD, J.S. & LOFGREN, G.E. 1991. Dehydration melting and water saturated melting of basaltic and andesitic greenstones and amphibolites at 1, 3 and 7 kb. *Journal of Petrology*, **32**, 365–401.

BEVIS, M., TAYLOR, F.W., SCHUTZ, B.E., RECY, J., ISACKS, B.L., HELU, S., SINGH, R., KENDRICK, E., STOWELL, J., TAYLOR, B. & CALMANT, S. 1995. Geodetic observations of very rapid convergence and back-arc extension at the Tonga arc. *Nature*, **374**, 249–251.

BLOOMER, S.H. & FISHER, R.L. 1987. Petrology and geochemistry of igneous rocks from the Tonga Trench – a non accreting plate boundary. *Journal of Geology*, **95**, 469–495.

BLOOMER, S.H., EWART, A., HERGT, J.M. & BRYAN, W.B. 1994. Geochemistry and origin of igneous rocks from the outer Tonga fore arc (Site 841). *In*: HAWKINS, J., PARSON, L., ALLAN, J. *et al. Proceedings of the Ocean Drilling Program, Scientific Results*, **135**, 625–646.

BLOOMER, S.H., STERN, R.J. & SMOOT, N.C. 1989. Physical volcanology of the submarine Mariana and Volcano arcs. *Bulletin of Volcanology*, **51**, 210–224.

BORG, L.E. & CLYNNE, M.A. 1998. The petrogenesis of felsic calc-alkaline magmas from the southernmost Cascades, California, origin by partial melting of basaltic lower crust. *Journal of Petrology*, **39**, 1197–1222.

BOTTINGA, Y. & WEILL, D.F. 1970. Densities of liquid silicate systems calculated from partial molar volumes of oxide components. *American Journal of Science*, **269**, 169–182.

BROTHERS, R.N. & SEARLE, E.J. 1970. The geology of Raoul Island, Kermadec Group, southwest Pacific. *Bulletin Volcanologique*, **34**, 7–37.

CANZ. 1997. *New Zealand Region Bathymetry.* New Zealand Oceanographic Institute Miscellaneous Charts No. 73. National Institute of Water and Atmospheric Research.

CARESS, D.W. 1991. Structural trends and back-arc extension in the Harvre Trough. *Geophysical Research Letters*, **18**, 853–856.

CHASE, T.E. 1985. Submarine topography of the Tonga–Fiji region and the southern Tonga Platform area. *In*: SCHOLL, D.W. & VALLIER, T.L. (eds) *Geology and Offshore Resources of Pacific Island Arcs – Tonga Region.* Circum-Pacific Council for Energy and Mineral Resources, Houston, TX, 21–22.

CLIFT, P.D. 1995. Volcaniclastic sedimentation and volcanism during the rifting of Western Pacific backarc basins. *In*: TAYLOR, B. & NATLAND, J. (eds) *Active Margins and Marginal Basins of the Western Pacific.* American Geophysical Union Monographs, **88**, 67–96.

CRAWFORD, A.J., GREENE, H.J. & EXON, N.F. 1988. Geology, petrology and geochemistry of submarine volcanoes around Epi Island, New Hebrides island arc. *In*: GREENE, H.G. & WONG, F.L. (eds) *Geology and Offshore Resources of Pacific Island Arcs – Vanuatu Region.* Circum-Pacific Council for Energy and Mineral Resources, Houston, TX, 301–327.

DEER, W.A., HOWE, R.A. & ZUSSMAN, J. 1966. *An Introduction to the Rock-forming Minerals.* Longman, London.

DEMETS, C., GORDON, R.G., ARGUS, D.F. & STEIN, S. 1994. Effects of recent revisions to the geomagnetic reversal time scale on estimates of current plate motions. *Geophysical Research Letters*, **21**, 2191–2194.

DUNCAN, R.A., VALLIER, T.L. & FALVEY, D.A. 1985. Volcanic episodes on Eua, Tonga. *In*: SCHOLL, D.W. & VALLIER, T.L. (eds) *Geology and Offshore Resources of Pacific Island Arcs – Tonga Region.* Circum-Pacific Council for Energy and Mineral Resources, Houston, TX, 281–290.

DUPONT, J. 1988. The Tonga and Kermadec Ridges. *In*: NAIRN, A.E.M., STEHLI, F.G. & UYEDA, S. (eds) *The Ocean Basins and Margins Volume 7b, The Pacific Ocean.* Plenum Press, New York, 375–409.

EWART, A., BROTHERS, R.N. & MATEEN, A. 1977. An outline of the geology and geochemistry and the possible petrogenetic evolution of the volcanic rocks of the Tonga–Kermadec–New Zealand island arc. *Journal of Volcanology and Geothermal Research*, **2**, 205–250.

FALLOON, T.J. & CRAWFORD, A.J. 1991. The Petrogenesis of high-calcium boninite lavas dredged from the northern Tonga Ridge. *Earth and Planetary Science Letters*, **102**, 375–394.

GAMBLE, J.A., CHRISTIE, R.H.K., WRIGHT, I.C. & WYSOCZANSKI, R.J. 1997. Primitive K-rich magmas from Clark Volcano, Southern Kermadec arc: a paradox in the K–depth relationship. *Canadian Mineralogist*, **35**, 275–290.

GAMBLE, J.A., WOODHEAD, J.D., WRIGHT, I.C. & SMITH, I.E.M. 1996. Basalt and sediment geochemistry and magma petrogenesis in a transect from oceanic island arc to rifted continental margin arc: the Kermadec–Hikurangi margin, southwest Pacific. *Journal of Petrology*, **37**, 1523–1546.

GEIST, E.L., CHILDS, J.R. & SCHOLL, D.W. 1988. The origin of summit basins of the Aleutian Ridge: implications for block rotations of an arc massif. *Tectonics*, **7**, 327–341.

GILL, J.B. 1981. *Orogenic Andesites and Plate Tectonics.* Springer, New York.

GILL, J.B., SEALES, C., THOMPSON, P., HOCHSTAEDTER, A.G. & DUNLAP, C. 1992. Petrology and geochemistry of Pliocene-Pleistocene volcanic rocks from the Izu arc, Leg 126. *In*: TAYLOR, B., FUJIOKA, K. *et al. Proceedings of the Ocean Drilling Program, Scientific Results*, **126**, 383–404.

GREEN, T.H. 1982. Anatexis of mafic crust and high pressure crystallization of andesite. *In*: THORPE, R.S. (ed.) *Andesites: Orogenic Andesites and Related Rocks*. John Wiley, Chichester, 499–487.

GREENE, H.G., MACFARLANE, A., JOHNSTON, D.P. & CRAWFORD, A.J. 1988. Structure and tectonics of the central New Hebrides arc. *In*: GREENE, H.G. & WONG, F.L. (eds) *Geology and Offshore Resources of Pacific Island Arcs – Vanuatu Region*. Council for Energy and Mineral Resources, Houston, TX, 377–412.

GUFFANTI, M., CLYNNE, M.A. & MUFFLER, L.J.P. 1996. Thermal and mass implications of magmatic evolution in the Lassen volcanic region, California, and minimum constraints on basalt influx to the lower crust. *Journal of Geophysical Research*, **101**, 3003–3013.

HAWKINS, J.W. 1995. Evolution of the Lau Basin – insights from ODP Leg 135. *In*: TAYLOR, B. & NATLAND, J. (eds) *Active Margins and Marginal Basins of the Western Pacific*. American Geophysical Union Monographs, **88**, 125–173.

HERGT, J.M. & HAWKESWORTH, C.J. 1994. Pb-, Sr-, and Nd-isotopic evolution of the Lau Basin: implications for mantle dynamics during backarc opening. *In*: HAWKINS, J., PARSON, L., ALLAN, J.F. *et al. Proceedings of the Ocean Drilling Program, Scientific Results*, **135**, 505–517.

HOCHSTEIN, M.P., SMITH, I.E.M., REGENAUER-LEIB, K. & EHARA, S. 1993. Geochemistry and heat transfer processes in Quaternary rhyolitic systems of the Taupo Volcanic Zone, New Zealand. *Tectonophysics*, **223**, 213–235.

LANGE, R.L. & CARMICHAEL, I.S.E. 1990. Thermodynamic properties of silicate liquids with emphasis on density, thermal expansion and compressibility. *Reviews in Mineralogy*, **24**, 25–64.

LEAT, P.T., SMELLIE, J.L, MILLAR, I.L. & LARTER, R.D. 2003. Magmatism in the South Sandwich arc. *In*: LARTER, R.D. & LEAT, P.T. (eds) *Intra-oceanic Subduction Systems: Tectonic and Magmatic Processes*. Geological Society, London, Special Publications, **219**, 285–313.

LLOYD, E.F. & NATHAN, S. 1981. Geology and tephrochronology of Raoul Island, Kermadec Group, New Zealand. *New Zealand Geological Survey, Bulletin*, **95**.

LLOYD, E.F., NATHAN, S., SMITH, I.E.M. & STEWART, R.B. 1996. Volcanic history of Macauley Island, Kermadec Group, New Zealand. *New Zealand Journal of Geology and Geophysics*, **39**, 295–308.

MCDOUGALL, I. 1994. Data report: dating of rhyolitic glass in the Tonga forearc (Hole 841b). *In*: HAWKINS, J., PARSON, L., ALLAN, J. *et al. Proceedings of the Ocean Drilling Program, Scientific Results*, **135**, 923.

MILLER, T.P. 1995. Late Quaternary caldera formation along the Aleutian arc: distribution, age and volume. *Eos, Transactions of the American Geophysical Union*, **76**, F680.

MONZIER, M., ROBIN, C. & EISSEN, J.-P. 1994. Kuwae (*c*. 1425 A.D.): the forgotten caldera. *Journal of Volcanology and Geothermal Research*, **59**, 207–218.

NAKAJIMA, K. & ARIMA, M. 1998. Melting experiments on hydrous low-K tholeiite: implications for the genesis of tonalitic crust in the Izu–Bonin–Mariana arc. *The Island Arc*, **7**, 359–373.

NGDC. 1996. *Terrainbase Global DTM Version 1.0*. National Geophysical Data Centre and World Data Centre–A, Solid Earth Geophysics, Boulder, CO.

NORTON, D. & KNIGHT, J. 1977. Transport phenomena in hydrothermal systems: cooling plutons. *American Journal of Science*, **277**, 937–981.

PARSON, L.M. & WRIGHT, I.C. 1996. The Lau–Havre–Taupo back-arc basin: a southward-propagating, multi-stage evolution from rifting to spreading. *Tectonophysics*, **263**, 1–22.

PEACOCK, S.M., RUSHMER, T. & THOMPSON, A.B. 1994. Partial melting of subducting oceanic crust. *Earth and Planetary Science Letters*, **121**, 227–244.

PEARCE, J.A., BAKER, P.E., HARVEY, P.K. & LUFF, L.W. 1995. Geochemical evidence for subduction fluxes, mantle melting and fractional crystallization beneath the South Sandwich island arc. *Journal of Petrology*, **36**, 1073–1109.

RAPP, R.P. 1995. Amphibole-out phase boundary in partially melted metabasalt, its control over liquid fraction and composition and source permeability. *Journal of Geophysical Research*, **100**, 15 601–15 610.

RAPP, R.P. & WATSON, E.B. 1995. Dehydration melting of metabasalt at 8–32 kbar: implications for continental growth and crust–mantle recycling. *Journal of Petrology*, **36**, 891–931.

ROBIE, R.A., HEMINGWAY, B.S. & FISHER, J.R. 1979. Thermodynamic properties of minerals and related substances at 298.15K and 1 bar (10^5 Pascals) pressure and at higher temperatures. *United States Geological Survey Bulletin*, **1452**.

ROBIN, C., EISSEN, J.-P. & MONZIER, M. 1993. Giant tuff cone and 12 km-wide associated caldera at Ambryn Volcano (Vanuatu, New Hebrides arc). *Journal of Volcanology and Geothermal Research*, **55**, 225–238.

RUSHMER, T. 1991. Partial melting of two amphibolites; contrasting experimental results under fluid-absent conditions. *Contributions to Mineralogy and Petrology*, **107**, 41–59.

SHOR, G.G., KIRK, H.K. & MENARD, H.W. 1971. Crustal structure of the Melanesian area. *Journal of Geophysical Research*, **76**, 2562–2586.

SISSON, T.W. & GROVE, T.L. 1993. Temperatures and H_2O contents of Low-MgO High-Alumina basalts. *Contributions to Mineralogy and Petrology*, **113**, 167–184.

SMITH, I.E.M., BROTHERS, R.N., MUIRURI, F.G. & BROWNE, P.R.L. 1988. The geochemistry of rock and water samples from Curtis Island Volcano, Kermadec Group, southwest Pacific. *Journal of Volcanology and Geothermal Research*, **34**, 233–240.

SMITH, I.E.M., STEWART, R.B. & PRICE, R.C. 2003. The petrology of a large-scale intra-oceanic felsic eruption: the Sandy Bay Tuff, Kermadec arc. *Journal of Volcanology and Geothermal Research*, **124**, 173–194.

SMITH, I.E.M., WORTHINGTON, T.J., PRICE, R.C. & GAMBLE, J.A. 1997. Primitive magmas in arc-type volcanic associations. *Canadian Mineralogist*, **35**, 257–273.

SMITH, W.H.F. & SANDWELL, D.T. 1997. Global seafloor topography from satellite altimetry and ship depth soundings. *Science*, **277**, 1956–1962.

SPEAR, F.S. 1993. *Metamorphic Phase Equilibria and Pressure–Temperature–Time Paths*. Mineralogical Society of America, Monographs, **1**.

SPRINGER, W. & SECK, H.A. 1997. Partial fusion of basic granulites at 5 to 15 kb: implications for the origin of TTG magmas. *Contributions to Mineralogy and Petrology*, **127**, 30–45.

STERN, R.J. & BLOOMER, S.H. 1992. Subduction zone infancy: examples from the Izu–Bonin–Mariana and Jurassic California arcs. *Geological Society of America, Bulletin*, **104**, 1621–1636.

STOFFERS, P., WRIGHT, I.C. & SHIPBOARD PARTY. 1999. *Havre Trough–Taupo volcanic zone: tectonic, magmatic and hydrothermal processes. Cruise Report Sonne 135*. Berichte – Reports, Institut für Geowissenschaften University of Kiel, **1**.

STOLPER, E., WALKER, R.J., HAGER, B. & HAYS, J.F. 1981. Melt segregation from partially molten source regions: the importance of melt density and source region size. *Journal of Geophysical Research*, **86**, 6261–6271.

TAGUDIN, J.E. & SCHOLL, D.W. 1994. The westward migration of the Tofua volcanic arc toward Lau Basin. *In*: STEVENSON, A.J., HERZER, R.H. & BALLANCE, P.F. (eds) *Geology and Submarine Resources of the Tonga–Lau–Fiji Region. SOPAC Technical Bulletin*, **8**, 121–129.

TAMURA, Y. & TATSUMI, Y. 2002. Remelting of an andesitic crust as a possible origin for rhyolitic magma in oceanic arcs: an example from the Izu–Bonin arc. *Journal of Petrology*, **43**, 1029–1047.

TAYLOR, B., KLAUS, A., BROWN, G.R., MOORE, G.F., OKAMURA, Y. & MURAKAMI, F. 1991. Structural development of the Sumisu Rift, Izu–Bonin arc. *Journal of Geophysical Research*, **96**, 16 113–16 129.

TURNER, S.P., HAWKESWORTH, C.J., ROGERS, N., BARLETT, J., WORTHINGTON, T.J., HERGT, J., PEARCE, J.A. & SMITH, I.E.M. 1997. ^{238}U–^{230}Th disequilibria, magma petrogenesis, and flux rates beneath the depleted Tonga–Kermadec island arc. *Geochimica et Cosmochimica Acta*, **61**, 4855–4884.

VAN DER HILST, R. 1995. Complex morphology of subducted lithosphere in the mantle beneath the Tonga Trench. *Nature*, **374**, 154–157.

WASSON, K. & KALLEMEYN, G.W. 1988. Compositions of chondrites. *Philosophical Transactions of the Royal Society of London, Series A*, **325**, 535–544

WINTHER, K.T. 1996. An experimentally based model for the origin of tonalitic and trondjemitic melts. *Chemical Geology*, **127**, 43–59.

WORTHINGTON, T.J. 1998. *Geology and petrology of Raoul Volcano: magma genesis and fractionation processes beneath the Tonga Kermadec arc*. PhD thesis, University of Auckland.

WORTHINGTON, T.J., GREGORY, M.R. & BONDARENKO, V. 1999. The Denham Caldera on Raoul Volcano: dacitic volcanism in the Tonga–Kermadec arc. *Journal of Volcanology and Geothermal Research*, **90**, 29–48.

WRIGHT, I.C. 1993. Pre-spread rifting and heterogeneous volcanism in the southern Havre Trough back-arc basin. *Marine Geology*, **113**, 179–200.

WRIGHT, I.C. 1994. Nature and tectonic setting of the southern Kermadec submarine arc volcanoes: an overview. *Marine Geology*, **118**, 217–236.

WRIGHT, I.C. & GAMBLE, J.A. 1999. Southern Kermadec submarine caldera arc volcanoes (SW Pacific): caldera formation by effusive and pyroclastic eruption. *Marine Geology*, **161**, 207–227.

WRIGHT, I.C., PARSON, L.M. & GAMBLE, J.A. 1996. Evolution and interaction of migrating cross-arc volcanism and back arc rifting: an example from the Southern Havre Trough (35°20′–37°S). *Journal of Geophysical Research*, **101**, 22 071–22 086.

Chemically rich and diverse submarine hydrothermal plumes of the southern Kermadec volcanic arc (New Zealand)

GARY J. MASSOTH[1], CORNEL E.J. DE RONDE[1], JOHN E. LUPTON[2], RICHARD A. FEELY[3], EDWARD T. BAKER[3], GEOFFREY T. LEBON[3] & STACY M. MAENNER[3]

[1]*Institute of Geological and Nuclear Sciences, Lower Hutt, New Zealand (e-mail: g.massoth@gns.cri.nz)*

[2]*Pacific Marine Environmental Laboratory, National Oceanic and Atmospheric Administration, Newport, OR 97365–5258, USA*

[3]*Pacific Marine Environmental Laboratory, National Oceanic and Atmospheric Administration, Seattle, WA 98115–6349, USA*

Abstract: The New Zealand American PLUme Mapping Expedition (NZAPLUME) provided the first systematic survey of chemical emissions along a submarine volcanic frontal arc. Chemical plumes emanated from seven of 13 volcanoes that line a 260 km-long section of the southern Kermadec arc northeast of New Zealand. Hydrothermal plumes ranged in depth from <200 to 1500 m and are generally more shallow than plumes over mid-ocean ridges (MORs). The chemical signatures of plumes along the southern Kermadec arc are unusually diverse and have concentration anomalies for CO_2, H_2S and Fe that can exceed those for MOR settings by 5–10 times, or more. Projected end-member fluid concentrations of carbon and sulphur gases at some volcanoes require a magmatic vapour source, while unusually high Fe concentrations and Fe/Mn values are consistent with venting an iron-rich magmatic brine. Thus, vent-fluid emissions on the Kermadec arc volcanoes often appear as hybrid mixtures of hydrothermally *evolved* sea water influenced by water–rock reaction with compositionally diverse arc lavas, and *exsolved* magmatic fluid present as gaseous (CO_2 and SO_2+H_2S) and liquid (Fe-rich brines) components. While rock-buffered fluids in arc settings are expected to vary compositionally from one another and from MOR fluids, it is the magmatic components that clearly differentiate arc emissions as being super-enriched in sulphur gases and ionic metals. These first systematic observations of spatially frequent and chemically robust fluid emissions from southern Kermadec arc forecast arcs as being a potentially important source of chemicals to the oceans.

Volcanic arcs are a natural and ubiquitous consequence of plate convergence and subduction. Constructional arc volcanism profoundly inflates our planetary morphology and globally contributes about 15% of crustal accretion (Crisp 1984). Magmatic volatiles discharged from subaerial arc volcanoes add significantly to the global atmospheric budgets of non-anthropogenic trace metals (Nriagu 1989). While magmatic–hydrothermal processes on submerged *divergent* plate boundaries (i.e. the *c.* 60 000 km-long system of mid-ocean ridge (MOR) spreading centres) clearly affect the chemistry of sea water (Von Damm 1995), generically similar processes on submarine volcanic arcs associated with oceanic *convergent* plate boundaries have been neither rigorously explored nor considered for effect. Volcanic arcs located within oceanic basins extend *c.* 21 500 km (Fig. 1) and are populated by at least 700 volcanoes, of which over 200 are submarine (de Ronde *et al.* 2003). Arguably, the most pronounced submarine emissions from arcs emanate from the western basin of the Pacific Ocean, where three intra-oceanic arcs (Izu–Bonin–Mariana, New Hebrides and Tonga–Kermadec) stretch *c.* 6400 km and host *c.* 150 submarine volcanoes (Bloomer *et al.* 1989; Worthington 1998; Glasby *et al.* 2000; de Ronde *et al.* 2003). While island arcs in adjacent seas may also contribute fluid emissions, their discharge is commonly subaerial and provides little direct input to the oceans (e.g. Baker *et al.* 2002*b*).

The New Zealand American PLUme Mapping Expedition (NZAPLUME) in March 1999 marked the first systematic reconnaissance of any oceanic arc for submarine hydrothermal activity (de Ronde *et al.* 2001; Baker *et al.* 2003). The southern Kermadec arc (SKA) northeast of

From: LARTER, R.D. & LEAT, P.T. 2003. *Intra-Oceanic Subduction Systems: Tectonic and Magmatic Processes.* Geological Society, London, Special Publications, **219**, 119–139. 0305-8719/03/$15.00

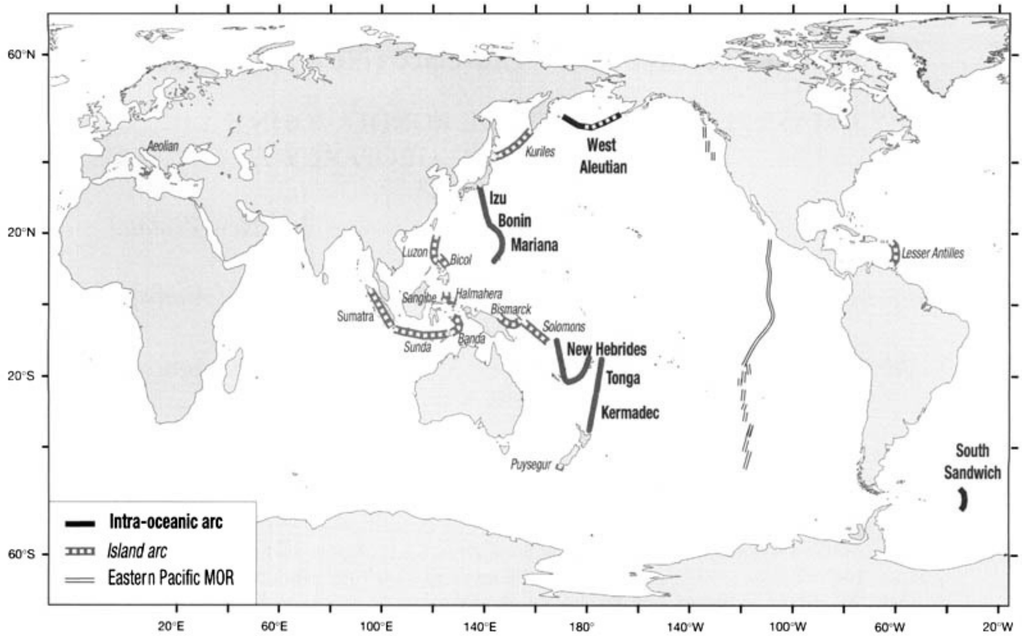

Fig. 1. Global distribution of active marine volcanic arcs (after Worthington 1998). Intra-oceanic arcs commonly are submarine, whereas island arcs typically have higher proportions of subaerial volcanoes. Almost 22 000 km of arc front exist globally, with *c.* 20 000 km of that within the western Pacific Basin and its boundary seas. Less than 3% of arc front has been surveyed for hydrothermal activity. Of the *c.* 9100 km of non-sedimented MOR located in the eastern Pacific Basin, *c.* 3200 km (35%) has been systematically explored for hydrothermal activity.

New Zealand was surveyed using conventional plume reconnaissance techniques (Baker *et al.* 1995). Seven of the 13 volcanoes that comprise this 260 km-long intra-oceanic arc section were confirmed to be hydrothermally active based on plume anomalies in optical light-scattering, ^3He, pH, H_2S, Mn, Fe and Cu. On average, one hydrothermally active volcano was found along each *c.* 33 km of arc front. While Baker *et al.* (2003) do not discriminate between venting frequency on the SKA and slow- and intermediate-rate spreading MORs (average frequency approximately one site per 100 km of ridge crest) due to uncertainties in the available data, it is clear that SKA venting is appreciable when compared to MORs.

Here we expand on the preliminary results of NZAPLUME reported by de Ronde *et al.* (2001), and the distribution and particle composition of plumes discussed by Baker *et al.* (2003) to more fully discern the chemical origins and nature of fluid emissions from the SKA volcanoes. We show that, in addition to having a high spatial frequency, the plumes also are commonly robust in concentration and chemically diverse relative to plumes on MORs. We interpret unusually high concentrations of CO_2, sulphur gases and Fe to be magmatic in origin, and seafloor discharges often to be hybrid mixtures of hydrothermal and magmatic fluids. Based on this first systematic assessment of venting at < 7% of known submarine arc volcanoes, we propose that submarine arcs may provide a significant contribution to sea-water chemistry.

Venting on submarine arc volcanoes

Hydrothermal systems on submarine arc volcanoes have much in common with MOR, back-arc basin (BAB) and hot-spot volcano venting (e.g. a magmatic heat source, permeable crust, subseafloor water–rock interaction, polymetallic mineral deposits and sea-water hydrothermal plumes; Fig. 2). It is, however, the largely unexplored differences in arc hydrothermal settings and the consequent effects on fluid emissions that make arc hydrothermalism valuable for chemical study. Important differences include a generally shallow depth of venting when compared to MORs and BABs (where discharge is volumetrically significant) and more highly differentiated compositions of arc magmas

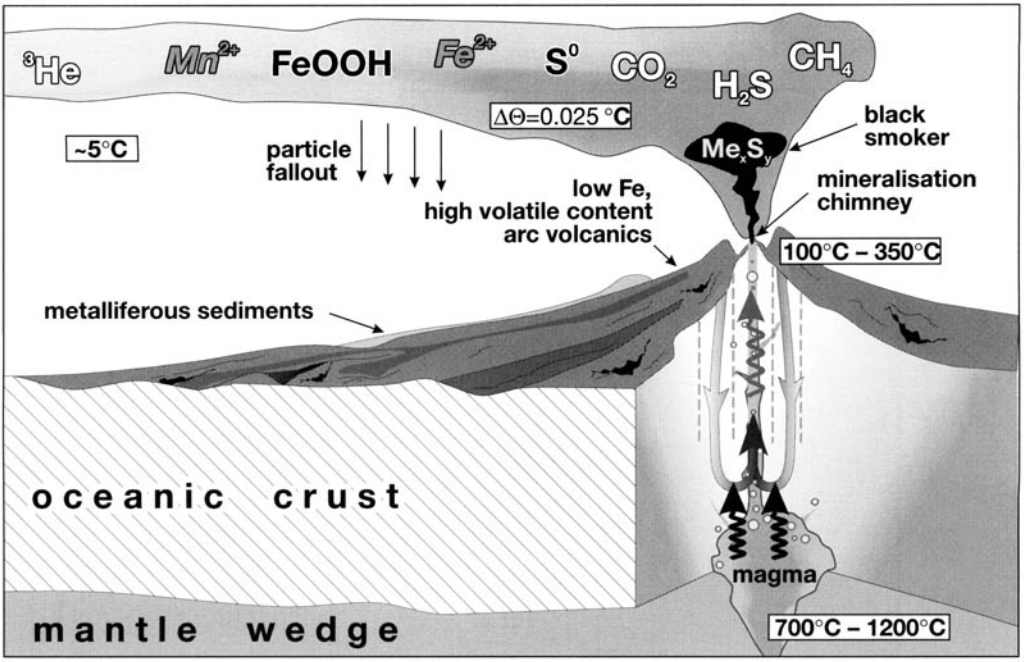

Fig. 2. Schematic cartoon of a venting system on a submarine arc volcano. These systems are driven by magma bodies that range in temperature depending on composition, typically 1100–1250°C for basalts, 1000–1150°C for andesites, 900–1050°C for dacites and 700–900°C for rhyolites. Dashed lines represent permeable crust into which sea water penetrates to form a hydrothermal circulation cell with ascending fluids discharging at *c.* 100–350°C, depending on depth (see text). White bubbles and sawtooth arrows represent exsolved magmatic fluid (vapour and liquid components, respectively) that may become incorporated into the hydrothermal circulation to form hybrid magmatic–hydrothermal (or *volcanic)* fluid. Some chemicals within volcanic vent fluid may precipitate near the seafloor interface as hydrothermal mineralization (e.g. volcanogenic massive sulphide (VMS) ore deposits). The remaining (most) chemicals will buoyantly rise to form 'black smoker' plumes characterized by metal sulphides (Me_xS_y) and horizontally dispersing neutrally buoyant hydrothermal plumes that are typically 7000- to >20 000-fold dilutions of vent fluids. Hydrothermal plumes are sensed as temperature anomalies ($\Delta\theta$) or optically detected as light scattered off iron oxyhydroxide (FeOOH) and native sulphur (S^0) particles and detected chemically as gas (^3He, CO_2, CH_4, and H_2S) and metal (Fe^{2+}, FeOOH, Mn^{2+}, Me_xS_y, S^0) concentration anomalies.

compared to basalt-dominated MORs. We discuss these differences below.

Discharge from active submarine hydrothermal systems on arcs occurs noticeably shallower than 1800 m, whereas MOR and BAB spreading centres vent predominantly at depths greater than this with a mode near 2600 m (Fig. 3a). Thus, hydrostatic confining pressures and maximum fluid discharge temperatures on arc volcano summits will be lower than on most ridge crests due to a lower pressure–temperature threshold for phase separation (i.e. boiling; Fig. 3b). To the extent that water–rock reactions and mineral stabilities are sensitive to lower physical property values, chemical transport and deposition may be affected.

From a chemical perspective, probably the most interesting aspect of arc hydrothermalism stems from the compositional diversity and high volatile contents of arc magmas (Ishibashi & Urabe 1995). In contrast to basalt-dominated MORs, arc lavas span a wide range of compositions ranging from basalt to andesite, dacite and rhyolite. As magmatic differentiation increases in this sequence the resulting lavas are progressively depleted in FeO-bearing minerals, become more oxidizing and are richer in water compared to basalt (Table 1).

The Fe(II)/Fe(III) rock buffer sets the redox (reduction–oxidation) poise for water–rock reaction within hydrothermal circulation cells on arc volcanoes (Giggenbach 1992). Hence, the relatively low abundance of FeO-bearing minerals in arc lavas can result in vent fluids with a low

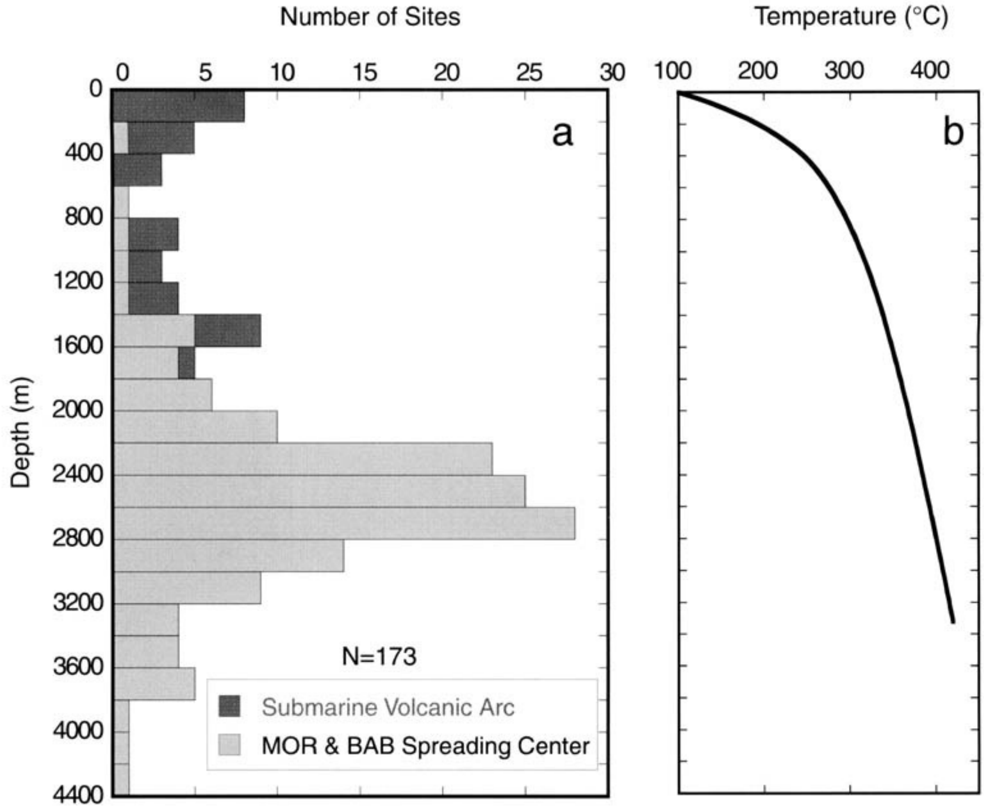

Fig. 3. Physical attributes of submarine hydrothermal venting. (**a**) Depth histogram for submarine venting on volcanic arcs and MOR and BAB spreading centres (references available from corresponding author). Sites include direct observations of seafloor venting and detections of hydrothermal plumes (binned as plume depth+100 m). (**b**) Two-phase boundary (boiling) curve for 3.2 wt% NaCl sea-water analogue solution (Bischoff & Rosenbauer 1988). Fluids at pressure/depth–temperature greater than that for venting will rise until intersection with the boiling curve, and then adiabatically boil–cool during continued ascent along this curve, thus constraining maximum venting temperature. Note steep gradient in boiling curve at temperatures <300°C and < *c.* 850 m depth. A smooth extrapolation was inferred between 100 and 250°C. Boiling curve extends to highest observed venting temperature *c.* 412°C.

buffer capacity. That is, when these fluids are titrated by oxidized sea water, mineral deposition may be accelerated and locally enhanced (Herzig *et al.* 1993). Rock-buffered vent fluids on arcs will be more oxidizing as the Fe content of host rock decreases and the oxidation index ($Fe_2O_3/(FeO + Fe_2O_3)$) increases (Table 1). Mineral phases deposited from these redox-moderated fluids should therefore reflect these conditions.

Intrusions of water-rich arc magmas are commonly accompanied by exsolution of magmatic fluid (Hedenquist & Lowenstern 1994). Magmatic fluid, as discussed in the context of this paper, is composed of two components – magmatic vapour (gaseous volatiles) and magmatic liquid (metalliferous brines) – which may or may not be simultaneously exsolved from the parent magma. Recent empirical evidence suggests magmatic brines may be some of the most chemically concentrated natural fluids on Earth (e.g. Ulrich *et al.* 2001). The necessary intimacy of hydrothermal circulation cells with subseafloor magma intrusions invokes the high probability that fluid *exsolved* from a given magma and local, hydrothermally *evolved* sea water will follow common pathways to the seafloor to form a hybrid and conceivably highly chemically enriched venting system (Fig. 2). We hereinafter refer to the hybrid magmatic–hydrothermal fluid as volcanic fluid.

Siliceous arc volcanoes have been referred to

Table 1. *Chemical properties of volcanic substrates*

Lava type	Total Fe as FeO* (wt%)	Oxidation index† ($Fe_2O_3/(FeO + Fe_2O_3)$)	H_2O‡ (wt%)
Basalt	9–11	0.25	0.28
Andesite	6–8	0.58	1.70
Rhyolite	1–2	0.68	4.50

*Representative data for Solomon arc suite (Stanton 1994).
†Oxidation index for Solomon lavas showing same general trend as broader literature base but 0.1–0.2 units more oxidized (Stanton 1994).
‡Values for melt inclusions (Giggenbach 1996).

as 'water volcanoes', compared to basaltic 'CO_2 volcanoes' when considering the main pressure-generating species in the respective magmas (Giggenbach 1996). Andesitic arc volcanoes have also been described as 'ventholes' allowing excess subducted volatiles to be recycled to the surface (Giggenbach 1992). After H_2O, the primary gases contributed from arc magmas are CO_2–CH_4 and SO_2–H_2S. Using subaerial White Island (New Zealand) as a model arc volcano system, Giggenbach (1987) showed that the redox poise of the magmatic vapour phase at high temperature (>400°C) is controlled by the sulphur gas buffer dominated by (oxidized) SO_2. At temperatures <300°C the carbon gases provide the primary buffer with (reduced) CH_4 dominant. The ultimate redox fate of hybrid magmatic–hydrothermal systems will depend on the outcome of the 'battle of the buffers' (rock: Fe(II)/Fe(III); fluid: CO_2–CH_4 and SO_2–H_2S; Giggenbach 1987) with both fluid and rock contributing to the so-called more oxidizing arc-venting environment. The high concentrations of sulphur gases present as magmatic volatiles (CO_2:S_t ≈ 10:3 for andesitic volcanoes, where $S_t = SO_2 + H_2S$; Giggenbach 1992) result in the production of acid and native sulphur when mixed with sea water:

$$4SO_2 + 4H_2O \rightarrow 3H_2SO_4 + H_2S \quad (1)$$

$$3SO_2 + 2H_2O \rightarrow S^0 + 2H_2SO_4 \quad (2)$$

$$H_2SO_4 \rightarrow HSO_4^- + H^+ \quad (3)$$

$$H_2S + 2H_2O \rightarrow SO_4^{2-} + 2\,H^+ \quad (4)$$

$$H_2S + \tfrac{1}{2}O_2 \rightarrow S^0 + H_2O. \quad (5)$$

Sulphur degassing at White Island has resulted in congruent dissolution of wallrock by acid condensates (i.e. advanced argillic alteration) and surface deposits of native sulphur (e.g. Giggenbach & Glasby 1977). Similar residues of magmatic sulphur degassing have been reported in the submarine environment at Esmeralda Bank and Kasuga volcanoes on the Mariana arc (Stüben *et al.* 1992; McMurtry *et al.* 1993) and in association with arc-like lavas at the Manus and Lau back-arc spreading centres (Gamo *et al.* 1997; Herzig *et al.* 1998).

Chloride complexing stabilizes metals in magmatic brines, allowing very high concentrations of metals to be transported to the seafloor where ore deposition may take place. For example, magmatic brines are the presumed source for ancient submarine Kuroko ore deposits (Fe–Zn–Pb±Cu±Au±Ag-rich; Urabe & Marumo 1991). High concentrations of metals in melt inclusions (Cu–Zn and Fe) derived from arc-like lavas hosting an actively forming polymetallic sulphide deposit (Cu–Zn–Pb–Ag–Au-rich) on the Manus back-arc spreading centre suggest an exsolved ore–metal-rich magmatic fluid may have contributed to the formation of that and other seafloor ore deposits (Yang & Scott 1996, 2002). These examples and others support an hypothesis that the bulk of heavy metals in some marine ore deposits is not derived from water–rock reaction inherent to hydrothermal circulation, but rather from magmatic fluids entrained in hydrothermal flowstreams (Stanton 1994). Unveiling modern magmatic–hydrothermal systems on arcs and associated seafloor mineral deposits provides a means to test the magmatic fluid hypothesis for ore genesis. The work presented here is an initial step in that direction on the southern Kermadec arc.

Southern Kermadec arc

The southernmost 260 km of active arc associated with the *c.* 2500 km-long Tonga–Kermadec subduction system is defined by 13 submarine volcanoes that comprise the southern Kermadec volcanic frontal arc (Fig. 4). The SKA lies within the back-arc region 20–30 km west of the Kermadec Ridge escarpment and *c.* 220 km west of the subduction trench (Wright 1993). The transition between New Zealand continental and oceanic arc crust occurs just south of Clark

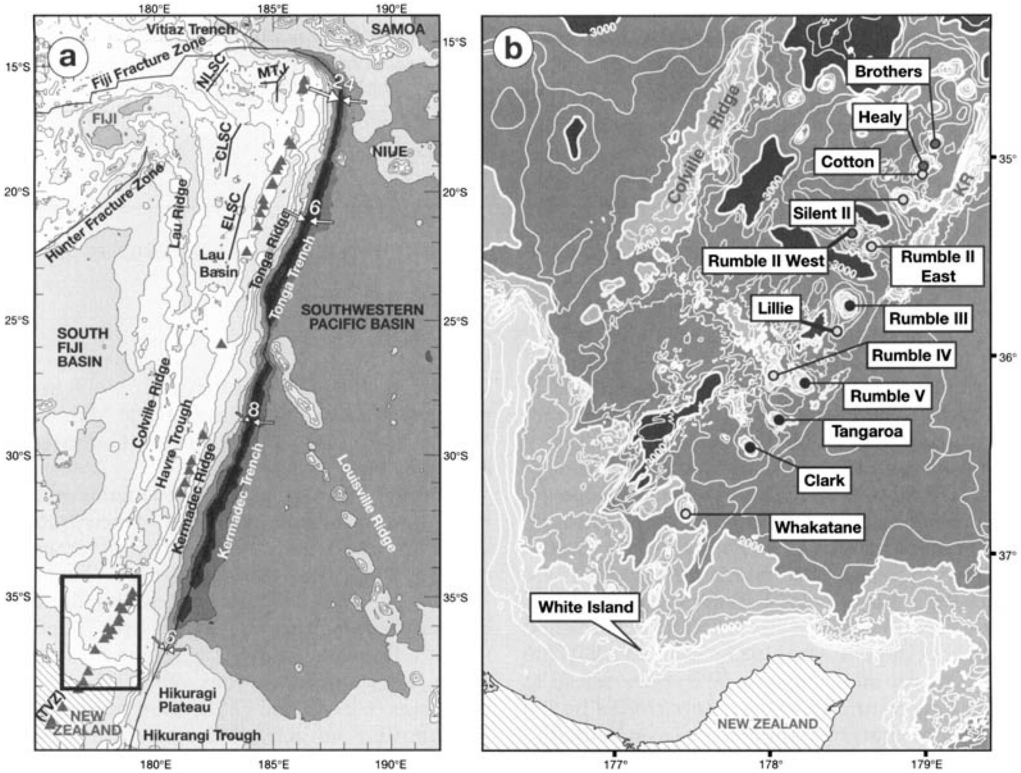

Fig. 4. (**a**) The Tonga–Kermadec subduction system extends *c.* 2500 km north of New Zealand, where the plate boundary lies along the Tonga and Kermadec trenches. The world record rate for plate convergence, 24 cm a^{-1} (white arrows and numbers) occurs at the northern end of this system and decreases to 25% that value near New Zealand. The active arc front is marked by a 40 km-wide zone of 34 known volcanoes (triangles) that lie up to 65 km west of the Tonga and Kermadec ridges. The southern Kermadec volcanic frontal arc domain is defined by the 13 southernmost oceanic volcanoes, which are all submarine (see boxed area). Modified after Worthington (1998). (**b**) Expanded view of NZAPLUME study area (shown as box in (**a**). The 13 volcanoes surveyed for hydrothermal activity are labelled and extend north from Whakatane to Brothers, along 260 km of arc front. Solid site markers indicate volcanoes confirmed to be hydrothermally active during the NZAPLUME expedition. KR, Kermadec Ridge. Modified after de Ronde *et al.* (2001) with permission from Elsevier Science.

volcano (Fig. 4b) (Gamble *et al.* 1997). Thus, with the exception of Whakatane Volcano, the SKA is intra-oceanic. The SKA volcanoes range widely in relief (900–2180 m height above the seafloor) and summit depth (220–1350 m). Brothers, Healy and Rumble II West volcanoes have calderas *c.* 2–3 km in breadth and 200–400 m in depth from the top of the caldera walls (Wright & Gamble 1999). The remaining 10 volcanic edifices are simple volcanic cones. Volcano spacing along the SKA varies from 7 to 52 km, with a mean of 24 km (Worthington 1998), similar to the apparent world average for oceanic arcs of *c.* 27 km (de Ronde *et al.* 2003). Volcanic rock compositions along the arc reflect various degrees of magmatic differentiation with compositions ranging from basalt to basaltic andesite, through to andesite, dacite and rhyolite. Overall, the SKA has a pronounced bimodal total alkali–silica distribution (Gamble *et al.* 1997; Wright & Gamble 1999).

Methods

Operational protocols developed over the past two decades for hydrothermal exploration on ridge crests (e.g. vertical casting, 'tow-yo' section profiling, and optical and chemical plume detection; Baker *et al.*1995; Lilley *et al.* 1995) were used to survey chemical plumes on the SKA. When applied to an active arc front several efficiencies were realized: detailed site surveys could be focused *a priori* near volcano tops and inter-volcano station spacing was commonly greater than when surveying ridge crests.

Continuous sensing for physical property plume anomalies in temperature ($\Delta\theta$) and optical light-scattering (Δ-NTU, where NTU refers to nepelometric turbidity units, a dimensionless optical standard) was performed using conventional profiling equipment and procedures described elsewhere (Baker *et al.* 2002*a* and references therein). Continuous profiling for chemical anomalies of dissolved H_2S was accomplished using The Submersible System Used to Assess Vented Emissions (SUAVE), an *in situ* chemical analyser fixed to the profiling tow-package (Massoth & Milburn 1997; Massoth *et al.* 1998). The H_2S data reported here were determined using the methylene blue method of Sakamoto-Arnold *et al.* (1986) with *in situ* calibration and a detection limit of *c.* 200 nmol l^{-1}.

Discrete samples were collected in Teflon-coated 19-l PVC bottles closed on demand using silicone tubing. Bottle closure was commonly coincident with maxima in Δ-NTU, which was monitored during profiling operations. Samples were drawn into copper tubes and cold-weld sealed (Young & Lupton 1983) for shore-based, independent determinations of He isotopes and concentration. He isotope measurements were made on a 21 cm-radius mass spectrometer with a 1σ precision of 0.2% in δ^3He. He concentrations were referenced to calibrated laboratory air standards with an accuracy of 1%. Sample pH was determined on board ship after attaining thermal equilibrium at 20–25°C (±0.2°C for any given station). Conventional potentiometric techniques and calibrations referenced to NBS (National Bureau of Standards) standards were employed with a precision of ±0.01 pH units. Samples for determinations of total dissolvable (TD) Fe and Mn (TDFe and TDMn) were drawn directly into I-Chem™ polyethylene bottles and acidified to pH *c.* 1.6 using ultra-clean HCl. TDFe was determined on board and in the laboratory using the direct injection N,N-dimethyl-*p*-phenylenediamine dihydrochloride colorimetric detection method of Measures *et al.* (1995). TDMn was determined simultaneously with Fe using a dual-channel linear photo-diode array detector and the leuco-malachite green method of Resing & Mottl (1992) modified by adding 4 g of nitrilotriacetic acid per litre of buffer. The 1σ precisions for the determinations of Fe and Mn were $\leq 8\%$ and $\leq 6\%$, respectively. Suspended particulate matter was collected by pressure filtration on to 0.4 μm-polycarbonate filters and analysed for particulate phosphorus (PP), sulphur (PS) and iron (PFe) by thin-film energy dispersive X-ray fluorescence (XRF) spectrometry following the methods described in Feely *et al.* (1991*a*). The analytical precision was 1, 2 and 11%, respectively, for particulate Fe, P and S. Native (volatile) sulphur was determined by taking the difference between PS concentrations measured before and after evacuation of the sample chamber (Feely *et al.* 1999). A broad spectrum of elements (Mg through to Zn plus several higher atomic number elements) was surveyed by XRF to detect unusual enrichments.

Results and discussion

A general overview of the results from the NZAPLUME expedition and details of the physical properties of plumes are presented elsewhere (de Ronde *et al.* 2001; Baker *et al.* 2003). Hydrothermal particle plumes detected shipboard by optical light-scattering at (in order of decreasing scattering intensity) Brothers, Rumble III, Tangaroa, Rumble V and Healy confirm hydrothermal activity at these volcanoes (Figs 4 and 5) (Baker *et al.* 2003). Two venting sources were identified at Brothers Volcano. A plume at >1300 m depth results from a vent site perched on the northwest caldera wall (henceforth referred to as Brothers NW) and a second, shallower plume emanates from a cone structure near the south crater rim (henceforth referred to as Brothers Cone). Two additional plumes over Clark and Rumble II West volcanoes (Fig. 5b, Table 2) (de Ronde *et al.* 2001) were verified (along with the five particle plume sites) by post-cruise laboratory determinations of δ^3He ($= 100[(R/R_A)-1]$, where $R = {}^3He/{}^4He$ and R_A is the ratio for air). Thus, 54% (seven of 13) of the arc volcanoes are known to be hydrothermally active. While the results for δ^3He demonstrate the utility of chemical plumes as sensitive markers of hydrothermal activity, our full suite of chemical data allow additional and useful insight into the subseafloor magmatic–hydrothermal processes responsible for the genesis of vent fluids and plumes. Here we present the results for five key chemical tracers of seafloor venting: ^3He, pH and H_2S as indicators of gaseous vent fluid components, and Fe and Mn as indicators of aqueous ionic vent fluid components.

Gaseous components

^{3}He. The single-most analytically sensitive and unequivocal tracer of seafloor hydrothermal activity (and ultimately a mantle-magmatic source) is ^3He. While past work has demonstrated that ^3He may transfer from the seafloor

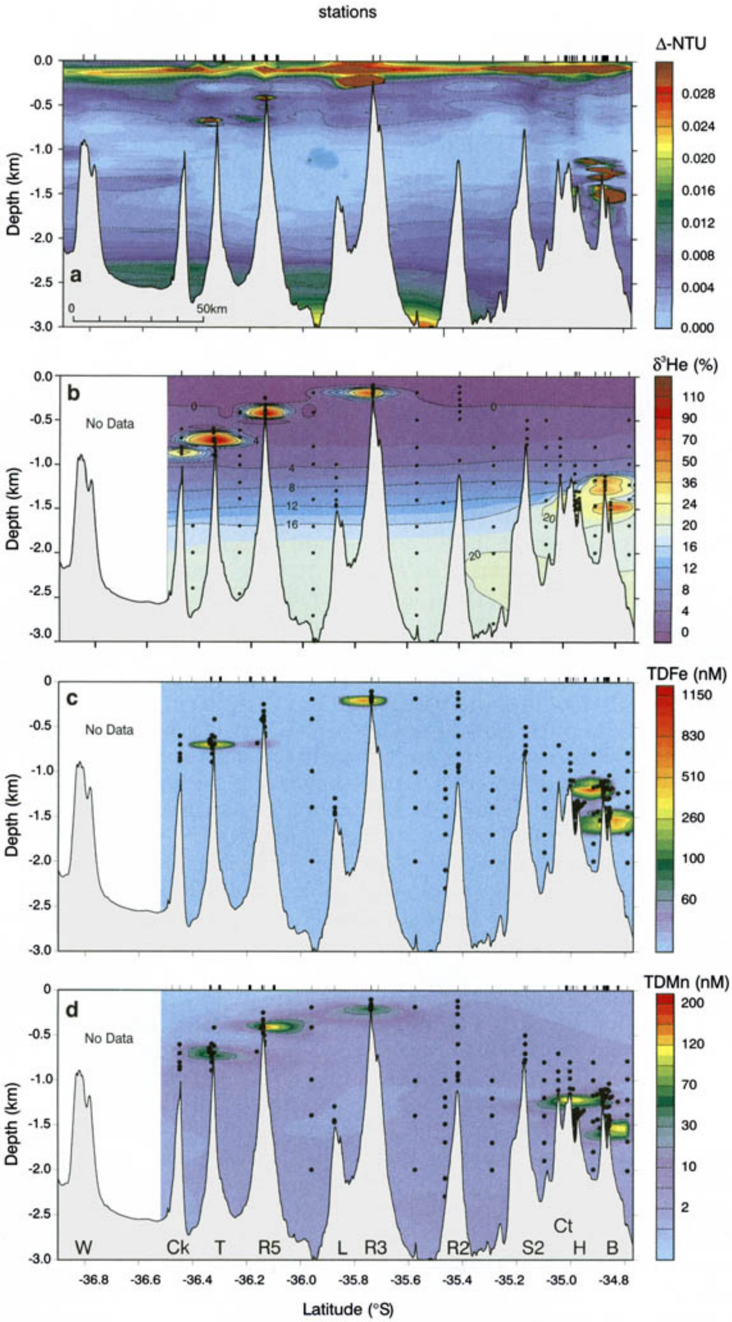

Fig. 5. Longitudinal sections along the southern Kermadec active frontal arc showing results for: (**a**) optical light-scattering expressed as Δ-NTU (nephelometric turbidity units, a non-dimensional optical standard); (**b**) δ^3He, the percentage increase in ^{3}He/^{4}He over air; (**c**) TDFe (total dissolvable iron); and (**d**) TDMn (total dissolvable manganese). Station distributions for the respective plume tracers are marked by ticks on the top of each panel, discrete sample points are indicated by dots. Contour intervals are indicated on side bar keys and are not constant for panels (b)–(d). W, Whakatane; Ck, Clark; T, Tangaroa; L, Lillie; R5, Rumble V; R3, Rumble III; R2, Rumble II East, S2, Silent II; Ct, Cotton; H, Healy; B, Brothers. (a) and (b) are reprinted from de Ronde *et al.* (2001) with permission from Elsevier Science.

Table 2. *Chemical characteristics of hydrothermal plumes over southern Kermadec arc volcanoes and selected mid-ocean ridge sites*

Volcano[1]	Depth (m)	δ^3He (%)	ΔpH	H_2S (nM)	PS (nM)	TDFe (nM)	TDMn (nM)	Fe/Mn (mol/mol)
Clark	880	37	–0.10	–		11	7	
Tangaroa	705	116	–0.22	–	32	560	98	5.7
Rumble V	405	105	–0.35	18700	98	39	200	0.2
	680					54	8	6.8
Rumble III	190	71	–0.28	360	167	1300	106	12.3
Rumble II West	1410	24	–	–		5	7	
Healy	1455	34	–0.04	–	16	203	148	9.9
Brothers								
Cone	1195	63	–0.27	4250	760	4720	260	18.2
NW	1455	74	–0.06	–	300	955	150	6.4
Rumble II East	115–2297		–	–	3.8±1.9	2.5±1.8	1.7±0.8	
MOR								
JdFR[2–4]	1900–2100	234		15	140	770	265	2.1 ± 1.2
EPR[5–7]	2200–2500	75	–0.04		260	500	193	3.0 ± 1.4
MAR[8–10]	1650–3300	68		450		175	42	3.2–7.8

Abbreviations: MOR, mid-ocean ridge; JdFR, Juan de Fuca Ridge (Cleft and Endeavour sites); EPR, East Pacific Rise (sites between 11°N and 32°S); MAR, Mid-Atlantic Ridge (23°, 26° and 37°N sites). ΔpH is the deviation from the regional depth trend (± 0.01), PS is particulate sulphur, TDFe and TDMn are total dissolvable Fe and Mn or the sum of dissolved and particulate Fe and Mn; nM, nanomoles per litre; mol, moles per litre. Values reported for volcanoes represent the most enriched samples from neutrally buoyant plumes, except for Healy where unpaired data are shown and Rumble II East where composite data reflect the concentration background. Discharge known to be influenced by magmatic intrusions has been excluded from MOR values; mean ± 1σ is given for Fe/Mn where large data sets exist, otherwise range is indicated; – , below detection; blank space, not analysed.

References: [1]this work and de Ronde *et al.* (2001); [2]Massoth *et al.* (1994); [3]Radford-Knoery *et al.* (2001); [4]R. A. Feely pers. comm. (2002); [5]Baker *et al.* (2002*a*); [6]Field & Sherrell (2000); [7]Lupton *et al.* (1993*a*); [8]Jenkins *et al.* (1980); [9]Radford-Knoery *et al.* (1998); [10]James & Elderfield (1996).

to the ocean independently of heat (Lupton *et al.* 1989; Baker & Lupton 1990) and other chemical species (Massoth *et al.* 1994), its exclusive transport through hydrothermal pathways is not disputed (Lupton 1983). Thus, the detection of ^{3}He plumes over seven SKA volcanoes (Figs 5b and 6a; Table 2) confirms magmatic sources and hydrothermal circulation at these sites. Particularly large δ^3He signals at Rumble III, Rumble V, Tangaroa (largest measured anomaly at 116%) and Brothers volcanoes coincide with the most intense particle plumes (Fig. 5a, b).

Our observations of ^{3}He plumes unaccompanied by particle plumes at Clark and Rumble II West (not shown in Fig. 5) are unusual. The lack of particle plumes indicates that high-temperature hydrothermal discharge is unlikely at these sites. If magmatic degassing is responsible for the ^{3}He signals, very high concentrations of CO_2 in the corresponding vent fluids (tens to hundreds of mM) would be expected (Butterfield *et al.* 1990; Sedwick *et al.* 1992*a*; Tsunogai *et al.* 1994). Because low-temperature (<200°C), CO_2-rich fluids are especially corrosive to volcanic wallrock (Bischoff & Rosenbauer 1996), Fe-rich vent fluids and particle plumes such as seen in association with CO_2 degassing at Loihi volcano (Sakai *et al.* 1987; Sedwick *et al.*1992*b*; Wheat *et al.* 2000) would be expected. Discoveries of massive sulphide mineralization at Clark (de Ronde pers. comm. 2002) and Rumble II West (Wright *et al.* 1998; de Ronde *et al.* 2002) confirm that high-temperature hydrothermal discharge has occurred on these volcanoes in the past. Whether the contemporary sources of ^{3}He at Clark and Rumble II West are magmatic or hydrothermal (i.e. liberation of ^{3}He trapped in vesicles or glass by high-temperature water–rock reaction), the relatively low intensity and near-seafloor proximity (< *c.* 20 m) of the ^{3}He signals imply diffuse discharge.

When the absolute concentrations of ^{3}He and ^{4}He for the SKA data set are compared, a single linear trend emerges, which is representative of the isotopic composition of the end-member

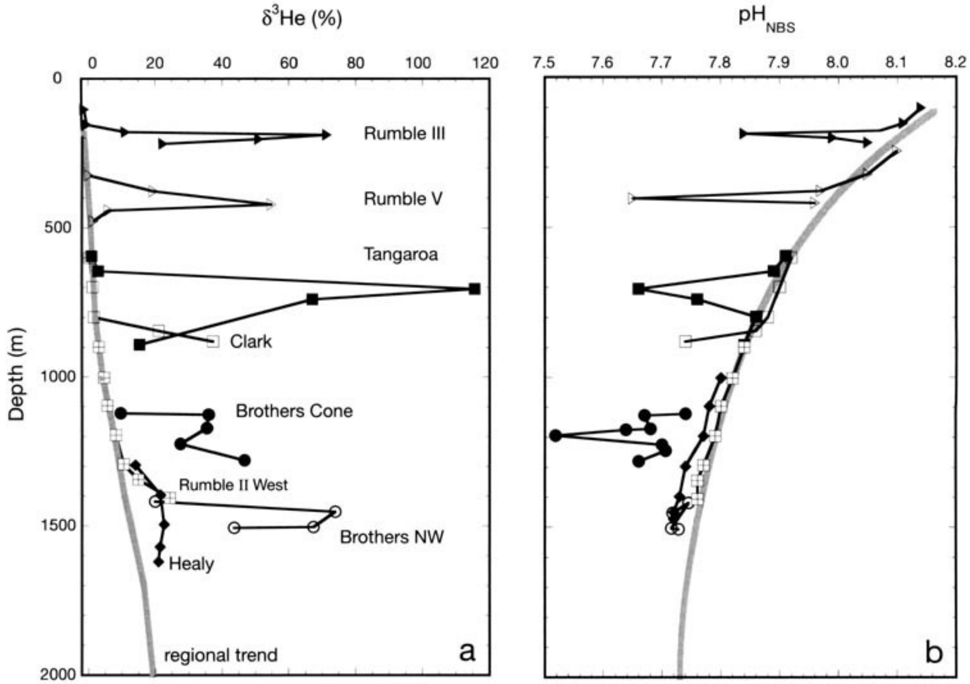

Fig. 6. Vertical distributions of (**a**) δ^3He and (**b**) pH_{NBS} showing maximum plume concentrations for these key indicators of gas emissions from the seven hydrothermally active southern Kermadec arc volcanoes. Note the wide range of venting depths extant over only 260 km of arc front. The two active sites at the Brothers Volcano (Cone and NW) are represented as plumes above and below 1300 m depth, respectively. The regional depth trends for δ^3He and pH_{NBS} are shown as broad grey lines and were determined from non-hydrothermally influenced samples collected throughout the study area.

vent fluids (Fig. 7). A linear regression fit to these data gives a slope of $8.34 \pm 1.1 \times 10^{-6}$, which corresponds to $R/R_A = 6.0 \pm 0.8$, identical to the average value given for subduction zone helium (Lupton 1983), and within the range for northwest Pacific subaerial arc volcanoes (6.5 ± 1.5; Poreda & Craig 1989). The R/R_A value for the SKA is slightly lower than found on MORs (e.g. along a similar length of the Juan de Fuca ridge, erupted MORBs range 7.6–8.9, and hydrothermal plumes average 8.3; Lupton *et al.* 1993*b*; J. E. Lupton pers. comm. 2002). However, it is the similarity of these values compared to that for crust ($R/R_A < 0.1$) that constrains the underlying mantle wedge and not subducting oceanic crust as being the major source for ^3He along the SKA (Lupton 1983; Poreda & Craig 1989).

Helium vented from submarine arc volcanoes may be less recognizable as a far-field oceanographic tracer compared to that emitted from MORs or hot-spot volcanoes due to the relatively lower R/R_A value for arcs. Tracing emissions of ^3He (discerned with highest resolution as δ^3He) from the Loihi Volcano near Hawaii provides an interesting comparison. Like arc volcanoes, Loihi is an insular source located at relatively shallow depth (*c.* 1100 m). However, unlike arc volcanoes, Loihi helium has a hotspot R/R_A signature value of *c.* 23, about four times the average value for arc helium. While the helium plume dispersing from Loihi clearly can be detected 400 km distant, and arguably discerned for >2000 km (Lupton 1996), analytical limitations will almost certainly preclude similar scale mapping from arcs.

The broad depth range for ^3He emissions along the SKA highlights an important contrast between arc and ridge crest venting, and a second reason why distal plumes of arc helium may be difficult to detect. If such depth-variable discharge is generally characteristic of submarine arcs, then basin-wide ^3He plumes, like those that congregate and disperse from long sections of near-constant-depth ridge crest in the eastern Pacific (Lupton 1998), may not emanate from western Pacific arcs, which also extend several thousands of kilometres in cumulative length. It therefore may be misleading to discount the relative significance of arc discharge within the Pacific Basin based on an

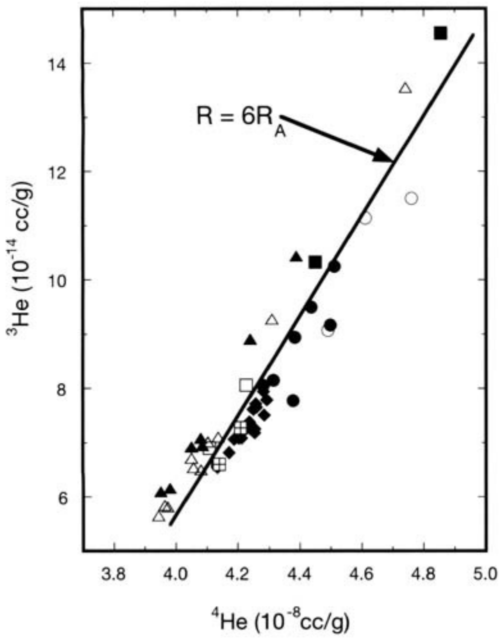

Fig. 7. Absolute ^3He concentration plotted against ^4He concentration for water column samples collected during the NZAPLUME expedition. Symbols as in Fig. 6.

absence of large, shallow isopycnal surface plumes of ^3He.

pH. pH does not provide a direct measure of dissolved gas concentration, although large negative anomalies in this property ($-\Delta$pH), such as observed during NZAPLUME (Fig. 6b, Table 2), may be taken as reliable indicators of magmatic gas discharge (Sakai *et al.* 1987; Resing & Sansone 1996). Proton additions resulting from the discharge of CO_2, H_2S and Fe can account for most of observed pH anomalies in hydrothermal plumes (Resing & Sansone 1996). Here we expand this reasoning to include volatile-rich arc magmas, which in subaerial settings typically discharge SO_2 in greater abundance than H_2S (Giggenbach 1996). Hence, we consider CO_2, H_2S, and SO_2 collectively as magmatic gas contributors to pH shifts in plumes originating from arc volcanoes.

Resing *et al.* (1999) related plume anomalies in pH to additions of CO_2 and protons resulting from post-discharge oxidation and hydrolysis reactions involving Fe and H_2S:

$$\Delta CO_2 + \Delta H^+ = X(-\Delta pH) \qquad (6)$$

where X represents a factor determined using measured carbon system variables, ambient seawater properties (temperature, salinity, and oxygen and nutrient concentrations) and the CO_2 system modelling program of Lewis & Wallace (1998). Using hydrographic data from World Ocean Circulation Experiment (WOCE) line P15S, station 107 (35°00.18′S, 169°59.58′W; website: cdiac.ornl.gov/oceans/home.html), values for X vary from 370 μM at Brothers to 500 μM at Rumble III. When applied to the maximum pH anomalies listed in Table 2, the predicted ΔCO_2 + ΔH^+ values range from 152 μM for the plume at Rumble V to 15 μM for the plume at Healy.

Every mole of discharged sulphur gas that does not oxidize to elemental sulphur (Equation 5) has the potential to generate 0.7–2 moles of protons through oxidation and hydrolysis (Equations 1–4). Every mole of Fe^{2+} will generate two moles of protons when fully oxidized:

$$Fe^{2+} + 2.5H_2O + 0.25O_2 \rightarrow Fe(OH)_3 + 2H^+. \qquad (7)$$

Using the most enriched TDFe values observed during NZAPLUME (Table 2) and assuming conservative behaviour of iron within near-field plumes (Feely *et al.* 1994; Massoth *et al.* 1998), we calculate maximum proton contributions from Fe to be less than 5% of the whole-plume values listed above. Unlike Fe, by-products of the dissociation of the sulphur gases do not provide a measurable indicator of proton generation. For example, H_2S values reflect instead the residual potential for acid generation (Equations 1, 3 and 4). Hence, we first estimate the total sulphur gas (S_t) contributions by assuming CO_2 and S_t are present at a ratio of *c.* 10: 3 (e.g. Giggenbach 1992). If we further assume a proton production efficiency with respect to our plume observations of one mole per mole of sulphur gas, then *c.* 70% of the measured pH anomalies are estimated to be due to CO_2 discharge (ignoring the small contributions from oxidation of Fe^{2+}). This corresponds to plume anomalies in CO_2 ranging from 11 to 106 μmol l^{-1} along the SKA, comparable to the value of 50 μmol l^{-1} excess CO_2 reported by Sakai *et al.* (1987) for a hydrothermal plume over magmatically degassing Loihi Seamount near Hawaii.

Vent fluid end-member concentrations of CO_2 can be estimated from paired plume samples, provided background concentrations and mixing ratios are known. Neutrally buoyant plumes are commonly sampled as 7000- to >20 000-fold dilutions of vent fluids (e.g. Field & Sherrell 2000), although rare samples collected within buoyantly rising plumes (e.g. Feely *et al.* 1994) can result in dilutions as low as *c.* 2000-fold. If we conservatively assume the SKA plume maxima reflect minimal 2000-fold dilutions of vent fluids, the estimated CO_2 end-member fluid concentrations are: *c.* 25 mM at Healy and Brothers NW, >50 mM at Clark, >100 mM at Tangaroa and Brothers cone, and *c.* 200 mM at Rumbles III and V. Even these potentially underestimated values suggest all of the SKA sites with pH anomalies are CO_2-rich by MOR hydrothermal vent fluid standards ($\leq$ 22 mM, Von Damm 1995). The higher concentrations (>50 mM CO_2) clearly require a freely degassing magmatic source (e.g. Butterfield *et al.* 1990; Sedwick *et al.* 1992*b*).

The contrasting pH observations at Clark and Rumble II West suggest different venting modes for the two volcanoes. The detection of a very large pH anomaly at Clark volcano (cf. Resing *et al.* 1999; Baker *et al.* 2002*a*) and no anomaly at Rumble II West (Fig. 6b), when combined with the ^3He data, is most consistent with diffuse magmatic and hydrothermal discharge at the respective sites. Similarly, the contrasting enrichments of δ^3He and CO_2 (as inferred from $-\Delta pH$ values) in the NW and Cone plumes at Brothers Volcano allow us to differentiate these plumes as deriving from chemically distinct sources, consistent with spatial plume mapping results (Baker *et al.* 2003). While both ^3He and high CO_2 concentrations have magmatic origins, the CO_2-rich Brothers Cone site is clearly volumetrically more enriched in magmatic gas. Whether the relatively low estimated vent-fluid concentration of CO_2 at Brothers NW (*c.* 25 mM) reflects robust hydrothermal discharge or is the result of differential fractionation of these gases by progressive degassing following a magma intrusion (e.g. Sedwick *et al.* 1992*a*) is beyond the scope of the available data. The plume above Healy Volcano is among the least enriched in CO_2 and ^3He, yet the erupted rhydacitic volcanic products that dominate this site (Wright & Gamble 1999; Wright *et al.* 2003) derive from the most highly differentiated and, by inference, most volatile-rich magma of any SKA volcano. This seeming disparity suggests the present magmatic source at Healy is compositionally different from previously erupted lavas. Alternatively, magmatic and hydrothermal discharge may follow different evolutionary time paths (e.g. Giggenbach 1987; Sedwick *et al.* 1992*a*), with perhaps the volumetrically most significant magmatic discharge having occurred in association with historic pyroclastic pumice eruptions at this site (Wright *et al.* 2003). Whatever the explanation, the Healy data illustrate an important observation: that the composition of erupted volcanic rocks may not be a good predictor of present-day fluid chemistry.

H_2S. The detection of H_2S within the plume above Rumble III and the very high concentrations determined at Rumble V and the Brothers Cone site (Table 2) are consistent with a magmatic origin. Concentrations at the latter two sites greatly exceed MOR plume values (Table 2). The coincidence of high concentrations of sulphur gases (if SO_2 is discharged some proportion will dissociate and be determined indirectly as H_2S; Equation 1) with highest inferred CO_2 emissions provides additional evidence for magmatic sulphur discharge. Making the conservative assumption that all vented sulphur at Rumble V and the Brothers Cone sites was diluted 2000-fold and sampled as plume H_2S, estimated vent-fluid concentrations at these sites are 37 and 8.5 mM, respectively. While these are minumum values (S_t is not expected to mix conservatively or uniquely as H_2S), they exceed the end-member values for most MOR fluids (Von Damm 1995).

Dissolved sulphur gases are the precursors of particulate sulphur (PS). The poor correlation between the concentrations of sulphur in the dissolved and particulate phases (Table 2) implies that phase transformations are complex and not only dependent on dissolved sulphur gas abundance. 'Black smoker' metal sulphides enriched in Fe and Cu are characteristic of venting at high temperatures ($T > c.$ 300°C) and contribute significantly to the PS compositions within Rumble III, Tangaroa and the Brothers NW and Cone site plumes (de Ronde *et al.* 2001; Baker *et al.* 2003). Native sulphur comprises 70% of total PS at Rumble V and 55% of PS in the plumes above the NW and Cone sites at Brothers. Large pieces (> 5 cm in diameter) of native sulphur recovered from the seafloor at Rumble V and Brothers Cone site (de Ronde *et al.* 2001) further attest to magmatic sulphur discharge (Cheminée *et al.* 1991; Sedwick *et al.* 1992*b*; McMurtry *et al.* 1993; Gamo *et al.* 1997; Herzig *et al.* 1998). Unusually high concentrations of particulate Al and Zn detected within the plume overlying Brothers Cone site suggest the seafloor here is being extensively altered by acid condensates resulting from magmatic sulphur degassing (e.g. Giggenbach & Glasby 1977).

Aqueous ionic components

Fe and Mn. Fe and Mn commonly are the most chemically enriched (*c.* 10^6-fold relative to sea water) ionic species (Fe^{2+} and Mn^{2+}) in vent fluids, and hydrothermal discharge is the major source of these metals in sea water. Thus, Fe and Mn are ideal tracers of hydrothermal emissions

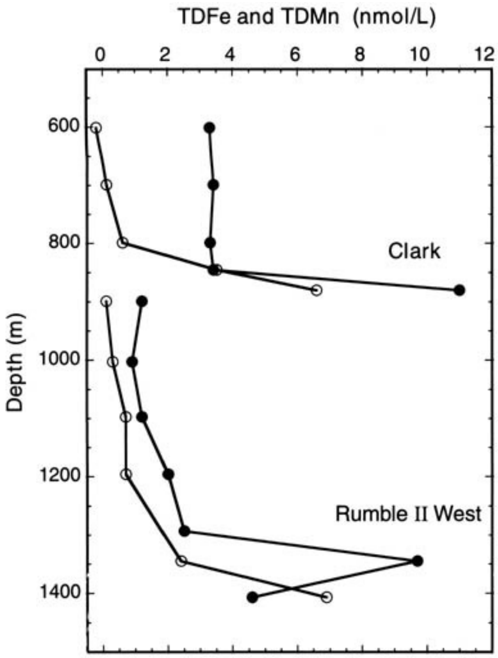

Fig. 8. Vertical distributions of TDFe (solid circles) and TDMn (open circles) over the Clark Volcano and within the caldera of Rumble II West Volcano. Lowermost samples were collected within 20±2 m of the seafloor.

when diluted as plumes, where they transform to particulate compounds that are important moderators of geochemical processes in sea water. Iron and Mn plumes were detected at all of the hydrothermally active SKA sites (Figs 5c, d and 8; Table 2). While there is generally good agreement among plume distributions reported previously for particles (Δ-NTU) and δ^3He (de Ronde *et al.* 2001) and reported here for TDFe, and TDMn (Fig. 5), the lack of an appreciable Fe plume over Rumble V is unusual (see below). Because iron oxyhydroxide particles formed after fluid discharge provide primary surfaces for light-scattering (Massoth *et al.* 1998; Baker *et al.* 2003), the low Fe concentrations at Rumble V are also shown as a weak particle plume (Fig. 5a). Even lower concentration anomalies for Fe and Mn detected near the seafloor at Clark and Rumble II West (Fig. 8) do not appear as plumes in Figure 5, although their coincidence with ^{3}He and pH (Clark only) plumes (Fig. 6) requires common seafloor origins. Whether these origins are magmatic or hydrothermal cannot be deduced from the low-level metal enrichments. Metal concentrations at Tangaroa, Rumble III, Rumble V (Mn only) and Brothers volcanoes are comparable to, or higher than, values for MOR plumes (e.g. Fe at Rumble III and the Brothers Cone sites is 1.7–6 times the highest MOR plume value, Table 2). If we accept that representative dilutions of vent fluids have been sampled everywhere, then predicted vent-fluid end-member concentrations for Fe and Mn at many of the active SKA volcanoes are similarly comparable to, or more enriched than, hydrothermal discharge along ridge crests.

Possible mis-interpretations due to sampling bias when comparing concentration data from different sites can be circumvented by normalizing the Fe and Mn values to hydrothermal heat and to each other. Unlike the situation at deep ridge crests in the eastern Pacific, where hydrographic variations within the ambient ocean are small and smoothly distributed, large and irregular gradients in potential temperature and density above the relatively shallow arc volcanoes commonly preclude resolution of a temperature anomaly (Δθ). Only within the deep caldera at Brothers Volcano were Δθ values quantified. Seven discrete samples collected within the deep Brothers NW plume had temperature anomalies that ranged from 0.008 to 0.054°C and corresponding Fe/heat and Mn/heat values that averaged 2.5±1.5 and 0.53±0.21 nmol J^{-1}, respectively; where:

$$\frac{\text{metal}}{\text{heat}} = \frac{\text{mol kg}^{-1}}{C_p\Delta\theta} \quad (8)$$

the heat capacity of sea water $C_p = 3915$ J kg^{-1}, and $\Delta\theta = \theta - (k_1\sigma_\theta + k_2\sigma_\theta^2 + b)$, where θ is potential temperature, σ_θ is potential density, and k and b are regression coefficients for the second-order fit of θ as a function of σ_θ (Baker *et al.* 2002*a*). Comparable Mn/heat values (means: 0.30–0.67 nmol J^{-1}) were obtained for plumes over the Juan de Fuca Ridge (Massoth *et al.* 1994, 1995; Resing *et al.* 1999), Gorda Ridge (Massoth *et al.* 1998) and Southern East Pacific Rise between 14°–18°30′S and 27°30′–32°18′S (Massoth & Hey 1998). By contrast, mean Fe/heat values for the eastern Pacific plumes (0.78–1.97 nmol J^{-1}) range consistently below the mean value for the deep plume at Brothers NW. An even greater contrast may exist for the plume above the Cone site at this volcano, where Fe concentrations were five times higher.

The availability of Fe/Mn values for all of the SKA plumes (Fig. 9a) allows a broader comparison to MOR and BAB fluids (Fig. 9b). Tangaroa, Healy and Brothers NW plumes have Fe/Mn values that lie primarily between 2 and 8, identical to the range for most MOR plumes and vent fluids. Rumble V plumes have very low

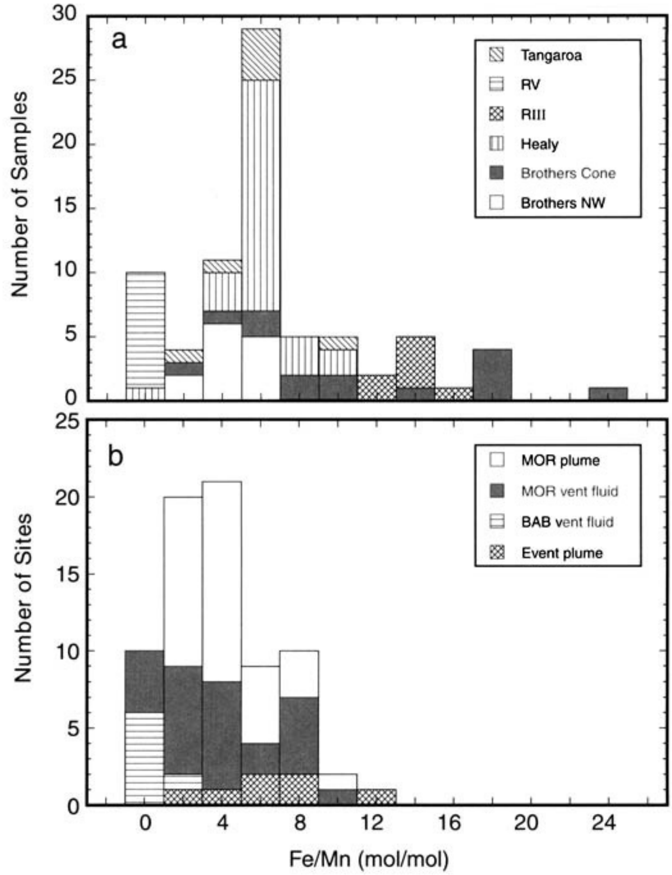

Fig. 9. Histogram distributions of Fe/Mn (mol/mol) for: (**a**) samples collected within hydrothermal plumes over SKA volcanoes (determined as TDFe and TDMn); and (**b**) average values for chronic and event plumes over MOR sites and vent fluids collected from non-sedimented MOR and BAB sites with temperatures greater than 60°C (references available from corresponding author). Event plumes are the result of magma intrusions near the seafloor (cf. Massoth *et al.* 1998 and references therein). The close correspondence in ranges for MOR vent fluids and plumes suggests that direct comparison of the respective Fe/Mn data is valid. While hot-spot volcano Fe/Mn values extend to 58 (not shown), they are not included here because these rare emissions are not likely be volumetrically important to sea-water chemistry.

Fe/Mn values (0.2 ± 0.1), consistent with vent fluids sampled at BAB sites, which generally are sulphur-dominated (i.e. Fe/S: 0.01–0.5). A similar situation may exist at Rumble V, where the concentration of H_2S in the plume is the highest observed on the SKA (18.7 μM, implying a high-temperature magmatic source as discussed above) and exceeds that for TDFe by almost 500-fold. Given that there are also high concentrations of Mn in the plume at Rumble V (again implying a high-temperature source), the most obvious explanation for the low Fe/Mn values is near-quantitative precipitation of Fe as iron sulphide minerals below the seafloor. This would require penetration of oxidized sea water into the subseafloor environment sufficient to destabilize the gas/rock-buffered Fe and S species responsible for the chemical mobility of these elements within volcanic fluids. An alternative explanation requires a stratabound Mn deposit on Rumble V. Such deposits, formed by diffuse discharge of low-temperature hydrothermal fluids, have been reported on arc volcanoes (including the northern Tonga–Kermadec arc) and back-arc ridges (average Fe/Mn *c.* 0.04; Hein *et al.* 1990, 1997). While it is conceivable that gas-rich hydrothermal warm springs could pass through a relict stratabound Mn deposit at Rumble V to create a plume with a low Fe/Mn value and high Mn concentration, observation of this phenomenon is unprecedented.

Of greater importance regarding the transport of metals to the oceans are the unusually high Fe/Mn values for plumes at Rumble III (13.7 ± 1.4) and Brothers Cone (11.6 ± 6.5) (Fig. 9a). As these ratios are also associated with extremely high Fe concentrations (Table 2), arc volcanoes such as Rumble III and Brothers may provide an enhanced source of Fe (and other associated elements) to sea water. Three processes, all magmatic in origin, may be responsible for the high Fe concentrations and Fe/Mn values. (i) Chemical weathering of wallrock by magmatic CO_2. An example of this is given by Loihi Volcano, where Fe/Mn values for vent fluids reach up to 58, which is near the value for the basaltic substrate (e.g. Sedwick *et al.* 1992*b*; Wheat *et al.* 2000). (ii) Congruent dissolution of wallrock by highly acidic fluids resulting from the discharge of SO_2 and H_2S, similar to that observed at White Island where Fe/Mn values in acid stream waters reach 42 (Giggenbach & Glasby 1977). (iii) Direct exsolution of liquid brine, possibly coincident with magmatic degassing. For example, fluid inclusions considered to have exsolved as brine from a dacitic magma intrusion have been analysed using laser ablation inductively coupled plasma-mass spectrometry (ICP-MS) and show Fe/Mn ratios as high as 12 and Fe concentrations as high as 4 M (Ulrich *et al.* 2001). Iron-rich brines also may be generated by physical phase separation. However, laboratory experiments (Bischoff & Rosenbauer 1987) and field data (e.g. phase-separated fluids are included in the MOR and BAB data presented in Fig. 9b) demonstrate that Fe and Mn do not fractionate during phase separation to produce high Fe/Mn values. Whether the Fe enrichments are secondary, i.e. induced by post-exsolution reaction of magmatic acid volatile gas(es) with volcanic rock, or primary, resulting from direct exsolution of liquid brine from magma, is difficult to discern at present.

Comparison of Fe/Mn data for SKA plumes to that for volcanic rock at the respective volcanoes provides insight regarding the nature of the Fe enrichments (Fig. 10). If either of the proposed secondary magmatic processes (i) and (ii) above were predominant, Fe/Mn values approaching that of wallrock and co-variant over the range of wallrock compositions extant along the SKA would be expected; clearly, this is not the case. This does not necessarily preclude these processes, only that their effects may be overprinted by secondary processes, such as incorporation of liberated Fe into alteration mineral phases. Nevertheless, the similarity of Fe/Mn values for

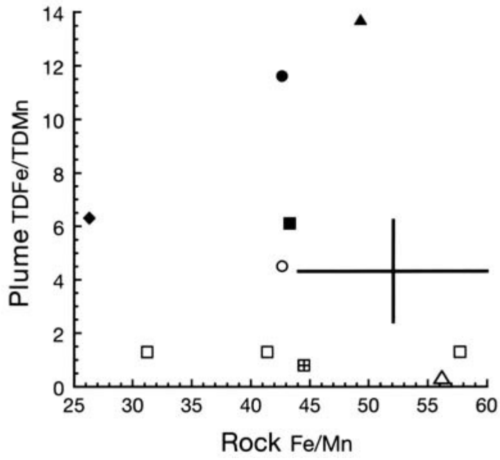

Fig. 10. Scatter plot of average TDFe/TDMn in plumes v. average Fe/Mn in volcanic rock dredged from the respective hydrothermally active volcanoes along the SKA. All values are mol/mol. Symbols as in Fig. 6. Multiple points for Clark Volcano reflect the diverse rock compositions reported for this site. Rock data are from Gamble *et al.* (1993, 1997), Gamble & Wright (1995), Wright & Gamble (1999) and T. Worthington (pers. comm.). The cross represents the range of values sampled along the Southern East Pacific Rise MOR between 14° and 32°S for plumes (*c.* 900 km of plume coverage; Baker *et al.* 2002*a*), and between 14° and 23°S for volcanic glasses (detailed sampling over >1000 km; Sinton *et al.* 1991).

magmatic brine fluid inclusions reported by Ulrich *et al.* (2001) and for plumes at the Rumble III and Brothers Cone sites poses an intriguing explanation of the high Fe/Mn values for these plumes. While it is unreasonable to suggest that magmatic fluid could volumetrically dominate volcanic discharge, it is conceivable that even small contributions of molar-level Fe-bearing liquids could elevate Fe concentrations, and, hence, Fe/Mn values in volcanic fluids and resulting plumes. For example, vent-fluid concentrations of Fe at the Rumble III and Brothers Cone sites are conservatively predicted from (2000-fold diluted) plume data to be 9.4 and 2.6 mM, respectively; 100–400 times less concentrated than magmatic fluids containing 1 M Fe.

Also evident in Figure 10 is a *c.* fourfold (or greater) disparity between Fe/Mn values for hydrothermal discharge and the respective host rock. This trend of lower hydrothermal values is universal for submarine hydrothermalism with the noted exception of hot-spot volcanoes. Until there is a firm understanding for why this large disparity exists, the relatively small variations in volcanic fluid Fe/Mn values (Fig. 9a) will be difficult to explain. It is incongruous that such widely differing Fe/Mn values should exist given that Fe and Mn co-vary as major components within the composition range of ferromagnesian silicates, consistent with affinities of both Mn^{2+} and Fe^{2+} for common lattice positions (Stanton 1994). Thus, any hydrothermal water–rock reaction pathway would be expected to first liberate these elements at bulk rock ratios and Fe/Mn then positively correlate in Figure 10.

The general scatter of Fe/Mn values along 260 km of the SKA is much greater than that observed along almost 900 km of MOR, represented by the large cross in Figure 10. This clearly illustrates the greater diversity of arc rock and fluid compositions compared to MOR settings, as well as the possible overprinting of rock-buffered signatures by geochemical processes active on arcs but not MORs. The scatter in SKA Fe/Mn values may be useful for regional plume tracking. For example, a weak plume *c.* 280 m beneath the summit on Rumble V not only lies on the same plume horizon as the adjacent Tangaroa Volcano plume, it has an almost identical Fe/Mn signature, which is distinctly different from the summit plume at Rumble V (Fig. 5c, Table 2). While the chemical data and our experience of summit venting argue that the deep Rumble V plume is a 22 km distal expression of Tangaroa fluid emissions, more detailed exploration will be required to rule out a deep source at Rumble V.

The effects of Fe on sea-water geochemical processes may be especially apparent near arc volcanoes. The colloidal iron oxyhydroxides formed following oxidation of vented Fe^{2+} are efficient scavengers of phosphate from sea water, potentially removing 10–30% of riverine P input (Feely *et al.* 1990, 1991*b* and references therein). Using data from two different oceans, Feely *et al.* (1991*b*) postulated that the efficiency of this removal, as reflected by the particulate P/Fe ratio, is directly proportional to the concentration of dissolved phosphate in sea water. The wide distribution of venting depths along the SKA allows the first vertical test of this hypothesis within a small area of the ocean. Plume samples collected over a range of venting depths at Rumble III (*c.* 120–220 m), Tangaroa (*c.* 650–780 m) and Brothers (*c.* 1070–1770 m) volcanoes have P/Fe values (mol/mol) of 0.06, 0.21 and 0.26, respectively (Fig. 11a). Phosphate concentrations over these venting intervals average 0.4 μM at Rumble III, 1.6 μM at Tangaroa and 2.3 μM at Brothers volcanoes (Fig. 11b). Normalizing these trends (to highest values at Brothers) for easier comparison shows similar progressions (P/Fe 1.00:0.81:0.23 and phosphate 1.00:0.70:0.17), verifying scavenging dependency on the availability of dissolved phosphate and demonstrating that arc discharge over a wide range of depths can have a variable effect on the oceans. Thus, while greater discharge of Fe from arcs may equate to greater removal of phosphate from the ocean, the efficiency of this removal in shallow sea water is likely to be only a small fraction of that for deeper arc discharge.

Summary

- The seven plumes first identified from particle and δ^3He signatures (de Ronde *et al.* 2001) are also recognizable as Fe and Mn anomalies. All of the volcano plumes, with the exception of the one at Rumble II West, have distinct pH anomalies. The spatial frequency of chemical plumes along the SKA is appreciable compared to MORs. The relatively shallow yet wide depth range of insular vent sites along 260 km of southern Kermadec arc front distributes hydrothermal emissions over a much broader depth range than seen along comparable lengths of MOR.
- The concentrations of measured (H_2S) and inferred (CO_2, SO_2) gases and of Fe within plumes at three (Rumble III, Rumble V and Brothers) of seven actively venting SKA volcanoes generally exceed concentrations reported for MOR and BAB hydrothermal plumes. The chemical intensity of Mn emissions appears to be similar at arc (as represented by the SKA) and MOR–BAB settings. Coupled with the high venting frequency and the appreciable arc length within the Pacific Basin (*c.* 6400 km for intra-oceanic arcs), the SKA chemical data suggest that fluid emissions from submarine arc volcanoes may be an important chemical source to the ocean.
- SKA volcano plumes are diverse in the magnitude of chemical signals and also with respect to MOR plume chemistry. While the composition of SKA volcanic rocks is also chemically variable compared to MORB, there does not appear to be a general correspondence between plume chemistry and the composition of erupted volcanic rocks at the respective SKA venting sites. This suggests that geochemical process(es) may provide a primary control (over 'apparent' magma source composition, i.e. Fe content, oxidation index, volatile content) on the chemistry of fluid emissions from some submarine arc volcanoes.

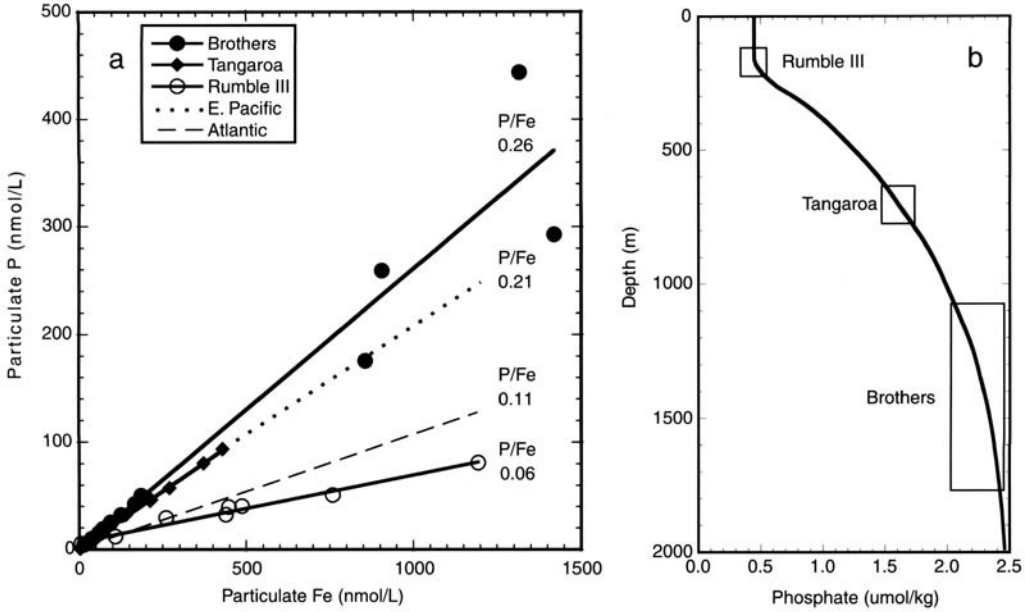

Fig. 11. (**a**) Particulate phosphorous (nmol) v. particulate iron (nmol) for plumes over Brothers (both NW and Cone plumes shown as solid circles), Tangaroa (solid diamonds) and Rumble III (open circles) volcanoes. Linear regression slopes are indicated for the respective volcano plume data and for hydrothermal plumes in the east Pacific (dotted line, note same as for Tangaroa) and Atlantic (dashed line) oceans (Feely *et al.* 1991*b*). (**b**) Vertical distribution of dissolved phosphate (μmol kg^{-1}) in regional waters north of New Zealand (WOCE line P14, station 7, 34°8.0′S, 175°18.1′E; website: cdiac.ornl.gov/oceans/home.html). Labelled boxes indicate depth ranges for plume data in (a).

- Magmatic iron enrichment may occur by direct injection of liquid brine from magma into the hydrothermal circulation, or as a result of secondary reactions between exsolved magmatic CO_2 and/or SO_2–H_2S and wallrock within the volcanic fluid circulation. The magmatic Fe signature may be masked by reaction with sulphur gas(es) prior to plume sampling (e.g. low plume values for Fe and Fe/Mn due to quantitative precipitation of iron below the sea floor as iron sulphides).

These early chemical results support further systematic investigation of the remaining estimated and largely unexplored >90% of submarine arc volcanoes. Better resolution of the spatial frequency of venting on arc fronts is needed in conjunction with more detailed chemical characterizations of plumes, particularly for magmatic components. Measurements of thermal and chemical flux at representative volcanoes are needed to quantify the magnitude of arc chemical emissions for comparison with MOR fluxes. Correlated temperature and chemical sampling of fluids venting from arc volcanoes are needed to compare arc sources with the existing global data set for hydrothermal emissions.

This research was funded by the New Zealand Foundation for Research Science and Technology and the NOAA VENTS Program. I. C. Wright, R. Greene, K. Faure, K. Britten, P. Hill, J. Mitchell and D. Singleton contributed to at-sea activities, and S.L. Walker assisted in shore-based processing of CTDO data and graphics presentation. We gratefully acknowledge reviews by Karen Von Damm and Jun-ichiro Ishibashi, and comments by Rob Larter that improved this manuscript. Contribution 2478 from the Pacific Marine Environmental Laboratory.

References

BAKER, E.T. & LUPTON, J.E. 1990. Changes in submarine hydrothermal ^3He/heat ratios as an indicator of magmatic/tectonic activity. *Nature*, **346**, 556–558.

BAKER, E.T., GERMAN, C.R. & ELDERFIELD, H. 1995. Hydrothermal plumes over spreading-center axes: Global distributions and geological inferences. *In*: HUMPHRIS, S.E., ZIERENBERG, R.A., MULLINEAUX, L.S. & THOMSON, R.E. (eds) *Seafloor Hydrothermal Systems: Physical, Chemical, Biological, and Geological Interactions.*

American Geophysical Union Monographs, **91**, 47–71.

BAKER, E.T., FEELY, R.A., DE RONDE, C.E.J., MASSOTH, G.J. & WRIGHT, I.C. 2003. Submarine hydrothermal venting on the southern Kermadec volcanic arc front (offshore New Zealand): location and extent of particle plume signatures. *In*: LARTER, R.D. & LEAT, P.T. (eds) *Intra-oceanic Subduction Systems: Tectonic and Magmatic Processes*. Geological Society, London, Special Publications, **219**, 141–161.

BAKER, E.T., HEY, R.N., LUPTON, J.E., RESING, J.A., FEELY, R.A., GHARIB, J.J., MASSOTH, G.J., SANSONE, F.J., KLEINROCK, M., MARTINEZ, F., NAAR, D.F., RODRIGO, C., BOHNENSTIEHL, D. & PARDEE, D. 2002*a*. Hydrothermal venting along Earth's fastest spreading center: East Pacific Rise, 27.5°–32.3°S. *Journal of Geophysical Research*, **107**(B7), 2130, 10.1029/2001JB000651.

BAKER, E.T., MASSOTH, G.J., DE RONDE, C.E.J., LUPTON, J.E. & MCINNES, B.I.A. 2002*b*. Observations and sampling of an ongoing subsurface eruption of Kavachi volcano, Solomon Islands, May 2000. *Geology*, **30**, 975–978.

BISCHOFF, J.L. & ROSENBAUER, R.J. 1987. Phase separation in sea floor geothermal systems: an experimental study of the effects of metal transport. *American Journal of Science*, **287**, 953–978.

BISCHOFF, J.L. & ROSENBAUER, R.J. 1988. An emperical equation of state for hydrothermal seawater (3.2 percent NaCl). *American Journal of Science*, **285**, 725–763.

BISCHOFF, J.L. & ROSENBAUER, R.J. 1996. The alteration of rhyolite in CO_2 charged water at 200 and 350°C: the unreactivity of CO_2 at higher temperatures. *Geochimica et Cosmochimica Acta*, **60**, 3859–3867.

BLOOMER, S.H., STERN, R.J. & SMOOT, N.C. 1989. Physical volcanology of the submarine Marianas and Volcano Arcs. *Bulletin of Volcanology*, **51**, 210–224.

BUTTERFIELD, D.A., MASSOTH, G.J., MCDUFF, R.E., LUPTON, J.E. & LILLEY, M.D. 1990. Geochemistry of hydrothermal fluids from Axial Seamount Hydrothermal Emissions Study vent field, Juan de Fuca Ridge: subseafloor boiling and subsequent fluid–rock interaction. *Journal of Geophysical Research*, **95**, 12 895–12 921.

CHEMINÉE, J.-L., STOFFERS, P., MCMURTRY, G., RICHNOW, H., PUTEANUS, D. & SEDWICK, P. 1991. Gas-rich submarine exhalations during the 1989 eruption of Macdonald Seamount. *Earth and Planetary Science Letters*, **107**, 318–327.

CRISP, J.A. 1984. Rates of magma emplacement and volcanic output. *Journal of Volcanology and Geothermal Research*, **20**, 177–211.

DE RONDE, C.E.J., BAKER, E.T., MASSOTH, G.J., LUPTON, J.E., WRIGHT, I.C., FEELY, R.A. & GREENE, R.R. 2001. Intra-oceanic subduction-related hydrothermal venting, Kermadec volcanic arc, New Zealand. *Earth and Planetary Science Letters*, **193**, 359–369.

DE RONDE, C.E.J., FAURE, K., BRAY, C.J., CHAPPELL, D.A. & WRIGHT, I.C. 2002. Hydrothermal fluids associated with seafloor mineralization at two southern Kermadec arc volcanoes, offshore New Zealand. *Mineralium Deposita*, **38**, 217–233, 10.1007/s00126-002-035-4.

DE RONDE, C.E.J., MASSOTH, G.J., BAKER, E.T. & LUPTON, J.E. 2003. Submarine hydrothermal venting related to volcanic arcs. *In*: SIMMONS, S.F. & GRAHAM, I.J. (eds) *Volcanic, Geothermal and Ore-forming Fluids: Rulers and Witnesses of Processes Within the Earth*. Society of Economic Geologists, Littleton, Colorado, Special Publications, in press.

FEELY, R.A., BAKER, E.T., LEBON, G.T., GENDRON, J.F., RESING, J.P. & COWEN, J.P. 1999. Evidence for sulfur enrichment in hydrothermal particles at Axial Volcano following the January–February 1998 eruption. *Geophysical Research Letters*, **26**, 3649–3652.

FEELY, R.A., MASSOTH, G.J., BAKER, E.T., COWEN, J.P., LAMB, M.F. & KROGSLUND, K.A. 1990. The effect of hydrothermal processes on midwater phosphorus distributions in the northeast Pacific. *Earth and Planetary Sciences Letters*, **96**, 305–319.

FEELY, R.A., MASSOTH, G.J. & LEBON, G.T. 1991*a*. Sampling of marine particulate matter and analysis by X-ray fluorescence spectrometry. *In*: HURD, D.C. & SPENCER, D.W. (eds) *Marine Particles: Analysis and Characterization*. American Geophysical Union Monographs, **63**, 251–257.

FEELY, R.A., MASSOTH, G.J., TREFRY, J.H., BAKER, E.T., PAULSON, A.J. & LEBON, G.T. 1994. Composition and sedimentation of hydrothermal plume particles from North Cleft segment, Juan de Fuca Ridge. *Journal of Geophysical Research*, **99**, 4985–5006.

FEELY, R.A., TREFRY, J.H., MASSOTH, G.J. & METZ, S. 1991*b*. A comparison of the scavenging of phosphorus and arsenic from seawater by hydrothermal iron oxyhydroxides in the Atlantic and Pacific Oceans. *Deep Sea Research*, **38**, 617–623.

FIELD, M.P. & SHERRELL R.M. 2000. Dissolved and particulate Fe in a hydrothermal plume at 9°45′N, East Pacific Rise: slow Fe(II) oxidation kinetics in Pacific plumes. *Geochimica et Cosmochimica Acta*, **64**, 619–628.

GAMBLE, J.A. & WRIGHT, I.C. 1995. The southern Havre Trough geological structure and magma pectrogenesis of an active backarc complex. *In*: TAYLOR, B. (ed.) *Backarc Basins: Tectonics and Magmatism*. Plenum Press, New York, 29–62.

GAMBLE, J.A., CHRISTIE, R.H.K., WRIGHT, I.C. & WYSOCZANSKI, R.J. 1997. Primitive K-rich magmas from Clark Volcano, southern Kermadec Arc: a paradox in the K–depth relationship. *The Canadian Mineralogist*, **35**, 275–290.

GAMBLE, J.A., WRIGHT, I.C. & BAKER, J.A. 1993. Sea floor geology and petrology in the oceanic to continental transition zone of the Kermadec–Havre–Taupo Volcanic Zone arc system, New Zealand. *New Zealand Journal of Geology and Geophysics*, **36**, 417–435.

GAMO, T., OKAMURA, K. CHARLOU, J.-L., URABE, T., AUZENDE, J.-M., ISHIBASHI, J. SHITASHIMA, K. & CHIBA, H. 1997. Acidic and sulfate-rich hydrothermal fluids from the Manus back-arc basin, Papua New Guinea. *Geology*, **25**, 139–142.

GIGGENBACH, W.F. 1987. Redox processes governing the chemistry of fumarolic gas discharges from White Island, New Zealand. *Applied Geochemistry*, **2**, 143–161.

GIGGENBACH, W.F. 1992. Magma degassing and mineral deposition in hydrothermal systems along convergent plate boundaries: SEG distinguished lecture. *Economic Geology*, **87**, 1927–1944.

GIGGENBACH, W.F. 1996. Chemical composition of volcanic gases. *In*: SCARPA, R. & TILLING, R.I. (eds) *Monitoring and Mitigation of Volcano Hazards*. Springer, Berlin, 222–255.

GIGGENBACH, W.F. & GLASBY, G.P. 1977. The influence of thermal activity on the trace metal distribtution in marine sediments around White Island, New Zealand. *New Zealand Department of Science and Industrial Research Bulletin*, **218**, 121–126.

GLASBY, G.P., IISASA, K., YUASA, M. & USUI, A. 2000. Submarine hydrothermal mineralization on the Isu–Bonin Arc, south of Japan: an overview. *Marine Georesources and Geotechnology*, **18**, 141–176.

HEDENQUIST, J.W. & LOWENSTERN, J.B. 1994. The role of magmas in the formation of hydrothermal ore deposits. *Nature*, **370**, 519–527.

HEIN, J.R., KOSCHINSKY, A., HALBACH, P., MANHEIM, F.T., BAU, M., KANG, J.-K. & LUBRICK, N. 1997. Iron and manganese oxide mineralization in the Pacific. *In*: NICHOLSON, K., HEIN, J.R., BÜHN, B. & DASGUPTA, S. (eds) *Manganese Mineralization: Geochemistry and Mineralogy of Terrestrial and Marine Deposits*. Geological Society, London, Special Publications, **119**, 123–138.

HEIN, J.R., SCHULZ, M.S. & KANG, J.-K. 1990. Insular and submarine ferromanganese mineralization of the Tonga–Lau region. *Marine Mining*, **9**, 305–354.

HERZIG, P.M., HANNINGTON, M.D. & ARIBAS, A., JR. 1998. Sulfur isotopic composition of hydrothermal precipitates from the Lau back-arc: implications for magmatic contributions to seafloor hydrothermal systems. *Mineralium Deposita*, **33**, 226–237.

HERZIG, P.M., HANNINGTON, M.D., FOUQUET, Y., VON STACKELBERG, U. & PETERSON, S. 1993. Gold-rich polymetallic sulfides from the Lau back arc and implications for the geochemistry of gold in seafloor systems of the southwest Pacific. *Economic Geology*, **88**, 2178–2205.

ISHIBASHI, J. & URABE, T. 1995. Hydrothermal activity related to arc-backarc magmatism in the western Pacific. *In*: TAYLOR, B. (ed.) *Backarc Basins: Tectonics and Magmatism*. Plenum Press, New York, 451–495.

JAMES, R.H. & ELDERFIELD, H. 1996. Dissolved and particulate trace metals in hydrothermal plumes at the Mid-Atlantic Ridge. *Geophysical Research Letters*, **23**, 3499–3502.

JENKINS, W.J., RONA, P.A. & EDMOND, J.M. 1980. Excess ^{3}He in the deep water over the mid-Atlantic Ridge at 26°N: evidence of hydrothermal activity. *Earth and Planetary Science Letters*, **49**, 39–44.

LEWIS, E. & WALLACE, D. 1998. *Program developed for CO_2 system calculations*, ORNL/CDIAC-105, Carbon Dioxide Information Analysis Center, Oak Ridge National Laboratory, US Department of Energy, Oak Ridge, TN. World Wide Web Address: http://cdiac.ornl.gov/oceans/co2rprt.html.

LILLEY, M.D., FEELY, R.A. & TREFRY, J.H. 1995. Chemical and biological transformations in hydrothermal plumes. *In*: HUMPHRIS, S.E, ZIERENBERG, R.A., MULLINEAUX, L.S. & THOMSON, R.E. (eds) *Seafloor Hydrothermal Systems: Physical, Chemical, Biological, and Geological Interactions*. American Geophysical Union Monographs, **91**, 369–391.

LUPTON, J. 1983. Terrestrial inert gases: isotope tracer studies and clues to primordial components in the mantle. *Annual Reviews in Earth and Planetary Sciences*, **11**, 371–414.

LUPTON, J. 1998. Hydrothermal helium plumes in the Pacific Ocean. *Journal of Geophysical Research*, **103**, 15 853–15 868.

LUPTON, J.E. 1996. A far-field hydrothermal plume from Loihi Seamount. *Science*, **272**, 976–979.

LUPTON, J.E., BAKER, E.T. & MASSOTH, G.J. 1989. Variable ^{3}He/heat ratios in submarine hydrothermal systems: evidence from two plumes over the Juan de Fuca Ridge. *Nature*, **337**, 161–164.

LUPTON, J.E., BAKER, E.T., MOTTL, M.J., SANSONE, F.J., WHEAT, C.G., RESING, J.A., MASSOTH, G.J., MEASURES, C.I. & FEELY, R.A. 1993*a*. Chemical and physical diversity of hydrothermal plumes along the East Pacific Rise, 8°45′N to 11°50′N. *Geophysical Research Letters*, **20**, 2913–2916.

LUPTON, J.E., GRAHAM, D.W., DELANEY, J.R. & JOHNSON, H.P. 1993*b*. Helium isotope variations in Juan de Fuca Ridge basalts. *Geophysical Research Letters*, **20**, 1851–1854.

MASSOTH, G.J. & HEY, R.N. 1998. SUAVE perspectives on the Southern East Pacific Rise. *Eos, Transactions, American Geophysical Union*, **79**, T11G-05.

MASSOTH, G.J. & MILBURN, H.B. 1997. SUAVE (SUbmersible System Used to Assess Vented Emissions): a diverse tool to probe the submarine hydrothermal environment. *In*: *Proceedings of Marine Analytical Chemistry for Monitoring and Oceanographic Research, Plouzane*. IUEM, Brest, France, 80–87.

MASSOTH, G.J., BAKER, E.T., FEELY, R.A., BUTTERFIELD, D.A., EMBLEY, R.E., LUPTON, J.E., THOMSON, R.E. & CANNON, G.A. 1995. Observations of manganese and iron at the CoAxial seafloor eruption site, Juan de Fuca Ridge. *Geophysical Research Letters*, **22**, 151–154.

MASSOTH, G.J., BAKER, E.T., FEELY, R.A., LUPTON, J.E., COLLIER, R.W., GENDRON, J.F., ROE, K.K., MAENNER, S.M. & RESING, J.A. 1998. Manganese and iron in hydrothermal plumes resulting from the 1996 Gorda Ridge event. *Deep Sea Research II*, **45**, 2683–2712.

MASSOTH, G.J., BAKER, E.T., LUPTON. J.E., FEELY, R.A., BUTTERFIELD, D.A., VON DAMM, K.L., ROE, K.K. & LEBON, G.T. 1994. Temporal and spatial variability of hydrothermal manganese and iron at Cleft segment, Juan de Fuca Ridge. *Journal of Geophysical Research*, **99**, 4969–4984.

McMurtry, G.M., Sedwick, P.N., Fryer, P., Vonderhaar, D.L. & Yeh, W.-H. 1993. Unusual geochemistry of hydrothermal vents on submarine arc volcanoes: Kasuga Seamounts, Northern Mariana Arc. *Earth and Planetary Science Letters*, **114**, 517–528.

Measures, C., Yuan, J. & Resing, J. 1995. Determination of iron in seawater by flow injection analysis using in-line preconcentration and spectrophotmetric detetection. *Marine Chemistry*, **50**, 3–12.

Nriagu, J.O. 1989. A global assessment of natural sources of atmospheric trace metals. *Nature*, **338**, 47–49.

Poreda, R. & Craig, H. 1989. Helium isotope ratios in circum-Pacific volcanic arcs. *Nature*, **338**, 473–478.

Radford-Knoery, J., Charlou, J.-L., Donval, J.-P., Aballea, M., Fouquet, Y. & Ondreas, H. 1998. Distribution of dissolved sulphide, methane, and manganese near the sea floor at the Lucky Strike (37°17′N) and Menez Gwen (37°50′N) hydrothermal vent sites on the mid-Atlantic Ridge. *Deep Sea Research*, **45**, 367–386.

Radford-Knoery, J., German, C.R., Charlou, J.-L., Donval, J.-P. & Fouquet, Y. 2001. Distribution and behaviour of dissolved hydrogen sulphide in hydrothermal plumes. *Limnology and Oceanography*, **46**, 461–464.

Resing, J.A. & Mottl, M.J. 1992. Determination of manganese in seawater by flow injection analysis using on-line preconcentration and spectrophotometic detection. *Analytical Chemistry*, **64**, 2682–2687.

Resing, J.A. & Sansone, F.J. 1996. Al and pH anomalies in the Manus Basin reappraised: comments on the paper by T. Gamo *et al.*, 'Hydrothermal plumes in the eastern Manus Basin, Bismark Sea: CH_4, Mn, Al, and pH anomalies'. *Deep Sea Research*, **43**, 1867–1872.

Resing, J.A., Feely, R.A., Massoth, G.J. & Baker, E.T. 1999. The water-column chemical signature after the 1998 eruption of Axial Volcano. *Geophysical Research Letters*, **26**, 3645–3648.

Sakai, H., Tsubota, H., Nakai, T., Ishibashi, J., Akagi, T., Gamo, T., Tilbrook, B., Igarashi, G., Kodera, K., Shitashima, K., Nakamura, S., Fujioka, K., Watanabe, M., McMurtry, G., Malahoff, A. & Ozima, M. 1987. Hydrothermal activity on the summit of Loihi Seamount, Hawaii. *Geochemical Journal*, **21**, 11–21.

Sakamoto-Arnold, C.M., Johnson, K.S. & Beehler, C.L. 1986. Determination of hydrogen sulfide in seawater using flow injection analysis and flow analysis. *Limnology and Oceanography*, **31**, 894–900.

Sawkins, F.J. 1990. *Metal Deposits in Relation to Plate Tectonics,* 2nd edition. Springer, Berlin.

Sedwick, P.N., McMurtry, G.M., Hilton, D.R. & Goff, F. 1992*a*. Carbon dioxide and helium in hydrothermal fluids from Loihi Seamount, Hawaii, USA: temporal variability and implications for the release of mantle volatiles. *Geochimica et Cosmochimica Acta*, **58**, 1219–1297.

Sedwick, P.N., McMurtry, G.M. & Macdougall, J.D. 1992*b*. Chemistry of hydrothermal solutions from Pele's Vents, Loihi Seamount, Hawaii. *Geochimica et Cosmochimica Acta*, **56**, 3643–3667.

Sinton, J.M., Smaglik, S.M., Mahoney, J.J. & Macdonald, K.C. 1991. Magmatic processes at superfast spreading mid-ocean ridges: glass compositional variations along the East Pacific Rise 13°–23°S. *Journal of Geophysical Research,* **96**, 6133–6155.

Stanton, R.L. 1994. *Ore Elements in Arc Lavas.* Oxford Monographs on Geology and Geophysics, **29**.

Stüben, D., Bloomer, S.H., Taïbi, N.E., Neumann, T., Bendel, V., Püschel, U., Barone, A., Lange, A., Shiying, W., Cuzhhong, L. & Deyu, Z. 1992. First results of study of sulphur-rich hydrothermal activity from an island-arc environment: Esmeralda Bank in the Mariana Arc. *Marine Geology*, **103**, 521–528.

Tsunogai, U., Ishibashi, J., Wakita, H., Gamo, T., Watanabe, K., Kajimura, T., Kanayama, S. & Sakai, H. 1994. Peculiar features of Suiyo Seamount hydrothermal fluids, Izu–Bonin Arc: differences from subaerial volcanism. *Earth and Planetary Science Letters*, **126**, 289–301.

Ulrich, T., Gunther, D. & Heinrich, C.A. 2001. The evolution of a porphyry Cu–Au deposit, based on LA-ICP-MS analysis of fluid inclusions: Bajo de la Alumbrera, Argentina. *Economic Geology*, **96**, 1743–1774.

Urabe, T. & Marumo, K. 1991. A new model for Kuroko-type deposits of Japan. *Episodes*, **14**, 246–251.

Von Damm, K.L. 1995. Controls on the chemistry and temporal variability of sea floor hydrothermal fluids. *In:* Humphris, S.E., Sierenberg, R.A., Mullineaux, L.S. & Thomson, R.E. (eds) *Seafloor Hydrothermal Systems: Physical, Chemical, Biological, and Geological Interactions.* American Geophysical Union Monographs, **91**, 222–247.

Wheat, C.G., Jannasch, H.W., Plant, J.N., Moyer, C.L., Sansone, F.J. & McMurtry, G.M. 2000. Continuous sampling of hydrothermal fluids from Loihi Seamount after the 1996 event. *Journal of Geophysical Research*, **105**, 19 353–19 367.

Worthington, T.J. 1998. *Geology and petrology of Raoul Volcano: magma genesis and fractionation processes beneath the Tonga–Kermadec arc.* PhD thesis, University of Auckland.

Wright, I.C. 1993. Pre-spread rifting and heterogeneous volcanism in the southern Havre Trough back-arc basin. *Marine Geology*, **113**, 179–200.

Wright, I.C. & Gamble, J.A. 1999. Southern Kermadec submarine caldera arc volcanoes (SW Pacific): caldera formation by effusive and pyroclastic eruption. *Marine Geology*, **161**, 207–227.

Wright, I.C., Gamble, J.A. & Shane, P.A.R. 2003. Submarine silicic volcanism of Healy caldera, southern Kermadec arc (SW Pacific): I – volcanology and eruption mechanisms. *Bulletin of Volcanology*, 10.1007/s00445–002–0234–1.

WRIGHT, I.C., DE RONDE, C.E.J., FAURE, K. & GAMBLE, J.A. 1998. Discovery of hydrothermal sulfide mineralasation from southern Kermadec arc volcanoes (SW Pacific). *Earth and Planetary Science Letters*, **164**, 335–343.

YANG, K. & SCOTT, S. 1996. Possible contribution of a metal-rich magmatic fluid to a sea-floor hydrothermal system. *Nature*, **383**, 420–423.

YANG, K. & SCOTT, S.D. 2002. Magmatic degassing of volatiles and ore metals into a hydrothermal system on the modern sea floor of the eastern Manus back-arc, western Pacific. *Economic Geology*, **97**, 1079–1100.

YOUNG, C. & LUPTON, J.E. 1983. An ultra-tight fluid sampling system using cold-welded copper tubing. *Eos, Transactions, American Geophysical Union*, **64**, 735.

This page intentionally left blank

Submarine hydrothermal venting on the southern Kermadec volcanic arc front (offshore New Zealand): location and extent of particle plume signatures

E.T. BAKER[1], R.A. FEELY[1], C.E.J. DE RONDE[2], G.J. MASSOTH[2] & I.C. WRIGHT[3]

[1]*Pacific Marine Environmental Laboratory, National Oceanic and Atmospheric Administration, Seattle, WA 98115–6349, USA (e-mail: baker@pmel.noaa.gov)*

[2]*Institute of Geological and Nuclear Sciences, PO Box 31–312, Lower Hutt, New Zealand*

[3]*National Institute of Water and Atmospheric Research, Private Bag 14–901, Wellington 6003, New Zealand*

Abstract: Hydrothermal activity on submarine volcanic arcs in the western Pacific Ocean is known but mostly unexplored. In March 1999, the New Zealand American PLUme Mapping Expedition (NZAPLUME) cruise conducted the first systematic exploration of hydrothermal venting along a sizeable section of an intra-oceanic arc, visiting 13 volcanoes along 260 km of the southern Kermadec arc, just northeast of New Zealand. Conclusive evidence of hydrothermal plumes exists for seven of the 13 volcanoes; at two other volcanoes plume indications were weak and uncertain. The hydrothermal origin of the particle plumes was confirmed by positive anomalies in the ratios of sulphur, iron and copper to titanium relative to non-plume particles, in mass concentrations similar to particles collected from hydrothermal plumes over mid-ocean ridges. The spatial density of active sites along the southern Kermadec arc is at least 2.7 per 100 km (2.7/100 km), probably not significantly different from the weakly constrained value of *c.* 1/100 km on slow- and intermediate-rate mid-ocean ridges. An analysis of the number of hydrothermal fields produced for the magma delivery rate in each of these environments suggests that the southern Kermadec arc presently has relatively abundant hydrothermal activity. While this result cannot yet be generalized to other Pacific arcs, submarine volcanoes may contribute significantly to the global hydrothermal budget.

Since the discovery of hydrothermal venting on mid-ocean ridges more than two decades ago, approximately 20% of the roughly 60 000 km of the Earth's divergent plate boundary has been surveyed for the presence of venting, resulting in the discovery of over 200 active vent fields (Baker *et al.* 1995; see also the InterRIDGE web site at http://triton.ori.u-tokyo.ac.jp/~intridge/). Conspicuously absent to date, however, has been the systematic mapping of hydrothermal venting within modern arc–back-arc systems along convergent plate boundaries. The first compilation of such hydrothermalism within these tectonic settings identified only 22 sites of active venting along 11 000 km of western Pacific Plate boundary extending from central Japan to New Zealand (Ishibashi & Urabe 1995). Fifteen of these sites occurred on back-arc spreading centres or rifts, with only seven submarine arc volcanoes reported to host active hydrothermal activity.

The paucity of information about such hydrothermalism within the western Pacific largely stems from our lack of data on arc volcano distribution. A compilation of volcano distribution along active margins (de Bremond d'Ars *et al.* 1995) listed the Tonga arc as including only nine. A more recent study of the Tonga–Kermadec arc identifies 20 subaerial and 17 submarine volcanoes, with satellite altimetry providing strong evidence for an additional 57 submarine volcanoes along the arc (Worthington 1998). If the submarine volcano population has been similarly underestimated along the rest of some 22 000 km of island arcs, then submarine arc volcanoes probably number in the hundreds (de Ronde *et al.* 2003).

The principal objective of the New Zealand American PLUme Mapping Expedition (NZAPLUME) cruise in March 1999 was a systematic investigation of all 13 volcanoes in the southern Kermadec arc (SKA). de Ronde *et al.* (2001) gave an overview of the NZAPLUME results with an emphasis on some of the unusual characteristics of arc-related venting; Massoth *et al.* (2003) characterize the chemistry of gaseous

From: LARTER, R.D. & LEAT, P.T. 2003. *Intra-Oceanic Subduction Systems: Tectonic and Magmatic Processes.* Geological Society, London, Special Publications, **219**, 141–161. 0305-8719/03/$15.00

and fluid emissions from the SKA volcanoes in an effort to identify the signature of a magmatic component. Here we present the first detailed observations of the distribution and composition of the particulate fraction of the SKA hydrothermal plumes, from which we estimate the location and extent of presently active hydrothermal discharge at each volcano. We use these new data to compare the spatial frequency of hydrothermal systems in arc and mid-ocean ridge environments and to speculate on the extent of volcano-hosted hydrothermalism in other volcanic arc settings.

Study area and methods

The Kermadec–Tonga complex is a classic example of an evolving arc–back-arc basin system (Karig 1971) (Fig. 1). West of the Kermadec and Tonga ridges back-arc extension progresses from full oceanic spreading in the Lau Basin, through rifting of arc crust along the Harve Trough, to rifting of the continental crust of New Zealand (Parson & Wright 1996; Delteil *et al.* 2002). The subduction rate (convergence plus back-arc widening) of this convergent boundary correspondingly decreases from *c.* 24 cm a^{-1} at 16°S to *c.* 5 cm a^{-1} at 38°S (Bevis *et al.* 1995; Parson & Wright 1996). The southern Harve Trough, 34°–37°S, is the southernmost section of rifting arc crust along the Kermadec–Tonga complex (Fig. 1). Here the active Kermadec volcanic arc forms a line of 13 submarine stratovolcanoes and calderas (Parson & Wright 1996; Wright *et al.* 1996) that extend some 260 km from Whakatane in the south to Brothers in the north (Fig. 1). The volcanoes range in depth from 220 m at the summit of simple cones (e.g. Rumble III) to 1850 m at the bottom of enclosed calderas (e.g. Brothers).

During the NZAPLUME cruise we deployed 61 conductivity–temperature–depth–optical (CTDO) vertical casts and 11 deep CTDO tow-yos to map optical and thermal anomalies along the SKA segment. The sensor and sampling package was identical to those used in previous plume studies (e.g. Baker 1998). For tow-yos the CTDO package followed a sawtooth path through the water column as the cable winch continuously payed in and out and the ship steamed steadily at a speed of *c.* 2.5–3.5 km h^{-1}. The sawtooth wavelength varied between *c.* 0.5 and 2 km according to the water depth.

Elemental composition of particulate matter was determined by X-ray primary- and secondary-emission spectrometry with a Pd source, and Mo, Ge, Co and Ti secondary targets using a non-destructive thin-film technique (Feely *et al.* 1991). Precision relative to standards averaged 2% for Fe, Ti and Cu, and 11% for sulphur.

Hydrothermal discharge from vents on deep mid-ocean ridges creates plumes that rise tens or hundreds of meters above the seafloor. These plumes are readily identified by enrichments in various dissolved and particulate species (e.g. ^3He, CH_4, CO_2, Mn, Fe, Cu) and by local anomalies in the turbidity and temperature of the plume waters (e.g. Lupton *et al.* 1985; Baker *et al.* 1995; Feely *et al.* 1996). Tracers that can be continually measured and observed in real time, such as light backscattering and temperature, are most useful for detecting and mapping hydrothermal plumes, and this paper uses these tracers to map the hydrothermal plume distributions around SKA volcanoes. Our principal plume mapping tool was a light backscattering sensor (LBSS) that yields nephelometric turbidity units (NTUs) (APHA, 1989) according to the expression

$$\Delta NTU = (V_r - V_b)/a_n$$

where ΔNTU = the plume LBSS anomaly above ambient water, V_r = the raw voltage reading of the LBSS, V_b = the background voltage of ambient water not affected by hydrothermal plumes and a_n = a factor unique to each LBSS determined from a laboratory calibration using formazine (Baker *et al.* 2001).

ΔNTU values were a good predictor of particle mass concentration (C_m) and an even better predictor of the particulate Fe+S (nmol l^{-1}) loadings in this study. For the entire set of 114 filtered (pore diameter = 0.4 μm) samples, a least-squares regression of C_m and ΔNTU yielded a correlation coefficient r^2 = 0.54. (The r^2 value increases to 0.80 while the regression slope and intercept remain unchanged by eliminating five samples collected in regions of extremely high vertical ΔNTU gradients. At these locations the sampling bottles probably did not collect water representative of the instantaneous ΔNTU value.) (See Fig. 2a.) For these samples a ΔNTU increment of 0.001 is equivalent to a C_m increment of *c.* 0.48 μg l^{-1}. The correlation coefficient between ΔNTU and the sum of Fe+S (nmol l^{-1}), the primary particulate hydrothermal elements, improves to 0.60 (and to 0.91 after again eliminating the five suspect samples) (Fig. 2b). Thus, the LBSS is a sensitive indicator of the mass concentration of hydrothermally precipitated particles suspended in the water column, as has been consistently observed within deep-sea hydrothermal plumes (Baker *et al.* 1995).

The other real-time tracer commonly used to track deep-sea hydrothermal plumes,

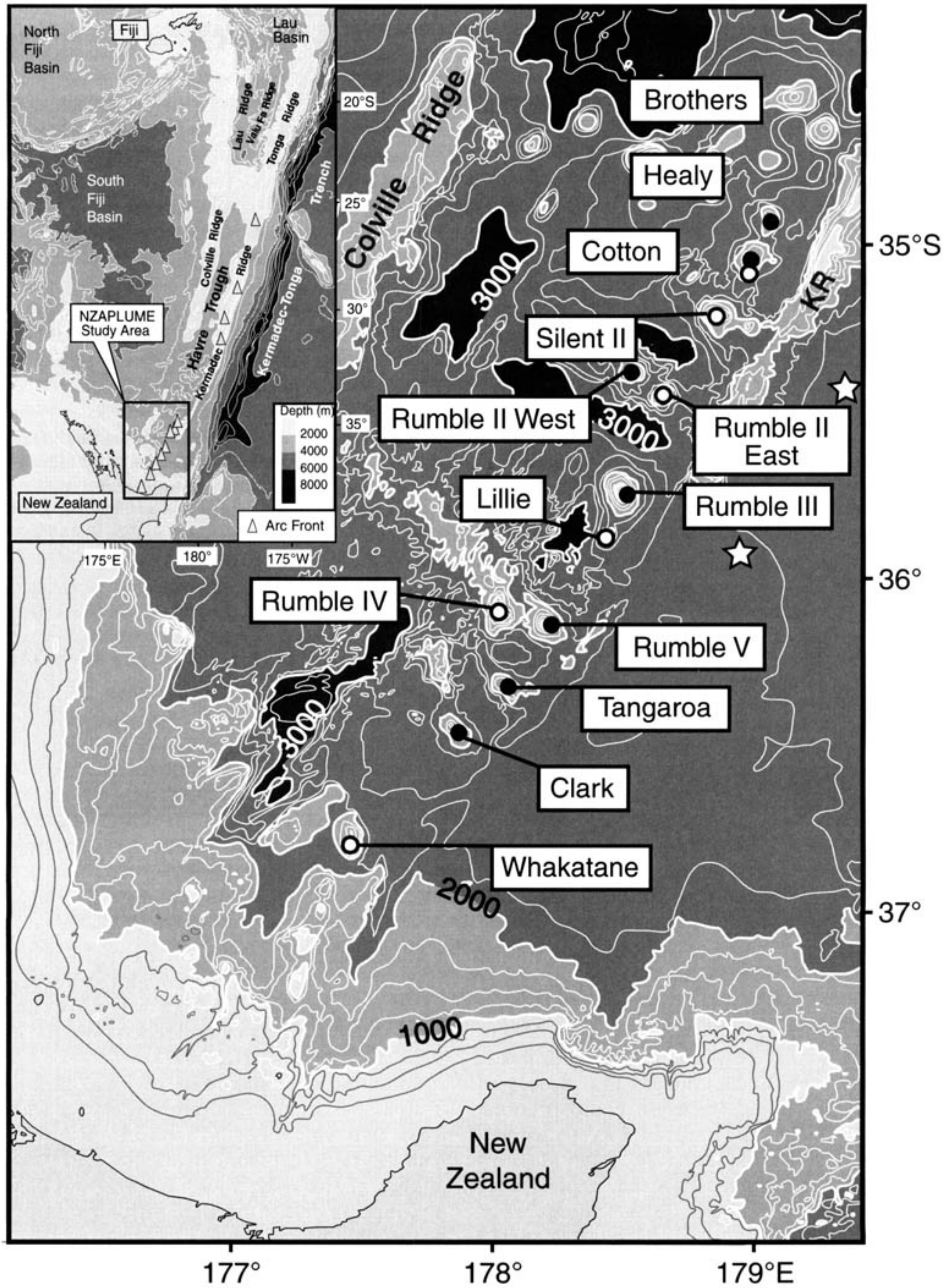

Fig. 1. Location of the 13 studied volcanoes along the southern Kermadec arc. Volcanoes marked by solid circles were confirmed hydrothermally active. Stars mark the location of core samples analysed for sediment chemistry (Table 1); a third core is off the map at 32°20.6′S, 178°32.3′W (Gamble *et al.* 1996) Inset map shows the regional setting of the study area and the trend of the Kermadec–Tonga volcanic arc front. Modified after de Ronde *et al.* 2001 with permission from Elsevier Science.

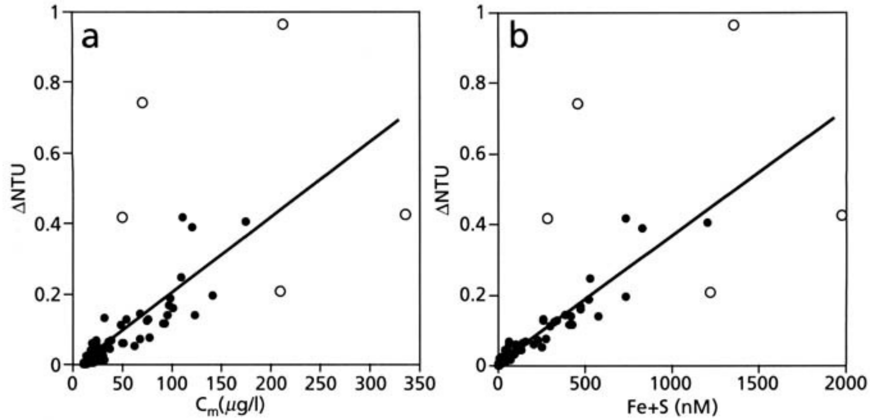

Fig. 2. (**a**) ΔNTU v. particle mass concentration (C_m) for all NZAPLUME samples. (**b**) ΔNTU v. Fe+S (nmol l^{-1}). Open circles denote five samples collected in regions of extremely high vertical gradients, where the instantaneous ΔNTU value may not be representative of the collected water sample. Solid lines are least-squares regression fits for all samples. For (a) $\Delta NTU = -0.025 + 0.0021C_m$ ($r^2 = 0.54$; 0.80 after removing the five suspect samples); for (b) $\Delta NTU = 0.0038 + 0.00036(Fe+S)$ ($r^2 = 0.60$; 0.91 after removing the five suspect samples).

temperature anomaly (Δθ) (Lupton *et al.* 1985), proved of limited use because of the shallow depths of many volcanoes and variability in the slope of the regional temperature–salinity profile (e.g. Lavelle *et al.* 1998). At depths < *c.* 1200 m (i.e. all plumes except those within the deep calderas of Brothers and Healy), the vertical temperature gradient is a minimum of *c.* 0.01°C m^{-1}. At these depths, even plumes with intense optical and hydrothermal chemical anomalies (Fig. 3a) do not create a resolvable hydrographic anomaly. The variability of the local temperature profile would conceal a robust Δθ as high as 0.1°C or more. In deeper waters with weaker temperature gradients, however, the hydrothermal Δθ mirrors the ΔNTU anomaly (Fig. 3b). In the absence of Δθ information there might be concern that processes such as sediment resuspension could produce optical anomalies misinterpreted as hydrothermal plumes. de Ronde *et al.* (2001) and Massoth *et al.* (2003) reassuringly show that plumes from each active volcano contain distinct anomalies of unmistakably hydrothermal species such as ^{3}He and dissolved Mn, anomalies that are generally congruent (although far less detailed) with the optical definition of the plumes as presented in this paper.

Regional overview

A transect of the ΔNTU distribution along the SKA defines four distinct particle layers (Fig. 4). A thin, high-intensity layer in the upper 200 m marks the influence of euphotic zone productivity. A layer of variable, but declining, ΔNTU between 200 and 700 m is likely to be a mixture of settling particles from surface production and hydrothermal discharge from shallow volcanoes. A broad mid-depth minimum in ΔNTU extends from 700 m to about 1500 m, coincident with low-salinity Antarctic Intermediate Water (McCave & Carter 1997). Below 1500 m a steadily increasing ΔNTU defines a bottom nepheloid layer that may represent, at least in part, filaments of Upper Circumpolar Deep Water flow leaking west through the Kermadec Ridge into the Harve Trough as it moves northward along the Kermadec Trench (Warren *et al.* 1994; McCave & Carter 1997).

Superimposed upon this regional trend are distinct particulate plumes associated with at least five volcanoes (Tangaroa, Rumble V, Rumble III, Healy and Brothers), and possible plumes at two others (Whakatane and Clark), discharging hydrothermal effluents into the water column at depths ranging from <200 to >1800 m. Similar plots showing the distribution of ^{3}He and total dissolvable Mn, two unambiguous hydrothermal tracers, match the particle plume distribution and additionally confirm hydrothermal sources at Clark and Rumble II West (de Ronde *et al.* 2001; Massoth *et al.* 2003). In the following section we examine the distribution of plumes at each volcano.

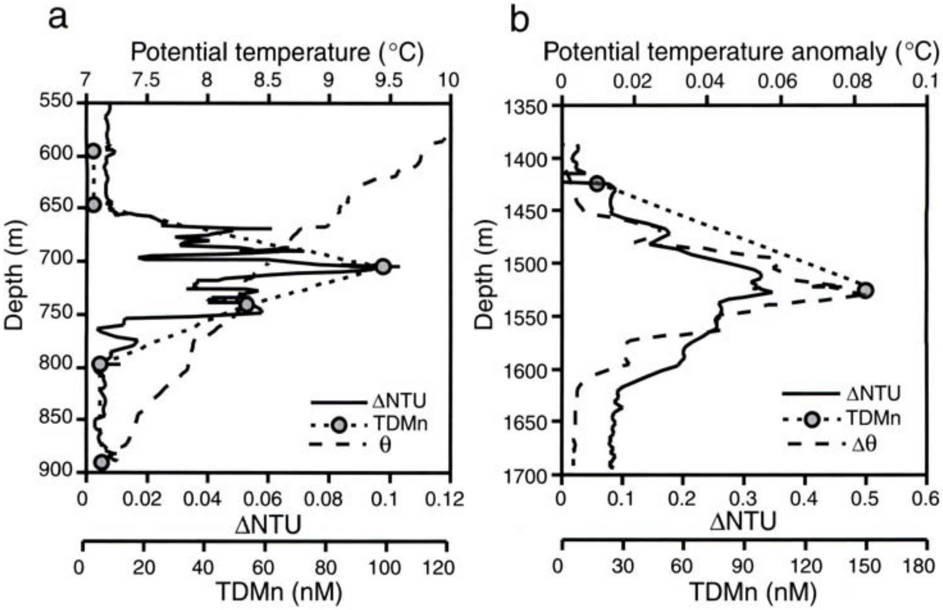

Fig. 3. (**a**) Vertical profiles of ΔNTU, potential temperature (θ) and total dissolved Mn through a hydrothermal plume emanating from Tangaroa. Note that any hydrothermal effect on the θ profile (typically of the order of 0.1°C) cannot be resolved within the variability of the ambient profile. (**b**) The same profiles through a plume within the Brothers caldera, but substituting the hydrothermal temperature anomaly, Δθ, for θ. Δθ at each depth $z = \theta(z) - (k_1\sigma_\theta(z) + k_2\sigma_\theta(z)^2 + b)$, where $\sigma_\theta(z)$ is potential density, and k and b are regression coefficients for a second-order fit of θ as a function of σ_θ immediately above the plume horizon. At these depths the vertical temperature gradient is small enough (c. 0.003°C m^{-1}) and smooth enough to reveal the Δθ signal.

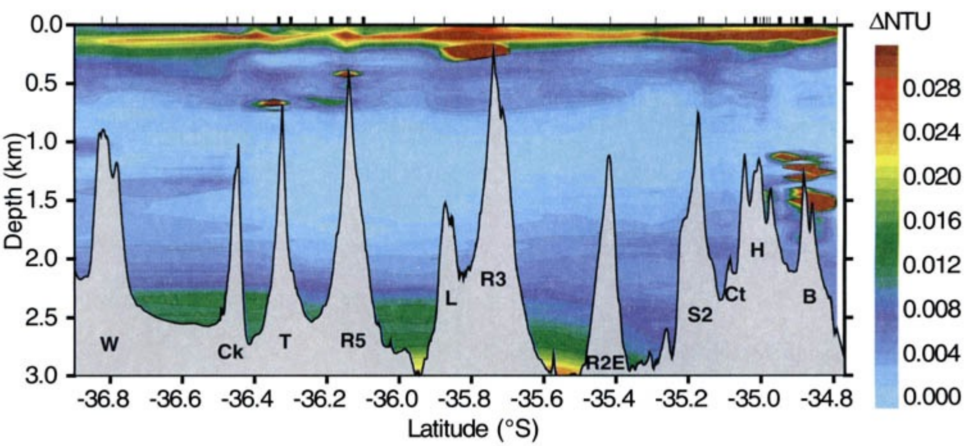

Fig. 4. Longitudinal section through the southern Kermadec arc of ΔNTU from vertical casts and tows; ticks along top axis indicate profile locations, which were concentrated over Tangaroa, Rumble V, Healy and Brothers. W, Whakatane; Ck, Clark; T, Tangaroa; R5, Rumble V; L, Lillie; R3, Rumble III; R2E, Rumble II East; S2, Silent II; Ct, Cotton; H, Healy; B, Brothers. Modified after de Ronde *et al.* 2001 with permission from Elsevier Science. Rumble IV is directly west of Rumble V, and Rumble II West is behind Rumble II East. Note that the ΔNTU maximum centred near 1300 m between Whakatane and Clark is not constrained by the data and is a gridding artifact.

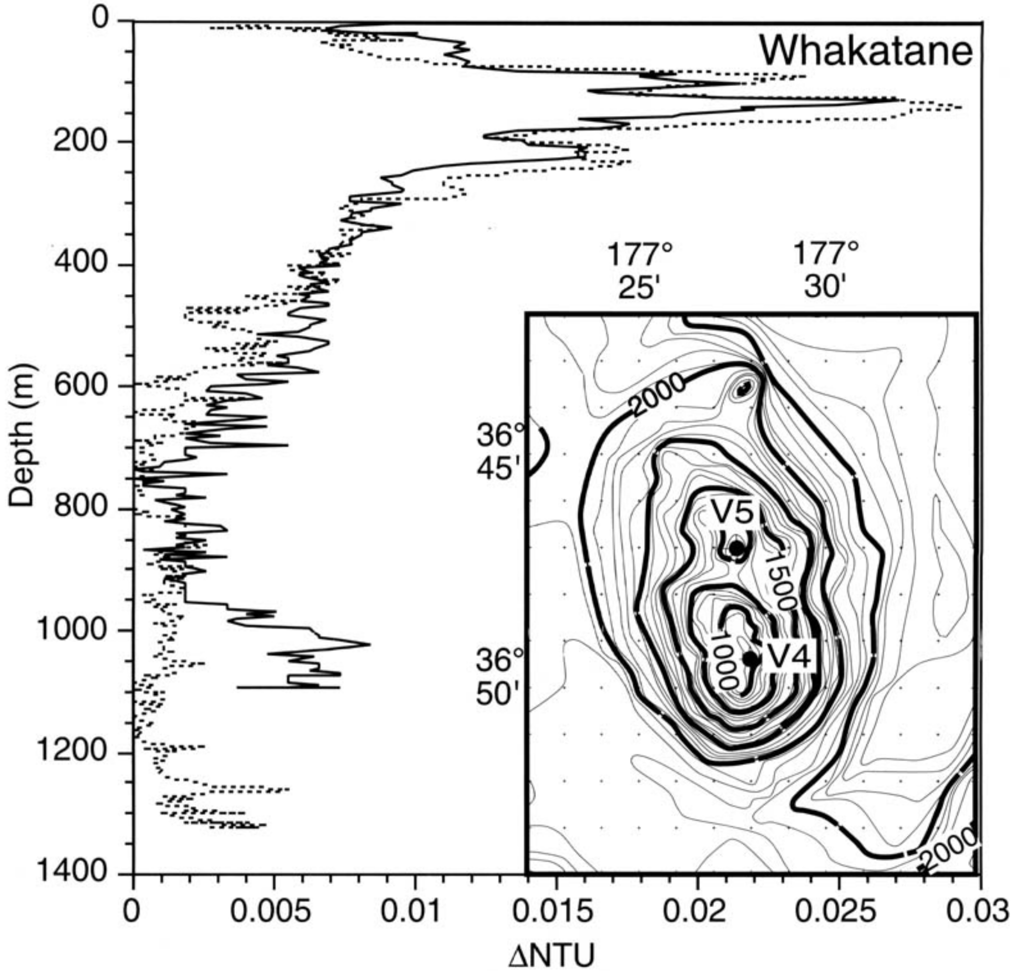

Fig. 5. Vertical profiles of ΔNTU for V4 (solid line) and V5 (dashed line) over Whakatane (inset). Both profiles show increased scattering near the seafloor, possibly indicative of hydrothermal venting. Map contour interval is 50 m.

Site plume mapping

Whakatane

Whakatane is a slightly elliptical edifice with two summits *c.* 4 km apart at depths of 1100 and 1350 m (Fig. 5). Water samples were not collected in the vicinity of Whakatane, so plume inferences rely solely on two CTDO profiles. Both profiles show near-bottom increases in ΔNTU, but only one, above the shallower summit, has a clear indication of an above-bottom ΔNTU maximum (*c.* 0.09) suggestive of a neutrally buoyant hydrothermal plume rather than a plume derived from sediment resuspension. The absence of supporting chemical data mean the presence of active hydrothermal discharge at Whakatane is equivocal and awaits further sampling.

Clark

Clark is also an elliptical, dual-cone edifice, with summits at depths of 900 and 1300 m (Fig. 6). Two vertical casts over the cones showed no clear optical evidence for hydrothermal plumes, but analysis of water samples at station V7 over the shallower, northern cone found elevated ^{3}He, Fe and Mn between 800 and 900 m (de Ronde *et al.* 2001; Massoth *et al.* 2003.). This

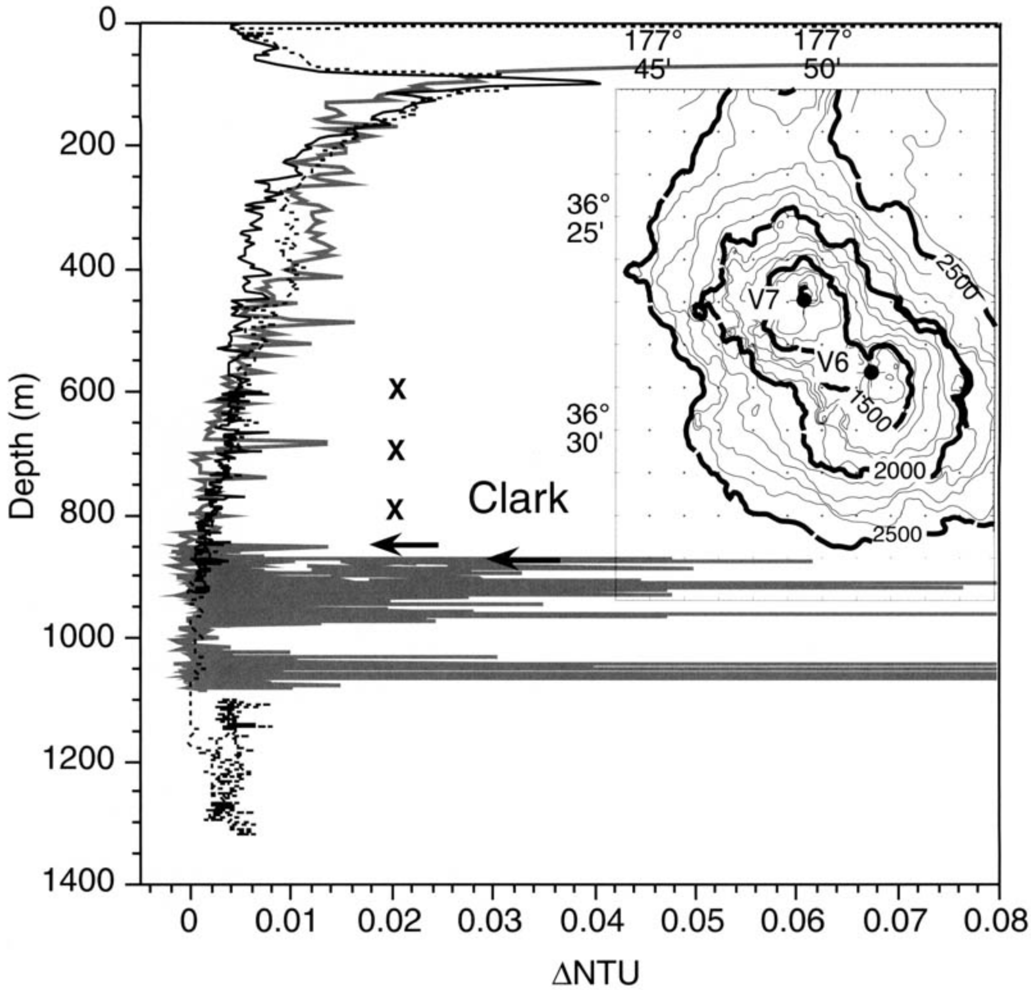

Fig. 6. Vertical profiles of ΔNTU for V6 (dashed line) and V7 (solid line) over Clark (inset). No strong optical plume signals were observed during NZAPLUME, but a 1998 camera tow during RV *Sonne*-135 (Stoffers *et al.* pers. comm.) (grey line) around the V7 position found exceptionally high ΔNTU. Arrows mark depths of V7 bottles with a δ(^{3}He)% anomaly, 'X' marks depths with no anomaly. Map contour interval is 100 m.

horizon corresponds exactly to the depth interval of intense ΔNTU mapped in October 1998 during a camera tow from *RV Sonne* cruise SO-135 (Stoffers *et al.* 1999; Wright *et al.* 2002*b*) around the peak of the northern cone. The *Sonne* camera tow also observed a barite chimney emitting shimmering water and surrounded by Fe-stained sediments.

Tangaroa

Tangaroa's summit shallows to <700 m and is one of high relief over a distance of *c.* 1 km aligned along a NW–SE trend (Fig. 7). The first station occupied found a thick, multilayered and intense optical plume *c.* 1 km southeast of the summit, but six subsequent casts encountered no significant plumes. Interactions between currents and the complex bathymetry apparently produced plumes of high spatial variability. To better map and sample the Tangaroa plumes we conducted three CTDO tow-yos in a roughly radial pattern over the summit. All three tows encountered spatially discontinuous plumes between 600 and 900 m, most strongly evident to the south and west of the summit. The most intense plumes congregated within the 650–750 m depth interval, where we sampled a δ(^{3}He)

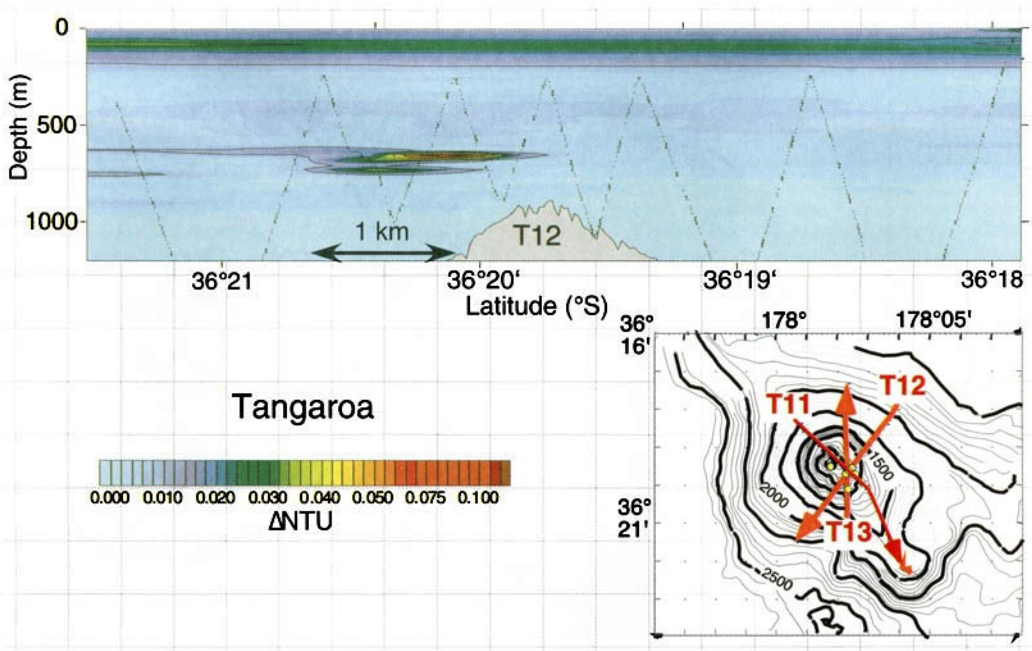

Fig. 7. Vertical transect of ΔNTU from tow T12 (dashed line) over Tangaroa. Tow paths (red arrows) and vertical casts (yellow dots) are shown on the inset map. Map contour interval is 50 m.

value of 116% at 705 m, the largest $\delta(^3He\%)$ value of the present study (de Ronde *et al.* 2001) ($\delta(^3He)\% = 100(R/R_{air} - 1)$; $R = {}^3He/{}^4He$ and R_{air} is this ratio normalized to air).

Rumble IV and Rumble V

Rumble IV and Rumble V are the most recent constructions of a long-lasting arc magma melt that has built a prominent cross-arc ridge (Wright *et al.* 1996). Rumble V, on the present arc front, is a near-symmetrical cone with a summit depth of *c.* 470 m (Fig. 8). The summit of older Rumble IV, about 16 km to the west, is a several kilometres-long ridge rising to a minimum depth of 440 m. One of four casts at the summit of Rumble V detected a moderate optical plume between 380 and 450 m; two subsequent tow-yos quartering the summit mapped more intense plumes in the same depth interval directly above the summit, plus weaker plumes centred at 520 and 660 m around the volcano flanks (Fig. 8). The plume horizon at 660 m was most broadly distributed, especially to the south. There was no convincing optical evidence for active discharge on Rumble IV, as a single tow along its summit found ΔNTU anomalies of only *c.* 0.002–0.003 at the same depth intervals as the much stronger Rumble V plumes (400 and 660 m). The origin of the 660 m plume is enigmatic. This plume occupied exactly the same depth (and density) interval as the more intense Tangaroa plume, and had both dissolved (de Ronde *et al.* 2001; Massoth *et al.* 2003) and particulate chemistry (Table 1) more similar to the Tangaroa plume than to the shallow Rumble V plume. The single cast between Tangaroa and Rumble V detected elevations in both ΔNTU (Fig. 4) and ^3He (a $\delta(^3He)$ increase of *c.* 6%; J. Lupton pers. comm.) between 600 and 700 m, at levels much lower than around Tangaroa but roughly comparable to those at the same depths near Rumble IV and V (de Ronde *et al.* 2001). The evidence is presently insufficient to determine if the deep plume originates from flank venting at Rumble V (or IV) or advection from Tangaroa.

Rumble III and Lillie

The Rumble III–Lillie complex appears to be two coalesced volcanoes, with a major summit shallowing to *c.* 220 m (Rumble III) and a minor summit 15 km south reaching only 1500 m (Lillie) (Fig. 9). A single cast over Lillie found no evidence of plumes. Two casts over the shallowest cone on Rumble III found intense particle plumes between 170 and 220 m, the

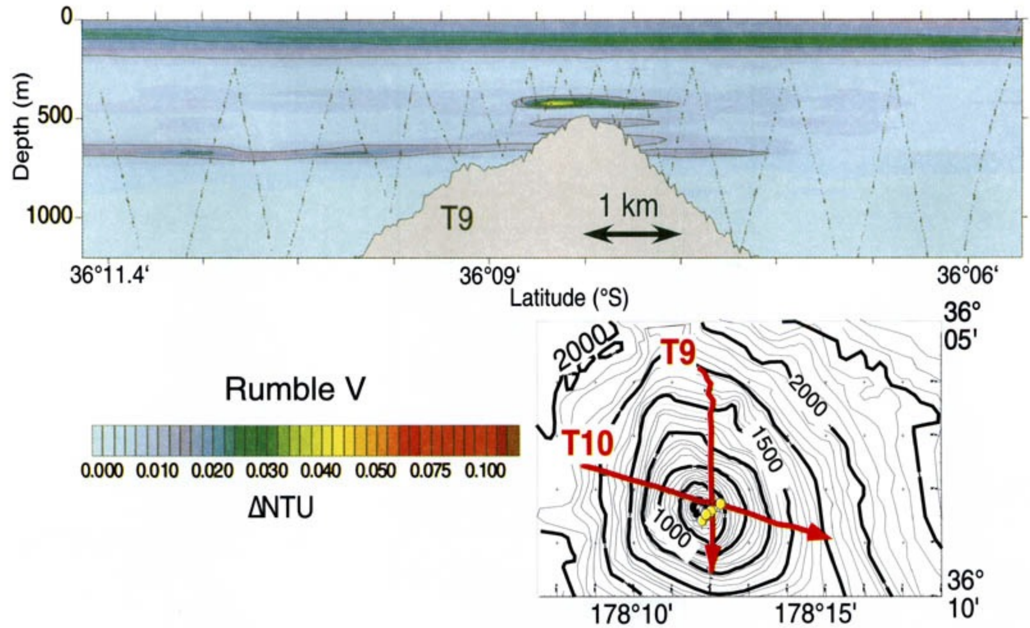

Fig. 8. Vertical transect of ΔNTU from tow T9 (dashed line) over Rumble V. Note the weak but pervasive plume centred at 660 m. Tow paths (red arrows) and vertical casts (yellow dots) are shown on the inset map. Map contour interval is 50 m.

same horizon where $\delta(^3He)$ values exceeded 70% (Massoth *et al.* 2003). A single cast over a 600 m-deep secondary cone 3 km to the northwest encountered no plumes. The complete absence of plumes only 3 km to the northwest of an intense plume source indicates a strong current with a dominant southward component at the time of the survey.

Rumble II (West and East)

Two casts over Rumble II (East), a symmetric cone rising to *c.* 1050 m, found no evidence of a particle plume. Rumble II (West) is a partially collapsed caldera with a diameter of *c.* 3 km and a summit floor at 1450 m supporting a *c.* 200 m-high volcanic dome at its centre (Wright & Gamble 1999). Four casts within the caldera found no optical evidence of plumes, but below *c.* 1300 m discrete samples were slightly elevated in total dissolvable Fe and Mn, and ^3He (Massoth *et al.* 2003). These samples, the recovery of massive sulphides from the caldera wall (Wright *et al.* 1998) and evidence from fluid inclusions within those sulphides for temperatures up to 268°C (de Ronde *et al.* 2002) imply that vents at Rumble II (West) presently discharge diffuse hydrothermal fluids and/or leak magmatic gases, and that high-temperature fluid discharge has occurred some time in the recent past. The inconsistency both here and at Clark of anomalies in dissolved tracers, despite the absence of a backscattering signal, furnishes cautionary testimony that some volcanoes can produce hydrothermal or magmatic emissions undetectable by optical methods.

Silent II and Cotton

Both these volcanoes are near-symmetrical edifices with cones rising to mid-water depths (Fig. 4). Casts over both found neither optical nor chemical (de Ronde *et al.* 2001) indications of hydrothermal venting.

Healy

Healy, along with Brothers, is one of two known dacitic–rhyodacitic calderas along the SKA (Wright & Gamble 1999; Wright *et al.* 2002*a*). The floor of the 3.5 km-diameter caldera reaches 1620 m, and the effective rim depth of the surrounding walls is *c.* 1420 m. The main edifice adjacent to the caldera shoals to a broad dome at 1150 m water depth (Fig. 10). We found evidence of hydrothermal activity over and around the Healy edifice crest, but the most intense plumes, with multiple maxima, were contained

Table 1. *Particulate chemistry of hydrothermal plumes*

Volcano	Number of samples	Fe	S	Ti	Cu	S/Fe	S/Ti	Fe/Ti	Cu/Ti
Tangaroa	11	144 ± 202	6.1 ± 2.8	0.42 ± 0.25	0.26 ± 0.26	0.63 ± 1.3	18 ± 10	449 ± 471	0.73 ± 0.58
Rumble V (*c.* 400 m)	4	2.26 ± 0.35	59 ± 28	0.25 ± 0.03	0.16 ± 0.20	26 ± 15	245 ± 143	9 ± 1	0.62 ± 0.44
Rumble V (*c.* 660 m)	1	43.9	3.8	0.82	0.03	0.09	4.6	54	0.036
Rumble III	9	390 ± 332	36 ± 50	0.41 ± 0.17	0.22 ± 0.20	0.35 ± 0.7	96 ± 136	1081 ± 1107	0.50 ± 0.37
Healy	32	34.8 ± 14.9	2.7 ± 2.2	0.39 ± 0.15	0.13 ± 0.21	0.09 ± 0.05	8 ± 11	99 ± 56	0.17 ± 0.14
Brothers (<1300 m)	20	242 ± 314	112 ± 208	0.31 ± 0.09	0.53 ± 0.81	0.94 ± 2.7	263 ± 445	738 ± 846	0.42 ± 1.04
Brothers (>1300 m)	14	214 ± 244	112 ± 142	0.50 ± 0.20	1.30 ± 1.45	0.94 ± 2.4	183 ± 245	379 ± 411	1.41 ± 1.73
Rumble II West (> 500 m)*	7	2.47 ± 0.88	1.9 ± 0.3	0.29 ± 0.08	0.05 ± 0.04	0.86 ± 0.3	7 ± 2	8 ± 2	0.17 ± 0.14
Local Sediments†	3	2.03 ± 0.22	–	0.20 ± 0.03	0.004 ± 0.001	–	–	10 ± 1	0.2 ± 0.03
SEPR (13°–19°S)‡	190	156 ± 243	34 ± 38	0.04 ± 0.05	1.2 ± 3	0.44 ± 0.6	628 ± 640	1428 ± 1000	0.57 ± 0.50
SJdFR§	123	47 ± 50	6 ± 6	0.47 ± 0.29	0.16 ± 0.14	0.2 ± 0.2	14 ± 12	112 ± 137	0.37 ± 0.31

Plume concentrations in units of nmol l^{-1}, sediment concentrations in wt%
*Background profile, no particle plume observed.
†Gamble *et al.* (1996).
‡Southern East Pacific Rise (Feely *et al.* 1996)
§Southern Juan de Fuca Ridge (Feely unpublished data)

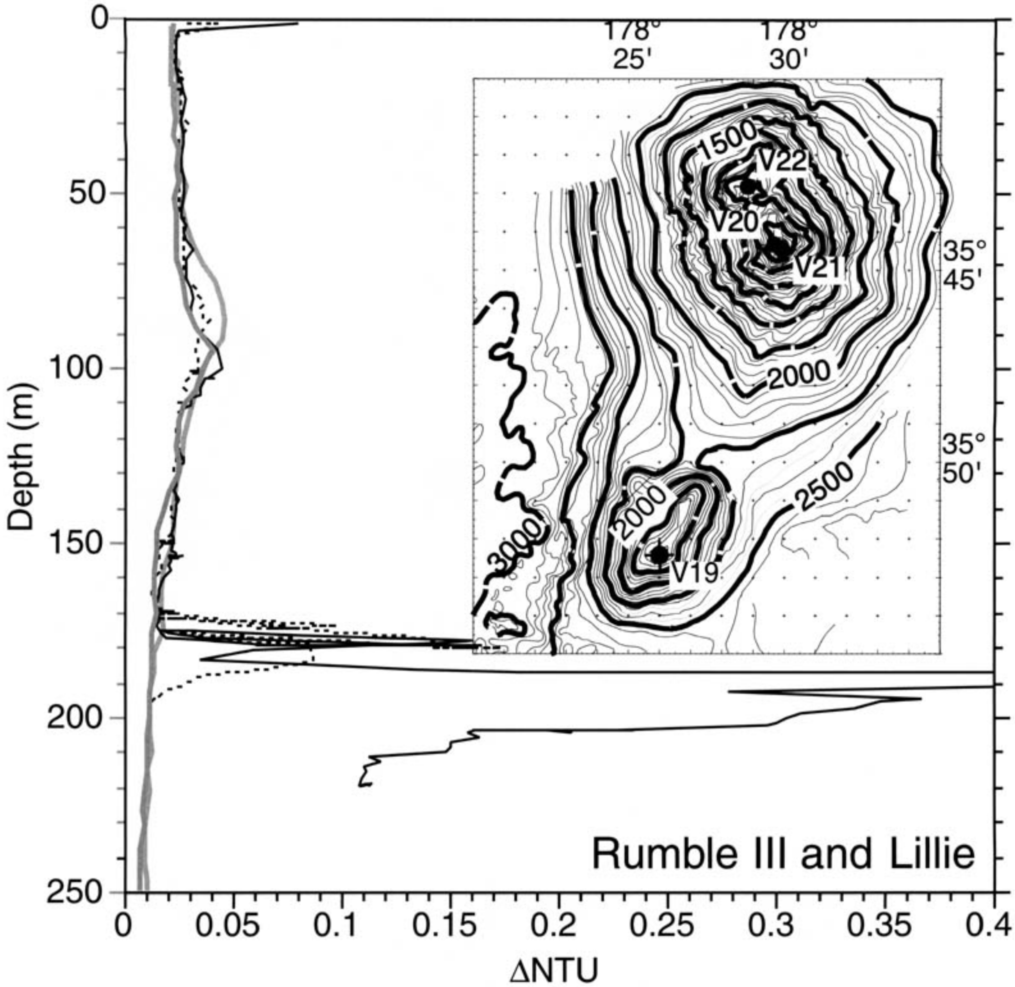

Fig. 9. Vertical profiles of ΔNTU for profiles V20 (dashed line) and V21 (solid line) over Rumble III (inset). No plume signatures were detected over Lillie (V19) or the deeper summit cone of Rumble III (V22) (both grey lines). Map contour interval is 50 m.

within the caldera, although some leakage occurred through topographic minima along the caldera wall. The strongest plumes were found on tow T5 near the western caldera wall between 1400 and 1500 m, the same interval in which the maximum $\delta(^3He)\%$ values were sampled (Massoth *et al.* 2003; J. Lupton pers. comm.). Similar, but weaker, plumes were present adjacent to the northern wall during tow T4. The common presence of intense plumes near the caldera walls, rather than its centre, suggests hydrothermal venting is most probably focused along normal faults bounding the west–south-west sectors of the caldera. This distribution of venting is common in hydrothermally active submarine volcanoes with calderas, such as Axial Volcano on the Juan de Fuca Ridge (Embley *et al.* 1990) and Myojin Knoll on the volcanic front of the Izu–Ogasawara arc (Iizasa *et al.* 1999).

Brothers

The other dacitic–rhyodacitic caldera, Brothers, hosts the most extensive and vigorous hydrothermal system yet discovered in the SKA. The caldera, slightly elongated along a NW–SE axis, has an outside diameter of *c.* 3.5 km. The inside depth of the caldera exceeds 300 m, from the floor at *c.* 1850 m up to an effective rim depth of *c.* 1500 m (Fig. 11). A volcanic cone coalesces

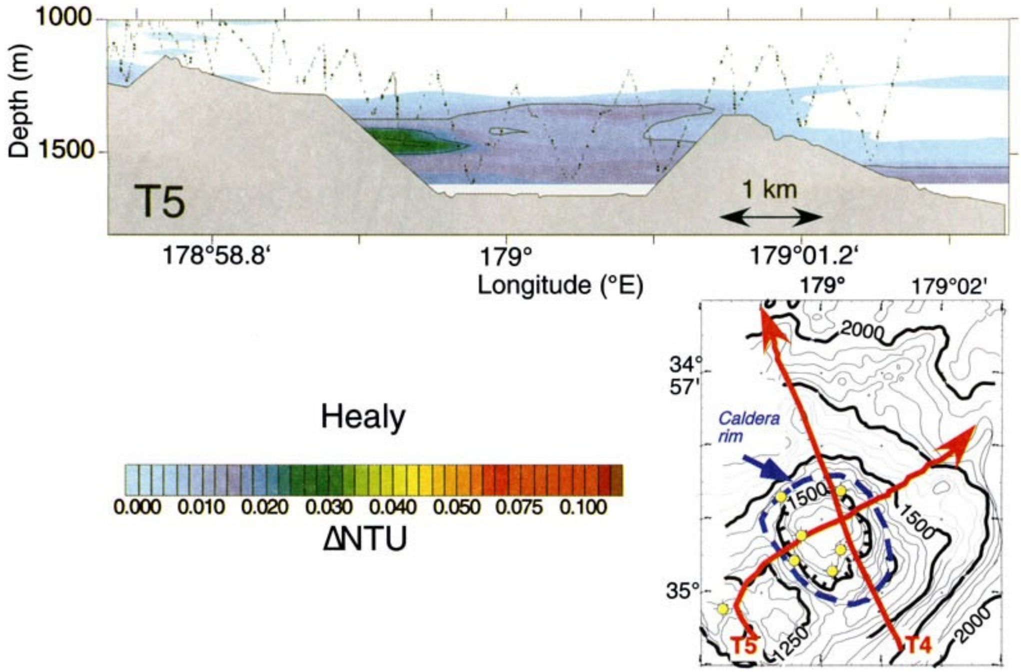

Fig. 10. Vertical transect of ΔNTU from tow T5 (dashed line) over Healy. Tow paths (red arrows) and vertical casts (yellow dots) are shown on the inset map. The blue dashed line traces the caldera rim. Map contour interval is 50 m.

with part of the southern wall and shoals to *c.* 1200 m.

Hydrothermal plumes apparently emanate from two separate sources: within the caldera itself (principally the northwest quadrant) and on the cone. Seafloor hydrothermal activity at both locations has been observed with camera tows (Stoffers *et al.* 1999). This combined discharge formed multiple thick plume layers that extended through more than 700 m of the water column, from the caldera floor to *c.* 1100 m depth (Fig. 11). Discharge within the caldera itself formed the deepest layer, most concentrated just below the rim depth at *c.* 1540 m. This layer may accumulate plumes from a range of source depths, as the negligible density gradient in the caldera allows plumes to rise quickly to the rim depth before spreading laterally. Transport of these plumes outside the caldera must be controlled by episodic flushing of the caldera waters, as has been inferred at the hydrothermally active Vailulu'u submarine caldera (Hart *et al.* 2000). The most intense plumes were found immediately over the cone at depths between 1150 and 1200 m, where ΔNTU values on tow T6 exceeded 1.0 (Fig. 11).

Particulate chemistry

We collected samples for particulate chemistry analysis at six of the active volcano edifices (Fig. 12, Table 1). For comparison, Table 1 also includes the particulate chemistry of documented hydrothermal plumes over the superfast-spreading southern East Pacific Rise (13°–19°S) where recent volcanic activity is thought to have occurred (Feely *et al.* 1996), the Cleft segment of the intermediate-spreading Juan de Fuca Ridge (Feely unpublished data), where no volcanic eruptions have been detected for at least a decade, and of local SKA sediment. The sediment composition is based on three surficial samples from gravity cores adjacent to the SKA volcanoes (Fig. 1) (Gamble *et al.* 1996). With the exception of Rumble II (West), all sites showed distinctive chemical signatures in the plume particulates.

The elements we discuss here include Fe and Cu, characteristic of metal-rich, high-temperature discharge, and S, which may precipitate as elemental sulphur from magmatic outgassing (e.g. H_2S) and/or as metal sulphides (Feely *et al.* 1990, 1999; Lilley *et al.* 1995). Element concentrations, particularly for Fe and Cu, varied

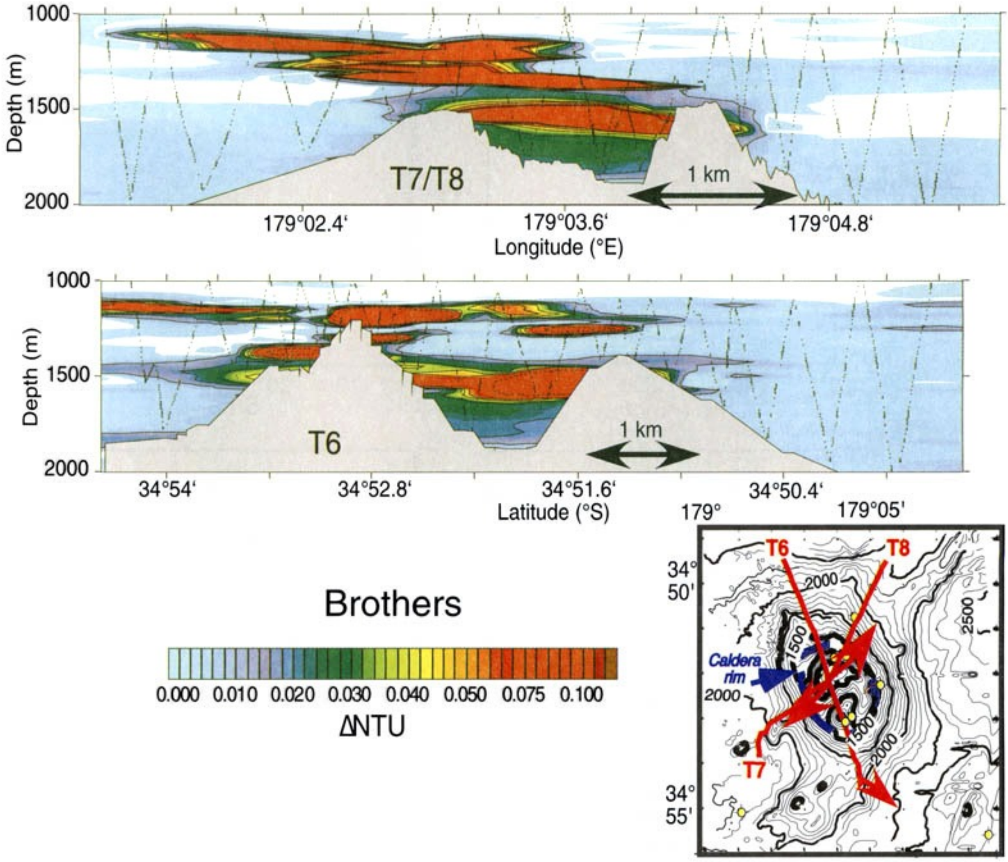

Fig. 11. Vertical transects of ΔNTU plumes in and around the Brothers caldera. CTD tow-yos shown by dashed lines in cross-sections. Tow paths (red arrows) and vertical casts (yellow dots) are shown on inset map. The blue dashed line traces caldera rim. Map contour interval is 50 m.

roughly as the optical intensity of plumes, with Brothers plumes having consistently high concentrations in all species. To separate the influence of plume composition from plume concentration we here compare each plume in terms of elements ratioed to Ti to identify hydrothermal enrichments in excess of detrital trends, as Ti has a negligible hydrothermal input and a nearly constant concentration in detrital materials (Feely *et al.* 1996, 1998). In addition, we compare the S/Fe ratio of each plume to identify plumes with sulphur enrichments beyond those of metal sulphides.

Plumes from every volcano except the shallow plume at Rumble V were elevated in particulate Fe relative to the background cast at Rumble II (West) (Fig. 12, Table 1). Iron concentrations were similar to those found in ridge crest plumes. Values of Fe/Ti in the plumes were *c.* 5–100 times those in local sediments, consistent with a hydrothermal origin for the plumes. The Rumble III plume had the highest Fe/Ti values sampled, followed closely by the shallow plumes (<1300 m) originating on the Brothers' cone. Plumes in the Healy caldera and the deep Rumble V plume had much lower enrichments in particulate Fe, while the shallow plume from Rumble V had Fe/Ti values indistinguishable from non-plume particles or the local sediments. Copper, generally indicative of high-temperature, black-smoker discharge (Feely *et al.* 1990, 1996), was significantly enriched only in the shallow and deep plumes at Brothers.

Fewer samples were more enriched in S than in metals. S/Ti values were elevated above background only in plumes from Rumble III and V, and in both the deep and shallow plumes from Brothers. In terms of S/Fe values, the shallow Rumble V plume showed enrichments 20 times

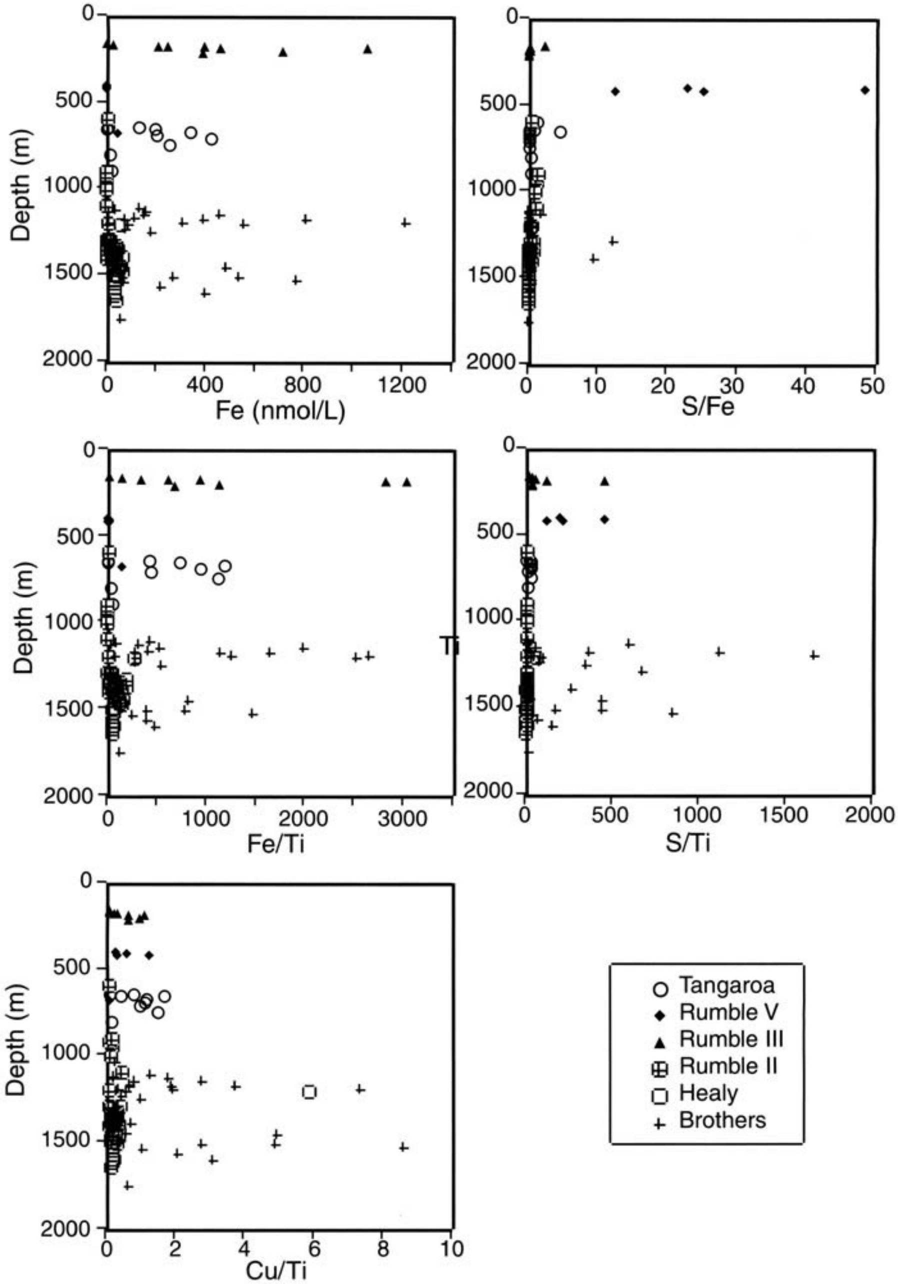

Fig. 12. Vertical profiles of the concentration of four particulate hydrothermal species in plumes overlying SKA volcanoes. Rumble II (West), where we detected no particle plumes, furnishes a non-hydrothermal background profile. Highest Fe loadings were sampled at Rumble III, Tangaroa and Brothers. High S/Ti and S/Fe values at Rumble V and Brothers suggest magmatic outgassing and/or recent volcanic activity at those volcanoes.

higher than any other volcano, thereby explaining the observation of an intense optical signal in the absence of Fe enrichments. The particulate S enrichments at Rumble V (and Rumble III and Brothers as well) probably result from the oxidation of sulphur gases (H_2S and SO_2) to elemental sulphur (Massoth *et al.* 2003). Hydrogen sulphide concentrations in the shallow Rumble V plume far exceeded those of any other SKA plume, and were also detected at Rumble III and the shallow Brothers' plume (de Ronde *et al.* 2001; Massoth *et al.* 2003). Fe/Ti, Cu/Ti and S/Ti values in SKA plumes span the range of mean values from the ridge crest sites, except for highly elevated Cu/Ti ratios in plumes from Brothers and S/Fe ratios from Rumble V.

Spatial frequency of hydrothermal systems

Of the 13 edifices investigated, seven (Clark, Tangaroa, Rumble V, Rumble III, Rumble II West, Healy and Brothers) were confirmed active by optical or chemical measurements at the time of the survey, and two more (Whakatane and Rumble IV) have suspected activity. As at least 200 submarine volcanoes may populate the 20 000 km of intra-oceanic and island arcs in the western Pacific (de Ronde *et al.* 2003), might arcs supply hydrothermal effluents at rates comparable to divergent plate boundaries? At present, the SKA provides our only reliable measure of along-arc hydrothermal frequency. With the conservative assumption that each active edifice represents a single vent field, active sites occur there at a spatial density of 2.7–3.5 per 100 km (2.7–3.5/100 km) of arc (depending on the eventual determination of activity on Whakatane and Rumble IV). For comparison with divergent boundaries we consider slow- to intermediate-spreading-rate (0–70 km Ma^{-1} full rate) mid-ocean ridges, which make up about 80% of the global total by length. Along these boundaries, magma delivery appears focused at discrete loci (Lin & Phipps Morgan 1992), analogous to the construction of individual volcanoes along arc fronts. Gravity and bathymetric 'bull's-eyes' occur along the Mid-Atlantic Ridge at wavelengths of *c.* 20–100 km (Lin *et al.* 1990; Detrick *et al.* 1995), a scale similar to the volcano spacing along arcs (de Ronde *et al.* 2003). Several studies have enumerated the location of confirmed or inferred (from plume observations) vent fields along sections of the Mid-Atlantic Ridge (German & Parson 1998), the Southwest Indian Ridge (German *et al.* 1998; Bach *et al.* 2002; Baker *et al.* 2002) and the Juan de Fuca Ridge (Baker & Hammond 1992; Fornari & Embley 1995) (Table 2). These ridge sections host at least 22 vent sites; a more detailed study may well discover additional sites. Hydrothermal site densities thus range from 0.2 to 1.7 sites/100 km (Table 2), and the mean ($\pm 1\sigma$) frequency over 2400 km of ridge crest is 1.0±0.6 sites/100 km, or roughly a factor of 2–3 lower than the SKA site density range.

Given our imperfect knowledge about the true distribution of vent fields on both arcs and mid-ocean ridges, these estimates of hydrothermal site density along the SKA and slow- to intermediate-spreading ridge crests seem equivalent at about 1–3/100 km. As magma supply and hydrothermal activity appear linearly correlated along mid-ocean ridges (Baker *et al.* 1996), should we expect also that a given magma supply produces comparable hydrothermal activity on arcs and ridges? Estimates of magma delivery, especially for arcs, are unavoidably approximate, and explorations of arc hydrothermal activity are only beginning. Even within these limitations, however, a first-order comparison between magma delivery and site density along arcs and ridges seems worthwhile, as the data needed to materially improve the analysis will require many years to accumulate.

The total magma delivery rate at mid-ocean ridges is the multiplicative product of crustal thickness (White *et al.* 2001) and by the full-rate plate divergence (DeMets *et al.* 1990). For the ridge sections mentioned above, this rate ranges from 36 to 390 $km^3\ Ma^{-1}\ km^{-1}$ of axis (Table 2). We calculate Q_t, the total heat carried by this magma (Table 2), by

$$Q_t = u_s H_c \rho_b (L_{melt} + c_p \Delta T)$$

where u_s is full-rate plate divergence, H_c is crustal thickness, ρ_b is basalt density (2800 kg m^{-3}), L_{melt} is the latent heat of melting, c_p is the specific heat of basalt (1330 J $kg^{-1}\,°C^{-1}$) and ΔT is the temperature change from molten lava (1200°C) to cooled basalt (350°C). Literature values for L_{melt} range between 367 and 676 J g^{-1} (e.g. Elderfield & Schultz 1996), so we use an intermediate value of 520 J g^{-1}. The portion of this heat available to power on-axis (±1 km from the ridge axis) hydrothermal venting is the neovolcanic zone heat flux (Table 2), given by the crustal thermal model of Chen & Phipps Morgan (1996) and Chen (2000). We call the percentage of total available heat that the model calculates as discharged within the neovolcanic zone the 'magma efficiency' and use it to estimate the 'effective magma delivery rate' available to drive hydrothermal venting (Table 2).

Calculating the effective magma delivery rate in volcanic arcs is more speculative because magma emplacement is not a spatially continuous process as along ridge crests. A minimum estimate of magma delivery to the seafloor

Table 2. *Comparison of hydrothermal activity and magma delivery at SKA volcanoes to mid-ocean ridges*

Plate boundary section	Convergence (–) or divergence (+) full rate (km Ma^{-1})	Hydrothermal site density (minimum) (sites per 100 km)	Total magma delivery rate (km^3 Ma^{-1} km^{-1})	Total magma heat flux (MW km^{-1})	Neovolcanic heat flux (MW km^{-1})	Magma efficiency (%)	Effective magma delivery rate (km^3 Ma^{-1} km^{-1})	Site production (sites per 100 km^3 per Ma)
Southern Kermadec arc	–80	2.7–3.5					2.5–9.3*	1.4–0.29
							8–28†	0.43–0.1
Juan de Fuca Ridge	+55	1.7	390	57	18	32	125‡	0.014
Mid-Atlantic Ridge (27°–30°N; 36°–38°N)	+24	1.1	170	25	7	28	48‡	0.022
Southwest Indian Ridge (57°–66°E)	+16	1.3	64	9	3	33	21‡	0.065
Southwest Indian Ridge (10°–24°E)	+9	0.2	36	5	2	40	14‡	0.017

*Volcano volumes only
†Volcanoes plus magma in upper crust cooled hydrothermally.
‡Total magma delivery rate × magma efficiency.

comes from direct measurement of the volume of volcano edifices rising above the local seafloor. Along the SKA, Wright *et al.* (1996) calculate a range of 2.5–9.3 km^3 Ma^{-1} km^{-1}, similar to the rate of *c.* 5–6 km^3 Ma^{-1} km^{-1} determined for the Mariana arc (Sample & Karig 1982; Bloomer *et al.* 1989). These are minimum estimates for the volume of hydrothermally cooled magma, as they include neither volcaniclastic material transported off the edifices themselves, reduction of eruption products to magma volume equivalents nor arc magma emplaced in the crust below the base of the volcanoes. Sample & Karig (1982), for example, calculated that the volcaniclastic apron surrounding the Marianas volcanoes has a volume roughly equal to the volcanoes themselves. Petrological considerations suggest that the mass of magmatic material within the lower crust is perhaps one–two times the volume of each volcano itself (Kay & Kay 1985; Bloomer *et al.* 1989). The likelihood of significant magma storage below the apparent base of a volcano is supported by recent seismic imaging of the Axial Volcano on the Juan de Fuca Ridge, where melt extends at least 6 km below the hydrothermally active summit caldera (West *et al.* 2001). Including these additional magma volumes might easily triple the effective magma delivery rate in the SKA, expanding the estimated range to 8–28 km^3 Ma^{-1} km^{-1}. Note that even these rates are well below recent estimates of 35–95 km^3 Ma^{-1} km^{-1} for the total magma supply to oceanic island arcs (Dimalanta *et al.* 2002).

The ratio of hydrothermal site density to effective magma delivery rate yields a site production rate (Table 2). The mean ($\pm 1\sigma$) site production on the four sections of ridge crest listed in Table 2 is 0.03±0.02 sites produced for every 100 km^3 of 'effective magma' supplied per Ma. The high variability reflects real differences between these sections of ridge, our uncertainty about the true number of vent fields and uncertainty in the model calculations of neovolcanic heat flux. Calculating the same ratio for volcanic arcs is hindered by the small sample presently available (the SKA) and a larger imprecision in the magma supply. At the high end, for perhaps unrealistically low magma delivery rates, the ratio is >1. At the low end, for high delivery rates, the ratio ≈ 0.1, a factor only *c.* 3 higher than the mid-ocean ridge ratio. While these estimates seem to favour the SKA magma being more efficient at producing hydrothermal sites than a comparable mid-ocean ridge section, the uncertainties involved are presently too large to generalize these results to all arcs. For example, a recent survey of submarine volcanoes along sections of the New Ireland and Solomon forearcs found only one hydrothermal site (de Ronde *et al.* 2003), so the average arc site production rate may be smaller than for the SKA. An overestimate of the ridge-crest magma efficiency, or an underestimate of the site density (not unlikely), would make the site production rates for ridges too small.

Vent field frequency, of course, is only a qualitative index of relative hydrothermal heat and mass flux. Making a quantitative comparison requires flux measurements at individual vent fields, measurements that are scarce on mid-ocean ridges and almost non-existent at arc volcanoes. Measured heat fluxes from mid-ocean ridge vent fields range from *c.* 15 to 5000 MW, although normalizing the data to vent field size lowers the variability to *c.* 40–200 MW km^{-1} of ridge crest length (Baker *et al.* 1996). Unfortunately, we cannot make analogous flux estimates at the SKA volcanoes, as none of the usual measurements (e.g. seafloor vent/buoyant plume observations, plume advection, samples of short-lived isotopes (such as ^{222}Rn)) are available. We can, however, make minimum estimates using a plume model and observations of plume rise height, although even these will be highly uncertain because we know neither the true depth of the source, the number of vents that contribute to the plume, nor the chemistry of the discharged fluids (which also affects plume rise). The source heat flux, H_s, is related to the maximum rise height, z^*, of a turbulent, axially symmetric plume rising through a linearly stratified, motionless environment by the expression

$$H_s = 1.6 \times 10^{-3}(z^*)^4 N^3 \rho c_p \pi / \alpha g$$

where N is the buoyancy frequency of the ambient water through which the plume rises, ρ is the background sea-water density (= 1027 kg m^{-3}), c_p is the specific heat of the dilute plume fluid (= 3915 J kg^{-1}°C^{-1}), α is the coefficient of thermal expansion of the fluid (= 1.3×10^{-4} °C^{-1}), and g is the gravitational constant (Morton *et al.* 1956; Turner 1973; Turner & Campbell 1987). (We assume a motionless environment in the absence of current measurements.) The volcanoes most amenable to this simple model were Rumble III and V, with cone-like summits and clearly defined plumes. Summit bathymetry at Tangaroa is rugged and the depths of the vent sources are highly speculative. Rumble III had a single plume layer with $z^* \approx 40$ m (assuming a vent source at the summit) and $N = 4.4 \times 10^{-3}$ Hz, yielding $H_s = 3$ MW. Rumble V had multiple layers, but the strongest plume horizon was between 380 and 450 m. For this layer, $z^* \approx 70$ m and $N = 3.7 \times 10^{-3}$ Hz, so H_s = 19 MW. Both these flux estimates, equivalent to a few black-smoker-type vents (Bemis *et al.* 1993), are low compared to many mid-ocean ridge fields. However, at both sites the plume profiles suggest multiple sources, so these minimum fluxes could be a few times larger. More significantly, note that as $H_s \propto (z^*)^4$, any underestimation of the rise height results in a considerably larger underestimate of H_s. If z^* in each case were just 50% higher, then H_s = 17 MW for Rumble III and 98 MW for Rumble V.

The most vigorous systems, at Healy and Brothers, are too complicated to model in this simple way. Some insight into their heat flux can be realized by comparing them to Vailulu'u, an intraplate volcano with a power output of *c.* 600 MW from hydrothermal discharge in its caldera (Hart *et al.* 2000, 2003). A qualitative comparison of the extent of plumes at each of these calderas suggests that the hydrothermal activity at Vailulu'u may be intermediate between Healy and Brothers. Given these largely qualitative estimates, the most we can say is that the variability of hydrothermal heat flux from the SKA volcano vent fields seems similar to that observed among mid-ocean ridge vent fields.

Summary

This first comprehensive survey of hydrothermal activity on island arc volcanoes found at least seven, and perhaps nine, of 13 volcanoes venting hydrothermal plumes into the surrounding water column. Particles suspended in plumes from Tangaroa, Rumble V, Rumble III, Healy and Brothers showed clear enrichments in Fe, S and Cu relative to background particles and regional sediment chemistry. The spatial density of hydrothermal sites along the SKA is 2.7–3.5/100 km of arc length, a factor of 2–3 higher than along four representative sections of slow- and intermediate-spreading mid-ocean ridges. Given the small length of arc studied here (260 km), this difference may not be significant. Normalizing the site density to the rate of magma supply in each environment finds an effective mean production of *c.* 0.03 ± 0.02 sites per 100 km^3 of magma per Ma on the ridge sections, and values ranging from 0.1 to 1.4 sites per 100 km^3 of magma per Ma for the SKA. The smaller SKA values reflect more reasonable magma supply rates, but the large uncertainty in the true, hydrothermally productive, magma delivery rate and the small sample size of the SKA (*c.* 1% of western Pacific arc length) makes any generalizations speculative. Until more arcs are surveyed and their magma delivery rates better quantified, it should be assumed that magma delivery is equally effective at producing hydrothermal activity on either island arc volcanoes or slow- and intermediate-spreading ridge crests. This conclusion is consistent with previous studies that find a linear correlation between hydrothermal activity and the magma budget on all mid-ocean ridges.

If a larger sampling of arc sections finds hydrothermal activity even half as common as on the SKA, then the hydrothermal output of volcanoes along the 20 000 km of convergent plate boundary in the western Pacific may be revealed as a heretofore unappreciated, but significant, component of the global hydrothermal budget.

This research was funded by the New Zealand Foundation for Research Science and Technology (FoRST) and the NOAA VENTS Programme. S.L. Walker assisted in processing the CTDO data and G.T. Lebon analysed the particulate samples for their elemental composition. We thank R. Greene, S.M. Maenner, K. Faure, K. Britten, P. Hill, J. Mitchell, and D. Singleton for contributing towards a successful cruise onboard RV *Tangaroa*. P. Stoffers and colleagues on RV *Sonne*-135 generously furnished optical data from camera tows on Clark. Contribution 2437 from the Pacific Marine Environmental Laboratory.

References

APHA. 1989. *Standard Methods for the Analysis of Water and Waste Water,* 17th edition. American Public Health Association, American Water Works Association. Water Pollution Control Federation, Washington, DC.

BACH, W., BANERJEE, N.R., DICK, H.J.B. & BAKER, E.T. 2002. Discovery of ancient and active hydrothermal systems along the ultra-slow spreading Southwest Indian Ridge, 10°–16°E. *Geochemistry, Geophysics, Geosystems*, **3**, 2001GC000279.

BAKER, E.T. 1998. Patterns of event and chronic hydrothermal venting following a magmatic intrusion: New perspectives from the 1996 Gorda Ridge eruption. *Deep Sea Research II*, **45**, 2599–2618.

BAKER, E.T. & HAMMOND, S.R. 1992. Hydrothermal venting and the apparent magmatic budget of the Juan de Fuca Ridge. *Journal of Geophysical Research*, **97**, 3443–3456.

BAKER, E.T., CHEN, Y.J. & PHIPPS MORGAN, J. 1996. The relationship between near-axis hydrothermal cooling and the spreading rate of midocean ridges. *Earth and Planetary Science Letters*, **142**, 137–145.

BAKER, E.T., EDMONDS, H.N., GERMAN, C.R., BACH, W., BANERJEE, N.R. & WALKER, S.L. 2002. The distribution of hydrothermal venting on ultraslow spreading ridges. *Eos, Transactions, American*

Geophysical Union, **83**(47), Fall Meeting Supplement, T11A-1228.

BAKER, E.T., GERMAN, C.R. & ELDERFIELD, H. 1995. Hydrothermal plumes over spreading-center axes: Global distributions and geological inferences. *In*: HUMPHRIS, S.E., ZIERENBERG, R.A., MULLINEAUX, L.S. & THOMSON, R.E. (eds) *Seafloor Hydrothermal Systems: Physical, Chemical, Biological, and Geological Interactions*. American Geophysical Union Monographs, **91**, 47–71.

BAKER, E.T., TENNANT, D.A., FEELY, R.A., LEBON, G.T. & WALKER, S.L. 2001. Field and laboratory studies on the effect of particle size and composition on optical backscattering measurements in hydrothermal plumes. *Deep Sea Research*, **48**, 593–604.

BEMIS, K.G., VON HERZEN, R.P. & MOTTL, M.J. 1993. Geothermal heat flux from hydrothermal plumes on the Juan de Fuca Ridge. *Journal of Geophysical Research*, **98**, 6351–6365.

BEVIS, M., TAYLOR, F.W., SCHULTZ, B.E., RACY, J., ISACKS, B.L., HELU, S., SINGH, R., KENDRICK, E., STOWELL, J., TAYLOR, B. & CALMANT, S. 1995. Geodetic observations of very rapid convergence and back-arc extension at the Tonga arc. *Nature*, **374**, 249–251.

BLOOMER, S.H., STERN, R.J. & SMOOT, N.C. 1989. Physical volcanology of the submarine Mariana and Volcano arcs. *Bulletin of Volcanology*, **51**, 210–224.

CHEN, Y.J. 2000. Dependence of crustal accretion and ridge axis topography on spreading rate, mantle temperature, and hydrothermal cooling. *In*: DILEK, Y., MOORES, E.M., ELTHON, D. & NICOLAS, A. (eds) *Ophiolites and Oceanic Crust: New Insights from Field Studies and the Ocean Drilling Program*. Geological Society of America, Special Papers, **349**, 161–179.

CHEN, Y.J. & PHIPPS MORGAN, J. 1996. The effects of spreading rate, the magma budget, and the geometry of magma emplacement on the axial heat flux at mid-ocean ridges. *Journal of Geophysical Research*, **101**, 11 475–11 482.

DE BREMOND D'ARS, J., JAUPART, C. & SPARKS, R.S.J. 1995. Distribution of volcanoes in active margins. *Journal of Geophysical Research*, **100**, 20 421–20 432.

DELTEIL, J., RUELLAN, E., WRIGHT, I.C. & MATSUMOTO, T. 2002. Structure and structural development of the Havre Trough (SW Pacific). *Journal of Geophysical Research*, **107**(B7), 2143, 10.1029/2001JB000494.

DEMETS, C., GORDON, R.G., ARGUS, D.F. & STEIN, S. 1990. Current plate motions. *Geophysical Journal International*, **101**, 425–478.

DE RONDE, C.E.J., BAKER, E.T., MASSOTH, G.J., LUPTON, J.E., WRIGHT, I.C., FEELY, R.A. & GREENE, R.R. 2001. Intra-oceanic subduction-related hydrothermal venting, Kermadec volcanic arc, New Zealand. *Earth and Planetary Science Letters*, **193**, 359–369.

DE RONDE, C.E.J., FAURE, K., BRAY, C.J., CHAPPELL, D.A. & WRIGHT, I.C. 2002. Hydrothermal fluids associated with seafloor mineralization at two southern Kermadec arc volcanoes, Offshore New Zealand. *Mineralium Deposita*, **38**, 217–233, 10.1007/s00126-002-0305-4.

DE RONDE, C.E.J., MASSOTH, G.J., BAKER E.T. & LUPTON J.E. 2003. Submarine hydrothermal venting related to volcanic arcs. *In*: SIMMONS, S.F. & GRAHAM, I.J. (eds) *Volcanic, Geothermal and Ore-forming Fluids: Rulers and Witnesses of Processes Within the Earth*. Society of Economic Geologists, Littleton, CO, Special Publications.

DETRICK, R.S., NEEDHAM, H.D. & RENARD, V. 1995. Gravity anomalies and crustal thickness along the Mid-Atlantic Ridge between 33°N and 40°N. *Journal of Geophysical Research*, **100**, 3767–3787.

DIMALANTA, C., TAIRA, A., YUMUL, G.P., JR, TOKUYAMA, H. & MOCHIZUKI, K. 2002. New rates of western Pacific island arc magmatism from seismic and gravity data. *Earth and Planetary Science Letters*, **202**, 105–115.

ELDERFIELD, H. & SCHULTZ, A. 1996. Mid-ocean ridge hydrothermal fluxes and the chemical composition of the ocean. *Annual Review of Earth and Planetary Sciences*, **24**, 191–224.

EMBLEY, R.W., MURPHY, K.M. & FOX, C.G. 1990. High-resolution studies of the summit of Axial Volcano. *Journal of Geophysical Research*, **95**, 12 785–12 812.

FEELY, R.A., BAKER, E.T., LEBON, G.T., GENDRON, J.F., MASSOTH, G.J. & MORDY, C.W. 1998. Chemical variations of hydrothermal particles in the 1996 Gorda Ridge Event and chronic plumes. *Deep Sea Research II*, **45**, 2637–2664.

FEELY, R.A., BAKER, E.T., LEBON, G.T., GENDRON, J.F., RESING, J.A. & COWEN, J.P. 1999. Evidence for iron and sulfur enrichments in hydrothermal plumes at Axial Volcano following the January–February 1998 eruption. *Geophysical Research Letters*, **26**, 3649–3652.

FEELY, R.A., BAKER, E.T., MARUMO, K., URABE, T., ISHIBASHI, J., GENDRON, J., LEBON, G.T. & OKAMURA, K. 1996. Hydrothermal plume particles and dissolved phosphate over the superfast-spreading southern East Pacific Rise. *Geochimica et Cosmochimica Acta*, **60**, 2297–2323.

FEELY, R.A., GEISELMAN, T.L., BAKER, E.T., MASSOTH, G.J. & HAMMOND, S.R. 1990. Distribution and composition of hydrothermal plume particles from the ASHES Vent Field at Axial Volcano, Juan de Fuca Ridge. *Journal of Geophysical Research*, **95**, 12 855–12 873.

FEELY, R.A., MASSOTH, G.J. & LEBON, G.T. 1991. Sampling of marine particulate matter and analysis by X-ray fluorescence spectrometry. *In*: HURD, D.C. & SPENCER, D.W. (eds) *Marine Particles: Analysis and Characterization*. American Geophysical Union Monographs, **63**, 251–257.

FORNARI, D.J. & EMBLEY, R.W. 1995. Tectonic and volcanic controls on hydrothermal processes at the mid-ocean ridge: An overview based on near-bottom and submersible studies. *In*: HUMPHRIS, S.E., ZIERENBERG, R.A., MULLINEAUX, L.S. & THOMSON, R.E. (eds) *Seafloor Hydrothermal Systems: Physical, Chemical, Biological, and*

Geological Interactions. American Geophysical Union Monographs, **91**, 1–46.

GAMBLE, J., WOODHEAD, J., WRIGHT, I. & SMITH, I. 1996. Basalt and sediment geochemistry and magma petrogenesis in a transect from oceanic island arc to ridged continental margin arc: the Kermadec–Hikurangi margin, SW Pacific. *Journal of Petrology*, **37**, 1523–1546.

GERMAN, C.R. & PARSON, L.M. 1998. Distributions of hydrothermal activity along the Mid-Atlantic Ridge: Interplay of magmatic and tectonic controls. *Earth and Planetary Science Letters*, **160**, 327–341.

GERMAN, C.R., BAKER, E.T., MEVEL, C., TAMAKI, K. & THE FUJI SCIENTIFIC TEAM. 1998. Hydrothermal activity along the southwest Indian Ridge. *Nature*, **395**, 490–493.

HART, S.R., STAUDIGEL, H., KOPPERS, A.A.P., BLUSZTAJN, J., BAKER, E.T., WORKMAN, R., JACKSON, M., HAURI, E., KURZ, M., SIMS, K., FORNARI, D., SAAL, A. & LYONS, S. 2000. Vailulu'u undersea volcano: The new Samoa. *Geochemistry, Geophysics, Geosystems*, **1**, 2000GC000108.

HART, S.R., STAUDIGEL, H., WORKMAN, R., KOPPERS, A.A.P. & GIRARD, A.P. 2003. A fluorescein tracer release experiment in the hydrothermally active crater of Vailulu'u Volcano, Samoa. *Journal of Geophysical Research*, in press.

IIZASA, K., FISKE, R.S., ISHIZUKA, O., YUASA, M., HASHIMOTO, J., ISHIBASHI, J., NAKA, J., HORII, Y., FUJIWARA, Y., IMAI, A. & KOYAMA, S. 1999. A kuroko-type polymetallic sulfide deposit in a submarine silicic caldera. *Science*, **283**, 975–977.

ISHIBASHI, J. & URABE, T. 1995. Hydrothermal activity related to arc-backarc magmatism in the western Pacific. *In*: TAYLOR, B. (ed.) *Backarc Basins: Tectonics and Magmatism*. Plenum Press, New York, 451–495.

KARIG, D.E. 1971. Origin and development of marginal basins in the western Pacific. *Journal of Geophysical Research*, **76**, 2542–2561.

KAY, S.M. & KAY, R.W. 1985. Role of crustal cumulates and the oceanic crust in the formation of the lower crust of the Aleutian arc. *Geology*, **13**, 461–464.

LAVELLE, J.W., BAKER, E.T. & MASSOTH, G.J. 1998. On the calculation of total heat, salt, and tracer fluxes from ocean hydrothermal events. *Deep Sea Research II*, **45**, 2619–2636.

LILLEY, M.D., FEELY, R.A. & TREFRY, J.H. 1995. Chemical and biological transformations in hydrothermal plumes. *In*: HUMPHRIS, S.E., ZIERENBERG, R.A., MULLINEAUX, L.S. & THOMSON, R.E. (eds) *Seafloor Hydrothermal Systems: Physical, Chemical, Biological, and Geological Interactions*. American Geophysical Union Monographs, **91**, 369–391.

LIN, J. & PHIPPS MORGAN, J. 1992. The spreading rate dependence of three-dimensional mid-ocean ridge gravity structure. *Geophysical Research Letters*, **19**, 13–16.

LIN, J., PURDY, G.M., SCHOUTEN, H., SEMPERE, J.-C. & ZERVAS, C. 1990. Evidence for focused magmatic accretion along the Mid-Atlantic Ridge. *Nature*, **344**, 627–632.

LUPTON, J.E., DELANEY, J.R., JOHNSON, H.P. & TIVEY, M.K. 1985. Entrainment and vertical transport of deep-ocean water by buoyant hydrothermal plumes. *Nature*, **316**, 621–623.

MASSOTH, G.J., DE RONDE, C.E.J., LUPTON, J.E., FEELY, R.A., BAKER, E.T., LEBON, G.T. & MAENNER, S.M. 2003. Chemically rich and diverse submarine hydrothermal plumes of the southern Kermadec volcanic arc (New Zealand). *In*: LARTER, R.D. & LEAT, P.T. (eds) *Intra-oceanic Subduction Systems: Tectonic and Magmatic Processes*. Geological Society, London, Special Publications, **219**, 119–139.

MCCAVE, I.N. & CARTER, L. 1997. Recent sedimentation beneath the Deep Western Boundary Current off northern New Zealand. *Deep Sea Research*, **44**, 1203–1237.

MORTON, B.R., TAYLOR, G.I. & TURNER, J.S. 1956. Turbulent gravitational convection from maintained and instantaneous sources. *Proceedings of the Royal Society of London*, **A234**, 1–23.

PARSON, L.M. & WRIGHT, I.C. 1996. The Lau–Havre–Taupo back-arc basin: A southward-propagating, multi-stage evolution from rifting to spreading. *Tectonophysics*, **263**, 1–22.

SAMPLE, J.C. & KARIG, D.E. 1982. A volcanic production rate for the Mariana Island arc. *Journal of Volcanology and Geothermal Research*, **13**, 73–82.

STOFFERS, P., WRIGHT, I.C., DE RONDE, C., HANNINGTON, M., VILLINGER, H., HERZIG, P. & THE SHIPBOARD SCIENTIFIC PARTY. 1999. Little-studied arc–backarc system in the spotlight. *Eos, Transactions, American Geophysical Union*, **80**, 353–359.

TURNER, J.S. 1973. *Buoyancy Effects in Fluids*. Cambridge University Press, New York.

TURNER, J.S. & CAMPBELL, I.H. 1987. Temperature, density and buoyancy fluxes in 'black smoker' plumes, and the criterion for buoyancy reversal. *Earth and Planetary Science Letters*, **86**, 85–92.

WARREN, B., WHITWORTH, T., MOORE, M.I. & NOWLIN, W.D. 1994. Slight northwestward inflow to the deep South Fiji Basin. *Deep Sea Research*, **41**, 953–956.

WEST, M., MENKE, W., TOLSTOY, M., WEBB, S. & SOHN, R. 2001. Magma storage beneath Axial volcano on the Juan de Fuca mid-ocean ridge. *Nature*, **413**, 833–836.

WHITE, R.S., MINSHULL, T.A., BICKLE, M.J. & ROBINSON, C.J. 2001. Melt generation at very slow-spreading oceanic ridges: Constraints from geochemical and geophysical data. *Journal of Petrology*, **42**, 1171–1196.

WORTHINGTON, T.J. 1998. *Geology and petrology of Raoul Volcano: magma genesis and fractionation processes beneath the Tonga–Kermadec Arc*. Ph. D. thesis, University of Auckland.

WRIGHT, I.C. & GAMBLE, J.A. 1999. Southern Kermadec submarine caldera arc volcanoes (SW Pacific): caldera formation by effusive and pyroclastic eruption. *Marine Geology*, **161**, 207–227.

WRIGHT, I.C., DE RONDE, C.E.J., FAURE, K. & GAMBLE, J.A. 1998. Discovery of hydrothermal sulfide mineralization from southern Kermadec volcanoes

(SW Pacific). *Earth and Planetary Science Letters*, **164**, 335–343.

WRIGHT, I.C., GAMBLE, J.A. & SHANE, P.A. 2002*a*. Submarine, silicic volcanism of the Healy caldera, southern Kermadec arc (SW Pacific): I – volcanology and eruption mechanisms. *Bulletin of Volcanology*, **65**, 15–29, 10.1007/s00445-002-0234-1.

WRIGHT, I.C., PARSONS, L.M. & GAMBLE, J.A. 1996. Evolution and interaction of migrating cross-arc volcanism and backarc rifting: An example from the southern Havre Trough (35°20′–37°S). *Journal of Geophysical Research*, **101**, 22 071–22 086.

WRIGHT, I.C., STOFFERS, P., HANNINGTON, M., DE RONDE, C.E.J., HERZIG, P., SMITH, I.E.M. & BROWNE, P.R.L. 2002*b*. Towed-camera investigations of shallow–intermediate water-depth submarine stratovolcanoes of the southern Kermadec arc, New Zealand. *Marine Geology*, **185**, 207–218.

This page intentionally left blank

Geodynamic setting of Izu–Bonin–Mariana boninites

ANNE DESCHAMPS[1] & SERGE LALLEMAND[2]

[1]*Japan Marine Science and Technology Centre (JAMSTEC), Deep Sea Research Department, 2–15 Natsushima-cho, Yokosuka 237–0061, Japan (e-mail: deschamps@jamstec.go.jp)*

[2]*Universite Montpellier 2, Lab. Geophysique, Tectonique & Sedimentologie, cc 060, Place E. Bataillon, 34095 Montpellier cedex 5, FRANCE*

Abstract: The Izu–Bonin–Mariana (IBM) forearc is characterized by the occurrence of boninite-like lavas. The study of the Cenozoic setting of the genesis of these boninitic lavas in light of modern geodynamic contexts in the Tonga and Fiji regions lead us to define three tectonic settings that favour the formation of boninites in back-arc basins in addition to previous settings that involve the presence of a mantle plume: (1) propagation at low angle between a spreading centre and the associated volcanic arc; (2) intersection at a high angle of an active spreading centre and a transform fault at the termination of an active volcanic arc; and (3) intersection at a right angle between an active spreading centre and a newly created subduction zone. A geodynamic model of the Philippine Sea Plate shows that boninites in the Bonin Islands are related to the second mechanism mentioned above, whereas Mariana forearc boninites are relevant to the third mechanism. In the early Eocene, the transform plate boundary bounding the eastern margin of the Philippine Sea Plate at the location of the present-day Mariana arc evolved into a subduction zone that trends perpendicular to the active spreading centre of the West Philippine Basin, somewhere around 43–47 Ma. The presence of a mantle plume in the vicinity of the subduction zone bounding the northern IBM arc explains boninites that erupted in its northern part, but only in early Eocene time.

Boninitic magmatism represents a distinctive style of subduction-related magmatism, which is interpreted to result from the melting of strongly depleted mantle that is variably metasomatized by slab-derived fluids or melts (Crawford *et al.* 1989; Pearce *et al.* 1992). Boninites are therefore a rare subduction-related magma type as they are the most H_2O rich, and require the most refractory sources, compared with normal island arc suites. These primitive arc rocks have distinctive geochemical characteristics, such as high magnesium, compatible element contents (Ni, Cr, Co) and Al_2O_3/TiO_2 ratios, low TiO_2, intermediate (andesitic) SiO_2 content (>53 wt%), U-shaped rare earth element (REE) patterns, extreme high-field-strength (HFSE) element depletions, and often, but not always, Zr and Hf enrichments relative to middle REE (Crawford *et al.* 1989; Pearce *et al.* 1992). Boninites are characterized by the absence of plagioclase phenocrysts, and by the presence of very magnesian olivine phenocrysts (Crawford *et al.* 1989).

The genesis of boninites requires unique thermal and petrological conditions: a depleted mantle peridotite, a source of (C–O–H) volatiles and an abnormally high geothermal gradient at relatively shallow levels in the mantle wedge. Based on experimental studies, it is now widely accepted that boninite petrogenesis requires temperatures of 1200–1350°C, even *c.* 1480°C according to Falloon & Danyushevsky (2000), and pressures below 10 kbars that are attained at about 25 km in depth (Crawford *et al.* 1989; Pearce *et al.* 1992; Hawkins 1994). Such temperatures are several hundred degrees higher than those postulated in geophysical models for the thermal structure of the mantle wedge under the modern forearc regions (Crawford *et al.* 1989). Boninite generation requires, therefore, a mechanism capable of raising the ambient temperatures in the shallow mantle wedge by up to 500°C.

Concerning the degree of depletion of the boninite source peridotites, its variations are reflected by a wide range of CaO/Al_2O_3 values (0.4–0.85, Crawford *et al.* 1989) in primitive boninites. On the basis of the CaO/Al_2O_3 ratio, boninites have therefore been divided into two groups: low-Ca and high-Ca boninites with a boundary set at CaO/Al_2O_3 *c.* 0.75 (Crawford *et al.* 1989). Low-Ca boninites are interpreted as being produced from relatively more depleted sources than high-Ca boninites. Variations in CaO/Al_2O_3 values and TiO_2 content recorded in several boninite suites (e.g. Howqua, Australia: Crawford & Cameron 1985; Izu–Bonin forearc:

From: LARTER, R.D. & LEAT, P.T. 2003. *Intra-Oceanic Subduction Systems: Tectonic and Magmatic Processes.* Geological Society, London, Special Publications, **219**, 163–185. 0305-8719/03/$15.00

Umino 1986; Pearce *et al.* 1992; Taylor & Mitchell 1992; Taylor *et al.* 1994) have been explained as the result of progressive source depletion during boninite magma genesis. The nature of depleted mantle sources involved in boninite petrogenesis is a subject of debate. Most workers propose a depleted mantle wedge, residual from prior extraction of mid-ocean ridge basalts (MORB) (Crawford *et al.* 1989). However, it is also suggested that at least some high-Ca boninites could originate from a refractory ocean island basalt (OIB) mantle source (Sharaskin *et al.* 1983*a*, *b*; Falloon & Crawford 1991; Macpherson & Hall 2001). A possible involvement of OIB-related melts as enriching components in boninite petrogenesis has been proposed in several studies (Hickey & Frey 1982; Rogers *et al.* 1989; Falloon & Crawford 1991; Stern *et al.* 1991; Kostopoulos & Murton 1992). However, many authors suggest that the source of boninite enrichment is the result of the metasomatism of the subforearc mantle by hydrous fluids or melts derived from the subducting Pacific Plate (Bougault *et al.* 1981; Sharaskin 1981; Wood *et al.* 1981; Hickey & Frey 1982; Murton *et al.* 1992).

Boninites or boninite-like lavas occurrences have been reported in a variety of settings, including modern forearc regions of intra-oceanic island arcs (Falloon & Crawford 1991; Pearce *et al.* 1992), back-arc basins (Kamenetsky *et al.* 1997), Phanerozoic and Proterozoic supra-subduction zone ophiolites (Rogers *et al.* 1989; Ballantyne 1991; Meffre *et al.* 1996; Bédard *et al.* 1998; Eissen *et al.* 1998; Bédard 1999; Wyman 1999), Achaean greenstone belts (Kerrich *et al.* 1998) and in continental or epicontinental settings (Rogers & Saunders 1989; Piercey *et al.* 2001). The best studied locations of Cenozoic–recent boninite lavas are the Izu–Bonin–Mariana forearc (Fig. 1) (Crawford *et al.* 1981, 1989; Umino 1985, 1986; Tatsumi & Maruyama 1989; Stern *et al.* 1991; Pearce *et al.* 1992; Stern & Bloomer 1992; Taylor *et al.* 1994; Hawkins & Castillo 1998; Hickey-Vargas 1989), the North Tonga Ridge (Fig. 2b) (Falloon *et al.* 1989; Falloon & Crawford 1991; Sobolev & Danyushevsky 1994; Danyushevsky *et al.* 1995), the southern termination of the New Hebrides island arc (Fig. 2c) (Monzier *et al.* 1993), the Valu Fa Ridge in Lau Basin (Fig. 2b) (Kamenetsky *et al.* 1997) and the Setouchi volcanic belt of Japan (Tatsumi & Maruyama 1989; Tatsumi *et al.* 2001).

A variety of models for the genesis of boninites have been proposed, such as arc infancy and catastrophic melting (Pearce *et al.* 1992; Stern & Bloomer 1992), ridge subduction beneath young and, hence, hot plate (Crawford *et al.* 1989), back-arc basin formation (Coish *et al.* 1982), mantle plume–island arc interaction (Kerrich *et al.* 1998; Macpherson & Hall 2001) and ridge propagation into a forearc region (Fallon & Crawford 1991; Monzier *et al.* 1993; Meffre *et al.* 1996). Concerning the genesis of Izu–Bonin–Mariana (IBM) arc boninitic lavas, different tectonic settings have been proposed (Pearce *et al.* 1992; Stern & Bloomer 1992; Macpherson & Hall 2001). However, the lack of constraints about the Tertiary behaviour of the West Philippine Basin, that was bordered on its eastern margin by the IBM arc during the production of boninites (Fig. 1), prevents an accurate definition of the geodynamic setting and, consequently, the cause of their eruption. Here, we propose a model for the formation of the IBM boninites with the help of tectonic reconstructions of the West Philippine Basin, as well as comparisons with modern analogues of boninite formation in the North Tonga Ridge, the Valu Fa Ridge (Lau Basin) and the New Hebrides Arc (North Fiji Basin).

Geodynamic setting of the Tonga and New Hebrides boninites

Occurrences of boninites are reported from the North Tonga Ridge (Falloon *et al.* 1989; Falloon & Crawford 1991; Sobolev & Danyushevsky 1994; Danyushevsky *et al.* 1995), the Valu Fa Ridge in the Lau Basin (Kamenetsky *et al.* 1997) and from the southern New Hebrides arc (Monzier *et al.* 1993) (Fig. 2). All these boninites were emplaced in the vicinity of active back-arc spreading centres intersecting active island arcs. They all are younger than Pliocene. From these modern examples, we aim to understand the relationships between the geodynamic context and the occurrence of boninites.

Intersection between the Tofua arc and the NE Lau spreading centre

High-Ca boninites, arc tholeiites and OIB-like lavas were dredged from the northernmost part of the Lau Basin (Falloon *et al.* 1989; Sharaskin *et al.* 1983*b*; Danyushevsky & Sobolev 1987; Fallon & Crawford 1991; Danyushevsky *et al.* 1995). Boninites occur close to the northern termination of the trench, where it swings west into a major transform fault (Fig. 2b). Boninites then erupt at the location of a tear fault within the Pacific Plate, just above the subducting plate edge (Millen & Hamburger 1998) (Fig. 3). They occupy a 50 km-long section of the trench slope.

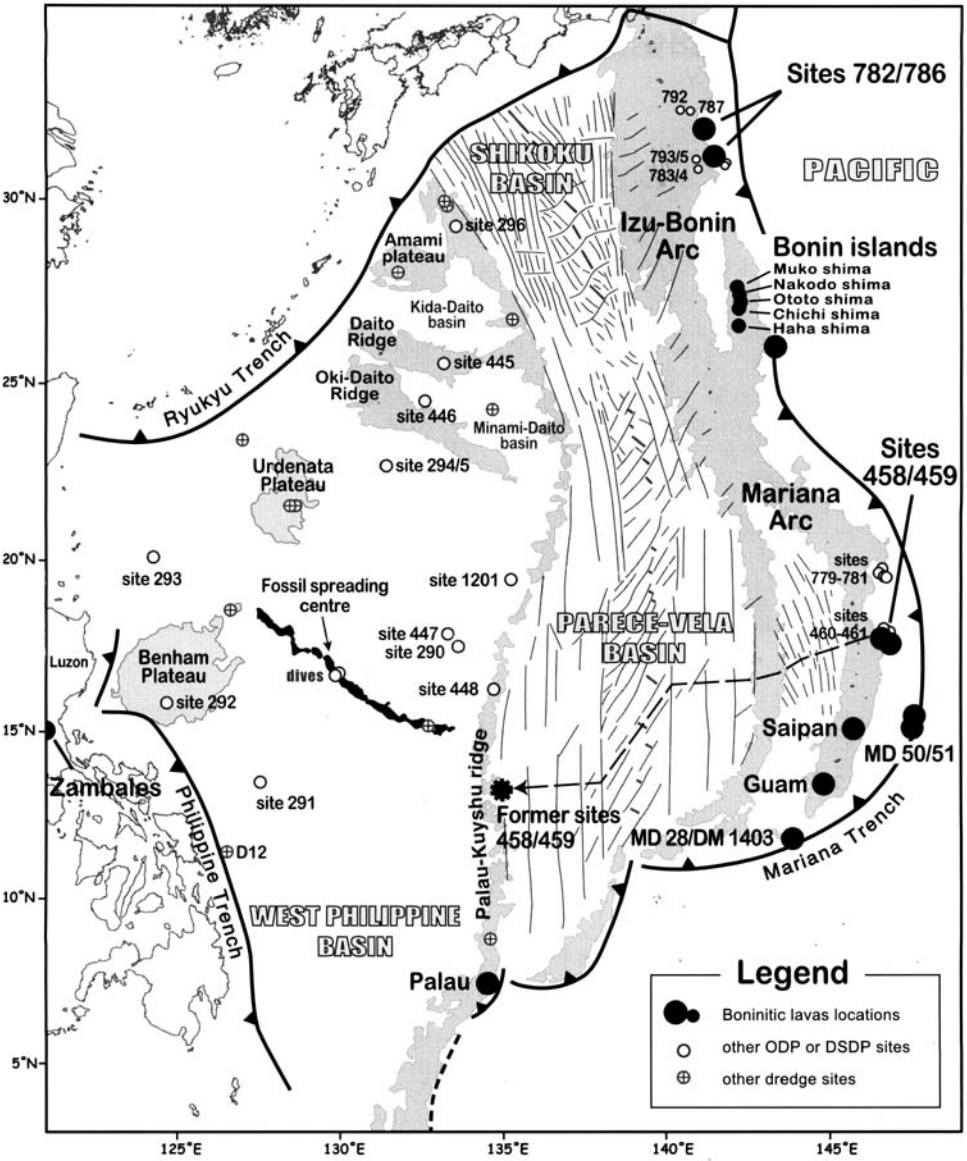

Fig. 1. Tectonic setting of the Philippine Sea Plate, with location of volcanic sites mentioned in the text and in Tables 1 and 2. Boninites are found along the Izu–Bonin–Mariana arc and within the Zambales ophiolite (Luzon). Tectonic and magnetic features in Shikoku, Parece–Vela and Mariana basins are indicated. They provide constraints about the direction of opening of these basins, and consequently about the former location of boninitic lavas sites along the Palau–Kyushu Ridge before the opening of these basins since 30 Ma. The arrow indicates as an example the path chosen to reconstruct the former position of sites 458/459 along the Palau–Kyushu Ridge.

Arc tholeiites were dredged 50 km east of the boninite outcrops (Sharaskin *et al.* 1983*a*). Alkaline OIB-like basalts, which have been shown to originate from the adjacent Samoan plume, are located 60 km to the west of boninite outcrops (Zlobin *et al.* 1991). Ages of boninites range from 1.4 to 2 Ma (Ar/Ar ages) (Danyushevsky *et al.* 1995).

The geodynamic context as the location of boninitic lavas is complex as the lavas occur not

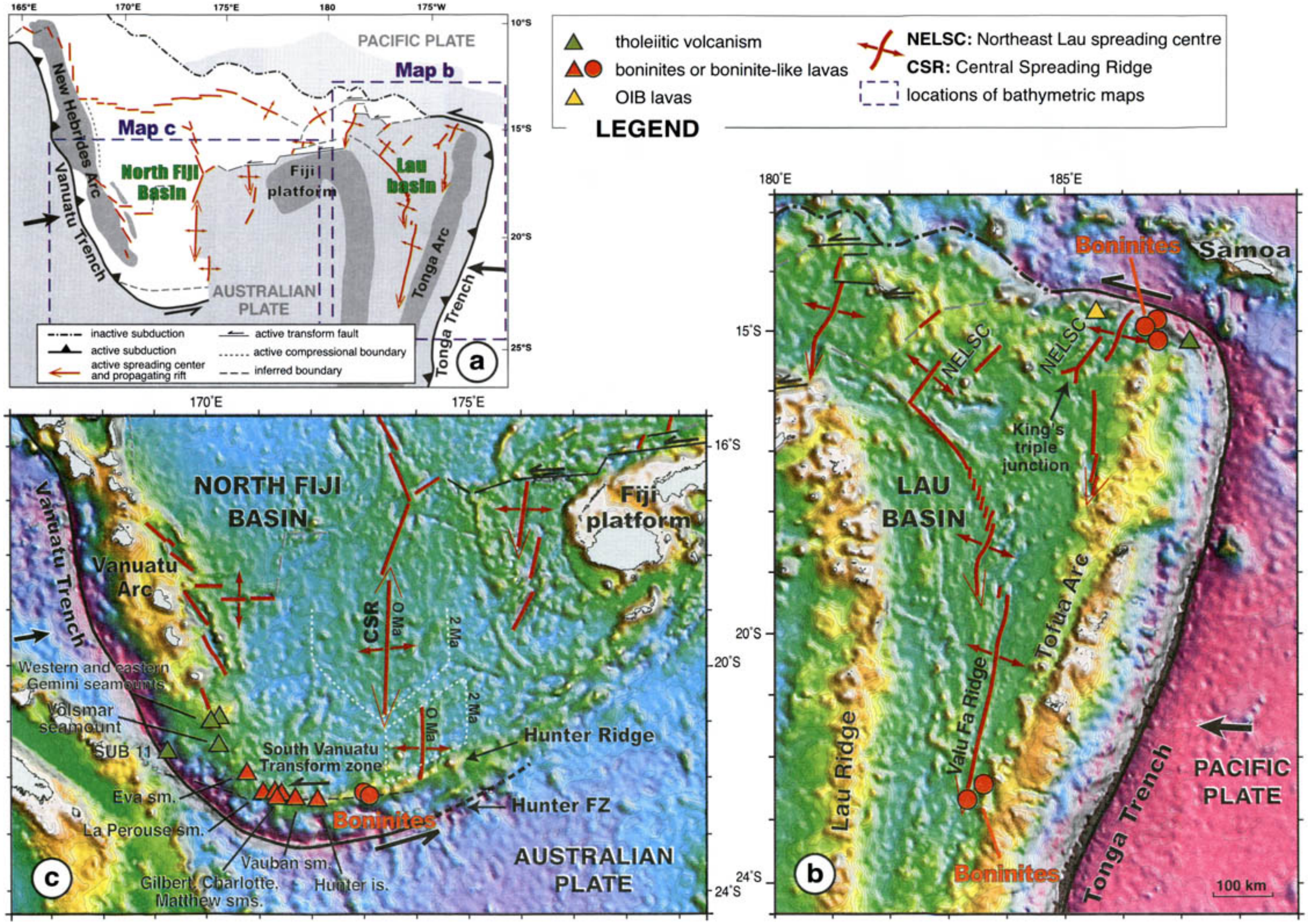
LEGEND
tholeiitic volcanism
boninites or boninite-like lavas
OIB lavas
NELSC: Northeast Lau spreading centre
CSR: Central Spreading Ridge
locations of bathymetric maps
PACIFIC PLATE
Map b
Map c
New Hebrides Arc
Vanuatu Trench
North Fiji Basin
Fiji platform
Lau basin
Tonga Arc
Tonga Trench
AUSTRALIAN PLATE
inactive subduction
active subduction
active spreading center and propagating rift
active transform fault
active compressional boundary
inferred boundary
a
NORTH FIJI BASIN
Vanuatu Arc
Vanuatu Trench
Fiji platform
CSR
0 Ma
2 Ma
Western and eastern Gemini seamounts
Volsmar seamount
SUB 11
South Vanuatu Transform zone
Hunter Ridge
Hunter FZ
Eva sm.
La Perouse sm.
Boninites
Vauban sm.
Gilbert, Charlotte, Matthew sms.
Hunter is.
AUSTRALIAN PLATE
c
Samoa
Boninites
NELSC
NELSC
King's triple junction
LAU BASIN
Tofua Arc
Valu Fa Ridge
Lau Ridge
Boninites
Tonga Trench
PACIFIC PLATE
b
100 km

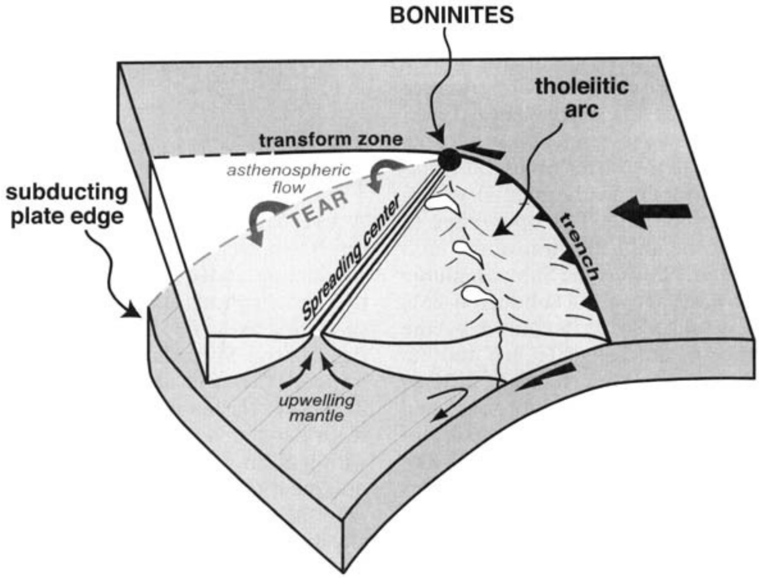

Fig. 3. Perspective cartoon illustrating the geometry of the subduction trench–transform transition in the vicinity of an active spreading centre. The open edge above the tear within the Pacific Plate favours upward asthenospheric flow and high heat flow. In the northern termination of the Tonga Trench, this tear allows the southward migration of the hot asthenospheric material related to the nearby Samoan plume. Boninites were formed at the termination of the active volcanic arc, at the intersection of the active spreading centre and the transform zone that accommodates the opening of the back-arc basin.

only in the vicinity of a trench–transform fault transition, but also near the Samoan active plume, and also at the termination of an active back-arc spreading centre (Falloon & Crawford 1991; Wright *et al.* 2000; Pelletier *et al.* 2001) (Fig. 2b). Because of this particular tectonic setting, different hypotheses have been proposed to explain the genesis of boninites in this northeastern part of the Lau Basin.

The first one, proposed by Falloon & Crawford (1991), is based on the isotopic (Sr, Nd) composition of lavas. The boninites mantle sources are part of a regional OIB mantle domain upwelling beneath the Tonga subduction zone system. This mantle source was of refractory lherzolite composition, depleted in basaltic components by prior generation of Lau Basin crust. It has been enriched in incompatible elements by one or more metasomatic phases, suggested to be a hydrous fluid from the subducting lithospheric slab, a carbonatite melt and a small-degree silicate partial melt, both derived from OIB source mantle. The genesis of boninites is explained by the presence of the NE Lau Spreading Centre, which intersects the northernmost Tofua Arc (Fig. 2b). Upwelling asthenospheric mantle beneath the spreading axis may, indeed, cause partial melting of the refractory peridotite located in the mantle wedge above the subducting Pacific Plate at shallow depth. According to this model, the source of heat flow that is necessary to melt the refractory mantle is thus the ascending diapirs of MORB magmas beneath the spreading ridge.

The other main hypothesis to explain the formation of boninites at the northern end of the

Fig. 2. Tectonic setting of the Lau and North Fiji basins. (**a**) is modified from Pelletier *et al.* (1998). Blue boxes indicate the location of maps (b) and (c). (**b**) Two-dimensional shaded bathymetric map of the Lau Basin, with location of boninitic lavas. Boninitic lavas are found at two places along the Tofua arc: at its northern end near the NE Lau Spreading Centre (NELSC) termination, and more to the south, close to the southern end of the Valu Fa Ridge. (**c**) Two-dimensional shaded bathymetric map of the southern part of the North Fiji Basin. Boninites are found at the intersection between the active Central Spreading Ridge (CSR) and the Hunter Fracture Zone, i.e. the eastern continuation of the New Hebrides (Vanuatu) Trench. The Vanuatu arc north of 21°N displays only normal island arc tholeiitic lavas. Bathymetric data are satellite derived (Smith & Sandwell 1997).

Lau Basin is suggested by Danyushevsky *et al.* (1995). These authors agree with Falloon & Crawford (1991) concerning the mantle source composition of boninitic magmas, but the source of heat flow to melt this refractory mantle differs in their model. They suggest that abnormal high heat flow results from the intrusion of hot residual plume mantle diapirs in the mantle wedge above the subduction zone. The open edge of the mantle wedge beneath the transform fault would have, indeed, allowed the Samoan plume to intrude southward above the subducted slab. This intrusion would also be favoured by the eastward rollback of the Tonga Trench and the southward asthenospheric flow beneath the Lau Basin (Smith *et al.* 2001). The variably enriched boninitic melts would be due to the mixing of these magmas with earlier formed OIB-like melts, during their ascent to the surface. This hypothesis of Danyushevsky *et al.* (1995) is supported by the presence of many recent seamounts in the northern part of the Lau Basin, whose lavas are isotopically similar to Samoan OIB-like basalts. This shows that either plume mantle, or mantle plume-derived melts, occupy a large area of the mantle wedge in this region.

Intersection between the Valu Fa Ridge and the Tofua arc

The Valu Fa Ridge is the southernmost active spreading axis of the Lau Basin. It is located 40 km west of Ata Island, a volcano belonging to the Tofua arc that results from volcanism related to the westward subduction of the Pacific Plate along the Tonga Trench (Fig. 2b). Several lava samples have been dredged at two sites from the southern termination of the Valu Fa Ridge, *c.* 50 km north of its southward propagating tip and close to its intersection with the Tofua arc (Frenzel *et al.* 1990; Sunkel 1990; von Stackelberg *et al.* 1990; Fouquet *et al.* 1991; Kamenetsky *et al.* 1997) (Fig. 2b). These rocks mainly consist of normal island arc basaltic and andesitic suites with strong geochemical affinities with subduction zone magmas (Jenner *et al.* 1987; Boespflug *et al.* 1990; Vallier *et al.* 1991). However, some rocks dredged close to the intersection between the active spreading axis and volcanic arc consist of low-Ca boninitic-like, primitive lavas (Kamenetsky *et al.* 1997). It is suggested that these boninitic lavas have been formed due to the melting of a shallow, refractory, hydrated mantle that has been metasomatized by fluids or melts coming from the subducting slab. The melting of the refractory mantle beneath the Tofua arc would be due to its juxtaposition against hot asthenospheric mantle that is currently supplying the Valu Fa Ridge (Kamenetsky *et al.* 1997).

The southern termination of the Vanuatu Trench

Active back-arc extension occurs in the North Fiji Basin, east of the Vanuatu (New Hebrides) subduction zone. The basin is characterized by the synchronous existence of several active spreading axes (Fig. 2 a, c). At least since 2 Ma, the Central Spreading Ridge of the basin has trended N–S and abuted the Hunter Fracture Zone, i.e. the eastern termination of the New Hebrides arc (Pelletier *et al.* 1998). It is active with a 8 cm a^{-1} full spreading rate in a N72°E oblique direction (Fig. 2c).

In the southern New Hebrides arc, two spatially distinct arc magmatic suites are described by Monzier *et al.* (1993) from analyses of several dredged rocks (see location of dredges on Fig. 2c). Between 21°S and 22°S, a normal island arc tholeiitic magmatic suite is essentially similar to those occurring in the main part of the New Hebrides arc central chain volcanoes, whereas south of 22°S, at the southern termination of the arc, a high magnesian andesite suite appears with the more mafic end-members having mineralogical and compositional affinities with high-Ca boninites (Monzier *et al.* 1993) (see location on Fig. 2c). Monzier *et al.* (1993) suggest that most of the sampled volcanoes are probably younger than 2 or 3 Ma, considering the recent evolution of the southern termination of the arc. This seems to be confirmed by ages of the Matthew and Hunter volcanoes that range from 0.8 to 1.4 Ma (Maillet *et al.* 1986; Monzier *et al.* 1993). True high-Ca boninites have been dredged only 100 km east of Hunter Island, in the area where the Central Spreading Ridge abuts the Hunter Fracture Zone (Sigurdsson *et al.* 1993). Monzier *et al.* (1993) suggest that the generation of high-Ca boninites or boninite-like magmas occurs by melting of a refractory mantle at a shallow level under the Hunter Ridge. The extra heat that is necessary to melt such a mantle would be provided by the rising diapirs supplying magmas to the intersecting spreading axis. Doleritic inclusions that are common in some Mg-rich acid andesites of Matthew and Hunter islands may represent quenched blobs of near parental boninitic high-Mg andesite magma incorporated into the acid andesite host magma prior to eruption. These inclusions are, indeed, certainly co-magmatic (Maillet *et al.* 1986; Monzier *et al.* 1993) and these authors suggest that magma mixing probably occurred along the termination of the New Hebrides arc.

Intersection between arc and back-arc volcanism: a geodynamic context favourable to the genesis of boninites

We learn from the above three recent tectonic settings of boninite eruptions that back-arc rifting or spreading occurs close to subduction-related arc volcanism:

- the southern Valu Fa spreading centre almost parallels and merges with the Tofua volcanic arc. Boninites are located at about 140 km above the subducting Pacific slab;
- the northern part of the NE Lau Spreading Centre and the southern part of the Central Spreading Ridge (North Fiji Basin) show similar geodynamic contexts. Boninites are found at the intersection between the back-arc spreading centre and a transform fault that connects at about right angle with the nearby subduction zones (Tonga or New Hebrides subduction zones). In northern Tonga, boninites erupt above the Pacific subducting slab whose top is 80 km deep, whereas, in southern New Hebrides, the Australian slab could reach depths around 80 km under the site of boninite eruption. Another similarity concerns their location just above the tear that allows the same plate to subduct along the trench and to slip along the transform fault (Fig. 3).

Earthquake distribution and source-mechanism determinations indicate progressive down-warping and tearing of the Pacific Plate as it enters the northernmost segment of the Tonga subduction zone (Millen & Hamburger 1998). Based on the same arguments, we suspect that the same situation occurs at the southernmost termination of the New Hebrides subduction zone. The occurrence of a tear is known to favour upward asthenospheric flow, unusual volcanic products and, thus, high heat flow (Lees 2000). As the subducting plate is torn beneath the transform fault, a slab window allows mantle material to flow around the exposed edge of the subducting plate. Slab rollback not only causes the entire wedge mantle to rise and decompress (Pearce *et al.* 1992; Bédard, 1999), but here also induces asthenospheric flow around the edge of the subducting plate, shearing of the edge and causing anomalously high magma production as seen at the Kamtchatka–Bering junction (Yogodzinski *et al.* 2001). The intrusion of the Samoan mantle plume into the mantle wedge above the Tonga slab evoked by Danyushevsky *et al.* (1995) is probably favoured by this asthenospheric flow.

We conclude that modern examples of boninitic eruptions all occur where back-arc spreading occurs above a subducting slab whose top is 80–140 km deep, commonly, but not always, above a tear in the subducting slab that could favour asthenospheric flow around the subducting plate edge, producing high heat flow (Fig. 3).

Occurrence of boninites along the Izu–Bonin–Mariana arc

The Izu–Bonin–Mariana (IBM) arc bounding the eastern margin of the Philippine Sea Plate is characterized by the presence of an important boninitic suite that occurs mainly within the present-day forearc domains (e.g. DSDP sites 782, 786, 458, Chichijima, Saipan, Guam, Palau islands, and dredge sites MD28, MD50, MD51, DM1403) (Fig. 1) (Dietrich *et al.* 1978; Sharaskin *et al.* 1980; Crawford *et al.* 1981, 1989; Umino 1985, 1986; Stern *et al.* 1991; Pearce *et al.* 1992; Taylor *et al.* 1994). The IBM region has been intensively studied and numerous geochronological and geochemical analyses were carried out. Boninites are found in close relationship with tholeiitic lavas, as well as other typical arc lavas, such as andesites, dacites and rhyolites (e.g. Crawford *et al.* 1981; Umino 1985; Pearce *et al.* 1992; Bloomer *et al.* 1995; Cosca *et al.* 1998). In Hole 458, on the Guam and on Chichijima islands, boninites are interbedded with tholeiites (see locations on Fig. 1). In Hole 786, they dominate the lowermost part of the deep crustal section through the outer arc, and are closely linked to bronzite andesites, andesites, dacites and rhyolites in the main part of the volcanic edifice. At this site, they are also found as younger sills or dykes that intrude the main volcanic edifice (Pearce *et al.* 1992). Radiometric dating of boninites and indirect palaeontological dating of their closely associated sediments show ages of emplacement that range between early Eocene and Oligocene times, with a principal phase of volcanism between 48 and 41 Ma, possibly followed by a second minor event around 35–34 Ma, which led to the emplacement of sills and dykes within the main volcanic edifice constructed during the first phase (Maruyama & Kuramoto 1981; Meijer 1983; Reagan & Meijer 1984; Mitchell *et al.* 1992; Pearce *et al.* 1992; Cosca *et al.* 1998) (Tables 1, 2,

Table 1. *Ages of arc volcanism along the Izu–Bonin Arc*

Site/sample[*]	Nature of sample[†]	K/Ar[§] (Ma)	Ar/Ar[§] (Ma)	Confidence[‡]	Ref.
Palau–Kyushu Ridge (northernmost part)					
GDP-8-12	plagiogranite	**37.4**	–	–	Malyarenko & Lelikov (1995)
N4-90	plagiogranite	**42.7**	–	–	Malyarenko & Lelikov (1995)
N4-91	plagiogranite	**31.2**	–	–	Malyarenko & Lelikov (1995)
N4-91	plagiogranite	**26.2**	–	–	Malyarenko & Lelikov (1995)
D-60	plagiogranite	**37.5**	–	–	Malyarenko & Lelikov (1995)
D-76	tonalite	**48.5**	–	–	Malyarenko & Lelikov (1995)
–	volcanic rock	**49**	–	–	Mizuno *et al.* (1977)
–	granodiorite	**38**	–	–	Shibata & Okuda (1975)
same	granodiorite	–	**51** (fission tracks)	–	Nishimura (1975)
Site 782A/B					
45X-1 31-35	clast, dacite	18.1	–	3	Mitchell *et al.* (1992)
50X-1 19-30	clast andesite	**30.7**	–	–	Mitchell *et al.* (1992)
1W-1 52-55	clast, andesite	**36.2**	–	2	Mitchell *et al.* (1992)
1W-1 52-55	clast, andesite	–	**35.5[t]**	2	Cosca *et al.* (1998)
Site 786 A/B					
12X-1 133-138	clast, basalt	9.2	–	3	Mitchell *et al.* (1992)
16X-1 24-29	clast, ICB	15.3	–	3	Mitchell *et al.* (1992)
2R-1 72-76	flow, ICBzA	**41.0**	–	–	Mitchell *et al.* (1992)
2R-1 72-76	flow, ICBzA	–	**46.6[t], 46.7[p], 45.7[i]**	–	Cosca *et al.* (1998)
2R-1 72-76	flow, ICBzA	–	**45.0[t], 45.8[p], 43.3[i]**	–	Cosca *et al.* (1998)
6R-2 135-137	dike, HCB	**17.3**	–	1	Mitchell *et al.* (1992)
8R-1 50-55	breccia, andesite	9.2	–	3	Mitchell *et al.* (1992)
11R-1 121-123	breccia, ICB	25.7	–	3	Mitchell *et al.* (1992)
16R-1 135-138	breccia, andesite	**33.7**	–	1	Mitchell *et al.* (1992)
20R-1 43-46	dike, ICB	12.0	–	3	Mitchell *et al.* (1992)
20R-1 124-128	flow, andesite	33.8	–	4	Mitchell *et al.* (1992)
21R-1 20-28	flow, andesite	16.7	–	3	Mitchell *et al.* (1992)
21R-2 85-94	dike, HCB	**33.8**	–	1	Mitchell *et al.* (1992)
21R-2 85-94	dike, HCB	–	**60[t], 54[p], 55.4[i]**	–	Cosca *et al.* (1998)
30R-1 0-7	flow, ICBzA	**39.8**	–	–	Mitchell *et al.* (1992)
30R-2 59-66	flow, ICBzA	**37.9**	–	–	Mitchell *et al.* (1992)
32R-2 83-85	flow, rhyolite	**41.1**	–	–	Mitchell *et al.* (1992)
34R-3 48-54	dike, HCB	**34**	–	1	Mitchell *et al.* (1992)
35R-1 122-126	flow, dacite	**38.2**	–	–	Mitchell *et al.* (1992)
40R-2 83-90	dike, HCB	**35.5**	–	1	Mitchell *et al.* (1992)
51R-1 75-79	breccia, ICB	33.6	–	4	Mitchell *et al.* (1992)
57R-2 122-125	pillow, LCB	**34.2**	–	4	Mitchell *et al.* (1992)
57R-4 7-13	pillow, LCB	**38.4**	–	–	Mitchell *et al.* (1992)
58R-1 121-126	pillow, LCB	33.7	–	3	Mitchell *et al.* (1992)
65R-1 25-32	dike, andesite	**36.0**	–	1	Mitchell *et al.* (1992)
66R-2 128-135	dike, rhyolite	**41.3**	–	–	Mitchell *et al.* (1992)
66R-2 128-135	same	–	**45.5[t], 45.7[p], 45.4[i]**	–	Cosca *et al.* (1998)
67R-1 56-59	dike, ICB	**41.1**	–	–	Mitchell *et al.* (1992)
70R-1 92-97	dike, LCBzA	**38.7**	–	–	Mitchell *et al.* (1992)
70R-4 27-35	dike, LCBzA	**43.9**	–	–	Mitchell *et al.* (1992)
70R-4 27-35	same		**45.9[t], 45.3[p], 46.6[i]**	–	Cosca *et al.* (1998)
72R-1 3-7	dike, ICB	**33.8**	–	1	Mitchell *et al.* (1992)
Sites 786/782					
Sediments over volcanics	nannofossils	**z. CP13c**	**44.4–47.0**	–	Xu & Wise (1992)
Same	foraminifers	**z. P10/P11**	**45–52**	–	Milner (1992)
Sediment intercalated	microfossil	–	**middle–late Eocene**	–	Milner (1992)
Mean values	–	–	**41.3 and 34.8**	–	Mitchell *et al.* (1992)
Conclusion:	–	–	**38–44 and 34–36**	–	Mitchell *et al.* (1992)

Table 1. *continued*

Site/sample*	Nature of sample†	K/Ar§ (Ma)	Ar/Ar§ (Ma)	Confidence‡	Ref.
Site 792E					
69R-1	amphibole in sed.	**37.7**	–	–	Taylor & Mitchell (1992)
71R-3	andesite	**33.3t**	–	–	Taylor & Mitchell (1992)
Site 793B					
96R-1	COBA	26.3t	–	3	Taylor & Mitchell (1992)
97R-1	COPBA	28.5t	–	3	Taylor & Mitchell (1992)
112R-2	COPBA	26.5t	–	3	Taylor & Mitchell (1992)
Sediments over volcanics		**chron 10R**	**30–33**	–	Taylor (1990)
Chichijima					
Chi-1	low-Ca boninite	**41.9**	**41.5[t], 44.8[p], 47.8[i]**	–	Cosca *et al.* (1998)
?	boninite glass	**48.1**	–	–	Dobson (1986)
CC01	boninite pillow	8.4/8.0	–	3	Tsunakawa (1983)
CC13	boninite	34.2	–	3	Tsunakawa (1983)
CC14	boninite	31.2	–	3	Tsunakawa (1983)
CC15	boninite	27.9	–	3	Tsunakawa (1983)
CC16	boninite	**41.3**	–	1	Tsunakawa (1983)
CC07	dacite	**38.6**	–	1	Tsunakawa (1983)
CC09	dacite	**43.0**	–	1	Tsunakawa (1983)
CC17	dacite	23.2	–	3	Tsunakawa (1983)
CC04	quartz dacite dike	5.5/3.9	–	3	Tsunakawa (1983)
CC06	quartz dacite	27.1	–	3	Tsunakawa (1983)
CC11	rhyolite	10.2	–	3	Tsunakawa (1983)
Ototojima			–		
OT01	andesite	22.4	–	3	Tsunakawa (1983)
Nakodojima			–		
NK01	dacite	**42.3**	–	1	Tsunakawa (1983)
Mukojima			–		
MK01	boninite	22.4	–	3	Tsunakawa (1983)
Hahajima			–		
HH01	andesite	23.3	–	3	Tsunakawa (1983)
HH02	andesite	9.6	–	3	Tsunakawa (1983)
HH03	basalt	29.9/29.4	–	3	Tsunakawa (1983)
HH04	dacite	32.6	–	3	Tsunakawa (1983)
?	pyroxene andesite	**41**	–	–	Kaneoka *et al.* (1970)
-	radiolarian	**43–47**	–	–	Kodama *et al.* (1983)
Bonin Islands	mean value	–	**40**	–	Tsunakawa (1983)

* Location of sites in Fig. 1.

† HCB, high-Ca boninite; ICB, intermediate-Ca boninite; ICBzA, intermediate-Ca bronzite–andesite; LCB: low-Ca boninite; LCBzA: low-Ca bronzite andesite; COBA, clinopyroxene–orthopyroxene phyric basaltic andesite; COPBA, clinopyroxene–orthopyroxene–plagioclase phyric basaltic andesite.

‡ Numbers 1, 2 and 3 in the 'Confidence' column indicate: (1) well constrained; (2) poorly constrained (altered sample or discrepancies between isochron and plateau ages for examples); (3) very poorly constrained (altered samples); and (4) reset ages due to the second boninitic event, according to authors (e.g. Cosca *et al.* 1998).

§ In the K/Ar and Ar/Ar columns, [p], [i], and [t] indicate plateau, isochron and whole rock ages, respectively. Palaeontological ages are also indicated, when they are determined on sediments that are closely associated with boninitic lavas. Those ages that are poorly constrained are given in normal type, and ages that are not poorly constrained are given in bold type.

Fig. 4). The low reliability of many dates prevents us from confirming continuous boninitic activity during this period. Younger ages ranging between 18 and 33 Ma have been determined from boninitic lavas in several sites, but they often conflict with palaeontological ages, leading some authors such as Cosca *et al.* (1998) to question their reliability.

Table 2. *Ages of arc volcanism along the Mariana arc*

Site/sample*	Nature	K/Ar (Ma)	Ar/Ar (Ma)	Confidence	Ref.
Site 458					
29R-3 3-8	bronzite	31.8	33.6^{i}	2	Takigami & Ozima (1981)
40R-2 38-45	basalt	–	40.5^{t}, 21.4^{p}, 19.1^{i}	2	Takigami & Ozima (1981)
32R-4	andesite	**36.9**	–	–	Cosca *et al.* (1998)
37R-1	andesite	**41.9**	**49.0^{t}, 49.3^{p}, 49.9^{i}**	–	Cosca *et al.* (1998)
39R-1	andesite	**28**	–	–	Cosca *et al.* (1998)
46R-1	pillow basalt	**43.6**	–	2	Cosca *et al.* (1998)
–	sediments	–	**30–34**	–	Hussong & Uyeda (1981)
Site 459B					
61R-1 133-138	clinopyroxene–plagioclase basalt		36.1^{t}	2	Takigami & Ozima (1981)
61R-1 133-138	same	**39.0**	–	–	Cosca *et al.* (1998)
60R-2	basalte	**39.9**	**43.0^{t}, 45.1^{p}, 44.9^{i}**	–	Cosca *et al.* (1998)
–	sediments		**42–45**		Hussong & Uyeda (1981)
Guam					
site 1403	boninite	**44**	–	–	Tsunakawa (1983)
G89–1	Facpi	33.0	–	2	Cosca *et al.* (1998)
G88–13	Facpi	27.3	–	2	Cosca *et al.* (1998)
G89–5	Facpi	16.3	–	2	Cosca *et al.* (1998)
G88–12	Facpi	36.2	–	2	Cosca *et al.* (1998)
G88–15	Facpi	34.9	–	2	Cosca *et al.* (1998)
G89–2	Facpi	24.2	–	2	Cosca *et al.* (1998)
–	Facpi	***c.* 44**	–	–	Hickey-Vargas & Reagan (1987)
G88–8	Alutom	21.4	–	2	Cosca *et al.* (1998)
–	Alutom	***c.* 36–32**	–	–	Hickey-Vargas & Reagan (1987)
Alutom	boninite	**35**	–		Meijer *et al.* (1983)
–	boninite pillow	**43.8**	–		Meijer *et al.* (1983)
Saipan					
SA88-13	Sankakayuma	**44.7**	**46.6^{t}, 46.1^{i}**	–	Cosca *et al.* (1998)
SA89-9	Sankakayuma	**44.6**	–	–	Cosca *et al.* (1998)
SA88-6	Sankakayuma	**45.3**	–	–	Cosca *et al.* (1998)
–	Sankakayuma	**41**			Meijer *et al.* (1983)
SA89-1	Hagman	**27.6**	–	–	Cosca *et al.* (1998)
SA89-6	Hagman	**26.2**	–	–	Cosca *et al.* (1998)
SA89-7	Hagman	**28.3**	–	–	Cosca *et al.* (1998)
Palau					
PA86-13	Babelduap	**25.7**	–	–	Cosca *et al.* (1998)
PA86-14	Babelduap	**47.9**	**58^{t}, 51^{p}**	–	Cosca *et al.* (1998)
PA86-18	Babelduap	**32.1**	**32.0^{t}**	–	Cosca *et al.* (1998)
PA86-19	Babelduap	**32.6**	–	–	Cosca *et al.* (1998)
PA86-22	Aimeliik	**31.9**	–	–	Cosca *et al.* (1998)
PA86-4	Arakabesan	**30.2**	**30.4^{t}**	–	Cosca *et al.* (1998)
PA89-7	Arakabesan	**34.3**	–	–	Cosca *et al.* (1998)
PA86-16	Arakabesan	**33.9**	–	–	Cosca *et al.* (1998)
PA86-24	Arakabesan	**32.2**	–	–	Cosca *et al.* (1998)

Location of sites in Fig. 1. On Guam Island, the Facpi Formation is Middle Eocene in age, and it consists in interbedded boninite pillow lavas and breccias, locally with tholeiitic rocks as the youngest member. The Alutom Formation paraconformably overlays the Facpi Formation, and is constituted by calc-alkaline, tholeiitic, and boninitic pyroclastic rocks and lavas (Meijer *et al.* 1983). On Palau, the Babelduap Formation is the oldest one, and contains boninitic lavas (Cosca *et al.* 1998). Boninites are also found in the Ameliik Formation. The youngest unit is called Arakabesan Formation. On Saipan, the Sankakuyama Formation is the lowest unit on this island, and it consists in boninite and dacite series. The younger Hagman Formation is composed of andesitic pyroclastic rocks and lavas flows (Meijer *et al.* 1983).
See Table 1 for the abbreviations used in the K/Ar, Ar/Ar and Confidence columns.

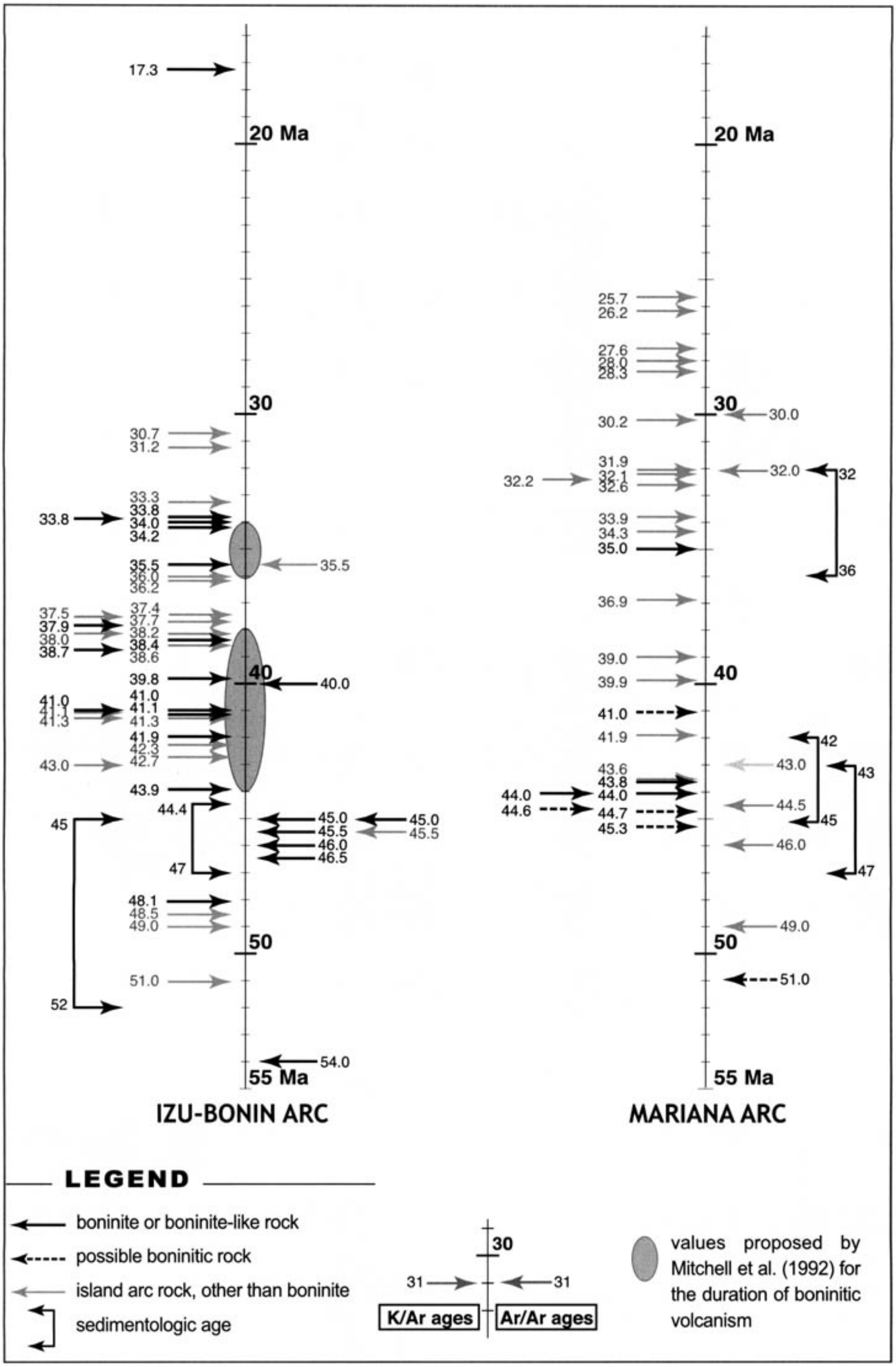

Fig. 4. Ages of volcanic events that are inferred along the Izu–Bonin arc between 55 and 15 Ma. Palaeontological and radiometric dating have been reported from Tables 1 (Izu–Bonin arc) and 2 (Mariana arc). Ages that are poorly constrained (in normal type in the K/Ar and Ar/Ar columns in Tables 1 and 2) are not reported on this figure.

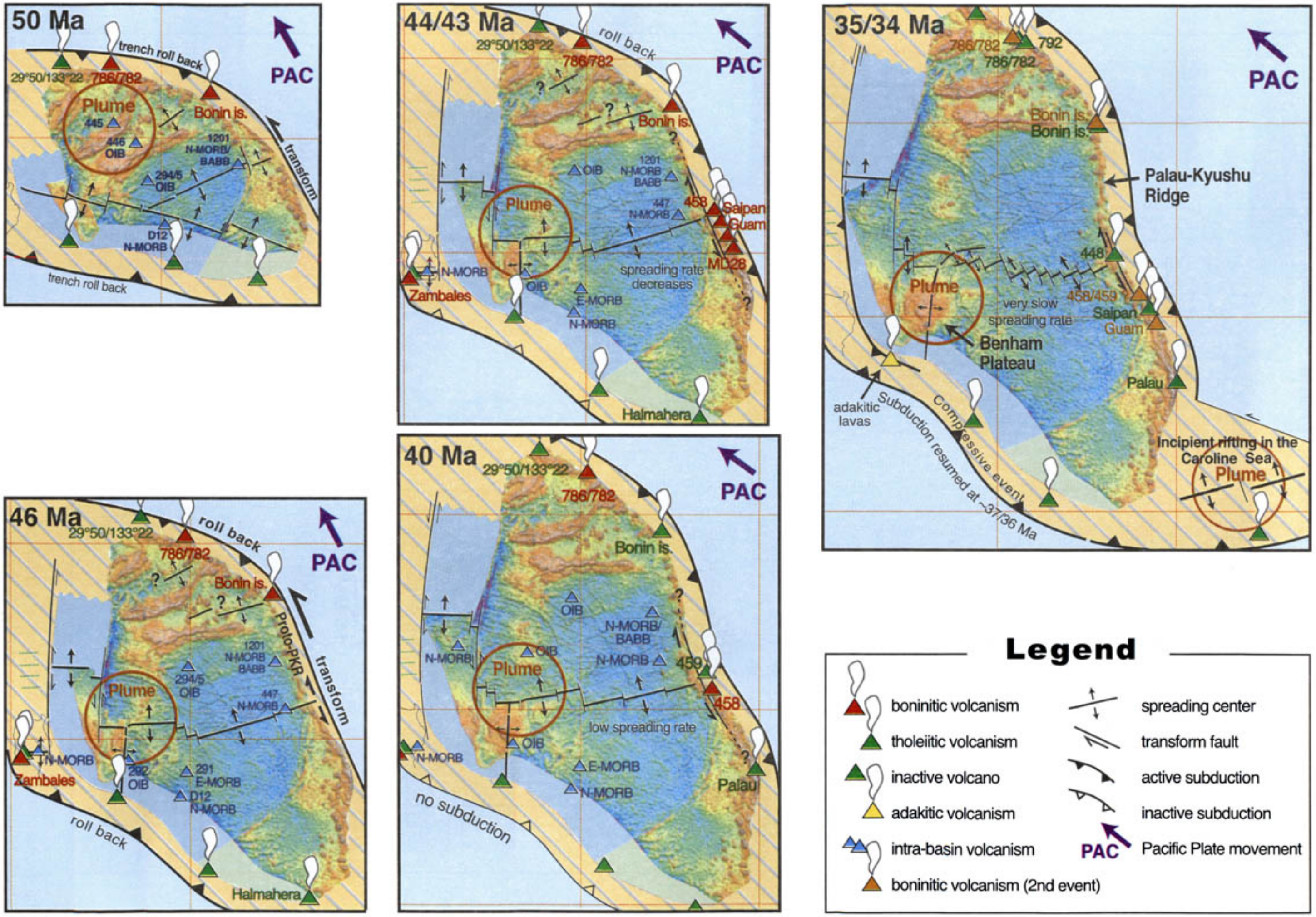

50 Ma
trench roll back
PAC
29°50/133°22
786/782
Bonin is.
Plume
445
446
OIB
1201
N-MORB/
BABB
294/5
OIB
transform
D12
N-MORB
trench roll back
44/43 Ma
29°50/133°22
786/782
roll back
PAC
Bonin is.
Plume
OIB
1201
N-MORB
BABB
447
N-MORB
458
Saipan
Guam
MD28
N-MORB
Zambales
OIB
E-MORB
N-MORB
spreading rate
decreases
Halmahera
35/34 Ma
786/782
792
786/782
PAC
Bonin is.
Bonin is.
Palau-Kyushu
Ridge
448
Plume
very slow
spreading rate
458/459
Saipan
Guam
Benham
Plateau
Palau
adakitic
lavas
Subduction resumed at ~37/36 Ma
Compressive event
Incipient rifting in the
Caroline Sea
Plume
46 Ma
29°50/133°22
786/782
roll back
PAC
Bonin is.
Proto-PKR
transform
1201
N-MORB
BABB
294/5
OIB
447
N-MORB
Plume
N-MORB
Zambales
292
OIB
291
E-MORB
D12
N-MORB
roll back
Halmahera
40 Ma
29°50/133°22
786/782
PAC
Bonin is.
OIB
N-MORB/
BABB
N-MORB
459
458
N-MORB
Plume
OIB
OIB
N-MORB
low spreading rate
E-MORB
N-MORB
Palau
no subduction
Legend
boninitic volcanism
tholeiitic volcanism
inactive volcano
adakitic volcanism
intra-basin volcanism
boninitic volcanism (2nd event)
spreading center
transform fault
active subduction
inactive subduction
PAC
Pacific Plate movement

Previous models for the formation of boninites along the Izu–Bonin–Mariana arc

The cause of the widespread boninitic volcanism along the IBM arc is the subject of considerable debate. Several hypotheses have been proposed. (1) According to Crawford *et al.* (1989), boninite formation is due to the subduction of an active spreading centre subparallel to the proto-Palau–Kyushu trench bounding the eastern margin of the Philippine Sea Plate at this time. As the hot lithosphere on either side of the spreading centre approached the trench, the dip of the slab probably decreased and isotherms in the mantle wedge were raised, causing partial melting of depleted subforearc oceanic lithosphere and generation of high-Ca boninites. (2) Pearce *et al.* (1992) and Taylor *et al.* (1994) suggested that the boninites formed due to the subduction of young, hot oceanic crust beneath hot, young, lithosphere of the Philippine Sea Plate. Subduction is supposed to have started along a ridge-to-ridge transform fault. (3) Stern & Bloomer (1992) proposed that boninites in the IBM forearc are due to the nucleation of subduction along an active transform boundary separating an active spreading ridge between Asia and Australia to the southwest, and the Kula–Pacific Ridge to the northeast. Because of its old age, the lithosphere east of the transform fault would have been gravitationally unstable and subsided, leading to the inception of a subduction zone. Migration of the asthenosphere over the subsiding lithosphere would have entailed adiabatic decompression, and water would have been released from the subducted lithosphere and sediments. These two processes should have led to extensive melting and production of boninites, particularly in the forearc region subjected to extension due to trench rollback. (4) Another hypothesis to explain the boninitic volcanism along the IBM arc is proposed by Macpherson & Hall (2001). These authors observe that regional uplift, ocean island basalt-style magmatism and high heat flow characterized the northern part of the Philippine Sea Plate in middle Eocene times. They also notice that the reconstructed middle Eocene location of the IBM arc and West Philippine Basin lies close to the present location of the Manus Basin, where there is evidence for the existence of a mantle plume. They therefore speculate that middle Eocene magmatism along the IBM arc developed its particular character because subduction was initiated above a mantle plume. The thermal anomaly in the mantle in the subduction zone would have provided the extra heat necessary to melt highly depleted mantle to form boninitic magmas along the volcanic arc. The OIB-like lavas that were recovered from the West Philippine Basin, and the uplift of the Amami–Oki–Daito province would also be due to the presence of the same mantle plume.

Geodynamic setting of the Philippine Sea Plate at the epoch of boninite formation: reconstruction

Any model of boninite genesis requires a good knowledge of the geodynamics of the Philippine Sea Plate during their emplacement. As the Parece–Vela and Shikoku basins started to open at *c.* 30 Ma (Okino *et al.* 1998), i.e. after the end of boninitic magmatism (Cosca *et al.* 1998), we focus on the Palaeogene history of the West Philippine Basin that was forming the Philippine Sea Plate at the time of boninitic volcanism. Deschamps *et al.* (1999, 2002), Fujioka *et al.* (1999) and Okino *et al.* (1999) studied the spreading mechanisms within the West Philippine Basin based on new data such as high-resolution bathymetry, magnetism and gravity, and on new radiometric dating on rocks recovered from the basin. Deschamps & Lallemand (2002) reconstructed the tectonic history of the Philippine Sea Plate between 54 and 30 Ma. We integrated results of these studies, as well as all available data within the region, such as geochronological and geochemical data, tectonic events and plate movements along the basin margins, and palaeomagnetic data from the basin and its surroundings.

We present in Figure 5 the reconstructed Philippine Sea Plate from early middle Eocene to late Eocene time, i.e. the time when most boninitic lavas were emplaced along the proto-IBM arc. The global model, and data used to establish it, are discussed in Deschamps (2001) and Deschamps & Lallemand (2002). Here we

Fig. 5. Evolutionary model from the Philippine Sea Plate between 55 and 34-35 Ma. The movement of the plate is constrained by palaeomagnetic data acquired in the West Philippine Basin, and from its northern and southern margins. The plate was restored every 5 Ma by successive rotations on a sphere that is tangential to the WGS84 ellipsoid (Deschamps 2001; Deschamps & Lallemand 2003). The Benham mantle plume is supposed to have remained fixed with respect to the mantle frame. Tholeiitic and boninitic volcanic events are reported, after Shikoku, Parece–Vela and Mariana basins are 'closed' perpendicularly to the spreading fabric and magnetic lineations, and parallel to the fracture zones (see Fig. 1).

focus on the Philippine Sea Plate itself and on evidence for arc and mid-ocean ridge lava eruption within the plate, in order to constrain the geodynamic setting of boninite eruption. In order to determine the location of the different parts of the proto-IBM arc before the opening of the Shikoku and Parece–Vela basins at 30 Ma (Okino *et al.* 1998) and of the Mariana Basin after 6 Ma (Hussong & Uyeda 1981), we have 'closed' these basins perpendicularly to the magnetic anomalies (when available) and to the spreading fabric (Shikoku and Parece–Vela basins: Chamot-Rooke *et al.* 1987; Okino *et al.* 1998; Sumisu Rift: Taylor 1992; Mariana Basin: Martinez *et al.* 1995; unpublished data of JAMSTEC and Kobe University) (Fig. 1).

At *c.* 50 Ma (Fig. 5), an efficient spreading system is established in the West Philippine Basin. The basin is characterized by the presence of two spreading axes. The driving force for its opening is provided by slab rollback along the two surrounding subduction zones. A mantle plume is active in the northernmost part of the basin. Its activity is responsible for the eruption of OIB-like lavas at sites 446 (Minami–Daito Basin) and 294/5 (northern West Philippine Basin) (Hickey-Vargas 1991, 1998; Macpherson & Hall 2001). The OIB-like lavas that erupted a few millions years later at Site 292 (Benham Rise) are probably also due to the same plume. Similarly enriched MORB (E-MORB) lavas found at Site 291 are interpreted to result from mixing of OIB and N-MORB sources. There are no age data for normal MORB (N-MORB)-like lavas recovered at DSDP Site 1201 (Shipboard Scientific Party 2001) or at dredge site D12 (Bloomer & Fisher 1988), but their locations in the northern and southwesternmost part of the basin, respectively, suggest that they erupted at about 50 Ma, according to the reconstruction (Deschamps & Lallemand 2002). Petrological and geochemical analyses of these samples demonstrate that their area of emplacement was not influenced by the mantle plume. Arc volcanism occurred along the northern part of the Palau–Kyushu Ridge after *c.* 51 Ma, possibly *c.* 55 Ma (see Table 1, Fig. 4). Boninitic or boninitic-like lavas of this age occur at sites 786 and 782, and in the Bonin Islands, but there is no evidence for arc volcanism along the southern part of the proto-Palau–Kyushu Ridge. Relative movement between the Philippine Sea Plate and the Pacific Plate, as well as the orientation of the proto-Palau–Kyushu Ridge, indicate that strike-slip movement was occurring along this boundary, accommodating the opening of the West Philippine Basin. It is very possible that a small amount of opening occurred within the Minami–Daito Basin in the early Middle Eocene, as indicated by ages of rocks at Site 446. We, unfortunately, lack reliable constraints about the opening of this basin.

At *c.* 46 Ma (Fig. 5), the transform fault separating the Philippine Sea Plate and the Pacific Plate still accommodated the opening of the West Philippine Basin at an intermediate spreading rate (Hilde & Lee 1984; Deschamps 2001). N-MORB lavas erupted at Site 447 located in the eastern part of the basin, and also possibly in its westernmost part. Some 46 Ma N-MORB lavas occur within the Coto Block of the Zambales ophiolite (Fuller *et al.* 1989), which is shown to be an autochthonous part of the Philippine Archipelago by Encarnacion *et al.* (1999). In the vicinity of the Benham Plateau, abundant volcanism occurs at the spreading axis due to the presence of the active mantle plume interacting with the spreading system. This is confirmed by eruption of OIB-like lavas at Site 292. In our reconstruction, the position of the mantle plume is fixed. Its size is constrained by: (1) the extent of volcanic plateaux in the West Philippine Basin; and (2) a constant size of the area where OIB-like and E-MORB lavas are found.

At *c.* 43–44 Ma (Fig. 5) a westward subduction zone initiated along the transform fault bounding the West Philippine Basin to the east, as shown by the onset of arc volcanism along the central and southern parts of the proto-Palau–Kyushu Ridge (Table 2, Fig. 4). This event likely correlates with a change of the Pacific Plate motion somewhere between 47 and 43 Ma, or simply to the progressive reorientation of the transform fault along the proto-Palau–Kyushu Ridge, due to the clockwise rotation of the Philippine Sea Plate. At this time, boninites erupted at sites 458, MD28, and on Saipan and Guam. Boninitic lavas of the same age are also found in the Zambales ophiolite. The spreading rate in the West Philippine Basin started to decrease significantly (Hilde & Lee 1984; Deschamps 2001).

The *c.* 40 Ma (Fig. 5) period marks the end of the main boninitic volcanic phase. Boninitic lavas were still erupting at Site 458, and possibly at sites 786 and 782. Tholeiitic arc volcanism occurs along the whole Palau–Kyushu Ridge. The mantle plume was still active beneath the Benham Rise in the western part of the West Philippine Basin, as shown by dating on OIB-like rocks from Site 292. The relief of the Benham Rise is almost fully developed at this epoch as the southern part of the Philippine Sea Plate remains stable above the mantle plume. This stability is due to the cessation of northward subduction along the proto-Philippine

Trench, and consequently, of the southwestward roll back that partly let the West Philippine Basin open after the early Eocene (Deschamps & Lallemand 2002).

At *c.* 34/35 Ma (Fig. 5) spreading rate in the West Philippine Basin continued to decrease. OIB-like lavas were still erupting in the vicinity of the Benham Rise, demonstrating the presence of the active mantle plume in this area. Rifting started in the Caroline Sea at *c.* 34 Ma (Hegarty & Wessel 1988). Hegarty & Wessel (1988) suggest that an active mantle plume was present under the basin at that time, and interacted with the spreading system, being responsible for important excess volcanism during spreading. Boninitic or boninitic-like lavas erupted at several places along the Palau–Kyushu Ridge (at least at sites 786/782, 458/459 and at Bonin and Guam islands). They are found as sills and dykes intruding former volcanic formations. However, the main volcanic products at this epoch are normal island arc lavas, such as tholeiites, andesites and dacites. Adakitic lavas erupted in Catanduanes Island, probably due to the onset of subduction of the young and hot lithosphere of the West Philippine Basin along the east Luzon Trough.

Inconsistencies between proposed models for boninites formation and the Cenozoic geodynamic setting of the Philippine Sea Plate

Our reconstruction shown in the previous section is generally incompatible with the existing models of boninite generation.

- The model of formation of boninitic lavas by subduction of a very young plate beneath the Philippine Sea Plate fails for several reasons: (i) The hypothesis implies that the new subduction zone was initiated close to an active spreading centre located on the subducting plate, and that very young and buoyant crust was the first crust to enter the trench over its entire length (Macpherson & Hall 2001). The formation of IBM boninites due to the subduction of an active spreading axis would thus require that the axis was almost parallel to the proto-IBM trench over a 700 km length, or even 2000 km according to Macpherson & Hall (2001), which is not very plausible. (ii) Kinematic reconstruction (Deschamps & Lallemand 2002) shows that, shortly after initiation of subduction along the proto-Palau–Kyushu Ridge (i.e. IBM arc), northward slab rollback was the main driving force for the opening of the West Philippine Basin between 54 and 33–30 Ma. It is now widely accepted that such a strong trench retreat cannot occur if the subducting crust is very young and, hence, buoyant. The subduction of a young plate and of its active spreading centre would therefore prevent the important trench rollback that is necessary to allow the basin to: (a) open since Early Eocene times; (b) migrate northward as indicated by palaeomagnetic data (e.g. Louden 1976, 1977; Haston & Fuller 1991; Haston *et al.* 1992; Koyama *et al.* 1992; Hall *et al.* 1995; Shipboard Scientific Party 2001); and (c) maintain a significant amount of convergence along the northern margin of the Philippine Sea Plate. Kinematic models (Deschamps 2001; Hall 2001, 2002; Deschamps & Lallemand 2003) show that the West Philippine Basin was surrounded by two subduction zones at the onset of its (rapid) opening, one being located along the Philippine arc and the other along the proto-IBM arc. The opening of the West Philippine Basin is essentially due to the northeastward migration of the proto-IBM trench. This strong rollback of the subducting slab probably requires the subduction of old lithosphere.

  The tectonic setting of the Izu–Bonin–Mariana system in the Eocene appears, therefore, to preclude Tertiary subduction of an active spreading centre on the Pacific Plate along the proto-Palau–Kyushu Ridge, suggesting that another mechanism is required to explain the generation of boninitic magmas.
- The hypothesis of genesis of boninites proposed by Stern & Bloomer (1992) does not account for the necessity of a high heat flow at the time of generation of the boninitic magmas. Secondly, according to this model, boninites would be expected at every subduction zone that is initiated at a boundary between plates of different ages. At present we do not have such evidence. Thirdly, the episode of boninite formation should be short in time (a few million years), but dating shows that it lasted for at least 14 Ma.
- Concerning the hypothesis of formation of boninitic lavas due to the presence of a mantle plume near the proto-IBM arc (Macpherson & Hall 2001), it can explain the formation of the first boninitic lavas erupted along the northern part of the IBM arc before *c.* 48 Ma. However, it fails to explain the genesis of younger boninitic lavas along the arc. As a matter of fact, the Amami–Oki–Daito region located in the northern part of the Philippine

Sea Plate was influenced by a mantle plume in Middle Eocene times (Hickey-Vargas 1991, 1998; Macpherson & Hall 2001) (Fig. 5). This is supported by geochemical analyses of rocks and by the shallow bathymetry of this region at this epoch. Concerning the West Philippine Basin itself, OIB-like lavas were described only in its northern and western parts. At *c.* 50 Ma, OIB-like lavas erupted only in the northern Philippine Sea Plate and the 46 Ma reconstruction clearly shows that the area influenced by the mantle plume is restricted to the western part of the plate (Fig. 5). This is demonstrated by: (i) the occurrence of typical N-MORB lavas in the eastern part of the basin; and (ii) the greater depth of the eastern part of the basin, contrasting with the much shallower western part. Moreover, detailed studies of the spreading mechanisms within the basin (Deschamps 2001; Deschamps & Lallemand 2002) show that the spreading system has been strongly disorganized in the western part of the basin due to the presence of an active hot spot during spreading, whereas its eastern part has been formed by normal seafloor spreading. We therefore suggest that an active mantle plume was present beneath the West Philippine Basin in middle Eocene times, but its influence was restricted to the northern part at *c.* 50 Ma, and then to the western part of the basin at *c.* 46 Ma and later. From the bathymetry and the distribution of different types of lavas, we propose that the zone of influence of the mantle plume was at most *c.* 500 km in diameter. An important consequence of this observation is that the boninitic volcanism that occurred after 48 Ma along the proto-IBM arc cannot be explained by the presence of a mantle plume interacting with the subduction zone (Fig. 5).

We have shown that the formation of boninites along the proto-IBM arc can be explained neither by the subduction of a very young and hot plate, nor by the nucleation of subduction along a transform boundary. It can be explained by the presence of a mantle plume in the vicinity of the subduction zone along the proto-IBM arc, but only in early middle Eocene times. We thus need to propose an alternative mechanism explaining the occurrence of boninitic lavas along the IBM arc after 48 Ma.

Geodynamic setting of boninites lavas

From our reconstruction, boninites observed in the Bonin Islands were generated near the termination of a volcanic arc, at the transition between a subduction zone and a transform fault (Fig. 5). As represented in our reconstruction, it is very possible that a spreading centre was active in the Minami–Daito Basin near the subduction–transform transition, at the time of boninite formation. This tectonic context appears to be similar to the setting of boninites from North Tonga and the southern New Hebrides (Figs 2, 3). The high heat flow that is necessary for the genesis of boninites may thus have been provided by the hot mantle upwelling beneath the spreading axis, and also by the active mantle plume in the northernmost part of the basin during early middle Eocene times. A slab window that formed due to the subduction–transform transition probably allowed hot mantle material to flow around the exposed edge of the subducting plate. Boninites found in the Zambales ophiolite are shown by our model to be formed by a similar mechanism. Reconstruction at *c.* 43–46 Ma (time of the boninitic episode) indeed shows that this region was at western termination of the Philippine arc, at the transition between the related subduction and a transform boundary. The eruptions of boninites at sites 458 and MD28, and Guam and Saipan in middle Eocene times are most probably due to incipient subduction along the transform plate boundary (along the proto-Palau–Kyushu Ridge) in the vicinity of a well-established spreading centre that connects at about a right angle with the subduction zone. In this case, the hot mantle upwelling beneath the spreading axis provided high heat flow. Boninites that erupted at *c.* 40 Ma near Site 458 would also have formed due to the interaction between the hot mantle feeding the active spreading centre and the subduction zone. Boninites erupted at sites 782 and 786 at *c.* 50 Ma would have originated due to the presence of a mantle plume in the vicinity of the subduction zone bounding the northern Philippine Sea Plate. Concerning boninites that were emplaced at the same location in the middle Eocene, it is possible that these are due to the interaction between hot mantle feeding a minor spreading axis in the Kita–Daito Basin and the same subduction zone. This hypothesis cannot be easily verified because of a diversity of age determination in the Amami–Oki–Daito region and the lack of reliable data. The occurrence of a minor episode of boninitic volcanism along the Palau–Kyushu Ridge at *c.* 34–35 Ma is still problematic. These boninites are observed as sills and dykes that intrude older volcanic sequences. However, our reconstruction at this epoch does not show any particularity in tectonic setting that can explain the occurrence of

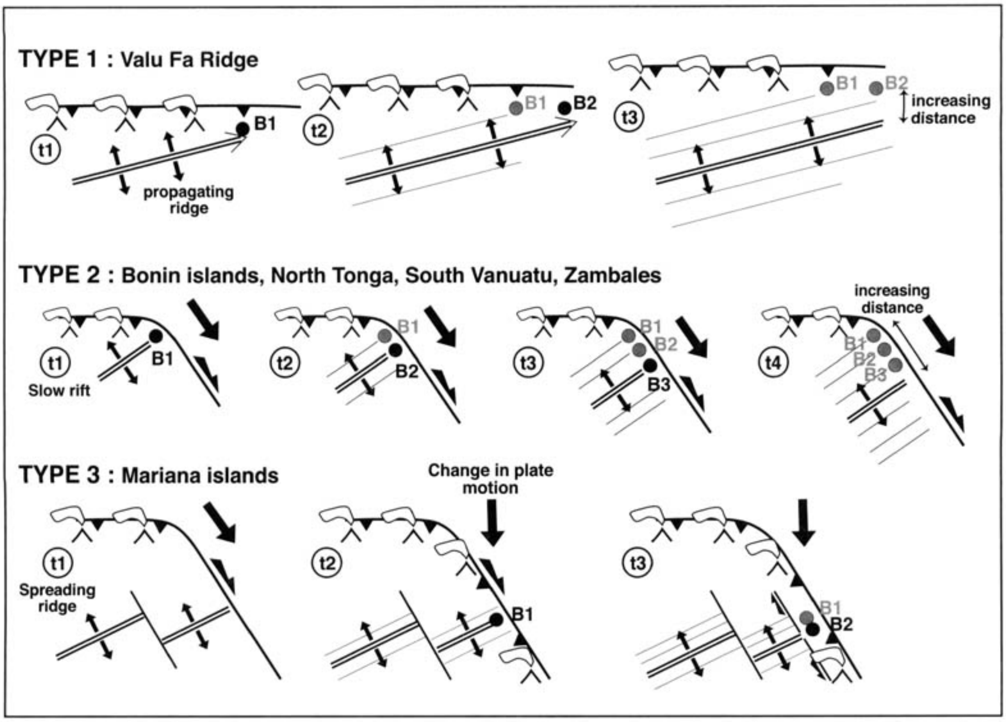

Fig. 6. Definition of three types of settings that favour the genesis of boninites lavas, without requiring the influence of a mantle plume. Black circles indicate location of possible boninite eruptions. Type 1 setting is most likely to favour the genesis of boninites along the central part of the Tofua arc. Type 2 setting is probably responsible for the production of boninitic lavas in the Bonin Islands, in the northern termination of the Tofua arc, in the southern termination of the Central Spreading Ridge in the North Fiji Basin and, perhaps, in the Zambales ophiolite. Similar settings are reported from the northern and southern margins of the Caribbean Plate, and near the southern termination of the Andaman Sea spreading ridge. We could thus expect to find boninitic lavas at these locations. Type 3 setting is probably the most unusual one, as this has probably operated for a limited length of time. It is likely to explain the genesis of boninites in the Mariana Islands.

these boninites. Incipient rifting in the Parece–Vela and Shikoku basins could explain the occurrence of such lavas, because of a possible mantle upwelling beneath the rift. Such a mechanism could be the origin of a short and minor episode of boninite formation, as suggested by Meffre *et al.* (1996) and Piercey *et al.* (2001). However, rifting in the eastern basins of the Philippine Sea Plate started at *c.* 30 Ma (Okino *et al.* 1998), which is not compatible with slightly older ages of boninitic lavas. From K/Ar and Ar/Ar dating, Cosca *et al.* (1998) seem to confirm the existence of such an episode at the southern part of the IBM arc at *c.* 35 Ma, but are unable to confirm it in its northern part, at sites 786 and 782. More information is, therefore, necessary about the existence and age of this second boninitic volcanic episode in order to determine its causes.

Discussion

The study of the Cenozoic tectonic setting of IBM arc boninite genesis in light of modern geodynamic contexts in Tonga and Fiji regions has led us to define three types of settings that favour the genesis of boninitic lavas, none of which require the influence of a mantle plume in the region (Fig. 6). In all three settings, the activity of a back-arc spreading centre is a key element for formation of boninites.

Type 1 (Fig. 6)

Most back-arc rifts and spreading centres propagate at a low angle (subparallel) to the associated volcanic arcs. The Valu Fa Ridge in the southern part of the Lau Basin is a typical example of a back-arc spreading system slightly oblique and close to the volcanic arc. It is propagating toward the arc from north to south. Boninites could erupt for a short period when the spreading axis is very close to the active arc. While the basin is opening, the spreading axis moves away from the arc and no more boninitic melts will be formed. However, if the tip of the spreading centre still propagates to the south, one may expect that the same favourable context will also propagate to the south. Similarly, further back in time, the same situation should have occurred more to the north, but no dredging or sampling is available to confirm this hypothesis. Many back-arc basins (Sumisu rift, Mariana Trough, Okinawa Trough, Havre Trough) begin to form along volcanic arcs, as attested by the presence of remnant arcs. Conversely, no boninites were found in these basins. One explanation is that boninites erupted during the rifting phase and were then buried shortly after their emplacement beneath N-MORB basalts when spreading starts. An alternative solution is that rifting conditions (for example, temperatures) are not compatible with boninite generation. One may observe that the Valu Fa Ridge already has the characteristics of a well-developed spreading centre with high heat flow.

Type 2 (Figs 3 and 6)

A favourable context for longer periods of boninite eruption is an intersection at a high angle between an active spreading centre and the transition between a subduction zone and a transform. There are a few examples of ridge segments almost perpendicular with arcs (Andaman Sea, Cayman Trough), all caused by a high obliquity in convergence. In these cases, short ridge segments are offset by long fracture zones more or less parallel to the arc. In other words, when a back-arc spreading ridge intersects a plate boundary, it is likely to be a transform fault, like in northern Tonga, southern New Hebrides or Scotia Sea, and rarely a subduction zone, or if it is, spreading segments are short indicating highly oblique plate convergence. In any case, spreading cannot occur in the forearc domain because the mantle wedge is absent. The subducting plate, indeed, cools the front of the overriding plate. Besides, no modern example of forearc spreading has been yet reported. Interestingly, nature offers us two modern examples where back-arc spreading ridges intersect the transition zone between subduction and strike-slip. At these transitions, the slab edge dips less than the rest of the slab and thus arc volcanism associated with boninite eruptions could occur during a significant amount of time as in northern Tonga (Millen & Hamburger 1998). We believe that a similar context occurred at the elbow along the Palau–Kyushu Ridge that coincides with the Bonin Islands after closure of the Shikoku Basin. We propose that subduction occurred along the palaeo-Izu–Bonin trench, whereas strike-slip occurred along the palaeo-Mariana segment between 55 and 47 Ma. We assume that a slow rift was active over a long period near the Palau–Kyushu Ridge elbow. There is evidence for a plume in this region at that time (Hickey-Vargas 1991, 1998; Macpherson & Hall 2001) that could have triggered either the generation of boninites by itself or by feeding such slow rifts. According to our reconstructions, the Zambales boninites were also in the same geodynamic context of subduction to strike-slip transition at the time of their emplacement (44–46 Ma).

Type 3 (Fig. 6)

Since 47 Ma, the main spreading centre of the West Philippine Basin was far from any subduction zone and intersected a major transform zone that evolved into a subduction zone between 47 and 43 Ma, according to volcanic records (Hussong & Uyeda 1981; Seno & Maruyama 1984; Stern & Bloomer 1992; Taylor 1992; Bloomer *et al.* 1995) and changes in Pacific Plate kinematics (e.g. Engebretson *et al.* 1985; Clague & Dalrymple 1989; Norton 1995; Rowley 1996; Gordon 2000; Hall 2002). Over a short period, boninites erupted near the edge of the spreading centre that formerly intersected the transform zone, which was progressively inactivated by incipient subduction of the Pacific Plate. When subduction started along the Mariana Trench, the spreading rate in the West Philippine Basin suddenly decreased from 4.5 to 2 cm a^{-1} (Hilde & Lee 1984; Deschamps 2001; Deschamps & Lallemand 2002). The transform motion required by the generation of oceanic crust on both sides of the spreading ridge of the West Philippine Basin was probably accommodated behind of the volcanic arc. Genesis of boninites in this type of setting is helped by migration of asthenosphere over the subsiding lithosphere, which would entail adiabatic decompression, and also by the presence of water released from the subducted lithosphere and sediments at a depth of 40 km (Peacock 1990; Stern & Bloomer 1992). The source of extra heat flow is provided by the nearby asthenospheric flow beneath the active spreading ridge in the forming upper plate.

Conclusions

Geodynamic models of the Philippine Sea Plate in Eocene times help us to define the tectonic setting of the Izu–Bonin–Mariana boninite genesis. It appears that in the early Eocene, the interaction between a subduction zone and a mantle plume could have contributed to the formation of boninitic lavas along the northern part of the IBM arc. However, our model clearly shows that the subduction zone along the arc was beyond the influence of this mantle plume since the middle Eocene. The genesis of boninites in the Bonin Islands at this time is thus rather due to the intersection at high angle between an active spreading centre and a subduction–transform fault transition. Modern examples of boninite tectonic settings show that the intersection between an active spreading axis and such a plate boundary is a context favourable to the genesis of boninites. The high heat flow associated with the upwelling of hot asthenospheric mantle beneath the spreading axis probably provides the extra heat that is necessary for the melting of a very depleted mantle, and the dehydration of the subducting slab provides fluids that help melting. The occurrence of a slab window at the location of the tear also probably favours upward asthenospheric flow around the exposed edge of the subducting plate, and hence high heat flow. Synchronous eruption of boninitic lavas within the Zambales ophiolites (Luzon) is likely to be due to a similar mechanism. The boninites that erupted along the central part of the IBM arc in the middle Eocene are probably formed due to the interaction between the active spreading centre of the West Philippine Basin and the transform fault that has accommodated the basin opening, and which was reconverted into a subduction zone at this time.

Finally, the study of the Cenozoic setting of the IBM arc boninites, considered in light of modern geodynamic contexts in the Tonga and Fiji regions, has led us to define three tectonic settings that favour the formation of boninitic lavas in back-arc basins, without requiring the influence of the mantle plume. The first setting is the propagation at a low angle of a spreading centre toward its associated volcanic arc. The second is the intersection at a high angle between an active spreading centre and the transition from subduction to a transform fault, which means the intersection between an active axis and the termination of an active volcanic arc. The third is the intersection at a high angle between an active spreading centre and a subduction zone. This last case of boninitic volcanism should be quite rare, as such a tectonic setting is probably limited in time. The definition of these three tectonic settings that favour the formation of boninitic lavas implies that such volcanic products should be found each time that an active spreading axis closely interacts with an active volcanic arc, or its termination near a transform boundary. We can then expect to find boninites at the southern termination of the Mariana Basin, where the active spreading axis approaches the southern termination of the active Mariana Arc. In the same way, boninites could be found along the border of the Andaman Sea, where the central valley (or Central Andaman Trough) approaches at a high angle to the active Andaman arc near the Nicobar Islands. The Caribbean–South America plate boundary could also be a context favourable to the genesis of boninites, at the southern termination of the Granada back-arc basin where the Lesser Antilles arc swings into a transform boundary. For same reasons, boninites could also occur at the northern end of the same arc, near the Virgin Islands.

We thank Y. Tatsumi and Y. Tamura for valuable discussions about conditions of boninitic lavas genesis. This contribution has been improved by constructive reviews by R. Taylor and J. Bédard. Some maps were made using Wessel & Smith (1995) G.M.T. 3.1 software. Smith & Sandwell's (1997) satellite-derived bathymetric data were used to draw some maps.

References

BALLANTYNE, P. 1991. Petrological constraints upon the provenance and genesis of the East Halmahera ophiolite. *In:* HALL, R., NICHOLS, G.J. & RANGIN, C. (eds) *Orogenesis in Action, Tectonics and Processes at the West Equatorial Pacific Margin. Journal of Southeast Asian Earth Sciences*, **6**, 259–270.

BÉDARD, J.H. 1999. Petrogenesis of boninites from the Betts Cove ophiolite, Newfoundland, Canada: identification of subducted source components. *Journal of Petrology*, **40**, 1853–1885.

BÉDARD, J.H., LAUZIÈRE, K., TREMBLAY, A. & SANGSTER, A. 1998. Evidence for forearc seafloor-spreading from the Betts Cove ophiolite, Newfoundland: oceanic crust of boninitic affinity. *Tectonophysics*, **284**, 233–245.

BLOOMER, S.H. & FISHER, R.L. 1988. Arc volcanic rocks characterize the landward slope of the Philippine Trench off northeastern Mindanao. *Journal of Geophysical Research*, **13**, 11 961–11 973.

BLOOMER, S.H., TAYLOR, B., MACLEOD, C.J., STERN, R.J., FRYER, P., HAWKINS, J.W. & JOHNSON, L. 1995. Early arc volcanism and the ophiolite problem: a perspective from drilling in the western Pacific. *In:*

TAYLOR, B. & NATLAND, J. (eds) *Active Margins and Marginal Basins of the Western Pacific*. American Geophysical Union Monographs, **88**, 1–30.

BOESPFLUG, X., DOSSO, L., BOUGAULT, H. & JORON, J.-L. 1990. Trace element and isotopic (Sr and Nd) geochemistry of volcanic rocks from the Lau Basin. *Geologisches Jahrbuch, (Reihe D)*, **92**, 503–516.

BOUGAULT, H., MAURY, R.C., AZZOUZI, M.E.R., JORON, J.-L., COTTEN, J. & TREUIL, M. 1981. Tholeiites, basaltic andesites and andesites from Leg 60 sites: geochemistry, mineralogy and low partition coefficient elements. *In*: HUSSONG, D.M., UYEDA, S. *et al. Initial Reports of the Deep Sea Drilling Project*, **60**, 657–678.

CHAMOT-ROOKE, N., RENARD, V. & LE PICHON, X. 1987. Magnetic anomalies in the Shikoku Basin: a new interpretation. *Earth and Planetary Science Letters*, **83**, 214–228.

CLAGUE, D.A. & DALRYMPLE, G.B. 1989. Tectonics, geochronology, and origin of the Hawaiian-Emperor volcanic chain. *In*: WINTERER, E.L., HUSSONG, D.M. & DECKER, R.W. (eds) *The Geology of North America, Vol. N, The Eastern Pacific Ocean and Hawaii*. Geological Society of America, Boulder, Colorado, 188–217.

COISH, R.A., HICKEY, R. & FREY, F.A. 1982. Rare earth element geochemistry of the Betts Cove ophiolite, Newfoundland: complexities in ophiolite formation. *Geochimica et Cosmochimica Acta*, **46**, 2117–2134.

COSCA, M.A., ARCULUS, R.J., PEARCE, J.A. & MITCHELL, J.G. 1998. $^{40}Ar/^{39}Ar$ and K–Ar geochronological age constraints for the inception and early evolution of the Izu–Bonin–Mariana arc system. *The Island Arc*, **7**, 579–595.

CRAWFORD, A.J. & CAMERON, W.E. 1985. Petrology and geochemistry of Cambrian boninites and low-Ti andesites from Heathcote, Victoria. *Contributions to Mineralogy and Petrology*, **91**, 93–104.

CRAWFORD, A.J., BECCALUVA, L. & SERRI, G. 1981. Tectono-magmatic evolution of the West Philippine-Mariana region and the origin of boninites. *Earth and Planetary Science Letters*, **54**, 346–356.

CRAWFORD, A.J., FALLOON, T.J. & GREEN, D.H. 1989. Classification, petrogenesis and tectonic setting of boninites. *In:* CRAWFORD, A.J. (ed.) *Boninites and Related Rocks*. Unwin Hyman, London, 1–49.

DANYUSHEVSKY, L.V. & SOBOLEV, A.V. 1987. New data on the petrology of boninites in Tonga. *Akademii Nauk USSR, Geology and Geophysics*, **12**, 100–103.

DANYUSHEVSKY, L.V., SOBOLEV, A.V. & FALLOON, T.J. 1995. North Tongan high-Ca boninite petrogenesis; the role of Samoan plume and subduction–transform fault transition. *Journal of Geodynamics*, **20**, 219–241.

DESCHAMPS, A. 2001. *Contribution à l'étude du Bassin Ouest Philippin: nouvelles données sur la bordure Ouest et la dorsale fossile*. PhD thesis, University of Montpellier 2.

DESCHAMPS, A. & LALLEMAND, S. 2002. The West Philippine Basin: a Paleocene–Oligocene back-arc basin opened between two opposed subduction zones. *Journal of Geophysical Research,* **107** (12)2322, 10.1029/2001 JB001706.

DESCHAMPS, A., LALLEMAND, S.E. & DOMINGEZ, S. 1999. The last spreading episode of the West Philippine Basin revisited. *Geophysical Research Letters*, **26**, 2073–2076.

DESCHAMPS, A., OKINO, K. & FUJIOKA, K. 2002. Late amagmatic extension along the central and eastern segments of the West Philippine Basin spreading axis. *Earth and Planetary Science Letters*, **203**, 277–293.

DIETRICH, V., EMMERMANN, R., OBERHAENSLI, R. & PUCHELT, H. 1978. Geochemistry of basaltic and gabbroic rocks from the West Mariana Basin and the Mariana Trench. *Earth and Planetary Science Letters*, **39**, 127–144.

DOBSON, P.F. 1986. *The petrogenesis of boninite: a field, petrologic and geochemical study of the volcanic rocks of Chichi-jima, Bonin Islands, Japan*. PhD thesis, Stanford University.

EISSEN, J-P., CRAWFORD, A.J., COTTEN, J., MEFFRE, S., BELLON, H. & DELAUNE, M. 1998. Geochemistry and tectonic significance of basalts in the Poya Terrane, New Caledonia. *Tectonophysics*, **284**, 203–219.

ENCARNACION, J., MUKASA, S.B. & EVANS, C.A. 1999. Subduction components and the generation of arc-like melts in the Zambales ophiolite, Philippines: Pb, Sr and Nd isotopic constraints. *Chemical Geology*, **156**, 343–357.

ENGEBRETSON, D.C., COX, A. & GORDON, R.G. 1985. *Relative motions between oceanic and continental plates in the Pacific Basin*. Geological Society of America, Special Papers, **206**.

FALLOON, T.J. & CRAWFORD, A.J. 1991. The petrogenesis of high calcium boninite lavas from the northern Tonga ridge. *Earth and Planetary Science Letters*, **102**, 375–394.

FALLOON, T.J., DANYUSHEVSKY, L.V. 2000. Melting of refractory mantle at 1.5, 2 and 2.5 GPa under anhydrous and H_2O undersaturated conditions: implications for the petrogenesis of high-Ca boninites and the influence of subduction components on mantle melting. *Journal of Petrology*, **41**, 257–283.

FALLOON, T.J., GREEN, D.H. & MCCULLOCH, M.T. 1989. Petrogenesis of high-Mg and associated lavas from the North Tonga Trench. *In:* CRAWFORD, A.J. (ed.) *Boninites and Related Rocks*. Unwin Hyman, London, 357–395.

FOUQUET, Y., VON STACKELBERG, U, CHARLOU, J.L., DONVAL, J.P., ERZINGER, J., FOUCHER, J.P., HERZIG, P.H., MÜHE, R., SOAKAI, S., WIEDICKE, M. & WHITECHURCH, H. 1991. Hydrothermal activity and metallogenesis in the Lau back-arc basin. *Nature*, **349**, 778–781.

FRENZEL, G., MÜHE, R. & STOFFERS, P. 1990. Petrology of the volcanic rocks from the Lau Basin, southwest Pacific. *Geologisches Jahrbuch*, **92**, 395–479.

FUJIOKA, K., OKINO, K., KANAMATSU, T., OHARA, Y., ISHISUKA, O., HARAGUCHI, S. & ISHII, T. 1999. Enigmatic extinct spreading center in the West Philippine backarc basin unveiled. *Geology*, **27**, 1135–1138.

FULLER, M., HASTON, R. & ALMASCO, J. 1989. Paleomagnetism of the Zambales ophiolite, Luzon, northern Philippines. *Tectonophysics*, **168**, 171–203.

GORDON, R.G. 2000. Plate tectonics – the Antarctic connection. *Nature*, **404**, 139–140.

HALL, R. 1998. The plate tectonics of Cenozoic SE Asia and the distribution of land and sea. *In*: HALL, R.D. & HOLLOWAY, J.D. (eds) *Biogeography and Geological Evolution of SE Asia*. Backhuys, Leide, 99–131.

HALL, R. 2001. Cenozoic reconstructions of SE Asia and the SW Pacific: changing patterns of land and sea. *In*: MATCALFE, I., SMITH, J.M.B., MORWOOD, M. & DAVIDSON, I.D. (eds) *Faunal and Floral Migrations and Evolution of SE Asia-Australia*. Swets and Zeitlinger, Lisse, 35–56.

HALL, R. 2002. Cenozoic geological and plate tectonic evolution of SE Asia and the SW Pacific: computer-based reconstructions, model and animations. *Journal of Asian Earth Sciences*, **20**, 353–431.

HALL, R., ALI, J.R., ANDERSON, C.D. & BAKER, S.J. 1995.Origin and motion history of the Philippine Sea Plate. *Tectonophysics*, **251**, 229–250.

HASTON, R.B. & FULLER, M. 1991. Paleomagnetic data from the Philippine Sea plate and their tectonic significance. *Journal of Geophysical Research*, **96**, 6073–6098.

HASTON, R.B., STOKKING, L.B. & ALI, J. 1992. Paleomagnetic data from Holes 782A, 784A, and 786A, Leg 125. *In*: FRYER, P., COLEMAN, P., PEARCE, J.A. & STOKKING, L.B. *Proceedings of the Ocean Drilling Program, Scientific Results*, **125**, 535–545.

HAWKINS, J.W. 1994. Petrologic synthesis, ODP Leg 135: Lau Basin transect. *In*: HAWKINS, J., PARSON, L., ALLAN, J. *et al. Proceedings of Ocean Drilling Program, Scientific Results*, **135**, 879–908.

HAWKINS, J.W. & CASTILLO, P.R. 1998. Early history of the Izu–Bonin–Mariana arc system: evidence from Belau and the Palau Trench. *The Island Arc*, **7**, 559–578.

HEGARTY, K.A. & WEISSEL, J.K. 1988. Complexities in the development of the Caroline Plate region, western equatorial Pacific. *In*: NAIRN, A.E.M., STEHLI, F.G. & UYEDA, S. (eds) *The Ocean Basins and Margins*. Plenum Press, New York, 277–301.

HICKEY, R.L. & FREY, F.A. 1982. Geochemical characteristics of boninite series volcanics: implications for their source. *Geochimica et Cosmochimica Acta*, **46**, 2099–2115.

HICKEY-VARGAS, R. 1989. Boninites and tholeiites from DSDP Site 458, Mariana forearc. *In*: CRAWFORD, A.J. (ed) *Boninites and Related Rocks*. Unwin Hyman, London, 339–356.

HICKEY-VARGAS, R. 1991. Isotope characteristics of submarine lavas from the Philippine Sea: implications for the origin of arc and basin magmas of the Philippine tectonic plate. *Earth and Planetary Science Letters*, **107**, 290–304.

HICKEY-VARGAS, R. 1998. Origin of the Indian Ocean-type isotopic signature in basalts from Philippine Sea plate spreading centers: an assessment of local versus large-scale processes. *Journal of Geophysical Research*, **103**, 20 963–20 979.

HICKEY-VARGAS, R. & REAGAN, M.K. 1987. Temporal variation of isotope and rare earth element abundances in volcanic rocks from Guam: implications for the evolution of the Mariana arc. *Contributions to Mineralogy and Petrology*, **97**, 497–508.

Hilde, T.W.C. & Lee, C.S. 1984. Origin and evolution of the West Philippine Basin: a new interpretation. *Tectonophysics*, **102**, 85–104.

HUSSONG, D. & UYEDA, S. 1981. Tectonic processes and the history of the Mariana arc: a synthesis of the results of Deep Sea Drilling Project Leg 60. *In*: HUSSONG, D.M., UYEDA S. *et al. Initial Reports of the Deep Sea Drilling Project*, **60**, 909–929.

JENNER, G.A., CAWOOD, P.A., RAUTENSCHLEIN, M. & WHITE, W.M. 1987. Composition of back-arc basin volcanics, Valu Fa Ridge, Lau Basin: evidence for a slab-derived component in their mantle source. *Journal of Volcanology and Geothermal Research*, **32**, 209–222.

KAMENETSKY, V.S., CRAWFORD, A.J., EGGINS, S. & MÜHE, R. 1997. Phenocryst and melt inclusion chemistry of near-axis seamounts, Valu Fa Ridge, Lau Basin: insight into mantle wedge melting and the addition of subduction components. *Earth and Planetary Science Letters*, **151**, 205–223.

KANEOKA, I., ISSHIKI, N. & ZASHU, S. 1970. K–Ar ages of the Izu–Bonin islands. *Geochemical Journal*, **4**, 53–60.

KERRICH, R., WYMAN, D., FAN, J. & BLEEKER, W. 1998. Boninite–low Ti-tholeiite associations from the 2.7 Ga Abitibi greenstone belt. *Earth and Planetary Science Letters*, **164**, 303–316.

KODAMA, K., KEATING, B.H. & HELSLEY, C.E. 1983. Paleomagnetism of the Bonin Islands and its tectonic significance. *Tectonophysics*, **95**, 25–42.

KOSTOPOULOS, D.K. & MURTON, B.J. 1992. Origin and distribution of components in boninite genesis: significance of the OIB component. *In*: PARSON, L.M., MURTON, B.J. & BROWNING, P. (eds) *Ophiolites and Their Modern Oceanic Analogues*. Geological Society, London, Special Publications, **60**, 133–154.

KOYAMA, M., CISOWSKI, S.M. & PEZARD, P.A. 1992. Paleomagnetic evidence for northward drift and clockwise rotation of the Izu–Bonin forearc since the Early Oligocene. *In*: TAYLOR, B., FUJIOKA, K. *et al. Proceedings of the Ocean Drilling Program, Scientific Results*, **126**, 353–370.

LEES, J.M. 2000. Implications of slab tear on geodynamics, seismology and volcano geochemistry. *Eos, Transactions, American Geophysical Union*, **81**, (48), Fall Meeting Supplement, T51E-06.

LOUDEN, K.E. 1976. Magnetic anomalies in the West Philippine Basin. *In*: SUTTON, G.H., MANGHNANI, M.H., & MOBERLY, R. (eds) *The Geophysics of the Pacific Ocean Basin and its Margin*. American Geophysical Union Monographs, **19**, 253–267.

LOUDEN, K.E. 1977. Paleomagnetism of DSDP sediments, phase shifting of magnetic anomalies and rotation of the West Philippine Basin. *Journal of Geophysical Research*, **82**, 2989–3002.

MACPHERSON, C.G. & HALL, R. 2001. Tectonic setting of Eocene boninite magmatism in the Izu–Bonin–Mariana forearc. *Earth and Planetary Science Letters*, **186**, 215–230.

MAILLET, P., MONZIER, M. & LEFEVRE, C. 1986. Petrology of Matthew and Hunter volcanoes, South New Hebrides island arc (Southwest Pacific).

Journal of Volcanology and Geothermal Research, **30**, 1–27.

MALYARENKO, A.N. & LELIKOV, E.P. 1995. Granites and associated rocks in the Philippine Sea and the East China Sea. *In*: TOKUYAMA, H., SHCHEKA, S.A. & ISEZAKI, N. (eds) *Geology and Geophysics of the Philippine Sea*. Terrapub, Tokyo, 311–328.

MARTINEZ, F., FRYER, P., BAKER, N.A. & YAMAZAKI, T. 1995. Evolution of backarc rifting: Mariana Trough, 20°–24°N. *Journal of Geophysical Research*, **100**, 3807–3827.

MARUYAMA, S. & KURAMOTO, T. 1981. Geology of Oto-jima, Ani-jima, and Chichi-jima, *Bulletin of the Volcanological Society of Japan*, **26**, 146 (in Japanese).

MEFFRE, S., AITCHISON, J.C. & CRAWFORD, A.J. 1996. Geochemical evolution and tectonic significance of boninites and tholeiites from the Koh ophiolite, New Caledonia. *Tectonics*, **15**, 67–83.

MEIJER, A. 1983. The origin of low-K rhyolites from the Mariana frontal arc. *Contributions to Mineralogy and Petrology*, **83**, 45–51.

MILLEN, D.W. & HAMBURGER, M.W. 1998. Seismological evidence for tearing of the Pacific Plate at the northern termination of the Tonga subduction zone. *Geology*, **26**, 659–662.

MILNER, G.J. 1992. Middle Eocene to early oligocene foraminifers from the Izu-Bonin forearc, hole 786A. *In*: FRYER, P., PEARCE, J.A., STOCKING, L.B. *et al. Proceeding of the Ocean Drilling Program, Scientific Results*, **125**, 71–90.

MITCHELL, J.G., PEATE, D.W., MURTON, B.J., PEARCE, J.A., ARCULUS, R.J. & VAN DER LAAN, S.R. 1992. K-Ar dating of samples from Sites 782 and 786 (Leg 125): the Izu-Bonin forearc region. *In*: FRYER, P., PEARCE, J.A., STOKKING, L.B. *et al. Proceedings of the Ocean Drilling Program, Scientific Results*, **125**, 203–210.

MIZUNO, A., SHIBATA, K., UCHIUMI, S., YUASA, M., OKUDA, Y., NOHARA, M. & KINOSHITA, Y. 1977. Granodiorite from the Minami-koho Seamount on the Kyushu–Palau Ridge, and its K–Ar age. *Chishitsu Chosajo Geppo Bulletin, Geological Survey* of *Japan*, **28**, 5–9.

MONZIER, M., DANYUSHEVSKY, L.V., CRAWFORD, A.J., BELLON, H. & COTTEN, J. 1993. High-Mg andesites from the southern termination of the New Hebrides island arc (SW Pacific). *Journal of Volcanology and Geothermal Research*, **57**, 193–217.

MURTON, B.J., PEATE, D.W., ARCULUS, R.J., PEARCE, J.A. & VAN DER LAAN, S.R. 1992. Trace-element geochemistry of volcanic rocks from Site 786: the Izu–Bonin forearc. *In*: FRYER, P., PEARCE J.A., STOKKING, L.B. *et al. Proceedings of the Ocean Drilling Program, Scientific Results*, **125**, 211–235.

NISHIMURA, S. 1975. On the value of the decay constant for spontaneous fission of uranium-238. *Memoirs of the Faculty of Science, Kyoto University*. Series of Geology and Mineralogy, **41**, 15–19.

NORTON, I.O. 1995. Tertiary relative plate motions in the North Pacific: the 43 Ma non-event. *Tectonics*, **14**, 1080–1094.

OKINO, K., KASUGA, S. & OHARA, Y. 1998. A new scenario of the Parece Vela Basin genesis. *Marine Geophysical Researches*, **20**, 21–40.

OKINO, K., OHARA, Y., KASUGA, S. & KATO, Y. 1999. The Philippine Sea: new survey results reveal the structure and history of the marginal basins. *Geophysical Research Letters*, **26**, 2287–2290.

PEACOCK, S.M. 1990. Fluid processes in subduction zones. *Science*, **248**, 329–337.

PEARCE, J.A., THIRLWALL, M.F., INGRAM, G., MURTON, B.J., ARCULUS, R.J. & VAN DER LAAN, S.R. 1992. Isotopic evidence for the origin of boninites and related rocks drilled in the Izu–Bonin (Ogasawara) forearc, Leg 125. *In*: FRYER, P., PEARCE, J.A., STOKKING, L.B. *et al. Proceedings of the Ocean Drilling Program, Scientific Results*, **125**, 237–261.

PELLETIER, B., CALMANT, S. & PILLET, R. 1998. Current tectonics of the Tonga–New Hebrides region. *Earth and Planetary Science Letters*, **164**, 263–276.

PELLETIER, B., LAGABRIELLE, Y., BENOIT, H., GABIOCH, G., CALNANT, S., GAREL, E. & GUIVEL, C., 2001. Newly identified segments of the Pacific–Australia plate boundary along the North Fiji transform zone. *Earth and Planetary Science Letters*, **193**, 347–358.

PIERCEY, S.J., MURPHY, D.C., MORTENSEN, J.K. & PARADIS, S. 2001. Boninitic magmatism in a continental margin setting, Yukon-Tanana terrane, southeastern Yukon, Canada. *Geology*, **29**, 731–734.

REAGAN, M.K. & MEIJER, A. 1984. Geology and geochemistry of early arc-volcanic rocks from Guam. *Geological Society of America Bulletin*, **95**, 701–713.

ROGERS, N.W. & SAUNDERS, A.D. 1989. Magnesian andesites from Mexico, Chile and the Aleutian Islands: implications for magmatism associated with ridge–trench collision. *In*: CRAWFORD, A.J. (ed.) *Boninites and Related Rocks*. Unwin Hyman, London, 416–445.

ROGERS, N.W., MACLEOD, C.J. & MURTON, B.J. 1989. Petrogenesis of boninitic lavas from the Limassol Forest complex, Cyprus. *In*: CRAWFORD, A.J. (ed.) *Boninites and Related Rocks*. Unwin Hyman, London, 288–313.

ROWLEY, D.B. 1996. Age of initiation of collision between India and Asia: a review of stratigraphic data. *Earth and Planetary Science Letters*, **145**, 1–13.

SENO, T. & MARUYAMA, S. 1984. Paleogeographic reconstruction and origin of the Philippine Sea. *Tectonophysics*, **102**, 53–84.

SHARASKIN, A.Y. 1981. Petrology and geochemistry of basement rocks from five Leg 60 sites. *In*: HUSSONG, D.M., UYEDA S. *et al. Initial Reports of the Deep Sea Drilling Project*, **60**, 647–656.

SHARASKIN, A.Y., DOBRETSOV, N.L. & SOBOLEV, N.V. 1980. Marianites: the clinoenstatite-bearing pillow-lavas associated with the ophiolite assemblage of Mariana Trench. *In*: PANAYIOTOU, A. (ed.) *Proceedings of the International Ophiolite Symposium, Nicosia, Cyprus*, 473–479.

SHARASKIN, A.Y., KARPENKO, S.F., LJALIKOK, A.V., ZOBLIN, S.K. & BALASHOV, Y.A. 1983*a*. Correlated $^{143}Nd/^{144}Nd$ and $^{87}Sr/^{86}Sr$ data on boninites from Mariana and Tonga arcs. *Ofioliti*, **8**, 326–342.

SHARASKIN, A.Y., PUSTCHIN, I.K., ZLOBIN, S.K. & KOLESOV, G.M. 1983*b*. Two ophiolitic sequences from the basement of the northern Tonga Arc. *Ofioliti*, **8**, 411–430.

SHIBATA, K. & OKUDA, Y. 1975. K–Ar age of a granite fragment dredged from the 2nd Komahashi Seamount. *Chishitsu Chosajo Geppo Bulletin, Geological Survey of Japan*, **26**, 19–20.

SHIPBOARD SCIENTIFIC PARTY. 2001. *Site 1201: ion seismic observatory, West Philippine Basin, Leg 195 Preliminary Report, Seafloor Observatories and the Kuroshio Current, 2 March–2 May 2001*. Ocean Drilling Program, Texas A & M University, World Wide Web address: http://www-odp.tamu.edu/publications/prelim/195_prel/195PREL.PDF.

SIGURDSSON, I.A., KAMENETSKY, V.S., CRAWFORD, A.J., EGGINS, S.M. & ZLOBIN, S.K. 1993. Primitive island arc and oceanic lavas from the Hunter Ridge–Hunter Fracture Zone – evidence from glass, olivine and spinel compositions. *Mineralogy and Petrology*, **47**, 149–169.

SMITH, G.P., WIENS, D.A., FISCHER, K.M., DORMAN, L.M., WEBB, S.C. & HILDEBRAND, J.A. 2001. A complex pattern of mantle flow in the Lau Backarc. *Science*, **292**, 713–716.

SMITH, W.H.F. & SANDWELL, D.T. 1997. Global sea floor topography from satellite altimetry and ship depth soundings. *Science*, **277**, 1956–1962.

SOBOLEV, A.V. & DANYUSHEVSKY, L.V. 1994. Petrology and geochemistry of boninites from the north termination of the Tonga Trench: constraints on the generation conditions of primary high-Ca boninite magmas. *Journal of Petrology*, **35**, 1183–1211.

STERN, R.J. & BLOOMER, S.H. 1992. Subduction zone infancy: examples from the Eocene Izu–Bonin–Mariana and Jurassic California arcs. *Geological Society of American Bulletin*, **104**, 1621–1636.

STERN, R.J., MORRIS, J., BLOOMER, S.H. & HAWKINS, J.W. 1991. The source of the subduction component in convergent margin magmas: trace element and radiogenic isotope evidence from Eocene boninites, Mariana forearc. *Geochimica et Cosmochimica Acta*, **55**, 1467–1481.

SUNKEL, G. 1990. Origin of petrological and geochemical variations of Lau basin lavas, SW Pacific. *Marine Mineralogy*, **9**, 205–234

TAKIGAMI, Y. & OZIMA, M. 1981. $^{40}Ar/^{39}Ar$ dating of rocks drilled at sites 458 and 459 in the Mariana fore-arc region during Leg 60. *In*: HUSSONG, D.M., UYEDA S. *et al. Initial Reports of the Deep Sea Drilling Project*, **60**, 743–746.

TATSUMI, Y. & MARUYAMA, S. 1989. Boninites and high-Mg andesites; tectonics and petrogenesis. *In*: CRAWFORD, A.J. (ed.) *Boninites and Related Rocks*. Unwin Hyman, London, 50–71.

TATSUMI, Y., ISHIKAWA, N., ANNO, K., ISHIZAKA, K. & ITAYA, T. 2001. Tectonic setting of high-Mg andesite magmatism in the SW Japan arc: K–Archronology of the Setouchi volcanic belt. *Geophysical Journal International*, **144**, 625–631.

TAYLOR, B. 1992. Rifting and the volcanic-tectonic evolution of the Izu–Bonin–Mariana arc. *In:* TAYLOR, B., FUJIOKA, K. *et al. Proceedings of the Ocean Drilling Program, Scientific Results*, **126**, 627–651.

TAYLOR, R.N. & MITCHELL J.G. 1992. K–Ar dating results from whole-rock and mineral separates of the Izu-Bonin forearc basement, Leg 126. *In:* TAYLOR, B. & FUJIOKA, K. *et al. Proceedings of the Ocean Drilling Program, Scientific Results*, **126**, 677–680.

TAYLOR, R.N., NESBITT, R.W., VIDAL, P., HARMON, R.S., AUVRAY, B. & CROUDACE, I.W. 1994. Mineralogy, chemistry and genesis of the boninite series volcanics, Chichijima, Bonin Islands, Japan. *Journal of Petrology*, **35**, 577–617.

TSUNAKAWA, H. 1983. K–Ar Dating on volcanic rocks in the Bonin Islands and its tectonic implication. *Tectonophysics*, **95**, 221–232.

UMINO, S. 1985. Volcanic geology of Chichijima, the Bonin Islands (Ogasawara Islands), Chishitsugaku Zasshi. *Journal of the Geological Society of Japan*, **91**, 505–523.

UMINO, S. 1986. Magma mixing in boninite sequence of Chichijima, Bonin Islands. *Journal of Volcanology and Geothermal Research*, **29**, 125–157.

VALLIER, T.L., JENNER, G.A., FREY, F.A., DAVIS, A.S., VOLPE, A.M., HAWKINS, J.M., CAWOOD, P.A., SCHOLL, D.W., RAUTENSCHLEIN, M., WHITE, W.M., WILLIAMS, R.W., STEVENSON, A.J. & WHITE, L.D. 1991. Subalkaline andesite from Valu Fa Ridge, a back-arc spreading center in southern Lau basin: petrogenesis, comparative chemistry, and tectonic implications. *Chemical Geology*, **91**, 227–256.

VON STACKELBERG, U., VON RAD, U. & RIECH, V. 1990. SONNE cruise SO-35 in the Lau and North Fiji basins, southwest Pacific Ocean. *Geologisches Jahrbuch*, **92**, 7–36.

WESSEL, P. & SMITH, W.H.F. 1995. New version of the Generic Mapping Tools released. *Eos, Transactions, American Geophysical Union*, **76**, 329.

WOOD, D.A., MATTEY, D.P., JORON, I.L., MARSH, N.G., TARNEY, J. & TREUIL, M. 1981. A geochemical study of 17 selected samples from basement cores recovered at sites 447, 448, 449, 450 and 451, Deep Sea Drilling Project Leg 59. *In:* KROENKE, L., SCOTT, R. *et al. Initial Reports of the Deep Sea Drilling Project*, **59**, 743–752.

WRIGHT, D.J., BLOOMER, S.H., MACLEOD, C.J., TAYLOR, B. & GOODLIKE, A.M. 2000. Bathymetry of the Tonga Trench and forearc: a map series. *Marine Geophysical Researches*, **21**, 489–511.

WYMAN, D.A. 1999. Paleoproterozoic boninites in an ophiolite-like setting, Trans-Hudson orogen, Canada. *Geology*, **27**, 455–458.

XU, Y. & WISE, S.W. JR. 1992. Middle Eocene to Miocene calcareous nannofossils of Leg 125 from the western Pacific Ocean. *In:* FRYER, P., PEARCE, J.A., STOKKING, L.B. *et al. Proceedings of the Ocean Drilling Program, Scientific Results*, **125**, 43–70.

YOGODZINSKI, G.M., LEES, J.M., CHURIKOVA, T.G., DORENDORF, F., WÖERNER, G. & VOLYNETS, O.N. 2001. Geochemical evidence for the melting of subducting oceanic lithosphere at plate edges. *Nature*, **409**, 500–504.

ZLOBIN, S.K., KOLESOV, G.M. & KONONKOVA, N.N. 1991. Development of within-plate magmatism on the landward and offshore slopes of the Tonga Trench. *Ofioliti*, **16**, 17–35.

This page intentionally left blank

Volcanic history of the back-arc region of the Izu–Bonin (Ogasawara) arc

OSAMU ISHIZUKA[1], KOZO UTO[1] & MAKOTO YUASA[2]

[1]*Institute of Geoscience, Geological Survey of Japan/AIST, Central 7, 1-1-1 Higashi, Tsukuba, Ibaraki, 305-8567, Japan (e-mail: o-ishizuka@aist.go.jp)*

[2]*Geoinformation Division, Geological Survey of Japan//AIST, Central 7, 1-1-1 Higashi, Tsukuba, Ibaraki, 305–8567, Japan*

Abstract: The laser-heating $^{40}Ar/^{39}Ar$ dating method was applied to volcanic rocks systematically collected from the back-arc region of the central part of the Izu–Bonin arc. Dating results combined with whole-rock chemistry and other geological information reveal the volcanic history of the back-arc region of the Izu–Bonin arc. In the back-arc seamount chains area, andesitic–basaltic volcanism initiated at *c.* 17 Ma, slightly before the Shikoku Basin ceased spreading, and continued until *c.* 3 Ma. Relatively old volcanism (>8 Ma) has been found only from the western part of the seamount chains, and younger volcanism mainly occurs in the eastern part of the chains, indicating the western margin of the active volcanic zone of the Izu–Bonin arc has migrated eastward with time. At around 2.8 Ma, volcanism initiated in the western part of the back-arc knolls zone. This volcanism is characterized by eruption of clinopyroxene–olivine basalt. In the first stage of rifting, this type of basalt erupted from N–S-trending fissures and/or vents aligned in this direction and formed N–S-trending ridges. Between 2.5 and 1 Ma, many small knolls were formed by eruption of basalt and minor felsic rocks. Volcanism younger than 1 Ma occurred only in the currently active rift zone and its adjacent area.

The active volcanic zone in the back-arc seamount chains area converged to the volcanic front with time from 17 to 3 Ma. Active rifting and rifting-related volcanism also migrated or converged eastward after 1 Ma. The observed temporal variation of locus of volcanism may be explained by rapid retreat of the Philippine Sea Plate relative to the Pacific Plate and resulting steepening of the subducting slab.

Oceanic island arcs in the western Pacific are generally associated with back-arc rifting or spreading. These processes significantly affect the volcanism and structure of the island arc including formation of rift basins and cessation of volcanism on the remnant arc.

The Izu–Bonin arc, which is one of the oceanic island arcs on the Philippine Sea Plate, experienced back-arc spreading (formation of the Shikoku Basin) and is being affected by ongoing back-arc rifting. The back-arc region of the Izu–Bonin arc exhibits complicated topographic features and structure, and is characterized by the existence of lines of back-arc seamount chains, a back-arc knolls zone and active back-arc rift basins. The complexity of submarine topography in this region is the result of the overprinting of volcanic activities of different ages. However, as the back-arc region is submerged below sea level with only limited erosion (Ishizuka *et al.* 2002*b*), volcano-tectonic features are well preserved.

Understanding the volcanic history of this area has been hampered by a lack of systematic sampling and reliable age data on volcanic rocks. Three K–Ar ages ranging from 2.2 to 3.3 Ma were reported from this region by Yuasa (1985) and Nakamura *et al.* (1987). The MW9507 cruise by R/V *Moana Wave* in 1995 provided systematically collected volcanic rocks from the back-arc region of the central part of the arc. K–Ar dating of these samples gave an estimate of the period of the volcanism in this region (Ishizuka *et al.* 1998*a*).

Submarine volcanic rocks are known to give ages different from their true eruption ages in some cases (e.g. Seidemann 1977). This is due to the existence of excess ^{40}Ar in the rapidly quenched glassy part or Ar loss and K remobilization caused by reaction with sea water or hydrothermal fluids. To establish a reliable and detailed volcanic history of the back-arc region of the Izu–Bonin arc, reliable and precise $^{40}Ar/^{39}Ar$ age data must be obtained on systematically collected volcanic rocks from the various topographic features in the region. Ishizuka *et al.* (2002*a*) focused on the rifting-related volcanism, and revealed the temporal variation of mode and locus of volcanism with the progress of rifting based on $^{40}Ar/^{39}Ar$ ages.

From: LARTER, R.D. & LEAT, P.T. 2003. *Intra-Oceanic Subduction Systems: Tectonic and Magmatic Processes.* Geological Society, London, Special Publications, **219**, 187–205. 0305-8719/03/$15.00

Here we present work on volcanic rocks mainly from the back-arc seamount chains that were dated by the laser-heating $^{40}Ar/^{39}Ar$ method. The $^{40}Ar/^{39}Ar$ data support the volcano-tectonic history partially revealed by K–Ar dating (Ishizuka *et al.* 1998*a*), and provide new and detailed information. Here we will summarize the current understanding of changing locus and characteristics of volcanism of the Izu–Bonin arc since the Miocene, using all the available age data from the back-arc region.

Tectonic setting

The Izu–Bonin arc is located in the northeastern margin of the Philippine Sea Plate and extends from southern Honshu to its intersection with the Mariana arc. The arc has a broad volcanic zone extending in a N–S direction and is bounded by the Izu–Bonin Trench on the east and the Shikoku Basin on the west (Fig. 1). Around the Sumisu Jima and Aoga Shima islands, situated in the middle of the arc (30°N–32°30′N), the volcanic zone exhibits four submarine topographic features from east to west (Figs 1, 2): volcanic front area, active rift zone, back-arc knolls zone and back-arc seamount chains area.

The volcanic front area includes stratovolcanoes (e.g. Aoga Shima) and large submarine calderas (e.g. Myojin Knoll), and the lava compositions range from basalt to rhyolite (e.g. Gill *et al.* 1992; Yuasa & Nohara 1992). These lavas are depleted in incompatible elements and light rare earth elements (LREE), and correspond to low-K tholeiite (Ikeda & Yuasa 1989; Tatsumi *et al.* 1992; Yuasa & Nohara 1992; Taylor & Nesbitt 1998). Volcanism at the volcanic front has been active since Middle Miocene times (Fujioka *et al.* 1992; Hiscott & Gill 1992). Within 10–15 km of the volcanic front, the active rift zone, including the Sumisu and Aogashima rifts, is bounded by N–S-trending faults (Klaus *et al.* 1992; Taylor 1992). Late Quaternary basalt lavas (<0.1 Ma) and hydrothermal activity occur along the central axis of the Sumisu Rift, whereas older lavas (*c.* 1.4 Ma) crop out along the rift walls (Hochstaedter *et al.* 1990*a*; Urabe & Kusakabe 1990). Lavas from the active rifts are compositionally bimodal (Hochstaedter *et al.* 1990*a*). These lavas show relatively flat REE patterns and are similar to enriched mid-ocean ridge basalts (E-MORB), except for a few characteristics including Nb depletion (Ikeda & Yuasa 1989; Fryer *et al.* 1990; Hochstaedter *et al.* 1990*a*, *b*). The back-arc knolls zone lies west of the active rifts. Originally defined by Honza & Tamaki (1985) on the basis of bathymetry and single-channel seismic profiles, the back-arc knolls zone consists of N–S-trending ridges and small volcanoes situated between the active rifts to the east and the larger seamounts of seamount chains to the west. Ishizuka *et al.* (2002*a*) presented a detailed bathymetric map of the back-arc knolls zone. A N–S-trending ridge up to 20 km long is overlain by small knolls. The knolls in this zone are relatively small, 500–1000 m high in most cases (Fig. 3). Seismic reflection data reveal that the northern part of the back-arc knolls zone is dominated by normal faults and small knolls, and had only small amount of subsidence (Honza & Tamaki 1985; Nakao *et al.* 1985). In contrast, the southern part of the back-arc knolls zone experienced large subsidence of the basement and a fault-bounded basin filled with thick sediment (>750 m) was formed. Based on detailed bathymetry and side-scan sonar data, Morita *et al.* (1999) concluded that the back-arc knolls zone is a region where seamount chain volcanoes have been dissected by N–S-trending lineations and fissure ridges.

The back-arc seamount chains extend into the Shikoku Basin from the western part of the back-arc knolls zone in an ENE–WSW direction, oblique to the trend of the volcanic front and extension-related features. Four seamount chains, i.e. the Kan'ei, Manji, Enpo and Genroku chains, occur in the central arc (Fig. 1). Isolated seamounts offset from these chains are also present. The seamounts in the western part of the chains are much larger than the knolls in the back-arc knolls zone, exceeding 2000 m high with basal diameters of up to 20 km (Fig. 3). Some of the seamounts have flat summits (e.g. Manji Seamount in the Manji Chain: Ishizuka *et al.* 2002*b*; Ten'na Seamount in the Enpo Chain) covered by reef limestones. This implies that their summits emerged above sea level and then subsided to their present depth (*c.* 130–1500 m).

Petrology

Volcanism in the back-arc seamount chains is mainly basaltic–andesitic, accompanied by minor amounts of felsic lavas. Andesite lavas are generally porphyritic, poorly vesiculated, and contain plagioclase, clinopyroxene and orthopyroxene as phenocrysts. These lavas do not show signs of rapid quenching and are well crystallized in general. Some andesites show different mineral assemblages, and contain hornblende and plagioclase as phenocrysts, pyroxene being absent. Basaltic lavas from the back-arc seamount chains are generally highly vesiculated, and contain olivine, clinopyroxene and plagioclase as phenocrysts. Olivine is more

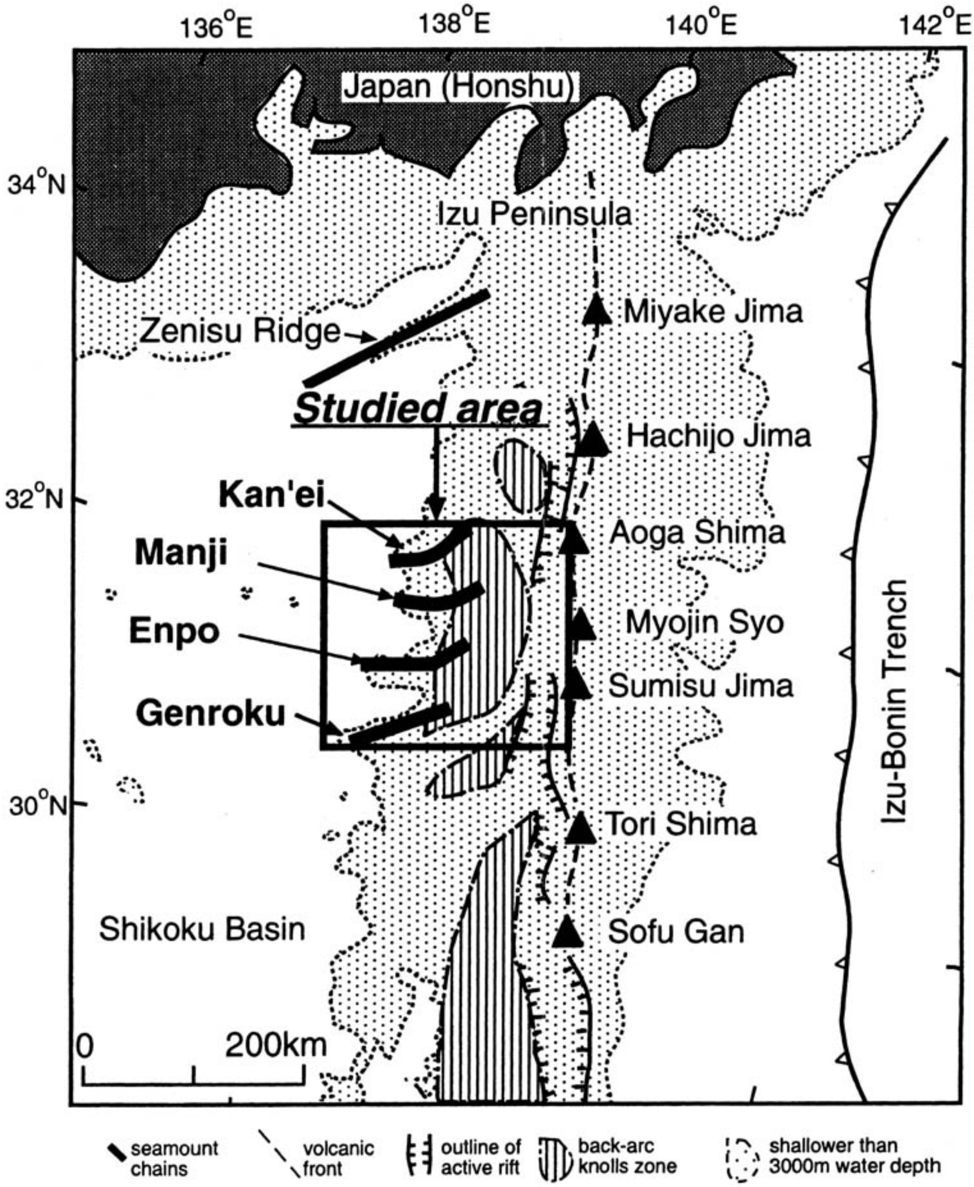

Fig. 1. Schematic map of the Izu–Bonin arc. The area containing the studied samples is indicated by the box.

abundant than orthopyroxene. Some basalts show signs of rapid cooling including glassy rind and swallowtail texture of plagioclase in the groundmass.

Lavas from the back-arc knolls zone are mainly clinopyroxene–olivine basalt accompanied by minor amounts of andesite, dacite and rhyolite. Basalts are generally vesiculated and contain more clinopyroxene than olivine as phenocrysts. Some of the basalts show swallowtail texture of plagioclase and dendritic growth of pyroxene in the groundmass, suggesting rapid cooling of these lavas. Andesitic–dacitic lavas from the back-arc knolls zone comprise both hornblende-bearing and hornblende-free lavas. Hornblende-bearing lavas contain plagioclase and hornblende as phenocrysts. Hornblende-free andesite lavas are generally glassy, and contain plagioclase, orthopyroxene and clinopyroxene as phenocrysts.

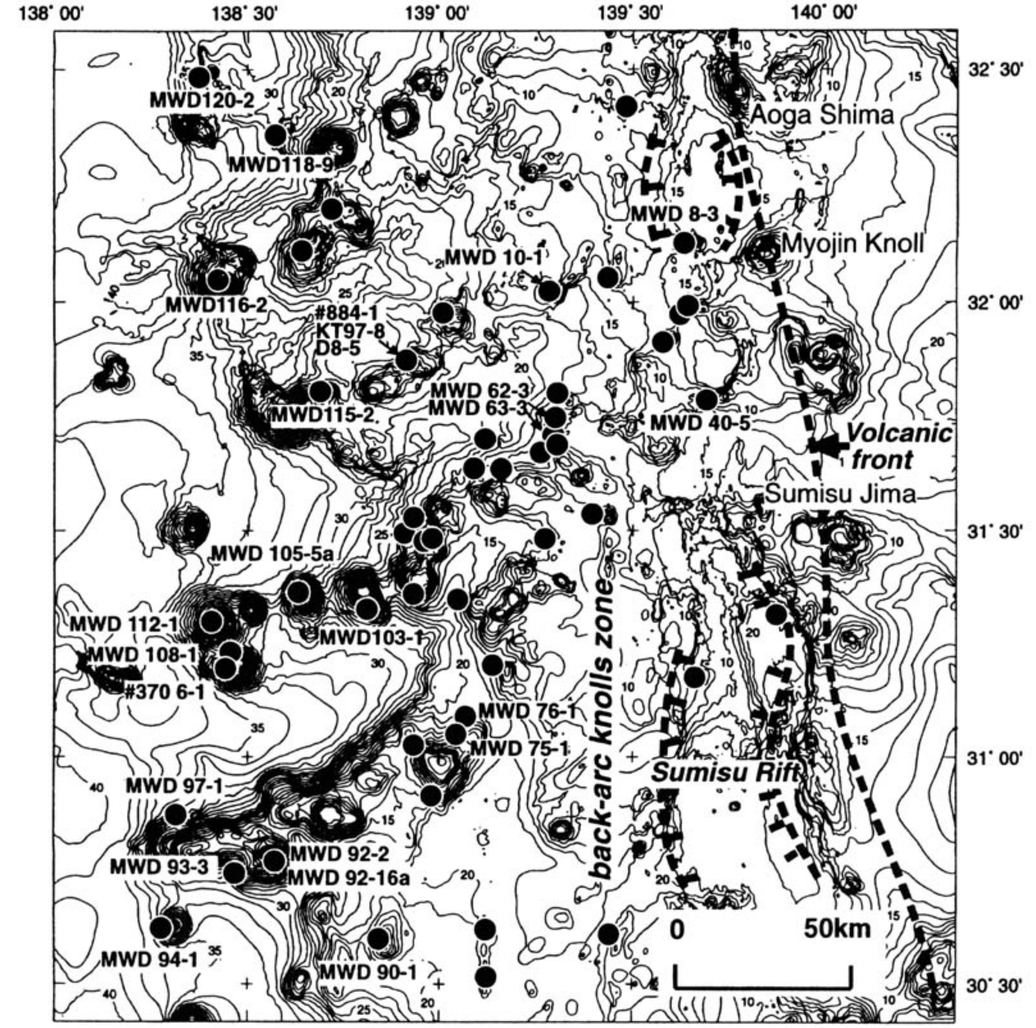

Fig. 2. Locality of the samples dated in this study (original map from Klaus unpublished data, contours at 125m intervals, labels in hundreds of metres). The localities of the samples whose age data were previously reported (Ishizuka *et al.* 1998*a*, 2002*a*) are also indicated (points not labelled with sample names).

Lavas from the active rift zones are bimodal in composition, and comprise basalt and rhyolite lavas. Basalt lavas are highly vesiculated, and often contain plagioclase, clinopyroxene and olivine as phenocrysts. Rhyolite lavas are glassy, and normally contain small amounts of phenocrysts of plagioclase, clinopyroxene, hornblende, biotite and quartz. Almost all of the samples dated in this study are covered with Mn-oxide crusts. The thickness of crusts generally increases westward in the seamount chains (Usui *et al.* 1996). Samples from the western margin of the back-arc knolls zone mostly have crusts less than 10 mm thick, while those from the western part of the chains have crusts 10–40 mm thick.

Samples studied

For the present study, 20 samples were selected for dating from more than 1000 samples collected during R/V *Moana Wave* cruise MW9507. Two samples collected from the back-arc seamount chains (the Manji and the Nishi Jokyo seamounts) by submersible survey (dive No. 884 of *Shinkai* 2000: Ishizuka *et al.* 2002; and dive No. 370 of *Shinkai* 6500: Ishizuka *et al.* 1998*b*) and one sample from the Manji Seamount

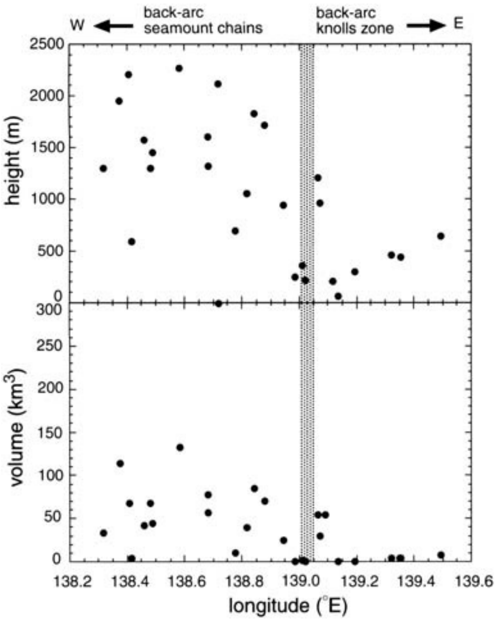

Fig. 3. Comparison of sizes of the volcanoes between the back-arc seamount chains and back-arc knolls zone. Longitude of summit of each seamount or knoll is plotted on the horizontal axis. (**a**) Longitude v. height of the volcanoes; (**b**) longitude v. volume. Dotted area indicates the boundary region of the back-arc knolls zone and back-arc seamount chains.

collected by R/V *Tansei-maru* during cruise KT97–8 were also dated. Localities of analysed samples are shown in Fig. 2 and descriptions of the samples can be found in Ishizuka *et al.* (1998*a*, *b*, 2002*b*). The localities of analysed samples cover the western part of the Kan'ei, Manji, Enpo and Genroku chains, and the western margin of the back-arc knolls zone. Two samples from isolated seamounts in the Shikoku Basin were also dated.

Sample selection for $^{40}Ar/^{39}Ar$ dating was based mainly on examination of thin sections. Less glassy samples (usually < 5% of total groundmass) with almost no visible groundmass alteration were regarded as suitable for dating, except in the case of some dacites and rhyolites, which were very fresh but with glassy groundmass. In addition, loss on ignition (LOI) was also taken into consideration, and samples showing < 2% LOI were considered suitable. In addition to the lava samples, essential blocks of volcanic breccia were dated where lava was not recovered.

Laser-heating $^{40}Ar/^{39}Ar$ dating

Age determination of volcanic rocks was achieved by the laser-heating $^{40}Ar/^{39}Ar$ dating system at the Geological Survey of Japan (Uto *et al.* 1997).

Stepwise heating of groundmass

Slabs 1 mm thick were taken from the freshest part of the samples with a water-cooled saw. This was partly because flat surfaces are required to precisely monitor the thermal energy distribution on the samples during laser heating. The slabs were gently crushed into small pieces of about 2–7 mg weight and then ultrasonically cleaned in distilled water. The pieces were further treated ultrasonically in 3N HCl for 10–15 min to remove alteration products (clays and carbonates). After this treatment, the samples were soaked in distilled water at 70°C for 3 days. After drying, the samples were wrapped in aluminium foil packets of around 2 × 2 mm in size. The packets were stacked in a pure aluminium (99.5% Al) irradiation capsule with flux monitor minerals. Sanidine from the Fish Canyon Tuff (FC3), whose age is 27.5 Ma (Lanphere & Baadsgaard 2001), was used as a flux monitor. We adopted 27.5 Ma as an age for Fish Canyon Tuff based on the calibration against our primary standard for our K–Ar laboratory, Sori biotite, whose age is 91.2 Ma (Uchiumi & Shibata 1980). Correction for interfering isotopes was achieved by analyses of $CaFeSi_2O_6$ and $KFeSiO_4$ glasses irradiated with the samples. Sample irradiation was performed at two reactors, the JMTR and the JRR3 reactors (Ishizuka 1998). Fast neutron flux in the JMTR was about 6.7×10^{12} neutrons (n) cm^{-2} s^{-1} and about 1.4×10^{12} n cm^{-2} s^{-1} for the JRR3.

Samples were baked at 250°C for 72 h after being placed in an extraction line before analysis. A continuous Ar ion laser was used for sample heating. The groundmass samples were heated for 3 min in each step, keeping laser power constant. Laser beam diameter was adjusted to 2 mm to ensure uniform heating of the sample. Extracted gas was purified for 10 min with three Zr–Al getters (SAES AP-10) and one Zr–Fe–V getter (SAES GP-50). Two Zr–Al getters were maintained at 400°C and other getters were at room temperature. Argon isotopes were measured on a VG Isotech VG3600 noble gas mass spectrometer. In this study, all the analyses were measured using the Daly collector. The sensitivity of the collector was about 5×10^{-10} ml (standard temperature and pressure) per volt (STP V^{-1}). Mass discrimination was monitored using diluted air. The blank of the system, including the mass spectrometer and the extraction line, was 7.5×10^{-14} ml STP for ^{36}Ar, 2.5×10^{-13} ml STP for ^{37}Ar, 2.5×10^{-13} ml STP for ^{38}Ar, 1.0×10^{-12} ml

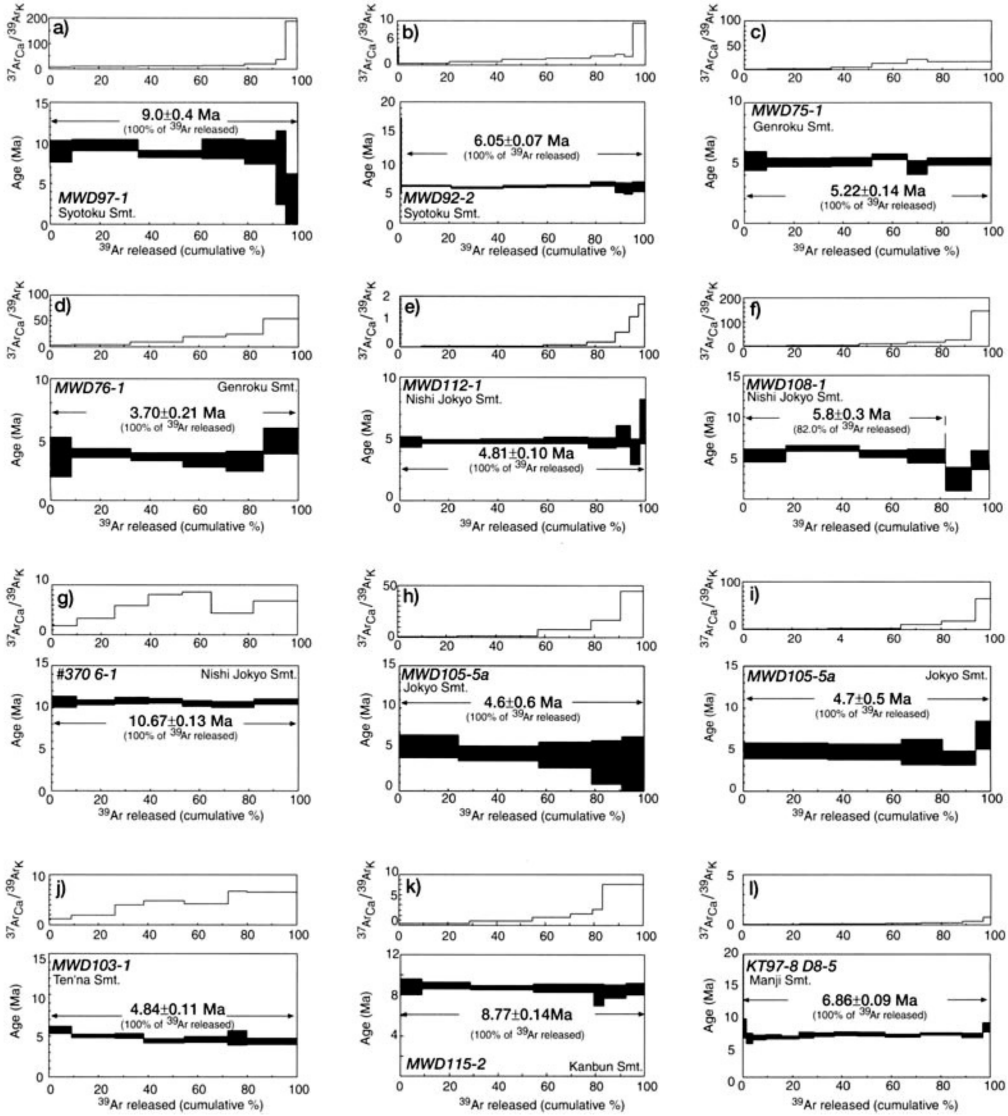

Fig. 4. $^{40}Ar/^{39}Ar$ age spectra with Ca/K plots for groundmass samples of lavas from the back-arc seamount chains.

STP for ^{39}Ar and 2.5×10^{-12} ml STP for ^{40}Ar. The blank analysis was performed every two or three step analyses.

Total fusion analysis of plagioclase phenocrysts

Slabs about 1 cm thick and 100 g in weight were taken from the freshest part of the samples and crushed to 250–500 μm using an iron pestle. After removal of the strongly magnetic fraction by a permanent magnet, mineral separation was achieved by conventional technique using an isodynamic magnetic separator, heavy liquids and hand-picking. Plagioclase separates were further treated ultrasonically in 0.2N HF for 10 min to remove groundmass and alteration products. Further treatment was achieved by cleaning with 3N HCl in an ultrasonic bath for 10 min to remove clay minerals, carbonates and fluoride that might have been produced during HF treatment. In total fusion analysis of plagioclase, laser power was raised quickly and several

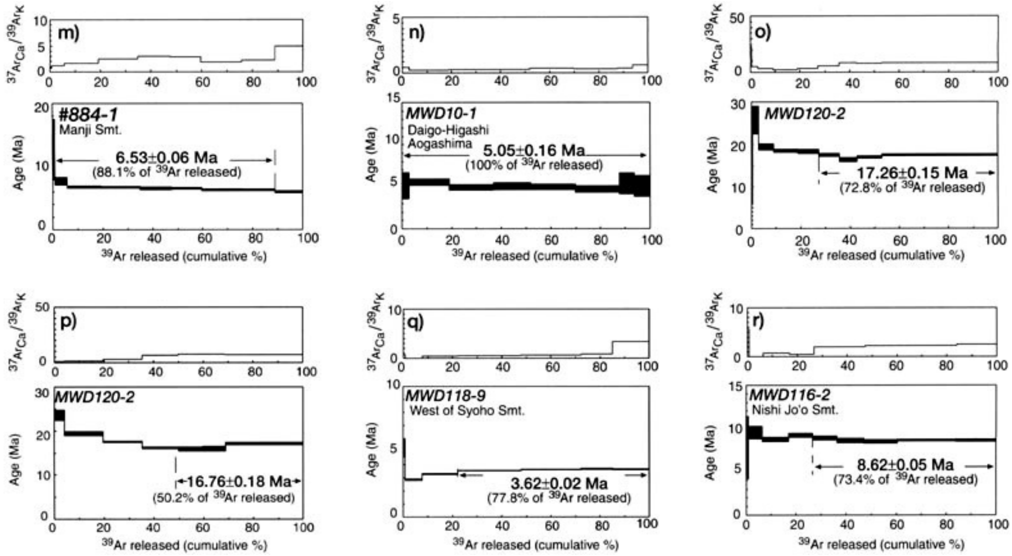

Fig. 4. *continued*

grains were fused completely within 1–2 min. The analysis for each sample was completed in a single step.

Error estimation and age calculation

All errors for $^{40}Ar/^{39}Ar$ results are reported at one standard deviation. Errors for ages include analytical uncertainties for Ar isotope analysis, correction for interfering isotopes and *J* value estimation. An error of 0.5% was assigned to *J* values as a pooled estimate during the course of this study.

Age spectra and inverse isochron ages were calculated from the stepwise heating analysis. Plateau ages were calculated as weighted means of ages of plateau-forming steps, where each age was weighted by the inverse of its variance. The age plateaux were determined following the definition by Fleck *et al.* (1977). Inverse isochrons were calculated using York's least-squares fit, which accommodates errors in both ratios and correlations of errors (York 1969).

Results

Validity of the stepwise heating analysis using laser-heating technique

The validity of stepwise heating analysis using laser-heating techniques has been a matter of debate. Sample heating by a laser beam could cause heterogeneous thermal energy distribution in the sample due to the Gaussian energy distribution profile of the laser beam (e.g. Turner *et al.* 1994). This characteristic of laser beams makes it difficult to heat relatively large amount of samples homogeneously. To overcome this problem, a homogenized laser beam 2 mm in diameter produced by the combination of an optical glass fibre and an optical objective lens (Uto *et al.* 1997) was applied to stepwise heating analysis of groundmass. This beam size is larger than the sample size. Replicate analyses were carried out to ensure the reproducibility of the analysis on some samples (MWD120-2: Fig. 4o, p, MWD105-5a: Fig. 4h, i) (GHD621-11 in Ishizuka *et al.* 2002*a*) showing slightly disturbed age spectra. All replicate analyses returned age spectra and $^{37}Ar_{Ca}/^{39}Ar_{K}$ variation diagrams that were consistent with the original measurements. The plateau age for each sample was also reproducible within analytical uncertainty at 2σ. Sample sizes used in the replicate analyses differed by up to 300% from the first analyses. If samples were heterogeneously heated by laser beam, high reproducibility of age spectrum obtained in this study should not be expected due to the artificial redistribution of argon in the samples. These results prove that samples were heated homogeneously, and artificial modification of Ar distribution in the sample by laser heating was minimal. Therefore, we consider that stepwise heating analysis of groundmass

Table 1. *$^{40}Ar/^{39}Ar$ dating results on the volcanic rocks from the back-arc seamount chains and back-arc knolls zone*

Sample No.	Seamount name	Rock type	Integrated age (±1σ) (Ma)	Plateau age (±1σ)					
				Weighted average (Ma)	inv. isochron age (Ma)	$^{40}Ar/^{36}Ar$ intercept	MSWD	Fraction of ^{39}Ar (%)	K–Ar age (Ma)
Genroku Chain									
MWD97-1	Syotoku	cpx-ol basalt	8.7±0.5	**9.0±0.4**	9.1±0.5	293±26	0.72	100.0	
MWD92-2	Syotoku	dacite	6.08±0.09	**6.05±0.07**	6.02±0.10	307±19	0.81	100.0	6.04±0.07
MWD75-1	Genroku	ol basalt	5.11±0.17	**5.22±0.14**	5.5±0.4	291±7	0.81	100.0	5.11±0.25
MWD76-1	Genroku	ol basalt	3.8±0.3	**3.70±0.21**	3.69±0.24	300±23	0.77	100.0	3.22±0.35
Enpo Chain									
MWD112-1	Nishi Jokyo	hb dacite	4.83±0.13	**4.81±0.10**	4.83±0.14	291±25	0.51	100.0	
MWD108-1	Nishi Jokyo	ol-cpx basalt	5.2±0.3	**5.8±0.3**	5.9±0.6	279±101	1.00	82.0	3.65±0.16
370 6-1	Nishi Jokyo	basaltic andesite	10.66±0.14	**10.67±0.13**	10.6±0.3	306±41	0.44	100.0	
MWD105-5a	Jokyo	ol-cpx basalt	4.4±0.7	**4.6±0.6**	4.2±1.3	430±384	0.37	100.0	
MWD105-5a	Jokyo	ol-cpx basalt	4.8±0.5	**4.7±0.5**	3.9±1.3	500±370	0.36	100.0	
			average	**4.7±0.4**					
MWD103-1	Ten'na	cpx andesite	4.76±0.14	**4.84±0.11**	4.92±0.24	291±11	1.32	100.0	4.54±0.19
Manji Chain									
MWD115–2	Kanbun	opx-cpx andesite	8.71±0.16	**8.77±0.14**	8.91±0.33	249±85	0.40	100.0	8.89±0.10
884-1	Manji	basaltic andesite	6.61±0.07	**6.53±0.06**	6.47±0.08	304±4	1.11	88.1	
KT97-8 D8-5	Manji	dacite	6.86±0.09	**6.86±0.09**	6.72±0.13	302±4	0.77	100.0	
MWD10-1		pl andesite	5.05±0.16	**5.05±0.16**	4.92±0.20	301±4	0.41	100.0	4.86±0.06
Kan'ei Chain									
MWD118-9	W of Syoho	cpx andesite	3.54±0.01	**3.62±0.02**	3.56±0.05	327±42	1.44	77.8	3.26±0.06
MWD116-2	Nishi Jo'o	cpx-opx andesite	8.66±0.05	**8.62±0.05**	8.53±0.12	309±12	0.59	73.4	
MWD120-2		cpx andesite	17.55±0.12	**17.26±0.15**	16.1±0.9	360±46	1.01	72.8	
MWD120-2		cpx andesite	17.43±0.13	**16.76±0.18**	14.5±1.6	667±259	0.35	50.2	
			average	**17.06±0.12**					
Isolated seamounts									
MWD90-1		cpx andesite	12.34±0.24	**12.34±0.24**	12.4±0.4	295±4	0.58	100.0	12.47±0.18
MWD94-1	Kyoho	ol-opx-cpx basalt	6.56±0.09	no plateau					4.82±0.16
Eastern margin of the back-arc knolls zone									
MWD63-3		cpx-ol basalt	0.33±0.10	**0.35±0.10**	<0.47	410±240	1.28	100.0	
MWD62-3		ol-cpx basalt	0.88±0.20	**0.92±0.17**	1.3±0.3	256±40	0.79	100.0	0.54±0.06

Inv. isochron age, inverse isochron age; MSWD, mean square of weighted deviates ((SUMS/(n–2))^0.5) in York (1969). Integrated ages were calculated using sum of the total gas released. K–Ar age: Ishizuka *et al.* (1998*a*). Weighted average ages and uncertainties are calculated using following equations (Taylor 1982):

$$T_{av} = \Sigma(T_i/\sigma_i^2)/\Sigma(1/\sigma_i^2)$$

$$\sigma_{av} = (\Sigma(1/\sigma_i^2))^{-0.5}$$

T_{av}, weighted average age; T_i, individual age; σ_{av}, uncertainty for the average age; σ_i, uncertainty for the individual age.

$\lambda_\beta = 4.962 \times 10^{-10} a^{-1}$, $\lambda_e = 0.581 \times 10^{-10} a^{-1}$, $^{40}K/K = 0.01167\%$ (Steiger & Jäger 1977).

Table 2. *Results of total fusion analyses of plagioclase of a lava from the Syotoku Seamount*

Sample No.	Number of grains	$^{40}Ar/^{39}Ar$	$^{37}Ar/^{39}Ar$	$^{36}Ar/^{39}Ar$ ($\times 10^{-3}$)	$^{37}Ar_{Ca}/^{39}Ar_K$	$^{40}Ar^*$ (%)	$^{40}Ar^*/^{39}Ar_K$	Age (Ma)
MWD92-16a	7–8	2.376±0.018	4.718±0.055	3.766±0.296	4.733	80.4	1.915±0.112	**3.12±0.18**

$^{40}Ar^*$, radiogenic ^{40}Ar.

using this laser-heating technique does produce geologically meaningful age spectra.

Back-arc seamount chains

Sixteen samples from 11 seamounts were dated by stepwise heating analysis (Fig. 4, Table 1). A sample from the Genroku Chain (MWD92-16a) was dated by total fusion analysis of plagioclase. K–Ar ages mentioned in the following sections were reported in Ishizuka *et al.* (1998*a*).

Genroku Chain. A basalt from a peak west of the Syotoku Seamount (MWD97–1) is partially affected by alteration, and the amount of fresh groundmass is limited. Stepwise heating analysis of fresh groundmass of this sample returned a plateau age of 9.0±0.4 Ma comprising of all seven steps (Fig. 4a). Inverse isochron calculation using all steps gave a concordant isochron age of 9.1±0.5 Ma and yielded an $^{40}Ar/^{36}Ar$ intercept of 293±26. A dacite from the southeastern slope of the Syotoku Seamount (MWD92-2) yielded a completely undisturbed age spectrum with a plateau age of 6.05±0.07 Ma (Fig. 4b). This plateau age is consistent with a K–Ar age for the same of 6.04±0.07 Ma. However, a plagioclase separate from another dacite from the same seamount (MWD92-16a) yielded a total fusion age of 3.12±0.18 Ma (Table 2), concordant with its K–Ar age of 2.95±0.04 Ma within analytical error. As both of the lavas from the Syotoku Seamount gave reliable ages, this seamount is presumed to have experienced at least two different periods of active volcanism. An olivine basalt (MWD75-1) from the northeastern slope of the Genroku Seamount yielded a completely undisturbed spectrum with a plateau age of 5.22±0.14 Ma (Fig. 4c), which is consistent with a K–Ar age of 5.11±0.25 Ma. Another olivine basalt sample (MWD76-1) from the northeastern slope of the Genroku Seamount gave a plateau age of 3.70±0.21 Ma comprising all the gas released (Fig. 4d). This plateau age is consistent with a K–Ar age of 3.22±0.35 Ma.

Enpo Chain. A dacite from the northern peak of the Nishi Jokyo Seamount (MWD112-1) located at the western end of the chain, yielded an undisturbed age spectrum with a plateau age of 4.81±0.10 Ma (Fig. 4e). From the southern peak of the Nishi Jokyo Seamount, two types of lava were dated. An olivine–clinopyroxene basalt (MWD108-1) from the northeastern slope yielded a plateau age of 5.8±0.3 Ma consisting of four contiguous steps with 82.0% of ^{39}Ar released (Fig. 4f). This plateau age is more than 2 Ma older than its K–Ar age of 3.65±0.16 Ma. On the other hand, a basaltic andesite collected by *Shinkai 6500* from the summit area (#370 6–1) yielded a completely undisturbed age spectrum with a plateau age of 10.67±0.13 Ma (Fig. 4g). Two different ages from the Nishi Jokyo Seamount indicate that there were at least two distinct periods of volcanism. A basalt from the Jokyo Seamount (MWD105-5a) located east of the Nishi Jokyo Seamount was analysed for two splits irradiated in different reactors (the JMTR and JRR3 reactors). The results were highly concordant, and both analyses yielded undisturbed age spectra with plateau ages of 4.6±0.6 and 4.7±0.5 Ma, respectively (Fig. 4h, i). An andesite from the Ten'na Seamount situated east of the Jokyo Seamount yielded a plateau age of 4.84±0.11 Ma consisting of 100% gas released (Fig. 4j), which is consistent with its K–Ar age of 4.54±0.19 Ma within analytical error.

Manji Chain. An andesite from the Kanbun Seamount at the western end of the Manji Chain (MW115–2) gave an undisturbed spectrum with a plateau age of 8.77±0.14 Ma (Fig. 4k), which is consistent with its K–Ar age of 8.89±0.10 Ma. From the Manji Seamount, two compositionally different lavas were dated (Ishizuka *et al.* 2002*b*). A dacite lava from the western slope gave a plateau age of 6.86±0.09 Ma (Fig. 4l). A basaltic andesite from the northeastern slope (#884–1) yielded a plateau age of 6.53±0.06 Ma (Fig. 4m). An andesite lava from the Daigo–Higashi Aogashima Knoll (MWD10-1) yielded an undisturbed age spectrum with a plateau age of 5.05±0.16 Ma (Fig. 4n), which is concordant with a K–Ar age of 4.86±0.06 Ma.

Kan'ei Chain. Two splits of an andesite from a seamount (MWD120-2) located north of the

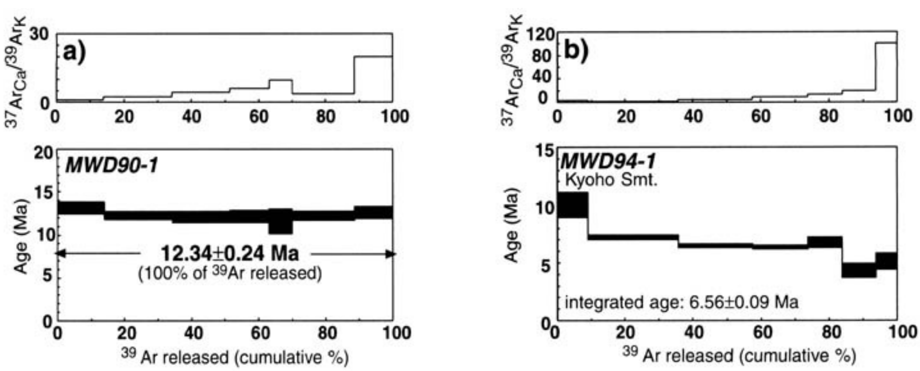

Fig. 5. $^{40}Ar/^{39}Ar$ age spectra with Ca/K plots for groundmass samples of lavas from the isolated back-arc seamounts.

Nishi Jo'o Seamount were analysed after irradiation in different reactors (JMTR and JRR3 reactors). Analysis of the sample irradiated in the JRR3 reactor yielded a slightly disturbed spectrum and gave a plateau age of 17.26±0.15 Ma comprising four steps with 72.8% of ^{39}Ar released (Fig. 4o). The other analysis of the sample irradiated in the JMTR reactor reproduced a similar spectrum to the first analysis and yielded a plateau age of 16.76±0.18 Ma with 50.2% of ^{39}Ar released (Fig. 4p). The plateau ages obtained in these two analyses are consistent within 2σ error. The age spectra obtained in the two analyses show a series of decreasing ages in the lower temperature steps. This feature is normally attributed to ^{39}Ar recoil loss (e.g. Turner & Cadogan 1974; Renne *et al.* 1992). The groundmass of this lava is relatively poorly crystalline and could have been affected by ^{39}Ar recoil loss. Another possible explanation for high ages in the lower temperature steps is the occurrence of excess ^{40}Ar in the phases such as clays. However, more stable phases (e.g. plagioclase in groundmass) that release gas at higher temperature steps are thought to have been free from ^{39}Ar recoil loss. The weighted average of the two plateau ages, 17.06±0.12 Ma, is a best estimate of eruption age for this andesite.

An andesite from a small peak located west of the Syoho Seamount (MWD118-9) yielded a slightly disturbed spectrum, but gave a plateau age of 3.62±0.02 Ma consisting of four steps with 77.8% of ^{39}Ar released (Fig. 4q). As low-temperature steps that gave younger ages than the plateau age are characterized by a high K/Ca ratio, partial alteration of K-rich groundmass to K-bearing clay minerals and oxide minerals might have caused radiogenic ^{40}Ar loss. The plateau age is regarded as a best estimate for the eruption age of this andesite. A slightly younger K–Ar age of 3.26±0.06 Ma is due to partial radiogenic ^{40}Ar loss in the alteration phases. An andesite from the Nishi Jo'o Seamount (MWD116-2) yielded a plateau age of 8.62±0.05 Ma comprising five steps with 73.4% of ^{39}Ar released (Fig. 4r).

Isolated seamounts

Samples from two isolated seamounts were dated. Andesite MWD90–1 from a seamount southeast of the Syotoku Seamount in the Genroku Chain yielded a completely undisturbed spectrum (Fig. 5a) with a plateau age of 12.34±0.24 Ma, which is in good agreement with the K–Ar age of 12.47±0.18 Ma. A basalt lava from the Kyoho Seamount (MWD94-1) located southwest of the Syotoku Seamount gave a disturbed age spectrum with no plateau (Fig. 5b). The integrated age of 6.56±0.09 Ma calculated using total released gas is older than the K–Ar age (4.82±0.16 Ma). The age spectrum for this sample shows a reversed staircase-like pattern, i.e. age decreases with increasing temperature. This pattern of age spectrum implies the redistribution of ^{39}Ar caused by recoil of K-derived ^{39}Ar out of high-K phases into low-K phases (e.g. Turner & Cadogan 1974). No reliable eruption age was obtained from this sample.

Eastern margin of the back-arc knolls zone

Basalts MWD63-3 and MWD62-3 are both from the eastern slope of a knoll in the eastern margin of the back-arc knolls zone. Basalt MWD63-3 yielded a well-defined plateau age of 0.35±0.10 Ma comprising all the gas released (Fig. 6a). Basalt MWD62-3 also gave a plateau age of 0.92±0.17 Ma consisting of all the steps (Fig. 6b).

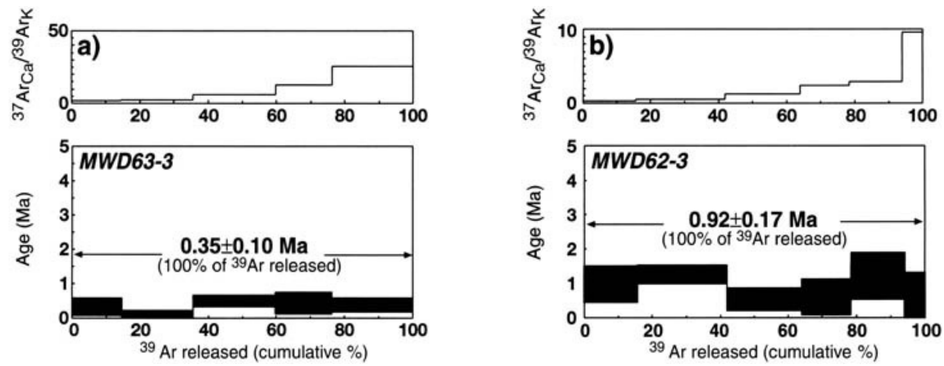

Fig. 6. $^{40}Ar/^{39}Ar$ **age spectra with Ca/K plots for groundmass samples of lavas from the eastern margin of the back-arc knolls zone.**

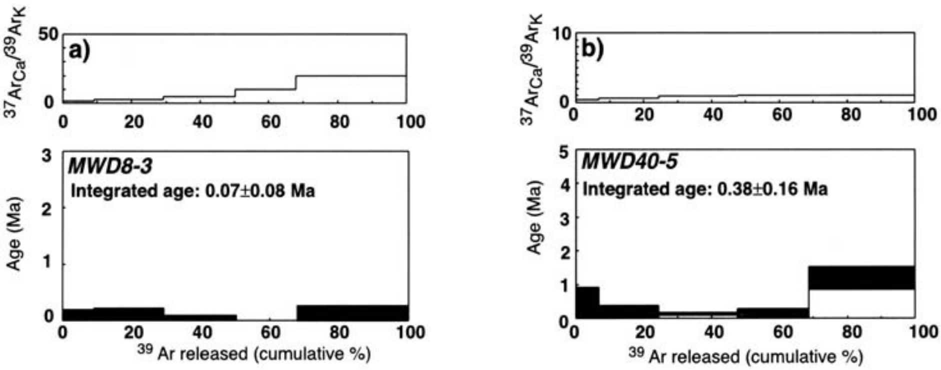

Fig. 7. $^{40}Ar/^{39}Ar$ **age spectra with Ca/K plot for groundmass samples of lavas from the active rift zone.**

Table 3. *$^{40}Ar/^{39}Ar$ dating results on the volcanic rocks from the active rift zone*

Sample No.	Seamount name	Rock type	Total age (±1σ)			
			Weighted average (Ma)	Inv. isochron age (Ma)	$^{40}Ar/^{36}Ar$ intercept	MSWD
Active rift zone						
MWD8-3	Aogashima Rift	cpx-ol basalt	**0.07±0.08**	0.03±0.03	295±21	0.77
MWD40-5	Myojin Rift	cpx-opx-hb dacite	(0.38±0.16)	<0.13	299.8±1.6	1.08

Inv. isochron age, inverse isochron age.
The weighted average age for MW40-5 is presumed to be affected by the presence of excess ^{40}Ar.

Active rift zone

Two basalts from the active rift zones were dated by stepwise heating analysis (Table 3). As uncertainty of age at each step is large due to the low yield of radiogenic ^{40}Ar, only integrated ages are reported here. Basalt (MWD8-3) from the Aogashima Rift gave an integrated age of 0.07±0.08 Ma (Fig. 7a). Regression of all the steps defines an inverse isochron age of 0.03±0.03 Ma with a $^{40}Ar/^{36}Ar$ intercept of 295±21. The integrated age is interpreted as a reasonable estimate for eruption age of this basalt, although analytical uncertainty spans zero. A basalt from the Myojin Rift (MW40-5) yielded an integrated age of 0.38±0.16 Ma (Fig. 7b). Inverse isochron calculation using all steps yielded a $^{40}Ar/^{36}Ar$ intercept of 299.8±1.6, which implies presence of excess ^{40}Ar. The high age obtained in the highest temperature step (the

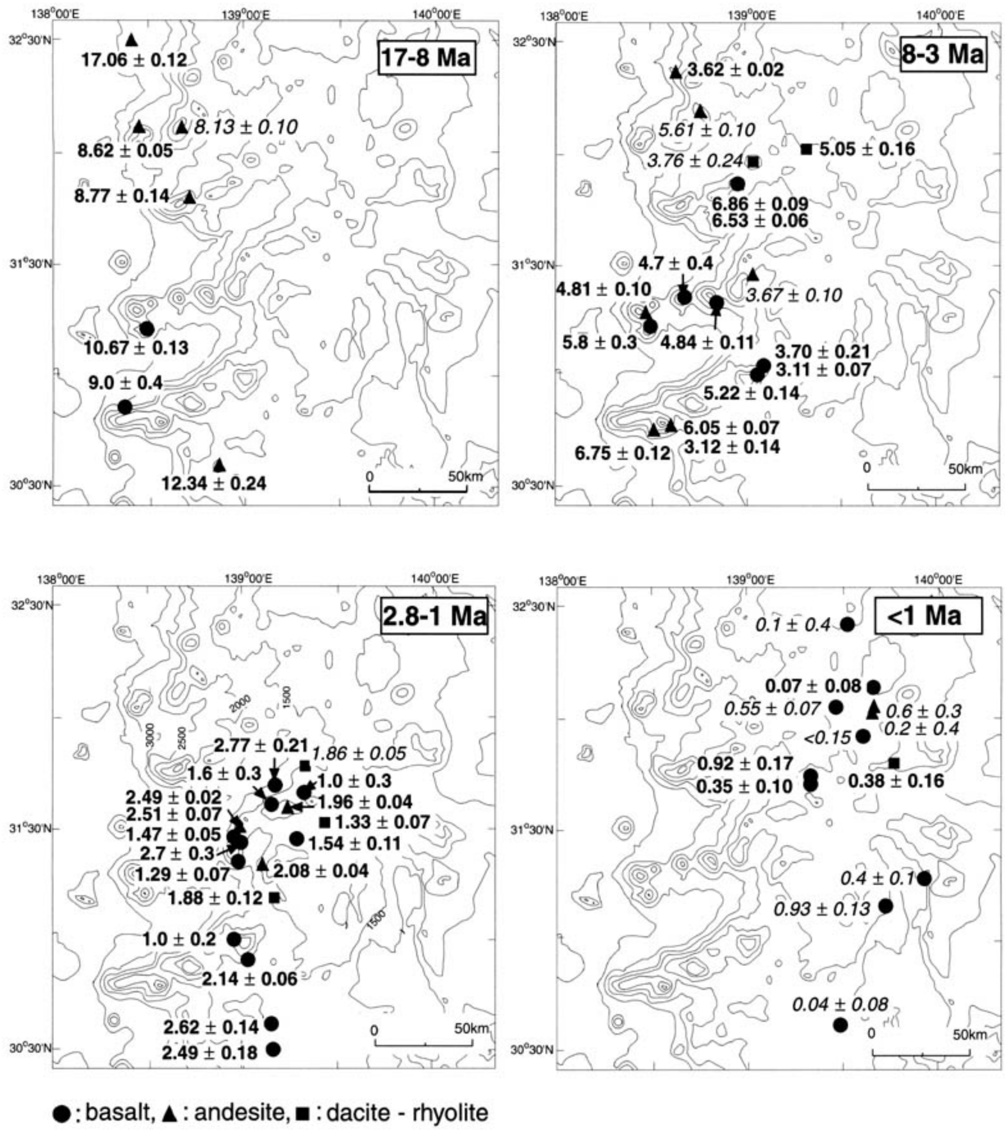

Fig. 8. Temporal variation of locations of volcanism in the back-arc region of the Izu–Bonin arc. Ages are designated in Ma. $^{40}Ar/^{39}Ar$ ages are shown in bold and K–Ar ages are shown in italics. Data sources: this study and Ishizuka *et al.* (2002*a*) for $^{40}Ar/^{39}Ar$ ages. Ishizuka *et al.* (1998*a*) for K–Ar ages.

last step) implies the presence of excess Ar in melt inclusions (e.g. Esser *et al.* 1997).

Discussion

Temporal variation of locus of volcanism in the back-arc region

Volcanic rocks from the back-arc region of the Izu–Bonin arc show a wide age range from *c.* 17 Ma to younger than 0.1 Ma. Each of the submarine topographic features in the region shows a different age range. The back-arc seamount chains yielded ages from *c.* 17 to 3 Ma (Figs 8, 9). The oldest age, 17.06±0.12 Ma, was obtained from a seamount on the slope marking the eastern margin of the Shikoku Basin. This age indicates that volcanism in the back-arc seamounts started at *c.* 17 Ma, i.e. about 2 Ma before the cessation of spreading of the Shikoku Basin. Start of volcanism in the back-arc

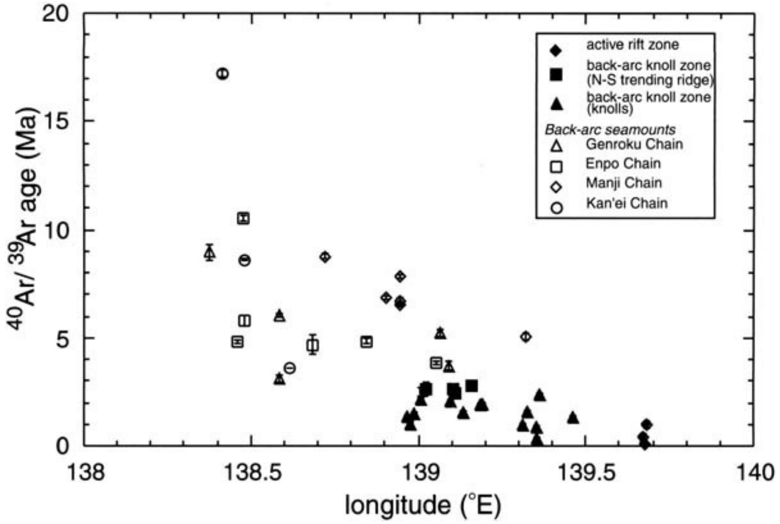

Fig. 9. Longitude v. $^{40}Ar/^{39}Ar$ age plot for the back-arc volcanics. The vertical axis is a plateau age of each sample. The horizontal axis represents the longitude of each sample locality.

seamount chains coincides with the resumption of arc volcanism at the volcanic front (Taylor 1992) after a dormant period during back-arc spreading forming the Shikoku Basin. Volcanism on the back-arc seamounts became more vigorous at *c.* 12 Ma, and continued until *c.* 3 Ma (Figs 9, 10). The increase of volcanic activity in the back-arc is almost coincident with that of the frontal arc volcanism (from 13 Ma: Leg 126 Shipboard Scientific Party 1989). Spatial variation of erupted volume of volcanism with time is examined in Figure 10. Figures 8–10 demonstrate that age of volcanism in the back-arc seamount chains in general becomes younger eastwards (i.e. toward volcanic front). Volcanism before 8 Ma only occurs in the western part of the seamount chains, and that after 8 Ma mainly occurs in the eastern part of the chains. Repeated and/or long-lasting volcanic activity and sampling effects (only rocks exposed on the surface of the seamounts were collected) could obscure the temporal variation of locus of active volcanism. Duration of volcanism at a single seamount is revealed to be up to 4.9 Ma. At the Nishi Jokyo Seamount in the Enpo Chain, olivine–clinopyroxene basalt (MWD108–1) yielded an age of 5.8±0.3 Ma, while basaltic andesite lava (#370 6–1) was dated to be 10.67±0.13 Ma (Fig. 9). Rocks from the Syotoku Seamount (MWD92–2 and MWD92–16a) also gave different ages by 3 Ma. Another feature of the volcanism in the back-arc seamount chains that should be considered is that the volcanism seems to have been active in a relatively wide area contemporaneously. For example, three seamounts in the Enpo Chain (north peak of the Nishi Jokyo Seamount, Jokyo Seamount and Ten'na Seamount), whose distances from the volcanic front range from 80 to 106 km, gave identical ages (4.7–4.8 Ma) within analytical error (Fig. 9).

Taking these characteristics of the volcanism into consideration, the locus of active volcanism in the back-arc seamount chains was not a spot, but instead formed a relatively wide zone. The western margin of the active volcanic zone migrated east with time. It is not clear from current knowledge whether the width of the zone narrowed with time or the volcanic zone migrated toward the east.

The youngest age from the back-arc seamount chains is 3.11 Ma, and no evidence of younger volcanism has been obtained. Isolated seamounts in the vicinity of the seamount chains are presumed to have been active in the same period as the seamount chains. Rocks with ages of *c.* 3–5 Ma also occur in the western margin of the back-arc knolls zone (Ishizuka *et al.* 1998*a*).

After 2.8 Ma, volcanism changed its locus and active volcanism took place in the western part of the back-arc knolls zone. At the earliest stage of this volcanism, eruption of basalt occurred along a N–S-trending line and formed ridges up to 20 km long and at least 200 m high based on the present-day bathymetry. From 2.5 to 1 Ma, bimodal volcanism formed knolls in a wide area of the back-arc knolls zone. Systematic temporal variation of the locus of volcanism is not

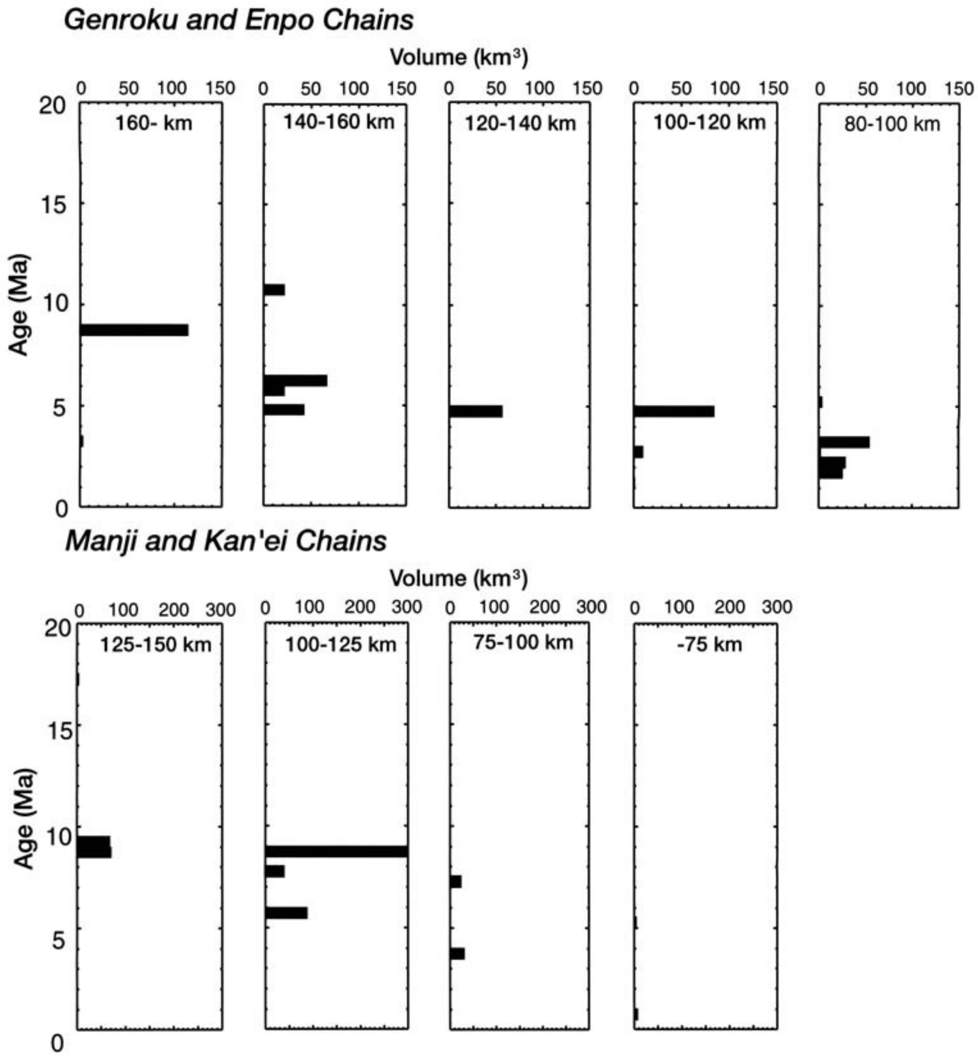

Fig. 10. Spatial and temporal variation of estimated volume of eruption. The horizontal axis is an estimated volume of eruption. The distance shown in each plot is the range of distance of seamounts from volcanic front used in each plot. Upper plots are for the Genroku and Enpo chains, and lower plots are for the Manji and Kan'ei chains. Volume of eruption was estimated using basal diameter and elevation of seamounts was determined following the procedure of Yuasa *et al.* (1991). When more than two ages are obtained for a single seamount, the estimated total volume is equally divided into the eruption of each age.

recognized in the back-arc knolls zone. Volcanism appears to have occurred sporadically in the back-arc knolls zone.

After *c.* 1 Ma, active volcanism was confined to the eastern part of the back-arc knolls zone and active rift zone. Active rifting is presumed to have been limited to the presently active rift zone including the Sumisu and the Myojin rifts.

Volcano-tectonic history of the back-arc region of the Izu–Bonin arc

Age data combined with whole-rock chemistry reveal the following volcanic history in the back-arc region of the Izu–Bonin arc.

- In the back-arc seamounts and adjacent isolated seamounts andesitic–basaltic volcanism, characterized by enrichment of incompatible elements, initiated at *c.* 17 Ma, slightly before the Shikoku Basin ceased spreading, and continued until *c.* 3 Ma.

- From 2.8 to 1 Ma, mainly basaltic volcanism is characterized by eruption of low-SiO_2 and low-Na_2O basalt (Ishizuka *et al.* 1998*a*).
- Volcanism younger than 1 Ma occurred in the active rift zone and its adjacent area.

Figure 11 is a schematic geological map based mainly on the age data of volcanic rocks and single-channel seismic reflection profiles (Honza & Tamaki 1985; Nakao *et al.* 1985). At around 2.8 Ma, the locus of active volcanism changed from the back-arc seamount chains to the western part of the back-arc knolls zone, and chemical characteristics of volcanic rocks also drastically changed at the same time. Ishizuka *et al.* (2002*a*) reported that the basalts from the N–S-trending ridges in the back-arc knolls zone gave ages between 2.4 and 2.8 Ma, and all the ages are concordant within analytical error. Ages of the basalts from the ridges are the oldest in the back-arc knolls, excluding the older basement samples. All of these ridges yield similar basalt lavas, i.e. low-SiO_2 and low-Na_2O basalt, which characteristically occur in the western part of the back-arc knolls zone. This volcanism forming N–S-trending ridges was followed by bimodal volcanism that formed many knolls in the wide area of the back-arc knolls zone. The back-arc knolls zone volcanic rocks are presumed to have been emplaced under an E–W extension, and the mode of volcanism changed in association with the progress of rifting (Ishizuka *et al.* 2002*a*). The age of 2.8 Ma is presumed to approximate the age of initiation of rifting-related volcanism. At the initiation of rifting, basalt with distinct chemical characteristics erupted under the control of the regional stress regime.

Taylor (1992) suggested that the back-arc rifting in the region west of Sumisu Jima Island initiated at around 2.35–2.9 Ma, based on the age of unconformity found in the Ocean Drilling Program (ODP) core from the eastern part of the Sumisu Rift. This age coincides well with the time when rifting is presumed to have initiated in the back-arc knolls zone. Rifting initiated at around 2.8 Ma and active volcanism related to rifting mainly occurred in the western part of the back-arc knolls zone. Rift basin formation was limited to the area east of the Genroku Chain where sediment fill reaches up to 1000 m (Honza & Tamaki 1985). As surface sediment is not disturbed by the faults that caused the offset of the basement of the back-arc knolls zone, these faults are not active at present. In the eastern part of the back-arc knolls zone, adjacent to the active Sumisu and Myojin rifts, basalts younger than 1 Ma were emplaced. The basalts younger than 1 Ma only occur in the easternmost part of the back-arc knolls zone, and have not been found in the western part. The eastern part of the back-arc knolls zone is presumed to have been affected by rifting later than the western part, and rifting-related volcanism had ceased by *c.* 1 Ma in the western part. However, active rifting seems now to have ceased also in the eastern part, and the amount of subsidence is much smaller than in the active rift.

Rifting in the back-arc knolls zone is presumed to have been extensive in the southern part of the surveyed area, i.e. east of the Genroku and Enpo chains. However, in the northern part of the surveyed area, i.e. east of the Kan'ei and Manji chains, the back-arc knolls zone is narrow and rifting appears to have been inactive. The amount of extension related to rifting may have been much smaller in the northern part than in the southern part. Furthermore, overprinting of rifting-related volcanism on the seamount chain structure seems to be very limited in the northern part and older rocks outcrop in the more eastern area in the Kan'ei and Manji chains than in the Enpo and Genroku chains. No low-SiO_2 and low-Na_2O basalt comparable to those found in the back-arc knolls zone have been collected from the northern part of the surveyed area.

Tectonic implication

The dating results revealed that the western margin of the active volcanism in the back-arc seamount chains migrated eastward with time during 17–3 Ma. Provided that the location of volcanic front did not change during this period, the active volcanic zone narrowed and converged to the volcanic front with time. This temporal variation of locus of volcanism might be explained by the oceanward retreat of trench or steepening of the subducting slab. If the trench retreats oceanward, location of volcanic front may also change, but this is not the case for the Izu–Bonin arc. On the other hand, steepening of the subducting Pacific Plate could narrow the zone beneath which slab dehydration occurs and, accordingly, the melting region beneath the back-arc. This process may explain the convergence of volcanism towards the volcanic front without significantly changing the position of volcanic front.

Carlson & Mortera-Gutierrez (1990) showed that the subduction hinge of the Pacific Plate is

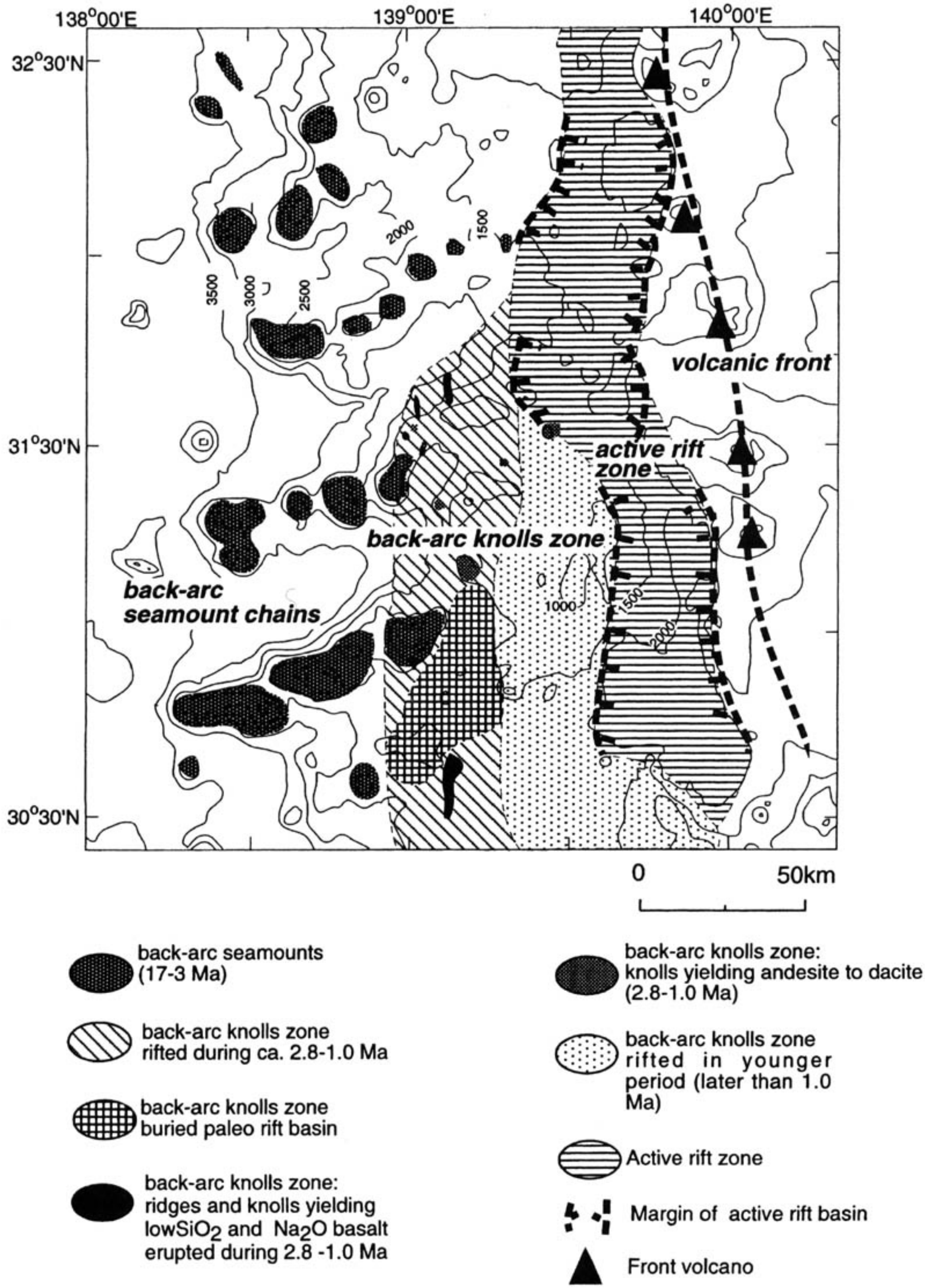

Fig. 11. Tectonic map of the back-arc region of the Izu–Bonin arc between 30°30′N and 32°30′N.

advancing, but the Philippine Sea Plate is retreating faster (10–15 mm a^{-1} at 30°–32°N). This circumstance might have existed during the last 17 Ma and rapid westward movement of the Philippine Sea Plate relative to the Pacific Plate may have caused steepening of the subducting slab. This hypothesis is supported by the synthesis of Carlson & Melia (1984), who pointed out that the dip of subducting slab is highly correlated with the rate of retreat of Philippine Sea Plate.

Steepening of the subducting slab may also explain the initiation of rifting at *c.* 2.8 Ma and eastward migration (or convergence) of the active rift zone after 1 Ma. Steepening of the subducting slab could cause decoupling of the subduction hinge from the Philippine Sea Plate and accordingly an extensional regime in the overriding plate (e.g. Uyeda & Kanamori 1979). Seno *et al.* (1988) proposed that the direction of Philippine Sea Plate motion may have changed from NW to NNW during the period 4–2 Ma. This estimated age for change of plate motion coincides with the age of initiation of rifting. This proposed change of plate motion may have changed the stress regime in the overriding plate and triggered the initiation of rifting. Further detailed reconstruction of plate motions will be required to determine the driving force for the onset of rifting and eastward migration of the locus of rifting.

Conclusions

New laser-heating $^{40}Ar/^{39}Ar$ ages combined with previously reported age data revealed the following volcanic history of the back-arc region of the Izu–Bonin arc.

- In the back-arc seamounts and adjacent isolated seamounts, mainly andesitic–basaltic volcanism initiated at *c.* 17 Ma, slightly before the Shikoku Basin ceased spreading, and continued until *c.* 3 Ma. Volcanism before 8 Ma occurred only in the western part of the back-arc seamount chains, and younger volcanism mainly occurred in the eastern part of the chains. The western margin of the active volcanic zone in the back-arc region had migrated eastward with time, although the volcanism seems to have been active in a relatively wide area contemporaneously.
- At around 2.8 Ma, active volcanism initiated in the western part of the back-arc knolls zone. This volcanism is characterized by eruption of clinopyroxene–olivine basalt. In the first stage of rifting, this basalt erupted from N–S-trending fissures and/or vents and formed N–S-trending ridges. After 2.5 Ma and until 1 Ma, many small knolls formed by eruption of this basalt and minor amounts of acidic rocks.
- Volcanism younger than 1 Ma occurred in the currently active rift zone and its adjacent area.
- The active volcanic zone in the back-arc seamount chains area converged toward the volcanic front with time from 17 to 3 Ma. The observed temporal variation of locus of volcanism may be explained by rapid retreat of the Philippine Sea Plate relative to the Pacific Plate and resulting steepening of the subducting slab. Initiation of rifting and migration or convergence of active rifting and rifting-related volcanism towards the east may be ascribed to the retreat of the subduction hinge, but may also have been triggered by the change of plate motion.

We are grateful to the members of the US–Japan cooperative study on the back-arc region of the Izu–Bonin arc including J. Gill, T. Ishii, S. Morita and A. Klaus. We also thank Mr M. Narui for providing important information on neutron irradiation at the JMTR reactor. Many helpful suggestions on the geology of the Izu–Bonin arc from Drs I. Sakamoto, A. Usui, A. Nishimura, F. Murakami and T. Ishihara are really appreciated. We thank the officers, crews and onboard scientists of the R/V *Moana Wave*, *Tansei-maru*, *Natsushima*, *Yokosuka* and *Hakurei-maru*. The authors greatly appreciate the constructive comments of R. Hickey-Vargas, S. Kelly, P. Leat and R. Larter.

References

CARLSON, R.L. & MELIA, P.J. 1984. Subduction hinge migration. *Tectonophysics*, **102**, 399–411.

CARLSON, R.L. & MORTERA-GUTIERREZ, C.A. 1990. Subduction hinge migration along the Izu–Bonin–Mariana arc. *Tectonophysics*, **181**, 331–344.

ESSER, R.P., MCINTOSH, W.C., HEIZLER, M.T. & KYLE, P.R. 1997. Excess argon in melt inclusions in zero-age anorthoclase feldspar from Mt. Erebus, Antarctica, as revealed by the $^{40}Ar/^{39}Ar$ method. *Geochimica et Cosmochimica Acta*, **61**, 3789–3801.

FLECK, R.J., SUTTER, J.F. & ELLIOT, D.H. 1977. Interpretation of discordant $^{40}Ar/^{39}Ar$ age-spectra of Mesozoic tholeiites from Antarctica. *Geochimica et Cosmochimica Acta*, **41**, 15–32.

FRYER, P., TAYLOR, B., LANGMUIR, C.H. & HOCHSTAEDTER, A.G. 1990. Petrology and geochemistry of lavas from the Sumisu and Torishima back-arc rifts. *Earth and Planetary Science Letters*, **100**, 161–178.

FUJIOKA, K., MATSUO, Y., NISHIMURA, A., KOYAMA, M. & RODOLFO, K.S. 1992. Tephras of the Izu-Bonin forearc (sites 787, 792, and 793). *In:* TAYLOR, B., FUJIOKA, K. *et al. Proceedings of the Ocean Drilling Program, Scientific Results*, **126**, 47–74.

GILL, J.B., SEALES, C., THOMPSON, P., HOCHSTAEDTER, A.G. & DUNLAP, C. 1992. Petrology and geochemistry of Pliocene–Pleistocene volcanic rocks from the Izu arc, Leg 126. *In*: TAYLOR, B., FUJIOKA, K. *et al. Proceedings of the Ocean Drilling Program, Scientific Results*, **126**, 383–404.

HISCOTT, R.N. & GILL, J.B. 1992. Major and trace element geochemistry of Oligocene to Quaternary volcaniclastic sands and sandstones from the Izu–Bonin arc. *In*: TAYLOR, B. & FUJIOKA, K. *et al. Proceedings of the Ocean Drilling Program, Scientific Results*, **126**, 467–486.

HOCHSTAEDTER, A.G., GILL, J.B., KUSAKABE, M., NEWMAN, S., PRINGLE, M., TAYLOR, B. & FRYER, P. 1990*a*. Volcanism in the Sumisu Rift, I. major element, volatile and stable isotope geochemistry. *Earth and Planetary Science Letters*, **100**, 179–194.

HOCHSTAEDTER, A.G., GILL, J.B. & MORRIS, J.D. 1990*b*. Volcanism in the Sumisu Rift, II. subduction and non-subduction related components. *Earth and Planetary Science Letters*, **100**, 195–209.

HONZA, E. & TAMAKI, K. 1985. The Bonin arc. *In*: NAIRN, A.E.M. & UYEDA, S. (eds) *The Ocean Basins and Margins, 7, The Pacific Ocean*. Plenum, New York, 459–502.

IKEDA, Y. & YUASA, M. 1989. Volcanism in nascent back-arc basins behind the Shichito Ridge and adjacent areas in the Izu–Ogasawara arc, northwest Pacific: evidence for mixing between E-type MORB and island arc magmas at the initiation of back-arc rifting. *Contributions to Mineralogy and Petrology*, **101**, 377–393.

ISHIZUKA, O. 1998. Vertical and horizontal variations of the fast neutron flux in a single irradiation capsule and their significance in the laser-heating $^{40}Ar/^{39}Ar$ analysis: case study for the hydraulic rabbit facility of the JMTR reactor, Japan. *Geochemical Journal*, **32**, 243–252.

ISHIZUKA, O., UTO, K., YUASA, M. & HOCHSTAEDTER, A.G. 1998*a*. K–Ar ages from the seamount chains in the back-arc region of the Izu–Ogasawara arc. *The Island Arc*, **7**, 408–421.

ISHIZUKA, O., YUASA, M. & USUI, A. 1998*b*. Low temperature hydrothermal activity on a back-arc seamount of the Izu–Ogasawara arc – submersible survey of the Nishi-Jokyo Seamount. *JAMSTEC Journal of Deep Sea Research*, **14**, 245–268 (in Japanese with English abstract).

ISHIZUKA, O., UTO, K., YUASA, M. & HOCHSTAEDTER, A.G. 2002*a*. Volcanism in the earliest stage of back-arc rifting in the Izu–Bonin arc revealed by laser-heating $^{40}Ar/^{39}Ar$ dating. *Journal of Volcanology and Geothermal Research,* **120**, 71–85.

ISHIZUKA, O., YUASA, M. & UTO, K. 2002*b*. Evidence of porphyry copper-type hydrothermal activity from a submerged remnant back-arc volcano of the Izu–Bonin arc – implications for the volcanotectonic history of back-arc seamounts. *Earth and Planetary Science Letters*, **198**, 377–395.

KLAUS, A., TAYLOR, B., MOORE, G.F., MACKAY, M., BROWN, G., OKAMURA, Y. & MURAKAMI, F. 1992. Structural and stratigraphic evolution of Sumisu Rift, Izu–Bonin arc. *In*: TAYLOR, B., FUJIOKA, K. *et al. Proceedings of the Ocean Drilling Program, Scientific Results*, **126**, 555–573.

LANPHERE, M.A. & BAADSGAARD, H. 2001. Precise K–Ar, $^{40}Ar/^{39}Ar$, Rb–Sr and U/Pb mineral ages from the 27.5 Ma Fish Canyon Tuff reference standard. *Chemical Geology*, **175**, 653–671.

LEG 126 SHIPBOARD SCIENTIFIC PARTY. 1989. Arc volcanism and rifting. *Nature*, **342**, 18–20.

MORITA, S., ISHIZUKA, O., HOCHSTAEDTER, A.G., ISHII, T., YAMAMOTO, F., TOKUYAMA, H. & TAIRA, A. 1999. Volcanic and structural evolution of the northern Izu–Bonin arc. *Chikyu Monthly*, **23**, 79–88 (in Japanese).

NAKAMURA, K., UCHIUMI, S. & SHIBATA, K. 1987. Chemistry and K–Ar age of igneous rocks dredged at the Zenisu Ridge. *Bulletin of the Volcanological Society of Japan*, **32**, 181 (in Japanese).

NAKAO, S., YUASA, M. & NOHARA, M. (eds). 1985. *Research on 'Submarine Hydrothermal Activity in Izu–Ogasawara Arc' 1985 FY Report.* Geological Survey of Japan, Tsukuba (in Japanese).

RENNE, P.R., ERNESTO, M., PACCA, I.G., COE, R.S., GLEN, J.M., PRÉVOT, M. & PERRIN, M. 1992. The age of Paraná flood volcanism, rifting of Gondwanaland, and the Jurassic–Cretaceous boundary. *Science*, **258**, 975–979.

SEIDEMANN, D.E. 1977. Effects of submarine alteration on K–Ar dating of deep-sea igneous rocks. *Geological Society of America Bulletin*, **88**, 1660–1666.

SENO, T., SEKIGUCHI, S. & YOSHIDA, A. 1988. Philippine Sea plate motions as determined by the slab pull forces for the past 4 My. *The Earth Monthly*, **10**, 646–654 (in Japanese).

STEIGER, R.H. & JÄGER, E. 1977. Subcommision on geochronology: convention on the use of decay constants in geo- and cosmochronology. *Earth and Planetary Science Letters*, **36**, 359–362.

TATSUMI, Y., MURASAKI, M. & NOHDA, S. 1992. Across-arc variation of lava chemistry in the Izu–Bonin arc: identification of subduction components. *Journal of Volcanology and Geothermal Research*, **49**, 179–190.

TAYLOR, B. 1992. Rifting and the volcanic–tectonic evolution of the Izu–Bonin–Mariana arc. *In*: TAYLOR, B., FUJIOKA K. *et al. Proceedings of the Ocean Drilling Program, Scientific Results*, **126**, 627–651.

TAYLOR, J.R., 1982. *An Introduction to Error Analysis.* University Science Books, Mill Valley, CA.

TAYLOR, R.N. & NESBITT, R.W. 1998. Isotopic characteristics of subduction fluids in an intra-oceanic setting, Izu–Bonin arc, Japan. *Earth and Planetary Science Letters*, **164**, 79–98.

TURNER, G. & CADOGAN, P.H. 1974. Possible effects of ^{39}Ar recoil in $^{40}Ar/^{39}Ar$ dating. *Geochimica et Cosmochimica Acta*, Supplement **5** (proceedings of the Fifth Lunar Science Conference), 1601–1615.

TURNER, S., REGELOUS, M., KELLY, S., HAWKESWORTH, C. & MANTOVANI, M. 1994. Magmatism and continental break-up in the South Atlantic: high precision $^{40}Ar/^{39}Ar$ geochronology. *Earth and Planetary Science Letters*, **121**, 333–348.

UCHIUMI, S. & SHIBATA, K. 1980. Errors in K–Ar age determinations. *Bulletin of Geological Survey of*

Japan, **31**, 267–273 [in Japanese with English abstract].

URABE, T. & KUSAKABE, M. 1990. Barite silica chimneys from the Sumisu Rift, Izu-Bonin arc: possible analogue to hematitic chert associated with Kuroko deposits. *Earth and Planetary Science Letters*, **100**, 283–290.

USUI, A., YUASA, M., ISHIZUKA, O. & HOCHSTAEDTER, A.G. 1996. Hydrogenetic and hydrothermal manganese crusts of the Nishi-Shichito Ridge: R/V *Moana Wave* cruise MW9507. (Abstract.) Japan Earth and Planetary Science Joint Meeting, 495.

UTO, K., ISHIZUKA, O., MATSUMOTO, A., KAMIOKA, H. & TOGASHI, K. 1997. Laser-heating $^{40}Ar/^{39}Ar$ dating system of the Geological Survey of Japan: system outline and preliminary results. *Bulletin of the Geological Survey of Japan*, **48**, 23–46.

UYEDA, S. & KANAMORI, H. 1979. Back-arc opening and the mode of subduction. *Journal of Geophysical Research*, **84**, 1049–1061.

YORK, D. 1969. Least squares fitting of a straight line with correlated errors. *Earth and Planetary Science Letters*, **5**, 320–324.

YUASA, M. 1985. Sofugan tectonic line, a new tectonic boundary separating northern and southern parts of the Izu-Ogasawara (Bonin) arc, northwest Pacific. *In*: NASU, N., KOBAYASHI, K., UEDA, S., KUSHIRO, I. & KAGAMI, H. (eds) *Formation of Active Ocean Margins*. Terra Scientific, Tokyo, 483–496.

YUASA, M. & NOHARA, M. 1992. Petrographic and geochemical along-arc variations of volcanic rocks on the volcanic front of the Izu-Ogasawara (Bonin) arc. *Bulletin of the Geological Survey of Japan*, **43**, 421–456.

YUASA, M., MURAKAMI, F., SAITO, E. & WATANABE, K. 1991. Submarine topography of seamounts on the volcanic front of the Izu-Ogasawara (Bonin) arc. *Bulletin of the Geological Survey of Japan*, **42**, 703–743.

This page intentionally left blank

Geochemical evolution of magmatism in an arc–arc collision: the Halmahera and Sangihe arcs, eastern Indonesia

COLIN G. MACPHERSON[1,2], EMILY J. FORDE[2], ROBERT HALL[2] & MATTHEW F. THIRLWALL[2]

[1]*Department of Earth Sciences, University of Durham, South Road, Durham DH1 3LE, UK (e-mail: colin.macpherson@durham.ac.uk)*

[2]*SE Asia Research Group, Department of Geology, Royal Holloway University of London, Egham, Surrey TW20 0EX, UK*

Abstract: The Molucca Sea Collision Zone in eastern Indonesia is the site of an orthogonal collision between two active subduction systems. Both the Halmahera subduction zone, to the east, and the Sangihe subduction zone, to the west, have subducted oceanic lithosphere of the Molucca Sea Plate, which has now been completely consumed. Both volcanic arcs were active since the Neogene and provide a means of probing the element fluxes through the two systems. The geochemistry of Neogene and Quaternary lavas from each volcanic arc is compared to constrain changes in the mass fluxes through the systems and the processes controlling these fluxes at different times during their history. Both arcs show increased evidence for sediment recycling as the collision progressed, but for contrasting reasons. In Halmahera this may represent an increased sediment flux through the arc front, while in Sangihe it may simply reflect a greater opportunity for melting of sediment-fluxed portions of the mantle wedge. In both cases the change in arc geochemistry can be related to the evolving architecture of that particular subduction zone. The Halmahera lavas also record a temporal change in the chemistry of the mantle component that resulted from induced convection above the falling Molucca Sea Plate drawing compositionally distinct peridotite into the mantle wedge.

The geochemistry of magmatism is an important tool for understanding the internal processes of active subduction zones and for providing constraints on the geodynamics of ancient convergent plate margins. Subduction-zone magmas are generated when melting occurs in the wedge of mantle trapped between the lower (subducted) plate and the upper (overriding) plate, onto which lavas are erupted. Geochemical evidence suggests that fluids are released from the subducted plate as pressure increases, causing hydrous mineral phases to break down and release volatiles. This provides a medium for mass transport from the subducted plate into the mantle wedge and may also encourage melting of the wedge by lowering its solidus temperature. Melting of sediment carried down on the surface of the subducted plate may provide another means of transporting subducted material into the source of lavas. Geochemical investigation of well-sampled traverses along and across arcs have shown that spatial changes in mass transfer processes, the material subducted and magma interaction with the overriding plate are all important features of active subduction systems (e.g. Ben Othman *et al.* 1989; Morris *et al.* 1990; Tatsumi *et al.* 1991; Edwards *et al.* 1993; Plank & Langmuir 1993; Vroon *et al.* 1993; Pearce *et al.* 1995; Davidson 1996; Ryan *et al.* 1996; Elliott *et al.* 1997; Peate *et al.* 1997; Turner & Hawkesworth 1997; Macpherson *et al.* 1998; Woodhead *et al.* 1998; Hochstaedter *et al.* 2001; van Soest *et al.* 2002). However, recent magmatic products from subduction systems provide less opportunity for studying temporal changes in these factors, especially on the timescales over which the architecture of subduction zones are likely to change, i.e. millions to tens of millions of years.

This contribution investigates the temporal evolution of two volcanic arcs in Indonesia. The Halmahera and Sangihe arcs are undergoing orthogonal collision after subducting a single piece of oceanic lithosphere (the Molucca Sea Plate) from the east and west, respectively. Neogene volcanic rocks are exposed, to varying degrees, in both arcs and their geochemistry can be compared with more recent lavas from the Quaternary arcs. Therefore, we are able to investigate magmatic systems that are reaching the end of their lifetime as island arcs and are becoming a single collision zone. There are significant differences between the architecture of these systems and the processes operating

From: LARTER, R.D. & LEAT, P.T. 2003. *Intra-Oceanic Subduction Systems: Tectonic and Magmatic Processes.* Geological Society, London, Special Publications, **219**, 207–220. 0305-8719/03/$15.00

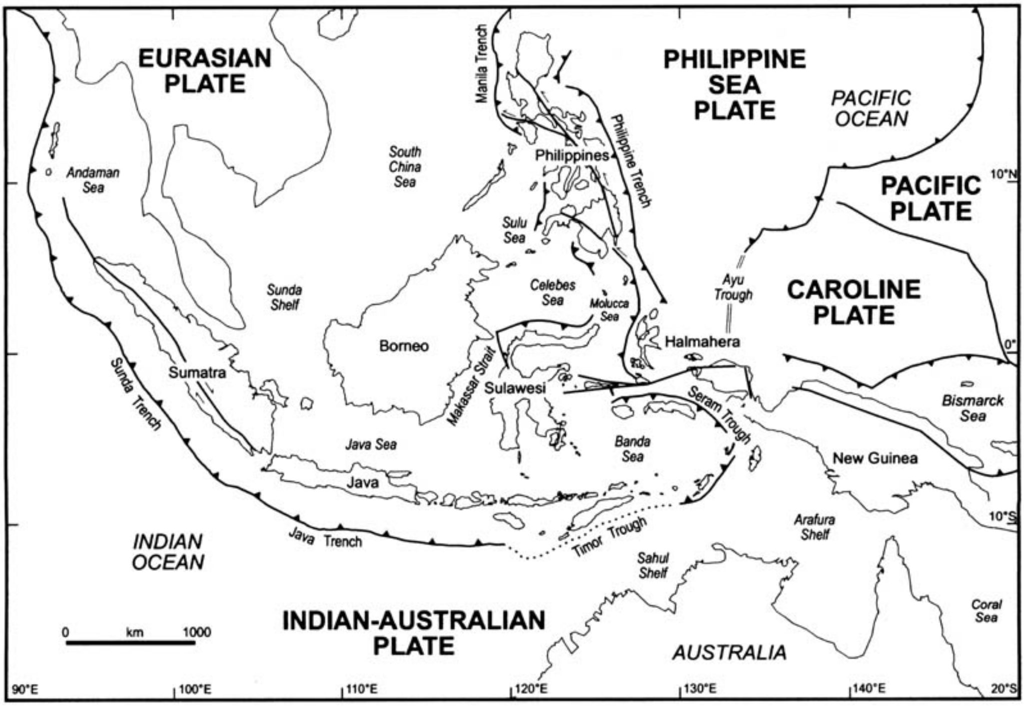

Fig. 1. Map of SE Asia highlighting major tectonic plates and plate boundaries. Plate names are shown in bold type and subduction zones are indicated by lines with barbs on the overriding plate.

within them that have important effects on the composition of the lavas erupted during the Neogene and Quaternary.

Geological setting of the Molucca Collision Zone

SE Asia and the SW Pacific are dominated by convergence between the Eurasian, the Indian–Australian and the Pacific plates (Fig. 1). In addition, the Philippine Sea Plate, which lies between the Pacific and Eurasian plates, has played a crucial role in the region's development. There are currently a large number of other small plates and plate fragments, and a similar complexity has probably existed throughout the Cenozoic (Hall 1996, 2002).

The Halmahera and Sangihe arcs form the Molucca Sea Collision Zone, which is itself part of an elongate zone of convergence extending north through the Philippines towards Taiwan (Fig. 1). The polarity and location of subduction varies along the length of this zone, and in the south the Halmahera and Sangihe arcs form the eastern and western margins of an orthogonal arc–arc collision (Fig. 2). During the Neogene, both arcs consumed oceanic lithosphere of the Molucca Sea Plate (Cardwell *et al.* 1980), which has now been entirely consumed such that the Sangihe arc is presently overriding the Halmahera forearc (Hall 2000) (inset to Fig. 2).

Neogene magmatic rocks in Halmahera overlie ophiolitic basement and arc volcanic rocks that represent an early Tertiary period of subduction (Hall *et al.* 1991). In the Halmahera arc Miocene magmatism is represented by exposures of volcanic rocks in the southern islands of Obi and Bacan, and in the centre of Halmahera itself where its four arms converge (Fig. 2). The oldest Neogene volcanic rocks, dated at about 11 Ma, are found in Obi at the southern end of the arc, but the most extensive areas of Neogene volcanic rocks are the Upper Miocene and Pliocene deposits of Bacan and Halmahera (Hakim & Hall 1991; Baker & Malaihollo 1996). These rocks are mainly andesitic with rare basalts and dacites (Hakim & Hall 1991; Malaihollo & Hall 1996). The active Halmahera arc extends along the north arm of Halmahera Island, through the islands of Tidore and Ternate, but Quaternary cones are present as far

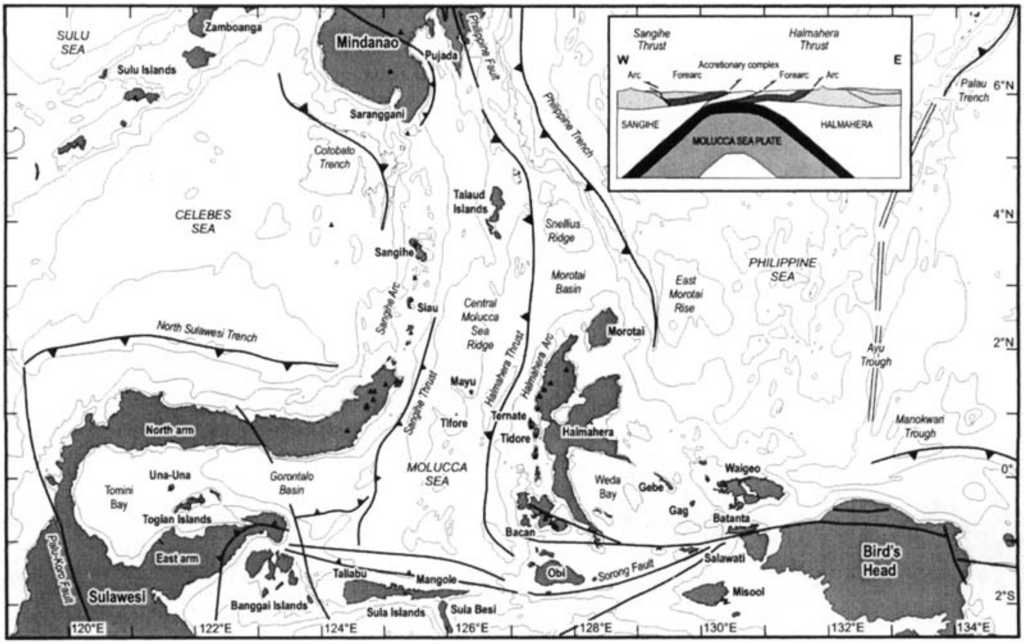

Fig. 2. Geographical features of the Molucca Sea and surrounding regions. Small black filled triangles are volcanoes from the Smithsonian database. Bathymetric contours at 200, 2000, 4000 and 5000 m from the *GEBCO Digital Atlas* (IOC, IHO & BODC 1997). Lines with large barbs are subduction zones and lines with small barbs are thrusts. Note that the direction of surface thrusting in the Molucca Sea is correctly shown. Thrusts on each side of the Molucca Sea are directed outwards towards the adjacent arcs, although the subducting Molucca Sea Plate dips east beneath Halmahera and west below the Sangihe arc. The Halmahera arc is being overridden by the Sangihe arc as shown in the inset figure.

south as Bacan (Fig. 2). Volcanic rocks erupted during the Quaternary range from basalt through to dacite, but are most commonly basaltic andesites and andesites (Morris *et al.* 1983; Malaihollo & Hall 1996).

The basement of the Sangihe arc is thought to comprise pre-Miocene ophiolitic or arc crust (Carlile *et al.* 1990). The arc extends from the northern tip of Sulawesi through the Sangihe islands, but terminates south of Mindanao due to a reversal in subduction polarity where the Cotobato Trench begins (Fig. 2). In the north, the arc is made up entirely of Quaternary volcanic islands and there is significant volcanic and geothermal activity on the eastern tip of the north arm of Sulawesi (Morrice *et al.* 1983; Morrice & Gill 1986) where older portions of the arc are also exposed. The oldest known Neogene volcanic rocks of the Sangihe arc occur on Sulawesi (Elburg & Foden 1998), where Late Miocene–Pliocene magmatism is also recognized (Polvé *et al.* 1997). Like Halmahera, lavas erupted throughout the history of this arc vary from basaltic to dacitic compositions, but andesitic rocks dominate (Morrice *et al.* 1983; Elburg & Foden 1998).

Data-set

Data are available from the Late Neogene and Quaternary segments of both the Halmahera and Sangihe arcs. Previous studies of both arcs have identified instances of crustal contamination and, for the purposes of this study, we have eliminated any analyses suspected of recording this process. Neogene volcanic rocks from central Halmahera, Bacan and Obi in the Halmahera arc were analysed by Forde (1997), while Morris *et al.* (1983) obtained data from the Quaternary arc. Elburg & Foden (1998) produced data from the entire range of known ages for the Sangihe arc. The Sangihe data-set is necessarily small due to the lack of published data suitable for comparison with the Halmahera data; however, Elburg & Foden's data-set represents the entire suite of analyses available at this time and so we make the assumption that these represent the magmatism of the Sangihe

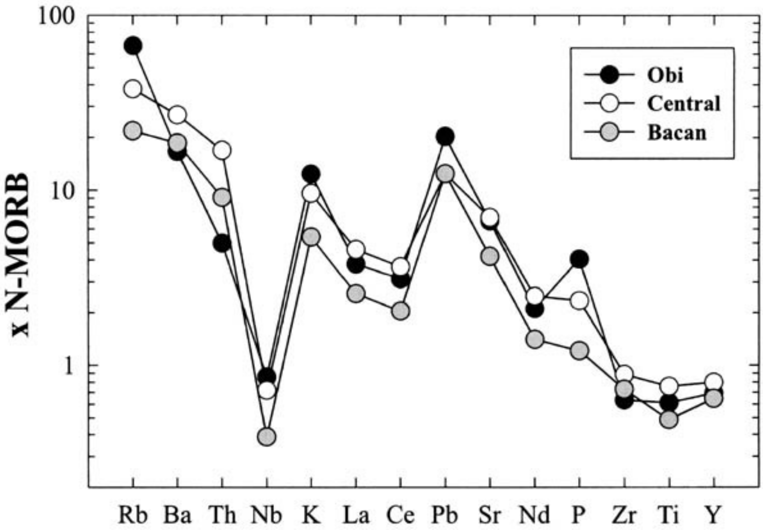

Fig. 3. Incompatible element abundances of the least-evolved Neogene Halmahera arc lavas, from the islands of Obi and Bacan and from central Halmahera, normalized to N-MORB (Sun & McDonough 1989).

arc. Where available, we have used other geochemical data from this arc to provide qualitative support for our conclusions. Conclusions reached below may have to be revised if the existing data-set for the Sangihe arc is shown to be unrepresentative. We have chosen to focus on a small number of key trace element and isotopic ratios to simplify the discussion. This is also forced on us by the less extensive coverage of trace element analyses for the Quaternary lavas from Halmahera, but the wider range of geochemical data for the remaining suites are consistent with the interpretations presented below. Finally, as the Molucca Sea Plate has been largely subducted, it is not possible to sample the crust itself or the sediments it carried. Therefore, we have not attempted to produce detailed geochemical models of particular processes discussed in this paper.

Geochemical evolution of the Molucca Sea Collision Zone

Neogene Halmahera arc

The geochemistry of Neogene magmatism in the Halmahera arc displays typical subduction zone characteristics (Forde 1997). Normalized incompatible element plots (Fig. 3) reveal that, relative to normal mid-ocean ridge basalt (N-MORB), the Neogene arc erupted lavas with elevated ratios of the large ion lithophile elements (LILEs) and the light rare earth elements (LREEs) to the high-field strength elements (HFSEs). Such patterns are considered typical of subduction zones in which the mantle wedge has been contaminated by fluid released from the subducted slab (e.g. McCulloch & Gamble 1991; Davidson 1996). Lead isotope ratios highlight two further important features of the sources contributing to the Neogene arc. First, the rocks with the lowest $^{206}Pb/^{204}Pb$, which are assumed to lie close to the composition of uncontaminated mantle wedge, have $^{207}Pb/^{204}Pb$ and $^{208}Pb/^{204}Pb$ ratios that are more elevated than MORB from the Pacific and Atlantic oceans (Fig. 4). This is a trait shared with Indian Ocean MORB (I-MORB) and suggests that during the Neogene the mantle wedge beneath Halmahera was part of the I-MORB domain which is consistent with the source inferred for lavas erupted to the north and west of the Molucca Sea during the Eocene and Oligocene (Hickey-Vargas 1998). Second, the data trend away from the main I-MORB array towards relatively high $^{207}Pb/^{204}Pb$ and $^{208}Pb/^{204}Pb$. This is another feature typical of island arc volcanics; such arrays are usually explained by the incorporation of subducted sediment into the source of the magmas (e.g. Morris *et al.* 1983).

More can be learned about the Neogene mantle wedge by considering elements that are likely to be relatively immobile during devolatilization of the slab, such as Nb and Zr, although these may become mobile if slab

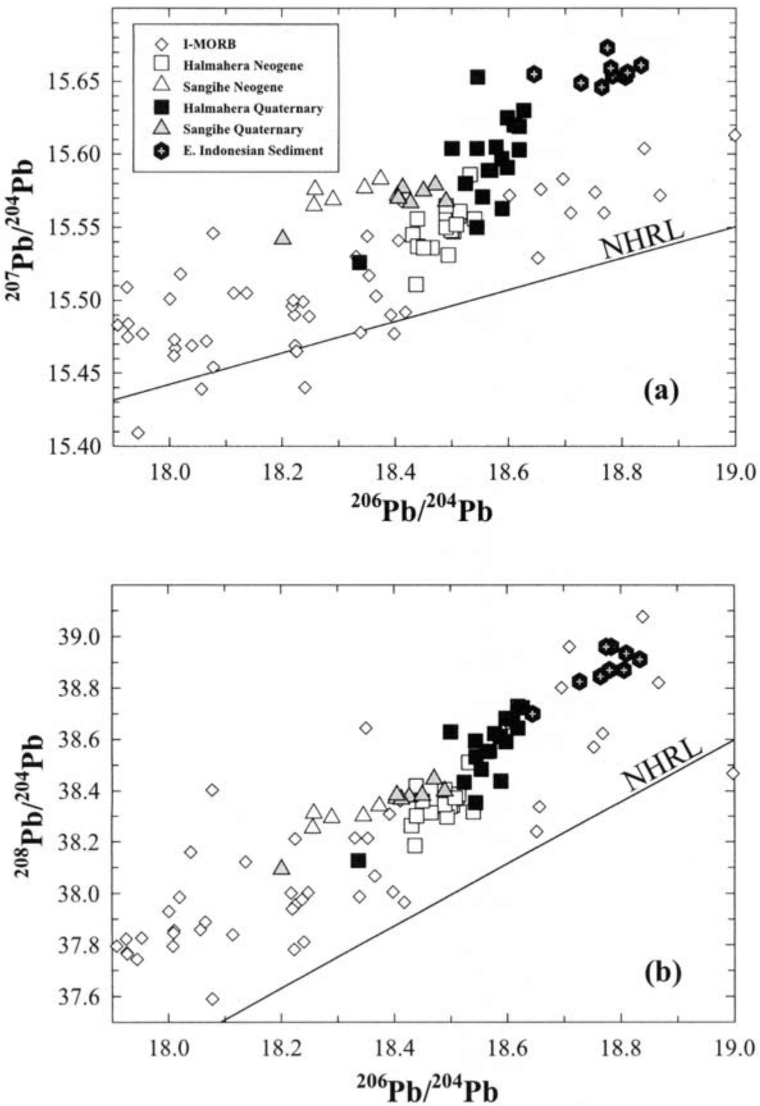

Fig. 4. **(a)** $^{207}Pb/^{204}Pb$ v. $^{206}Pb/^{204}Pb$ and **(b)** $^{208}Pb/^{204}Pb$ v. $^{206}Pb/^{204}Pb$ in Neogene and Quaternary lavas from the Molucca Sea Collision Zone (Morris *et al.* 1983; Forde 1997; Elburg & Foden 1998). The Northern Hemisphere Reference Line (NHRL; Hart 1984), I-MORB (Michard *et al.* 1986; Dosso *et al.* 1988; Le Roex *et al.* 1989; Mahoney *et al.* 1989, 1992; Danyushevsky *et al.* 2000) and East Indonesia sediments (Vroon *et al.* 1995) are shown for comparison.

components melt (Elliott *et al.* 1997). Most MORB display a restricted range in Zr/Nb in contrast to subduction zone lavas in which Zr/Nb varies up to high values (e.g. McCulloch & Gamble 1991). High Zr/Nb lavas cannot be generated directly by melting MORB-source peridotite (Woodhead *et al.* 1993). Instead, the high Zr/Nb signature is thought to characterize mantle that has previously lost a basaltic melt fraction, leaving behind a source that is more depleted in the most highly incompatible elements, such as Nb. Furthermore, refractory sources require high fluid fluxes to lower the solidus and assist the melting process, therefore, high Zr/Nb ratios are consistent with fluid fluxing as an important recycling mechanism. Source contamination by sediments, or partial melts derived from sediments, would most probably reduce the Zr/Nb ratio of the source of arc lavas (Elliott *et al.* 1997).

Neogene lavas from Halmahera display considerable Zr/Nb variation with a strong spatial control (Fig. 5). The southernmost, and oldest, lavas from Obi possess a narrow range in Zr/Nb that is similar to the mean value of MORB. This suggests that the mantle wedge beneath Obi contained relatively fertile mantle similar to the source of MORB from the major ocean basins. The Neogene lavas from Central Halmahera and Bacan also show quite restricted ranges for Zr/Nb, but at progressively higher values with only minor overlap between the different centres. This suggests that during the Neogene the sources of Central Halmahera and Bacan lavas were increasingly depleted relative to the source of MORB. Prior depletion of the mantle wedge is consistent with HFSE concentrations, which are consistently less than N-MORB (Fig. 3). Zr/Nb is similar to, or greater than, N-MORB in rocks from all three sites suggesting sediments made an insufficient contribution to modify this ratio in the source of the Neogene arc. The Central Halmahera and Bacan suites were probably erupted at similar distances from the trench, so their contrasting Zr/Nb implies along-arc variations in the degree of mantle wedge depletion.

The relationship between the mantle wedge and the recycled component in the Neogene Halmahera arc is explored further in Figure 6. There is a broad positive correlation between Ba/Nb and Zr/Nb, with some scatter to higher Ba/Nb at intermediate Zr/Nb. This is consistent with an important role for fluid fluxing of the mantle wedge. Ba is highly mobile in fluids released from both subducted oceanic crust and its sedimentary cover (Brennan *et al.* 1995; Keppler 1996; You *et al.* 1996), so high Ba/Nb ratios represent a high fluid flux. More depleted (higher Zr/Nb) mantle will possess lower concentrations of trace elements, so incoming fluids will be more visible in any mixture, thus producing a broad correlation between Zr/Nb and Ba/Nb (Fig. 6). Scatter to higher Ba/Nb at constant Zr/Nb could represent more variable fluid fluxes at any location. This seems to be particularly true for Central Halmahera lavas, in which Zr/Nb values lie between 30 and 50.

In summary, Neogene Halmahera arc magmatism was generated from a mantle wedge that was part of the I-MORB domain. This mantle had experienced prior melt extraction and there is evidence that the amount of depletion varied along the strike of the arc. Slab dehydration added fluid-mobile elements to the source and may have helped promote melting. Lead isotope ratios indicate that relatively modest quantities of sediment were also incorporated into the source of the lavas.

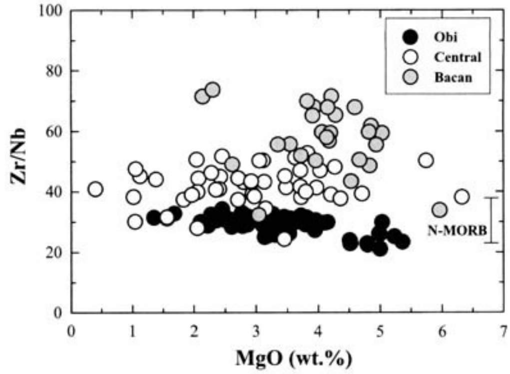

Fig. 5. Zr/Nb v. MgO for Neogene lavas from the islands of Obi and Bacan and from central Halmahera, in the Halmahera arc (Forde 1997).

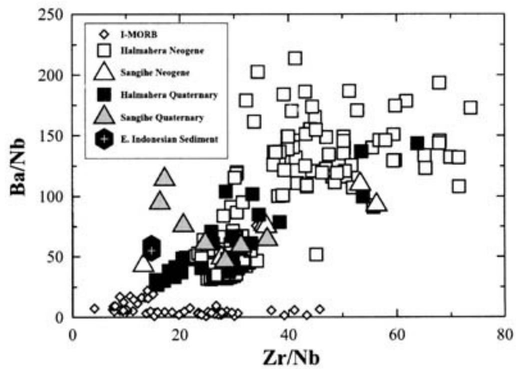

Fig. 6. Ba/Nb v. Zr/Nb for Molucca Sea Collision Zone lavas, with I-MORB and sediment from eastern Indonesia for comparison (see Fig. 4 for data sources).

Quaternary Halmahera arc

Quaternary lavas from the Halmahera arc (Morris *et al.* 1983) differ from the Neogene arc in their lead isotope and trace element ratios. One Quaternary lava lies at the low $^{206}Pb/^{204}Pb$ end of the Neogene array, but still within the I-MORB field, and represents our best estimate of uncontaminated mantle presently lying beneath Halmahera (Fig. 4). The majority, however, are displaced to higher $^{206}Pb/^{204}Pb$, $^{207}Pb/^{204}Pb$ and $^{208}Pb/^{204}Pb$ values, and extend the Neogene array well beyond the I-MORB field. This

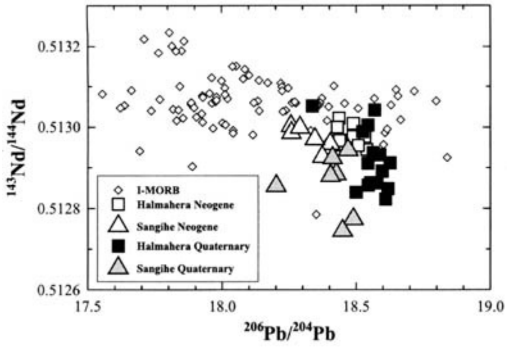

Fig. 7. $^{143}Nd/^{144}Nd$ v. $^{206}Pb/^{204}Pb$ for Molucca Sea Collision Zone lavas and I-MORB. Data sources as in Figure 4 plus Rehkämper & Hofmann (1997) and references therein.

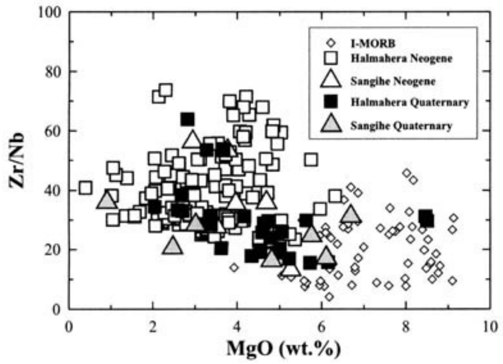

Fig. 8. Zr/Nb v. MgO for Molucca Sea Collision Zone lavas and I-MORB (see Fig. 4 for data sources).

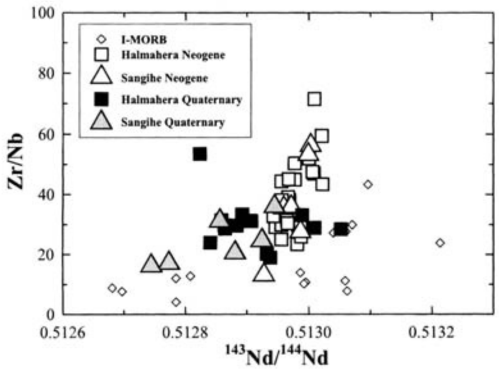

Fig. 9. Zr/Nb v. $^{143}Nd/^{144}Nd$ for Molucca Sea Collision Zone lavas and I-MORB. Data sources as in Figure 4.

suggests that the components recycling Pb into the sourse of the Halmahera arc were similar from the Neogene until the present day, but this process contributed a greater fraction to the source of Quaternary lavas. As noted above, such arrays are commonly interpreted as reflecting an increased sediment input to the source of lavas. An important role for sediment recycling can also be inferred from Nd isotope ratios as $^{143}Nd/^{144}Nd$ is substantially lower in the high-$^{206}Pb/^{204}Pb$ Quaternary lavas, which again extend beyond the vast majority of I-MORB rocks (Fig. 7). Hochstaedter *et al.* (2001) observed Pb isotope variations resembling the Halmahera arrays in Figure 4 in transects across the Izu–Bonin arc. These were explained as the result of contamination of variably depleted mantle wedge by fluids derived at different stages of slab devolatilization. An important conclusion of their work was that the ratio of material derived from subducted oceanic crust and sediment remained constant in all slab-derived fluids. If this were true in Halmahera the strongly increased $^{206}Pb/^{204}Pb$, $^{207}Pb/^{204}Pb$ and $^{208}Pb/^{204}Pb$ (Fig. 4) and decreased $^{143}Nd/^{144}Nd$ (Fig. 7) values of the Quaternary suite, relative to the Neogene, would require a substantial increase in either the fluid flux through the arc or the depletion of the mantle wedge to make the recycled signature more visible. Neither scenario is supported by the trace element data leaving the alternative explanation; that the extent of sediment recycling increased from the Neogene to the Quaternary.

The Zr/Nb data also differ through the history of the Halmahera arc. Quaternary lavas have ratios that are, for the most part, similar to or lower than N-MORB (Fig. 8). As mentioned above, addition of a subducted sedimentary component can lower Zr/Nb levels of arc sources (Elliott *et al.* 1997). However, a comparison of the isotopic and trace element data for the Quaternary arc does not provide convincing support for this. For example, there is no clear correlation between Zr/Nb and $^{143}Nd/^{144}Nd$ (Fig. 9), suggesting either that sediment addition has not influenced trace element ratios or that some additional factor has influenced the source of the Quaternary arc.

Ba/Nb data also suggest that a distinctive component has affected the Quaternary lavas. There is a global correlation between the Ba flux entering a particular subduction zone in sediment and the Ba contents of arc lavas erupted by that subduction zone (Plank & Langmuir 1993; Peate *et al.* 1997). Therefore, we assume, as a broad approximation, that Ba partitioning during partial melting of sediment varies relatively little between arcs. If increased sediment recycling is the main control on the changing trace element inventory of the Halmahera arc sources, the Quaternary array in Figure 6 requires any sedimentary component added to their source to have relatively low Ba/Nb. Pelagic clays and volcaniclastic sediment are two possible low Ba/Nb sediments (Elliott *et al.* 1997; Peate *et al.* 1997). As the Molucca Sea Plate cannot be sampled, we have no way of estimating the proportion of these relative to other types of sediment that were subducted beneath Halmahera. However, we note that the volcaniclastic sediments are unlikely to possess sufficiently low $^{143}Nd/^{144}Nd$ to produce the isotopic shift apparent in the Quaternary lavas (Fig. 7). Therefore, pelagic clay, similar to that found in the western Pacific (Elliott *et al.* 1997), appears to provide the most likely sedimentary contaminant.

An alternative explanation for the Zr/Nb and Ba/Nb characteristics of the Quaternary arc is that the composition of the mantle wedge beneath Halmahera may have changed. The trace element characteristics of the youngest Halmahera lavas include a tendency towards more enriched mid-ocean ridge basalt (MORB) compositions (low Ba/Nb, relative to other arc lavas, and low Zr/Nb; Figs 6 and 8) found in various parts of the Indian Ocean (Le Roex *et al.* 1989; Mahoney *et al.* 1989, 1992). In addition to the change in the recycled component, the mantle wedge composition may have changed in the Halmahera arc with the introduction of enriched I-MORB. Over the lifetime of an arc, peridotite is cycled through the mantle wedge as a result of convection induced by 'slab rollback' (Andrews & Sleep 1974; Hamilton 1995). Volcanic rocks erupted at spreading centres in the Indian Ocean (Fig. 6) demonstrate that the I-MORB mantle domain contains low-Ba/Nb, low-Zr/Nb portions, which could be drawn into the mantle wedge as a source for the Quaternary lavas. Plate reconstruction of the Molucca Sea region suggests that Halmahera was particularly susceptible to this type of mantle wedge circulation due to the large amount of rollback associated with the arc between the Neogene and Quaternary (see Macpherson & Hall 2002, figs 4 and 7). Therefore, the Quaternary arc appears to have experienced a greater flux of recycled sediment than the Neogene arc, but the mantle wedge may also have sampled compositionally distinctive parts of the I-MORB domain. Using the possible sediment components suggested by Elburg & Foden (1998) and our best estimate of the mantle wedge, the estimated sediment contributions are 0.3–1% during the Neogene and 0.1–2.2% during the Quaternary.

Sangihe arc

Elburg & Foden (1998) studied changes in the geochemistry of Sangihe arc lavas from the Neogene to Recent. They demonstrated a characteristic subduction zone signature with elevated LILE/HFSE and LREE/HFSE ratios and distinctive isotope ratios. Like Halmahera, Elburg & Foden (1998) identified an I-MORB affinity for the mantle wedge beneath Sangihe and suggested that low concentrations of HFSE and the heavy rare earth elements (HREEs) indicate that the mantle wedge had previously experienced partial melting. There are also differences between the trace element and isotopic characteristics of the Neogene and Quaternary Sangihe arcs. Elburg & Foden (1998) attributed these changes to (i) a decrease in the extent of prior depletion with time coupled with (ii) a change from fluid-dominated to sedimentary melt-dominated recycling from the Neogene to the present day.

Elburg & Foden (1998) interpreted lower Zr/Nb, lower $^{143}Nd/^{144}Nd$ and higher Pb isotope ratios as evidence that partial melt from sediment became the dominant recycling mechanism in the Sangihe arc during the Quaternary. Like Halmahera, the isotope ratios changed with time (Figs 4 and 7). Furthermore, decreasing $^{143}Nd/^{144}Nd$ in the Quaternary lavas correlates well with decreasing Zr/Nb (Fig. 9), which is consistent with adding a partial melt of subducted sediment to the source of the younger lavas (Elliott *et al.* 1997; Elburg & Foden 1998). In contrast to Halmahera, low Zr/Nb ratios are associated with higher Ba/Nb (Fig. 6) in the Sangihe arc, which could also be generated by partial melting of sediment with moderate Ba/Nb, such as East Indonesian sediment (Fig. 6).

Geodynamic evolution of the Molucca Sea Collision Zone

Geochemical evidence has resulted in similar conclusions regarding the evolution of the Halmahera and Sangihe arcs. Both appear to have experienced an increase in the amount of sediment incorporated into their sources and both have seen an evolution in the composition of the mantle wedge. Because it is not possible to sample either the oceanic crust of the Molucca Sea Plate or its sedimentary cover, the processes discussed above have not been modelled in detail. Nevertheless, there are significant differences between the geochemistry of the lavas erupted in the two arcs that provide clues as to the tectonic processes that have affected each. First, the Halmahera and Sangihe data-sets form oblique arrays in plots of $^{207}Pb/^{204}Pb$ v. $^{206}Pb/^{204}Pb$ and $^{208}Pb/^{204}Pb$ v. $^{206}Pb/^{204}Pb$ (Fig. 4). This indicates that each arc sampled isotopically distinct mantle wedges and that these were contaminated by different recycled components. The wedge beneath Halmahera has higher $^{206}Pb/^{204}Pb$ values than Sangihe, while the sediment incorporated beneath Halmahera has higher $^{207}Pb/^{204}Pb$ and $^{208}Pb/^{204}Pb$ at a given $^{206}Pb/^{204}Pb$ value (similar to the least radiogenic East Indonesian sediment, Fig. 4). The difference is also apparent in Figure 7, where the whole Halmahera array is displaced to higher $^{206}Pb/^{204}Pb$. Second, the Quaternary Halmahera lavas display less coupling between $^{143}Nd/^{144}Nd$ and trace element ratios than contemporary Sangihe magmatism (Fig. 9), indicating that the former may not have experienced a simple increase in the amount of recycled sediment. Finally, the Quaternary arcs show divergent arrays in Ba/Nb v. Zr/Nb sapce. As discussed above, the latter two observations may reflect distinctive mantle wedges and recycled sedimentary components beneath the two arcs. In this section we shall discuss the geodynamic controls that were responsible for this contrasting evolution in the different parts of the collision zone.

Halmahera

In the Halmahera arc, the increased $^{206}Pb/^{204}Pb$, $^{207}Pb/^{204}Pb$ and $^{208}Pb/^{204}Pb$, and decreased $^{143}Nd/^{144}Nd$, are found at centres along the entire length of the arc interspersed with, or even at the same centres as, rocks containing a weaker sedimentary imprint. This suggests that the increase in sediment fluxing is a ubiquitous feature of the arc and requires a mechanism to increase the sediment flux close to the volcanic front. Following the models of Elliott *et al.* (1997), this can be achieved by compressing the distance between the parts of the mantle wedge where fluid fluxing and sediment melting dominate mass transfer. Steepening of the subducted slab provides a mechanism whereby this compression could occur. Hall *et al.* (1988) proposed that localized deformation and tilting of fault-bounded blocks throughout the main island of Halmahera, and an unconformity in the Weda Basin to the southeast of Halmahera, resulted from steepening of the eastern limb of the Molucca Sea Plate during the Pleistocene. The dip of the Molucca Sea slab may have increased due to a downward force from the Philippine Sea Plate at the newly formed Philippine Trench to the north, or through westward motion of continental fragments along splays of the Sorong Fault at the southern end of the arc (Hall *et al.* 1988). As slab dehydration and sediment melting are thought to be pressure-dependent, slab steepening would bring the locus of sediment melting closer to the arc front during the Quaternary than it had been during the Neogene, therefore increasing the flux of recycled sediment in volcanic arc lavas. Steepening of the slab would also increase the effects of slab rollback in the mantle, in turn increasing the rate of replenishment of the mantle wedge. Therefore, slab steepening can also explain the way in which peridotite with distinctive trace element characteristics (Fig. 6) could be incorporated into the Halmahera mantle wedge.

Sangihe arc

Elburg & Foden (1998) argued that the low $^{143}Nd/^{144}Nd$ and high $^{206}Pb/^{204}Pb$ of the Quaternary Sangihe lavas are consistent with the input of a component derived from subducted sediment, and proposed two mechanisms to explain the increased sedimentary contribution to younger lavas in their data-set. First, they suggested that as the two arcs collided their accretionary wedges may have overlapped and thickened, thus increasing the likelihood of sediment being subducted. Recent models of the Molucca Sea Collision Complex have suggested that segments of the Halmahera forearc may have penetrated to depth approaching the magma genesis zone beneath the northern Sangihe arc (Lallemand *et al.* 1998; Hall 2000), but whether this is the case in the south is not clear. Second, they suggested that subduction of the Molucca Sea Plate may have slowed down and stopped as the arcs collided, allowing sediment on its upper surface to heat up and melt. However, this assumes that the downward velocity of the Molucca Sea Plate became negligible when the collision occurred or, for subduction more generally, that the motion of overriding plates drives the descent rate of subducted plates. An alternative perspective is that subduction is driven largely by 'slab pull' (e.g. Hamilton 1988, 1995) so that the descent of subducted lithosphere is controlled by the weight of the slab, with the extreme case that overriding plates move passively (or deform) in response to their subducting neighbours. This process must be invoked for models that interpret isolated seismic and tomographic anomalies in the mantle up to 400 km beneath Mindanao, which is thought to be a northern, more advanced extension of the Molucca Sea Collision Zone, as slabs of oceanic lithosphere (Lallemand *et al.*

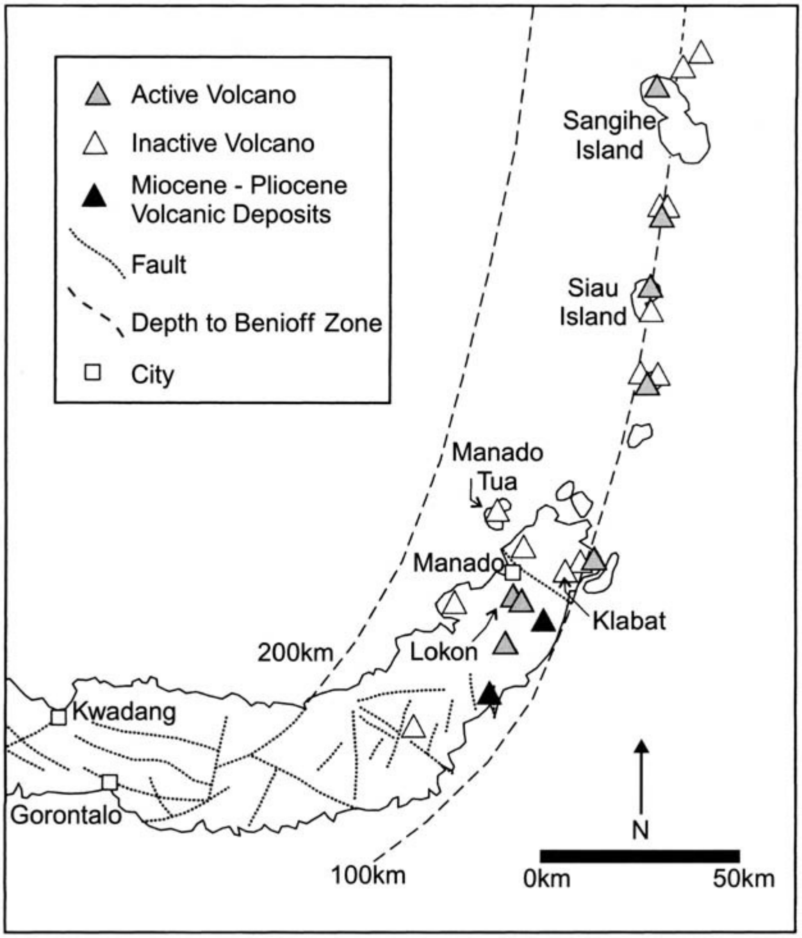

Fig. 10. Map of the southern Sangihe arc collated from Morrice *et al.* (1983), Carlile *et al.* (1990) and Kavalieris *et al.* (1992). Locations of active and inactive Quaternary cones are shown along with the locations of Miocene and Pliocene volcanic rocks sampled by Elburg & Foden (1998).

1998; Rangin *et al.* 1999). If slab pull drove subduction in the Molucca Sea Collision Complex the ever increasing mass in the two limbs of subducted lithosphere acting on the diminishing area of the Molucca Sea Plate at the Earth's surface (Fig. 2, inset) may actually have accelerated the descent rate of the subducted portions. Note also that this may also have contributed to increasing the slab dip beneath Halmahera (see above).

We note that Gill & Williams (1990) used ^{226}Ra- and ^{238}U-excesses to demonstrate the importance of fluid fluxing of the mantle wedge in the very youngest lavas from the Sangihe arc, and Vroon & van Bergen (2000) have also questioned the importance of sedimentary signal at the active Sangihe arc front. This raises the possibility that the change in recycling mechanism may have a spatial, rather than temporal, control as the strongest sediment signature is found in lavas from Manado Tua Volcano, which lies at a considerably greater depth to the Benioff zone than most of the arc (Fig. 10). In this case, the appearance of recycled sediment in the Quaternary Sangihe arc would not be due to an increase in the amount of recycling but to a greater opportunity for melting of the parts of the mantle wedge containing recycled sediment.

Elliott *et al.* (1997) proposed two models in which slab fluid and sediment melts are added to the mantle wedge at different times, in different parts of the wedge. In one of these models sediment melting occurs at greater depth than, and therefore to the backarc side of, the dehydration process that initiates melting beneath the volcanic front. This could provide a means of generating a gradient in the intensity of the sediment signal, decreasing from the backarc region to the arc front. Sediment-modified mantle encountering the zone of fluid-fluxed melting would contribute to the main volcanic arc, as envisaged by Elliott *et al.* (1997). However, without some external process to extract melt from the backarc mantle there would be little magmatism bearing a stronger recycled sediment signature. Manado Tua lies just north of an inferred NW–SE strike-slip fault that crosses the north arm of Sulawesi from Manado to Bitung (Fig. 10). Mt Klabat lies a similar distance north of the same fault where it crosses the Sangihe arc front, and Kavalieris *et al.* (1992) indicated the presence of a further young cone in an intermediate position between Manado Tua and Klabat. Young strike-slip faulting generated in a collision zone may provide a pathway for melts in the back-arc region to reach the surface and be erupted. Alternatively, older strike-slip faults may have been reactivated as the stress field changed during the collision between the Halmahera and Sangihe arcs (Pearson & Caira 1999). In these circumstances new zones of compression and dilation may occur, the latter providing the opportunity for decompression and melting of mantle wedge modified by sedimentary melts (Macpherson & Hall 1999).

Summary

The Molucca Sea Collision Zone magmatism reveals several similarities but a number of differences between the two arc systems involved. These findings have implications for understanding the dynamics of subduction systems and for using geochemistry as a tectonic probe in ancient collision zones.

Magma geochemistry evolved through time in both Halmahera and Sangihe. The mantle wedge beneath both arcs was peridotite from the I-MORB domain that had experienced variable depletion, probably by melting, prior to the onset of Neogene arc magmatism. Both wedges were contaminated by fluid derived from the oceanic crust of the subducted Molucca Sea Plate. In both subduction zones Quaternary magmatism displays an increase in the amount of sediment incorporated into the source of arc lavas. There are geochemical differences between the Quaternary arcs that can be related to the composition of the mantle wedge, the composition of subducted sediment and the processes causing the increased sediment flux. Distinctive peridotite, with enriched I-MORB trace element chemistry, became incorporated into the source of the Quaternary Halmahera arc as a result of induced convection in the mantle wedge. Halmahera arc lavas were contaminated by a sediment with elevated $^{207}Pb/^{204}Pb$ and $^{208}Pb/^{204}Pb$ at a particular $^{206}Pb/^{204}Pb$ value relative to the sediment affecting Sangihe. Finally, the increased sediment flux at Halmahera appears in arc front lavas and is interpreted as reflecting a change in the dip of the subducted plate and a decrease in the horizontal separation between the locus of slab dehydration and sediment melting. In Sangihe the sediment signature is predominantly found in back-arc Quaternary lavas suggesting that deformation of the upper plate (North Sulawesi) provided a pathway for these melts to reach the surface and/or induced decompression melting in the underlying, sediment-enriched mantle.

Financial support has been provided by NERC, the Royal Society, the London University Central Research Fund and the Royal Holloway SE Asia Research Group. J.B. Gill, R.D. Larter and an anonymous reviewer provided valuable, constructive comments on an earlier manuscript.

References

ANDREWS, D.J. & SLEEP, N.H. 1974. Numerical modelling of tectonic flow behind island arcs. *Geophysical Journal of the Royal Astronomical Society*, **38**, 237–251.

BAKER, S. & MALAIHOLLO, J. 1996. Dating of Neogene igneous rocks in the Halmahera region: arc initiation and development. *In*: HALL, R. & BLUNDELL, D.J. (eds) *Tectonic Evolution of Southeast Asia*. Geological Society, London, Special Publications, **106**, 499–509.

BEN OTHMAN, D., WHITE, W.M. & PATCHETT, P. 1989. The geochemistry of marine sediments, island arc magma genesis and crust–mantle recycling. *Earth and Planetary Science Letters*, **94**, 1–21.

BRENNAN, J., SHAW, H.F., PHINNEY, D.L. & RYERSON, J.F. 1995. Mineral–aqueous fluid partitioning of trace elements at 900°C and 2.0 GPa: Constraints on the trace element chemistry of mantle and deep crustal fluids. *Geochimica et Cosmochimica Acta*, **59**, 3331–3350.

CARDWELL, R.K., ISACKS, B.L. & KARIG, D.E. 1980. The spatial distribution of earthquakes, focal mechanism solutions and subducted lithosphere in the Philippine and northeastern Indonesian islands. *In*: HAYES, D.E. (ed.) *The Tectonic and Geologic Evolution of Southeast Asian Seas and Islands*. American Geophysical Union, Geophysical Monographs, **23**, 1–36.

CARLILE, J.C., DIGDOWIROGO, S. & DARIUS, K. 1990. Geological setting, characteristics and regional exploration for gold in the volcanic arcs of North Sulawesi, Indonesia. *Journal of Geochemical Exploration*, **35**, 105–140.

DANYUSHEVSKY, L.V., EGGINS, S.M., FALLOON, T.J. & CHRISTIE, D.M. 2000. H_2O abundance in depleted to moderately enriched mid-ocean ridge magmas; Part I: Incompatible behaviour, implications for mantle storage, and origin of regional variations. *Journal of Petrology*, **41**, 1329–1364.

DAVIDSON, J.P. 1996. Deciphering mantle and crustal signatures in subduction zones. *In*: BEBOUT, G.E., SCHOLL, D.W., KIRBY, S.H. & PLATT, J.P. (eds) *Subduction: Top to Bottom*. American Geophysical Union, Geophyscial Monographs, **96**, 251–262

DOSSO, L., BOUGAULT, H., BEUZART, P., CALCEZ, J.Y. & JORON, J.L. 1988. The geochemical structure of the Southeast Indian Ridge. *Earth and Planetary Science Letters*, **88**, 47–59.

EDWARDS, C.M.H., MORRIS, J.D. & THIRLWALL, M.F. 1993. Separating mantle from slab signatures in arc lavas using B/Be and radiogenic isotope systematics. *Nature*, **362**, 530–533.

ELBURG, M.A. & FODEN, J.D. 1998. Temporal changes in arc magma geochemistry, north Sulawesi, Indonesia. *Earth and Planetary Science Letters*, **163**, 381–398.

ELLIOTT, T., PLANK, T., ZINDLER, A., WHITE, W. & BOURDON, B. 1997. Element transport from slab to volcanic front at the Mariana arc. *Journal of Geophysical Research*, **102**, 14 991–15 019.

FORDE, E. 1997. *The geochemistry of the Neogene Halmahera Arc, eastern Indonesia*. PhD Thesis, University of London.

GILL, J.B. & WILLIAMS, R.W. 1990. Th isotope and U-series studies of subduction-related volcanic rocks. *Geochimica et Cosmochimica Acta*, **54**, 1427–1442.

HAKIM, A.S. & HALL, R. 1991. Tertiary volcanic rocks from the Halmahera arc, eastern Indonesia. *Journal of Southeast Asian Earth Sciences*, **6**, 271–287.

HALL, R. 1996. Reconstructing Cenozoic SE Asia. *In*: HALL, R. & BLUNDELL, D.J. (eds) *Tectonic Evolution of Southeast Asia*. Geological Society, London, Special Publications, **106**, 153–184.

HALL, R. 2000. Neogene history of collision in the Halmahera region, Indonesia. *In*: *Proceedings of the Indonesian Petroleum Association 27th Annual Convention*, Indonesian Petroleum Association, Jakarta, 487–493.

HALL, R. 2002. Cenozoic geological and plate tectonic evolution of SE Asia and the SW Pacific: computer-based reconstructions, model and animations. *Journal of Asian Earth Sciences*, **20**, 353–431.

HALL, R., AUDLEY-CHARLES, M.G., BANNER, F.T., HIDAYAT, S. & TOBING, S.L. 1988. Late Palaeogene–Quaternary geology of Halmahera, eastern Indonesia: initiation of a volcanic island arc. *Journal of the Geological Society, London*, **145**, 577–590.

HALL, R., NICHOLS, G., BALLANTYNE, P., CHARLTON, T. & ALI, J. 1991. The character and significance of basement rocks of the southern Molucca Sea region. *Journal of Southeast Asian Earth Sciences*, **6**, 249–258.

HAMILTON, W.B. 1988. Plate tectonics and island arcs. *Geological Society of America Bulletin*, **100**, 1503–1527.

HAMILTON, W.B. 1995. Subduction systems and magmatism. *In*: SMELLIE, J.L. (ed.) *Volcanism Associated with Extension at Consuming Plate Margins*. Geological Society, London, Special Publications, **81**, 3–28.

HART, S.R. 1984. A large-scale isotope anomaly in the Southern Hemisphere mantle. *Nature*, **309**, 753–757

HICKEY-VARGAS, R. 1998. Origin of the Indian Ocean-type isotopic signature in basalts from Philippine Sea Plate spreading centres: an assessment of the local versus large-scale processes. *Journal of Geophysical Research*, **103**, 20 963–20 979.

HOCHSTAEDTER, A., GILL, J., PETERS, R., BROUGHTON, P. & HOLDEN, P. 2001. Across-arc geochemical trends in the Izu–Bonin arc: Contributions from the subducting slab. *Geochemistry, Geophysics, Geosystems*, **2**, 2000GC000105.

IOC, IHO & BODC. 1997. *GEBCO-97: The 1997 Edition of the GEBCO Digital Atlas*. British Oceanographic Data Centre, Bidston Observatory, Merseyside. World Wide Web address: http://www.bodc.ac.uk/projects/gebco/index.html

KAVALIERIS, I., VAN LEEUWEN, T.H. & WILSON, M. 1992. Geological setting and styles of mineralization, north arm of Sulawesi, Indonesia. *Journal of Southeast Asian Earth Sciences*, **7**, 113–129.

KEPPLER, H. 1996. Constraints from partitioning experiments on the composition of subduction-zone fluids. *Nature*, **380**, 237–240.

LALLEMAND, S.E., POPOFF, M., CADET, J.P., BADER, A.G., PUBELLIER, M., RANGIN, C. & DEFFONTAINES, B. 1998. Genetic relationship between the central and southern Philippine Trench and the Sangihe Trench. *Journal of Geophysical Research*, **103**, 933–950.

LE ROEX, A.P., DICK, H.J.B. & FISHER, R.L. 1989. Petrology and geochemistry of MORB from 25°E to 46°E along the Southwest Indian Ridge: Evidence for contrasting styles of mantle enrichment. *Journal of Petrology*, **30**, 947–986.

MACPHERSON, C.G. & HALL, R. 1999. Tectonic controls of geochemical evolution in arc magmatism of SE Asia. *Proceedings PACRIM '99 Congress, Australian Institute of Mining and Metallurgy Publication Series*, **4/99**, 359–368.

MACPHERSON, C.G. & HALL, R. 2002. Timing and tectonic controls in the evolving orogen of SE Asia and the western Pacific and some implications for ore generation. *In*: BLUNDELL, D.J., NEUBAUER, F. & VON QUADT, A. (eds) *The Timing and Location of Major Ore Deposits in an Evolving Orogen*. Geological Society, London, Special Publications, **204**, 49–67.

MACPHERSON, C.G., GAMBLE, J.A. & MATTEY, D.P. 1998. Oxygen isotope geochemistry of an oceanic to continental arc transition, Kermadec–Hikurangi margin, SW Pacific. *Earth and Planetary Science Letters*, **160**, 609–621.

MAHONEY, J.J., LE ROEX, A.P., PENG, Z., FISHER R.L. & NATLAND, J.H. 1992. Southwestern limits of Indian ocean ridge mantle and the origin of low $^{206}Pb/^{204}Pb$ mid-ocean ridge basalt: isotope systematics of the central southwest Indian ridge. *Journal of Geophysical Research*, **97**, 19 771–19 790.

MAHONEY, J.J., NATLAND, J.H., WHITE, W.M., POREDA, R.J., FISHER, R.L. & BAXTER, A.N. 1989. Isotopic and geochemical provinces of the western Indian Ocean spreading centers. *Journal of Geophysical Research*, **94**, 4033–4052.

MALAIHOLLO, J.F.A. & HALL, R. 1996. The geology and tectonic evolution of the Bacan region, east Indonesia. *In*: HALL, R. & BLUNDELL, D.J. (eds) *Tectonic Evolution of Southeast Asia*. Geological Society, London, Special Publications, **106**, 483–497.

MCCULLOCH, M.T. & GAMBLE, J.A. 1991. Geochemical and geodynamical constraints on subduction zone magmatism. *Earth and Planetary Science Letters*, **102**, 358–374.

MICHARD, A., MONTIGNY, R. & SCHLICH, R. 1986. Geochemistry of the mantle beneath the Rodruiguez Triple Junction and the South-East Indian Ridge. *Earth and Planetary Science Letters*, **78**, 104–114.

MORRICE, M.G. & GILL, J.B. 1986. Spatial patterns in the mineralogy of island arc magma series: Sangihe arc, Indonesia. *Journal of Volcanology and Geothermal Research*, **29**, 311–353.

MORRICE, M.G., JEZEK, P.A., GILL, J.B., WHITFORD, D.J. & MONOARFA, M. 1983. An introduction to the Sangihe arc: Volcanism accompanying arc–arc collision in the Molucca Sea, Indonesia. *Journal of Volcanology and Geothermal Research*, **19**, 135–165.

MORRIS, J.D., JEZEK, P.A., HART, S.R. & GILL, J.B. 1983. The Halmahera Arc, Molucca Sea Collision Zone, Indonesia: A geochemical survey. *In*: HAYES, D.E. (ed.) *The Tectonic and Geologic Evolution of Southeast Asian Seas and Islands: Part 2*. American Geophysical Union, Geophysical Monographs, **27**, 373–387.

MORRIS, J.D., LEEMAN, W.P. & TERA, F. 1990. The subducted component in island arc lavas: constraints from Be isotopes and B-Be systematics. *Nature*, **344**, 31–36.

PEARCE, J.A., BAKER, P.E., HARVEY, P.K. & LUFF, I.W. 1995. Geochemical evidence for subduction fluxes, mantle melting and fractional crystallisation beneath the South Sandwich island arc. *Journal of Petrology*, **36**, 1073–1109

PEARSON, D.P. & CAIRA, N.M. 1999. The geology and metallogeny of central north Sulawesi. *Proceedings PACRIM '99 Congress, Australian Institute of Mining and Metallurgy Publication Series*, **4/99**, 359–368.

PEATE, D.W., PEARCE, J.A., HAWKESWORTH, C.J., COLLEY, H., EDWARDS, C.M.H. & HIROSE, K. 1997. Geochemical variations in Vanuatu arc lavas: the role of subducted material and a variable mantle wedge composition. *Journal of Petrology*, **38**, 1331–1358.

PLANK, T. & LANGMUIR, C.H. 1993. Tracing trace elements from sediment input to volcanic output at subduction zones. *Nature*, **362**, 739–743.

POLVÉ, M., MAURY, R.C., BELLON, H., RANGING, C., PRIADI, B., YUWONO, S., JORON, J.L. & SOERIA ATMADJA, R. 1997. Magmatic evolution of Sulawesi (Indonesia): constraints on the Cenozoic geodynamic history of the Sundaland active margin. *Tectonophysics*, **272**, 69–92.

RANGIN, C., SPACKMAN, W., PUBELLIER, M. & BIJWAARD, H. 1999. Tomographic and geological constraints on subduction along the eastern Sundaland continental margin (South-east Asia). *Bulletin de la Societé Geologique de France*, **170**, 775–788.

REHKÄMPER, M. & HOFMANN, A.W. 1997. Recycled ocean crust and sediment in Indian Ocean MORB. *Earth and Planetary Science Letters*, **147**, 93–106.

RYAN, J., MORRIS, J., BEBOUT, G. & LEEMAN, W.P. 1996. Describing chemical fluxes in subduction zones: Insights from 'depth-profiling', studies of arc and forearc rocks. *In*: BEBOUT, G.E., SCHOLL, D.W., KIRBY, S.H. & PLATT, J.P. (eds) *Subduction: Top to Bottom*. American Geophysical Union, Geophyscial Monographs, **96**, 263–268.

SUN, S.-S. & MCDONOUGH, W.F. 1989. Chemical and isotopic systematics of oceanic basalts: implications for mantle composition and processes. *In*: SAUNDERS, A.D. & NORRY, M.J. (eds) *Magmatism in the Ocean Basins*. Geological Society, London, Special Publications, **42**, 313–345.

TATSUMI, Y., MURASAKI, M., ARSADI, E.M. & NOHDA, S. 1991. Geochemistry of Quaternary lavas from NE Sulawesi: transfer of subduction components into the mantle wedge. *Contributions to Mineralogy and Petrology*, **107**, 137–149

TURNER, S.P. & HAWKESWORTH, C.J. 1997. Constraints on flux rates and mantle dynamics beneath island arcs from Tonga–Kermadec lava geochemistry. *Nature*, **389**, 568–573.

VAN SOEST, M.C., HILTON, D.R., MACPHERSON, C.G. & MATTEY, D.P. 2002. Resolving sediment subduction and crustal contamination in the Lesser Antilles island arc: a combined He–O–Sr isotope approach. *Journal of Petrology*, **43**, 143–170.

VROON, P.Z. & VAN BERGEN, M.J. 2000. Geochemical evidence for two subducting plates beneath North Sulawesi (Indonesia). *Journal of Conference Abstracts*, **5**, 1060.

VROON, P.Z., VAN BERGEN, M.J., KLAVER, G.J. & WHITE, W.M. 1995. Strontium, neodymium and lead isotopic and trace element signatures of the east Indonesian sediments – provenance and implications for Banda arc magma genesis. *Geochimica et Cosmochimica Acta*, **59**, 2573–2598.

VROON, P.Z., VAN BERGEN, M.J., WHITE, W.M. & VAREKAMP, J.C. 1993. Sr–Nd–Pb isotope systematics of the Banda arc, Indonesia: Combined subduction and assimilation of continental material. *Journal of Geophysical Research*, **98**, 22 349–22 366.

WOODHEAD, J.D., EGGINS, S. & GAMBLE, J.A. 1993. High field strength and transition element systematics in island arc and back-arc basin basalt:

evidence for multi-phase melt extraction and a depleted mantle wedge. *Earth and Planetary Science Letters*, **114**, 491–504.

WOODHEAD, J.D., EGGINS, S.M. & JOHNSON, R.W. 1998. Magma genesis in the New Britain island arc: further insights into melting and mass transfer processes. *Journal of Petrology*, **39**, 1641–1668.

YOU, C.-F., CASTILLO, P.R., GIESKES, J.M., CHAN, L.H. & SPIVAK, A.J. 1996. Trace element behaviour in hydrothermal experiments: implications for fluid processes at shallow depths in subduction zones. *Earth and Planetary Science Letters*, **140**, 41–52.

Some geochemical constraints on hot fingers in the mantle wedge: evidence from NE Japan

Y. TAMURA

Institute for Frontier Research on Earth Evolution (IFREE), Japan Marine Science and Technology Centre (JAMSTEC), Yokosuka 237–0061, Japan

(e-mail: tamuray@jamstec.go.jp)

Abstract: Mantle melting and the production of magmas along the NE Japan arc may be controlled by hot regions in the mantle wedge (hot fingers) that move toward the volcanic front along upward-sloping trajectories. At depths equivalent to 1–2 GPa, where magmas are expected to segregate from mantle diapirs, the hot-finger structures result in a decreasing thermal gradient away from volcanic front. Low-alkali tholeiite is therefore formed by the greater degree of diapiric melting near the volcanic front; high-alumina basalt and alkali olivine basalt are produced by lesser degrees of diapiric melting to the west. The grouping of volcanoes at the volcanic front is interpreted as being controlled by thermal structure in the mantle wedge, and groups are concentrated above the tips of the hot fingers. Map-view variations of minimum $^{87}Sr/^{86}Sr$ of NE Japan volcanoes are interpreted as resulting from transport of fertile and high-$^{87}Sr/^{86}Sr$ mantle material into the magma source region in the hot fingers. Given that mantle diapirs are formed in the lower part of the mantle wedge, a greater proportion of fertile material will be contained in the diapirs at the tips of the hot fingers, resulting in higher $^{87}Sr/^{86}Sr$ magmas along the volcanic front. Conveyor-like return flow carries the sheet-like remnants of the fingers to depth along the top of the subducting slab.

Tamura *et al.* (2001, 2002) showed that Quaternary volcanoes in NE Japan arc can be grouped into 10 elongate volcanic groups striking transverse to the arc; each of these has an average width of 50 km and linear separations of 30–75 km (Fig. 1). This grouping of volcanic centres is closely correlated with linear topographic highs, low-velocity regions in the mantle wedge and local negative Bouguer gravity anomalies behind the volcanic arc (Tamura *et al.* 2002). Mantle melting and the production of magmas in NE Japan may be controlled by locally developed hot regions within the mantle wedge that have the form of inclined, 50 km-wide fingers (Tamura *et al.* 2001, 2002) (Fig. 1). Although these hot fingers have been imaged by seismic tomography (e.g. Zhao *et al.* 1992), the role they play in arc magma genesis is not fully understood. Do these hot mantle fingers melt to produce arc magmas, or, alternatively, do they play a role mainly as heat sources? Are arc magmas generated from mantle diapirs, which form in the lower part of the mantle wedge and rise through the overlying hot fingers in the mantle wedge (Tamura 1994)? Across-arc variations of isotope and trace element compositions in volcanoes of NE Japan (e.g. Shibata & Nakamura 1997) do not support the concept of melting of a uniform mantle source. Kersting *et al.* (1996), on the other hand, identified along-strike isotopic variations and suggested that crustal contamination contributed to arc magmatism in NE Japan. The chief objective of this paper is to explore further the two-dimensional geochemical variations among volcanic clusters in NE Japan and to clarify the role that hot fingers might play in the production of arc magmas.

$^{87}Sr/^{86}Sr$ data from 44 volcanoes are reviewed to identify systematic variations of magma sources in the mantle wedge. These data include those derived from basalt, andesite, dacite and rhyolite. In addition, I present across- and along-arc variations of major element compositions from Quaternary basalts in NE Japan. While pursuing this goal, two previously unrecognized relationships emerged: (1) some volcano groups consist only of andesite and dacite; and (2) basalt-bearing volcanoes are larger than basalt-free volcanoes. Locally developed hot regions within the mantle wedge (hot fingers) may also play a role in these relationships.

Variations in basalt composition across and along the NE Japan arc

Present-day volcanism along the NE Japan arc is dominated by andesites (Aramaki & Ui 1978),

From: LARTER, R.D. & LEAT, P.T. 2003. *Intra-Oceanic Subduction Systems: Tectonic and Magmatic Processes.* Geological Society, London, Special Publications, **219**, 221–237. 0305-8719/03/$15.00

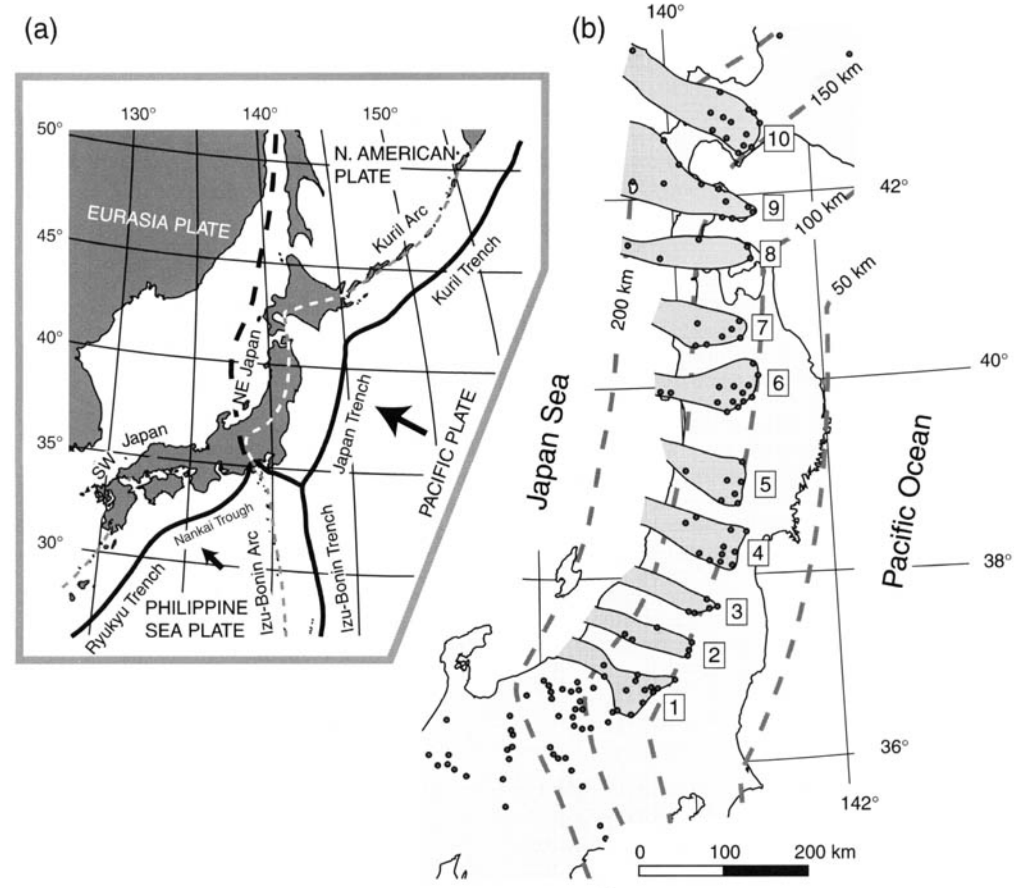

Fig. 1. (**a**) Location map, showing plate configurations, subduction directions and volcanic fronts (thin dashed lines). The approximate boundary between the North American and Eurasia plates is shown by a thick dashed line. (**b**) Quaternary volcanoes in NE Japan (Committee for Catalogue of Quaternary Volcanoes in Japan 1999); these have been used to define 10 volcanic groups (hot fingers) striking transverse to the volcanic front (Tamura *et al.* 2002). The dashed lines are depth contours to the top of the subducting Pacific Plate.

and in many Quaternary volcanoes there are no analyses to indicate that basalts were erupted (Committee for Catalogue of Quaternary Volcanoes in Japan 1999 and references therein). Basalt is, however, conspicuous in some volcanoes (Table 1). Basalt compositions are discussed here because there is a broad consensus that basalt magma is mantle-derived. Figure 2 and Table 1 present the distribution and data sources of basalt-bearing volcanoes in NE Japan. Basalts are defined here simply as volcanic rocks with $SiO_2 < 53$ wt% calculated on an anhydrous basis. All discussions in this paper refer to analyses that have been normalized to 100% on a volatile-free basis with total iron calculated as FeO.

Total alkalis, Al_2O_3 and K_2O

Transverse geochemical variations across volcanic arcs have been reported from many areas (Kuno 1960, 1966; for summary, see Gill 1981, p. 209). Chemical analyses of basalt from 20 Quaternary volcanoes in NE Japan arc are reviewed to evaluate across- and along-arc variations (Table 1). A plot of total alkalis (Na_2O + K_2O) against SiO_2 of basalts in NE Japan (Fig. 3a) serves to identify the three roughly parallel zones: (1) low-alkali tholeiite with low Al_2O_3 and alkalis (LAT) lying along the volcanic front; (2) high-alumina basalt with higher Al_2O_3 and intermediate alkalis (HAB) lying just west of the front; and (3) alkali (olivine) basalt with variable Al_2O_3 and higher alkalis (AOB) lying further to

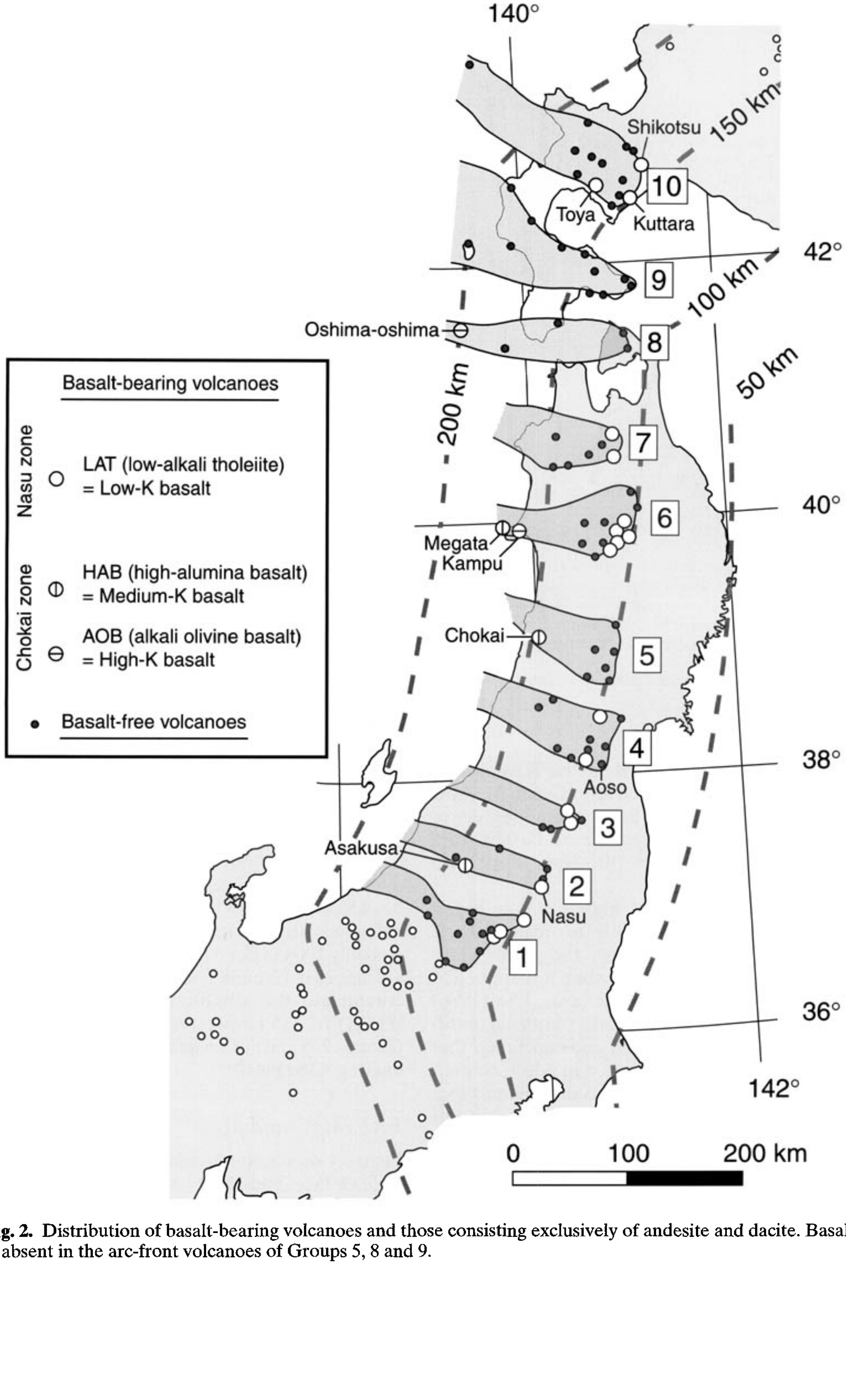

Fig. 2. Distribution of basalt-bearing volcanoes and those consisting exclusively of andesite and dacite. Basalt is absent in the arc-front volcanoes of Groups 5, 8 and 9.

Table 1. *Sources of analytical data of the Quaternary basalt-bearing volcanoes in NE Japan*

Group*	Volcano (number of analyses)	Basalt (% of analyses)	Constructional shape	References	Volcano No.†
Nasu Zone					
1	Nantai & Nyoho-Akanagi (22)	13	S	Sasaki *et al.* (1986)	111 and 112
1	Takahara (54)	7	S	Ban *et al.* (1992)	113
2	Nasu (58)	17	VG	Ban *et al.* (1987); Ban (1991)	114
3	Adatara (29)	3	VG	Fujinawa *et al.* (1984)	121
4	Zao (44)	27	VG	Sakayori *et al.* (1984, 1987)	123
4	Funagata (77)	18	VG	Yoshida *et al.* (1987)	128
6	Akita-komagatake (37)	54	S	Nakagawa *et al.* (1985)	140
6	Iwate (44)	34	VG	Ishikawa *et al.* (1984)	142
6	Hachimantai (100)	9	VG	Ohba & Umeda (1999)	143
7	Towada (27)	3	VG, C	Hunter & Blake (1995)	152
7	Hakkoda (26)	23	VG, C	Sasaki *et al.* (1985, 1987)	154
10	Toya (13)	23	VG, C	Oba *et al.* (1985)	193
10	Kuttara (33)	27	C	Yamazaki (1991)	196
10	Shikotsu (5)	20	VG, C	Katsui *et al.* (1978)	198
Chokai Zone					
2	Asakusa (76)	32	S	Asakusa Volcano Collaborative Research Group (1991)	116
5	Chokai (56)	4	S	Hayashi *et al.* (1984)	135
6	Kampu (17)	35	S	Hayashi *et al.* (1991)	146
6	Megata (41)	34	Maar	Sakuyama & Koyaguchi (1984); Aoki & Yoshida (1986); Yoshinaga & Nakagawa (1999)	147
8	Oshima-oshima (20)	50	S	Yamamoto (1984)	184

*Grouping of volcanoes in NE Japan defined by Tamura *et al.* (2002) and shown in Figure 1.
†Volcano number in catalogue of Quaternary volcanoes in Japan (Committee for Catalogue of Quaternary Volcanoes in Japan 1999).
S, single volcano; VG, volcano group; C, caldera.

the west. AOB and HAB in the Kampu and Megata volcanoes, respectively (Figs 2, 3), show that HAB and AOB have some degree of overlap. Importantly, however, all basalts from volcanic front volcanoes (the Nasu Zone) are LAT (Figs 2, 3).

Kuno (1960) defined high-alumina basalt (HAB) in a study that only involved aphyric rocks. Practically, however, the term 'high-alumina basalt' is confusing when it is applied to both aphyric and porphyritic lavas. Uto (1986) studied Al_2O_3 variation in late Cenozoic undifferentiated basalts in Japan and concluded that there is no significant variation in Al_2O_3 content among the three parental basalt magma types (LAT, HAB and AOB). Data presented in this study confirm Uto's findings for the basalt bearing volcanoes of NE Japan (Fig. 3b).

A striking characteristic of orogenic andesites and associated rocks within many volcanic arcs of modest width is the consistent increase of their incompatible element concentrations, most notably K_2O, away from the plate boundary (Gill 1981). Apparently, K_2O is a more sensitive variable than total alkalis (Fig. 3c); basalts along the NE Japan volcanic front contain significantly less K_2O than those from the rear of the arc (Figs 2, 3c).

Interestingly, however, along-arc K_2O values in NE Japan are not simply related to local slab depth (Fig. 2). For example, the subducting slab lies 150 km beneath the low-K (LAT) Group 10 volcanoes Toya, Kuttara and Shikotsu, whereas it is only 100 km deep beneath the volcanic front volcanoes in Groups 1–4 to the south. To further complicate the situation, medium-K basalts (HAB) 70–115 km west of the volcanic front in Groups 2, 5 and 6, also lie 150 km above the subducting slab (Fig. 2).

FeO/MgO and MgO*

Figure 4 shows along- and across-arc variations of FeO*/MgO and MgO in basalts from the NE Japan arc. FeO*/MgO and wt% MgO of basalts range from 0.9 to 3.2 and from 2.5 to 11, respectively. Lavas erupting at the volcanic front in three of the Groups (Nos 5, 8 and 9) do not contain basalts (Fig. 2). Moreover, it is rare for volcanoes in Group 3 to have basalts, and the

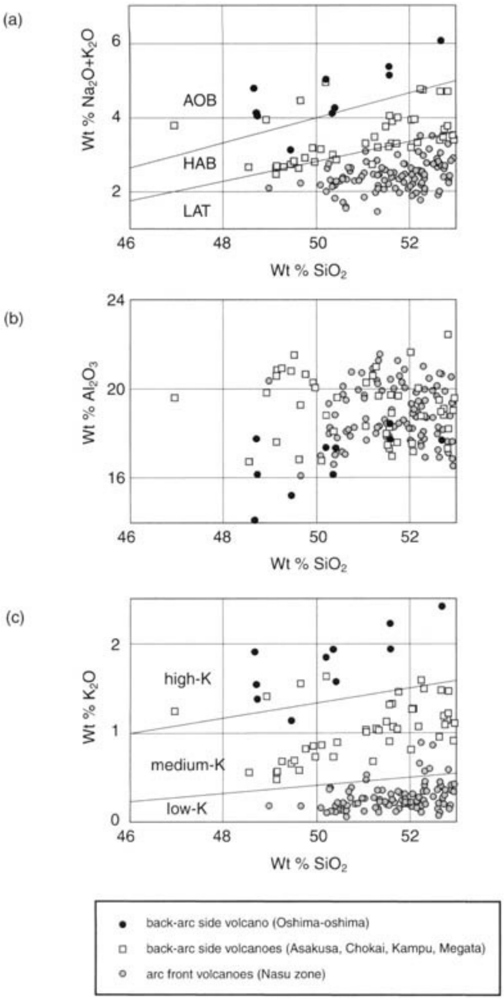

Fig. 3. Plots of total alkalis, Al_2O_3 and K_2O against SiO_2 for NE Japan basalts. (**a**) Total alkalis v. SiO_2. The two lines (after Kuno 1966) mark the boundaries of low-alkali tholeiite (LAT), high-alumina basalt (HAB) and alkali olivine basalt (AOB). (**b**) Al_2O_3 v. SiO_2, showing HAB, LAT and AOB have overlapping Al_2O_3 contents, but note that not all HAB is rich in Al_2O_3. (**c**) K_2O v. SiO_2. The boundary lines, originally defined by Gill (1981) to subdivide the andesite field (>53 wt% SiO_2), are here extrapolated into the basalt field.

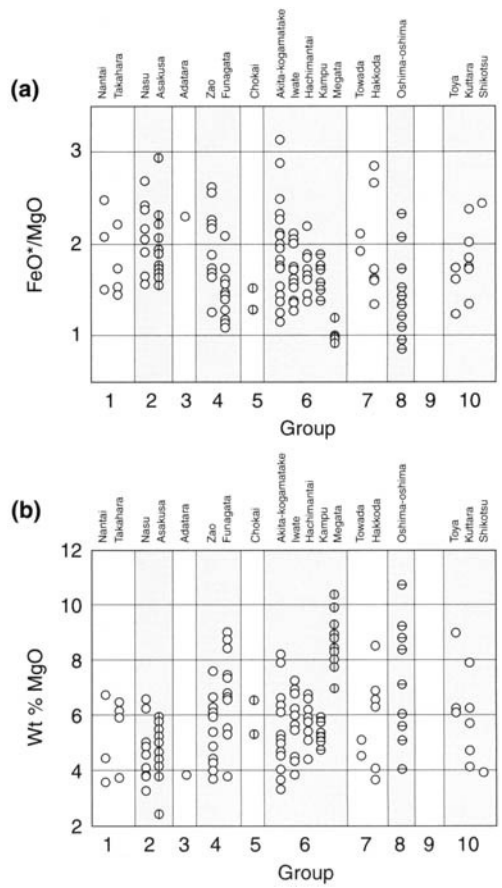

Fig. 4. Variation of along- and across-arc basalt composition in terms of: (**a**) FeO*/MgO; and (**b**) MgO. Data from volcanoes in each group plotted in order of increasing distance from the volcanic front; symbols are the same in Fig. 2. Volcanic front volcanoes in Groups 5, 8 and 9 do not contain basalts.

only basalt reported in the Group 3, Adatara Volcano (Fujinawa *et al.* 1984), is fairly differentiated and contains higher FeO*/MgO (2.3) and lower MgO (3.9 wt%) than other primitive volcanic front basalts. In contrast, two volcanoes in Group 4 (Zao and Funagata volcanoes) and three volcanoes in Group 6 (Akita-komagatake, Iwate and Hachimantai volcanoes) contain more primitive basalts (wt% MgO = 7–9, FeO*/MgO < 1.5).

Basalts from Megata and Oshima-oshima volcanoes, located furthest from the volcanic front (Fig. 2), contain the lowest FeO*/MgO (*c.* 1) and the greatest MgO content (>10 wt%), as shown in Figure 4. These volcanoes are made up of calc-alkaline andesites and basalts, both of which contain mantle-derived or cumulate ultramafic xenoliths, suggesting the primary nature of these magmas. It should be noted, however, that the extent of fractional crystallization does not decrease monotonously across the arc. The Chokai Zone HAB, such as those in Asakusa and Chokai volcanoes, are generally more

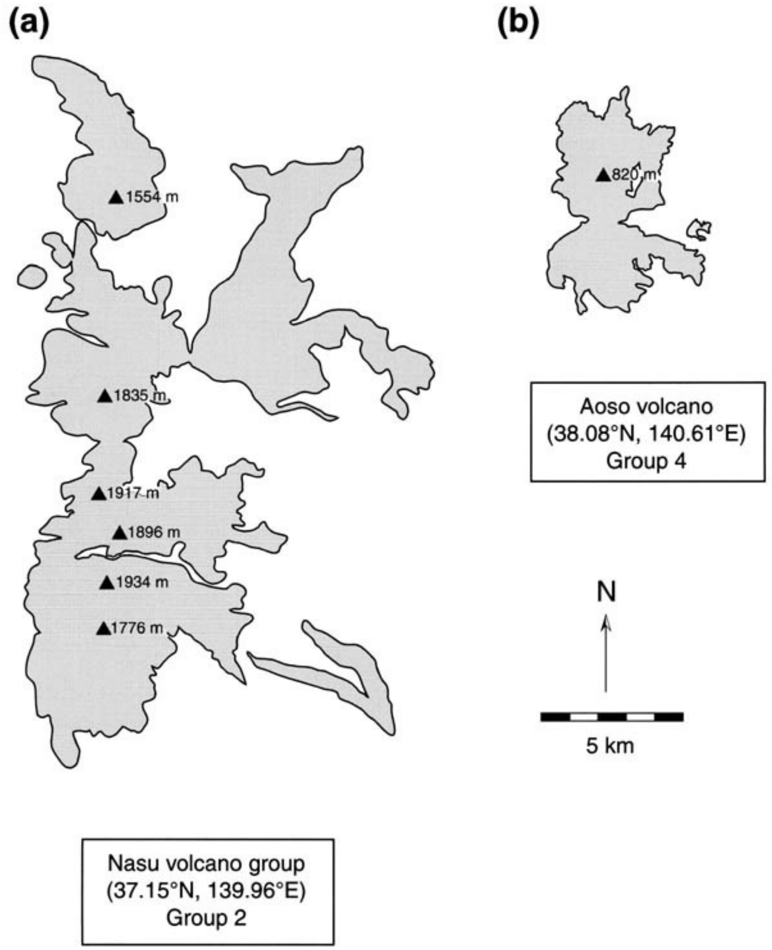

Fig. 5. Two contrasting volcanoes having different degrees of complexity; each is shown as a single dot in Figures 1and 2. (**a**) A complex volcano, Nasu volcano group (37.15°N, 139.96°E) (Ban & Takaoka 1995), consists of six individual edifices. (**b**) A simple volcano, Aoso (38.08°N, 140.61°E) (Toya & Ban 2001).

fractionated than those in the volcanic front volcanoes (Fig. 4).

Elevation–composition relationships

Individual dots on Figure 1b represent either a small single volcano or a much larger volcano group consisting of clustered and overlapping edifices. Figure 5 shows two such volcanoes that exhibit striking differences in size and complexity. Both, however, are shown by a single dot on the map. One is the Nasu Volcano group, which consists of six volcanic edifices extending for 25 km in a N–S direction (Ban & Takaoka 1995). The other is Aoso Volcano, which is a small single volcano (Toya & Ban 2001). Interestingly, the Nasu volcanic suite contains basalt, andesite and dacite, but the smaller Aoso Volcano consists only of andesite and dacite.

A simple measure of eruptive volume might be related to the height of a volcano above its local basement. Magmatic volumes produced in the mantle wedge are the total of the eruptive volumes plus the intrusive volumes remaining in the crust. Although the latter volumes are uncertain, basement elevations probably reflect intrusive volumes in NE Japan, because: (1) volcanic basement might well have been uplifted by repeated intrusion of Quaternary magmas; and (2) Tamura *et al.* (2002) showed that taller volcanoes rest on higher basements, and that most of the basement peaks have

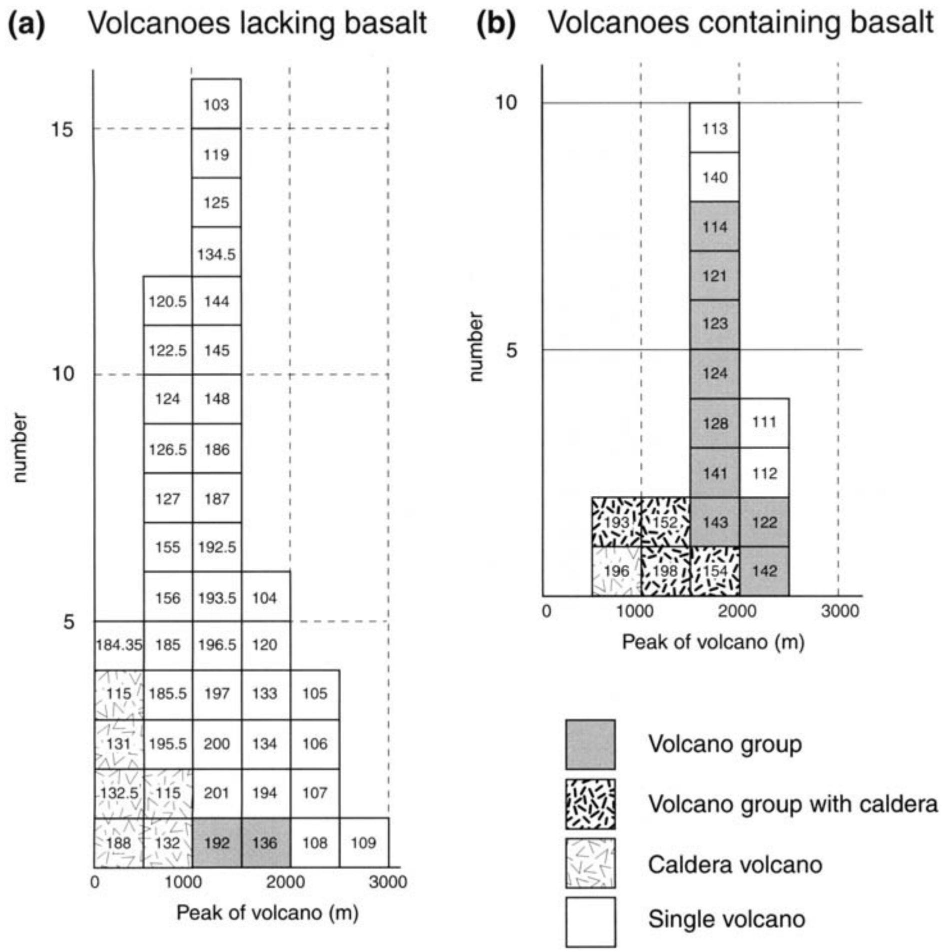

Fig. 6. Histograms of highest (metres above sea level) volcanoes along the volcanic front (the Nasu Zone) in the NE Japan arc. Volcano groups, volcano groups with calderas, caldera volcanoes and single volcanoes are shown by different patterns. The number in each box is the volcano number assigned by the Committee for Catalogue of Quaternary Volcanoes in Japan (1999). Nasu Volcano is No. 114 and Aoso Volcano is No. 122.5. (**a**) Volcanoes in which basalt (SiO_2 < 53 wt%) is absent. (**b**) Volcanoes containing basalt.

elevations more than half the height of the volcanoes.

I conclude that volcano elevations (as measured above sea level) are another useful factor to consider, because the topographic profiles are likely to reflect masses of magmas derived from the mantle wedge (Tamura *et al.* 2002). Figure 6 shows histograms of peak volcano height of: (a) volcanoes free of basalt lavas; and (b) those containing basalts in the Nasu Zone, and distinctions among single volcano, volcano group, caldera volcano and volcano group with caldera are shown by different patterns. The summits of most basalt-bearing volcanoes are higher than 1500 m, but those of volcanoes free of basalts are lower than 1500 m. Moreover, most basalt-bearing volcanoes are parts of volcano clusters, such as Nasu Volcano (Fig. 5a), or a volcano complex containing a caldera. On the other hand, most basalt-free volcanoes are single edifices, similar to, or slightly larger than, Aoso Volcano (Fig. 5b).

I conclude that the basalt-bearing volcanoes along the volcanic front of the NE Japan arc are generally larger than the basalt-free ones.

Across- and along-arc $^{87}Sr/^{86}Sr$ variations

Forty-four Quaternary volcanoes are reviewed to evaluate two-dimensional strontium isotopic

Table 2. *Compilation of $^{87}Sr/^{86}Sr$ data for NE Japan arc Quaternary volcanoes*

Group*	Volcano (number of analyses)	Range of $^{87}Sr/^{86}Sr$ values	References	Volcano No.†
1	Takahara (4)	0.70559–0.71052	Notsu (1983); Kersting *et al.* (1996)	113
1	Nyoho-Akanagi (3)	0.70578–0.70605	Kersting *et al.* (1996)	112
1	Nantai (7)	0.70594–0.71528	Kersting *et al.* (1996)	111
1	Nikko (2)	0.7060–0.7064	Kurasawa (1984)	110
1	Sukai (1)	0.70639	Notsu (1983)	106
1	Nikko-Shirane (3)	0.70593–0.70956	Notsu (1983); Kersting *et al.* (1996)	109
1	Akagi (30)	0.70603–0.70879	Notsu (1983); Kersting *et al.* (1996); Kobayashi & Nakamura (2001)	104
1	Hiuchigatake(2)	0.70518–0.70538	Notsu (1983); Notsu *et al.* (1987)	108
1	Ayamedaira (1)	0.70491	Notsu *et al.* (1987)	107
1	Hotaka (4)	0.70516–0.70577	Notsu (1983); Notsu *et al.* (1987)	105
1	Komochi (2)	0.70555–0.70568	Notsu *et al.* (1987)	103
2	Nasu (31)	0.70430–0.70630	Notsu (1983); Ban & Fujimaki (1992); Togashi *et al.* (1992); Kersting *et al.* (1996)	114
2	Shirakawa (2)	0.70465–0.70555	Shirahase *et al.* (1989)	115
2	Asakusa (2)	0.70391–0.70425	Notsu (1983)	116
2	Sumon (2)	0.70414–0.70437	Notsu (1983)	117
3	Adatara (34)	0.70473–0.70571	Kurasawa *et al.* (1986); Togashi *et al.* (1992); Kersting *et al.* (1996)	121
3	Azuma (6)	0.70463–0.70517	Notsu (1983); Kersting *et al.* (1996)	122
3	Nekoma (12)	0.70491–0.70524	Kimura *et al.* (2002)	119
4	Adachi (4)	0.70435–0.70447	Kanisawa & Shibata (1987)	126.5
4	Zao (7)	0.70375–0.70440	Notsu (1983); Kersting *et al.* (1996)	123
4	Funagata (7)	0.70406–0.70425	Notsu (1983); Kersting *et al.* (1996); Shibata & Nakamura (1997)	128
4	Gassan (2)	0.70347–0.70352	Notsu (1983)	129
5	Kurikoma (2)	0.70416–0.70425	Notsu (1983)	133
5	Chokai (5)	0.70305–0.70352	Notsu (1983); Shibata & Nakamura (1997)	135
6	Nanashigure (?)	0.7044–0.7051	Ohba & Umeda (1999)	148
6	Iwate (9)	0.70421–0.70510	Notsu (1983); Togashi *et al.* (1992); Shibata & Nakamura (1997)	142
6	Hachimantai (16)	0.70400–0.70430	Ohba & Umeda (1999)	143
6	Akita-komagatake (3)	0.70412–0.70430	Shibata & Nakamura (1997)	140
6	Akita-Yakeyama (14)	0.70379–0.70411	Ohba (1993)	144
6	Moriyoshi (17)	0.70365–0.70409	Notsu (1983); Nakagawa (1991); Shibata & Nakamura (1997)	145
6	Kampu (5)	0.70300–0.70350	Notsu (1983); Shibata & Nakamura (1997)	146
6	Megata (11)	0.70300–0.70365	Zashu *et al.* (1980); Sakuyama & Koyaguchi (1984)	147
7	Towada (28)	0.70392–0.70438	Notsu (1983); Hunter & Blake (1995)	152
7	Hakkoda (3)	0.70399–0.70405	Notsu (1983); Shirahase *et al.* (1989)	154
7	Taira-komagatake (2)	0.70390–0.70410	Kurasawa (1984)	150
7	Iwaki (4)	0.70407–0.70437	Notsu (1983)	153
8	Osore-zan (7)	0.70381–0.70419	Notsu (1983); Togashi *et al.* (1992)	155
8	Oshima-oshima (4)	0.70311–0.70330	Notsu (1983); Kurasawa (1984)	184
9	Esan (1)	0.70439	Kimura & Yoshida (pers. comm. 2002)	185
9	Komagatake (1)	0.70390	Kimura & Yoshida (pers. comm. 2002)	187
9	Kariba (2)	0.7034–0.7037	Kurasawa (1984)	190
10	Toya (13)	0.7040–0.7042	Oba *et al.* (1985)	193
10	Yotei (2)	0.7043–0.7046	Kurasawa (1984)	194
10	Niseko (2)	0.7039–0.7042	Kurasawa (1984)	192

*Grouping of volcanoes in NE Japan defined by Tamura *et al.* (2002) and shown in Figure 1.
†Volcano number in catalogue of Quaternary volcanoes in Japan (Committee for Catalogue of Quaternary Volcanoes in Japan 1999).

variations (Table 2). It can be seen that isotopic variability from the same volcano with more than 10 analyses of $^{87}Sr/^{86}Sr$, ranges from <0.0003 (Hachimantai and Toya volcanoes) to >0.002 (Akagi and Nasu volcanoes) (Table 2). To investigate $^{87}Sr/^{86}Sr$ variability from the same volcano, Tamura & Nakamura (1996) reviewed isotopic data from 38 arc volcanoes worldwide. The ranges of $^{87}Sr/^{86}Sr$ values are < 0.0003 in 12 of the 38 volcanoes that are situated on thin continental crust. Those volcanoes located on thicker crust exhibit much larger, but systematic, $^{87}Sr/^{86}Sr$ ranges; rocks with intermediate compositions (andesite and dacite) yield the lowest and the highest $^{87}Sr/^{86}Sr$; basalts and rhyolites are intermediate in terms of $^{87}Sr/^{86}Sr$ values

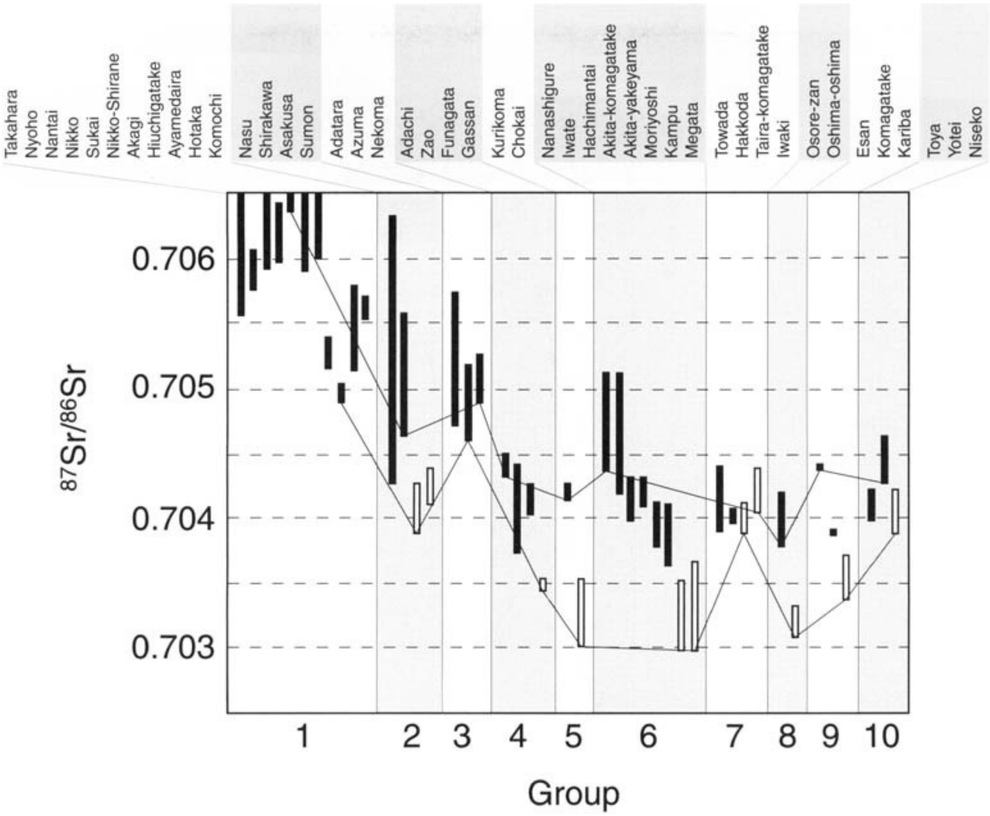

Fig. 7. Ranges of $^{87}Sr/^{86}Sr$ of volcanic rocks in the 10 volcanic groups in the NE Japan arc. Solid and open bars show $^{87}Sr/^{86}Sr$ ranges in individual volcanoes of the Nasu and the Chokai zones, respectively.

(Tamura & Nakamura 1996). Such features preclude simple mantle-source heterogeneity. If the mantle diapir model of Tamura (1994) is applicable to other arc volcanoes, isotopic variability within an arc volcano could be ascribed to crustal contamination (Tamura & Nakamura 1996).

On the other hand, Rb-poor lower crust could have relatively low $^{87}Sr/^{86}Sr$, and assimilation of such lower crust could result in lavas having lower $^{87}Sr/^{86}Sr$ than source-mantle values. The lower crust in NE Japan, however, has much higher $^{87}Sr/^{86}Sr$ values than mantle-derived magma (Kobayashi & Nakamura 2001; Kimura *et al.* 2002). Generally, volcanoes from Group 1 to Group 3 have higher $^{87}Sr/^{86}Sr$ values than the volcanoes in the other groups further to the north. Kobayashi & Nakamura (2001) concluded that assimilation of lower crust with $^{87}Sr/^{86}Sr > 0.707$ by mantle-derived hydrous magmas ($^{87}Sr/^{86}Sr$ *c.* 0.7043) produced the highly enriched, isotopically varied magmas of Akagi Volcano (Group 1). Kimura *et al.* (2002) showed that extremely low-K lavas at Nekoma Volcano (Group 3) ($^{87}Sr/^{86}Sr$ *c.* 0.7049) were produced from melts that originated in the lower crust. Thus, the lowest $^{87}Sr/^{86}Sr$ values of individual volcanoes may be close to source-mantle values in the NE Japan arc.

Figure 7 shows ranges of $^{87}Sr/^{86}Sr$ values of individual volcanoes from the front to the rear of the arc for each of the 10 volcano groups. Volcanoes along the volcanic front generally have higher $^{87}Sr/^{86}Sr$ than those to the west, except for those in Group 7, as pointed out previously by Notsu (1983). Moreover, these across-arc variations are not independent of the along-arc variations. In Figure 7, lines are shown connecting the minimum $^{87}Sr/^{86}Sr$ values of the highest $^{87}Sr/^{86}Sr$ volcano and the lowest $^{87}Sr/^{86}Sr$ volcano of each group, respectively. This shows that as the minimum values of the highest $^{87}Sr/^{86}Sr$ volcanoes decrease from Group 2 through Group 4 to Group 5, those of the lowest

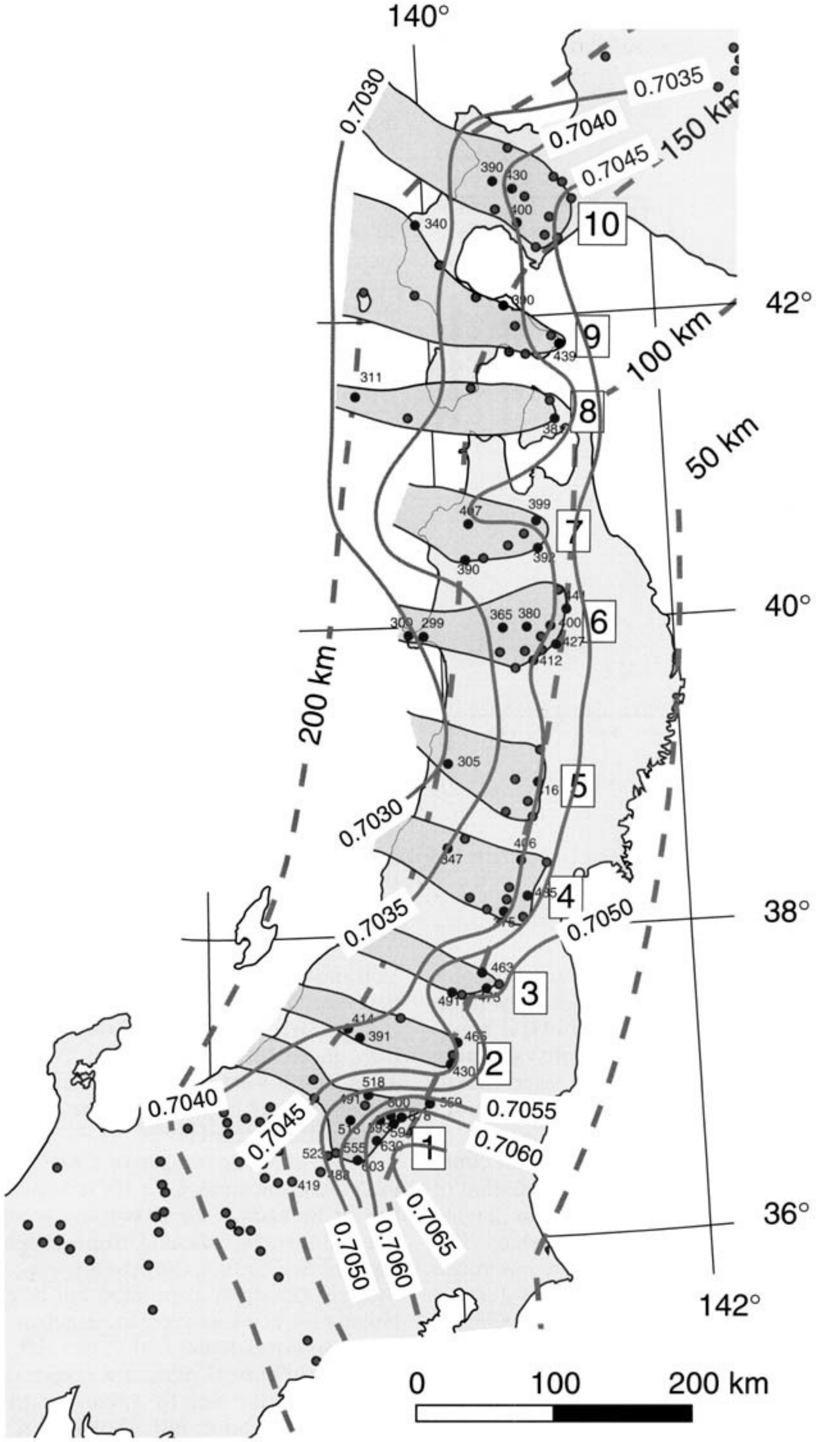

Fig. 8. Map showing inferred $^{87}Sr/^{86}Sr$ in mantle sources for selected volcanoes in the NE Japan arc. The $^{87}Sr/^{86}Sr$ values shown are abbreviated as follows (lowest $^{87}Sr/^{86}Sr$ –0.7) $\times$ 10^5. Lines show $^{87}Sr/^{86}Sr$ contours of the source mantle based on the lowest $^{87}Sr/^{86}Sr$.

$^{87}Sr/^{86}Sr$ volcanoes also decrease in the same along-strike direction. These two-dimensional variations of lowest $^{87}Sr/^{86}Sr$ values of individual volcanoes and inferred $^{87}Sr/^{86}Sr$ contours of the source mantle are shown together in Figure 8. Although there is a general decrease in minimum $^{87}Sr/^{86}Sr$ ratios from the volcanic front to the back-arc, the slope of the $^{87}Sr/^{86}Sr$ surface is irregular. For example, the $^{87}Sr/^{86}Sr$ surface slopes more steeply to the west in Groups 4 and 5 than it does in Groups 8 and 9 (Fig. 8).

As noted by Notsu (1983), volcanic front volcanoes from Group 4 to Group 10 have almost constant $^{87}Sr/^{86}Sr$ values, mostly between 0.7040 and 0.7045, Because the depth of the subducting slab beneath these volcanic front volcanoes increases from <100 km in Group 4 to >150 km in Group 10, slab depth seems to have a questionable relationship to the constant $^{87}Sr/^{86}Sr$ values observed.

Discussion

Why does basalt erupt?

Differences in crystallization histories of ascending primary basalt beneath individual volcanoes may explain why some arc volcanoes contain basalt and others do not. Basalts from the Megata and Oshima-oshima volcanoes in the Chokai Zone are the most primitive and have the lowest FeO*/MgO values (*c.* 1) and the highest MgO (> 10 wt%) (Fig. 4). Kushiro (1983) showed that the density of primary tholeiite magma exceeds that of primary alkali magma by 0.07–0.08 g cm^{-3} at pressures between 5 and 10 kbar, based on density measurements using the falling sphere method. The density of alkali basalt would be further reduced if it contains H_2O and other volatiles such as F and CO_2. Kushiro (1983) concluded that primary alkali basalt would probably ascend buoyantly at greater rates than primary tholeiites, resulting in less fractionation.

There is no evidence for H_2O heterogeneity in the basalt lavas along the NE Japan volcanic front. The low-alkali tholeiites (LAT) near the front contain no hydrous minerals, and plagioclase crystallizes early, indicating that there was little H_2O in the primary tholeiite magma (Sakuyama 1983). Similarly, basalt magmas on the volcanic front of the Izu–Bonin arc, south of Japan, are either anhydrous or contain very little water (Tamura & Tatsumi 2002). Thus, along-strike variations of FeO*/MgO and MgO of basalt magmas along the volcanic front (Fig. 4), and possibly the presence or absence of basalt in individual volcanoes, cannot be explained simply by volatile-induced differences in buoyancy.

Basalt-bearing volcanoes along the volcanic front in NE Japan tend to have higher elevations and are more complex than basalt-free volcanoes (Fig. 6). The absence of extrusive basalt, however, does not preclude the presence of basalt at depth. Moreover, I assume that fractional crystallization of basalt magmas played an important role, despite its absence at the surface. If masses of primary basalt magma are of larger volume and/or if the mantle wedge through which they pass is hotter, the eruption of non-fractionated basalts would be favoured. Thus, the basalt-bearing criterion could be another surface expression of large sizes and/or hotter thermal structure of the magma plumbing system below individual volcanoes along the volcanic front. The hot fingers beneath the volcanoes in Groups 5, 8 and 9, where no basalt is present, may be slightly cooler than the other fingers, which would result in a slightly cooler mantle wedge (or crust) above these fingers. Rising primary basalt magma passing through these cooler regions would have a greater opportunity to fractionate into andesite. Such a process may explain the absence of basalt at the surface in these three andesite-bearing volcano groups.

Slab depth v. thermal structure in the mantle wedge (hot fingers)

Cross-arc geochemical variations have been thought to be a function of slab depth (e.g. Ryan *et al.* 1995; Shibata & Nakamura 1997). Such a relationship, however, is not valid along the total length of the NE Japan arc (Figs 2, 3, 8). Along the axis of any of the 10 volcano groups, K_2O increases from east to west (Figs 2, 3). Group 10 volcanoes, offset slightly to the northwest, contain low-K basalts or LAT, which are similar to lavas erupting at the volcanic front to the south, but are different from the medium-K basalts or HAB erupting at volcanoes lying at the same distance above the subducting slab (Fig. 2).

Isotopically, mantle sources for NE Japan arc lavas are apparently not uniform (Fig. 8). However, at a similar $^{87}Sr/^{86}Sr$ ratio (0.704), Zao Volcano in the volcanic front (Group 4) produces LAT, but Asakusa Volcano behind the front (Group 2) contains HAB. At $^{87}Sr/^{86}Sr$ *c.* 0.703, Chokai Volcano and the Oshima-oshima volcanoes produce HAB and AOB, respectively (Figs 3, 7). Sakuyama & Nesbitt (1986) presented major and trace element data for a series of lavas from 17 volcanic centres in the NE Japan arc. They suggested that the main control on melt chemistry (except for Pb, Rb and Th content) is the degree of partial melting of a common source. Kushiro (1994) showed the variations of SiO_2 and total alkalis (Na_2O + K_2O) in partial melts formed from peridotite (PHN-1611) to be functions of pressure and degree of melting. The partial melt composition changes from higher alkalis to lower alkalis with increasing degree of melting at each pressure. At 10 and 15 kbar, low-alkali tholeiite is produced by relatively high degrees of partial melting (>20 wt%), but alkali basalt is produced by less than 10 wt% melting at more than 15 kbar (Kushiro 1994). Thus, I suggest that across-arc variation of basalt types from LAT through HAB to AOB or from low- to high-K in the NE Japan arc mainly reflects a decrease in the degree of partial melting.

One model for decrease in degree of partial melting with increasing distance from the volcanic front is the one proposed by Martinez & Taylor (2002). They suggested that this trend is a consequence of the mantle above the slab and behind the volcanic front having been depleted by extraction of arc magmas. This is not the case in NE Japan. The experimental results of Tatsumi *et al.* (1983) show that the mantle residue after the production of primary LAT in NE Japan is harzburgite. Primary AOBs from NE Japan and SW Japan are, however, saturated with lherzolitic minerals at mantle depths (Takahashi 1981; Tatsumi *et al.* 1983). Thus, AOB sources are no more depleted than the LAT sources.

I suggest that the decrease in degree of partial melting with increasing distance from the volcanic front in NE Japan is controlled by the thermal structure in the mantle wedge. The configuration of the thermal structure at depth thus appears to be independent of both of slab depth and mantle isotopic composition.

Magma source material at depth

Shibata & Nakamura (1997) suggested that the volume of fluid expelled from the subducted material (oceanic sediments and altered MORB), and added to the mantle wedge, decreases with increasing distance from the volcanic front. They suggested that the melting of the mantle wedge, having been metasomatized by rising fluids, would produce arc magmas showing the isotopic variations of Pb, Sr and Nd observed in the Quaternary volcanoes of NE Japan.

High $^{87}Sr/^{86}Sr$ ratios in magmatic arc magmas are widely thought to be the result of direct addition of subducted sediments from the slab to the mantle wedge (Turner *et al.* 1996; Hawkesworth *et al.* 1997). However, volcanoes in the volcanic front have similar $^{87}Sr/^{86}Sr$ values of 0.7040–0.7045 (Fig. 8), despite the increase in slab depth of <100 km in the south to >150 km in the north. Moreover, across-arc variation in $^{87}Sr/^{86}Sr$ is not observed in Group 7. Thus, the isotopic composition of magma source materials at depth again indicates little relationship to slab depth. Fluid from subarc devolatilization of the subducted material would definitely lower the mantle wedge solidus, but it is not always certain that Sr within this fluid plays a major role in $^{87}Sr/^{86}Sr$ variations in arc lavas. I suggest that these variations are mainly the result of processes acting at the tips of the hot mantle fingers.

There is evidence that the isotopic variation in NE Japan mantle pre-dates the formation of the Quaternary volcanic arc. Tamaki *et al.* (1992) noted that vigorous volcanism accompanied the opening of the Japan Sea at about 28–18 Ma. Cousens & Allan (1992), Tamaki *et al.* (1992) and Cousens *et al.* (1994) found that basaltic rocks from this area have the same range of isotopic characteristics as those of the Quaternary arc volcanic rocks in NE Japan, suggesting widespread and similar mantle isotopic variability. Cousens *et al.* (1994) further concluded that the subduction of devolatilized sediments prior to the Japan Sea opening (long before the formation of the Quaternary NE Japan arc) might have contributed to the enriched component of this variation.

Kushiro (1990) discussed evolution of the crust in the NE Japan arc based on melting experiments of a peridotite under hydrous conditions and crustal compositions estimated from deep crustal xenoliths and seismic velocity data. He concluded that the mass of the present mantle wedge is not sufficient to produce the present crust and cumulates in the NE Japan arc, and he suggested that the mantle wedge may have been replenished several times by the addition of fertile mantle materials (Kushiro 1990).

I extend the models presented by Kushiro (1990) and Cousens *et al.* (1994) to my present study and suggest that a MORB-like mantle source ($^{87}Sr/^{86}Sr$ *c.* 0.703) in the mantle wedge is replenished by fertile mantle materials ($^{87}Sr/^{86}Sr$ *c.* 0.705) through convection induced by the subducting lithosphere. These fertile mantle materials would be the result of mixing between partial melts of sediments and depleted mantle (Cousens *et al.* 1994). They would be preferentially entrained into upward-convecting masses (mantle fingers) because they would be produced just above the subducting slab and down-dragged mantle layer, the region where the mantle fingers originate. Such convection, coupled with the mantle diapir model of Tamura (1994), could explain the two-dimensional variations in degrees of melting and $^{87}Sr/^{86}Sr$ values in the volcanoes of NE Japan.

A dynamic model

The exact ways in which melt is generated in subduction zones and transported to the surface remain uncertain. According to the model of Tamura (1994), mantle diapirs consisting of hydrous peridotite form in the lower part of the mantle wedge and rise through anhydrous peridotite. Hall & Kincaid (2001) presented the results of laboratory experiments that indicated that the interaction between buoyantly upwelling diapirs and subduction-induced mantle flow creates a network of low-density, low-viscosity conduits. The formation of interconnected conduit networks is consistent with a number of observational constraints, including the rapid transport time required by recent U–Th disequilibrium (e.g. Hawkesworth *et al.* 1997).

Turner *et al.* (2001) documented ^{226}Ra excesses in island arc lavas and concluded that preservation of this signal requires very rapid transport of magma to the surface – only a few hundred to a few thousand years after fluid addition. The mantle diapir model cannot explain such ultrafast source-to-surface movement if the ^{226}Ra excesses originate at the base of mantle wedge. Turner *et al.* (2000), however, interpret that the U and Ra were added by fluids that were spatially and temporally separated, and it is possible that a slowly rising mantle diapir could be overtaken by much faster high-^{226}Ra melts.

Figure 9a shows my proposed model for dynamic convection within the mantle wedge and genesis of arc magmas by mantle diapirs. As suggested by previous workers (e.g. Furukawa 1993; Kincaid & Sacks 1997), subduction of a rigid oceanic slab into the viscous mantle induces convection in the mantle wedge. Tamura *et al.* (2002) refined this concept and suggested that in NE Japan this convection takes the form of hot, finger-like regions in the mantle wedge that move toward the volcanic front. Conveyor-like return flow is interpreted to carry the remnants of these fingers to depth along the top of the subducting slab. In the act of returning, it is likely that the fingers lose their identity and are smeared out to take the form of a thin, continuous sheet near the base of the wedge. Given that mantle diapirs are formed in the lower part of the mantle wedge (Tamura 1994), greater amounts of fertile material would be incorporated in diapirs beneath the volcanic front, and lesser amounts would be incorporated in areas behind the front (Fig. 9a). Thus, mantle diapirs are mixtures between depleted mantle ($^{87}Sr/^{86}Sr$ *c.* 703) and fertile mantle ($^{87}Sr/^{86}Sr$ *c.* 705) and the ratio of this mixing is schematically shown in the two circles in Figure 9a. As a result, the magmas formed beneath the volcanic front would have higher $^{87}Sr/^{86}Sr$, and those formed further 'back' would have lower $^{87}Sr/^{86}Sr$.

The hot fingers interpreted in this paper extend from deeper than 150 km below the back-arc region towards the shallower mantle (*c.* 50 km) beneath the volcanic front (Tamura *et al.* 2002). Across-arc variation of basalt type (Figs 2, 3) may be controlled by the configuration of hot fingers in the mantle wedge (Fig. 9a). When mantle diapirs cease their ascent, those below the volcanic front are still enclosed within the hot fingers and, therefore, still heated, but those beneath the back-arc region will have risen above the hot fingers and will cool before magma segregation. Thus, primary basaltic magmas near the volcanic front are formed by higher degrees of partial melting, whereas those further west are formed by smaller degrees of partial melting.

Conclusions

- I propose that hot fingers in the mantle wedge play a role in producing across-arc variation of basalt type from LAT through HAB to AOB in the NE Japan arc. Hot fingers are inclined within the mantle wedge (Tamura *et al.* 2001, 2002), but magma sources (mantle diapirs) stop ascending at similar depths (Kushiro 1994), which results in higher degrees of partial melting below the volcanic front and lower degrees of partial melting beneath the regions behind the front (Sakuyama & Nesbitt 1986).
- There is evidence that the isotopic variation in NE Japan mantle pre-dates the formation of the Quaternary volcanic arc (Cousens & Allan 1992; Tamaki *et al.* 1992; Cousens *et al.* 1994). I suggest that a mid-ocean ridge basalt (MORB)-like mantle source ($^{87}Sr/^{86}Sr$ *c.* 0.703) in the mantle wedge is replenished by fertile mantle materials ($^{87}Sr/^{86}Sr$ *c.* 0.705) through convection induced by the subducting lithosphere. These fertile mantle materials would be the result of mixing between partial melts of sediments and depleted mantle

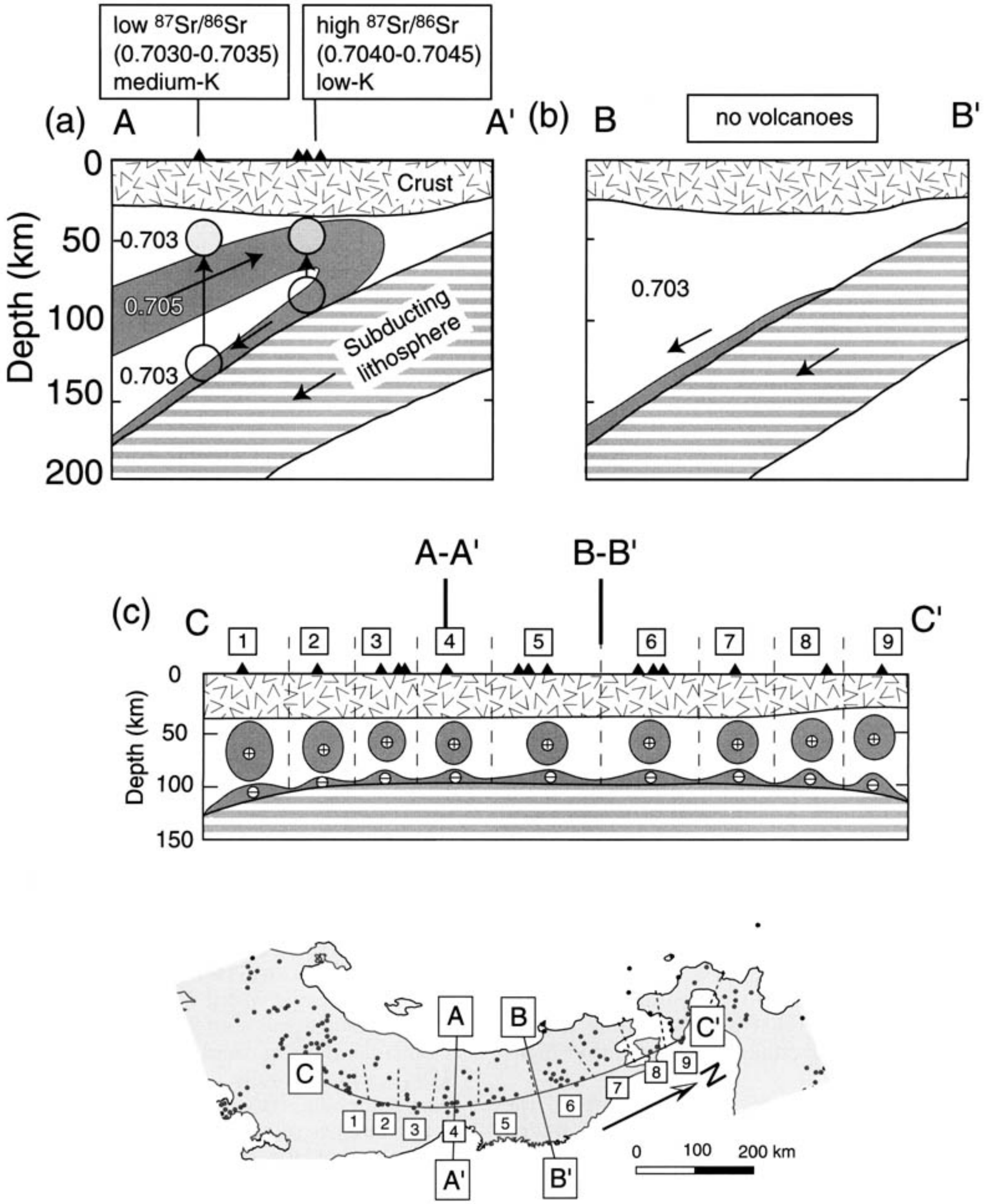

Fig. 9. Schematic cross-sections collectively showing proposed model for three-dimensional convection within the mantle wedge of the NE Japan subduction zone. Solid triangles denote NE Japan volcanoes. Insert map shows cross-front sections A–A′, B–B′ and a front-parallel section (C–C′). Numbers enclosed in squares denote volcano groups. (**a**) Section along the axis of a hot finger. A MORB-like mantle in the ambient mantle wedge ($^{87}Sr/^{86}Sr$ *c.* 0.703) is replenished by fertile mantle materials ($^{87}Sr/^{86}Sr$ *c.* 0.705) by conveyor-like convection. See text for explanation. (**b**) Section along an area lying between two hot fingers. The upper, finger-like part of the system is absent, but its lower (down-going) part is the result of lateral spreading of material from the vestiges of adjacent downgoing fingers. (**c**) Front-parallel section; tips of hot fingers (+) are moving toward the viewer; sheet-like return flow (–) is moving away.

(Cousens *et al.* 1994), and would be produced just above the subducting slab and down-dragged mantle layer, the region from which upward convecting masses (mantle fingers) originate.

- I suggest that the hot fingers represent the irregular advancing front of hot and fertile mantle material in the mantle wedge. After reaching the volcanic front, this material turns over, cools and spreads laterally to form continuous sheet moving downward along the top of subducting slab. Mantle diapirs formed in the lower part of the mantle wedge (Tamura 1994; Hall & Kincaid 2001) would incorporate greater amounts of fertile material below the volcanic front and lesser amounts of fertile material away from the volcanic front, which could explain the observed map-view variations of minimum $^{87}Sr/^{86}Sr$ in volcanoes in NE Japan.

I thank I. Kushiro, Y. Tatsumi and T. Hanyu for helpful discussions, and I much appreciate the comments and reviews of J.F. Allan, W.P. Leeman and R.D. Larter. R.S. Fiske helped with manuscript revision.

References

AOKI, K. & YOSHIDA, T. 1986. Minor element composition of volcanic rocks and xenoliths from lower crust of Ichinomegata volcano, Akita Prefecture. *Kakuriken Houkoku*, **19**, 279–287 (in Japanese).

ARAMAKI, S. & UI, T. 1978. Major element frequency distribution of the Japanese Quaternary volcanic rocks. *Bulletin Volcanologique*, **41**, 390–407.

ASAKUSA VOLCANO COLLABORATIVE RESEARCH GROUP. 1991. Petrology of Asakusa Volcano – petrography and bulk rock chemistry. *Chikyu Kagaku*, **45**, 113–130 (in Japanese with English abstract).

BAN, M. 1991. A petrological model for the Minamigassan volcano, Nasu volcanoes, Northeast Japan arc. *Bulletin of the Volcanological Society of Japan*, **36**, 255–267.

BAN, M. & FUJIMAKI, H. 1992. Petrology of Nasu volcanic Group, Northeast Japan arc. *Abstracts of the Volcanological Society of Japan*, **2**, 95.

BAN, M. & TAKAOKA, N. 1995. Evolutionary history of the Nasu volcano Group, Northeast Japan arc. *Journal of Mineralogy, Petrology and Economic Geology*, **90**, 195–214.

BAN, M., YAMANAKA, T., INOUE, M., YOSHIDA, T., HAYASHI, S. & AOKI, K. 1992. Geochemistry of volcanic rocks of Takahara volcano, Northeast Japan. *Kakuriken Houkoku*, **25**, 199–226 (in Japanese).

BAN, M., YOSHIDA, T. & AOKI, K. 1987. Bulk chemistry of volcanic rocks from Nasu volcano Group. *Kakuriken Houkoku*, **20**, 165–178.

COMMITTEE FOR CATALOGUE OF QUATERNARY VOLCANOES IN JAPAN. 1999. *Catalogue of Quaternary Volcanoes in Japan.* Volcanological Society of Japan, Tokyo.

COUSENS, B.L. & ALLAN, J.F. 1992. A Pb, Sr, and Nd isotopic study of basaltic rocks from the Sea of Japan, Legs 127/128. *In*: TAMAKI, K., SUYEHIRO, K., ALLAN, J., MCWILLIAMS, M. *et al. Proceedings of the Ocean Drilling Program, Scientific Results*, **127/128**, 805–817.

COUSENS, B.L., ALLAN, J.F. & GORTON, M.P. 1994. Subduction-modified pelagic sediments as the enriched component in back-arc basalts from the Japan Sea: Ocean Drilling Program Sites 797 and 794. *Contributions to Mineralogy and Petrology*, **117**, 421–434.

FUJINAWA, A., YOSHIDA, T. & AOKI, K. 1984. Geochemical study of Adatara volcano, Northeast Japan. *Kakuriken Houkoku*, **17**, 356–374 (in Japanese).

FURUKAWA, Y. 1993. Magmatic processes under arcs and formation of the volcanic front. *Journal of Geophysical Research*, **98**, 8309–8319.

GILL, J. 1981. *Orogenic Andesites and Plate Tectonics.* Springer, Berlin.

HALL, P.S. & KINCAID, C. 2001. Diapiric flow at subduction zones: a recipe for rapid transport. *Science*, **292**, 2472–2475.

HAWKESWORTH, C.J., TURNER, S.P., MCDERMOTT, F., PEATE, D.W. & VAN CALSTEREN, P. 1997. U–Th isotopes in arc magmas: implications for element transfer from the subducted crust. *Science,* **276**, 551–555.

HAYASHI, S., YOSHIDA, T. & AOKI, K. 1984. Geochemical study of Chokai volcano, Northeast Japan. *Kakuriken Houkoku*, **17**, 382–390 (in Japanese).

HAYASHI, S., YOSHIDA, T., TAKASHIMA, K. & AOKI, K. 1991. Minor element compositions of Kanpu volcano, Northeast Japan. *Kakuriken Houkoku*, **24**, 274–285.

HUNTER, A.G. & BLAKE, S. 1995. Petrological evolution of a transitional tholeiitic-calc-alkaline series: Towada volcano, Japan. *Journal of Petrology*, **36**, 1579–1605.

ISHIKAWA, K., YOSHIDA, T. & AOKI, K. 1984. Crystallization differentiation of magmas in the Quaternary Iwate volcano, northern Nasu zone. *Kakuriken Houkoku*, **17**, 330–345 (in Japanese).

KANISAWA, S. & SHIBATA, K. 1987. Strontium isotope ratios of the products from the Adachi volcano, Northeast Japan. *Journal of Japanese Association of Mineralogists, Petrologists, and Economic Geologists*, **82**, 81–84 (in Japanese with English abstract).

KATSUI, Y., OBA, Y., ANDO, S., NISHIMURA, S., MASUDA, Y., KURASAWA, H. & FUJIMAKI, H. 1978. Petrochemistry of the Quaternary volcanic rocks of Hokkaido, North Japan. *Journal of Faculty of Science, Hokkaido University, Series IV*, **18**, 449–484.

KERSTING, A.B., ARCULUS, R.J. & GUST, D.A. 1996. Lithospheric contributions to arc magmatism: isotope variations along strike in volcanoes of Honshu, Japan. *Science*, **272**, 1464–1468.

KIMURA, J., YOSHIDA, T. & IIZUMI, S. 2002. Origin of low-K intermediate lavas at Nekoma volcano, NE Honshu arc, Japan: geochemical constraints for lower-crustal melts. *Journal of Petrology*, **43**, 631–661.

KINCAID, C. & SACKS, I.S. 1997. Thermal and dynamical evolution of the upper mantle in subduction zones. *Journal of Geophysical Research*, **102**, 12 295–12 315.

KOBAYASHI, K. & NAKAMURA, E. 2001. Geochemical evolution of Akagi volcano, NE Japan: Implications for interaction between island-arc magma and lower crust, and generation of isotopically various magmas. *Journal of Petrology*, **42**, 2303–2331.

KUNO, H. 1960. High-alumina basalt. *Journal of Petrology*, **1**, 121–145.

KUNO, H. 1966. Lateral variation of basalt magma type across continental margins and island arcs. *Bulletin Volcanologique*, **29**, 195–222.

KURASAWA, H. 1984. Strontium isotopic consequence of the volcanic rocks from Fuji, Hakone and Izu areas. *Bulletin of Geological Survey of Japan*, **35**, 637–659.

KURASAWA, H., FUJINAWA, A. & LEEMAN, W.P. 1986. Calc-alkaline and tholeiitic rock series magmas coexisting within volcanoes in Japanese island arcs – Strontium isotopic study. *Journal of Geological Society of Japan*, **92**, 255–268.

KUSHIRO, I. 1983. On the lateral variations in chemical composition and volume of Quaternary volcanic rocks across Japanese arc. *Journal of Volcanology and Geothermal Research*, **18**, 435–447.

KUSHIRO, I. 1990. Partial melting of mantle wedge and evolution of island arc crust. *Journal of Geophysical Research*, **95**, 15 929–15 939.

KUSHIRO, I. 1994. Recent experimental studies on partial melting of mantle peridotites at high pressures using diamond aggregates. *Journal of Geological Society of Japan*, **100**, 103–110.

MARTINEZ, F. & TAYLOR, B. 2002. Mantle wedge control on back-arc crustal accretion. *Nature*, **416**, 417–420.

NAKAGAWA, M. 1991. Model for the generation of andesitic–dacitic magma of Moriyoshi volcano, Northeastern Japan. *Bulletin of the Volcanological Society of Japan*, **36**, 223–239.

NAKAGAWA, M., YOSHIDA, T. & AOKI, K. 1985. Geochemical study of volcanic materials from Akita–Komagatake volcano, Northeast Japan. *Kakuriken Houkoku*, **18**, 189–202.

NOTSU, K. 1983. Strontium isotope composition in volcanic rocks from the Northeast Japan arc. *Journal of Volcanology and Geothermal Research*, **18**, 531–548.

NOTSU, K., ARAMAKI, S., OSHIMA, O. & KOBAYASHI, Y. 1987. Two overlapping slabs subducting beneath central Japan as revealed by strontium isotope data. *Journal of Volcanology and Geothermal Research*, **32**, 195–207.

OBA, Y., YOSHIDA, T. & AOKI, K. 1985. Geochemistry of Usu volcano, Hokkaido. *Kakuriken Houkoku*, **18**, 189–202 (in Japanese).

OHBA, T. 1993. Geology and petrology of Akita-yakeyama volcano 2. Evolutional history of magma composition. *Journal of Mineralogy, Petrology and Economic Geology*, **88**, 1–19.

OHBA, T. & UMEDA, K. 1999. Geology of Hachimantai volcanic field and temporal–spatial variation of the magma compositions. *Journal of Mineralogy, Petrology and Economic Geology*, **94**, 187–202.

RYAN, J.G., MORRIS, J., TERA, F., LEEMAN, W.P. & TSVETKOV, A. 1995. Cross-arc geochemical variations in the Kurile arc as a function of slab depth. *Science*, **270**, 625–627.

SAKAYORI, A., YOSHIDA, T. & AOKI, K. 1984. Geochemical study of Minami–Zao volcano, northern Nasu zone. *Kakuriken Houkoku*, **17**, 346–355 (in Japanese).

SAKAYORI, A., YOSHIDA, T. & AOKI, K. 1987. Geochemical study of Zao volcano, Northeast Japan. *Kakuriken Houkoku*, **20**, 153–164 (in Japanese).

SAKUYAMA, M. 1983. Petrology of arc volcanic rocks and their origin by mantle diapirs. *Journal of Volcanology and Geothermal Research*, **18**, 297–320.

SAKUYAMA, M. & KOYAGUCHI, T. 1984. Magma mixing in mantle xenolith-bearing calc-alkalic ejecta, Ichinomegata volcano, Northeastern Japan. *Journal of Volcanology and Geothermal Research*, **22**, 199–224.

SAKUYAMA, M. & NESBITT, R.W. 1986. Geochemistry of the Quaternary volcanic rocks of the Northeast Japan arc. *Journal of Volcanology and Geothermal Research*, **29**, 413–450.

SASAKI, M., YOSHIDA, T. & AOKI, K. 1986. Geochemical study of Nikko volcano Group, Northeast Japan. *Kakuriken Houkoku*, **19**, 307–319 (in Japanese).

SASAKI, N., YOSHIDA, T. & AOKI, K. 1985. Geochemical study of Kita–Hakkoda volcano Group, northern Nasu zone. *Kakuriken Houkoku*, **18**, 175–188 (in Japanese).

SASAKI, N., YOSHIDA, T., AOKI, K. 1987. Geochemical study of Stage-1 tholeiitic magmas of the Hakkoda volcano Group, northern Nasu zone. *Kakuriken Houkoku*, **20**, 363–374 (in Japanese).

SHIBATA, T. & NAKAMURA, E. 1997. Across-arc variations of isotope and trace element compositions from Quaternary basaltic volcanic rocks in northeastern Japan: Implications from interaction between subducted oceanic slab and mantle wedge. *Journal of Geophysical Research*, **102**, 8051–8064.

SHIRAHASE, T., TAMANYU, S. & TOGASHI, S. 1989. Sr isotope geochemistry of voluminous acidic pyroclastics erupted at 1–3 Ma in Northeast Japan. *Journal of Mineralogy, Petrology and Economic Geology*, **84**, 200–207.

TAKAHASHI, E. 1981. Melting relations of an alkali–olivine basalt to 30 kbars, and their bearing on the origin of alkali basalt magmas. *Carnegie Institution of Washington Year Book*, **79**, 271–276.

TAMAKI, K., SUYEHIRO, K., ALLAN, J., INGLE, J.C., JR & PISCIOTTO, K.A. 1992. Tectonic synthesis and implications of Japan Sea ODP drilling. *In*: TAMAKI, K., SUYEHIRO, K., ALLAN, J., MCWILLIAMS, M. *et al. Proceedings of the Ocean Drilling Program, Scientific Results*, **127/128**, 1333–1348.

TAMURA, Y. 1994. Genesis of island arc magmas by mantle-derived bimodal magmatism: evidence from the Shirahama Group, Japan. *Journal of Petrology*, **35**, 619–645.

TAMURA, Y. & NAKAMURA, E. 1996. The arc lavas of the Shirahama Group, Japan: Sr and Nd isotopic data indicate mantle-derived bimodal magmatism. *Journal of Petrology*, **37**, 1307–1319.

TAMURA, Y. & TATSUMI, Y. 2002. Remelting of an andesitic crust as a possible origin for rhyolitic magma oceanic arcs: an example from the Izu–Bonin arc. *Journal of Petrology*, **43**, 1029–1047.

TAMURA, Y., TATSUMI, Y., ZHAO, D., KIDO, Y. & SHUKUNO, H. 2001. Distribution of Quaternary volcanoes in the Northeast Japan arc: geologic and geophysical evidence of hot fingers in the mantle wedge. *Proceedings of the Japan Academy*, **77**, 135–139.

TAMURA, Y., TATSUMI, Y., ZHAO, D., KIDO, Y. & SHUKUNO, H. 2002. Hot fingers in the mantle wedge: new insights into magma genesis in subduction zones. *Earth and Planetary Science Letters*, **197**, 105–116.

TATSUMI, Y., SAKUYAMA, M., FUKUYAMA, H. & KUSHIRO, I. 1983. Generation of arc basalt magmas and thermal structure of the mantle wedge in subduction zones. *Journal of Geophysical Research*, **88**, 5815–5825.

TOGASHI, S., TANAKA, T., YOSHIDA, T., ISHIKAWA, K., FUJINAWA, A. & KURASAWA, H. 1992. Trace elements and Nd–Sr isotopes of island arc tholeiites from frontal arc of Northeast Japan. *Geochemical Journal*, **26**, 261–277.

TOYA, N. & BAN, M. 2001. Volcanic history and major element bulk chemistry of the Aoso volcano, Northeast Japan arc. *Japanese Magazine of Mineralogical and Petrological Sciences*, **30**, 105–116.

TURNER, S., BOURDON, B., HAWKESWORTH, C. & EVANS, P. 2000. ^{226}Ra–^{230}Th evidence for multiple dehydration events, rapid melt ascent and the time scales of differentiation beneath the Tonga–Kermadec island arc. *Earth and Planetary Science Letters*, **179**, 581–593.

TURNER, S., EVANS, P. & HAWKESWORTH, C. 2001. Ultrafast source-to-surface movement of melt at island arcs from ^{226}Ra–^{230}Th systematics. *Science*, **292**, 1363–1366.

TURNER, S., HAWKESWORTH, C., VAN CALSTEREN, P., HEATH, E., MACDONALD, R. & BLACK, S. 1996. U-series isotopes and destructive plate margin magma genesis in the Lesser Antilles. *Earth and Planetary Science Letters*, **142**, 191–207.

UTO, K. 1986. Variation of Al_2O_3 content in late Cenozoic Japanese basalts: a re-examination of Kuno's high-alumina basalt. *Journal of Volcanology and Geothermal Research*, **29**, 397–411.

YAMAMOTO, M. 1984. Origin of calc-alkaline andesite from Oshima-Oshima volcano, North Japan. *Journal of the Faculty of Science, Hokkaido University*, **21**, 77–131.

YAMAZAKI, T. 1991. Geology and petrology of the Somma Stage effusives from Kuttara volcano, south-eastern Hokkaido, Japan. *Chikyu Kagaku*, **45**, 51–60 (in Japanese with English abstract).

YOSHIDA, T., ABE, T., TANIGUCHI, M. & AOKI, K. 1987. Geochemical study of volcanic rocks from Funagata volcano in the Northeast Japan arc. *Kakuriken Houkoku*, **20**, 131–151 (in Japanese).

YOSHINAGA, T. & NAKAGAWA, M. 1999. Finding of primary basalt from Sannome-gata volcano, northeastern Japan, and its compositional variation. *Journal of Mineralogy, Petrology and Economic Geology*, **94**, 241–253.

ZHAO, D., HASEGAWA, A. & HORIUCHI, S. 1992. Tomographic imaging of P and S wave velocity structure beneath Northeastern Japan. *Journal of Geophysical Research*, **97**, 19 909–19 928.

ZASHU, S., KANEOKA, I. & AOKI, K. 1980. Sr isotope study of mafic and ultramafic inclusions from Itinome-gata, Japan. *Geochemical Journal*, **14**, 123–128.

This page intentionally left blank

Mantle genesis and crustal evolution of primitive calc-alkaline basaltic magmas from the Lesser Antilles arc

M. PICHAVANT[1] & R. MACDONALD[2]

[1]*Institut des Sciences de la Terre d'Orléans (ISTO), UMR 6113 CNRS-UO, 1A rue de la Férollerie, 45071 Orléans, France (e-mail: pichavan@cnrs-orleans.fr)*

[2]*Environmental Science Division, IENS, Lancaster University, Lancaster LA1 4YQ, UK*

Abstract: Most eruptive rocks in the Lesser Antilles arc are compositionally evolved. However, lavas with primitive characteristics do occur including, in the central part of the arc, a suite of rocks from Soufriere, St Vincent, and the Ilet à Ramiers basalt from Martinique. High-pressure experiments performed on a Soufriere basalt point to a spinel lherzolite source. Glass inclusion data and phase equilibria analysis suggest extraction of the Soufriere melt under relatively dry conditions (*c.* 2 wt% H_2O in melt). Using estimates of the H_2O content of mantle sources fluxed by an hydrous slab-derived component, H_2O concentrations as high as 5 wt% are considered possible for primary mantle melts in the Lesser Antilles arc. Experiments at low pressures (4 kbar) simulate the evolution of primitive melts within the arc crust. For elevated melt H_2O concentrations (6–8.5 wt%), derivative liquids ranging from low-MgO basalt to basaltic andesite are generated at 1050–1100°C. Their crystallization at 950–1000°C yield andesitic liquids similar to those erupting at active volcanic centres such as Mt Pelée, Martinique, and Soufriere Hills, Montserrat. Therefore, experimental data support the derivation of Lesser Antilles arc eruptives by different degrees of fractionation from primary mantle melts.

Near-primary magmas, such as high-MgO (MgO $\geq$ 8 wt%) basalts, are scarce in intra-oceanic arcs. Nevertheless, they occur in virtually every arc and are of great petrological importance as these basalts possibly represent one type of primary magma in subduction zones (e.g. Tatsumi & Eggins 1995 and references therein). As such, they constitute valuable sources of information on the conditions of partial melting and the thermal structure and composition of the mantle wedge beneath island arcs. In addition, knowledge of the H_2O content of primary arc magmas is important in assessing processes of volatile recycling in subduction zones and for understanding the causes of explosive volcanism. Experimental studies at upper mantle pressures constitute our main source of information on the conditions of genesis of high-MgO basalts in arc settings (Tatsumi 1982; Tatsumi *et al.* 1983, 1994; Gust & Perfit 1987; Kushiro 1987; Bartels *et al.* 1991; Draper & Johnston 1992; Baker *et al.* 1994; Myers & Johnston 1996; Falloon *et al.* 1999; Pichavant *et al.* 2002*b*).

At most island arcs, volcanism is dominated by non-primary compositions (basaltic andesite–andesite, see also below and Davidson 1996; Macdonald *et al.* 2000). It is uncertain whether these evolved compositions can be related to the near-primary magmas by simple petrogenetic processes such as fractional crystallization, or whether more complex scenarios involving, for example, large-scale assimilation of the arc crust by mantle melts need to be considered. Experiments performed at crustal pressures on examples of near-primary magmas can provide an efficient test of these different possibilities. To date, the number of such studies in the literature is limited (Sisson & Grove 1993*a*, *b*), mainly because of technical difficulties.

In this paper we focus on the Lesser Antilles intra-oceanic arc, the surface manifestation of the subduction of the American Plate beneath the Caribbean Plate (Fig. 1). We first identify among the Lesser Antilles eruptive rocks those that have the geochemical characteristics of near-primary magmas. We then discuss some recently obtained experimental results pertaining to: (1) the conditions of genesis of these magmas in the mantle wedge; and (2) their evolution in the arc crust. These data lead to a quantitative petrogenetic model for the present-day calc-alkaline magmatism in the Caribbean.

Compositions of Lesser Antilles eruptive rocks

Results of a recent compilation of the major element composition of eruptive rocks from the Lesser Antilles arc are shown in Figure 2

From: LARTER, R.D. & LEAT, P.T. 2003. *Intra-Oceanic Subduction Systems: Tectonic and Magmatic Processes.* Geological Society, London, Special Publications, **219**, 239–254. 0305-8719/03/$15.00

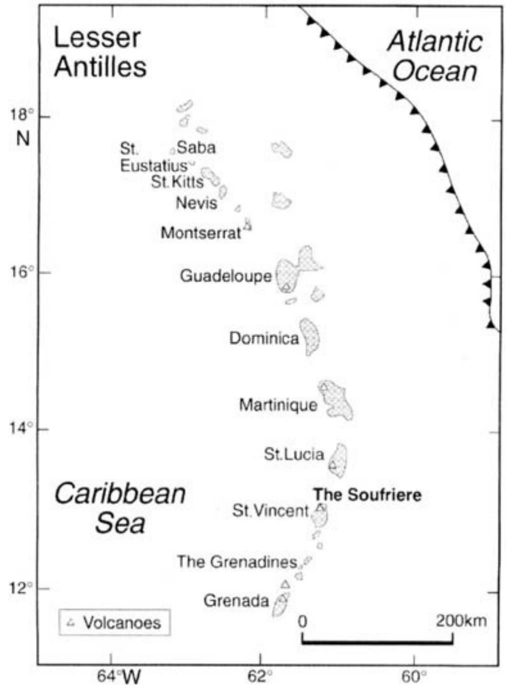

Fig. 1. Map of the Lesser Antilles island arc showing location of the Soufriere Volcano, St Vincent.

(Macdonald *et al.* 2000). The arc contains a wide range of magma types (e.g. Brown *et al.* 1977; Westercamp 1979), from low-K tholeiites (north), calc-alkaline basalts (central islands) to alkalic basalts in Grenada (south), the distinction between these different series being made mainly on the basis of the minor and trace elements (Macdonald *et al.* 2000). As in most other oceanic arcs (Davidson 1996), the Lesser Antilles compilation underlines the fact that the majority of lavas have MgO contents <6 wt% and can hence be considered evolved. As reference points, the composition of andesites now erupting at Soufriere Hills, Montserrat (Murphy *et al.* 2000) or emitted during the recent activity of Mt Pelée, Martinique (Pichavant *et al.* 2002*a*) (Table 1), would plot near the low end of the range in Figure 2 (about 2 wt% MgO). At both Soufriere Hills and Mt Pelée, the most mafic rocks erupted are relatively evolved basaltic andesites or basalts with MgO contents <5–6 wt% (Table 1).

There are, however, a few eruptive rocks with primitive characteristics. Most occur in the southern part of the arc, i.e. in Grenada (Fig. 2). In the central part of the arc, primitive compositions are restricted to a very limited suite of samples which includes some calc-alkaline lavas

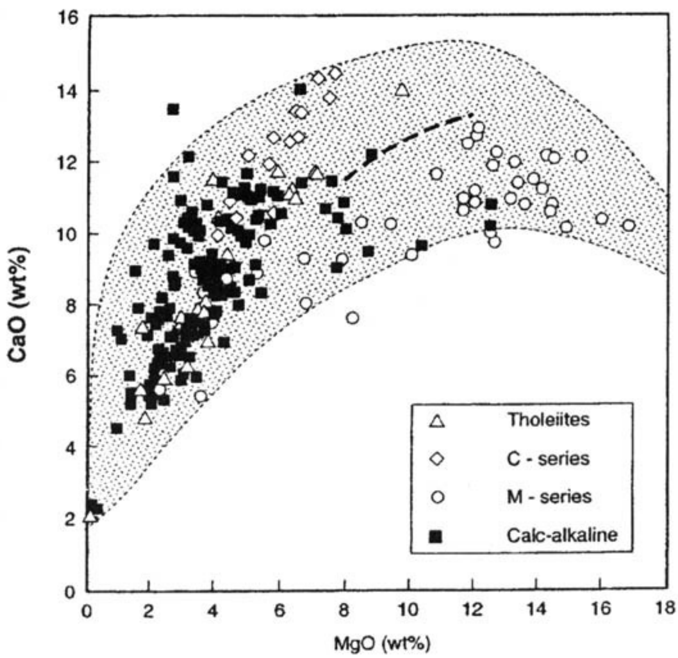

Fig. 2. MgO–CaO plot for Lesser Antilles eruptive rocks, after Macdonald *et al.* (2000). The stippled field encloses rocks from oceanic arcs compiled by Davidson (1996). The dashed line separates high-Ca from low-Ca suites.

Table 1. *Whole-rock compositions*

Sample	STV301[1]	ID 16[2]	IK85060803[3]	STV303[4]	031-22b[5]	MT33S[6]
(wt%)						
SiO_2	47.01	48.94	49.03	51.43	53.00	60.97
TiO_2	1.07	0.70	0.64	0.91	0.78	0.45
Al_2O_3	15.28	16.01	13.95	17.97	19.00	17.47
FeO_t	8.79	8.90	8.95	8.07	7.96	5.96
MnO	0.16	0.17	0.15	0.18	0.17	0.18
MgO	12.50	11.42	12.38	5.23	4.24	2.20
CaO	10.96	10.89	10.75	9.20	9.60	6.15
Na_2O	2.23	2.21	1.93	2.59	2.79	3.53
K_2O	0.47	0.52	0.27	0.40	0.67	1.03
H_2O	nd	nd	1.90	nd	0.57	0.77
Total	98.47	99.76	99.95	95.98	98.78	98.71
(ppm)						
Cr	728	662	820	116	13	nd
Ni	250	266	nd	45	8	nd

[1] Olivine basalt, St Vincent, Lesser Antilles (Heath *et al.* 1998).
[2] High-magnesia basalt, Umnak, Aleutians (Draper & Johnston 1992).
[3] Olivine tholeiite, Ryozen, NE Japan (Kushiro 1987).
[4] Basalt, St Vincent, Lesser Antilles (Heath *et al.* 1998).
[5] Basaltic andesite, Mt Pelée, Lesser Antilles (Pichavant *et al.* 2002*a*).
[6] Andesite, Mt Pelée, Lesser Antilles (Pichavant *et al.* 2002*a*).
nd, not determined.

from Soufriere, St Vincent (Heath *et al.* 1998) and the Ilet à Ramiers basalt, Martinique (Westercamp 1979).

Primitive calc-alkaline basalts from Soufriere, St Vincent

The Soufriere Volcano, located in the north of St Vincent, is composed almost entirely of calc-alkaline basalts and basaltic andesites (Heath *et al.* 1998). Basalts were volumetrically most abundant during the earlier stages of volcanic activity (Pre-Somma lavas, Heath *et al.* 1998). Some Pre-Somma basalts have primitive geochemical characteristics (MgO > 10 wt%, Ni > 200 ppm, Cr > 500 ppm; Fig. 3), contrasting with basaltic andesites from both the Pre-Somma lava stage and the present stage of activity, as represented by products from the 1979 eruption (Fig. 3). These primitive lavas are good candidates for representing primary mantle melts (Table 1). They are comparable to high-MgO and picritic basalts in other arcs, for example Vanuatu (Eggins 1993), NE Japan (Kushiro 1987; Tatsumi *et al.* 1994) and the Aleutians (Nye & Reid 1986; Draper & Johnston 1992). The Ilet à Ramiers basalt from Martinique (Westercamp 1979) is geochemically similar to the primitive basalts from Soufriere, St Vincent (Fig. 3). This suggests that, although rare, compositions of this type are found throughout the arc and may have a common petrogenetic origin.

The primitive Soufriere basalts range from microphyric fine-grained rocks with abundant (up to 30%) microphenocrysts of olivine (ol), spinel (sp) and clinopyroxene (cpx), to more coarsely porphyritic rocks also containing phenocrystic plagioclase (pl). Olivines up to $Fo_{89.7}$ have been found (Marcelot *et al.* 1981; Heath *et al.* 1998). The ol–sp thermometer of Ballhaus *et al.* (1991) yields temperatures of between 1026 and 1130°C for these basalts (Heath *et al.* 1998). The higher end of this range is in agreement with older temperature estimates on the same rocks and probably corresponds to crystallization temperatures (Heath *et al.* 1998). The St Vincent basalts record fairly oxidizing redox conditions (FMQ+1.5 < fO_2 < FMQ+1.8; Heath *et al.* 1998). (FMQ = the feyalite-magmetite-quartz oxygen buffer; fO_2 = fugacity of oxygen).

The most magnesian basaltic lava (STV301, 12.5 wt% MgO, Table 1; see also Marcelot *et al.* 1981) from Black Point is slightly nepheline-normative, a feature shared with some Grenada picrites (Thirlwall *et al.* 1996). The other St Vincent basalts are silica-oversaturated (Heath *et al.* 1998). Calculation of the olivine/whole-rock Fe–Mg partition coefficient yields a value of 0.33 (Heath *et al.* 1998), indicating no significant olivine accumulation. The chondrite-normalized rare earth element (REE) patterns for the magnesian basalts (Fig. 4) are flat to slightly

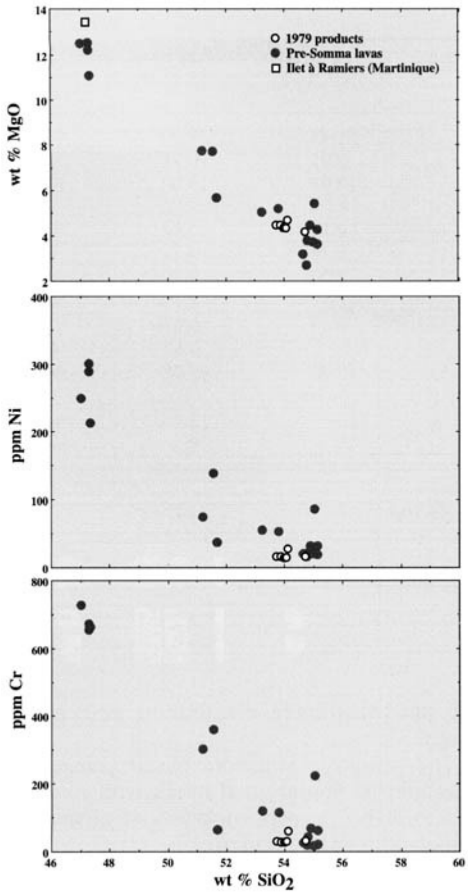

Fig. 3. Variation diagrams for selected rocks from Soufriere Volcano, St Vincent. Data from Graham & Thirlwall (1981) for the 1979 eruption products and from Heath *et al.* (1998) for the Pre-Somma lavas. The composition of the Ilet à Ramiers primitive basalt from Martinique (Westercamp & Mervoyer 1976) is plotted for comparison on the MgO variation diagram.

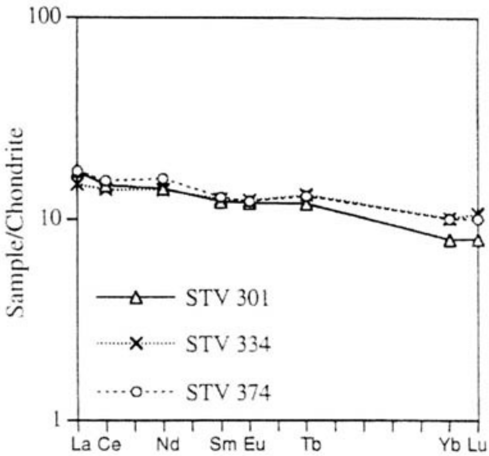

Fig. 4. Chondrite-normalized REE abundances in selected basalts from Soufriere, St Vincent. After Heath *et al.* (1998).

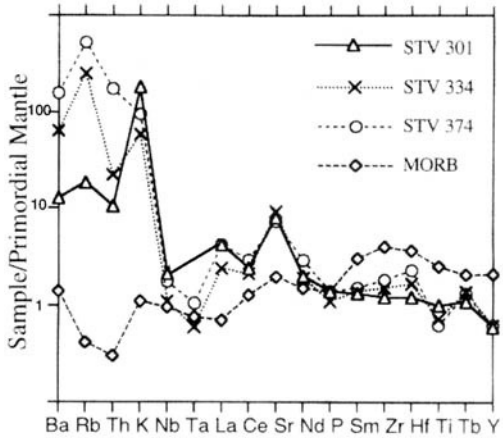

Fig. 5. Primitive mantle-normalized trace element plots for selected basalts, Soufriere, St Vincent, and MORB. Modified from Heath *et al.* (1998).

light REE (LREE)-enriched. Mantle-normalized element abundances (Fig. 5) show patterns characteristic of arc basalts, namely high concentrations of large ion lithophile elements (LILE), low concentrations of high-field-strength elements (HFSE), hence high LILE/HFSE, high LREE/HFSE, negative Nb anomalies and relatively high Ba/La. Relative to mid-ocean ridge basalts (MORB), the Soufriere basalts show LILE and LREE enrichment and heavy REE (HREE) depletion (Fig. 5). The geochemical characteristics of the Soufriere basalts are consistent with generation from a mantle wedge similar to the MORB source, and metasomatized by addition of a fluid phase from the subducting slab (e.g. Heath *et al.* 1998).

Mantle genesis of the Soufriere basalts

Experimental

High-pressure piston-cylinder experiments have recently been carried out to test the possible

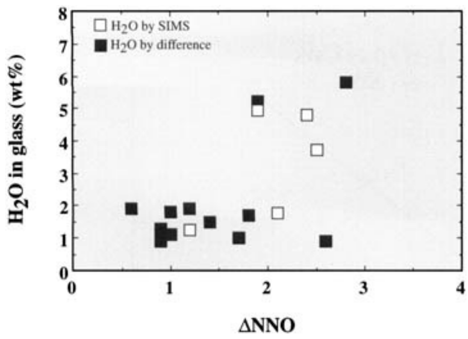

Fig. 6. H_2O content of glasses from high-pressure experiments on STV301 plotted as a function of the experimental fO_2, expressed as deviation from the log fO_2 of the NNO buffer (ΔNNO). (■), H_2O in glass analysed with the by-difference technique; (□), H_2O in glass analysed with ion microprobe. Note the oxidizing conditions of the experiments, comparable to fO_2 in arc settings. See Pichavant *et al.* (2002*b*) for more details.

origin of the St Vincent basalt STV301 by partial melting of the mantle (Pichavant *et al.* 2002*b*). To do so, the inverse approach was used (e.g. Myers & Johnston 1996; Falloon *et al.* 1999). Phase relations were studied near the liquidus of STV301. If the studied rock type is multiply saturated with olivine + orthopyroxene + clinopyroxene on its liquidus, then it is considered to be in equilibrium with a lherzolite and thus primary (e.g. Thompson 1974; Tatsumi *et al.* 1983, 1994; Kushiro 1987; Draper & Johnston 1992; Myers & Johnston 1996; Falloon *et al.* 1999). In such a case, the pressure–temperature (*P–T*) conditions of multiple saturation provide an estimate of the conditions of magma segregation from (or of last equilibration with) its mantle source (e.g. Tatsumi *et al.* 1983, 1994; Falloon *et al.* 1999). The *P–T* conditions of multiple saturation also define one point on the mantle geotherm.

Full information on the experimental starting materials and techniques have been reported elsewhere (Pichavant *et al.* 2002*b*). For the purpose of this paper, it is sufficient to stress that, in comparison with previous inverse experiments on primitive high-MgO arc basalts (Tatsumi 1982; Tatsumi *et al.* 1983, 1994; Gust & Perfit 1987; Kushiro 1987; Bartels *et al.* 1991; Draper & Johnston 1992), the new experiments on STV301 were performed under: (1) hydrous conditions; and (2) oxidizing fO_2. Two series of melt H_2O concentrations were investigated (1.5 and 4.5 wt% H_2O on average) and the experimental glasses were analysed for H_2O either using an ion microprobe or the by-difference technique or both (Pichavant *et al.* 2002*b*). Redox conditions, computed from either olivine–spinel or spinel–melt equilibria, range from NNO + 0.5 to NNO + 3 (Fig. 6). Therefore, experimental conditions realistic for arc settings were successfully imposed.

Fe-loss was minimized, although not totally suppressed, by using $Au_{70}Pd_{30}$ capsules as containers. For example, below 1200°C, Fe-losses of a few per cent (relative to the total Fe present) were found in all but a few charges. Quench crystallization was commonly observed in the 4.5 wt% H_2O series of experiments but was never important enough to affect the glass compositions, as demonstrated by mass-balance calculations (Pichavant *et al.* 2002*b*).

A lherzolitic mantle source for the St Vincent basalt

The near-liquidus phase equilibria for the Soufriere basalt STV301 are represented on two *P–T* diagrams (Fig. 7), each for a given H_2O concentration in the melt. Liquidus phase assemblages divide into three groups: (1) ol + sp; (2) ol + sp + cpx; and (3) cpx + opx ± sp. Spinel is present at the lowest pressures investigated (7.5 kbar) but there is no sp + liquid field. Spinel is absent in a number of charges, especially at pressures > 15 kbar.

In both phase diagrams (Fig. 7), the ol + sp assemblage is located at low pressures and the cpx + opx ± sp assemblage at high pressures. The ol + cpx + sp field was found in an intermediate pressure domain and only in the 1.5 wt% H_2O experiments. At low pressures, olivine and spinel crystallize simultaneously below the liquidus. At higher pressures, both cpx and opx (± sp) appear together on the liquidus. Neither a cpx + liquid nor an opx + liquid field has been found. In both diagrams, the intersection of the low- and high-pressure liquidus fields defines multiple saturation points, where the study composition would be simultaneously saturated with an ol + cpx + opx + sp phase assemblage. These points are located at 1235°C, 11.5 kbar and 1185°C, 16 kbar, for 1.5 and 4.5 wt% H_2O in the melt, respectively (Fig. 7). Varying the melt H_2O concentration mainly changes the *P–T* location of the multiple saturation points.

Electron microprobe analysis of the experimental charges yielded olivine compositions between $Fo_{92.4}$ and $Fo_{89.9}$ in the 1.5 wt% H_2O series of experiments, and between $Fo_{92.3}$ and $Fo_{92.1}$ in the 4.5 wt% H_2O series of experiments. Experimental orthopyroxenes

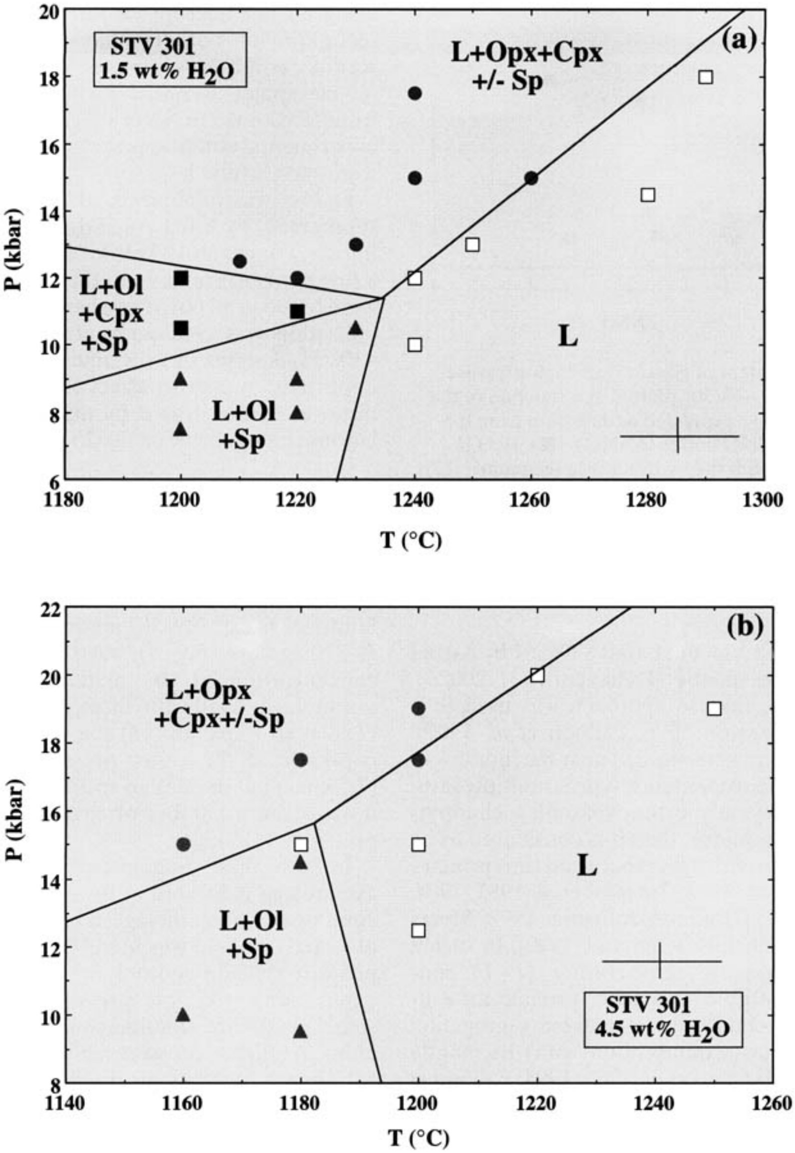

Fig. 7. Near-liquidus phase relations for STV301 with 1.5 wt% H_2O (**a**) and 4.5 wt% H_2O in the melt (**b**). Symbols: (▲), l + ol + sp; (●), l + opx + cpx ± sp; (■), l + ol + cpx + sp; (□), l (above liquidus). Abbreviations: ol, olivine; opx, orthopyroxene; cpx, clinopyroxene; sp, Cr–Al spinel; l, glass. The cross shown in both diagrams represents the experimental uncertainty.

($Wo_{2.7-4.9}En_{81.8-87}Fs_{10.2-13.8}$) have elevated Al_2O_3 (6.8–10.6 wt%), Al^{IV} (0.16–0.23 pfu (per formula unit), 6 O basis) and Al^{VI} (0.12–0.21 pfu). Orthopyroxenes from the 4.5 wt% H_2O series of experiments tend to be slightly richer in En, and poorer in Wo, Al_2O_3 and TiO_2 than those from the 1.5 wt% H_2O series of experiments. Clinopyroxenes ($Wo_{36-42.9}En_{49.7-56.2}Fs_{7.1-12.2}$) are Ca-rich with Wo content increasing from the 1.5 to the 4.5 wt% H_2O experiments (Gaetani *et al.* 1993). They have high Al_2O_3 (8.0–11.0 wt%), Al^{IV} (0.18–0.23 pfu, 6 O basis) and Al^{VI} (0.15–0.25 pfu). The Cr–Al spinels have Cr# (= Cr/(Cr + Al) mostly between 20 and 28. The experimental glasses are all basaltic and characterized by a narrow range of SiO_2 content. The most evolved glasses (i.e. the least MgO-rich) have SiO_2

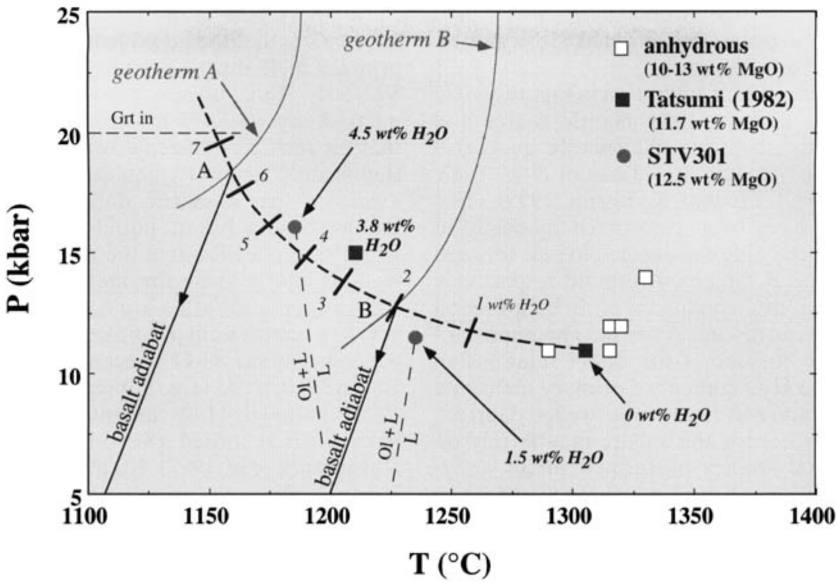

Fig. 8. *P–T* conditions of multiple saturation for high-MgO arc basalts with MgO concentrations between *c.* 10 and 13 wt%. Source of data, anhydrous conditions: Kushiro (1987), Bartels *et al.* (1991), Draper & Johnston (1992), Tatsumi *et al.* (1994); hydrous conditions: Tatsumi (1982), Pichavant *et al.* (2002*b*). The heavy dashed curve yields the *P–T–*H_2O in melt conditions of equilibrium of a high-MgO basalt, such as STV301, with either a spinel or a garnet lherzolite source, the spinel to garnet transition being located at 20 kbar. Numbers along the curve are H_2O concentrations in the melt. A and B are two different *P–T–*H_2O conditions of extraction of STV301 with its mantle source (see text). Basalt adiabats are calculated with a slope of 1°C km^{-1}. The low-pressure liquidi for STV301 with 1.5 and 4.5 wt% H_2O in the melt (light dashed lines) are from Fig. 7. The two geotherms, drawn schematically through points A and B, illustrate the relationship between the H_2O concentration of primary melts and the thermal regime of the mantle.

content near 50 wt% and Al_2O_3 near 19 wt% at 7.5 wt% MgO. In other words, these glasses approach the composition of certain high-alumina basalts, as discussed by Gust & Perfit (1987) and Draper & Johnston (1992).

In summary, the experimental phase diagrams allow ol + cpx + opx + sp multiple saturation points to be defined for each series of H_2O concentration in the melt. This, combined with the observation that the phases crystallizing on the liquidus have compositions typical of upper mantle minerals (i.e. Mg-rich olivines and pyroxenes, Cr-bearing spinels), demonstrates that STV301 could be a product of partial melting of a spinel lherzolite mantle. This conclusion is robust and does not depend on the melt H_2O concentrations imposed in the experiments (Pichavant *et al.* 2002*b*).

Conditions of melt extraction from the mantle

The *P–T* conditions of multiple saturation for several high-MgO basalts are summarized in Figure 8. The data include results for both dry and hydrous conditions (only two studies available) and are for basalts with MgO concentrations ranging between 10 and 13 wt%. The two multiple saturation points from this study are in good agreement with the data of Tatsumi (1982), also for basalts with similar MgO contents (respectively, 12.5 and 11.7 wt% MgO). Interpolation and extrapolation of the available multiple saturation points defines a *P–T–*H_2O in melt locus along which STV301 would be in equilibrium with a lherzolitic phase assemblage. By increasing the H_2O concentration of the melt, conditions of multiple saturation progressively evolve toward lower temperatures and higher pressures. In other words, the higher the H_2O concentration of a STV301 melt, the deeper the level of extraction from the lherzolitic mantle. Assuming that garnet replaces spinel on the STV301 liquidus above 20 kbar (Nicholls & Ringwood 1973; Falloon *et al.* 1999), extrapolation of the multiple saturation *P–T* locus (Fig. 8) yields a minimum melt H_2O concentration of *c.* 7 wt% for STV301 to be multiply saturated with a garnet lherzolite. This shows that very high H_2O contents are needed for STV301 to be last-equilibrated with a garnet-bearing lherzolite source.

Conditions of melt extraction in Figure 8 yield the *P–T* conditions of the mantle source and consequently constrain the mantle geotherm beneath the volcanic arc (Tatsumi *et al.* 1983; Kushiro 1987; Tatsumi & Eggins 1995). Two geotherms have been drawn schematically in Figure 8, each being constructed to pass through points A and B, which correspond respectively to 'wet' and 'dry' conditions of melt extraction for STV301, as discussed below. The important point to be stressed is the direct relationship between the H_2O content of primary melts and the temperature in the mantle wedge. Current thermal models for the subarc mantle rely on experimental studies performed under anhydrous conditions (Fig. 8), which imply temperatures in excess of 1350°C in the mantle wedge (Tatsumi *et al.* 1983; Kushiro 1987; Tatsumi & Eggins 1995). However, were primary basalts more hydrous, the mantle wedge could be much cooler, as shown in Figure 8.

H_2O content of primitive basalts from St Vincent

From the *P–T–*H_2O locus of Figure 8, it is now possible to discuss the question of the H_2O content of the STV301 melt. Different types of approaches can be followed. Knowledge of the depth of extraction of the STV301 melt from the mantle would allow direct use of the *P–T–*H_2O locus of Figure 8. However, this type of information is usually unavailable. The observation that calc-alkaline magmas from the central islands of the Lesser Antilles arc do not have a signature indicative of their derivation from a garnet-bearing source (Macdonald *et al.* 2000) implies melt extraction in the spinel stability field. From the previous section, this implies H_2O concentrations less than *c.* 7 wt% for the STV301 primary melt. Another method would be to use the dependence on temperature of the multiple saturation *P–T–*H_2O locus. Thermometric estimates for the most primitive St Vincent basalts have yielded values between 1026 and 1130°C (see above and Heath *et al.* 1998). A basalt adiabat consistent with the upper end of this temperature range would meet the STV301 *P–T–*H_2O multiple saturation locus at about 1160°C, 18.5 kbar, corresponding to a melt H_2O content of *c.* 6.5 wt% (point A, Fig. 8). As discussed below, this is a very elevated H_2O concentration, which is inconsistent with constraints from glass inclusions and phase-equilibria analysis. The main difficulty with such an approach is that the liquidus temperature of the primary melt must be known. In the case of STV301, the presence of clinopyroxene microphenocrysts (Heath *et al.* 1998) indicates that the melt crystallized down to temperatures significantly below its liquidus. Therefore, the available thermometric data most probably underestimate basalt liquidus temperatures, with the implication that the melt H_2O concentrations inferred with this method are too high. Thus, other approaches are needed.

Glass inclusions in primitive arc magmas have yielded average H_2O concentrations between 1.5 and 2.0 wt% (e.g. Sobolev & Chaussidon 1996), although H_2O contents up to 6–7 wt% have been recorded (Sisson & Layne 1993; Roggensack *et al.* 1997). No glass inclusion data are available for the primitive St Vincent basalts. There is, however, a large body of data available for products of the 1979 eruption of Soufriere (Devine & Sigurdsson 1983; Bardintzeff 1992; Toothill 1999). Basaltic inclusions trapped in olivine have average H_2O concentrations of about 3 wt% (Macdonald *et al.* 2000). These glass inclusions do not represent primitive liquids but rather correspond to derivative compositions (i.e. MgO $\leq$ 3–4 wt%). By taking 3 wt% as the H_2O content of the derivative liquids and assuming that they represent products of 40% closed-system fractionation from parents such as STV301 (Sisson & Grove 1993*a*, *b*), a value of 1.8 wt% H_2O is obtained for the primitive liquids. For comparison, Devine (1995) and Devine & Sigurdsson (1995) have suggested that the H_2O contents of relatively magnesian (close to primary) basalts of Grenada were 1–2 wt% and that the melts parental to the Kick'em Jenny basalts initially contained *c.* 2 wt% H_2O. If 2 wt% is accepted as the H_2O concentration of the STV301 melt, the *P–T–*H_2O locus suggests *c.* 1230°C and *c.* 13 kbar as the conditions of melt extraction from the mantle, corresponding to point B (Fig. 8).

This range of H_2O concentrations is consistent with constraints from the phase equilibria. For a basalt such as STV301 to preserve its status as a primary magma, it is necessary that olivine crystallization is limited during magma ascent. Basaltic magma ascent in the subarc mantle is commonly viewed to occur via dykes. Consequently, little or no chemical reaction with wallrocks is expected during ascent, and the process can be considered as adiabatic (e.g. Tatsumi & Eggins 1995). The basalt adiabats shown in Figure 8 are calculated with a constant slope of $dT/dP = 1°C\ km^{-1}$ (McKenzie & Bickle 1988). Melt crystallization during ascent will be controlled by the relative *P–T* slopes of the adiabat and of the low-pressure liquidus (ol + liquid = liquid). If the slope of the low-pressure liquidus is flatter than the adiabat, the melt may ascend unmodified. Alternatively, if the low-pressure liquidus has a negative slope, olivine crystallization will occur during ascent. The former situation is the one expected for anhydrous basaltic melts. However, hydrous systems, either H_2O saturated or at equilibrium with a H_2O-rich fluid, have liquidi with negative slopes (e.g. Nicholls & Ringwood 1973; Yoder 1976) so that the latter situation is expected. An STV301 melt, if extracted from the mantle under anhydrous conditions, will have the ability to reach the surface largely unmodified and will thus preserve its primary geochemical characteristics. Conversely, if last-equilibrated with its mantle source under H_2O-rich conditions, an STV301 melt will crystallize a significant amount of ol during ascent and thus will not reach the surface unmodified. Therefore, phase-equilibria considerations dictate that STV301 was extracted from the mantle relatively dry.

Inversion of the incompatible trace element concentrations in STV301 represents another possible approach to estimating the water content of the basaltic products (Stolper & Newman 1994). Recent studies have shown that there are four components reflected in the trace element and isotopic compositions of primitive basalts of the Lesser Antilles. These are the mantle wedge, an aqueous fluid, a component derived from subducted sediment and a shallow crustal sediment (Smith *et al.* 1996; Thirlwall *et al.* 1996; Turner *et al.* 1996; Macdonald *et al.* 2000). Unfortunately, the proportions of the different components are not precisely constrained. In particular, the water content of the fluid component is unknown. It must be concluded, therefore, that the water content of the source mantle of STV301 cannot be sensibly determined by this method.

To summarize, several approaches have been used to constrain the H_2O content of primary, mantle-derived, melts from St Vincent. Phase-equilibria constraints, and in particular the necessity of preserving the mantle signature seen in the high-MgO basalt STV301, indicate its extraction from a spinel lherzolite mantle source under relatively dry conditions. This conclusion is corroborated by the available glass inclusion data. It is worth emphasizing that this range of H_2O concentrations applies to primitive basalts that erupt virtually unmodified at the surface. Because originally more hydrous melts will crystallize during ascent and will not be present unmodified at the surface, it should not be concluded that all primary basalts in the Lesser Antilles arc are extracted from their mantle source under similarly dry conditions. Evidence for more hydrous melts may come from the petrology of plutonic blocks that are common on all the islands (Arculus & Wills 1980). While amphibole phenocrysts are largely restricted, in the eruptive rocks, to silicic andesites and dacites, amphibole is an abundant phase (up to 78% modally) in the more mafic plutonic assemblages. Mg# are as high as 86, consistent with crystallization from high-magnesia, hydrous, basalts.

Using the available constraints on the H_2O content of the mantle source

One complementary approach is to constrain the H_2O content of primary arc melts by using information available on the H_2O content of the subarc mantle source. Melting models for the mantle wedge commonly assumes a H_2O content of 0.2 wt% (e.g. Kushiro 1987), which would yield a basalt melt with 2 wt% H_2O for 10% melting if it is assumed that H_2O is perfectly incompatible. However, more precise estimates of the H_2O content of the subarc mantle are now becoming available through the use of oxygen isotopes (Eiler *et al.* 2000). From the $\delta^{18}O$ values of primitive arc lavas mostly from Vanuatu–Fiji–New Caledonia, Eiler *et al.* (2000) concluded that their mantle sources were fluxed with about 0.5–1.0 wt% (2.5 wt% was suggested in some cases) of slab-derived hydrous component. By using the composition of the slab-derived component given by Eiler *et al.* (2000), this corresponds to a mantle H_2O content of about 0.45–0.9 wt%. These H_2O estimates are model-dependent and may not be directly applicable to the Lesser Antilles arc, but they constitute a useful basis for further discussion.

We have used the peridotite melting experiments of Hirose & Kushiro (1993) and Hirose & Kawamoto (1995), both performed on the KLB-1 starting peridotite material, to estimate degrees of melting for STV301. Degrees of melting and MgO concentrations of the partial melts (recalculated on an anhydrous basis), respectively, have been regressed as a function of pressure, temperature and melt H_2O content. The empirical regressions reproduce the experimental data (Hirose & Kushiro 1993; Hirose & Kawamoto 1995) within 15% (degrees of melting) and 6% (MgO concentrations of partial melts), respectively. These regressions enable the degree of melting and the MgO content of the partial melt generated from a KLB-1

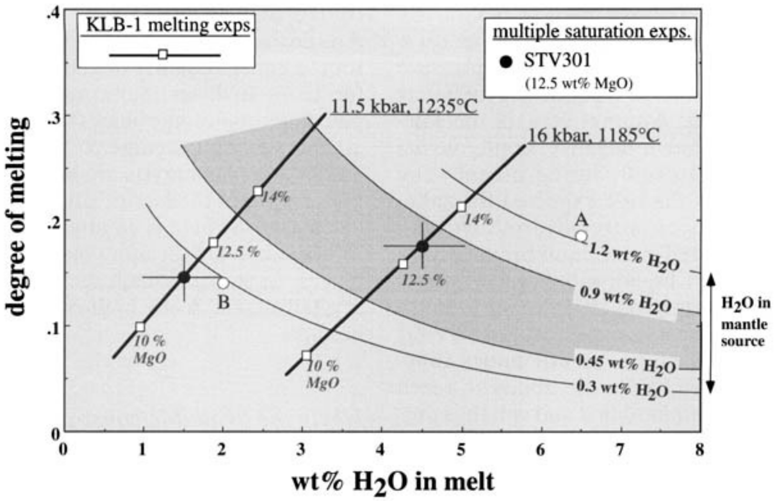

Fig. 9. Degrees of melting for KLB-1 lherzolite expressed as a function of H_2O and MgO concentrations of partial melts (bold lines). They are obtained from the experimental data of Hirose & Kushiro (1993) and Hirose & Kawamoto (1995), and are calculated for the *P–T* conditions of multiple saturation experimentally determined for STV301 with 1.5 and 4.5 wt% H_2O in the melt (11.5 kbar, 1235°C and 16 kbar, 1185°C, Fig. 7). Under these conditions, STV301 is in equilibrium with a lherzolite assemblage similar to KLB-1 and degrees of melting can be determined for each melt H_2O concentration (1.5, 4.5 wt%). Experimental (STV301) and calculated points for 12.5 wt% MgO in the melt are in good agreement. Note the weak dependence of the degree of melting on the melt H_2O content for a given MgO (10, 12.5 and 14 wt% in the melt). Degrees of melting for the two *P–T–*H_2O conditions of multiple saturation detailed in Figure 8 are shown as points A and B. The light curves are partial melting curves for four initial H_2O concentrations in the mantle source (0.3, 0.45, 0.9 and 1.2 wt%), calculated by assuming that H_2O is perfectly incompatible during melting.

peridotite source to be calculated if *P*, *T* and H_2O in melt are given.

A STV301 melt with 1.5 and 4.5 wt% H_2O is in equilibrium with a spinel lherzolite at 11.5 kbar, 1235°C and 16 kbar, 1185°C, respectively (Fig. 7). Under these conditions, degrees of partial melting calculated with the KLB-1 regression are 14.6 and 17.7%, and MgO concentrations of partial melts calculated with the KLB-1 regression are 11.47 and 12.98 wt%, respectively (Fig. 9). The fact that the MgO concentrations calculated from the KLB-1 regression agrees within 8% or better with that of STV301 (12.50 wt%, Table 1) indicates that KLB-1 can, at a first approximation and with respect to MgO, be taken as a model peridotite source for STV301. One aspect of general significance is that degrees of melting vary relatively little for the two *P–T–*H_2O conditions (Fig. 9), i.e. along the multiple saturation locus (Fig. 8). Therefore, the melt MgO concentration is a very robust indicator of the degree of melting, even in the presence of water. Degrees of melting estimated for STV301 (14–18% for melt H_2O concentrations from 1.5 to 4.5 wt%) are consistent with previous estimates based on trace elements (Heath *et al.* 1998).

Different contours of the H_2O concentration of the mantle source are also shown in Figure 9. The calculations assume perfectly incompatible behaviour for H_2O during melting. Two of the H_2O concentrations (0.3 and 1.2 wt% H_2O) generate contours that pass very close to the points A and B (Fig. 8). For a STV301 melt to be extracted under conditions of point B, the mantle source would have to contain less than about 0.3 wt% H_2O (Fig. 9), which seems perfectly feasible if 0.2 wt% is taken as the H_2O content of 'normal' subarc mantle (Kushiro 1987). If extracted under conditions represented by A, a mantle source distinctly more hydrous (1.2 wt% H_2O) would be required. It remains to be established whether such amounts of H_2O are realistic for the Lesser Antilles subarc mantle, especially considering that the low rate of subduction in the arc (Macdonald *et al.* 2000) would limit the amount of subducted hydrous component added to the source region. For a mantle source with H_2O contents between 0.45 and 0.9 wt% (see above and Eiler *et al.* 2000), H_2O

concentrations between *c.* 2 and *c.* 3 wt% for MgO concentrations between *c.* 13 and *c.* 15 wt% would be expected if melts are extracted at 11.5 kbar, 1235°C, and between *c.* 4 and *c.* 5 wt% H_2O for *c.* 12–*c.* 13 wt% MgO at 16 kbar, 1185°C (Fig. 9). Therefore, depending on the water content of the mantle source, the possibility exists that some high-MgO primary melts have H_2O concentrations as high as 5 wt%, i.e. well exceeding that inferred previously for STV301 (*c.* 2 wt% H_2O).

Evolution of primitive magmas in the arc crust

Experimental methods and results

In order to model the first stages of differentiation of primary melts in the arc crust, STV301 melts were crystallized in gas vessels at 4 and 10 kbar between 1200 and 1050°C. Arculus & Wills (1980) have shown from the study of gabbroic cumulates that crystallization of basaltic magmas takes place over a substantial pressure range (4–10 kbar) in the Lesser Antilles crust. The crystallization experiments were performed in the presence of variable H_2O contents, with H_2O being analysed in the glass run products either by ion microprobe or with the by-difference technique. Redox conditions were kept between NNO and NNO+1. Crystallization of the STV301 melt was obtained either by lowering the melt H_2O content under isothermal conditions or by varying the temperature at constant melt H_2O contents (e.g. Pichavant *et al.* 2002*a*). Previous studies of this type on Lesser Antilles mafic lavas include those of Cawthorn *et al.* (1973) and Graham (1981). The main difference between the new experiments and these previous studies resides in the systematic use of a rapid-quench device that allowed the capsules (either made of Au, AgPd or AuPd alloys) to be quenched at rates of about 100°C s^{-1}. This effectively limited the proportion of quench crystals in the charges and allowed the compositions of derivative liquids to be determined. Therefore, the evolution of the liquid composition during equilibrium crystallization and fractionation of the STV301 primary melt could be directly determined.

The detailed presentation of these experimental results is now in preparation. In this paper we focus on the experimental results at 4 kbar, where most of the data have been obtained. Temperatures of appearance of mineral phases were found to depend strongly on the melt H_2O content. Olivine and spinel are the liquidus phases. They are followed on decreasing temperature either by clinopyroxene for $H_2O > 3$ wt% in the melt or by plagioclase for $H_2O < 3$ wt%. At 1050°C for 6–8 wt% H_2O in the melt, the phase assemblage is ol + cpx + plag + sp. Note that amphibole is not present under these conditions. For comparison, temperatures ≤ 1000°C are necessary for amphibole to crystallize at 4 kbar in a basaltic andesite from Mt Pelée (Pichavant *et al.* 2002*a*). In contrast, at 10 kbar, amphibole was successfully crystallized from STV301 at 1100°C, which stresses the strong positive dependence of the amphibole stability curve on pressure (Holloway & Burnham 1972).

Generation of evolved basaltic liquids

The compositions of residual liquids are shown in Figures 10 and 11. The presence of several groups of data points for a given temperature reflects differences in melt H_2O contents (and consequently differences in phase assemblages, compositions and melt fractions) between experimental charges. The experimental data points are compared in Figures 10 and 11 with representative compositions of mafic volcanic rocks from Soufriere, St Vincent and Mt Pelée, Martinique (Table 1). In Figure 10, the main trend of increasing Al_2O_3 at decreasing MgO contents in the melt corresponds to the fractionation of ol ± cpx ± sp. This trend generates high-Al_2O_3 melt compositions with 18 wt% Al_2O_3 for 7–8 wt% MgO (1150°C) and 22 wt% Al_2O_3 for 4–6 wt% MgO (1100 and 1050°C). When plagioclase appears in the fractionating assemblage, melt Al_2O_3 contents start to drop (Fig. 10). Overall, the ol ± cpx ± sp fractionation trend neatly reproduces the evolution of the natural compositions, from the high-MgO basalt (STV301), medium-MgO basalts (STV315 and STV303) to basaltic andesites (BA, the latter from Mt Pelée, Table 1). In particular, the experimental glasses at 1100 and 1050°C have Al_2O_3 concentrations higher than, but still close to, the evolved basaltic rocks (low-MgO high-alumina basalts, and basaltic andesites 303 and BA). These glasses have CaO contents of 10–11 wt% at 4–5 wt% MgO (Fig. 11) and are nearly identical to the reference evolved basaltic rocks plotted (see also Fig. 2 for comparison). It is concluded that crystallization of primary magmas such as STV301 can generate residual liquids similar to the evolved basaltic compositions that contribute the present-day volcanic activity along the arc.

Experimental glasses produced by crystallizing a high-MgO basalt, compositionally very

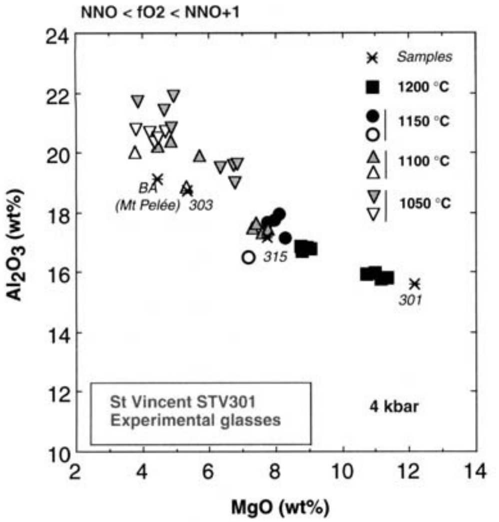

Fig. 10. MgO–Al_2O_3 plot showing the composition of experimental glasses produced from STV301 at 4 kbar, 1200–1050°C under variable water contents. Selected compositions of mafic lavas from Soufriere, St Vincent and Mt Pelée are shown for reference: samples 301 (STV301, Table 1) and 315 (STV315, Heath *et al.* 1998), 303 (STV303, Table 1) and BA (031-22b, Table 1). At 1150, 1100 and 1050°C, plagioclase-bearing charges are labelled with open symbols, and plagioclase-free charges with solid symbols. Note the trend of progressively increasing glass Al_2O_3 concentrations on decreasing MgO and temperature, and the drop of glass Al_2O_3 contents in plagioclase-bearing charges compared to plagioclase-free charges at the same temperature. Glasses at 1100 and 1050°C approach the composition of evolved, low-magnesia, basaltic rocks (303, BA).

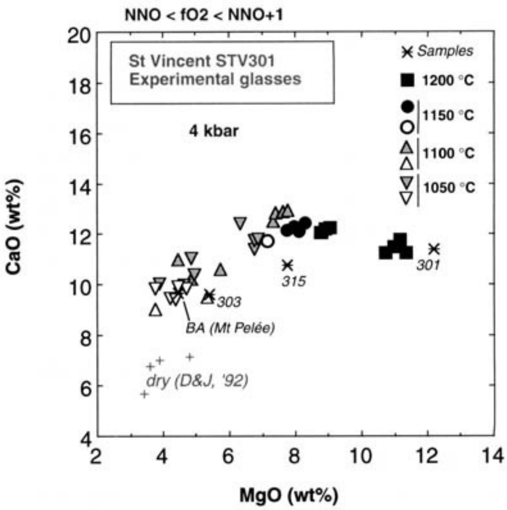

Fig. 11. MgO–CaO plot showing the composition of experimental glasses produced from STV301 at 4 kbar, 1200–1050°C under variable water contents. Selected compositions of mafic lavas from Soufriere, St Vincent and Mt Pelée are shown for reference: 301 (STV301, Table 1), 315 (STV315, Heath *et al.* 1998), 303 (STV303, Table 1) and BA (031-22b, Table 1). At 1150, 1100 and 1050°C, plagioclase-bearing charges are labelled with open symbols, and plagioclase-free charges with solid symbols. Glasses at 1050 and 1100°C approach the composition of evolved, low-magnesia, basaltic rocks (303, BA). See also Fig. 2. Crosses are experimental glasses produced by crystallizing a high-MgO basalt (Table 1) under anhydrous conditions at high pressures (Draper & Johnston 1992). Note their lower CaO content at equivalent MgO (4–5 wt%) in comparison with glasses produced from STV301 in presence of water.

close to STV301 (ID16, Table 1), under anhydrous conditions at high pressures (Draper & Johnston 1992) are also plotted in Figure 11. Note their lower CaO content at equivalent MgO (4–5 wt%) in comparison with glasses produced from STV301 in the presence of H_2O. This stresses the need for H_2O to be present for trends such as those shown in Figures 10 and 11 to be generated. How much H_2O needs to be present? At 1150°C and for melt H_2O contents ≤ 3 wt%, plagioclase crystallizes relatively early and glass Al_2O_3 contents are limited to a maximum of about 18 wt% (Fig. 10). In contrast, at 1100 and 1050°C (about 6–8.5 wt% H_2O dissolved in melt), plagioclase crystallization is delayed and glass Al_2O_3 contents reach values >19 wt% and as high as 22 wt% (Fig. 10). In other words, a melt H_2O concentration of ≤ 3 wt% would prevent formation of Al_2O_3-rich melt compositions typical of evolved island arc basaltic rocks. In contrast, generation of Al_2O_3-rich compositions would be promoted with melt H_2O concentrations, as in the 1100 and 1050°C glasses (about 6–8.5 wt%). Both experimental (Sisson & Grove 1993*b*; Pichavant *et al.* 2002*a*) and glass inclusion (Sisson & Layne 1993; Roggensack *et al.* 1997) studies have shown that H_2O concentrations > 6 wt% are attained in some compositionally evolved subduction zone mafic melts. Therefore, experimental melt H_2O concentrations, as in the 1050 and 1100°C glasses (6–8.5 wt%), are realistic.

Approximately 40% crystallization is needed to generate low-MgO high-alumina basalts and basaltic andesites at 1050°C starting from a high-MgO basalt parent such as STV301 (see also Sisson & Grove 1993b). If fractionation occurs under a closed system and assuming a perfectly incompatible behaviour for H_2O, 6–8.5 wt%

H_2O in the derivative liquids corresponds to 3.6–5.1 wt% H_2O in the parental liquids. This H_2O concentration range is higher than inferred above for the STV301 melt (*c.* 2 wt% H_2O), but is comparable to the maximum H_2O concentrations estimated possible for primary melts extracted from a mantle source fluxed with a slab-derived hydrous component (5 wt% H_2O). Therefore, the experimental constraints on the H_2O concentration of derivative melts strengthens the possibility of H_2O concentrations as high as 5 wt% in some primary arc melts.

Fractionation of evolved basaltic liquids and the origin of andesites in the Lesser Antilles arc

The fractionation of evolved basaltic liquids similar to those produced at 1100 and 1050°C in the STV301 crystallization experiments has been recently investigated (Pichavant *et al.* 2002*a*). The aim was to test the origin of the Mt Pelée andesites by crystallization–differentiation from evolved mafic liquids. The experiments were performed at 4 kbar between 950 and 1025°C, and started from the basaltic andesite composition BA in Figures 10 and 11. Experimental and analytical methods are detailed elsewhere (Pichavant *et al.* 2002*a*); these are, for the most part, identical to those previously mentioned in this paper. The compositions of residual liquids are shown in Figure 12. With progressive crystallization, liquids range continuously from basaltic andesite through andesite to dacite, becoming progressively enriched in SiO_2, K_2O and Na_2O, and depleted in Al_2O_3, FeO_t, MgO and CaO. The redox conditions control the proportion of magnetite present, the TiO_2, FeO_t concentrations and FeO_t/MgO ratios. Melts with compositions identical to the andesites erupted during the recent stage of activity of Mt Pelée are generated by about 30–50% crystallization of the basaltic andesite (Fig. 12). Therefore, the main petrogenetic mechanism responsible for the genesis of andesites at Mt Pelée is fractionation of evolved basaltic magmas.

Conclusions

- Experiments at upper mantle pressures on a natural lava representative of rare primitive calc-alkaline compositions in the Lesser Antilles arc demonstrate derivation by partial melting of a lherzolitic mantle source. These primitive rocks may serve as probes of processes and conditions in the mantle wedge. There is a strong interdependence between the *P–T* conditions of melt extraction (hence, the local mantle geotherm) and the H_2O content of the melt.
- For primary basaltic magmas to be erupted at the surface, little or no crystallization during ascent is required. This is most easily obtained if the melt is extracted relatively dry (e.g. 1–2 wt% H_2O) from its mantle source. Glass inclusion data available for Lesser Antilles primitive basalts support this conclusion. Melts extracted under wet conditions will crystallize on ascent and their primary characteristics will be lost. Therefore, the primitive basalts erupted at the surface in the Lesser Antilles may give an incomplete, biased, view of the H_2O content of primary mantle melts. Melt H_2O contents up to 5 wt% are expected for mantle sources fluxed with a slab-derived hydrous component. Oxygen isotope systematics on primitive Lesser Antilles rocks would be very helpful to put precise constraints on the H_2O content of the subarc mantle.
- Crystallization of primary mantle melts under crustal conditions progressively produces low-MgO and Al_2O_3-rich derivative liquids. CaO melt concentrations peak at about 13 wt% for 7–8 wt% MgO. Melt H_2O contents $\geq$ 3 wt% delay plagioclase crystallization and promote olivine + clinopyroxene + spinel fractionation. H_2O-rich (6–8.5 wt%) derivative liquids at 1050 and 1100°C are compositionally close to the low-MgO high-alumina basalts and basaltic andesites erupting at active volcanic centres along the arc.
- Crystallization of hydrous evolved basaltic compositions produces residual liquids ranging from basalt to dacite. The main mechanism responsible for the genesis of andesites in the Lesser Antilles arc is fractionation of low-magnesia basaltic magmas. The range of evolved compositions seen in the arc (basalt/basaltic andesite to andesite and more rarely dacite) can be produced by different degrees of crystallization–differentiation from primary mantle melts. The experimental data show that it is not necessary to appeal to large amounts of crustal contamination to generate the evolved compositions. Direct evidence for the crystallization, in the arc crust, of basaltic magmas of variable composition and H_2O content is provided by the gabbroic cumulates that are common along the arc.
- For compositions such as low-magnesia basalts and basaltic andesites to be produced from the crystallization of STV301, between 6 and 8.5 wt% H_2O in the melt is necessary. These H_2O concentrations are in the same

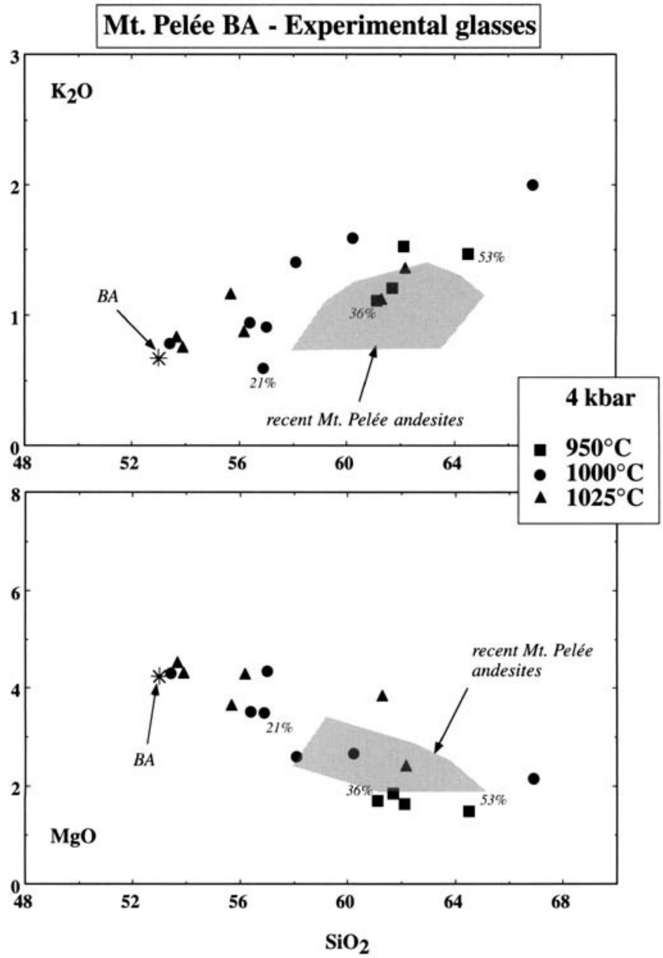

Fig. 12. K_2O and MgO variation diagrams for experimental glasses generated by crystallization of the Mt Pelée basaltic andesite BA (Figs 10 and 11, Table 1). Source of data: Pichavant *et al.* (2002*a*). Proportions (wt%) of crystals are shown for three charges having similar fO_2 (ΔNNO = + 1.2–1.3) and H_2O contents (6–8 wt%), to illustrate the effect of progressive crystallization on melt composition. Glasses generated from the crystallization of the basaltic andesite plot within or very close to the field of recent Mt Pelée eruption products.

range as those inferred for a number of subduction zone mafic melts, including the basaltic magmas feeding the Mt Pelée magmatic system. From mass-balance calculations, such H_2O concentrations in the derivative liquids imply about 3.5–5 wt% H_2O in the primary melts, a range consistent with the maximum H_2O concentrations estimated possible for mantle melts extracted from sources fluxed with a slab-derived hydrous component. Experimental constraints on the H_2O concentrations of primary and derivative arc melts are thus mutually consistent and suggest the possibility of elevated H_2O concentrations in primitive arc magmas.

This paper has benefited from reviews from M. Thirlwall, Ph. Leat and an anonymous reviewer.

References

ARCULUS, R.J. & WILLS, K.J.A. 1980. The petrology of plutonic blocks and inclusions from the Lesser Antilles island arc. *Journal of Petrology*, **21**, 743–799.

BAKER, M.B., GROVE, T.L. & PRICE, R. 1994. Primitive basalts and andesites of the Mt. Shasta region, N.

California: products of varying melt fraction and water content. *Contributions to Mineralogy and Petrology*, **118**, 111–129.

BALLHAUS, C., BERRY, R.F. & GREEN, D.H. 1991. High pressure experimental calibration of the olivine–orthopyroxene–spinel oxygen barometer: implications for the oxidation state of the upper mantle. *Contributions to Mineralogy and Petrology*, **107**, 27–40.

BARDINTZEFF, J.-M. 1992. Magma mixing processes in volcanic contexts, a thermodynamic approach with the examples of St. Vincent Soufrière Volcano, West Indies and Cerro Chiquito, Guatemala. *Terra Nova*, **4**, 553–566.

BARTELS, K.S., KINZLER, R.J. & GROVE, T.L. 1991. High-pressure phase relations of primitive high-alumina basalts from Medecine Lake Volcano, northern California. *Contributions to Mineralogy and Petrology*, **108**, 253–270.

BROWN, G.M., HOLLAND, J.G., SIGURDSSON, H., TOMBLIN, J.F. & ARCULUS, R.J. 1977. Geochemistry of the Lesser Antilles island arc. *Geochimica et Cosmochimica Acta*, **41**, 785–801.

CAWTHORN, R.G., CURRAN, E.B. & ARCULUS, R.J. 1973. A petrogenetic model for the origin of the calc-alkaline suite of Grenada, Lesser Antilles. *Journal of Petrology*, **14**, 327–337.

DAVIDSON, J.P. 1996. Deciphering mantle and crustal signatures in subduction zone magmatism. *In*: BEBOUT, G.E., SCHOTT, D.W., KIRBY, S.H. & PLATT, J.P. (eds) *Subduction: Top to Bottom*. American Geophysical Union Monographs, **96**, 251–262.

DEVINE, J.D. 1995. Petrogenesis of the basalt–andesite–dacite association of Grenada, Lesser Antilles island arc, revisited. *Journal of Volcanology and Geothermal Research*, **69**, 1–33.

DEVINE, J.D. & SIGURDSSON, H. 1983. The liquid composition and crystallization history of the 1979 Soufrière magma, St. Vincent. *Journal of Volcanology and Geothermal Research*, **16**, 1–31.

DEVINE, J.D. & SIGURDSSON, H. 1995. Petrology and eruption styles of Kick'em Jenny submarine volcano, Lesser Antilles island arc. *Journal of Volcanology and Geothermal Research*, **69**, 35–58.

DRAPER, D.S. & JOHNSTON, A.D. 1992. Anhydrous PT phase relations of an Aleutian high-MgO basalt: an investigation of the role of olivine–liquid reaction in the generation of arc high-alumina basalts. *Contributions to Mineralogy and Petrology*, **112**, 501–519.

EGGINS, S. 1993. Origin and differentiation of picritic arc magmas, Ambae (Aoba), Vanuatu. *Contributions to Mineralogy and Petrology*, **114**, 79–100.

EILER, J.M., CRAWFORD, A., ELLIOTT, T., FARLEY, K.A., VALLEY, J.W. & STOLPER, E.M. 2000. Oxygen isotope geochemistry of oceanic-arc lavas. *Journal of Petrology*, **41**, 229–256.

FALLOON, T.J., GREEN, D.H., JACQUES, A.L. & HAWKINS, J.W. 1999. Refractory magmas in back-arc basin settings – experimental constraints on the petrogenesis of a Lau basin example. *Journal of Petrology*, **40**, 255–277.

GAETANI, G.A., GROVE, T.L. & BRYAN, W.B. 1993. The influence of water on the petrogenesis of subduction-related igneous rocks. *Nature*, **365**, 332–334.

GRAHAM, A.M. 1981. Melting relations of island arc lavas from Grenada, Lesser Antilles. *In:* Ford, C.E. (ed.) *Progress in Experimental Petrology*. NERC Publications Series D, **18**, 126–132.

GRAHAM, A.M. & THIRLWALL, M.F. 1981. Petrology of the 1979 eruption of Soufriere volcano, St. Vincent, Lesser Antilles. *Contributions to Mineralogy and Petrology*, **76**, 336–342.

GUST, D.A. & PERFIT, M.R. 1987. Phase relations of a high-Mg basalt from the Aleutian island arc: implications for primary island arc basalts and high-Al basalts. *Contributions to Mineralogy and Petrology*, **97**, 7–18.

HEATH, E., MACDONALD, R., BELKIN, H.E. & HAWKESWORTH, C.J. 1998. Magmagenesis at the Soufriere St. Vincent Volcano, Lesser Antilles arc. *Journal of Petrology*, **39**, 1721–1764.

HIROSE, K. & KAWAMOTO, T. 1995. Hydrous partial melting of lherzolite at 1 GPa – the effect of H_2O on the genesis of basaltic magmas. *Earth and Planetary Science Letters*, **133**, 463–473.

HIROSE, K. & KUSHIRO, I. 1993. Partial melting of dry peridotites at high pressures: determination of compositions of melts segregated from peridotites using aggregates of diamond. *Earth and Planetary Science Letters*, **114**, 477–489.

HOLLOWAY, J.R. & BURNHAM, C.W. 1972. Melting relations of basalt with equilibrium water pressure less than total pressure. *Journal of Petrology*, **13**, 1–29.

KUSHIRO, I. 1987. A petrological model for the mantle wedge and lower crust in the Japanese island arcs. *In*: MYSEN, B.O. (ed.) *Magmatic Processes: Physicochemical Principles*. Special Publications, Geochemical Society, University Park, PA, **1**, 165–181.

MACDONALD, R., HAWKESWORTH, C.J. & HEATH, E. 2000. The Lesser Antilles volcanic chain: a study in arc magmatism. *Earth Science Reviews*, **49**, 1–76.

MARCELOT, G., LE GUEN DE KERNEIZON, M. & BOHN, M. 1981. Zonation du nickel et du chrome dans les minéraux ferromagnésiens d'un basalte de Saint-Vincent (Petites Antilles); conséquences pétrogénétiques. *Comptes Rendus de l'Académie des Sciences, Paris*, **293**, 1079–1082.

MCKENZIE, D. & BICKLE, M.J. 1988. The volume and composition of melt generated by extension of the lithosphere. *Journal of Petrology*, **29**, 625–679.

MURPHY, M.D., SPARKS, R.S.J., BARCLAY, J., CARROLL, M.R. & BREWER, T.S. 2000. Remobilization of andesite magma by intrusion of mafic magma at the Soufriere Hills volcano, Montserrat, West Indies. *Journal of Petrology*, **41**, 21–42.

MYERS, J.D. & JOHNSTON, A.D. 1996. Phase equilibria constraints on models of subduction zone magmatism. *In*: BEBOUT, G.E., SCHOTT, D.W., KIRBY, S.H. & PLATT, J.P. (eds) *Subduction: Top to Bottom*. American Geophysical Union Monographs, **96**, 229–249.

NICHOLLS, I.A. & RINGWOOD, A.E. 1973. Effect of water on olivine stability in tholeiites and production of silica-saturated magmas in the island arc environment. *Journal of Geology*, **81**, 285–300.

NYE, C.J. & REID, M.R. 1986. Geochemistry of primary and least fractionated lavas from Okmok volcano, Central Aleutians: implications for arc magma genesis. *Journal of Geophysical Research*, **91**, 10 271–10 287.

PICHAVANT, M., MARTEL, C., BOURDIER, J.-L. & SCAILLET, B. 2002*a*. Physical conditions, structure and dynamics of a zoned magma chamber: Mt. Pelée (Martinique, Lesser Antilles arc). *Journal of Geophysical Research*, **107**, ECV 2-1–2-3, 10.1029/2001JB000315.

PICHAVANT, M., MYSEN, B.O. & MACDONALD, R. 2002*b*. Source and H_2O content of high-MgO magmas in island arc settings: an experimental study of a primitive calc-alkaline basalt from St. Vincent, Lesser Antilles arc. *Geochimica et Cosmochimica Acta*, **66**, 2193–2209.

ROGGENSACK, K., HERVIG, R.L., MCKNIGHT, S.B. & WILLIAMS, S.N. 1997. Explosive basaltic volcanism from Cerro Negro volcano: influence of volatiles on eruptive style. *Science*, **277**, 1639–1642.

SISSON, T.W. & GROVE, T.L. 1993*a*. Experimental investigations of the role of H_2O in calc-alkaline differentiation and subduction zone magmatism. *Contributions to Mineralogy and Petrology*, **113**, 143–166.

SISSON, T.W. & GROVE, T.L. 1993*b*. Temperatures and H_2O contents of low-MgO high-alumina basalts. *Contributions to Mineralogy and Petrology*, **113**, 167–184.

SISSON, T.W. & LAYNE, G.D. 1993. H_2O in basalt and basaltic andesite glass inclusions from four subduction-related volcanoes. *Earth and Planetary Science Letters*, **117**, 619–635.

SMITH, T.E., THIRWALL, M.F. & MACPHERSON, C. 1996. Trace-element and isotope geochemistry of the volcanic rocks of Bequia, Grenadine Islands, Lesser Antilles arc: a study of subduction enrichment processes. *Journal of Petrology*, **37**, 117–143.

SOBOLEV, A.V. & CHAUSSIDON, M. 1996. H_2O concentrations in primary melts from supra-subduction zones and mid-ocean ridges. *Earth and Planetary Science Letters*, **137**, 45–55.

STOLPER, E.M. & NEWMAN, S. 1994. The role of water in the petrogenesis of Mariana trough magmas. *Earth and Planetary Science Letters*, **121**, 293–325.

TATSUMI, Y. 1982. Origin of high-magnesian andesites in the Setouchi volcanic belt, southwest Japan II. Melting phase relations at high pressures. *Earth and Planetary Science Letters*, **60**, 305–317.

TATSUMI, Y. & EGGINS, S.M. 1995. *Subduction Zone Magmatism*. Blackwell, Cambridge, MA.

TATSUMI, Y., FURUKAWA, Y. & YAMASHITA, S. 1994. Thermal and geochemical evolution of the mantle wedge in the northeast Japan arc 1. Contribution from experimental petrology. *Journal of Geophysical Research*, **99**, 22 275–22 283.

TATSUMI, Y., SAKUYAMA, M., FUKUYAMA, H. & KUSHIRO, I. 1983. Generation of arc basalt magmas and thermal structure of the mantle wedge in subduction zones. *Journal of Geophysical Research*, **88**, 5815–5825.

THOMPSON, R.N. 1974. Primary basalts and magma genesis. *Contributions to Mineralogy and Petrology*, **43**, 317–341.

THIRLWALL, M.F., GRAHAM, A.M., ARCULUS, R.J., HARMON, R.S. & MACPHERSON, C.G. 1996. Resolution of the effects of crustal assimilation, sediment subduction and fluid transport in island arc magmas: Pb–Sr–Nd–O isotope geochemistry of Grenada, Lesser Antilles. *Geochimica et Cosmochimica Acta*, **60**, 4785–4810.

TOOTHILL, J. 1999. *The role of hydrous fluids in the generation of magmas in the Lesser Antilles*. Unpublished PhD thesis, University of Lancaster.

TURNER, S., HAWKESWORTH, C.J., VAN CALSTEREN, P., HEATH, E., MACDONALD, R. & BLACK, S. 1996. U-series isotopes and destructive plate margin magma genesis in the Lesser Antilles. *Earth and Planetary Science Letters*, **142**, 191–207.

WESTERCAMP, D. 1979. Diversité, contrôle structural et origines du volcanisme récent dans l'arc insulaire des Petites Antilles. *Bulletin du Bureau de Recherches Géologiques et Minières, BRGM Section IV*, **3/4**, 211–226.

WESTERCAMP, D. & MERVOYER, B. 1976. Les séries volcaniques de la Martinique et de la Guadeloupe (F.W.I.). *Bulletin du Bureau de Recherches Géologiques et Minières, Section IV*, **4**, 229–242.

YODER, H.S., JR 1976. *Generation of Basaltic Magma*. National Academy of Sciences, Washington, DC.

Structure and tectonic evolution of the South Sandwich arc

ROBERT D. LARTER[1], LIEVE E. VANNESTE[1], PETER MORRIS[1] & DAVID K. SMYTHE[2,3]

[1]*British Antarctic Survey, High Cross, Madingley Road, Cambridge CB3 0ET, UK (e-mail: r.larter@bas.ac.uk)*

[2]*Department of Geology and Applied Geology, University of Glasgow, UK*

[3]*Present address: GeoLogica Ltd, 191 Wilton Street, Glasgow G20 6DF, UK*

Abstract: Detailed analysis of marine magnetic profiles from the western part of the East Scotia Sea confirms continuous, organized back-arc spreading since at least 15 Ma ago. In the eastern part of the East Scotia Sea, the South Sandwich arc lies on crust that formed at the back-arc spreading centre since 10 Ma ago, so older back-arc crust forms the basement of the present inner forearc. Interpretations of two multichannel seismic reflection profiles reveal the main structural components of the arc at shallow depth, including evidence of trench-normal extension in the mid-forearc, and other features consistent with ongoing subduction erosion. The seismic profile interpretations have been used to constrain simple two-dimensional gravity models. The models were designed to provide constraints on the maximum possible thickness of the arc crust, and it is concluded that this is 20 and 19.2 km on the northern and southern lines, respectively. On the northern line the models indicate that the forearc crust cannot be much thicker than normal oceanic crust. Even with such thin crust, however, the magmatic growth rate implied by the cross-section of the arc crust is within the range recently estimated for two other arcs that have been built over a much longer interval.

The South Sandwich island arc is a classic intra-oceanic arc in the southernmost Atlantic Ocean (Fig. 1). The arc is situated on the small Sandwich Plate, which is overriding the southernmost part of the South American Plate at the South Sandwich Trench at a rate of 67–81 mm a^{-1} (Pelayo & Wiens 1989; Thomas *et al.* 2003) (Fig. 1). Further west, the Sandwich Plate is separating from the Scotia Plate at the East Scotia Ridge (ESR) back-arc spreading centre, where the full spreading rate is 60–70 mm a^{-1} (Thomas *et al.* 2003).

Early studies of marine magnetic profiles from the East Scotia Sea showed that E–W back-arc spreading had been active since at least 8 Ma ago (Barker 1970, 1972; Barker & Hill 1981). More recently Barker (1995) identified lineated magnetic anomalies out to at least anomaly 5 (9.7–10.9 Ma) and probably out to anomaly 5B (*c.* 15 Ma) on the western flank of the ESR. On the eastern flank of the ESR, the central part of the South Sandwich island arc lies on crust formed at the ESR during anomaly 5. Therefore, the identification of anomalies older than anomaly 5, if confirmed, has important implications for the tectonic evolution of the arc and can provide a basis for quantitative estimates of rates of processes such as sediment subduction and subduction erosion (Vanneste & Larter 2002).

In this paper we present a detailed analysis of new and archive magnetic profiles across the western margin of the East Scotia Sea, confirming that organized back-arc spreading has been active since at least 15 Ma ago. We speculate that spreading was probably preceded by a phase of arc rifting, as observed in other back-arc basins (e.g. Parson & Hawkins 1994; Martinez *et al.* 1995; Baker *et al.* 1996; Parson & Wright 1996), and that rifting was triggered by a change in South American–Antarctic plate motion about 20 Ma ago. We also present interpretations of two multichannel seismic (MCS) reflection profiles that cross the trench, arc and ESR, and use these to constrain two-dimensional gravity models. Implications of the MCS interpretations and gravity modelling results are discussed in the context of the confirmed history of >15 Ma of continuous, organized back-arc spreading.

Marine magnetic record of back-arc spreading

Marine magnetic profiles were examined to constrain the time of onset and early history of back-arc spreading in the East Scotia Sea. Several long profiles were selected for analysis, including eight that cross the oldest back-arc crust at the western limit of the East Scotia Sea

From: LARTER, R.D. & LEAT, P.T. 2003. *Intra-Oceanic Subduction Systems: Tectonic and Magmatic Processes.* Geological Society, London, Special Publications, **219**, 255–284. 0305-8719/03/$15.00

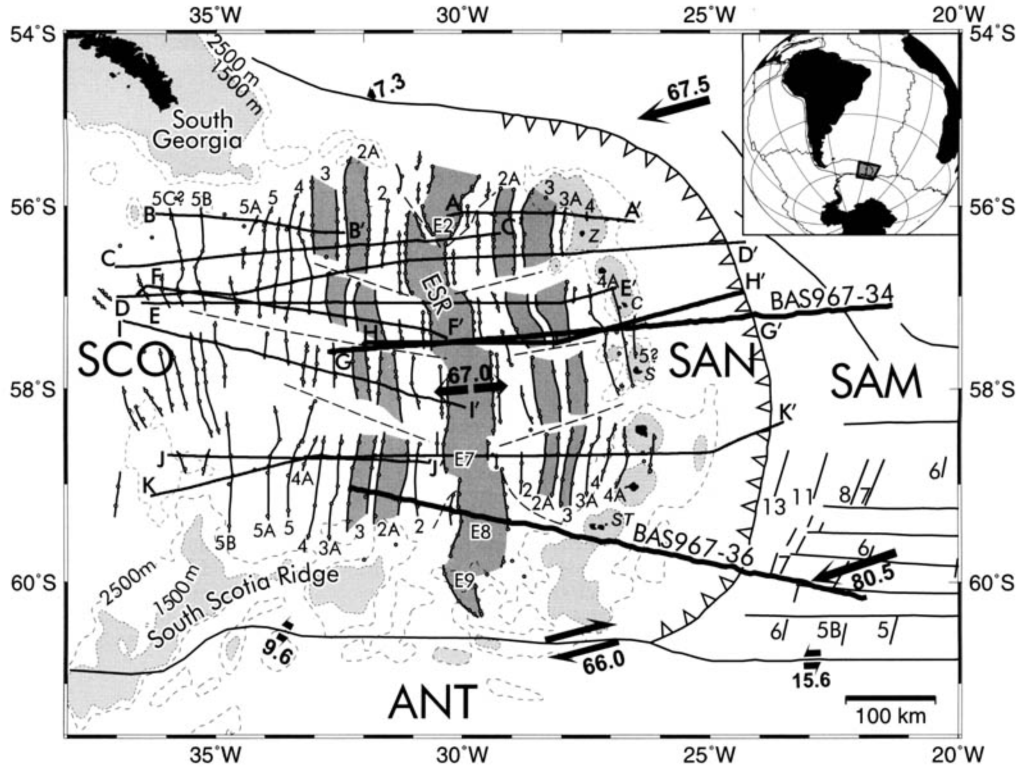

Fig. 1. Location map showing the tectonic setting of the South Sandwich island arc, and marine magnetic anomalies in the East Scotia Sea, modified from Vanneste *et al.* (2002). The grey-filled box on the globe in the inset shows the location of the main map. Magnetic anomaly picks are represented by small open circles. The central Brunhes anomaly and anomalies 2A and 3 are shaded dark grey. Segments E2 and E7–E9 of the East Scotia Ridge (ESR) are labelled. Long-dashed lines represent pseudofaults formed by ridge-segment propagation (Livermore *et al.* 1994, 1997). Magnetic anomaly identifications on the South American Plate are based on Barker & Lawver (1988). Arrows indicate vectors of relative motion between the Scotia (SCO), Sandwich (SAN), South American (SAM) and Antarctic (ANT) plates, based on Euler vectors of Thomas *et al.* (2003). Arrow lengths are proportional to rates (annotated in mm a^{-1}). Locations of magnetic and bathymetry profiles A–A′ to K–K′ that are shown in Figure 2 and 3 are shown as solid lines. Locations of Sandwich Lithospheric and Crustal Experiment (SLICE) multichannel seismic lines BAS967-34 and BAS967-36 are shown as thicker black lines. The 2500 m (short-dashed lines) and 1500 m (filled, light grey) bathymetric contours, based on global seafloor topography data of Smith & Sandwell (1997), define the South Sandwich arc, South Georgia microcontinental block and South Scotia Ridge. The barbed line represents the trench. Island labels (italics): C, Candlemas Island; S, Saunders Island; ST, Southern Thule; Z, Zavodovski Island.

(Fig. 1). In previous interpretations of East Scotia Sea spreading history the existence of long, approximately E–W-trending fracture zones was inferred (Barker & Hill 1981; Barker 1995). However, a swath sonar investigation of the entire ESR revealed no stable fracture zone offsets (Livermore *et al.* 1995, 1997; Bruguier & Livermore 2001), and therefore we consider it likely that the prominent WNW–ESE-trending gravity anomalies in the western part of the East Scotia Sea (Livermore *et al.* 1994) represent the loci of migrating ridge offsets (i.e. pseudofaults). Some magnetic profiles used in previous interpretations of East Scotia Sea spreading history probably included unrecognized offsets across these pseudofaults. Magnetic lineations between pseudofaults trend N–S, and it is likely that the extension direction has been approximately E–W throughout the development of the East Scotia Sea.

In selecting magnetic profiles for analysis of spreading rates we gave priority to those that avoid crossing pseudofaults. After removal of the International Geomagnetic Reference Field

(IGRF; Barton 1996), the selected profiles were projected onto E–W lines and compared to synthetic magnetic anomaly profiles to identify anomalies (Fig. 2). Six of the 11 profiles shown in Figure 2 were collected during cruises in 1995 and 1997, and thus were not included in the analysis of Barker (1995). The geomagnetic polarity timescale of Cande & Kent (1995) was used in the generation of the synthetic magnetic anomaly profiles, and is the basis for all magnetic anomaly ages quoted in this paper. Initial identifications of anomalies were made by comparison with a set of synthetic profiles generated using a range of constant spreading rates. The variable spreading rates used to generate the synthetic profiles shown in Figure 2 were based on reduced distance analyses (see below).

Six of the eight profiles that extend to the western limit of the East Scotia Sea show a pair of positive anomalies that are a very close match to anomalies 5AC and 5AD (13.9 and 14.4 Ma, respectively) on the synthetic profiles. Anomaly 5B (15.0 Ma) is a subtle feature on the synthetic profiles, but also appears to be present on several of the observed profiles. A little further west, another positive anomaly is observed on most of these profiles and is in approximately the position where anomaly 5C (16.4 Ma) would be expected to occur, given a constant spreading rate. However, to the west of this anomaly magnetic profiles are less consistent, so identification of it as 5C must remain tentative. Sharp offsets in seafloor depth occur near to this anomaly on several of the profiles (Fig. 3), perhaps indicating that it approximates the limit of back-arc crust formed by organized seafloor spreading.

On the eastern side of the back-arc basin, the crest of the northern end of the modern arc is approximately coincident with anomaly 4 (e.g. profiles A–A′ and D–D′ in Fig. 2), while the central part of the arc is approximately coincident with anomaly 5 (e.g. profiles G–G′, H–H′ and K–K′). Therefore, if an arc existed between 15 Ma ago and chron 5 (9.7–10.9 Ma), it must have been located farther east relative to the Sandwich Plate.

The interpretation of magnetic anomalies on the eastern side of the back-arc basin north of about 57°S, shown in Figures 1 and 2, is slightly different from that recently published in Vanneste & Larter (2002) and Vanneste *et al.* (2002). The revised interpretation results from careful comparison of the profiles in Figure 2 with synthetic profiles and consideration of reduced distance analyses (see below). In our revised interpretation, anomaly 3n in this part of the back-arc basin is wider than it was in the earlier interpretation, and we now think that the positive anomaly previously interpreted as 3An (6.2 Ma) is actually 3n.4n (5.1 Ma). This change also implies that the anomalies previously interpreted as 4n and 4An (7.9 and 8.9 Ma) on profiles in this area are actually 3An and 4n, respectively.

In general, there is a close correspondence between the observed magnetic profiles and the synthetic profiles in Figure 2. This close correspondence, and the continuity of the reversal sequence on the observed profiles, shows that the greater width of the western side of the East Scotia Sea compared to its eastern side cannot be attributed to ridge jumps. The crust formed on the eastern flank of the ESR prior to chron 5 must now lie beneath the inner forearc. Our analysis of spreading rates (see below) shows that the half spreading rates between chrons 5B and 5r (15.0–11.5 Ma) on the western side of the ESR were 17–20 mm a^{-1}, decreasing to 12–14 mm a^{-1} during chrons 5r and 5n (11.5–10.0 Ma). If spreading during this interval was symmetrical, then the crust formed on the eastern flank of the ESR during chron 5B now lies about 80 km east of the central part of the present arc.

Studies in other back-arc basins have shown that the earliest stages of back-arc extension typically involve asymmetrical rifting and that a spreading axis tends to develop near, or propagate into, the trenchward flank of the rifted crust (Parson & Hawkins 1994; Martinez *et al.* 1995; Parson & Wright 1996). Furthermore, it has been suggested that magnetic lineations may be developed even in the rifting phase by systematic migration of zones of magmatism across the rift zone (Martinez *et al.* 1995). However, the asymmetrical extension described in these studies occurs during the arc-rifting phase that precedes organized back-arc spreading. The close correspondence between the observed magnetic profiles and the synthetic profiles shown in Figure 2, and the continuity of magnetic lineations along strike, leaves little doubt that extension in the East Scotia Sea had already progressed to organized spreading by 15 Ma ago. Even if it is assumed that quite extreme asymmetrical extension persisted into the spreading phase, with the western flank of the ESR spreading twice as fast as the eastern flank until 10 Ma ago, the crust formed on the eastern flank during chron 5B still must lie 40 km or more east of the central part of the present arc. As the present arc–trench gap is only 140–160 km, this implies that either spreading began unusually close to the trench or a substantial amount of subduction erosion has taken place.

Figure 4 shows the magnetic anomaly interpretation from Figure 1 overlaid on the

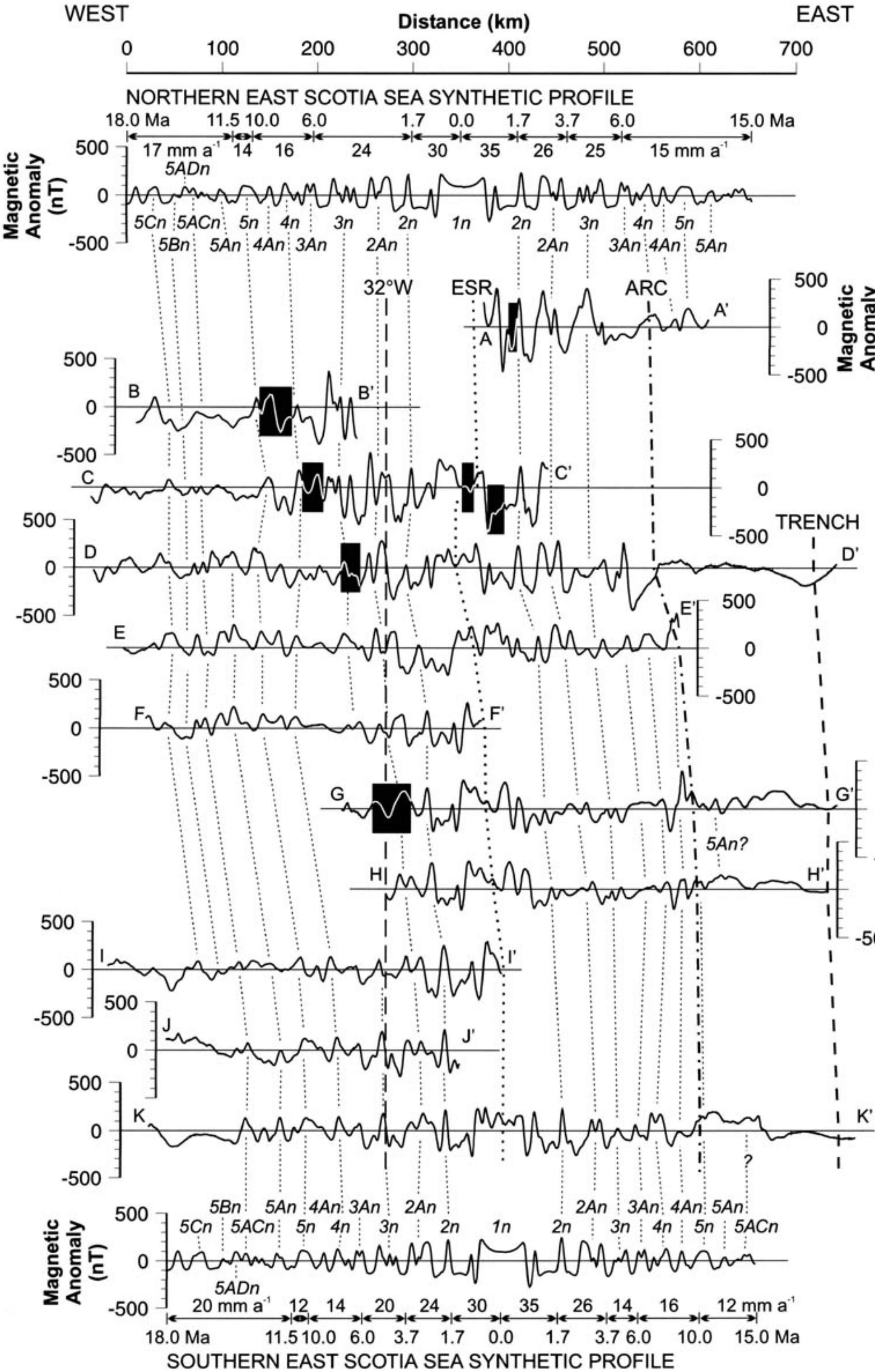
WEST
Distance (km)
EAST
0 100 200 300 400 500 600 700
NORTHERN EAST SCOTIA SEA SYNTHETIC PROFILE
Magnetic Anomaly (nT)
32°W
ESR
ARC
TRENCH
5An?
SOUTHERN EAST SCOTIA SEA SYNTHETIC PROFILE

regional magnetic anomaly field. The regional field was calculated by subtracting the IGRF from all available marine magnetic profiles, carrying out cross-over error analysis on data from different cruises and sections of cruises (cruise files were subdivided where there was a significant break in data acquisition), applying constant corrections to data from each cruise section and then gridding the corrected anomaly data. Figure 4 confirms that most of our magnetic anomaly picks are on the peaks or edges of lineated magnetic anomalies, and also shows that lineated anomalies are present as far west as, and even beyond, the position where we have identified anomaly 5B. Furthermore, Figure 4 confirms that the interpreted pseudofaults correspond to discontinuities in the lineated magnetic anomalies.

The close correspondence between the observed and synthetic magnetic profiles in Figure 2 permits detailed analysis of spreading rates using the enhanced sensitivity of the reduced distance method (Barker 1979). On a reduced distance graph the distance along a profile at which a particular peak, trough or zero crossing is observed is shown after subtraction of the distance at which it occurs along a synthetic magnetic profile generated using a constant spreading rate, and the resulting value is plotted versus age. A spreading rate matching that of the synthetic profile would produce a horizontal line on a reduced distance graph, and this form of display is more sensitive to variations in spreading rate than a simple plot of distance v. time. The sensitivity of a reduced distance graph is greatest at spreading rates close to those of the reference synthetic profile.

Barker (1995) published reduced distance graphs based on comparison of six East Scotia Sea magnetic profiles with a synthetic profile generated using a constant half spreading rate of 25 mm a^{-1}. These graphs indicated that half spreading rates prior to 4 Ma averaged about 15 mm a^{-1}. In order to examine the early history of East Scotia Sea spreading in more detail we have plotted reduced distance graphs based on comparison of the projected profiles shown in Figure 2 with a synthetic profile generated using a constant half spreading rate of 15 mm a^{-1} (Fig. 5). The distances on which these graphs are based were measured from a confidently identified peak or trough, rather than from the spreading axis. As it is the gradient of the graph that represents spreading rate, absolute values of reduced distance are unimportant.

The overall positive gradients on the reduced distance graphs in Figure 5 indicate that half spreading rates prior to 4 Ma averaged more than 15 mm a^{-1}. The graphs also reveal some significant N–S and temporal variations. Between 15 and 11.5 Ma ago half rates on the western flank of the ESR (Fig. 5a, b) were slightly slower on the northern (17 mm a^{-1}) than on the central and southern parts of the ridge (20 mm a^{-1}). About 11.5 Ma ago spreading rates along the whole ridge slowed abruptly, and from then until 4 Ma ago spreading at the northern part of the ESR was faster than at its central and

Fig. 2. Selected East Scotia Sea marine magnetic profiles compared to synthetic magnetic anomaly profiles. Locations of profiles A–A′ to K–K′ are shown in Figure 1. All of the profiles are projected on to 090°. The observed magnetic profiles are aligned at 32°W (long-dashed line), except for profiles A–A′ and B–B′, which are positioned such that the youngest anomalies are aligned with the equivalent anomalies on profile C–C′. The parts of profiles shown as white lines on a black background are interpreted as being affected by pseudofault crossings. ESR, East Scotia Ridge axis (dotted line); ARC, crest of island arc (dash–dot line); TRENCH, South Sandwich Trench axis (medium-dashed line). Short-dashed lines represent interpreted correlations between magnetic anomalies on observed and synthetic profiles. The synthetic profiles were calculated using the spreading rates shown, the geomagnetic polarity timescale of Cande & Kent (1995), the Definitive Geomagnetic Reference Field (DGRF) for 1985.0 (Barton 1996), the age–depth relationship for oceanic crust of Parsons & Sclater (1977), and a magnetic layer of 1 km thickness and susceptibility that decreases with increasing age (susceptibility (SI) 0.045 at 0 Ma, 0.024 at 0.68 Ma, 0.014 at 10 Ma, then constant for ages >10 Ma). Remanent magnetization vector inclinations, based on the assumptions that the time-averaged magnetic field approximates an axial geocentric dipole and there has been no significant change in latitude of the crust since its formation, were –72° for the northern synthetic profile and –73° for the southern one, with declination of 0° in both cases. The calculation of synthetic anomalies is based only on remanent magnetization, but the DGRF is used to calculate the component of the anomaly in the direction of the present magnetic field, as this is what observed total field anomalies measure. The reason that decreasing susceptibility with crustal age is used is to simulate the widely observed decay in anomaly amplitudes with increasing crustal age. The top of the magnetic layer in the model used to calculate the synthetic profiles was based on an oceanic age–depth relationship, rather than on observed bathymetric profiles, because the synthetic profiles are compared to a suite of observed magnetic profiles, and the bathymetry differs between profiles. Furthermore, using observed bathymetry would result in the top of the magnetic layer being too shallow wherever there is a significant thickness of sediment.

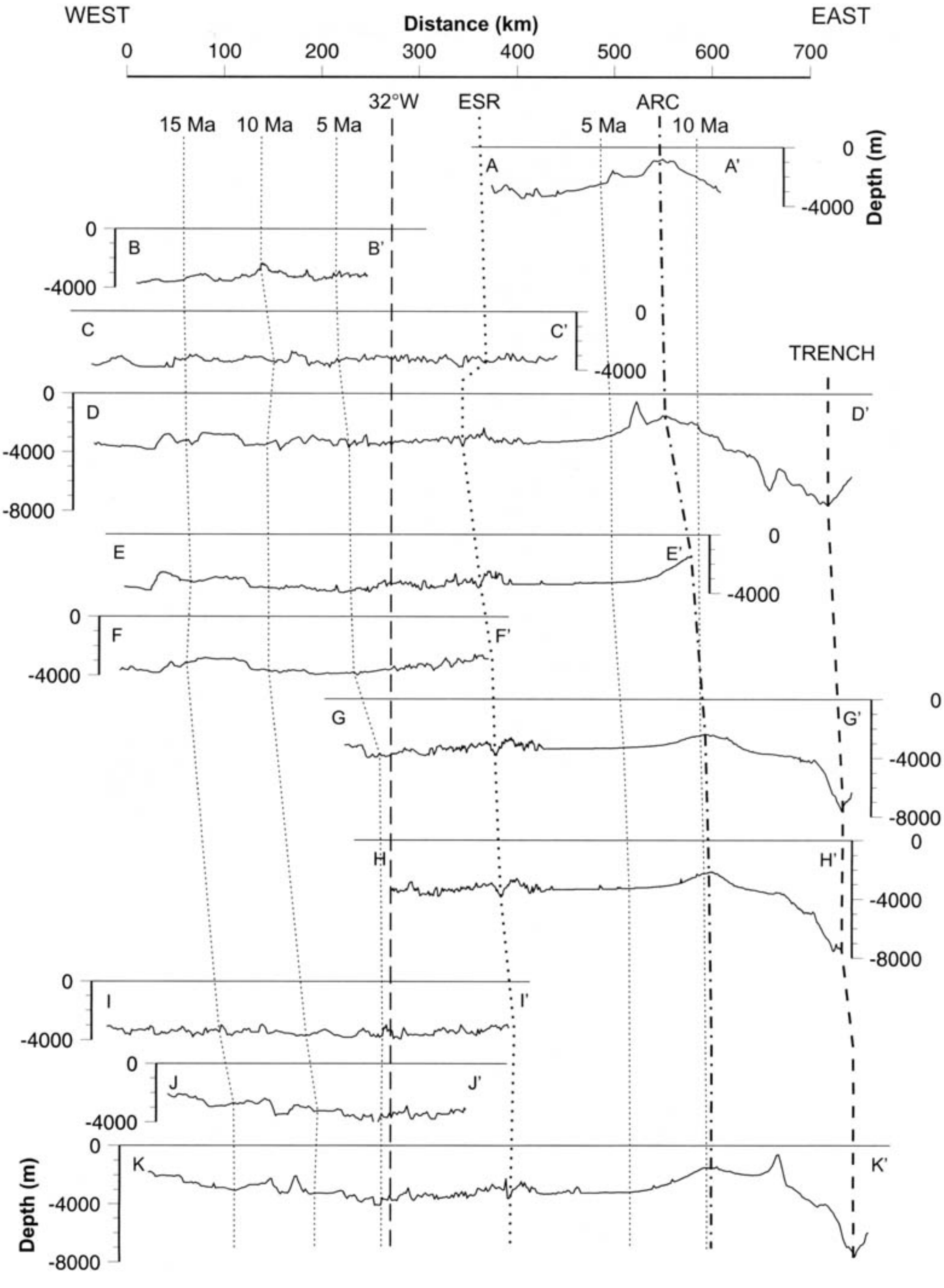

Fig. 3. East Scotia Sea bathymetry profiles along the same ship tracks as the magnetic profiles shown in Figure 2. Locations of profiles A–A′ to K–K′ are shown in Figure 1. All of the profiles are projected on to 090° . The profiles are aligned at 32°W, except for profiles A–A′ and B–B′, which are shown in the same relative positions as the coincident magnetic profiles in Figure 2. ESR, East Scotia Ridge axis (dotted line); ARC, crest of island arc (dash–dot line); TRENCH, South Sandwich Trench axis (medium-dashed line). Short-dashed lines represent lines of constant crustal age, based on interpretation of the coincident magnetic profiles, with ages annotated at the top of these lines.

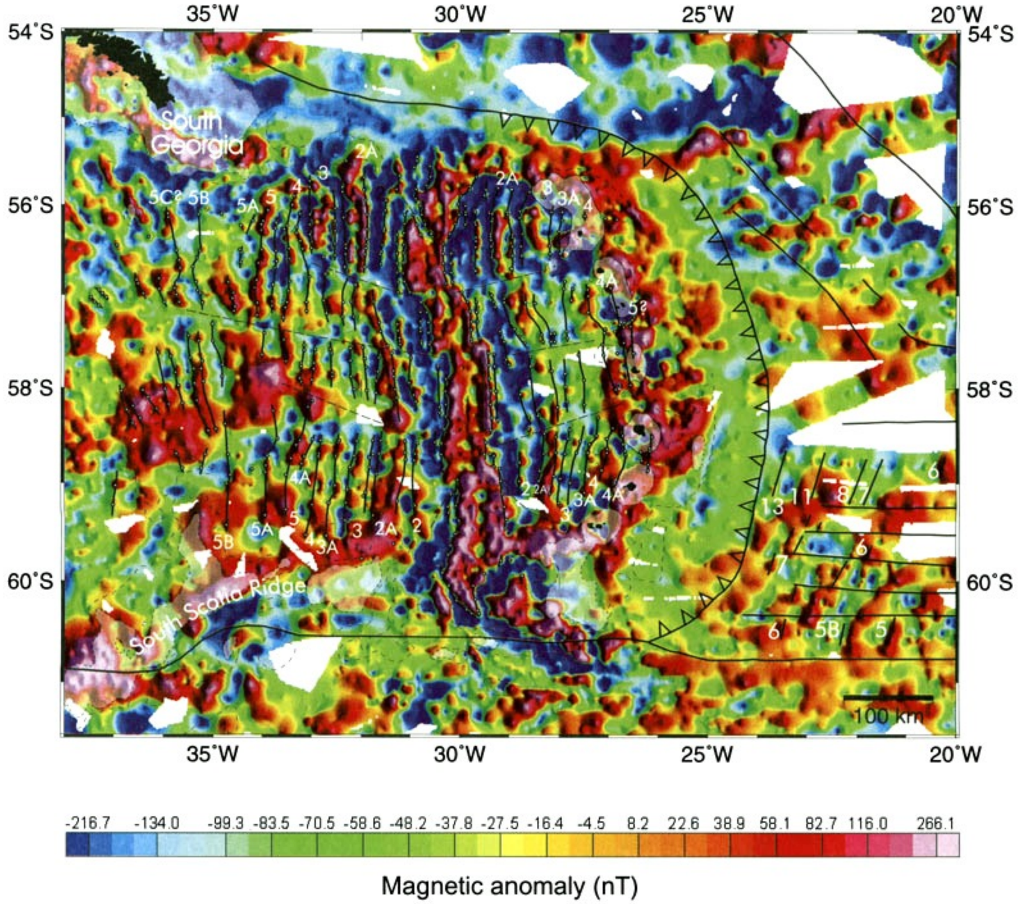

Fig. 4. Regional magnetic anomaly field, overlaid with the magnetic anomaly interpretation from Figure 1. The 2500 m (short-dashed lines) and 1500 m (pale, semi-transparent fill) bathymetric contours from Figure 1 are also shown. The regional field was calculated by subtracting the IGRF from all available marine magnetic profiles, carrying out cross-over error analysis on data from different cruises and sections of cruises, applying constant corrections to data from each cruise section and then gridding the corrected anomaly data. Interpolation was limited to 16 km from profiles, and areas further from the nearest profile appear white.

southern parts. Since the decrease in spreading rates 11.5 Ma ago, all subsequent spreading rates changes have been increases (Figs 2 and 5). Rates have increased in a series of steps on all parts of the ESR, eventually reaching the modern full rate of about 65 mm a^{-1} 1.7 Ma ago. About 10 Ma ago half rates on the western flank of the ESR increased from 14 to 16 mm a^{-1} in the north and from 12 to 14 mm a^{-1} in the south. Spreading rates increased again 6 Ma ago, with western flank half rates increasing to 24 mm a^{-1} in the north and 20 mm a^{-1} in the south.

On the eastern flank of the ESR only magnetic anomalies younger than 10 Ma can be identified with confidence. Older back-arc crust must now lie beneath the inner forearc, but magnetic profiles across the forearc do not reveal consistent lineations, probably because the original magnetic record has been disturbed and overprinted as a result of arc magmatism (Vanneste & Larter 2002). Our tentative identifications of anomaly 5A (12.2 Ma) on profiles G–G′ and H–H′ imply that half rates between 12.2 and 10 Ma ago on the eastern flank of the ESR were about 13 mm a^{-1} (Figs 2 and 5c). If these anomaly identifications are correct, spreading during this interval was approximately symmetrical. On the basis of more confidently identified anomalies, the reduced distance graphs indicate that spreading was approximately symmetrical between 10 and 6 Ma ago, with half rates on the eastern flank of

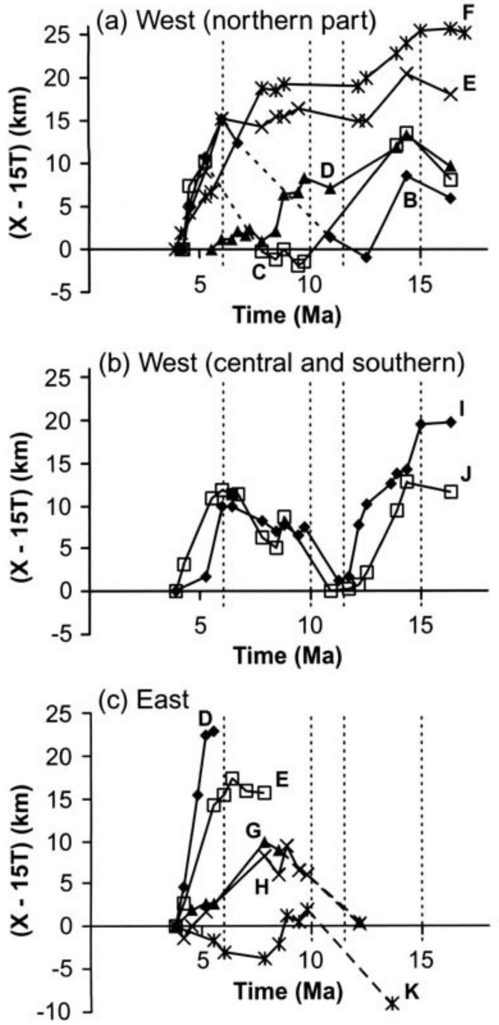

Fig. 5. Reduced distance graphs for the magnetic profiles shown in Figure 2, based on comparison with a synthetic profile generated using a constant half-spreading rate of 15 mm a^{-1}. Graph lines labelled B to K represent reduced distance data calculated from profiles B–B′ to K–K′, which are located in Figure 1. Vertical dotted lines indicate interpreted times of spreading rate changes. (**a**) Reduced distance graphs for profiles crossing the northern part of the west side of the East Scotia Sea. Short-dashed lines indicate probable pseudofault crossings. (**b**) Reduced distance graphs for profiles crossing the central and southern parts of the west side of the East Scotia Sea. (**c**) Reduced distance graphs for profiles crossing the east side of the East Scotia Sea. Long-dashed lines indicate parts of the graphs based on tentative identification of anomalies in the forearc.

the ESR averaging 16 mm a^{-1}. For the interval between 6 and 4 Ma ago, the fan-shaped pattern of graph lines in Figure 5c indicates substantial N–S variation in half spreading rates on the eastern flank of the ESR. During this interval eastern flank half rates ranged from about 25 mm a^{-1} in the north to 14 mm a^{-1} in the south. The systematic variation in spreading rates from north to south during this interval emerges as a result of our revised interpretation of anomalies in the NE part of the back-arc basin (see above). The earlier interpretation implied rates that increased from the southern to the central part of the ESR but were approximately constant along the central and northern part of the ESR, a pattern that is inconsistent with a rigid Sandwich Plate.

The most significant changes in spreading rate revealed by Figure 5 occurred 11.5 and 6 Ma ago. There was an overall reduction in spreading rates on the ESR 11.5 Ma ago, but the reduction was much greater in the south than in the north. About 6 Ma ago there was an overall increase in spreading rates, but the increase was much smaller in the south than in the north. Investigations of the South Scotia Ridge have revealed evidence for collisions between ancestors of the South Sandwich Trench and more westerly segments of the South American–Antarctic Ridge (Barker *et al.* 1984; Hamilton 1989). After each collision it appears that subduction stopped at the section of trench involved and rearrangement of plate boundaries transferred a sliver of back-arc lithosphere to the Antarctic Plate. However, the precise ages of collisions are poorly constrained. We suggest that such collisions are the most likely cause of the changes in spreading rates 11.5 and 6 Ma ago revealed by Figure 5. After each collision, spreading at the southern part of the ESR was probably slower than spreading at the northern part of the ridge while a new southern boundary to the Sandwich Plate became established (Fig. 6).

Bathymetry profiles and age–depth relationships

Bathymetry data collected on the same ship tracks as the magnetic profiles shown in Figure 2 generally show a gradual increase in water depth with increasing distance from the ESR axis on its western flank (Fig. 3). On most of the profiles water depth increases from slightly less than 3000 m on the flanks of the axial troughs to between 3500 and 4000 m in the vicinity of anomaly 3A (5.9–6.6 Ma). This amount of subsidence is consistent with predictions of oceanic age–depth relationships (Trehu 1975; Parsons & Sclater 1977). However, farther west most profiles show seafloor depths becoming slightly shallower with increasing crustal age between

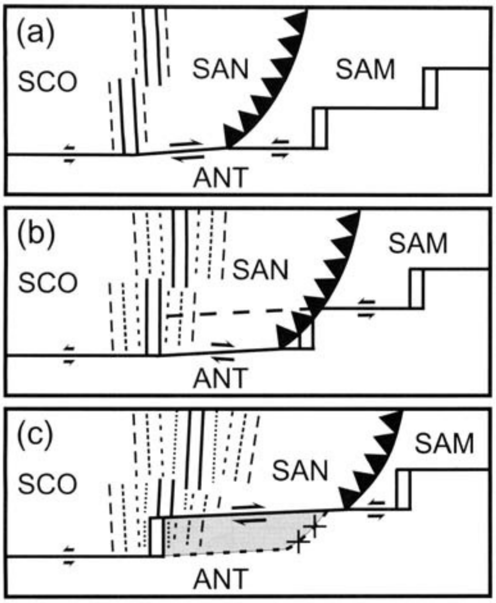

Fig. 6. Schematic illustrations showing postulated sequence of events resulting from collision of a South American–Antarctic Ridge segment with the southern end of the South Sandwich Trench. The positions of all features are shown relative to a fixed Antarctic Plate. (**a**) Pre-collision tectonic setting. Dashed lines represent magnetic anomalies recently formed at the East Scotia Ridge (SCO–SAN boundary). (**b**) Syncollision tectonic setting. Entry of young Antarctic Plate ocean floor into the southernmost part of the trench increases forces resisting subduction. This results in a N–S variation in spreading rates along the East Scotia Ridge, illustrated by short-dashed lines representing recently formed magnetic anomalies, and incipient rupture through the Sandwich Plate to form a new plate boundary north of the collision zone (long dashes). (**c**) Post-collision tectonic setting. Plate boundary north of the collision zone becomes established, resulting in transfer of a sliver of back-arc lithosphere to the Antarctic Plate (grey-shaded area), and creating a short spreading segment or transtensional zone on the South Scotia Ridge (SCO–ANT boundary). Spreading on East Scotia Ridge becomes uniform again, illustrated by dotted lines representing recently formed magnetic anomalies. Crosses represent the collision zone, where subduction has ceased.

anomalies 3A and 5r (6.6–11.5 Ma). In the vicinity of anomaly 5A (11.9–12.4 Ma) several profiles show a sharp decrease westwards in seafloor depths by more than 500 m, so the surface of some of the oldest crust in the East Scotia Sea lies at a similar depth to crust recently formed at the ESR. Seismic reflection profiles coincident with the western part of profiles E–E′ and F–F′ show that the sediment cover in that area is fairly uniform and has a thickness of 0.5 s two-way travel time (TWT) or less (<500 m), so the anomalous seafloor depths cannot be explained by thick sediment cover. Most of the back-arc basement on the eastern side of the ESR is buried beneath an arcward-thickening sediment apron (see the following section), so examination of age–depth relationships on that side of the back-arc basin would be a more complex exercise involving laterally variable correction for sediment loading.

Martinez & Taylor (2002) recently proposed a model for mantle wedge control on back-arc crustal accretion in which there are systematic variations in magma supply with distance from the arc volcanic front. The model predicts enhanced magma supply when a back-arc ridge is close to the arc volcanic front, on the basis that it is drawing on the arc mantle source, which is enriched in volatiles from the subducting slab. For a back-arc ridge located somewhat further from the arc volcanic front, the model predicts diminished magma supply, on the basis that melt at such a ridge is generated by advection of mantle that has been entrained above the subducting slab and has already been depleted by the extraction of arc magmas. This model provides a plausible explanation for the anomalous seafloor depths in the western part of the East Scotia Sea. During the formation of the oldest crust (before about 12 Ma) the back-arc ridge was probably close to the arc volcanic front, and enhanced magma supply would have produced anomalously thick back-arc crust, the surface of which would be shallower than predicted by standard oceanic age–depth relationships. As spreading continued the back-arc ridge migrated away from the arc volcanic front, and diminishing magma supply would have produced progressively thinner back-arc crust, resulting in the inverse age–depth relationship we observe today. The sharp change in seafloor depths observed on several profiles in the vicinity of anomaly 5A may indicate that there is an abrupt boundary within a broader transition region between the zones of 'enhanced' and 'diminished' magmatism.

Seismic reflection profiles

MCS lines BAS967–34 and BAS967–36 (hereinafter referred to simply as 'line 34' and 'line 36', respectively) were acquired during RRS *James Clark Ross* cruise JR18 as part of the Sandwich Lithospheric and Crustal Experiment (SLICE; Larter *et al.* 1998). The locations of these lines are shown in Figure 1, and Figure 7 shows interpreted line drawings of the processed

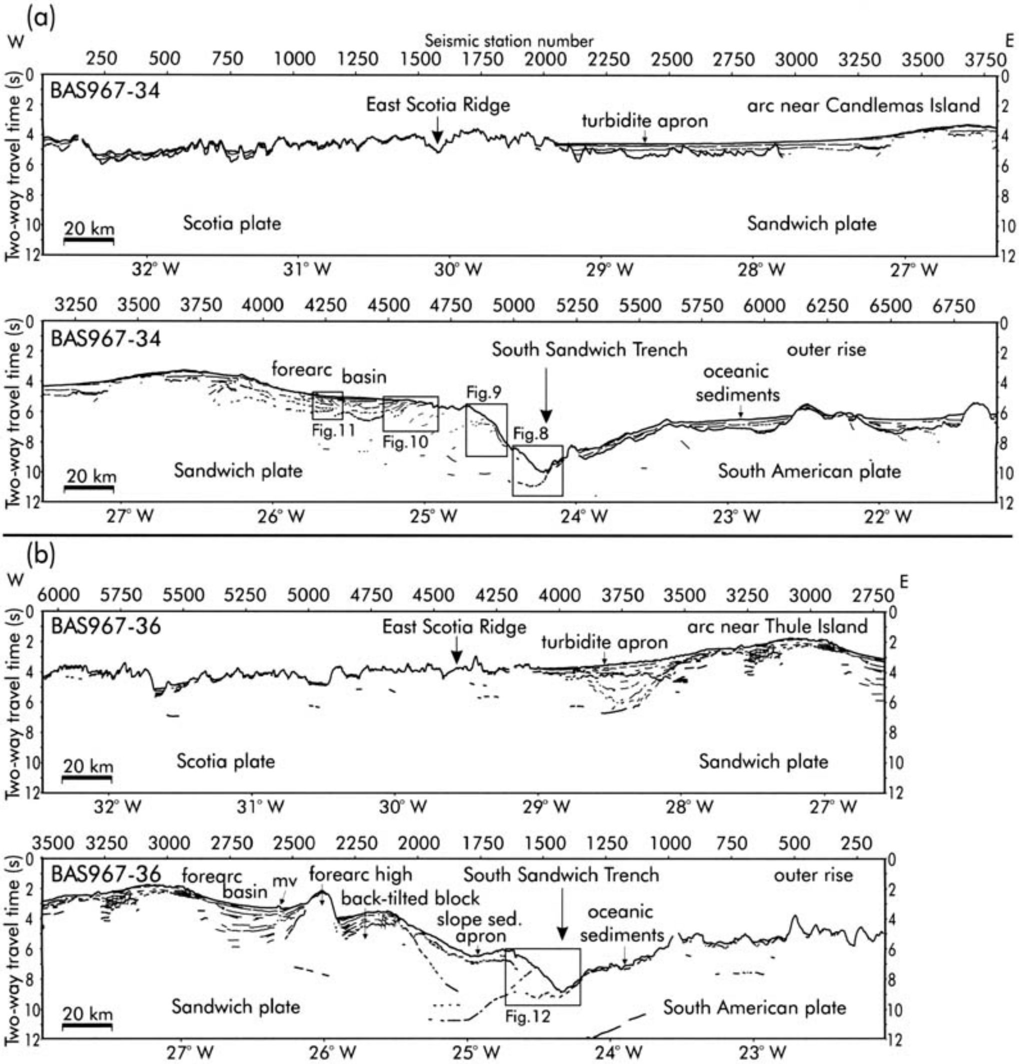

Fig. 7. Interpreted line drawings of multichannel seismic reflection profiles: (**a**) line BAS967-34; and (**b**) line BAS967-36. mv indicates mud volcano. Vertical exaggeration at the seafloor is 8: 1.

seismic profiles. The seismic source consisted of an array of 14 airguns with a total volume of 98 l (5976 in.^{3}). Shots were fired at a nominal spacing of 100 m to allow a sufficient interval between shots for simultaneous recording of wide-angle data on ocean-bottom seismometers (Larter *et al.* 2001). Ninety-six data channels were recorded at a 2 ms-sampling interval from a hydrophone streamer with an active length of 2400 m.

The standard processing sequence for both lines included resampling to 4 ms, bandpass filtering, predictive deconvolution, velocity analysis, stack (25 m common-depth point bins), Stolt *f–k* migration (where *f* is frequency and *k* is wavenumber), time-variable bandpass filter, weighted trace mix and automatic gain control. The central part of line 34 was acquired in extremely adverse conditions that resulted in most of the hydrophone streamer towing at an undesirably shallow depth, introducing high levels of noise into the data. For the part of the line between the ESR and the trench, only data from the leading 12 channels of the streamer were processed, as these remained at an acceptable depth throughout this period. On line 36 additional processes were carried out on certain parts of the line. Before deconvolution, a weighted trace mix was applied to shot gathers between station numbers (SN) 1–1250 and 4175–6066 to attenuate coherent noise from the rough surface of oceanic basement. Before stacking the data, an *f–k* filter and inner-trace mute were applied to common-depth point gathers between SN 2018 and 4175 to suppress seafloor multiple reverberations.

Lines 34 and 36 both cross the entire South Sandwich subduction system, running from the outer rise in the east to the western flank of the back-arc basin. Line 34 crosses the northern part of the arc and is about 700 km long. It passes over the deepest saddle in the arc, which lies at a depth of 2400 m between Candlemas and Saunders islands (Fig. 1). Line 36 crosses the arc close to the southernmost group of islands, Southern Thule, and is about 600 km long (Fig. 1).

Line BAS967-34

The eastern end of line 34 shows a variable thickness of sediment cover over the oceanic basement of the South American Plate on the outer rise (Fig. 7a), in the range 0–1 s TWT. On the basis of typical velocity–depth relationships for deep-water sediments (Hamilton 1979; Carlson *et al.* 1986) these travel times indicate a maximum sediment thickness of <1 km. The oceanic basement in this area has an age of about 55 Ma and was formed by NW–SE-directed spreading at the South American–Antarctic Ridge (Barker & Lawver 1988; Livermore & Woollett 1993). The basement highs between seismic station numbers (SN) 6100–6200 and 6800–6900 probably represent oblique crossings of ridges associated with small-offset fracture zones. When these highs are excluded, the average depth of the seafloor over the crest of the outer rise is 4700 m.

The trench axis on the line lies at a depth of 7600 m (Figs 7a and 8). Swath bathymetric data have shown that the axial depth of the trench is quite variable in this area, ranging from <7300 to >8100 m within 50 km either side of this line (Vanneste & Larter 2002).

The arc–trench gap measured along line 34 is 145 km (Fig. 7a). Among modern subduction zones only the New Hebrides, Solomon and New Britain systems have narrower arc–trench gaps (Jarrard 1986). The forearc can be divided into a broad inner forearc, with an average seafloor dip <1°, and a narrow outer forearc with an average seafloor dip >6° . Between these two areas there is an abrupt 'trench-slope break' at SN 4820, where the water depth is 4150 m (Figs 7a and 9).

Discontinuous reflections between 10 and 11 s TWT beneath the outer forearc probably represent the top of the subducted oceanic basement (Figs 7a and 8). A 'velocity pull-up' effect resulting from the dipping seafloor causes this surface to appear approximately horizontal on a travel time display, even though its true dip is to the west. Few other reflections are observed beneath the lower part of the outer forearc on this line, either on migrated or unmigrated data. Although data quality on the part of the line crossing the arc and forearc is compromised by the rough sea conditions that prevailed during acquisition, we do not think the scarcity of reflections beneath the outer forearc is caused by poor data quality. Subsurface features are clearly imaged beneath the upper part of the outer forearc and beneath the inner forearc (Figs 9 and 10) on data of similar quality, so if extensive coherent structures were present in the toe of the outer forearc slope we believe that they would be imaged.

A strong, horizontal reflection is observed beneath the upper part of the outer forearc slope at about 6.8 s TWT (Figs 7a and 9). The eastern end of this reflection terminates shortly before reaching the seafloor, at a point where the material beneath it is covered by a layer of slope sediment that is about 0.15 s TWT (<150 m) thick. However, the position where the projection of this reflection meets the seafloor coincides with an abrupt break in slope (at SN 4925). To the west of this point, the uppermost part of the outer forearc slope has a dip of 5°, while to the east a slope with a dip of 13° continues over a change in water depth of >800 m. This latter slope is much steeper than that on any modern accretionary prism (Lallemand *et al.* 1994) and lies within 20 km of the trench axis.

Analysis of the mechanics of accretionary prisms as critically tapered wedges suggests that such a steep surface slope could only be produced if the wedge material was unusually weak (had low 'effective internal friction'), the basal coupling was unusually strong or the basal décollement was at an unusually low angle (Davis *et al.* 1983). On the basis of this consideration, together with interpretation of gravity and four-channel seismic reflection data, Vanneste & Larter (2002) suggested that any frontal prism present along this part of the forearc is restricted to within a few kilometres of the trench.

In contrast, if the dominant process controlling evolution of the lower forearc in this area has been subduction erosion, as proposed by Vanneste & Larter (2002), the abrupt break of

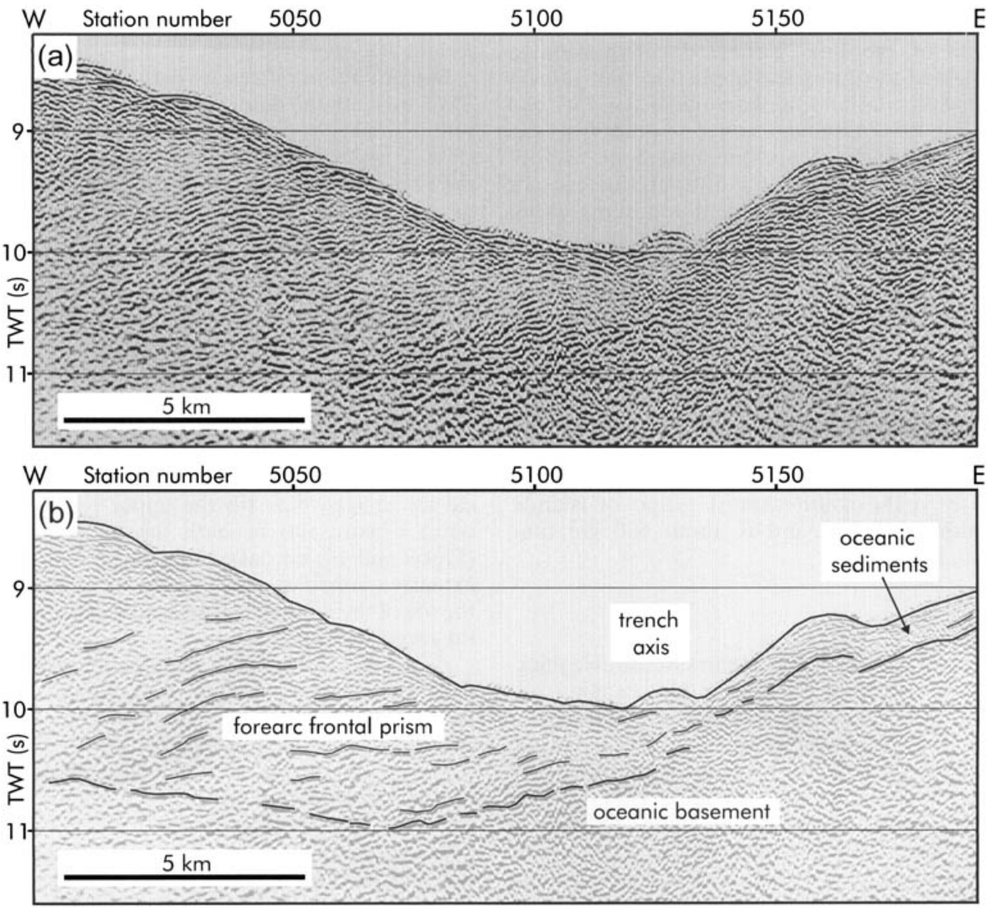

Fig. 8. Section of *f–k* migrated multichannel seismic line BAS967–34 crossing the trench and frontal prism. Vertical exaggeration at sea floor is 3.4: 1. Location of the section shown in Figure 7. TWT, two-way travel time. (**a**) Seismic data. (**b**) Interpretation of selected reflections overlaid on seismic data.

slope at SN 4925 suggests that the material beneath the reflector at 6.8 s TWT is significantly stronger than the overlying material. We speculate that this reflector is the top of the crustal basement on which the arc and forearc were built. Further detailed survey may reveal locations where the slope sediment cover is absent, allowing the supposed basement to be sampled by dredging.

A sedimentary basin extends across most of the inner forearc on line 34, with reflections being clearly imaged to depths of 1–1.5 s TWT (Figs 7a, 10 and 11). Velocity analyses on the MCS data, and wide-angle seismic data recorded on ocean-bottom seismometers, indicate that the average seismic interval velocity in the forearc basin sediments is about 2.5 km s^{-1}. Therefore, the thickness of sediments imaged on the MCS data in the central part of the basin varies between 1.2 and 1.9 km.

Forearc basin reflections at shallow depth near the eastern edge of the basin have a slight arcward dip and are truncated at the seafloor (Fig. 10). Deeper basin reflections in the same area dip more steeply and are truncated beneath an unconformity 0.17 s TWT below the seafloor. These reflection configurations indicate that the eastern part of the forearc basin has been subject to recent erosion, and there has been at least one previous episode of erosion during the development of the basin.

The MCS data show that the eastern edge of the forearc basin is affected by normal faults, most of which downthrow to the east and offset

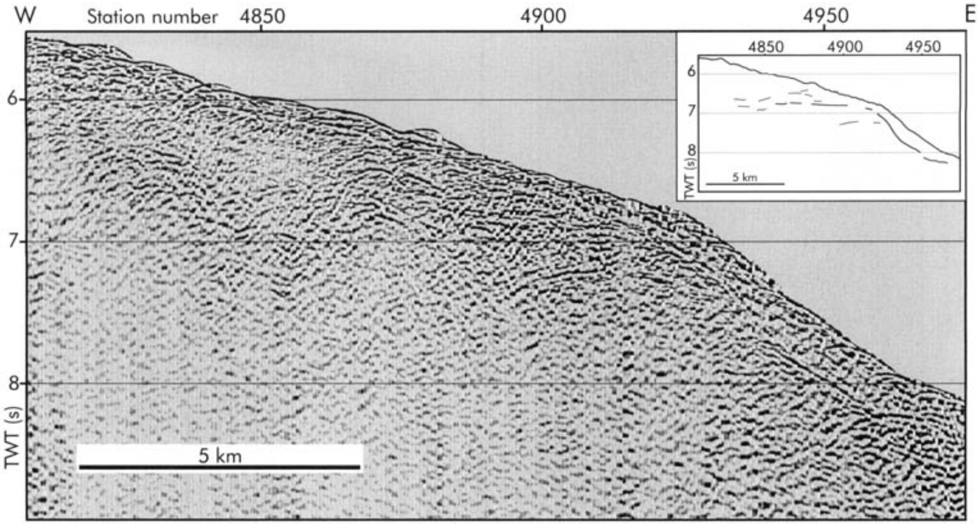

Fig. 9. Section of *f–k* migrated multichannel seismic line BAS967–34 crossing a break of slope on outer forearc. Location of the section shown in Figure 7. Inset shows interpreted reflections, including flat lying reflections at *c*. 6.8 s two-way travel time (TWT) that appear to be associated with the break in slope. Vertical exaggeration at the seafloor is 3.4: 1.

the seafloor (Fig. 10). Vanneste & Larter (2002) previously presented evidence for trench-parallel normal faults near the eastern edge of the basin in this area, based on side-scan sonar and four-channel seismic reflection data. Further west, however, the main part of the basin appears to be unaffected by such faulting. The only structural disruption affecting the main part of the basin is a set of low-angle extensional faults that sole out within the basin sediments (Fig. 11).

The MCS data do not reveal a distinct western boundary to the forearc basin. Reflections at shallow depth appear to continue across the saddle in the arc between Candlemas and Saunders islands, while deeper basin reflections become progressively less continuous westward and eventually disappear into a unit with chaotic seismic facies beneath the arc crest (Fig. 7a).

A sedimentary apron up to 1 s TWT thick (up to *c*. 1 km) extends to about 160 km west of the arc crest on line 34 and covers most of the back-arc basement east of the ESR (Fig. 7a). Reflections within the sediment apron are subhorizontal and very continuous, suggesting that it consists mostly of arc-derived turbidites.

Line 34 crosses the middle of segment E5 of the ESR about 210 km west of the arc crest. At this point segment E5 exhibits a median valley approximately 8 km wide with 600–750 m relief. No subseafloor reflections have been identified beneath the axial valley, but the seafloor profile across its eastern flank suggests the presence of a ‘staircase’ of normal faults with about 3 km spacing and downthrows to the west (Fig. 7a). Further away from the ridge both its flanks exhibit asymmetric basement topography, with parts of the basement surface that dip towards the ridge generally having steeper gradients than parts that dip away from the ridge. We interpret this observation as evidence that the spreading process involved rotational block faulting.

To the west of the ESR sediment thickness generally increases with increasing distance from the ridge, and hence with increasing crustal age. The sediment thickness reaches about 0.6 s TWT (<600 m) near the western end of the line, where the oceanic basement age is 6 Ma (Fig. 1). The basement ridge at SN 100–200 coincides with an oblique crossing of a pseudofault (Figs 1 and 2).

Line BAS967-36

A *f–k* migrated profile showing data from the entire length of line 36 has been published previously (Vanneste *et al.* 2002). Below we describe the main differences between this line and line 34.

The oceanic basement presently entering the trench where line 36 crosses it has an age of about 27 Ma. Although fracture zones to the east

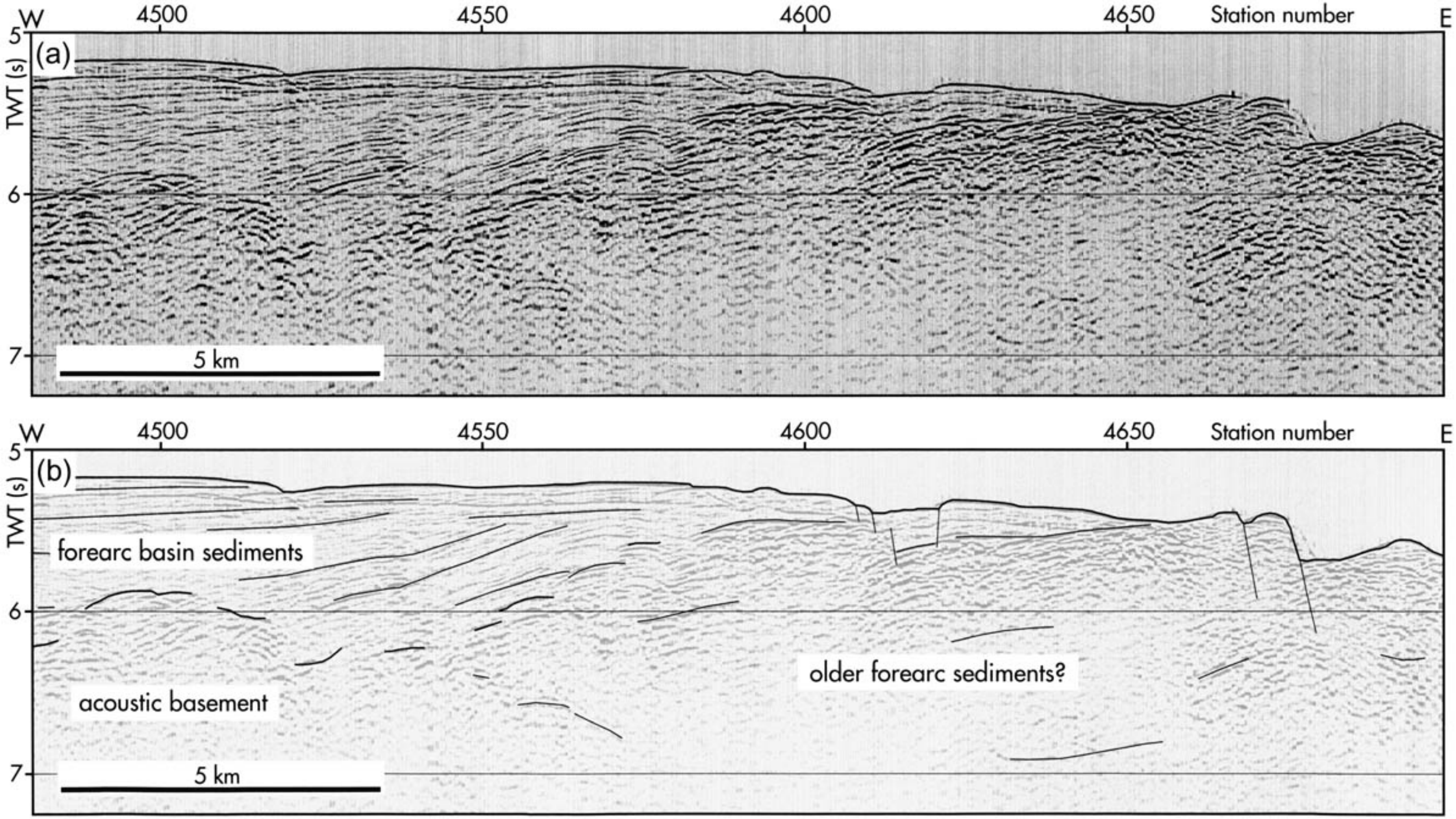

Fig. 10. Section of *f–k* migrated multichannel seismic line BAS967-34 crossing the eastern edge of the inner forearc basin. Vertical exaggeration at seafloor is 3.4:1. Location of the section shown in Figure 7. TWT, two-way travel time. (**a**) Seismic data. (**b**) Interpretation of selected reflections overlaid on seismic data.

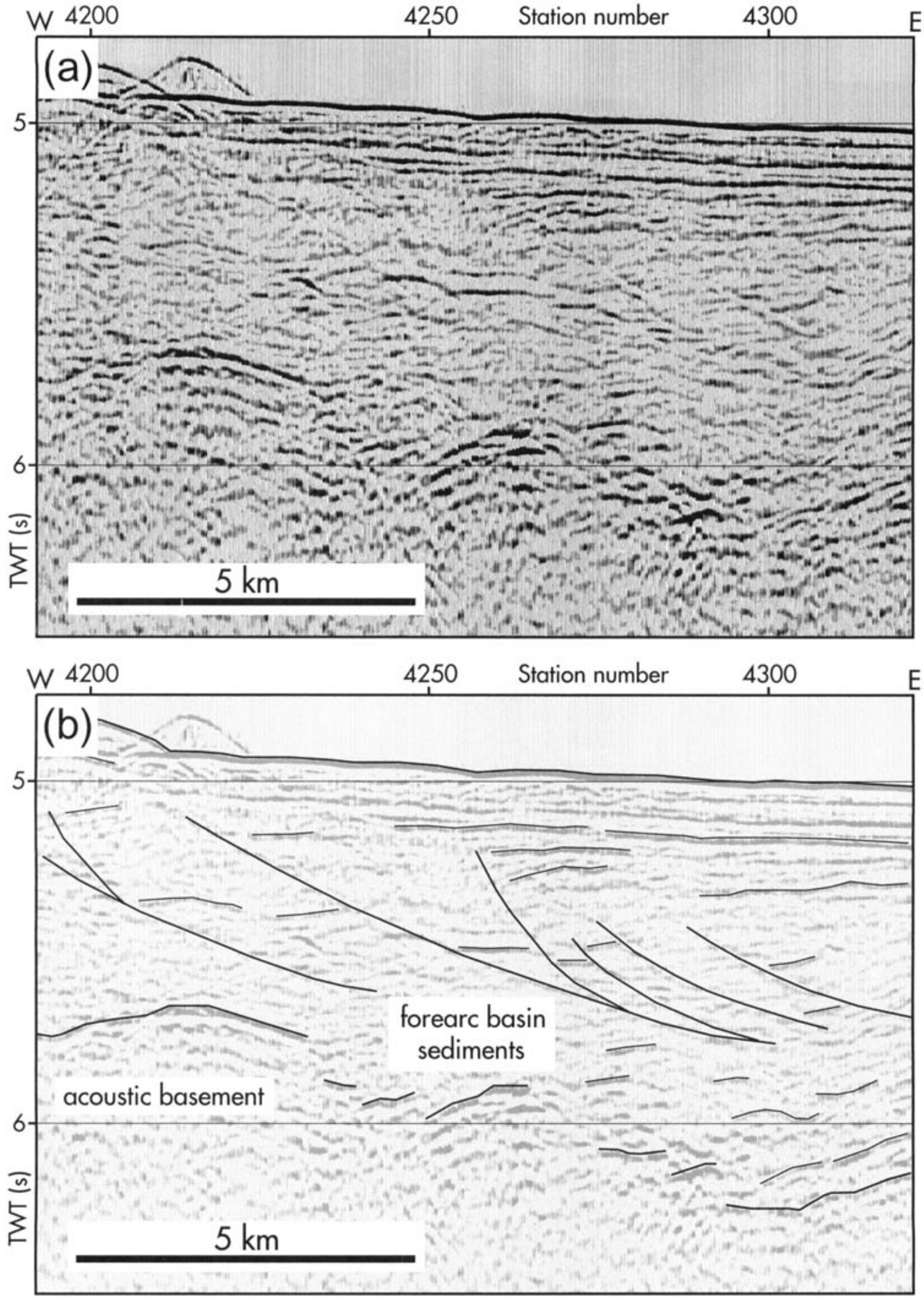

Fig. 11. Section of *f–k* migrated multichannel seismic line BAS967–34 crossing the central part of the inner forearc basin, showing low-angle extensional faulting within the forearc basin sediments. Vertical exaggeration at the seafloor is 6.8: 1. Location of the section shown in Figure 7. TWT, two-way travel time. (**a**) Seismic data. (**b**) Interpretation of selected reflections overlaid on seismic data. The mound that is observed centred about SN 4215 is interpreted as being out of the plane of the section.

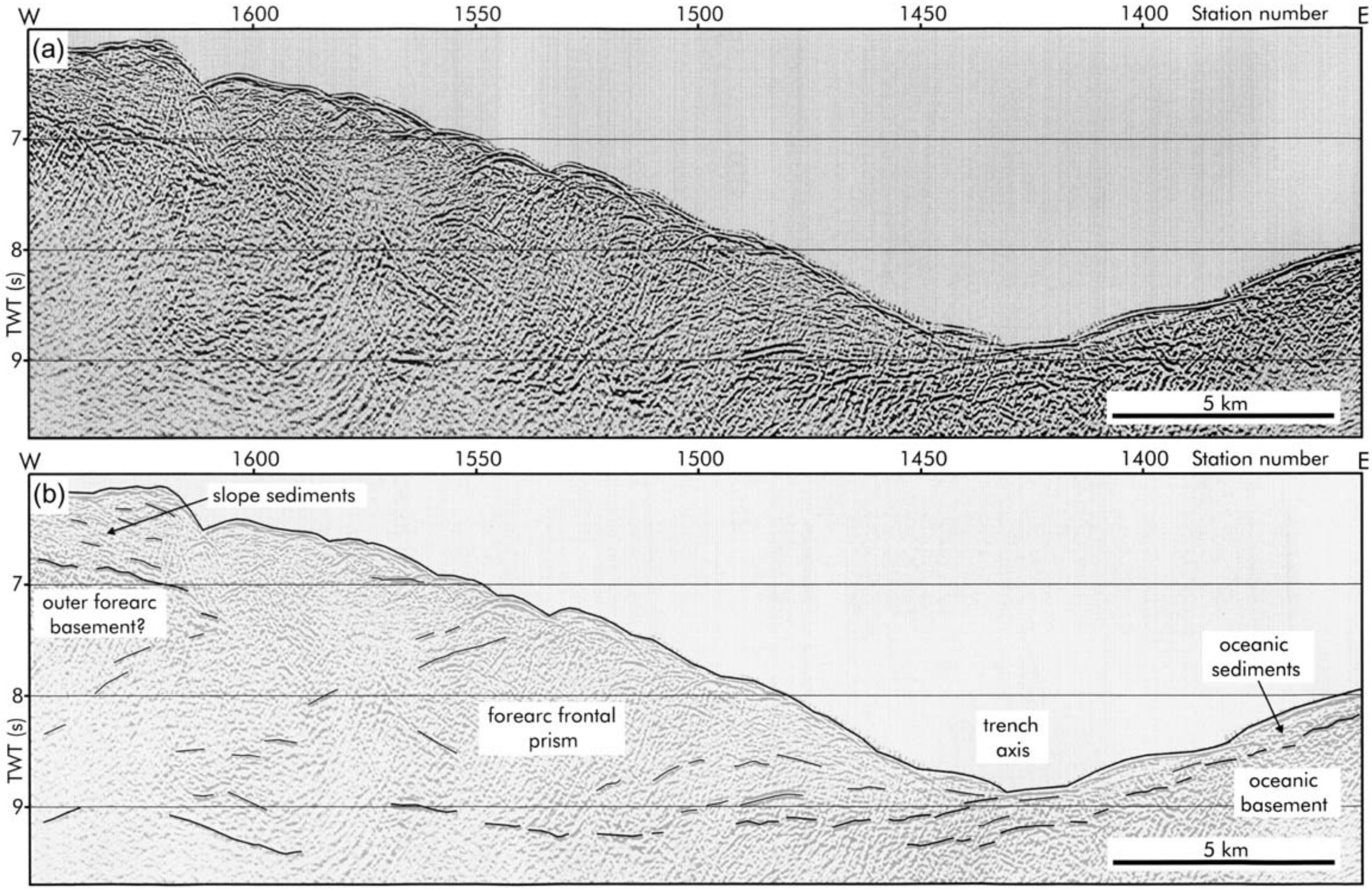

Fig. 12. Section of *f–k* migrated multichannel seismic line BAS967–36 crossing the trench and frontal prism. Vertical exaggeration at the seafloor is 3.4:1. Location of the section shown in Figure 7. TWT, two-way travel time. (**a**) Seismic data. (**b**) Interpretation of selected reflections overlaid on seismic data.

of the southern part of the trench trend E–W (Fig. 1), they have formed since a change in the direction of South American–Antarctic relative motion at about 20 Ma (Barker & Lawver 1988). Prior to this the spreading direction at the South American–Antarctic Ridge was NW–SE, and all of the South American ocean floor consumed at the South Sandwich Trench thus far was formed by spreading with this earlier orientation.

The sediment cover overlying oceanic basement on the outer rise on line 36 is 0–0.2 s TWT thick (<200 m), which is much less than the average thickness of the cover on the older basement on line 34. The average seafloor depth over the crest of the outer rise (3900 m) is also much shallower on line 36, as is the depth of the trench axis, at 6680 m (Figs 7b and 12).

The arc–trench gap measured along line 36 is 160 km (Fig. 7b), which is slightly greater than on line 34. However, the biggest difference between the two lines is in the topography and structure of the forearc.

On line 36 a forearc high separates a narrow inner forearc from a broad outer forearc (Fig. 7b). The outer forearc slope has a stepped appearance, as it includes two gently arcward-dipping terraces. Across most of the outer forearc slope, a sediment apron that is 0.2–0.7 s TWT thick (*c.* 200–700 m) and has a chaotic seismic facies overlies a band of strong reflections. This band of reflections ends abruptly at SN 1610, 18 km west of the trench (Fig. 12). Between this point and the trench axis is the steepest part of the outer forearc slope, with an average seafloor dip of 6.6°. This part of the slope is the surface of a frontal prism that has a thickness of up to 2.5 s TWT (>2.5 km). The base of the frontal prism is constrained by a strong and fairly continuous reflection that can be traced for nearly 50 km from the trench beneath the outer forearc and has been interpreted as the top of subducted oceanic basement (Vanneste *et al.* 2002).

The frontal prism on line 36 has a chaotic seismic facies similar to that of the slope sediment apron, but distinct from the almost reflection-free material beneath the slope apron to the west (Fig. 12). The frontal prism appears to taper arcward beneath the material to its west. Only one extensive reflection is clearly imaged within the prism, dipping arcward from just below the seafloor at SN 1530 (Fig. 12). We interpret this reflection as a thrust fault. As on line 34, we interpret the scarcity of reflections beneath the toe of the outer forearc slope as indicating that extensive coherent structures, such as those imaged in frontal prisms where active sediment accretion is taking place (Westbrook *et al.* 1988; Moore *et al.* 1990; Bangs *et al.* 1996; Park *et al.* 2002), are rare here.

The eastern flank of the forearc high on line 36 is a 1200 m-high escarpment that exposes reflection-free forearc basement and stands above a 20 km-wide arcward-dipping terrace. The MCS data show that stratified sediments up to 1.3 s TWT thick (>1 km) lie beneath the terrace, and within these sediments there are upward transitions in reflection configurations from parallel with the top of basement, to arcward divergent, to parallel and horizontal (Fig. 7b). These reflection configurations indicate rotation of a 20 km-wide fault block underlying the terrace. The seismic data also reveal small normal faults that offset the seafloor near the trenchward edge of the terrace. To the east of the terrace, breaks in slope of the seafloor (at SN 2040) and of the base of the slope sediment apron (at SN 2020) coincide with the upward projection of a 20 km-long, trenchward-dipping, weak and discontinuous reflection (Fig. 7b), which we interpret as a low-angle detachment fault.

A sedimentary basin extends across most of the inner forearc on line 36, as on line 34 (Fig. 7). Once again, only the eastern edge of the basin appears to have been subject to structural disturbance, and a 100 m-high mound that has been interpreted as a mud volcano is situated above the westernmost fault (Vanneste *et al.* 2002). Shallow earthquake hypocentres (Engdahl *et al.* 1998) and focal mechanisms are consistent with the interpretation that the western limit of active faulting is near the eastern edge of the forearc basin (Vanneste *et al.* 2002).

The forearc basin on line 36 differs from the one on line 34 in that its maximum thickness is considerably greater and the seismic data do not suggest that any part of the basin has been subject to recent erosion. Velocity analyses on the MCS data, and wide-angle seismic data recorded on ocean-bottom seismometers, indicate that seismic interval velocities in the forearc basin sediments on line 36 increase from <2.0 km s^{-1} near the seafloor to >2.5 km s^{-1} at 1 km below seafloor (bsf) and to >4.0 km s^{-1} at 3 km bsf. The velocity data imply that the deepest clearly imaged reflection in the basin, at 2.85 s TWT bsf, is at a depth of >4 km bsf.

As on line 34, the MCS data on line 36 do not reveal a distinct western boundary to the forearc basin. Reflections become progressively less continuous westward until they disappear into a unit with chaotic seismic facies beneath the arc near Southern Thule. Another similarity is the presence of a sedimentary apron that is up to 1 s TWT thick (up to *c.* 1 km) on the western flank of the arc, although on line 36 it only extends to about 105 km west of the arc crest (Fig. 7b).

Line 36 crosses the middle of segment E8 of the ESR about 140 km west of the arc crest (Fig. 7b). Swath bathymetric data have shown that along most of its 90 km length, ridge segment E8 exhibits a median valley approximately 12 km wide with 300–800 m relief (Bruguier & Livermore 2001). However, a topographic high, offset towards the eastern wall, occurs within the valley where line 36 crosses it (SN 4350–4480).

The volcanic basement to the west of the ESR on line 36 exhibits a similar asymmetric topography to that observed on line 34, with parts of the basement surface that dip towards the ridge generally having steeper gradients than parts that dip away from the ridge (Fig. 7b). Sediment cover to the west of the ESR on line 36 is generally thinner and more unevenly distributed than on line 34. The thickest sediment cover on this part of line 36 is in the deepest trough (SN 5580–5610), and is about 0.5 s TWT (<500 m). However, the average sediment thickness between this trough and the western end of the line, over basement that ranges in age between 3.3 and 5.3 Ma, is <0.2 s TWT (<200 m).

Gravity modelling

Gravity data were collected on cruise JR18 using a LaCoste and Romberg marine gravity meter. Base ties at Port Stanley, Falkland Islands at the start and end of the 55 day-long cruise indicated an overall meter drift of only +0.13 mGal.

The gravity data collected along MCS lines 34 and 36 were modelled to constrain crustal thickness variations across the arc and forearc, and to estimate the density of the outer forearc crust. The objectives of modelling were not to determine precise or detailed crustal cross-sections, but to examine what constraints gravity data place on crustal thickness and outer forearc density. Two-dimensional gravity models were constructed for each line, starting with the bathymetry data that were collected along the MCS lines.

In any marine gravity model the largest contribution to local free-air gravity anomaly variations is from seafloor topography, which commonly represents a density contrast of >1 Mg m^{-3} (i.e. 10^6 g m^{-3}). Unless there are large variations in sediment thickness, the second largest contribution is usually from the base of the crust (the Moho), which typically represents a density contrast of approximately 0.4 Mg m^{-3}. Therefore, simple gravity models comprising only sea water, crust and mantle can provide a quick estimate of crustal thickness variations, assuming that no other significant density contrasts are present.

Jull & Kelemen (2001) recently calculated that some arc lower crust lithologies have densities similar to, or greater than, the underlying mantle at pressures >0.8 GPa and temperatures <800°C. Therefore, gravity models may be insensitive to arc lower crust at depths where the pressure is >0.8 GPa. However, for crust consisting mainly of basaltic and gabbroic lithologies, 0.8 GPa is equivalent to a depth of about 28 km. Our gravity modelling results indicate a maximum crustal thickness that is significantly less than this threshold, so it is unlikely that such ultra-high-density lower crust is present beneath the South Sandwich arc.

To obtain absolute crustal thickness estimates from simple gravity models of the kind described above it is necessary for the thickness of the crust to be known or assumed at one point within the model. In the models presented here (Figs 13 and 14) the initial assumption was that the crust on the South American Plate is normal oceanic crust with a thickness of 7 km. On the

Fig. 13. Gravity models for multichannel seismic line BAS967–34. For each model the calculated free-air anomaly profile is shown as a dashed line and the observed profile is shown as a solid line. The apparent thinning of subducted crust with increasing slab dip is an artefact of the 4.3: 1 vertical exaggeration. (**a**) Model assuming a uniform crustal density, a uniform mantle density, and that crust to the east of the trench and subducted crust have a constant thickness of 7 km. (**b**) Model assuming a uniform crustal density, and that crust to the east of the trench, subducted crust and back-arc crust all have a constant thickness of 7 km, but allowing different mantle densities either side of the subducted crust. (**c**) Model modified from that in (**b**) by the introduction of sediment bodies observed on a multichannel seismic line, adjustment of arc Moho to compensate for effect of sediments, and the introduction of additional intermediate-density bodies required to match the calculated anomaly to the observed anomaly over the outer forearc and trench. Inset shows detail of the outer forearc and trench part of model. (**d**) Model modified from that in (**c**) by extension of the base of model to 150 km depth, introduction of an eclogite layer in place of subducted crust below 60 km and adjustment of the mantle density beneath the back-arc and arc. Then Moho beneath arc and forearc was adjusted to compensate for other changes. Models in (**a**)–(**c**) continue 200 km to either end of the observed anomaly profile to minimize edge effects on the calculated profile. Model (**d**) continues 400 km to either end of the observed profile.

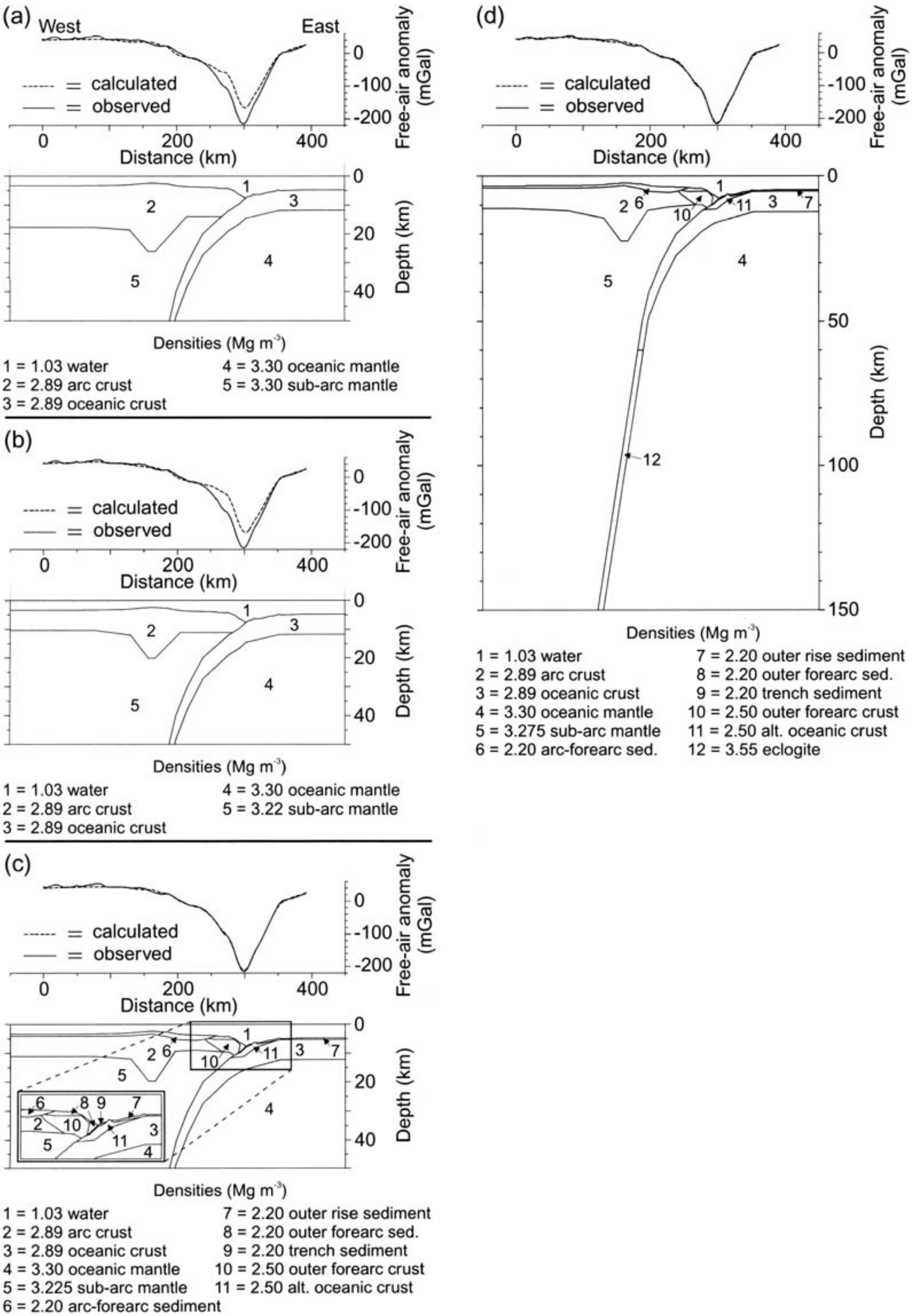
(a)
West
East
----- = calculated
—— = observed
Free-air anomaly (mGal)
Distance (km)
Depth (km)
Densities (Mg m⁻³)
1 = 1.03 water
2 = 2.89 arc crust
3 = 2.89 oceanic crust
4 = 3.30 oceanic mantle
5 = 3.30 sub-arc mantle
(b)
----- = calculated
—— = observed
Free-air anomaly (mGal)
Distance (km)
Depth (km)
Densities (Mg m⁻³)
1 = 1.03 water
2 = 2.89 arc crust
3 = 2.89 oceanic crust
4 = 3.30 oceanic mantle
5 = 3.22 sub-arc mantle
(c)
----- = calculated
—— = observed
Free-air anomaly (mGal)
Distance (km)
Depth (km)
Densities (Mg m⁻³)
1 = 1.03 water
2 = 2.89 arc crust
3 = 2.89 oceanic crust
4 = 3.30 oceanic mantle
5 = 3.225 sub-arc mantle
6 = 2.20 arc-forearc sediment
7 = 2.20 outer rise sediment
8 = 2.20 outer forearc sed.
9 = 2.20 trench sediment
10 = 2.50 outer forearc crust
11 = 2.50 alt. oceanic crust
(d)
----- = calculated
—— = observed
Free-air anomaly (mGal)
Distance (km)
Depth (km)
Densities (Mg m⁻³)
1 = 1.03 water
2 = 2.89 arc crust
3 = 2.89 oceanic crust
4 = 3.30 oceanic mantle
5 = 3.275 sub-arc mantle
6 = 2.20 arc-forearc sed.
7 = 2.20 outer rise sediment
8 = 2.20 outer forearc sed.
9 = 2.20 trench sediment
10 = 2.50 outer forearc crust
11 = 2.50 alt. oceanic crust
12 = 3.55 eclogite

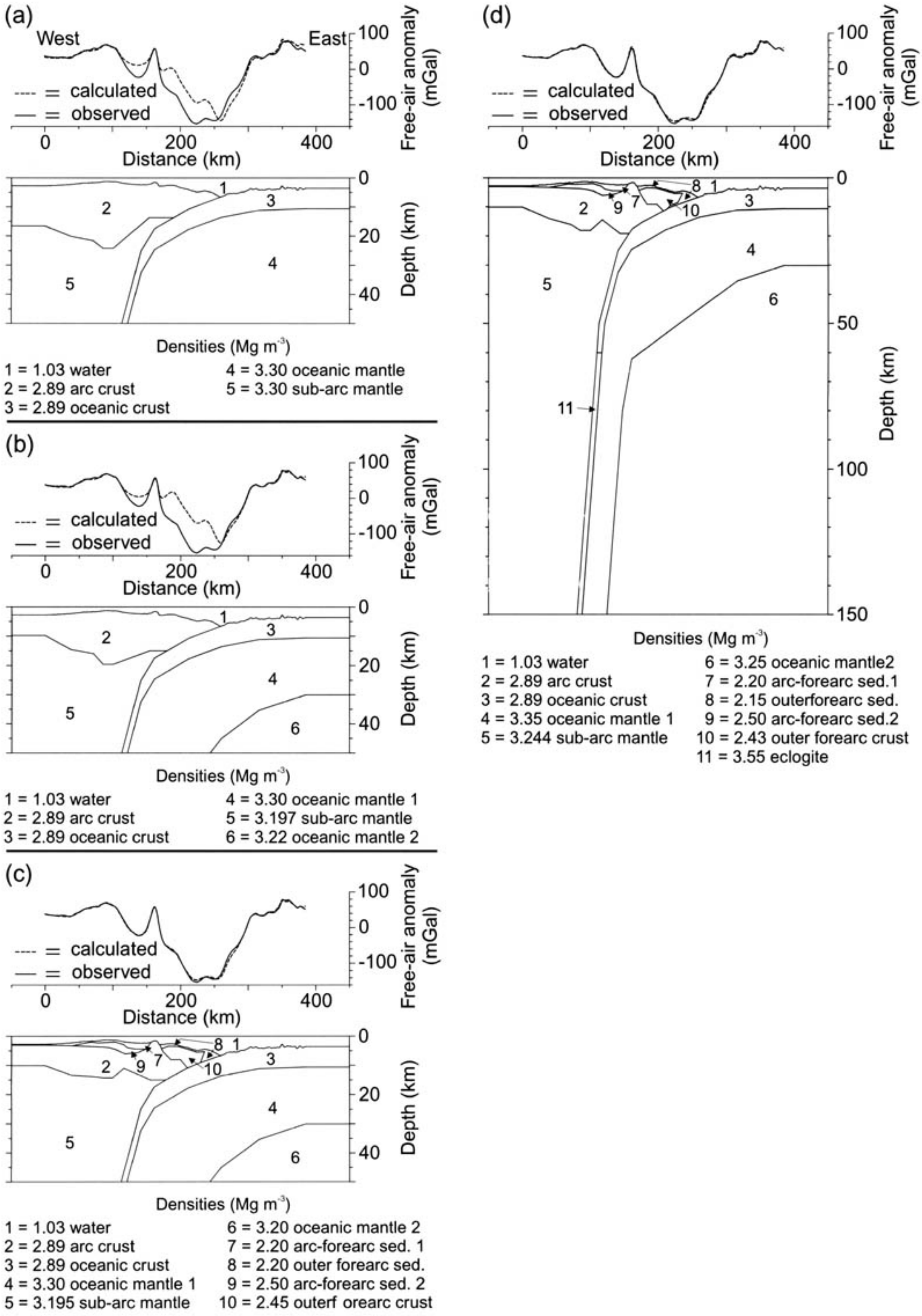

(a)
West
East
--- = calculated
— = observed
Free-air anomaly (mGal)
100
0
-100
0
200
400
Distance (km)
Depth (km)
0
20
40
1
2
3
4
5
Densities (Mg m^{-3})
1 = 1.03 water
2 = 2.89 arc crust
3 = 2.89 oceanic crust
4 = 3.30 oceanic mantle
5 = 3.30 sub-arc mantle
(b)
--- = calculated
— = observed
Free-air anomaly (mGal)
Distance (km)
Depth (km)
1
2
3
4
5
6
Densities (Mg m^{-3})
1 = 1.03 water
2 = 2.89 arc crust
3 = 2.89 oceanic crust
4 = 3.30 oceanic mantle 1
5 = 3.197 sub-arc mantle
6 = 3.22 oceanic mantle 2
(c)
--- = calculated
— = observed
Free-air anomaly (mGal)
Distance (km)
Depth (km)
1
2
3
4
5
6
7
8
9
10
Densities (Mg m^{-3})
1 = 1.03 water
2 = 2.89 arc crust
3 = 2.89 oceanic crust
4 = 3.30 oceanic mantle 1
5 = 3.195 sub-arc mantle
6 = 3.20 oceanic mantle 2
7 = 2.20 arc-forearc sed. 1
8 = 2.20 outer forearc sed.
9 = 2.50 arc-forearc sed. 2
10 = 2.45 outerf orearc crust
(d)
--- = calculated
— = observed
Free-air anomaly (mGal)
Distance (km)
Depth (km)
0
50
100
150
1
2
3
4
5
6
7
8
9
10
11
Densities (Mg m^{-3})
1 = 1.03 water
2 = 2.89 arc crust
3 = 2.89 oceanic crust
4 = 3.35 oceanic mantle 1
5 = 3.244 sub-arc mantle
6 = 3.25 oceanic mantle2
7 = 2.20 arc-forearc sed.1
8 = 2.15 outerforearc sed.
9 = 2.50 arc-forearc sed.2
10 = 2.43 outer forearc crust
11 = 3.55 eclogite

basis of a compilation of seismic refraction results, White *et al.* (1992) concluded that the igneous section of oceanic crust averages 7.1±0.8 km thick away from anomalous regions such as fracture zones and hot spots. Regional bathymetry data from the South American Plate to the east of the outer rise are generally in close agreement with depths predicted from oceanic age–depth relationships (Barker & Lawver 1988), suggesting that the crust in this area is of normal thickness.

On both lines 34 and 36 it was found that simple models of the type described above imply unrealistically thick back-arc crust, and cannot explain the full magnitude of the negative anomaly over the outer forearc and trench (Figs 13a and 14a). The models were extended 200 km from both ends of the modelled gravity profile to minimize edge effects. The position of the subducted oceanic crust was based on consideration of earthquake hypocentre locations (Engdahl *et al.* 1998; Vanneste *et al.* 2002; Livermore 2003). All of the crust in these models was assigned a density of 2.89 Mg m^{-3}, the average density of igneous oceanic crust estimated by Carlson & Raskin (1984). The average density of the arc crust and forearc crust is probably slightly lower than that of oceanic crust due to the presence of a larger proportion of lithologies with higher Si contents, and thick volcanic and volcaniclastic units. However, using lower densities for the arc and forearc crust would result in the modelled crust being thinner in these areas. Therefore, models including oceanic crustal density are used to examine the constraints gravity data place on maximum thickness of the crust. The mantle in the initial models was assigned a uniform density of 3.3 Mg m^{-3}, which approximates the average density of abyssal peridotite above 100 km-depth for an intermediate geothermal gradient (Christensen & Mooney 1995; Jull & Kelemen 2001).

On both lines the western limit of the modelled gravity data is over crust that formed at the ESR since 2 Ma. Line 36 crosses segment E8 of the ESR about 140 km west of the arc. A lone earthquake hypocentre at a depth of 273 km and located 20 km east of segment E8 (Engdahl *et al.* 1998) provides the only clue to the depth of the slab beneath this part of the ESR. At this distance from the volcanic front and this elevation above the slab, subduction-related processes probably have only a minor influence on magma supply to back-arc spreading ridges (Martinez & Taylor 2002, 2003). Line 34 crosses segment E5 of the ESR about 210 km west of the arc crest, and earthquake hypocentres suggest that the top of the slab has already reached a depth of 300 km more than 100 km to the east. Therefore, we consider it unlikely that subduction influence would have caused the crust produced recently at either of these segments to be thicker than normal oceanic crust.

Swath bathymetry data (Bruguier & Livermore 2001; Livermore 2003) show that the average depth over the flanks of the axial troughs on segments E5 and E8 is about 2.8 km. This is slightly deeper than the 2.5 km average for the world's mid-ocean ridges calculated by Parsons & Sclater (1977) and suggests that the young back-arc crust may, in fact, be slightly thinner than normal oceanic crust.

As it seems unlikely that the back-arc crust is thicker than normal oceanic crust, another pair of gravity models was produced in which the additional assumption was made that the back-arc crust is 7 km thick (Figs 13b and 14b). The observed regional anomaly trend was then matched by reducing the density of the mantle body beneath the back-arc and arc. In a similar

Fig. 14. Gravity models for multichannel seismic line BAS967–36. For each model the calculated free-air anomaly profile is shown as a dashed line and the observed profile is shown as a solid line. The apparent thinning of subducted crust with increasing slab dip is an artefact of the 4.3: 1 vertical exaggeration. (**a**) Model assuming a uniform crustal density, a uniform mantle density, and that crust to the east of the trench and subducted crust have a constant thickness of 7 km. (**b**) Model assuming a uniform crustal density, and that crust to the east of the trench, subducted crust and back-arc crust all have a constant thickness of 7 km, but allowing different mantle densities either side of the subducted crust. The mantle on the eastern side of the model is divided into two bodies to simulate the lateral density variation in young oceanic lithosphere that is the probable cause of the different calculated and observed anomaly gradients observed on this part of the model in (**a**). (**c**) Model modified from that in (**b**) by the introduction of sediment bodies observed on multichannel seismic line, adjustment of arc Moho to compensate for effect of sediments, and the introduction of additional intermediate-density bodies required to match the calculated anomaly to the observed anomaly over the outer forearc and trench. (**d**) Model modified from that in (**c**) by extension of the base of the model to 150 km depth, introduction of eclogite layer in place of subducted crust below 60 km and adjustment of mantle densities. Then the outer forearc structure and Moho beneath the arc were adjusted to compensate for other changes. Models in (**a**)–(**c**) continue 200 km to either end of the observed anomaly profile to minimize edge effects on the calculated profile. Model (**d**) continues 400 km to either end of the observed profile.

gravity modelling exercise on a profile across the Mariana arc, Sager (1980) also found that it was necessary to include a low-density mantle body beneath the back-arc in order to allow the overlying crust to have a normal thickness. Furthermore, Sager (1980) calculated that the required density anomaly depended on the depth chosen as the base of the anomalous mantle body, decreasing from –0.057 Mg m^{-3} for a body with its base at 100 km depth to –0.033 Mg m^{-3} for a body with its base at 200 km depth.

The base of most of the models presented here was fixed at a depth of 50 km, and it was found that mantle density anomalies of –0.078 (line 34) and –0.083 Mg m^{-3} (line 36) were required to match the regional anomaly trend. We recognize that these density anomalies are unrealistically high and have used them as a crude way of approximating a mass deficiency that probably extends to greater depth. The lower density contrast at the Moho beneath the arc results in the arc crust in the model being slightly thicker than it would be if a more normal mantle density was used and the regional anomaly trend was matched by adjusting the model in a different way (e.g. extending it to greater depth or increasing the density of the South American Plate mantle).

A model for line 34 extended to 150 km depth (Fig. 13d) requires a back-arc and arc mantle with a density anomaly of –0.025 Mg m^{-3}, which seems more realistic and is equivalent to an average temperature anomaly of about +300°C relative to the South American Plate mantle (using a volumetric coefficient of thermal expansion for peridotite of 2.4×10^{-5} K^{-1}). The back-arc and arc mantle density anomaly in a model for line 36 extended to 150 km depth (Fig. 14d) cannot be described so simply, as it was found to be necessary to divide the South American mantle into two bodies to simulate lateral density variation in the young oceanic lithosphere approaching the trench in this area. The extension of the models to greater depth required only minor changes to the crustal profile across the arc, so we consider that this justifies our approach of limiting initial models to a depth of 50 km for preliminary estimation of crustal thickness variations. The deeper models were also extended an additional 200 km from both ends of the modelled gravity profile to minimize edge effects (i.e. 400 km from each end in total). The changes to the crustal profiles after extending the models to 150 km depth were mainly due to the inclusion of an eclogite layer at the top of the subducted slab rather than to the depth extension itself.

The simple gravity models considered thus far do not take account of the effect of sediment bodies. Insertion of a sediment body into these models introduces a mass deficit that requires adjustment of the underlying Moho to shallower depth to maintain the same calculated anomaly. Therefore, the models without sediments (Figs 13b and 14b) constrain the maximum possible crustal thickness, subject to the assumptions described above.

A third pair of gravity models was produced including sediment bodies observed on the MCS lines (Figs 13c and 14c). Our aim was still to use these models to constrain the maximum possible crustal thickness beneath the arc and forearc, and for this reason sediment bodies extending to a depth of <2 km below seafloor were all assigned the relatively high density of 2.2 Mg m^{-3}. This density is equivalent to a seismic velocity of 2.5–3.0 km s^{-1} according to the velocity–density relationships of Ludwig *et al.* (1970) and Gardner *et al.* (1974), which is quite a high average velocity for the upper 2 km of deep ocean sedimentary successions (Hamilton 1979; Carlson *et al.* 1986). More deeply buried inner forearc basin sediments on line 36 were assigned a density of 2.5 Mg m^{-3}, which is equivalent to a seismic velocity of 4.3–4.8 km s^{-1} according to the above relationships. We also used this pair of models to investigate what average density of outer forearc crust was required to account for the large negative anomaly over the outer forearc on each line (Figs 13c and 14c).

Travel-time inversion of wide-angle seismic data recorded on ocean-bottom seismometers will provide additional constraints on, and more detailed models of, crustal structure for both profiles. The results of this work will be published in separate papers. However, preliminary results for line 36 are consistent with the gravity modelling results described below.

Line BAS967-34

The total range of free-air anomalies observed along line 34 is >260 mGal. An interesting characteristic of the observed profile along this line is that there is no peak in free-air anomaly associated with the topography of the arc, which suggests that the topography is perfectly compensated by a crustal root. However, this line crosses the deepest saddle in the arc, and regional free-air anomaly maps show large positive free-air anomalies centred on each of the South Sandwich Islands (Livermore *et al.* 1994; Vanneste & Larter 2002).

Gravity and bathymetry data along line 34 used in two-dimensional gravity modelling were projected on to a line trending 085°. As this direction is nearly perpendicular to both the trench and the arc we consider that errors related to the two-dimensional assumption will be insignificant on this line. Our initial model for line 34, based on the assumptions that the crust on the South American Plate is 7 km thick and the mantle density is uniform, shows the Moho beneath the crest of the arc at a depth of 26.1 km (Fig. 13a). As the seafloor depth over the crest of the arc on this line is 2.4 km, the thickness of arc crust in the model is 23.7 km. However, the back-arc crust in the same model is 14.4 km thick, which seems implausible for reasons outlined above. When the additional assumption was made that the back-arc crust is 7 km thick and the density of the underlying mantle was reduced to match the regional anomaly trend, the modelled crustal thickness beneath the arc decreased to 17.7 km (Fig. 13b). Inclusion of sediments observed on the MCS line in the model resulted in the thickness of the arc crust, including the sediment thickness, being reduced further to 17.3 km (Fig. 13c).

One surprising feature of the model in Figure 13c is that it shows the forearc crust as being even thinner than normal oceanic crust. This is probably a consequence of the fact that a uniform density has been used for the entire mantle to the west of the subducting crust. In reality there will be a gradient of increasing mantle density towards the slab due to its cooling effect. Furthermore, the mantle directly beneath the forearc is probably cooler and denser than most of the mantle wedge because it is most distant from the main flux of the corner flow that is predicted to take place above subducting slabs (Davies & Stevenson 1991; Winder & Peacock 2001). Assuming that a denser mantle beneath the forearc would result in a greater modelled thickness of crust in this area.

The main difficulty encountered in extending subduction-zone gravity models to greater depth is how to represent the transformation of igneous oceanic crust to eclogite. This change is thought to take place at a depth between 40 and 80 km, the precise depth probably being dependent on temperature and water pressure (Ahrens & Schubert 1975; Anderson *et al.* 1976; Delany & Helgeson 1978). In the model shown in Figure 13d this boundary was placed at a depth of 60 km and a density of 3.55 Mg m^{-3} was assigned to the eclogite layer. Before the eclogite body was added, extending of the model to 150 km depth and increasing the mantle density beneath the arc and back-arc had resulted in a decrease in calculated anomaly over the arc, relative to the back-arc, by about 20 mGal. Inserting the eclogite body contributed an additional, broad positive anomaly approximately centred on the arc with amplitude about 55 mGal. Thus, the net effect of extending the model to 150 km depth was a positive residual anomaly of about +35 mGal centred over the arc. In the model shown in Figure 13d, the thickness of the arc crust was increased to eliminate this residual anomaly. The crust beneath the crest of the arc was increased in thickness by 2.7 km to 20.0 km, and the thickness of the crust on both flanks of the arc was increased by smaller amounts. In view of the fact that the densities used for both average arc crust and sediments are towards the high end of the acceptable range, we consider that this model constrains the crustal thickness beneath the crest of the arc on line 34 to be no greater than 20 km.

The effect of the transformation of igneous oceanic crust to eclogite has probably been slightly overestimated in the modelling exercise described above, because no reduction in the thickness of the layer of subducted crust was made to allow for the >20% increase in density. The effect of this overestimation will be to bias the model further towards including thicker arc crust. In reality an eclogite layer may persist deeper than 150 km, but extending the model to greater depth would have very little effect on the crustal section because any density contrast at such great depth would produce a very long wavelength anomaly.

The top of the slab in Figure 13d is at a depth of 90 km beneath the crest of the arc. An alternative model with an increased slab dip was produced, so that the top of the slab was at 110 km depth beneath the arc. This change produced a residual anomaly of about –15 mGal centred over the western flank of the arc. It was found that this residual anomaly could be eliminated by reducing the thickness of the crust on the western flank of the arc by about 1 km, and without any change to the Moho beneath the crest of the arc.

In modifying the model in Figure 13b to produce the model in Figure 13c, the outer forearc material above the reflection at 6.8 s TWT (Fig. 9) was interpreted as sediment and assigned a density of 2.2 Mg m^{-3}. The thin layer of sediment over the steepest part of the slope and a small frontal prism were included in a continuation of this body towards the trench. Even after introduction of this body there remained a substantial positive residual anomaly over the lower forearc and trench. We found that the residual anomaly over the outer forearc could be accounted for by reducing the density of the main part of the outer forearc crust to 2.5

$Mg\ m^{-3}$. However, it was not possible to account for the entire residual anomaly over the trench, and the fact that the calculated anomaly over the eastern flank of the trench has a lower gradient than the observed anomaly, by changes to the outer forearc alone. This problem was not apparent in a gravity model for a nearby profile presented by Vanneste & Larter (2002) because that profile only extended about 25 km east of the trench.

Sager (1980) observed a similar kind of discrepancy on a profile across the Mariana Trench and arbitrarily reduced the crustal thickness beneath the outer rise to make the calculated and observed anomalies match over that part of the profile. In our model we found it would be necessary to make the crustal thickness between the outer rise and the trench differ by more than 6 km if the difference in calculated and observed anomaly was to be explained by this means alone. Instead, we chose to keep the thickness of the oceanic crust constant in the models in Figure 13c and d, and accounted for the difference by introducing a new body with a lower density in the upper part of the crust. It was found to be possible to account for the observed anomaly by making this body 2.5 km thick beneath the trench and reducing its density to 2.5 $Mg\ m^{-3}$.

Line BAS967-36

The total range of free-air anomalies observed along line 36 is 230 mGal. This range is smaller than on line 34 mainly because the trench is shallower. On this line, which passes close to Southern Thule, there is a free-air anomaly high over the crest of the arc with amplitude +30 mGal relative to the back-arc basin. An interesting characteristic of the observed profile along this line is that the deepest negative anomaly lies about 35 km west of the trench axis, suggesting the presence of a large mass deficit beneath the outer forearc.

Gravity and bathymetry data along line 36 used in two-dimensional gravity modelling were projected on to a line trending 105° . This direction is nearly perpendicular to the trench and forearc high, but the strike of the arc is about 25° clockwise from perpendicular to the projected line. As a result, the positive anomaly associated with the arc will be broader along the projected profile than it would be if the arc were perpendicular to the line. The effect of this on the two-dimensional gravity models in Figure 14 will be to smooth out the Moho relief beneath the arc, with the modelled crust being fractionally too thin beneath the crest of the arc and too thick beneath the flanks of the arc. However, a three-dimensional effect that is probably more significant is the large positive free-air anomaly centred on Southern Thule. The peak of the anomaly is >120 mGal relative to the back-arc region (see fig. 2 in Vanneste & Larter 2002), and line 36 approaches within 12 km of this island group (Fig. 1), cutting across the distal part of the anomaly. The effect of this on the models in Figure 14 will be to make the modelled arc crust slightly too thin, as additional shallow subarc mantle is required to simulate the gravity effect of a mass that is out of the plane of the section. However, even if the entire +30 mGal anomaly over the arc, relative to the back-arc basin, were an out-of-plane effect, the amount by which the models in Figure 14 underestimate the thickness of the arc crust would be <2.5 km.

Our simplest model for line 36, based on the assumptions described above, shows the Moho beneath the crest of the arc at a depth of 24.2 km (Fig. 14a). As the seafloor depth over the crest of the arc on this line is 1.3 km, this is a crustal thickness of 22.9 km. However, once again, the back-arc crust in this model is implausibly thick (13.9 km). When the additional assumption was made that the back-arc crust is 7 km thick and the density of the underlying mantle was reduced to match the regional anomaly trend, the modelled crustal thickness beneath the arc decreased to 18.3 km (Fig. 14b).

An additional change in the model shown in Figure 14b is that the mantle to the east of the trench has been divided into two bodies. This change was made in order to match the observed free-air anomaly gradient on the eastern flank of the trench, which is less steep than the calculated anomaly in Figure 14a. We suspect that this discrepancy is a consequence of lateral density variation being significant in the young oceanic lithosphere approaching the trench here. This variation was simulated by dividing the mantle into two bodies along a boundary that lies approximately along the 1000°C isotherm predicted by a cooling-plate model (Parsons & Sclater 1977).

Inclusion of sediments observed on the MCS line in the model resulted in the thickness of the crust beneath the crest of the arc, including the sediment thickness, being reduced to 13.0 km (Fig. 14c). In this model the body representing the deeper part of the forearc basin (body 9 in Fig. 14c) was continued across the crest of the arc. The MCS data do not show a distinct western boundary to the basin, and if the body was terminated east of the arc crest then even more extreme Moho topography than that in Figure 14c would be needed to cancel out the gravity effect from such a boundary. The thin (<200 m) and patchy sediments on the outer rise were not included in the model as their effect would be insignificant.

In modifying the model in Figure 14b to produce the model in Figure 14c, the stratified sediments on top of the large fault block, the outer slope sediments and the frontal prism observed on the MCS data were represented by a single body with a density of 2.2 Mg m^{-3} (body 8). Even after introduction of this body there remained a substantial positive residual anomaly over the lower forearc and trench. We found that the residual anomaly over the outer forearc could be accounted for by reducing the density of the main part of the outer forearc crust to 2.45 Mg m^{-3}.

A model for line 36 extended to 150 km depth, and with the subducted oceanic crust below 60 km depth replaced by eclogite, is shown in Figure 14d. The two-layer South American mantle used in the 50 km-depth models (Fig. 14b, c) to simulate lateral density variation in the young oceanic lithosphere presented an additional difficulty when increasing the basal depth of the model. An unrealistically low density (3.2 Mg m^{-3}) had been used for the deeper of the two mantle bodies as a crude way of approximating a density contrast that extends to greater depth. Simply extending this body to 150 km depth would add a large volume of mantle with an unrealistically low density to the eastern end of the model. Instead, the density of this body was increased to 3.25 Mg m^{-3} and that of the shallower mantle body was increased to 3.35 Mg m^{-3}, thus preserving the density contrast between them. After making these changes and extending the model to 150 km depth it was found necessary to increase the density of the mantle body beneath the back-arc and arc to 3.244 Mg m^{-3} to match the observed regional anomaly trend.

Extending of the model to 150 km depth and increasing the mantle densities as described above resulted in a decrease in calculated anomaly over the arc, relative to the back-arc, by about 15 mGal. Inserting the eclogite body contributed an additional, broad positive anomaly approximately centred on the arc with amplitude about 60 mGal. Thus, the net effect of extending the model to 150 km depth was a positive residual anomaly of about +45 mGal centred over the arc. In the model shown in Figure 14d, the thickness of the arc crust was increased and some changes were made to the outer forearc structure to eliminate this residual anomaly. The crust beneath the crest of the arc was increased in thickness by 3.7 km to 16.7 km, and the thickness of the crust on both flanks of the arc was increased by smaller amounts. As explained above, non-two-dimensional effects resulting from the proximity of the line to Southern Thule could mean the arc crust is up to 2.5 km thicker than this. Therefore, in view of the fact that the densities used for both average arc crust and sediments are towards the high end of the acceptable range and, as explained previously, the effect of the transformation of igneous oceanic crust to eclogite has probably been slightly overestimated, we consider that this model constrains the crustal thickness beneath the crest of the arc on line 36 to be no greater than 19.2 km. This is consistent with preliminary results from modelling wide-angle seismic data recorded along this line, which have been interpreted as indicating a maximum crustal thickness of 15 km beneath the arc crest (Larter *et al.* 2001).

Discussion

Detailed analysis of marine magnetic profiles confirms that organized back-arc spreading in the East Scotia Sea started at least 15 Ma ago, making it the world's longest-lived extant back-arc basin. The back-arc spreading ridge 15 Ma ago was already more than 350 km long (Fig. 1), and spreading has continued to the present day without any detectable ridge jumps. The stability of this spreading regime has probably been facilitated by the stability of motions of the surrounding major plates during this period (Barker & Lawver 1988). The fact that the South Sandwich subduction system has not interacted with any other subduction systems, or encountered features such as aseismic ridges or oceanic plateaux, has probably also been important in contributing to the longevity of the back-arc spreading regime.

The cause for the start of East Scotia Sea extension may have been a change in the direction of South American–Antarctic relative motion, from 120°–300° to the present E–W direction, at about 20 Ma (Barker & Lawver 1988). Drilling results from the western flank of the Lau Basin have been interpreted as evidence of a period of asymmetrical arc rifting that predated organized seafloor spreading (Parson & Hawkins 1994), and extension in the East Scotia Sea may have started in a similar way between 20 and 15 Ma ago. Such asymmetrical arc rifting appears to be taking place at the present day in the northern Mariana Trough (Martinez *et al.* 1995; Baker *et al.* 1996) and the Havre Trough (Parson & Wright 1996; Wright *et al.* 1996), and it has been suggested that magnetic lineations may be developed even in this rifting phase by systematic migration of zones of magmatism across the rift zone (Martinez *et al.* 1995). Arc rifting is therefore a possible explanation for the origin of the crust with unidentified linear magnetic anomalies that lies between about 35° and 37°W, west of anomaly 5B, in the East Scotia Sea (Fig. 5).

Magnetic anomalies in the eastern part of East Scotia Sea indicate that the central part of the South Sandwich arc is built on crust that was formed at the back-arc spreading ridge about 10 Ma ago. The northernmost and southernmost arc islands are situated on even younger back-arc crust. Therefore, no part of the present arc could have existed when organized back-arc spreading began. It is thought that back-arc spreading is usually initiated close to the line of a pre-existing arc (Karig 1971; Taylor & Karner 1983; Taylor 1992). In some cases initial rifting occurs on the forearc side of the volcanic front (Cole *et al.* 1990; Taylor 1992). The only bathymetric highs along the western edge of the East Scotia Sea that might represent substantial remnant arc volcanic edifices are two circular highs about 150 km south of South Georgia (Fig. 1). Hence, if there was a pre-existing arc, it seems likely that initial rifting was on the back-arc side along most of its length.

If back-arc extension was symmetrical following a transition from arc rifting to organized spreading about 15 Ma ago (chron 5B), then the early spreading rates we have measured imply that crust originally formed at the ESR extends about 80 km east of the central part of the present arc. Even if spreading between 15 and 10 Ma ago was highly asymmetrical, with the rate on the eastern flank of the ESR only half of that on the western flank, crust formed on the eastern flank 15 Ma ago must lie more than 40 km east of the central part of the present arc. Any pre-existing arc must have been even farther east relative to the Sandwich Plate. Analyses of peridotites dredged from the trench-slope break 75–85 km ENE of Zavodovski Island suggest that there was indeed a pre-existing arc in such a position. The peridoites have geochemical characteristics that demonstrate they originated as the residue from melting at a ridge, probably the early ESR, and were subsequently modified by interaction with South Sandwich arc magmas (Pearce *et al.* 2000).

The present arc–trench gap of 140–160 km is one of the narrowest among modern subduction systems, so if the pre-existing arc was situated more than 40–80 km east of the present arc it seems likely that a substantial part of the earlier forearc has been removed by subduction erosion. Even if there was no pre-existing arc, it seems improbable that a 350 km-long back-arc spreading ridge could have developed only about 100 km from the trench, so once again substantial subduction erosion is implied. If it is assumed that the arc has retreated by 80 km and that the pre-existing forearc was as wide as the modern forearc, then the average rate of forearc slope retreat over 15 Ma has been 5.3 km Ma^{-1}. However, if arc–trench gaps tend to increase with time, as proposed by Dickinson (1973) and Jarrard (1986), then the average rate of forearc slope retreat could have been somewhat slower than the rate calculated by assuming that the slope retreated as far as the arc has (Vanneste & Larter 2002).

Subduction erosion provides a possible explanation for the absence of relict volcanic edifices of the supposed pre-existing arc from the modern forearc. Forearc slope retreat, and steepening of the forearc slope as a result of basal subduction erosion (Clift & MacLeod 1999), may have made such edifices gravitationally unstable so that they collapsed towards the trench. The only large bathymetric and gravity high that lies far enough east in the forearc for it to possibly represent a relict arc volcano is between 58°30′ and 59°S (Fig. 1). The peak of this high is close to where 15 Ma-old back-arc crust would be predicted to lie if back-arc spreading between 15 and 10 Ma was symmetrical, and within 40 km of the edge of such old back-arc crust even if the ratio of west:east asymmetry in spreading rate at the ESR is assumed to have been 2: 1 during this interval. Dredges from the eastern slope of the high yielded calc-alkaline basalts, basaltic andestites and andesites, and K/Ar ages determined on three samples range from 28.5 to 32.8 Ma (Barker 1995). Such old ages close to where back-arc spreading started about 15 Ma ago are surprising, and results from Ar/Ar dating are awaited with interest. However, a possible interpretation based on the published ages is that these dredged samples represent the exhumed deeper parts of a pre-existing arc volcano that had grown in this position over about 15 Ma prior to the start of East Scotia Sea spreading. If Ar/Ar dating confirms the published ages, then these dredges constrain the maximum extent of old back-arc crust beneath the inner forearc. The present elevation of the high is probably related to more recent tectonic processes, similar to those responsible for the uplift of the forearc high observed on line 36 (Vanneste *et al.* 2002), and this may have promoted erosion of the younger parts of a pre-existing volcanic succession.

If a pre-existing arc migrated gradually to the position of the modern arc as a consequence of subduction erosion, it might be expected that relict volcanic edifices would be found on the modern inner forearc. Vanneste & Larter (2002) suggested such edifices could have formed and subsequently been removed as part of a cyclic process of accumulation and denudation on the inner forearc. An alternative possibility is that the arc moved to its present position in a single jump, as appears to have happened in the northern Lesser Antilles during the Miocene (Westbrook & McCann 1986).

If the northern part of the South Sandwich arc moved to its present position in a single jump, this may partly explain why the forearc crust on line 34 is so thin. As already noted, the forearc crust on line 34 is probably not as thin as shown in Figure 13c and d, because these gravity models do not take into account lateral density variation in the mantle wedge. However, Figure 13a shows that, even using the most extreme assumptions, the forearc crust on this line cannot be much thicker than normal oceanic crust. If the arc migrated gradually to its present position, then either the arc magma supply was small prior to 10 Ma or the forearc crust has been thinned by extension. Recent trench-normal extension in this area appears to be restricted to the outer forearc (Vanneste & Larter 2002), but this does not preclude the possibility that the inner forearc may have been extended at an earlier stage in the history of the arc.

The crust on the western side of the back-arc basin that we interpret as being conjugate to the inner forearc basement on this line is anomalously elevated, which suggests that it is thicker than normal back-arc crust (profiles D–D′, E–E′ and F–F′ in Fig. 3). Therefore, the constraint on thickness of the inner forearc crust derived from gravity modelling is evidence in favour of the inner forearc in this area having been extended earlier in the history of the arc. Vanneste & Larter (2002) suggested that the lack of extensional strain indicators in the inner forearc and arc at the present day may be a consequence of the fact that the East Scotia Sea is a mature back-arc basin, and therefore is expected to contribute a substantial ridge-push force to the stress balance. On this basis, extension induced by subduction erosion near the trench might be expected to have affected a wider area of the forearc during earlier stages of development of the East Scotia Sea. Another possible cause of forearc extension distant from the trench is basal subduction erosion, which can cause mid-forearc subsidence and basin formation (e.g. Laursen *et al.* 2002).

The excess volume of the arc crust in Figure 13d compared to normal, 7 km-thick, oceanic crust is about 720 km^3 km^{-1} along the arc. If this volume has all been added since a jump in the locus of arc magmatism about 10 Ma ago, it represents an arc growth rate of 72 km^3 Ma^{-1} for each km along the arc. This rate is similar to the rates estimated for the Aleutian and Izu–Bonin arcs by Holbrook *et al.* (1999) based on travel-time inversion of wide-angle seismic data. It should be remembered that the gravity models presented here were constructed based on assumptions designed to constrain the maximum thickness of the crust. Nevertheless, any over-estimation of crustal thickness must be offset against the fact that the modelled section crosses the deepest saddle in the arc and therefore does not include representation of the volume of the volcanic edifices around the arc islands, or any three-dimensional crustal root associated with them. Moreover, the errors resulting from these factors are probably small compared to the overall uncertainties in estimates of arc growth rates, so it is interesting that Figure 13d suggests a growth rate within the range calculated for arcs that have been built over a much longer interval.

The gravity models shown in Figure 14c and d suggest that the crust beneath the forearc high on line 36 is of similar thickness to the arc crust on the same line. Assuming symmetrical spreading during the early stages of back-arc opening, we estimate that the crust beneath the forearc high on line 36 has an age of $\leq$12.5 Ma (chron 5Ar.1r). In view of the age and thickness of the crust beneath the forearc high, it seems possible that the arc front could have been located in this area before moving to its present position. However, the structural setting of the forearc high suggests that its present elevation results from flexural footwall uplift related to trench-normal extension in the outer forearc (Vanneste *et al.* 2002), so we do not consider the high to be simply the eroded root of a former volcanic edifice.

The nature of the intermediate-density bodies (2.43–2.5 Mg m^{-3}) inferred to form the bulk of the outer forearc crust is uncertain. These densities are too high for the material to be recently accreted ocean-floor sediments. Furthermore, travel-time inversion of wide-angle seismic data indicates a P-wave velocity of 5.1±0.2 km s^{-1} for the eastern part of the intermediate-density body on line 36 (N.J. Bruguier pers. comm. 2001). However, the estimated densities are also considerably lower than the average density of the oceanic crust as a whole (2.89 Mg^{-3}), and lower even than estimates of the average density of layer 2 of the oceanic crust (in the range

2.64–2.86 Mg m^{-3}; Carlson & Raskin 1984). We speculate that these bodies represent igneous crust that has been pervasively fractured and hydrated. The same explanation may also apply to the intermediate-density body that occupies the upper part of the oceanic crust beneath the trench in the models in Figure 13c and d. Faulting resulting from flexure of the oceanic lithosphere as it approaches the trench may allow water to penetrate deep into the crust and oceanic mantle (Peacock 2001).

Conclusions

Analysis of magnetic data from the western part East Scotia Sea confirms that the present regime of organized back-arc spreading has been active since at least 15 Ma ago. Extension may have been initiated as a result of a change in direction of South American–Antarctic relative motion about 20 Ma ago. On the eastern side of the East Scotia Sea, crust formed at the ESR forms the basement underlying the South Sandwich arc and inner forearc.

Samples dredged from the forearc provide indications of a previous arc that existed before the start of spreading in the East Scotia Sea and was located more than 80 km east of the modern arc on the Sandwich Plate. The proximity of this former arc to the modern trench suggests that substantial subduction erosion has taken place, with the forearc slope retreat rate perhaps being as high as 5.3 km Ma^{-1}.

Gravity models constrained by MCS reflection data indicate that the crust beneath the northern forearc cannot be much thicker than normal oceanic crust. This may indicate that the northern part of the arc moved to its present position in a single jump at some time since 10 Ma, rather than migrating gradually. However, alternative explanations for the thin forearc crust are also possible. If it is assumed that the northern part of the present arc has developed since a jump in the locus of arc magmatism 10 Ma ago, the volume of arc crust in the gravity models represents an arc growth rate of 72 km^3 Ma^{-1} km^{-1}, which is within the range of growth rates estimated for the Aleutian and Izu-Bonin arcs (Holbrook *et al.* 1999). Models for a line across the southernmost part of the forearc indicate that the mid-forearc crust there is of similar thickness to the arc crust, making a stepwise migration of the arc front more plausible in this area. The gravity models indicate that intermediate-density bodies (2.43–2.5 Mg m^{-3}) constitute the bulk of the outer forearc crust in both areas, perhaps representing igneous crust that has been pervasively fractured and hydrated.

We thank everyone who participated in the many cruises over the past 33 years from which we have used magnetic and bathymetry data. In particular we thank all those who sailed with us on RRS *James Clark Ross* cruises JR09a (1995) and JR18 (1997). We are grateful to Fernando Martinez, David Scholl and Tim Minshull for constructive reviews.

References

AHRENS, T.J. & SCHUBERT, G. 1975. Gabbro-eclogite reaction rate and its geophysical significance. *Reviews of Geophysics and Space Physics*, **13**, 383–400.

ANDERSON, R.N., UYEDA, S. & AKIHO, M. 1976. Geophyscial and geochemical constraints at converging plate boundaries – part 1: dehydration in the downgoing slab. *Geophysical Journal of the Royal Astronomical Society*, **44**, 333–357.

BAKER, N., FRYER, P., MARTINEZ, F. & YAMAZAKI, T. 1996. Rifting history of the northern Mariana trough: SeaMARC II and seismic reflection surveys. *Journal of Geophysical Research*, **101**, 11 427–11 455.

BANGS, N.L., SHIPLEY, T.H. & MOORE, G.F. 1996. Elevated fluid pressure and fault zone dilation inferred from seismic models of the northern Barbados Ridge decollement. *Journal of Geophysical Research*, **101**, 627–642.

BARKER, P.F. 1970. Plate tectonics of the Scotia Sea region. *Nature*, **228**, 1293–1296.

BARKER, P.F. 1972. A spreading centre in the East Scotia Sea. *Earth and Planetary Science Letters*, **15**, 123–132.

BARKER, P.F. 1979. The history of ridge-crest offset at the Falkland–Agulhas Fracture Zone from a small-circle geophysical profile. *Geophysical Journal of the Royal Astronomical Society*, **59**, 131–145.

BARKER, P.F. 1995. Tectonic framework of the East Scotia Sea. *In*: TAYLOR, B. (ed.) *Backarc Basins: Tectonics and Magmatism*. Plenum, New York, 281–314.

BARKER, P.F. & HILL, I.A. 1981. Back-arc extension in the Scotia Sea. *Philosophical Transactions of the Royal Society of London*, **A 300**, 249–262.

BARKER, P.F. & LAWVER, L.A. 1988. South American–Antarctic plate motion over the past 50 Myr, and the evolution of the South American–Antarctic ridge. *Geophysical Journal International*, **94**, 377–386.

BARKER, P.F., BARBER, P.L. & KING, E.C. 1984. An early Miocene ridge crest–trench collision on the South Scotia Ridge near 36°W. *Tectonophysics*, **102**, 315–332.

BARTON, C.E. 1996. Revision of the International Geomagnetic Reference Field released. World Wide Web address: http://www.agu.org/eos_elec/95242e.html

BRUGUIER, N.J. & LIVERMORE, R.A. 2001. Enhanced magma supply at the southern East Scotia Ridge: evidence for mantle flow around the subducting slab? *Earth and Planetary Science Letters*, **191**, 129–144.

CANDE, S.C. & KENT, D.V. 1995. Revised calibration of the geomagnetic polarity timescale for the Late Cretaceous and Cenozoic. *Journal of Geophysical Research*, **100**, 6093–6095.

CARLSON, R.L. & RASKIN, G.S. 1984. Density of the ocean crust. *Nature*, **311**, 555–558.

CARLSON, R.L., GANGI, A.F. & SNOW, K.R. 1986. Empirical reflection travel time versus depth and velocity versus depth functions for the deep sea sediment column. *Journal of Geophysical Research*, **91**, 8249–8266.

CHRISTENSEN, N.I. & MOONEY, W.D. 1995. Seismic velocity structure and composition of the continental crust: a global view. *Journal of Geophysical Research*, **100**, 9761–9788.

CLIFT, P.D. & MACLEOD, C.J. 1999. Slow rates of subduction erosion estimated from subsidence and tilting of the Tonga forearc. *Geology*, **27**, 411–414.

COLE, J.W., GRAHAM, I.J. & GIBSON, I.L. 1990. Magmatic evolution of late Cenozoic volcanic rocks of the Lau Ridge, Fiji. *Contributions to Mineralogy and Petrology*, **104**, 540–554.

DAVIES, J.H. & STEVENSON, D.J. 1992. Physical model of source region of subduction zone volcanics. *Journal of Geophysical Research*, **97**, 2037–2070.

DAVIS, D., SUPPE, J. & DAHLEN, F.A. 1983. Mechanics of fold-and-thrust belts and accretionary wedges. *Journal of Geophysical Research*, **88**, 1153–1172.

DELANY, J.M. & HELGESON, H.C. 1978. Calculation of the thermodynamic consequences of dehydration in subducting ocean crust to 100 kb and >800°C. *American Journal of Science*, **278**, 638–686.

DICKINSON, W.R. 1973. Widths of modern arc–trench gaps proportional to past duration of igneous activity in associated magmatic arcs. *Journal of Geophysical Research*, **78**, 3376–3389.

ENGDAHL, R.E., VAN DER HILST, R. & BULAND, R. 1998. Global teleseismic earthquake relocation with improved travel times and procedures for depth determination. *Bulletin of the Seismological Society of America*, **88**, 722–743.

GARDNER, G.H.F., GARDNER, L.W. & GREGORY, A.R. 1974. Formation velocity and density: the diagnostic basics for stratigraphic traps. *Geophysics*, **39**, 770–780.

HAMILTON, E.L. 1979. Sound velocity gradients in marine sediments. *Journal of the Acoustical Society of America*, **65**, 909–922.

HAMILTON, I.W. 1989. *Geophysical investigations of subduction-related processes in the Scotia Sea*. PhD Thesis, University of Birmingham, UK.

HOLBROOK, W.S., LIZARRALDE, D., MCGEARY, S., BANGS, N. & DIEBOLD, J. 1999. Structure and composition of the Aleutian island arc and implications for continental crustal growth. *Geology*, **27**, 31–34.

JARRARD, R.D. 1986. Relations among subduction parameters. *Reviews of Geophysics*, **24**, 217–284.

JULL, M. & KELEMEN, P.B. 2001. On the conditions for lower crustal convective instability. *Journal of Geophysical Research*, **106**, 6423–6446.

KARIG, D.E. 1971. Origin and development of marginal basins in the western Pacific. *Journal of Geophysical Research*, **76**, 2542–2561.

LALLEMAND, S.E., SCHNÜRLE, P. & MALAVIEILLE, J. 1994. Coulomb theory applied to accretionary and nonaccretionary wedges: possible causes for tectonic erosion and/or frontal accretion. *Journal of Geophysical Research*, **99**, 12 033–12 055.

LARTER, R.D., BRUGUIER, N.J. & VANNESTE, L.E. 2001. Structure, composition and evolution of the South Sandwich island arc: implications for rates of arc magmatic growth and subduction erosion. *Eos, Transactions, American Geophyscial Union*, **82**(47), Fall Meeting Supplement, T32D-10.

LARTER, R.D., KING, E.C., LEAT, P.T., READING, A.M., SMELLIE, J.L. & SMYTHE, D.K. 1998. South Sandwich slices reveal much about arc structure, geodynamics, and composition. *Eos, Transactions, American Geophyscial Union*, **79**, 281, 284–285.

LAURSEN, J., SCHOLL, D.W. & VON HUENE, R. 2002. Neotectonic deformation of the central Chile margin: deepwater forearc basin formation in response to hot spot ridge and seamount subduction. *Tectonics*, **21**, 2-1–2-27, 1038, 10.1029/2001TC901023.

LIVERMORE, R. 2003. Back-arc spreading and mantle flow in the East Scotia Sea. *In*: LARTER, R.D. & LEAT, P.T. (eds) *Intra-oceanic Subduction Systems: Tectonics and Magmatic Processes*. Geological Society, London, Special Publications, **219**, 315–331.

LIVERMORE, R.A. & WOOLLETT, R.W. 1993. Seafloor spreading in the Weddell Sea and southwest Atlantic since the Late Cretaceous. *Earth and Planetary Science Letters*, **117**, 475–495.

LIVERMORE, R., CUNNINGHAM, A., VANNESTE, L. & LARTER, R. 1997. Subduction influence on magma supply at the East Scotia Ridge. *Earth and Planetary Science Letters*, **150**, 261–275.

LIVERMORE, R.A., LARTER, R.D., CUNNINGHAM, A.P., VANNESTE, L., HUNTER, R.J. & THE JR09 TEAM 1995. HAWAII-MR1 sonar survey of the East Scotia Ridge. *BRIDGE Newsletter*, **8**, 51–53.

LIVERMORE, R., MCADOO, D. & MARKS, K. 1994. Scotia Sea tectonics from high-resolution satellite gravity. *Earth and Planetary Science Letters*, **123**, 255–268.

LUDWIG, W.J., NAFE, J.E. & DRAKE, C.L. 1970. Seismic refraction. *In*: MAXWELL, A.E. (ed.) *The Sea, Ideas and Observations in the Study of the Seas*. Wiley, New York, 53–84.

MARTINEZ, F. & TAYLOR, B. 2002. Mantle wedge control on back-arc crustal accretion. *Nature*, **416**, 417–420.

MARTINEZ, F. & TAYLOR, B. 2003. Controls on back-arc crustal accretion: insights from the Lau, Manus and Mariana basins. *In*: LARTER, R.D. & LEAT, P.T. (eds) *Intra-oceanic Subduction Systems: Tectonics and Magmatic Processes*. Geological Society, London, Special Publications, **219**, 19–54.

MARTINEZ, F., FRYER, P., BAKER, N.A. & YAMAZAKI, T. 1995. Evolution of backarc rifting: Mariana Trough, 20°–24°N. *Journal of Geophysical Research*, **100**, 3807–3827.

MOORE, G.F., SHIPLEY, T.H., STOOFA, P.L., KARIG, D.E., TAIRA, A., KURAMOTO, H., TOKUYAMA, H. & SUYEHIRO, K. 1990. Structure of the Nankai

Trough accretionary zone from multichannel seismic reflection data. *Journal of Geophysical Research*, **95**, 8753–8765.

PARK, J.-O., TSURO, T., TAKAHASHI, N., HORI, T., KODAIRA, S., NAKANISHI, A., MIURA, S. & KENADA, Y. 2002. A deep strong reflector in the Nankai accretionary wedge from multichannel seismic data: implications for underplating and interseismic shear stress release. *Journal of Geophysical Research*, **107**(B4), ESE3-1–ESE3-17, 2061, 10.1029/2001JB000262.

PARSON, L.M. & HAWKINS, J.W. 1994. Two-stage ridge propagation and the geological history of the Lau backarc basin. *In*: HAWKINS, J.W., PARSON, L.M., ALLAN, J.F. *et al. Proceedings of the Ocean Drilling Program, Scientific Results*, **135**, 819–828.

PARSON, L.M. & WRIGHT, I.C. 1996. The Lau–Havre–Taupo back-arc basin: a southward-propagating, multi-stage evolution from rifting to spreading. *Tectonophysics*, **263**, 1–22.

PARSONS, B. & SCLATER, J.G. 1977. An analysis of the variation of ocean floor bathymetry and heat flow with age. *Journal of Geophysical Research*, **82**, 803–827.

PEACOCK, S.M. 2001. Are the lower planes of double seismic zones caused by serpentine dehydration in subducting oceanic mantle? *Geology*, **29**, 299–302.

PEARCE, J.A., BARKER, P.F., EDWARDS, S.J., PARKINSON, I.J. & LEAT, P.T. 2000. Geochemistry and tectonic significance of peridotites from the South Sandwich arc–basin system, South Atlantic. *Contributions to Mineralogy and Petrology*, **139**, 36–53.

PELAYO, A.M. & WIENS, D.A. 1989. Seismotectonics and relative plate motion in the Scotia Sea region. *Journal of Geophysical Research*, **94**, 7293–7320.

SAGER, W.W. 1980. Mariana arc structure inferred from gravity and seismic data. *Journal of Geophysical Research*, **85**, 5382–5388.

SMITH, W.H.F. & SANDWELL, D.T. 1997. Global sea floor topography from satellite altimetry and ship depth soundings. *Science*, **277**, 1956–1962.

TAYLOR, B. 1992. Rifting and the volcano-tectonic evolution of the Izu–Bonin–Mariana arc. *In*: TAYLOR, B., FUJIOKA, K. *et al. Proceedings of the Ocean Drilling Program, Scientific Results*, **126**, 627–651.

TAYLOR, B. & KARNER, G.D. 1983. On the evolution of marginal basins. *Reviews of Geophysics and Space Physics*, **21**, 1727–1741.

THOMAS, C., LIVERMORE, R. & POLLITZ, F. 2003. Motion of the Scotia Sea plates. *Geophysical Journal International*, in press.

TREHU, A.M. 1975. Depth versus (age)$^{1/2}$: A perspective on mid-ocean rises. *Earth and Planetary Science Letters*, **27**, 287–304.

VANNESTE, L.E. & LARTER, R.D. 2002. Sediment subduction, subduction erosion and strain regime in the northern South Sandwich forearc. *Journal of Geophysical Research*, **107**(B7), EPM5-1–EPM5-24, 2149, 10.1029/2001JB000396.

VANNESTE, L.E., LARTER, R.D. & SMYTHE, D.K. 2002. A slice of intraoceanic arc: insights from the first multichannel seismic reflection profile across the South Sandwich island arc. *Geology*, **30**, 819–822.

WESTBROOK, G.K. & MCCANN, W.R. 1986. Subduction of Atlantic lithosphere beneath the Caribbean. *In*: VOGT, P.R. & TUCHOLKE, B.E. (eds) *The Geology of North America, Volume M, The Western North Atlantic Region*. Geological Society of America, Boulder, Colorado, 341–350.

WESTBROOK, G.K., LADD, J.W., BUHL, P., BANGS, N. & TILEY, G.J. 1988. Cross section of an accretionary wedge: Barbados Ridge complex. *Geology*, **16**, 631–635.

WHITE, R.S., MCKENZIE, D. & O'NIONS, R.K. 1992. Oceanic crustal thickness from seismic measurements and rare earth element inversions. *Journal of Geophysical Research*, **97**, 19 683–19 715.

WINDER, R.O. & PEACOCK, S.M. 2001. Viscous forces acting on subducting lithosphere. *Journal of Geophysical Research*, **106**, 21 937–21 951.

WRIGHT, I.C., PARSON, L.M. & GAMBLE, J.A. 1996. Evolution and interaction of migrating cross-arc volcanism and backarc rifting: an example from the southern Havre Trough (35°20′–37°S). *Journal of Geophysical Research*, **101**, 22 071–22 086.

Magmatism in the South Sandwich arc

P.T. LEAT[1], J.L. SMELLIE[1], I.L. MILLAR[2] & R.D. LARTER[1]
[1]*British Antarctic Survey, High Cross, Madingley Road, Cambridge CB3 0ET, UK (e-mail: p.leat@bas.ac.uk)*
[2]*British Antarctic Survey, c/o NERC Isotope Geoscience Laboratory, Kingsley Dunham Centre, Keyworth, Nottingham NG12 5GG, UK*

Abstract: The South Sandwich Islands are one of the world's classic examples of an intra-oceanic arc. Formed on recently generated back-arc crust, they represent the earliest stages of formation of arc crust, and are an excellent laboratory for investigating variations in magma chemistry resulting from mantle processes, and generation of silicic magmas in a dominantly basaltic environment. Two volcanoes are examined. Southern Thule in the south of the arc is a complex volcanic edifice with three calderas and compositions that range from mafic to silicic and tholeiitic to calc-alkaline. It is compared to the Candlemas–Vindication edifice in the north of the arc, which is low-K tholeiitic and strongly bimodal from mafic to silicic. Critically, Southern Thule lies along a cross-arc, wide-angle seismic section that reveals the velocity structure of the underlying arc crust. Trace element variations are used to argue that the variations in both mantle depletion and input of a subducted sediment component produced the diverse low-K tholeiite, tholeiite and calc-alkaline series. Primitive, mantle-derived melts fractionally crystallized by *c.* 36% to produce the most Mg-rich erupted basalts and a high-velocity cumulitic crustal keel. Plagioclase cumulation produced abundant high-Al basalts (especially in the tholeiitic series), and strongly influenced Sr abundances in the magmas. However, examination of volumetric and geochemical arguments indicates that the silicic rocks do not result from fractional crystallization, and are melts of amphibolitic arc crust instead.

The South Sandwich Islands, situated in the South Atlantic, form a 350 km-long, N–S-orientated, crescent-shaped volcanic arc that is regarded as one of the classic global examples of an intra-oceanic arc (Baker 1968). The islands are small, typically 3–8 km across, and entirely volcanic in origin (Baker 1978, 1990; Holdgate & Baker 1979). The islands typically rise 500–1000 m above sea level (asl), and are the subaerial summits of edifices that rise some 3 km above the surrounding seafloor. The arc is tectonically simple in that no collisions are taking place between the arc and features such as oceanic plateaux, seamounts or ocean ridges. Moreover, there have been no major changes in the arrangement of plate boundaries or relative plate motion directions since the start of the current phase of back-arc opening at >15 Ma. All sediment arriving at the trench is subducted (Vanneste & Larter 2002) and there is virtually no accretionary prism. The volcanoes of the arc are dominated by mafic compositions. The arc is therefore an excellent natural laboratory for studying the influence of the subducting slab on processes in the mantle wedge.

The South Sandwich arc is situated on the Sandwich microplate, below which the South American Plate is subducting in a westerly direction (Fig. 1) at a rate of 70–85 km Ma^{-1} (Pelayo & Wiens 1989). The Sandwich microplate is separating from the Scotia Plate to the west along the back-arc East Scotia Ridge at an intermediate spreading rate of 65–70 km Ma^{-1} (full rate) (Livermore *et al.* 1997). The major plates in the area, the Antarctic, South American and Scotia plates are all slow moving (<22 km Ma^{-1}), and the relatively high rate of subduction is therefore accommodated mostly by rapid E-directed movement of the Sandwich Plate (Barker 1995). Most of the Sandwich Plate is constructed of oceanic lithosphere that was generated at the East Scotia Ridge, which has been active for at least 15 Ma (Larter *et al.* 2003). The South Sandwich arc is built on such back-arc crust formed since 10 Ma (Barker & Hill 1981; Barker 1995; Larter *et al.* 2003). If volcanic arcs are the sites where continental crust is initially formed, the South Sandwich Islands represent a very immature stage of this process.

The volcanic arc consists of the islands (from north to south): Zavodovski, Visokoi, the Candlemas–Vindication group, Saunders, Montagu, Bristol and the Southern Thule group (Fig. 1b). The submarine Protector Shoal represents a continuation of the arc to the northwest of Zavodovski. The tiny Leskov Island is in

From: LARTER, R.D. & LEAT, P.T. 2003. *Intra-Oceanic Subduction Systems: Tectonic and Magmatic Processes.* Geological Society, London, Special Publications, **219**, 285–313. 0305-8719/03/$15.00

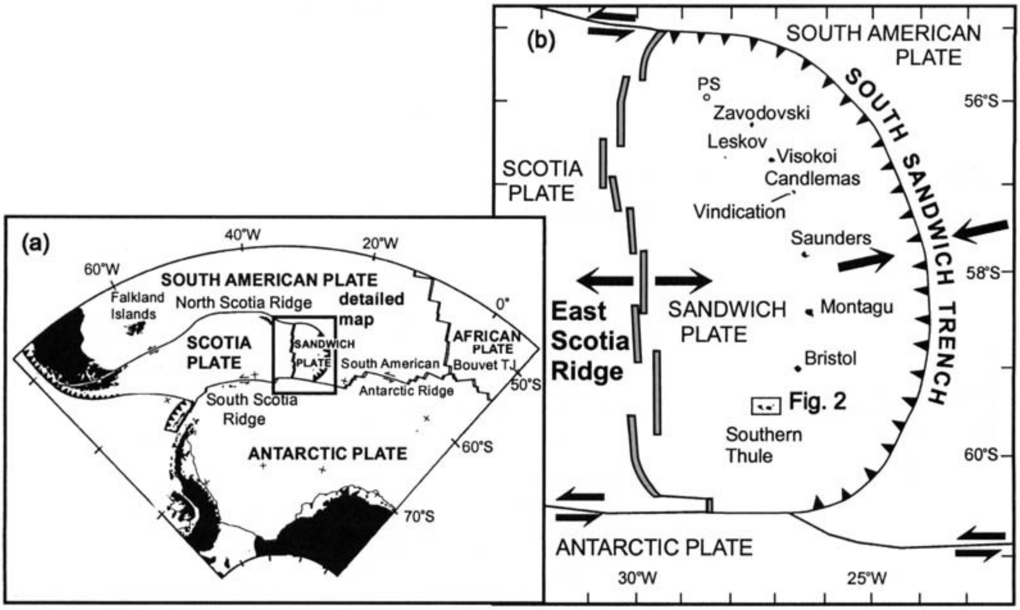

Fig. 1. Location of the South Sandwich arc. The tectonic map (**a**) shows plate boundaries. The map of the Sandwich Plate (**b**) shows locations of the islands of the South Sandwich arc in relation to the trench and back-arc spreading centre. Arrows depict approximate relative plate motions. PS, Protector Shoal.

a rear-arc position (Fig 1b). The only radiometric dates for the arc are four K–Ar ages on volcanic rocks, the oldest being 3.1±0.3 Ma, reported by Baker *et al.* (1977). Attempts by the authors (with S.P. Kelley) to date plagioclase crystals from basalts from the islands by Ar–Ar failed owing to the paucity of potassium and extreme youth of the samples. The South Sandwich arc is volcanically active. There is intense fumarolic activity on several of the islands and there have been at least six historic eruptions viz.: Zavodovski, 1830; Bristol, 1935 and 1956; Protector Shoal, 1962; Bellingshausen (in the Southern Thule group) between 1964 and 1997; Saunders (recurrent lava lake, 1995–1998) (Gass *et al.* 1963; Holdgate & Baker 1979; Baker 1990; Lachlan-Cope *et al.* 2001).

This paper examines selected aspects that are critical to understanding the magmatism in the island arc: the variable degree of depletion of the mantle source, the compositions of components derived from the slab, the nature of the primary magmas, the origin of high-alumina basalts, constraints on magmatic processes from the seismic refraction results and the origin of silicic magmas. We shall concentrate on the two island groups; Southern Thule and Candlemas–Vindication. These island groups are chosen because: (i) both contain significant volumes of silicic volcanic rocks; (ii) they belong to contrasting magma series – Candlemas and Vindication consist of low-K tholeiites, whereas Southern Thule is calc-alkaline – tholeiitic; and (iii) Southern Thule lies very close to a seismic reflection and refraction line that ran from back-arc to fore-arc (Larter *et al.* 1998, 2001; Vanneste *et al.* 2002).

Southern Thule

Southern Thule (centred on 59°27′S, 27°15′W) is an archipelago that forms the southernmost part of the South Sandwich Islands. Southern Thule consists of three main islands: Cook, Thule and Bellingshausen (Fig. 2). Cook Island (4.5 × 6.5 km) is mainly covered by snow and ice. Rock exposures only occur around the edges of the island, where they form precipitous cliffs. The island rises to over 1000 m asl at Mount Harmer. The island is accessible only by helicopter at only two places, Resolution Point and Reef Point.

Thule Island (5.5 × 7.0 km) is also mainly covered by snow and ice, with outcrop restricted to the coastline. The coastline is generally less precipitous that that of Cook Island, and the highest point (Mount Larsen) is lower (725 m asl). At Hewison Point, an ice-free, 1 × 0.6 km

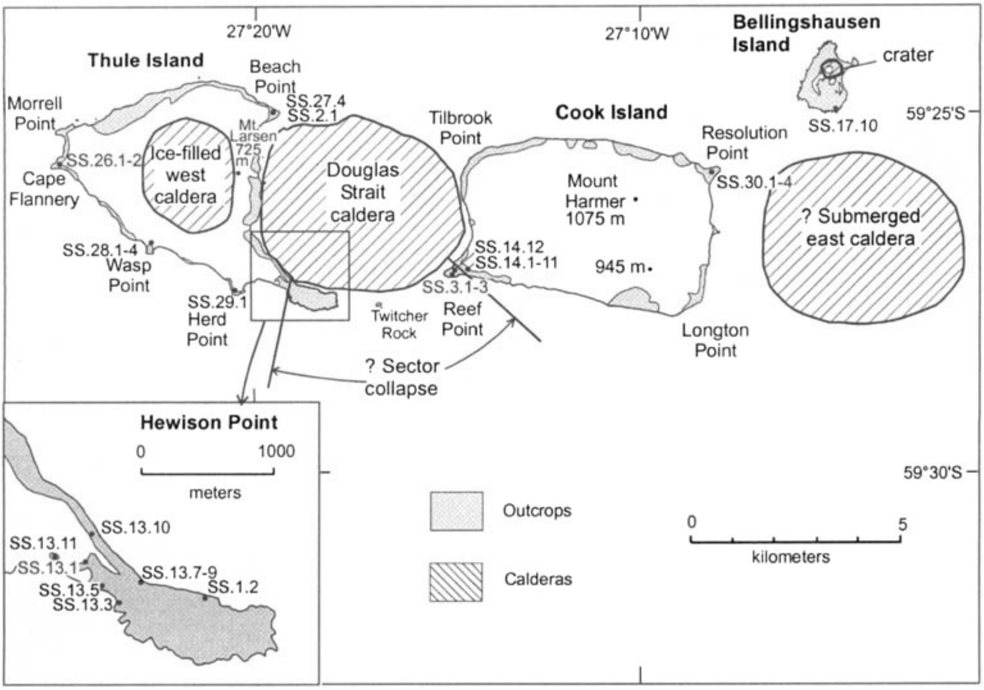

Fig. 2. Sketch map of Southern Thule, showing major geological features and sample locations.

lava platform is joined to the rest of the island by a low-lying neck of land that has developed beaches along its N- and S-facing coasts. A chain of three calderas lying along an E–W trend is a notable feature (Fig. 2). The 1.5–2 km-diameter west caldera occupies the central part of Thule and is ice filled. Douglas Strait caldera is 4.5 km in diameter, with a subhorizontal bottom surface about 600–625 m below sea level (Smellie *et al.* 1998). The submerged east caldera has a floor about 110 m below sea level, based on evidence from soundings.

Sequences at Beach Point and east of Reef Point dip away from a former centre in Douglas Strait, and shallow-dipping lava platforms at Reef Point and Hewison Point unconformably overlie these older sequences (Smellie *et al.* 1998). It is likely that there was a S-directed sector collapse that pre-dates Douglas Strait caldera. Some units can therefore be assigned as pre-sector collapse, or post-sector collapse and pre-Douglas caldera in age. The lava platforms at Hewison and Reef points are overlain by a matrix-supported, poorly sorted, non-graded deposit containing blocks up to 1.85 m across and weakly vesicular juvenile clasts up to 0.5 m across. The deposit mantles topography and ranges up to 25 m thick northwest of Hewison Point. It is interpreted as an air fall pyroclastic deposit of approximately the same age as Douglas Strait caldera. The only known post-caldera unit is a 50 m-thick scoria deposit on Hewison Point.

Bellingshausen Island (1.8 × 1.5 km) is the most recently active island of Southern Thule. It consists of lavas and scoria forming a shield-like volcano. There is a summit crater 450 m in diameter that is intensely fumarolic, and several smaller (probably phreatic) craters. Some of these craters probably formed between the 1964 and 1997 surveys.

Candlemas and Vindication Islands

These two islands in the north part of the arc are about 4.5 km apart (Fig. 3), and belong to the same edifice. Vindication Island (2.8 × 1.5 km) is an eroded sequence of lavas and scoria cut by dykes. It is up to 432 m high, and with an ice cap. Candlemas (57°05'S, 26°43'W, 6.0 × 4.0 km) consists of two volcanic centres, joined by shingle beaches (Tomblin 1979). To the south, an older sequence of lavas, scoria and epiclastic rocks cut by dykes forms the area around the

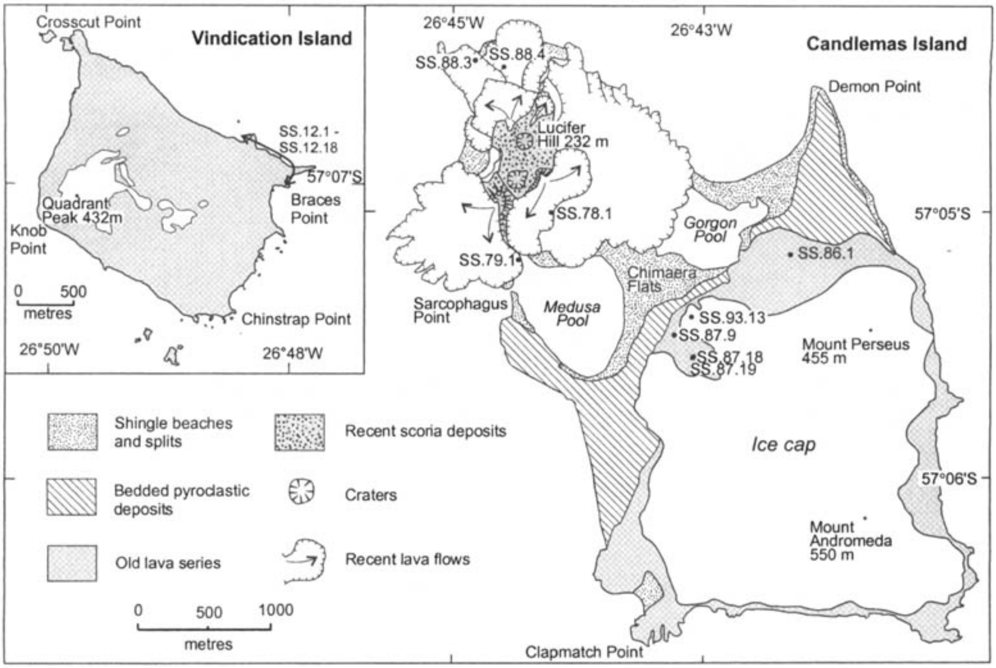

Fig. 3. Sketch map of Candlemas and Vindication islands, showing major geological features and sample locations.

550 m high, ice-covered Mount Andromeda. This sequence is exposed in accessible cliffs representing a former coastline south of Chimaera Flats (Fig. 3). The sequence dips to the southwest, and is apparently related to an eroded former centre northeast of Mount Perseus. A sequence dominated by bedded pyroclastic deposits and blocky orthobreccias at least 20 m thick crop out between Demon Point and Sarcophagus Point (Fig. 3). The deposits are unconsolidated, stratified and dip up to 6° away from Lucifer Hill. They are interpreted as interbedded air fall, pyroclastic surge and mass flow deposits representing the flanks of an edifice centred around the present Lucifer Hill, which was mostly removed by wave erosion or caldera collapse. To the north, lavas and pyroclastic rocks form the much more recent, 232 m-high, Lucifer Hill Volcano, which has abundant active fumaroles. It is ice-free and easily accessible by foot. The blocky surfaces of the lavas and some boccas and associated scoria cones are virtually non-eroded. The Mount Andromeda ice cap contains at least two air fall deposits. One of these is well exposed, 1 m thick and contains pumice clasts up to 30 cm across. Both deposits are interpreted to have been derived from Lucifer Hill.

History of research

Southern Thule and Candlemas and Vindication islands were discovered by the British naval captain James Cook in 1775. In 1819–1820, the Russian captain von Bellingshausen first demonstrated that Southern Thule comprises three main islands (Holdgate & Baker 1979). During the nineteenth century, activity around the islands was virtually restricted to sealing and whaling (Holdgate 1963; Holdgate & Baker 1979). The first geological description of the islands resulted from the 1930 voyage of RRS *Discovery II* (Kemp & Nelson 1931), during which a landing at Beach Point, Thule Island was made. Kemp & Nelson (1931) first suggested that Douglas Strait was the site of a submerged volcanic crater, and that Cook and Thule islands originally formed a single edifice. Several of the South Sandwich Islands were visited by scientific parties during the 1950s and early 1960s (Holdgate 1963; Holdgate & Baker 1979).

In 1964, a comprehensive survey of the South Sandwich Islands, including Cook, Thule, Bellingshausen, Vindication and Candlemas islands, was undertaken by scientists aboard HMS *Protector* (Baker 1978; Holdgate & Baker 1979; Tomblin 1979). Specimens collected during that survey were used for elemental and isotopic work, which established input of subducted material to the arc magmas (Hawkesworth *et al.* 1977; Cohen & O'Nions 1982; Barreiro 1983). Luff (1982) documented the petrographic, mineralogical and geochemical variations between islands, and modelled the variations as results of fractional crystallization of a basaltic parent derived by partial melting of peridotite. He also argued that high-Al basalts had been generated by accumulation of plagioclase. Johnston (1986), on the other hand, determined that the liquidus phases of a high-Al basalt from Saunders Island are garnet, clinopyroxene and plagioclase at high, moderate and low pressures, respectively, and suggested that the basalt was a primary melt generated by partial melting of subducting slab. Pearce *et al.* (1995) developed models for generation of the primary arc magmas by dynamic melting of depleted peridotite in the mantle wedge following enrichment of the source by components derived from the slab.

In 1997, British Antarctic Survey scientists (including P.T. Leat and J.L. Smellie) visited all the main islands as part of the multidisciplinary SLICE (Sandwich Lithospheric and Crustal Experiment) project (Larter *et al.* 1998, 2003; Smellie *et al.* 1998). At the same time, seismic reflection and refraction data were collected along back-arc to forearc traverses (Larter *et al.* 1998, 2001; Vanneste *et al.* 2002). The arc and back-arc were also studied by a group working from R/V *Polarstern* in 1997–1998 (Ackermand *et al.* 2003). Associated geochemical and geophysical work on the back-arc spreading centre has been documented by Livermore *et al.* (1997, 2003), Leat *et al.* (2000), Bruguier & Livermore (2001), Pearce *et al.* (2001), Fretzdorff *et al.* (2002), Harrison *et al.* (2003) and Larter *et al.* (2003). At the same time, Vanneste & Larter (2002) documented extensional tectonic features in the fore-arc region and Pearce *et al.* (2000) described peridotites from the forearc mantle rocks exposed by such extension. This paper is based on the results of the SLICE fieldwork on the island arc.

Analytical methods

Most of the geochemical data described in this paper are for samples collected in 1997 by the authors. Major elements and some trace elements were determined by standard X-ray fluorescence analysis (XRF) methods at the University of Keele (UK). Trace elements determined by inductively couple plasma-mass spectrometry (ICP-MS) were analysed using a Plasmaquad at the University of Durham (UK). ICP-MS methods, precision and detection limits are similar to, or better than, those of Pearce *et al.* (1995). Sr, Nd and Pb isotopic ratios were determined on a Finnigan MAT 262 mass spectrometer at the NERC Isotope Geosciences Laboratory (UK), using standard techniques (Pankhurst & Rapela 1995). The $^{87}Sr/^{86}Sr$ ratios were normalized to $^{86}Sr/^{88}Sr$ = 0.1194. Seven analyses of NBS987 during the course of the study gave $^{87}Sr/^{86}Sr = 0.710152 \pm 0.000024$ (2σ). Data in Table 2 are normalized to a preferred value of 0.710240. The $^{143}Nd/^{144}Nd$ ratios were normalized to $^{146}Nd/^{144}Nd$ = 0.7219. Eleven analyses of the La Jolla standard yielded $^{143}Nd/^{144}Nd = 0.511875 \pm 0.000014$ (2σ). Pb analyses followed procedures summarized in Kempton *et al.* (1997). All whole-rock powders were leached in 6 M HCl before dissolution. Pb isotope ratios are corrected for fractionation using the standard values of Todt *et al.* (1984). Long-term reproducibility of Pb isotope ratios in the NBS981 solution standard is better than $\pm 0.1\%$ (1σ). Long-term reproducibility of the BHVO-1 rock standard is better than $\pm 0.2\%$ (1σ). Laboratory blanks for Sr, Nd and Pb at the time of analysis were better than 500, 250 and 150 pg, respectively.

Selected major and trace element analyses from Southern Thule, Candlemas and Vindication are presented in Table 1, and isotope analyses are presented in Table 2.

Classification

Compositionally, the volcanic rocks forming the volcanoes of the arc range from basalt to rhyolite, with mafic rocks (basalts and basaltic andesites) being volumetrically dominant (Baker 1968, 1978). In Figure 4, data for South Sandwich Islands rocks are plotted on the K_2O v. SiO_2 classification diagram (after Pearce *et al.* 1995). Samples from the arc as a whole form three trends, low-K tholeiitic, tholeiitic and calc-alkaline. Samples from Candlemas and Vindication islands lie along the low-K tholeiite trend (although there is some scatter toward the tholeiitic trend at low Si abundances). Southern Thule samples plot along the tholeiitic and calc-alkaline trends. In the arc as a whole, most rocks are basalts or basaltic andesites, confirming the view of Baker (1968) that the islands are dominantly basaltic. However, Candlemas Island and Southern Thule have significant proportions of andesites and dacites (the only other silicic rocks in the island arc are on Protector Shoal and the tiny rear-arc Leskov Island, and rare andesites on Montagu, Bristol, and the adjacent Freezland Rock). The Candlemas and Vindication samples

Table 1. *Major and trace element analyses of volcanic rocks from Southern Thule and Candlemas and Vindication islands*

Sample number	SS.14.1	SS.14.2	SS.14.3	SS.14.4	SS.14.5	SS.14.6	SS.14.7	SS.14.8	SS.14.9	SS.14.10	SS.14.11	SS.27.4	SS.2.1	SS.30.1	SS.30.4A	SS.13.11	SS.17.10
Chemical group	t	t	t	t	t	t	t	t	t	t	t	t	t	t	t	t	t
Location	Reef	Reef	Reef	Reef	Reef	Reef	Reef	Reef	Reef	Reef	Reef	Beach	Beach	Resltn	Resltn	Hewison	Bell
Rock type	dyke	lava	lava	lava	lava	lava	lava	lava	lava	lava	lava	dyke	lava	lava	lava	lava	lava
Rock unit	1	1	1	1	1	1	1	1	1	1	1	2	2	3	3	1	4
Major elements by XRF																	
SiO_2	52.56	51.01	51.04	50.89	51.13	51.19	51.13	51.22	51.25	51.51	52.64	49.19	55.70	53.65	67.11	67.93	56.55
TiO_2	0.59	0.55	0.56	0.55	0.56	0.55	0.56	0.55	0.56	0.56	0.60	0.68	0.76	0.64	0.53	0.51	0.93
Al_2O_3	19.45	21.20	20.98	20.89	21.11	21.07	20.95	21.16	21.17	21.09	19.50	19.75	16.80	19.57	14.30	14.03	15.19
Fe_2O_3(T)	9.54	8.72	8.87	8.70	8.76	8.79	8.78	8.77	8.78	8.77	9.52	10.24	10.01	8.99	6.92	6.29	11.80
MnO	0.17	0.15	0.15	0.15	0.15	0.15	0.16	0.15	0.15	0.15	0.17	0.17	0.18	0.16	0.16	0.14	0.19
MgO	4.13	4.28	4.40	4.39	4.28	4.29	4.36	4.32	4.27	4.28	4.10	4.59	3.59	4.04	1.03	1.35	3.24
CaO	10.87	11.73	11.69	11.76	11.69	11.64	11.70	11.76	11.72	11.72	10.91	12.26	8.59	10.49	3.97	4.53	8.22
Na_2O	2.57	2.29	2.35	2.25	2.34	2.35	2.30	2.37	2.34	2.32	2.57	1.97	3.20	2.86	4.87	4.48	3.25
K_2O	0.28	0.22	0.22	0.21	0.22	0.23	0.22	0.21	0.21	0.22	0.28	0.12	0.55	0.35	1.10	1.07	0.53
P_2O_5	0.07	0.06	0.06	0.06	0.06	0.07	0.06	0.06	0.06	0.07	0.08	0.06	0.13	0.08	0.13	0.15	0.15
LOI	–0.33	–0.23	–0.29	–0.24	–0.32	–0.24	–0.31	–0.28	–0.30	–0.27	–0.36	0.06	0.11	–0.33	–0.14	–0.22	–0.53
Total	99.92	99.99	100.04	99.61	99.99	100.11	99.91	100.29	100.23	100.42	100.00	99.09	99.63	100.50	99.98	100.27	99.53
Trace elements by XRF																	
V	218	197	220	211	223	212	224	220	218	221	235	305	198	207	51	40	269*
Cr	n.d.	8	14	10	7	5	7	8	7	3	2	1	n.d.	8	n.d.	2	5*
Ni	7	13	12	13	15	12	13	13	11	11	6	8	7	14	4	4	9*
Cu	88	85	88	83	82	89	79	85	92	82	95	116	109	163	56	43	97*
Zn	67	61	63	59	61	62	62	64	61	64	72	71	87	68	103	71	87*
Y	17	16	15	14	15	15	16	15	14	16	18	15	27	19	46	42	
Zr	63	56	56	55	54	54	56	54	56	56	63	57	95	45	147	145	
Trace elements by ICP																	
Sc	37.8	33.5				33.0				34.7	37.3	37.1	32.5			18.9	34.74
Co	28.5	29.4				28.9				29.3	28.7	31.7	26.8			10.1	31.0
Ga	17.1	17.1				16.8				17.3	17.0	16.6	16.4			15.8	16.5
Rb	4.52	4.61				4.71				4.76	4.67	2.72	11.78			19.74	11.92
Sr	164	185				181				186	165	169	158			122	131
Y	16.5	14.6				14.7				14.8	16.5	14.4	26.2			41.3	28.5
Zr	34.7	27.9				27.8				28.8	34.4	27.5	63.3			129.7	73.4
Nb	0.64	0.96				0.95				1.00	0.66	0.71	1.71			2.98	1.11
Cs	0.12	0.16				0.18				0.14	0.14	0.13	0.46			0.19	0.52
Ba	62.8	54.5				55.2				55.1	63.0	42.4	116.3			211.7	118.1
La	2.12	1.88				1.89				1.92	2.12	1.85	4.15			7.24	3.92
Ce	6.02	5.13				5.15				5.17	6.08	5.20	11.29			19.70	11.04
Pr	0.94	0.81				0.81				0.81	0.95	0.83	1.72			2.94	1.76
Nd	4.92	4.18				4.26				4.26	4.90	4.32	8.85			14.27	9.29
Sm	1.60	1.41				1.40				1.42	1.62	1.44	2.78			4.34	2.95
Eu	0.62	0.57				0.58				0.58	0.63	0.58	0.95			1.17	0.96
Gd	2.13	1.85				1.84				1.87	2.10	1.89	3.52			5.32	3.84
Tb	0.39	0.34				0.34				0.34	0.39	0.35	0.64			0.96	0.68
Dy	2.56	2.24				2.24				2.24	2.53	2.28	4.15			6.29	4.46
Ho	0.57	0.49				0.49				0.49	0.55	0.49	0.90			1.37	0.98
Er	1.62	1.44				1.42				1.45	1.63	1.43	2.63			4.05	2.77
Tm	0.257	0.223				0.224				0.226	0.254	0.219	0.414			0.652	0.438
Yb	1.64	1.45				1.44				1.45	1.64	1.41	2.64			4.18	2.88
Lu	0.26	0.23				0.22				0.23	0.26	0.22	0.41			0.65	0.44
Hf	1.06	0.84				0.85				0.85	1.04	0.84	1.91			3.67	2.19
Ta	0.056	0.068				0.069				0.071	0.050	0.054	0.117			0.196	0.098
Pb	0.97	1.16				1.09				1.08	0.93	1.01	2.23			2.05	2.88
Th	0.39	0.30				0.30				0.30	0.39	0.34	0.84			1.79	0.85
U	0.120	0.088				0.086				0.087	0.124	0.095	0.247			0.542	0.281

Chemical group: c, calc-alkaline; t, tholeiite; low-K, low-K tholeiite.
Location: Reef, Reef Point, Cook; Beach, Beach Point, Thule; Resltn, Resolution Point, Cook; Hewison, Hewison Point, Thule; Bell, Bellingshausen; Wasp, Wasp Point, Thule; Flannery, Cape Flannery, Thule; Herd, Herd Point, Thule; Candl, Candlemas; Vind, Vindication.
Rock unit: 1, pre-sector collapse series; 2, pre-caldera; 3, no stratigraphic control; 4, recent Bellingshausen lava; 5, block in moraine; 6, post-sector collapse lavas; 7, post-sector collapse scoria; 8, bomb in syncaldera deposit; A, Old lava series, Candlemas Island; B, Lucifer Hill lavas, Candlemas Island; C, air fall deposit in ice cap, Candlemas Island; D, Braces Point, Vindication Island.
* Trace elements by ICP-MS. n.d. = not detected.

Table 1. *continued*

Sample number	SS.28.2	SS.28.1	SS.28.3	SS.26.2	SS.29.1	SS.30.2A	SS.13.10	SS.1.2	SS.3.1	SS.13.5	SS.13.1	SS.13.3	SS.13.7	SS.13.9	SS.13.8	SS.14.12	SS.3.3
Chemical group	c	c	c	c	c	c	c	c	c	c	c	c	c	c	c	c	c
Location	Wasp	Wasp	Wasp	Flannery	Herd	Resltn	Hewison	Hewison	Reef	Hewison	Hewison	Hewison	Hewison	Hewison	Hewison	Reef	Reef
Rock type	block	Block	block	lava	lava	obsidian	lava	lava	lava	scoria	scoria	bomb	bomb	bomb	bomb	bomb	bomb
Rock unit	5	5	5	3	3	3	1	6	6	7	7	8	8	8	8	8	8
Major elements by XRF																	
SiO_2	49.96	53.41	54.01	52.07	52.11	63.35	58.45	57.64	60.72	55.26	56.66	54.21	60.77	61.34	63.15	58.69	59.25
TiO_2	0.72	0.76	0.61	0.68	0.72	0.90	1.22	1.03	1.16	1.19	1.15	1.34	1.02	0.98	0.86	1.16	1.16
Al_2O_3	15.12	15.79	17.74	16.85	16.44	13.93	14.26	14.28	14.23	15.47	14.88	14.74	13.73	14.09	13.18	13.96	14.46
$Fe_2O_3(T)$	11.25	11.29	9.37	10.81	10.52	10.23	12.57	11.66	11.76	13.04	12.91	13.95	11.48	11.24	10.51	12.10	11.92
MnO	0.19	0.19	0.16	0.19	0.18	0.19	0.21	0.20	0.19	0.21	0.20	0.22	0.22	0.21	0.19	0.20	0.20
MgO	8.20	5.36	4.64	5.90	6.01	1.22	2.40	2.71	1.89	3.50	3.34	3.58	1.15	1.13	0.99	1.97	2.37
CaO	12.80	10.44	10.35	11.61	11.33	5.14	6.61	6.89	5.85	7.69	7.71	7.79	5.31	5.06	4.83	6.28	6.46
Na_2O	1.76	2.46	2.50	2.15	2.27	4.13	3.75	3.48	3.83	3.23	3.38	3.01	4.04	3.92	4.20	4.08	3.84
K_2O	0.26	0.44	0.55	0.35	0.40	1.36	1.01	0.93	1.17	0.80	0.78	0.83	1.41	1.34	1.43	1.23	1.03
P_2O_5	0.08	0.10	0.07	0.08	0.10	0.29	0.29	0.21	0.22	0.16	0.16	0.21	0.30	0.31	0.27	0.25	0.21
LOI	–0.32	–0.32	–0.14	–0.25	–0.33	–0.45	–0.39	–0.34	–0.62	–0.47	–0.61	–0.51	0.06	0.21	0.16	–0.42	–0.54
Total	100.02	99.92	99.86	100.44	99.75	100.28	100.38	98.69	100.41	100.08	100.58	99.35	99.50	99.83	99.79	99.50	100.35
Trace elements by XRF																	
V	307	282	242	277	261	35	165	219	123	347	366	338	28	29	27	130	156
Cr	168	13	3	28	57	n.d.	n.d.	n.d.	n.d.	43	n.d.	44	20	19	n.d.	n.d.	n.d.
Ni	40	16	12	18	24	3	3	6	5	16	12	15	9	10	3	6	5
Cu	157	46	75	115	31	87	135	130	122	144	181	179	64	63	70	139	163
Zn	73	83	74	77	74	119	113	112	123	119	113	120	130	129	137	126	126
Y	18	21	20	19	20	49	42	39	45	34	35	36	56	56	54	45	44
Zr	65	82	88	67	78	167	135	129	133	95	100	101	164	162	164	132	136
Trace elements by ICP																	
Sc	52.6			45.5	41.7	23.9	32.5	33.2	28.8						24.9	28.3	30.5
Co	45.9			38.3	37.8	14.5	24.7	26.1	22.8						10.1	22.9	25.5
Ga	13.8			15.7	15.6	17.9	17.6	17.4	17.9						17.3	17.5	17.7
Rb	5.78			7.74	9.43	32.76	23.61	22.41	27.21						35.66	27.56	25.11
Sr	127			150	148	138	146	148	141						130	141	143
Y	16.8			17.4	19.6	50.2	42.4	38.3	45.4						55.5	44.9	42.0
Zr	34.1			38.0	47.7	155.7	117.8	109.8	137.7						173.3	134.6	123.2
Nb	0.67			0.80	1.08	3.31	3.03	2.55	2.96						4.21	2.96	2.67
Cs	0.25			0.33	0.35	1.35	0.86	0.92	0.97						1.41	1.14	1.09
Ba	61.8			79.2	91.3	273.5	205.2	198.0	244.4						294.4	240.9	222.5
La	2.19			2.67	3.20	9.94	7.89	7.22	8.65						11.21	8.58	7.92
Ce	6.38			7.35	8.79	26.95	21.53	19.77	23.49						30.04	23.31	21.53
Pr	1.00			1.10	1.30	3.92	3.19	2.92	3.46						4.42	3.40	3.17
Nd	5.25			5.73	6.73	19.45	16.01	14.52	17.16						21.52	16.87	15.63
Sm	1.73			1.83	2.09	5.74	4.78	4.42	5.05						6.47	5.02	4.70
Eu	0.63			0.66	0.72	1.51	1.40	1.28	1.42						1.64	1.40	1.35
Gd	2.26			2.31	2.60	6.96	5.91	5.36	6.17						7.68	6.13	5.71
Tb	0.42			0.41	0.47	1.21	1.03	0.94	1.11						1.36	1.08	1.00
Dy	2.70			2.74	3.08	7.80	6.60	6.11	7.14						8.67	6.92	6.58
Ho	0.59			0.59	0.67	1.68	1.42	1.32	1.53						1.86	1.50	1.42
Er	1.69			1.71	1.92	4.88	4.11	3.83	4.45						5.45	4.38	4.12
Tm	0.259			0.269	0.298	0.773	0.628	0.610	0.708						0.846	0.685	0.649
Yb	1.65			1.71	1.90	4.84	4.08	3.82	4.57						5.49	4.41	4.11
Lu	0.25			0.27	0.30	0.75	0.63	0.60	0.69						0.85	0.69	0.64
Hf	1.07			1.13	1.40	4.41	3.37	3.23	4.04						4.97	3.93	3.56
Ta	0.054			0.055	0.079	0.218	0.197	0.174	0.197						0.270	0.195	0.184
Pb	1.34			1.69	1.64	5.65	4.03	4.18	4.88						5.92	5.18	4.74
Th	0.42			0.59	0.70	2.46	1.79	1.72	2.17						2.70	2.15	1.93
U	0.122			0.169	0.206	0.740	0.528	0.513	0.661						0.806	0.648	0.579

Chemical group: c, calc-alkaline; t, tholeiite; low-K, low-K tholeiite.
Location: Reef, Reef Point, Cook; Beach, Beach Point, Thule; Resltn, Resolution Point, Cook; Hewison, Hewison Point, Thule; Bell, Bellingshausen; Wasp, Wasp Point, Thule; Flannery, Cape Flannery, Thule; Herd, Herd Point, Thule; Candl, Candlemas; Vind, Vindication.
Rock unit: 1, pre-sector collapse series; 2, pre-caldera; 3, no stratigraphic control; 4, recent Bellingshausen lava; 5, block in moraine; 6, post-sector collapse lavas; 7, post-sector collapse scoria; 8, bomb in syncaldera deposit; A, Old lava series, Candlemas Island; B, Lucifer Hill lavas, Candlemas Island; C, air fall deposit in ice cap, Candlemas Island; D, Braces Point, Vindication Island.
* Trace elements by ICP-MS. n.d. = not detected.

Table 1. *continued*

Sample number	SS.86.1	SS.87.9	SS.87.18	SS.87.19	SS.78.1	SS.79.1	SS.88.3	SS.88.4	SS.93.13	SS.12.1	SS.12.2	SS.12.4	SS.12.5	SS.12.7	SS.12.13	SS.12.16	SS.12.18
Chemical group	low-K	low-K	low-K	low-K	low-K	low-K	low-K	low-K	low-K	low-K	low-K	low-K	low-K	low-K	low-K	low-K	low-K
Location	Candl	Candl	Candl	Candl	Candl	Candl	Candl	Candl	Candl	Vind	Vind	Vind	Vind	Vind	Vind	Vind	Vind
Rock type	lava	Lava	lava	lava	lava	lava	lava	lava	pumice	lava	lava	dyke	dyke	bomb	lava	lava	dyke
Rock unit	A	A	A	A	B	B	B	B	C	D	D	D	D	D	D	D	D
Major elements by XRF																	
SiO_2	51.14	49.74	50.15	50.58	64.61	61.38	65.00	65.43	58.34	49.84	51.23	50.93	50.53	50.70	51.10	49.60	49.59
TiO_2	0.49	0.56	0.59	0.60	0.90	0.97	0.88	0.90	0.92	0.51	0.56	0.52	0.56	0.59	0.66	0.64	0.56
Al_2O_3	19.05	18.51	18.13	18.57	14.00	14.33	14.19	14.23	15.85	17.94	19.80	20.28	19.95	17.34	19.33	18.67	18.05
Fe_2O_3(T)	9.68	9.44	9.71	10.15	8.99	9.85	8.82	8.67	9.93	9.67	8.54	8.69	8.90	10.12	9.16	9.98	10.29
MnO	0.17	0.16	0.17	0.18	0.17	0.18	0.17	0.17	0.18	0.18	0.16	0.16	0.16	0.19	0.16	0.17	0.19
MgO	6.33	7.16	6.83	6.60	1.76	2.07	1.58	1.54	3.05	6.54	5.31	5.18	5.34	6.48	5.14	5.40	5.82
CaO	11.62	12.57	12.25	11.67	5.82	6.52	5.48	5.38	7.84	13.10	12.36	12.45	12.68	12.35	12.01	12.98	13.15
Na_2O	1.76	1.71	1.67	1.83	4.16	4.14	4.24	4.27	3.33	1.82	1.79	1.85	1.89	1.95	2.01	2.16	1.98
K_2O	0.12	0.18	0.21	0.13	0.48	0.42	0.50	0.50	0.34	0.14	0.09	0.10	0.10	0.10	0.09	0.10	0.12
P_2O_5	0.05	0.06	0.06	0.04	0.13	0.12	0.13	0.13	0.09	0.04	0.04	0.04	0.04	0.03	0.04	0.04	0.04
LOI	0.01	0.23	–0.30	–0.34	–0.45	–0.37	–0.20	–0.13	–0.01	–0.11	0.01	–0.28	–0.27	–0.14	–0.25	–0.19	–0.30
Total	100.43	100.31	99.45	100.01	100.57	99.60	100.79	101.09	99.87	99.65	99.89	99.91	99.86	99.70	99.45	99.55	99.50
Trace elements by XRF																	
V	237	248	269	274	113*	174	93	102	268	251	231	241	248	271	300	269	258
Cr	64	59	59	82	3*	n.d.	n.d.	n.d.	1	45	25	36	23	64	49	51	8
Ni	23	27	31	31	n.d.	4	4	4	7	21	18	16	17	19	17	18	12
Cu	84	100	114	94	68*	179	126	135	145	92	82	86	137	103	99	100	25
Zn	74	75	70	77	83*	94	101	103	100	69	66	64	63	72	71	70	93
Y	10	13	15	13		35	38	40	29	13	13	12	13	13	13	15	15
Zr	23	28	53	27		82	94	96	66	21	21	20	21	19	22	22	22
Trace elements by ICP																	
Sc	42.9	39.9	41.1	47.0	30.8	33.8	34.6	31.9	39.3	43.2	38.9	37.5	38.3	46.6	38.8	40.3	42.1
Co	35.1	35.9	39.0	37.4	15.4	17.8	17.6	14.7	23.5	34.8	29.8	29.9	29.1	34.3	30.8	31.6	33.4
Ga	15.6	17.0	15.1	16.3	17.1	16.9	17.2	17.3	17.5	14.8	16.1	15.8	15.6	15.7	16.1	16.4	15.3
Rb	1.48	2.10	4.41	2.82	9.70	5.87	5.54	11.97	8.22	3.67	2.10	1.96	1.19	2.15	2.22	1.57	1.07
Sr	117	148	124	123	105	119	122	120	125	111	115	115	112	104	111	113	115
Y	12.6	14.2	13.0	14.5	38.4	34.8	35.0	40.4	29.9	12.0	12.3	12.0	12.0	12.9	13.7	14.0	12.7
Zr	19.4	23.7	23.7	23.1	82.8	73.6	75.5	88.3	60.6	19.7	18.0	17.6	17.6	17.6	19.8	19.6	20.6
Nb	0.21	0.30	0.31	0.26	0.87	0.77	0.83	0.94	0.64	0.26	0.23	0.23	0.22	0.17	0.23	0.21	0.27
Cs	0.07	0.07	0.18	0.13	0.43	0.17	0.16	0.62	0.44	0.16	0.09	0.09	0.03	0.13	0.09	0.09	0.04
Ba	30.8	41.2	50.7	34.7	112.7	110.3	107.5	122.2	88.9	38.8	27.0	26.2	25.8	24.9	25.6	26.1	36.1
La	0.80	1.19	1.41	1.00	3.34	3.04	2.87	3.56	2.57	0.98	0.77	0.78	0.77	0.67	0.75	0.75	1.02
Ce	2.60	3.58	3.97	3.27	10.46	9.57	9.24	11.22	7.98	3.01	2.46	2.43	2.42	2.23	2.54	2.51	3.14
Pr	0.48	0.62	0.64	0.60	1.76	1.68	1.65	1.97	1.41	0.50	0.45	0.43	0.43	0.42	0.47	0.46	0.52
Nd	2.83	3.46	3.56	3.48	9.85	9.42	9.28	10.91	7.87	2.85	2.56	2.52	2.55	2.48	2.78	2.75	2.94
Sm	1.04	1.23	1.22	1.27	3.42	3.25	3.23	3.75	2.73	1.03	0.98	0.97	0.99	1.00	1.11	1.09	1.08
Eu	0.48	0.55	0.53	0.56	1.12	1.12	1.15	1.26	0.98	0.46	0.48	0.45	0.46	0.48	0.53	0.51	0.47
Gd	1.59	1.80	1.80	1.90	4.78	4.61	4.59	5.28	3.89	1.45	1.46	1.39	1.43	1.49	1.58	1.59	1.57
Tb	0.30	0.34	0.33	0.35	0.87	0.85	0.85	0.96	0.72	0.28	0.28	0.27	0.27	0.28	0.31	0.31	0.29
Dy	1.93	2.14	2.12	2.23	5.80	5.37	5.38	6.16	4.61	1.89	1.87	1.85	1.84	1.95	2.09	2.10	1.99
Ho	0.43	0.48	0.46	0.50	1.29	1.18	1.18	1.37	1.01	0.42	0.42	0.41	0.41	0.44	0.46	0.47	0.44
Er	1.21	1.35	1.28	1.40	3.77	3.33	3.38	3.90	2.88	1.22	1.25	1.20	1.19	1.28	1.36	1.37	1.30
Tm	0.209	0.233	0.226	0.243	0.599	0.572	0.576	0.664	0.492	0.200	0.197	0.192	0.190	0.204	0.216	0.216	0.208
Yb	1.28	1.42	1.37	1.47	3.90	3.50	3.53	4.07	3.00	1.24	1.27	1.23	1.23	1.31	1.40	1.42	1.33
Lu	0.22	0.24	0.23	0.25	0.62	0.58	0.59	0.69	0.51	0.19	0.20	0.20	0.20	0.21	0.22	0.22	0.21
Hf	0.61	0.72	0.74	0.72	2.56	2.19	2.27	2.65	1.83	0.62	0.59	0.56	0.57	0.58	0.65	0.63	0.66
Ta	0.025	0.032	0.025	0.029	0.069	0.061	0.061	0.068	0.054	0.028	0.025	0.025	0.023	0.019	0.023	0.022	0.024
Pb	0.89	0.83	0.61	0.68	2.49	1.73	1.34	2.97	1.92	1.39	0.79	0.57	0.44	0.64	0.50	0.59	0.64
Th	0.11	0.20	0.25	0.13	0.54	0.49	0.52	0.61	0.42	0.16	0.09	0.09	0.09	0.06	0.07	0.07	0.16
U	0.038	0.064	0.070	0.045	0.191	0.169	0.163	0.219	0.145	0.052	0.031	0.031	0.030	0.022	0.024	0.023	0.049

Chemical group: c, calc-alkaline; t, tholeiite; low-K, low-K tholeiite.
Location: Reef, Reef Point, Cook; Beach, Beach Point, Thule; Resltn, Resolution Point, Cook; Hewison, Hewison Point, Thule; Bell, Bellingshausen; Wasp, Wasp Point, Thule; Flannery, Cape Flannery, Thule; Herd, Herd Point, Thule; Candl, Candlemas; Vind, Vindication.
Rock unit: 1, pre-sector collapse series; 2, pre-caldera; 3, no stratigraphic control; 4, recent Bellingshausen lava; 5, block in moraine; 6, post-sector collapse lavas; 7, post-sector collapse scoria; 8, bomb in syncaldera deposit; A, Old lava series, Candlemas Island; B, Lucifer Hill lavas, Candlemas Island; C, air fall deposit in ice cap, Candlemas Island; D, Braces Point, Vindication Island.
* Trace elements by ICP-MS. n.d. = not detected.

Table 2. *New isotope analyses of samples from Southern Thule*

Sample number	SS14.2	SS14.6	SS14.10	SS14.11	SS27.4	SS.2.1	SS13.11	SS28.2	SS26.2	SS29.1	SS30.2A	SS13.10	SS.1.2
Chemical group	t	t	t	t	t	t	t	c	c	c	c	c	c
Location	Reef	Reef	Reef	Reef	Beach	Beach	Hewison	Wasp	Flannery	Herd	Resolution	Hewison	Hewison
$^{87}Sr/^{86}Sr$	0.703748	0.703786	0.703782	0.703782	0.703747	0.703699	0.703766	0.703643	0.703757	0.703816	0.703773	0.703835	0.703773
Sr±	7	7	6	7	8	7	7	7	7	7	6	6	9
$^{143}Nd/^{144}Nd$	0.512998		0.512995	0.513027		0.513013	0.513002	0.513012		0.512995	0.513005	0.513019	0.512984
Nd±	4		3	4		3	4	5		4	4	4	4
$^{206}Pb/^{204}Pb$	18.546	18.561	18.562	18.574	18.572	18.573	18.581	18.591	18.611	18.600	18.599	18.592	18.598
6/4 ±	0.0013	0.0011	0.0016	0.0015	0.0016	0.0005	0.0007	0.0011	0.0011	0.0016	0.0005	0.0005	0.0004
$^{207}Pb/^{204}Pb$	15.599	15.597	15.597	15.598	15.597	15.602	15.599	15.602	15.611	15.606	15.602	15.602	15.604
7/4 ±	0.0012	0.001	0.0014	0.0012	0.0014	0.0004	0.0006	0.0009	0.001	0.0013	0.0005	0.0005	0.0003
$^{208}Pb/^{204}Pb$	38.475	38.484	38.486	38.479	38.487	38.503	38.495	38.508	38.542	38.528	38.516	38.509	38.518
8/4 ±	0.0029	0.0023	0.0035	0.0031	0.0035	0.001	0.0015	0.0024	0.0024	0.0032	0.0014	0.0012	0.0008

Chemical groups: t, tholeiite; c, calc-alkaline.

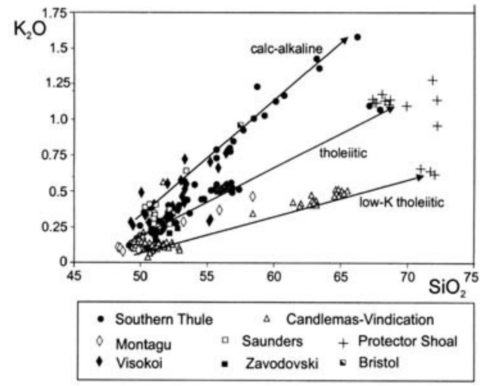

Fig. 4. K_2O v. SiO_2 plot for the South Sandwich arc. Data are from this study supplemented by data for Southern Thule from Pearce *et al.* (1995). Arrows show generalized trends of the calc-alkaline, tholeiitic and low-K tholeiitic groups.

form a distinctly bimodal series in Figure 4. Similar bimodality possibly exists in the tholeiitic series of Southern Thule, but no bimodality is evident in the calc-alkaline series.

Geochemical variations and volcano histories

Southern Thule

On Cook and Thule islands, the scattered distribution of most outcrops, separated by inaccessible cliffs or ice caps, means that stratigraphic control is poor, except for Hewison and Reef points. The oldest known rocks comprise a 50 m-thick sequence of 10 lavas exposed at Reef Point (Fig. 2). The sequence consists of strongly plagioclase–phyric mafic tholeiites with relatively homogenous compositions (50.9–52.6 wt% SiO_2, 4.1–4.4 wt% MgO) among the most mafic in Southern Thule (Fig. 5a, b). This sequence was cut by the sector collapse feature (Fig. 2). In contrast, probable pre-sector collapse lavas on Hewison Point are silicic (Fig. 5b). The post-sector collapse lavas of Reef and Hewison points are aphyric andesites (57.6–60.1 wt% SiO_2). Juvenile clasts from the possible syn-Douglas caldera air fall deposit range from basaltic andesite to dacite (54.2–63.2 wt% SiO_2), and the latter are among the most silicic samples from Southern Thule (Fig. 5b). Compositions

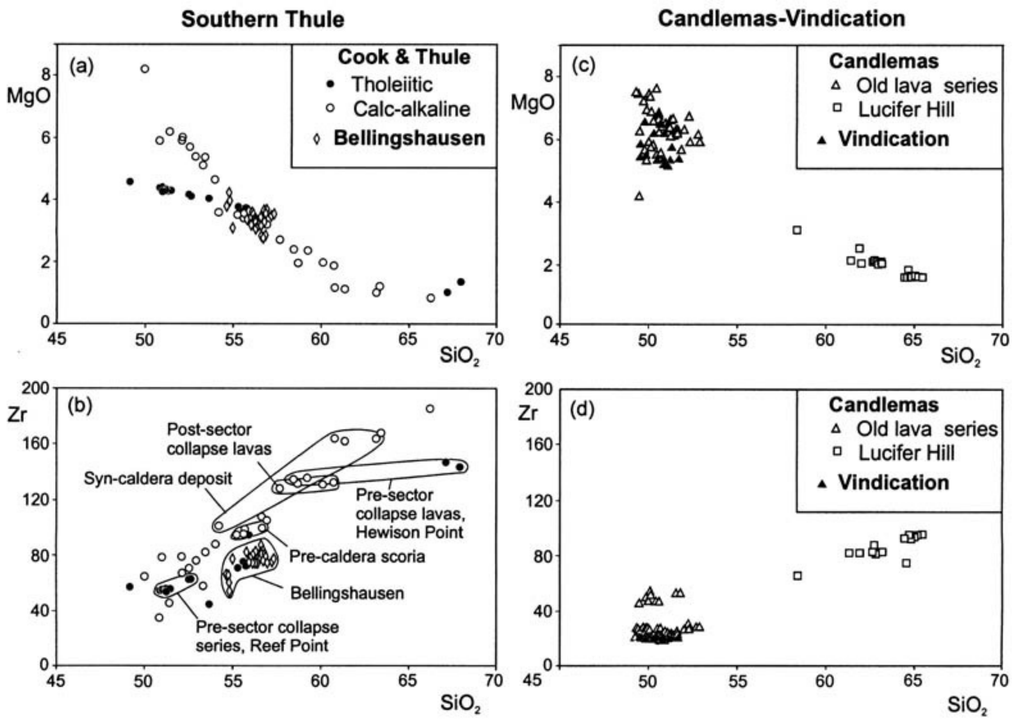

Fig. 5. Plots of MgO and Zr v. SiO_2 for (**a**, **b**) Southern Thule and (**c**, **d**) Candlemas and Vindication islands to illustrate magmatic evolutions of the islands. Data are from this study and Pearce *et al.* (1995).

therefore tended to become more silicic with time, and caldera formation was probably associated with some of the most silicic erupted compositions. There was also a tholeiitic to calc-alkaline change with time.

Bellingshausen Island, the youngest focus of volcanism in Southern Thule, is only known to have erupted relatively homogenous tholeiitic basaltic andesite magma compositions (Fig. 5), which are distinctly more evolved than the pre-sector collapse basalts.

Candlemas–Vindication

The oldest parts of this volcano are the sequences on Vindication Island and the southern part of Candlemas Island. The relative ages of these two sequences are unknown. Both sequences entirely consist of low-K tholeiitic mafic rocks. Over 400 m of section of the old lava sequence on Candlemas is exposed in cliffs south of Chimaera Flats (Fig. 3). The lavas contain abundant plagioclase phenocrysts and are notably homogenous in major and trace element composition, with all lavas in the range 49.3–52.9 wt% SiO_2 and 4.1–7.5 wt% MgO (Fig. 5c). Vindication samples are also strongly plagioclase phyric and similar to the low-Zr Candlemas group (Fig. 5d). All the lavas and pyroclastic deposits erupted from the younger, active volcano of Lucifer Hill are phenocryst-poor and are andesites and dacites (58.3–65.4 wt% SiO_2 and 1.5–3.1 wt% MgO). The compositional gap between the mafic and silicic rocks is pronounced.

Crustal structure from seismic studies

Larter *et al.* (2001) reported the results of a wide-angle seismic section along the approximately E–W-trending line BAS967–36, which crosses the arc near Southern Thule (Larter *et al.* 1998). The seismic results, which were constrained by gravity data, show a 14–15 km-thick crust with two notable features, both of which are absent from the adjacent oceanic crust.

- The lowest part of the crust beneath the South Sandwich arc consists of a 3 km-thick keel inferred from wide-angle reflections and gravity modelling, with a P-wave seismic velocity of 7.0–7.5 km s^{-1}. Similar lower crustal layers with velocities of about 7.0–7.5 km s^{-1} have been seismically identified in the intra-oceanic Izu–Bonin and Aleutian arcs (Suyehiro *et al.* 1996; Fliedner & Klemperer 1999; Holbrook *et al.* 1999). In the uplifted and exposed Kohistan arc, Pakistan, lithologies with seismic velocities of about 7.5 km s^{-1} are pyroxenites, garnet gabbros and wehrlites that occur at the base of the crust, and are interpreted as cumulates from mafic magmas (Miller & Christensen 1994). Similar olivine–pyroxene cumulates occur at the base of the exposed Talkeetna (Alaska) and Canyon Mountain (Oregon) intra-oceanic arcs (Pearcy *et al.* 1990; DeBari & Sleep 1991), and would appear to be a universal feature of intra-oceanic arcs.
- The mid-crust of the South Sandwich arc contains a 2 km-thick layer with a P-wave velocity of 6.0–6.5 km s^{-1}. This structure is very similar to the mid-crustal layer with seismic velocities of about 6.0 km s^{-1} found in the Izu–Bonin arc (Suyehiro *et al.* 1996), although the South Sandwich layer is about a third of the thickness of the Izu–Bonin example. A similar layer may exist beneath most of the length of the Lesser Antilles arc (Boynton *et al.* 1979). Such structures are not found in all arcs, not being present, for example, in seismic sections of the Aleutian arc (Fliedner & Klemperer 1999; Holbrook *et al.* 1999). P-wave velocities of 6.0–6.5 km s^{-1} are characteristic of virtually all intermediate and granitic plutonic rocks found in the arc environment (Chroston & Simmons 1989; Miller & Christensen 1994; Christensen & Mooney 1995), and it is highly likely that the mid-crustal layer in the South Sandwich arc consists of such intermediate–granitic plutonic rocks (Larter *et al.* 2001). Suyehiro *et al.* (1996) interpreted the mid-crustal layer in the Izu–Ogasawara arc as tonalitic, based on lateral correlation of the seismically identified layer with tonalitic outcrops.

These two features are critical to understanding of the magmatic evolution of the South Sandwich arc, and are further discussed below.

The nature of the mantle source

Source depletion

Pearce *et al.* (1995) demonstrated that the mantle source of the South Sandwich arc is variably depleted relative to normal mid-ocean ridge basalt (N-MORB)-source mantle, with the low-K tholeiites having been derived from the most depleted mantle. Among trace elements that are not affected by additions from the subducting slab, those that are highly incompatible in mantle assemblages have lower abundances, relative to MORB, than less incompatible

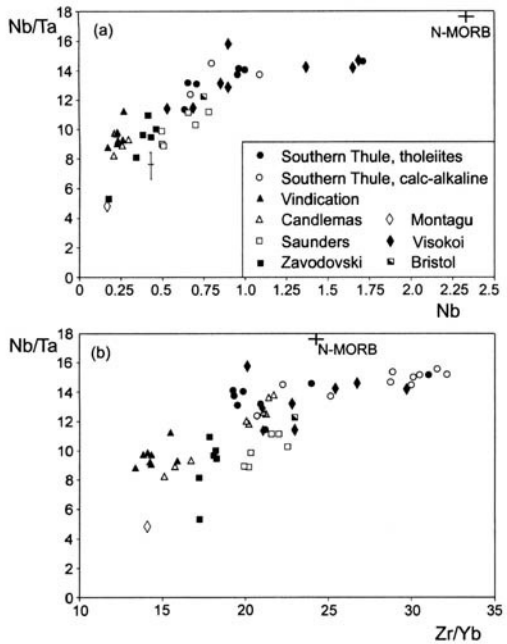

Fig. 6. Plots of Nb/Ta v. Nb and Zr/Yb for volcanic rocks from the South Sandwich arc (data from this study). In (**a**) only mafic rocks with <57 wt% SiO_2 are plotted; in (**b**) mafic and silicic rocks are plotted. The N-MORB composition is that of Sun & McDonough (1989). The error bars give typical errors in precision for a low-Nb basalt.

elements. The most likely explanation is that the mantle, which was originally N-MORB-source in composition, lost a proportion of its most incompatible elements during partial melting and melt extraction from the mantle sources in an event prior to the melting event which generated the arc basalts (Woodhead *et al.* 1993; Pearce *et al.* 1995).

Figure 6 illustrates some of the effects of the source depletion. All the volcanic rocks of the South Sandwich arc have subchondritic Nb/Ta ratios, in the range 4.9–15.8, contrasting with MORB (and ocean island basalt (OIB)), which have chondritic Nb/Ta ratios of about 17.5 (Sun & McDonough 1989). The samples with the lowest Nb/Ta ratios are those having the lowest Nb abundances (Fig. 6a), in agreement with the findings of Plank & White (1995), Eggins *et al.* (1997) and Woodhead *et al.* (1998). The relationship is unlikely to be a result of analytical errors at low Ta and Nb abundances. Subchondritic Nb/Ta ratios have been well documented in arc lavas of the New Britain (Nb/Ta ≥ 11.6; Woodhead *et al.* 1998) and the Mariana arcs (Nb/Ta ≥ 10.1; Elliott *et al.* 1997) and also occur in the Tonga–Kermadec arc (Nb/Ta ≥ 9.8; Ewart *et al.* 1998). In all these cases, the lavas with the lowest Nb/Ta ratios are the ones with the lowest Nb abundances. The South Sandwich arc has the lowest Nb/Ta ratios of any arc of which we are aware. There is a positive correlation of Nb/Ta with Zr/Yb (Fig. 6b).

There is substantial evidence that Nb is more incompatible than Ta in mantle assemblages (e.g. Forsythe *et al.* 1994; Green 1994), so the decrease in Nb/Ta ratio cannot be the result of a single partial melting event of mantle. However, the low Nb/Ta ratios could be produced if the more incompatible Nb was preferentially removed in a melt during a partial melting event before the generation of the arc basalts (Plank & White 1995; Eggins *et al.* 1997; Elliott *et al.* 1997). This interpretation is supported by the positive correlation of Nb/Ta with Zr/Yb. The latter ratio is well constrained as recording variable depletion of the South Sandwich subarc mantle (Pearce *et al.* 1995), and it is likely that Nb/Ta records the same process. It has been widely proposed that the depletion events that preceded the mantle melting to produce arc magmas occur at back-arc spreading centres associated with individual arcs (Woodhead *et al.* 1993, 1998; Plank & White 1995). This seems to be the case in the South Sandwich system for the following reasons: (i) all the arc magmas have subchondritic Nb/Ta, indicating that the depletion is not taking place by generation of magmas within the arc; (ii) most of the back-arc magmas (segments E2–E9) have Nb/Ta ratios in the range 14.8–18.0 (Leat *et al.* 2000; Fretzdorff *et al.* 2002), consistent with this being the location of extraction of relatively high Nb/Ta melts; and (iii) peridotites in the forearc show a history of melt extraction, probably at the back-arc spreading centre before being overridden by the arc (Pearce *et al.* 2000).

The compositions of components derived from subducted material

Recent studies of island arcs have shown that it is possible to identify two main chemical components, sediment (or more likely, a melt derived from sediment) and aqueous fluid, within the overall subduction signature. The sediment component is variable in composition and characterized by high La/Sm, Th/Nb and Th/Yb ratios (Elliott *et al.* 1997; Woodhead *et al.* 1998), and sometimes has high $^{87}Sr/^{86}Sr$ and low $^{143}Nd/^{144}Nd$ ratios (Turner *et al.* 1996; Elliott *et al.* 1997; Hawkesworth *et al.* 1997; Class *et al.*

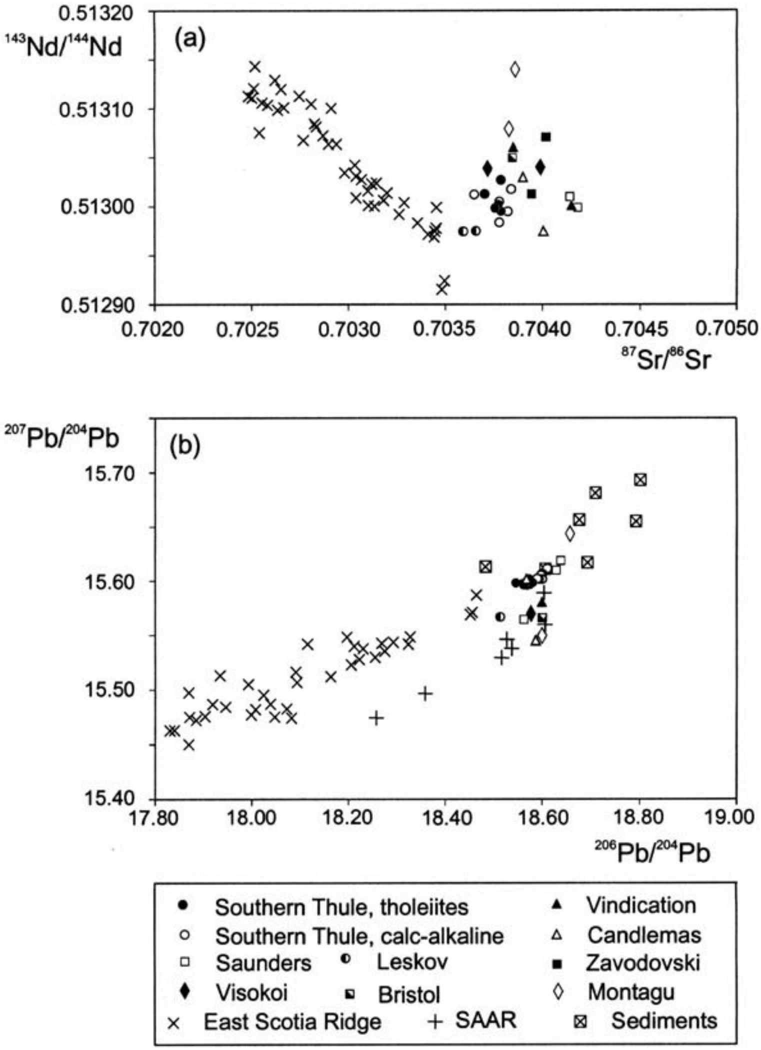

Fig. 7. Isotope plots for the South Sandwich Islands. (**a**) Plot of ^{143}Nd/^{144}Nd v. ^{87}Sr/^{86}Sr for the South Sandwich Islands and the East Scotia Ridge. Data for the tholeiitic and calc-alkaline series of Southern Thule are from Table 2, and other South Sandwich data from the compilation of Pearce *et al.* (1995). The East Scotia Ridge data are from Leat *et al.* (2000) and Fretzdorff *et al.* (2002). (**b**) Plot of ^{207}Pb/^{204}Pb v. ^{206}Pb/^{204}Pb for the South Sandwich Islands, East Scotia Ridge, South American–Antarctic Ridge and South Atlantic sediments. Data for the tholeiitic and calc-alkaline series of Southern Thule are from Table 2, and other South Sandwich data from Cohen & O'Nions (1982) and Barreiro (1983). The East Scotia Ridge data are from Leat *et al.* (2000, the Bouvet-like component is omitted) and Fretzdorff *et al.* (2002), the South American–Antarctic Ridge (SAAR) data are from Kurz *et al.* (1998), and the South Atlantic sediment data are from Barreiro (1983).

2000). The aqueous fluid, derived by dehydration of basaltic slab and dewatering of sediments, is characterized by high Ba/Th, Ba/Nb, B/Be and ^{238}U/^{230}Th ratios (Ryan *et al.* 1995; Elliott *et al.* 1997; Hawkesworth *et al.* 1997; Turner & Hawkesworth 1997). The aqueous fluid component is also sometimes associated with high Sr/Nd and Sr/Th ratios in excess of those produced by plagioclase cumulation (see later section). The existing Sr, Nd and Pb isotope ratio data for the South Sandwich Islands have a small range, and there is no apparent correlation with trace element ratios defining the component end-members. In Figure 7a, new Sr and Nd isotope data for Southern Thule are plotted relative to previous data for the South Sandwich

Islands and the back-arc East Scotia Ridge. The new data have a limited range compared to the older data, and plot as a group in the low $^{87}Sr/^{86}Sr$, low $^{143}Nd/^{144}Nd$ part of the scatter of data points from the South Sandwich Islands, close to the high $^{87}Sr/^{86}Sr$ end of the isotopic array of East Scotia Ridge lavas. In most of the islands, however, there is no systematic variation of either $^{87}Sr/^{86}Sr$ or $^{143}Nd/^{144}Nd$ with geographic position in the arc, or with compositional series. Within the Southern Thule data, there is no difference in $^{87}Sr/^{86}Sr$ between the tholeiitic and calc-alkaline rocks, but the calc-alkaline rocks have marginally lower $^{143}Nd/^{144}Nd$ than the tholeiites.

New Pb data for Southern Thule are plotted relative to published data in Figure 7b. Also plotted are data for South American–Antarctic Ridge basalts and South Atlantic sediments, which are the best available data representing slab and sediment, respectively, subducting at the South Sandwich trench. The new data form a very tight cluster and do not extend the field for the South Sandwich Islands. However, the calc-alkaline rocks have slightly higher $^{206}Pb/^{204}Pb$ and $^{207}Pb/^{204}Pb$ ratios than the tholeiites within Southern Thule. This relationship is consistent with higher sediment input to the calc-alkaline than the tholeiitic magmas. The scatter in the older Pb analyses from the arc does not relate in any obvious way to either geographic position in the arc, or with compositional series, and some of the scatter may be due to greater analytical errors in Pb isotope analysis two decades ago. The Pb isotope data can be explained in terms of mixing of Pb from subducted sediment, mantle wedge and subducted slab (Pearce *et al.* 1995), with the subducted sediment being the main control on arc magma compositions.

The East Scotia Ridge and South American–Antarctic Ridge form closely spaced parallel trends in Figure 7b. Southern Thule samples plot on a continuation of the East Scotia Sea trend, indicating their Pb may have been dominated by wedge plus sediment. By contrast, some samples from Candlemas, Vindication, Montagu and Bristol islands plot below this trend, and can be modelled by mixing of Pb from sediment and subducting slab (Pearce *et al.* 1995).

Nevertheless, both main slab components have been identified in the South Sandwich arc (Leat *et al.* 2000). In the plot of Ba/Th v. Th/Nb (Fig. 8a), there is an overall negative correlation in South Sandwich Island lavas, with the high Ba/Th samples interpreted to be dominated by the aqueous fluid component, and the high Th/Nb samples interpreted to be dominated by the sediment component, in line with observations from other arcs (Elliott *et al.* 1997; Hawkesworth *et al.* 1997) and experimental results (Johnson & Plank 1999 and references therein).

In detail, the South Sandwich Islands data form two trends in Figure 8a. One trend, defined by the low-K tholeiite series of Candlemas–Vindication, Zavodovski and Montagu islands, shows strongly increasing Ba/Th ratios with decreasing Th/Nb, and a maximum Ba/Th ratio of about 400. This trend is similar to that shown by the central islands of the Mariana arc (Fig. 8a), and probably by other intra-oceanic arcs showing comparable high Ba/Th end-members (Hawkesworth *et al.* 1997). The other trend is defined by the tholeiitic and calc-alkaline series from Southern Thule, and shows minor increase in Ba/Th with decreasing Th/Nb, producing an almost horizontal trend in the diagram. Maximum Ba/Th in the trend is less than 200. A similar trend is absent from the Mariana arc.

The Southern Thule (and Leskov) samples, which have a high sediment component according to their high Th/Nb and low Ba/Th ratios, have some of the lowest $^{87}Sr/^{86}Sr$ ratios in the arc (Fig. 7). Moreover, while these samples have among the lowest $^{143}Nd/^{144}Nd$ ratios in the arc, they fall within the range of $^{143}Nd/^{144}Nd$ shown by the low-K tholeiites. This lack of correlation of Sr and Nd isotopes with the subducted sediment component is in strong contrast to behaviour in other arcs (e.g. Mariana arc, Elliott *et al.* 1997; Lesser Antilles arc, Turner *et al.* 1996; Aleutian arc, Class *et al.* 2000).

Ba/Th and Th/Nb are plotted against Nb/Ta in Figure 8b, c. Nb/Ta indicates the degree of depletion of the subarc mantle prior to addition of the subduction components, with the lowest Nb/Ta samples being the most depleted. There is poor positive correlation of Th/Nb with Nb/Ta, and a better negative correlation of Ba/Th with Nb/Ta. The negative correlation of Ba/Th is expected, given the general observation that large ion lithophile element/high-field-strength elements (LILE/HFSE) ratios are highest in the most depleted arc rocks (Hawkesworth *et al.* 1997 and references therein).

Elliott *et al.* (1997), in their model for the Mariana arc, argued that the overall inverse correlations of indices of fluid addition, such as Ba/Th, with indices of sediment addition, such as Th/Nb, demand that an approximately constant fluid flux was added to mantle that was already variably enriched in the sediment component. They further argued that the inverse correlation of Th/Nb with Ta/Nb in the Mariana Arc lavas (Fig. 8c) was a result of variable addition of the sediment component to depleted mantle. They thus implied, but did not explicitly state, that their variation in Nb/Ta was a result of variable sediment component addition to a uniformly depleted mantle. Peate & Pearce (1998) equivocated whether magmas from the northern Mariana arc having high Th/Nb and super-chondritic Nb/Ta resulted from sediment melt addition or from pre-existing variation in the mantle wedge. Such models can be examined with respect to the South Sandwich arc samples.

In Figure 8c, the variation in Th/Nb v. Nb/Ta in the South Sandwich samples cannot be satisfactorily modelled by mixing of a single depleted mantle composition with a sediment component. The data are scattered, and clearly do not plot along a single mixing line, although there is a very weak overall positive correlation of Th/Nb with Nb/Ta. Variable depletion of N-MORB source mantle will produce melts with progressively decreasing Nb/Ta with increasing depletion. As Th is more incompatible in mantle assemblages than Nb (Green 1994), melts from increasingly depleted mantle will also produce melts with progressively decreasing Th/Nb (Fig. 8c). The sediment component has Th/Nb > 0.9, and is likely to have chondritic Nb/Ta. Samples from Southern Thule plot along a steep trend at a high angle to the weak overall trend. Candlemas–Vindication samples form another trend at a lower angle to the overall weak trend. The Central Mariana samples plot on yet another trend, probably toward high Th/Nb, super-chondritic Nb/Ta compositions (Peate & Pearce 1998). Our interpretation for the South Sandwich arc is that melts derived from sources representing mixtures of variable amounts of the sediment component and variably depleted mantle will produce the observed fan-shaped array. In this model the amount of sediment added is independent from the degree of mantle depletion.

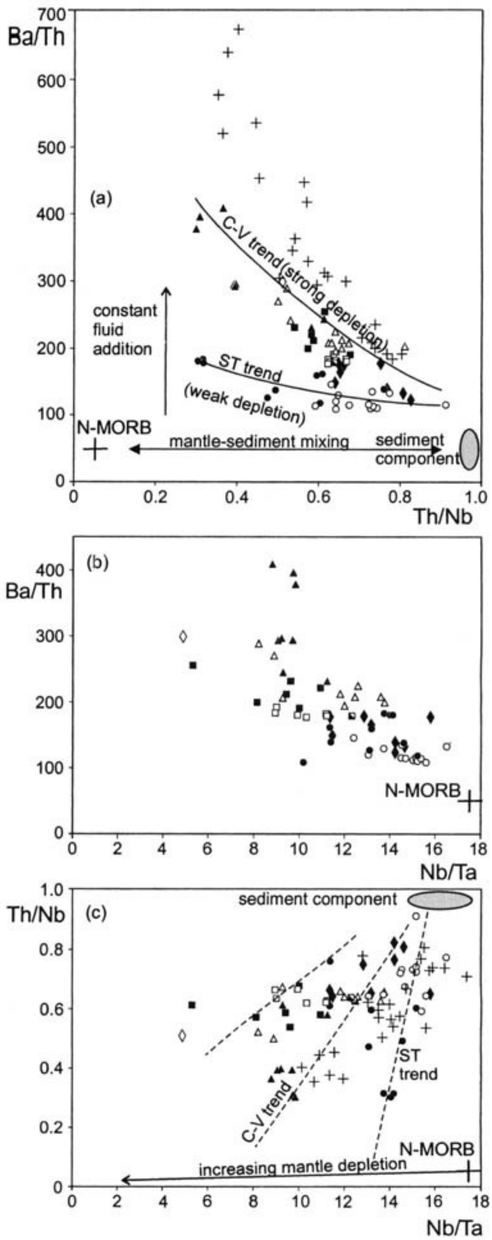

Fig. 8. Trace element ratio diagrams showing the relationships of mantle depletion and enrichment events in the generation of the South Sandwich arc magmas. Data are from this study, supplemented by data for Southern Thule from Pearce *et al.* (1995), and the N-MORB composition is from Sun & McDonough (1989). Symbols are as in Fig. 6. Small vertical crosses are data from the central island province of the Mariana arc (Elliott *et al.* 1997). (**a**) Ba/Th v. Th/Nb showing the effects of addition of aqueous fluid and sediment components to mantle of various degrees of depletion. A mantle–sediment mixing line is drawn between N-MORB and a sediment component (probably a sediment melt, and defined only by having higher Th/Nb than any of the arc samples, together with low Ba/Th). Trend C–V illustrates the effect of adding a constant amount of Ba-bearing fluid to variable proportions of strongly depleted mantle and sediment component, whereas trend ST illustrates the effect of adding a constant amount of Ba-bearing fluid to variable proportions of weakly depleted mantle and sediment component. (**b**) Ba/Th v. Nb/Ta, showing higher Ba/Th in more depleted (lower Nb/Ta) samples. (**c**) Th/Nb v. Nb/Ta showing absence of good correlation between these ratios. Dashed lines show possible trends for individual island groups, labelled as in (a).

The overall inverse correlation of Ba/Th with Th/Nb (Fig. 8b) can be adequately modelled as the result of addition of constant amounts of aqueous fluid, carrying Ba but no Th, into a source that is variably enriched in Th due to input of the sediment component (Elliott *et al.* 1997; Peate & Pearce 1998). The existence of at least two diverging trends in Figure 8a shows that the situation is more complicated than two-component mixing. The arguments made from Figure 8c demand that Th is controlled by both the sediment component and by the variably depleted mantle. Two trends (representing different degrees of mantle depletion) in Figure 8a show the effects of addition of constant aqueous fluid (carrying Ba) to two different sediment component-depleted mantle mixtures. Differences are greatest at the low sediment component (low Th/Nb) ends, where the effects of removal of Th due to mantle depletion are greatest. Strongly depleted mantle, with minor sediment addition, will produce very high Ba/Th ratios by addition of a fluid-borne batch of Ba. By contrast, weakly depleted mantle, with the same minor sediment addition, will produce relatively low Ba/Th ratios by addition of the same fluid-borne batch of Ba. At the high sediment component ends of the trends, the Th budgets are both dominated by the sediment components and strongly converge. The result is that samples in Figure 8a plot as a fan-shaped array, and not as a two-component mixing curve.

These considerations suggest the following model for the South Sandwich arc:

- variable depletion of the mantle source, reducing Nb/Ta and Th/Nb;
- variable addition of the sediment component to the variably depleted mantle, producing weakly depleted sources that are either sediment-poor or sediment-rich (≡Southern Thule), as well as strongly depleted sources that are either sediment-poor or sediment-rich (≡Candlemas–Vindication). This result is intuitive, given that the processes of mantle depletion and addition of the sediment component are thought to be independent of each other (Woodhead *et al.* 1993; Pearce *et al.* 1995);
- addition of approximately constant amounts of aqueous fluid to the sources that carried Ba into the source, as well as triggering melting (Elliott *et al.* 1997).

The difference between the origin of the tholeiitic–calc-alkaline series of Southern Thule, on the one hand, and that of the low-K tholeiite series of Candlemas–Vindication, on the other, is the weak mantle depletion of the former relative to the latter. In the Southern Thule magmas, the difference between the origin of the calc-alkaline and tholeiitic magmas lies in the greater sediment component input to the former (in accord with Pb isotope data).

The nature of the primary magmas

Knowing the compositions of primary magmas erupted in magmatic arcs is important in order to answer questions about the compositions and melting processes in their mantle sources. Primary magmas, that have not been modified since leaving their sources, are very rare in magmatic arcs, but primitive magmas, which have experienced only minimal fractionation or contamination since leaving their sources, are much more common. The primitive magmas have FeO*/MgO ratios <1 (≡Mg#>64) and high Ni and Cr abundances (>200 and >400 ppm, respectively) (Tatsumi & Eggins 1995). In this paper, FeO* and Fe* are total iron as FeO and Fe, respectively, and Mg# is calculated as 100×Mg/(Mg+Fe*), after Tatsumi & Eggins (1995). The primitive magmas of arc volcanic sequences generally contain 9–16 wt% MgO. At first sight, the thin crust and dominantly mafic composition of the South Sandwich arc make it a likely arc in which to find primitive magmas. Figure 9 shows that this is not the case. There are very few South Sandwich samples having Mg# > 60, and none > 64, except for a group of 'oceanite' lavas from Allen Point, Montagu Island (Baker 1978, 1990). These rocks contain 50–80% clinopyroxene, plagioclase and olivine (Fo_{60-82}) phenocrysts, are unlikely to represent primitive, mantle-derived compositions and probably are cumulitic in origin (Luff 1982).

All other mafic magmas erupted in the South Sandwich arcs have <8–8.5 wt% MgO, (Mg# <63) (Fig. 9), and have clearly experienced considerable fractional crystallization during ascent. Nevertheless, Figure 9 demonstrates that none of the South Sandwich Islands lavas are related to the boninite suite. Instead, they appear to be related to the group of primitive arc magmas that is thought to have been generated by partial melting of peridotites in mantle wedges above subducting slabs (e.g. Nye & Reid 1986; Gust & Perfit 1987; Eggins 1993; Tatsumi & Eggins 1995). Such primitive arc magmas, although relatively rarely erupted in magmatic arcs, are widely regarded as parental to most volcanic arc magma series. Known examples are distributed in roughly equal amounts in continental and oceanic arcs (Leat *et al.* 2002), and their eruption does not appear to be especially

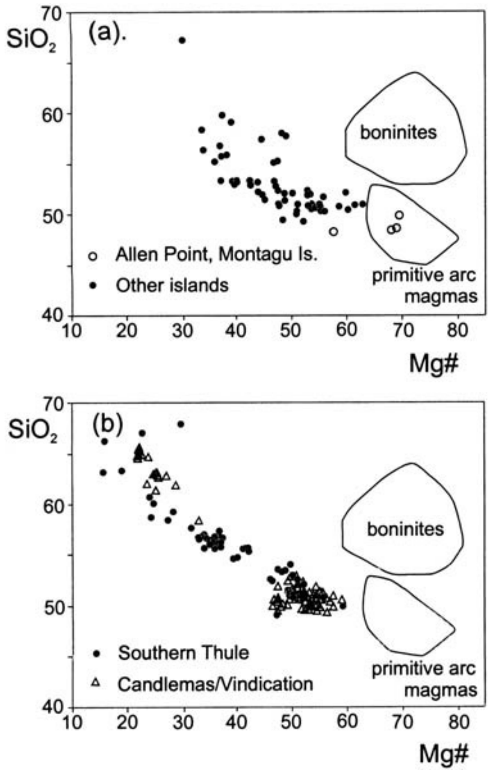

Fig 9. SiO_2 v. Mg# plots for South Sandwich Islands volcanic rocks, compared to fields for boninites (Crawford *et al.* 1989) and primitive and primary magmas from magmatic arcs (Leat *et al.* 2002). **(a)** Samples from Bristol, Freezland, Montagu, Saunders, Visokoi, Leskov and Zavodovski islands, and Protector Shoal (data from this study and Pearce *et al.* 1995). Oceanite samples from Allen Point, Montagu Island are shown as open circles. **(b)** Samples from Southern Thule and Candlemas and Vindication Islands (this study and Pearce *et al.* 1995).

favoured by thin, mafic, oceanic crust. Various explanations for their rarity of eruption in magmatic arcs include insufficient buoyancy to ascend through the crust (Smith *et al.* 1997), and tendency to be trapped in magma chambers at or near the Moho (Leat *et al.* 2002). In view of the fact that the South Sandwich Islands represent the emergent parts of large volcanoes that are likely to have well-developed magma plumbing systems, it not surprising that all the magmas were trapped on their way to the surface in magma chambers in which fractional crystallization occurred, and that primitive magmas are therefore lacking.

Fractionation crystallization

Because of the complex magmatic evolution of the South Sandwich magmas it is not possible to model the magma compositions along simple lines of descent by fractional crystallization. Pearce *et al.* (1995) provided a workable summary for fractional crystallization of South Sandwich magmas from basalt to dacite, in good agreement with results of Luff (1982) for the South Sandwich arc and of Woodhead (1988) for the Mariana arc. The main features are that the fractionating assemblage consists of olivine, clinopyroxene and plagioclase, with magnetite being significant at more than about 56% silica, and orthopyroxene being significant after more than about 63% silica. Approximately 52% fractional crystallization is required to generate basaltic andesite from the least evolved erupted basalt, and a further 16% fractionation is required to generate andesite from basaltic andesite. The fractionation paths are complicated by accumulation of plagioclase (common) and olivine and clinopyroxene (Luff, 1982; Pearce *et al.* 1995).

The origin of high-Al basalts

The origin of high-Al basalts, which are characteristic of volcanic arcs, is controversial, and origins by partial melting of subducting slab (Johnston 1986), fractional crystallization of hydrous basalt (Sisson & Grove 1993; Pichavant & Macdonald 2003) and accumulation of plagioclase (Crawford *et al.* 1987) have been suggested. In the Al_2O_3 v. MgO plot (Fig. 10a), all basalts of Candlemas and Vindication islands and of the tholeiitic series on Southern Thule have significantly greater Al_2O_3 abundances than nearly all primitive magmas of volcanic arcs. With >17.5 wt% Al_2O_3, they classify as high-Al basalts. They contrast with the relatively low Al_2O_3 contents of calc-alkaline basalts of Southern Thule (Fig. 10a). The absence of primitive magmas in the South Sandwich Islands, and the gap between global primitive magmas and the bulk of South Sandwich basalts in Figure10a, means that fractionation trajectories are not certain. Nevertheless, it is highly likely that, in this case, all the high-Al compositions were caused by accumulation of plagioclase. Evidence includes the modal abundance of up to 40% plagioclase phenocrysts, the correlation of Al_2O_3 abundances with modal plagioclase contents (Luff 1982), Eu/Eu* ratios of >1 in basaltic rocks (Fig 10c) and correlation of high Eu/Eu* with high Al_2O_3 abundances (Fig. 11). These features are among those used by

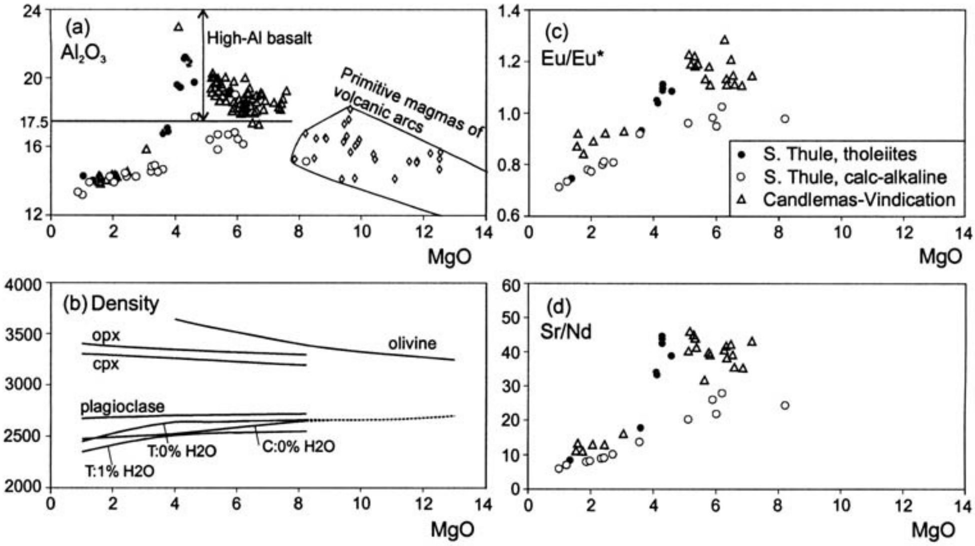

Fig. 10. Plots of Al_2O_3, density, Eu/Eu* and Sr/Nd v. MgO for Southern Thule and Candlemas–Vindication. In (**a**), the field for primitive magmas of volcanic arcs is from the compilation from numerous arcs of Leat *et al.* (2002). In (**b**) magma densities (kg m^{-3}) are calculated after the method of Bottinga & Weill (1970), as modified by Lange & Carmichael (1990). The curves T: 0% H_2O and T: 1% H_2O are calculated for Southern Thule tholeiites containing 0 and 1% H_2O, respectively; the curve C: 0% H_2O is for Southern Thule anhydrous calc-alkaline magmas. Data are from this study and Pearce *et al.* (1995).

Crawford *et al.* (1987) to argue that high-Al basalts of arcs in general formed by accumulation of plagioclase.

In Figure 10b, density of phenocrysts and South Sandwich magmas is plotted against magma MgO contents. Olivine and pyroxenes have densities that are at least 500 kg m^{-3} greater than all the magmas. On the other hand, plagioclase and anhydrous tholeiitic magma have the same densities to within ± 72 kg m^{-3} for all compositions more mafic than MgO = 4%. The extremely high proportion of basalts that experienced plagioclase accumulation suggests that these density contrasts are petrogenetically significant. The calc-alkaline magmas have lower densities than the tholeiites at MgO contents between 2 and 8 wt% (Fig. 10b), which might explain why the calc-alkaline magmas did not experience significant plagioclase accumulation.

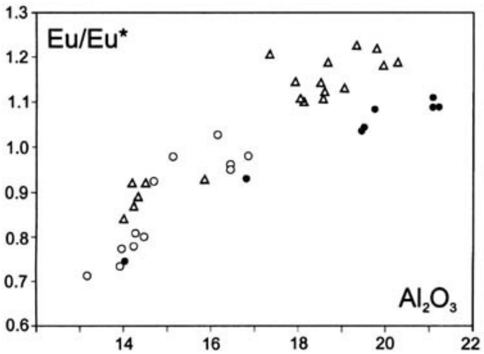

Fig. 11. Plot of Eu/Eu* v. Al_2O_3 MgO for Southern Thule and Candlemas–Vindication islands. Data are from this study and Pearce *et al.* (1995). Symbols as in Fig 10.

Eu is concentrated in plagioclase relative to other rare earth elements. The tholeiitic basalts of Candlemas, Vindication and Southern Thule have high Eu/Eu* ratios of >1, indicating plagioclase accumulation. This contrasts with the calc-alkaline basalts of Southern Thule, which have Eu/Eu* ratios of about 1.0, indicating no net plagioclase removal or accumulation. Silicic magmas having MgO <4 wt% in all series have Eu/Eu* ratios <1.0, which would be consistent with net removal of plagioclase from any mafic parent. Very similar relationships are shown in the Sr/Nd v. MgO plot (Fig. 10d). Sr is much more compatible in plagioclase than Nd, but both elements are incompatible in other phenocryst phases. The high-Al tholeiitic basalts of Candlemas, Vindication and Southern Thule have Sr/Nd ratios of 33–46, much higher than the calc-alkaline basalts of Southern Thule. Rocks

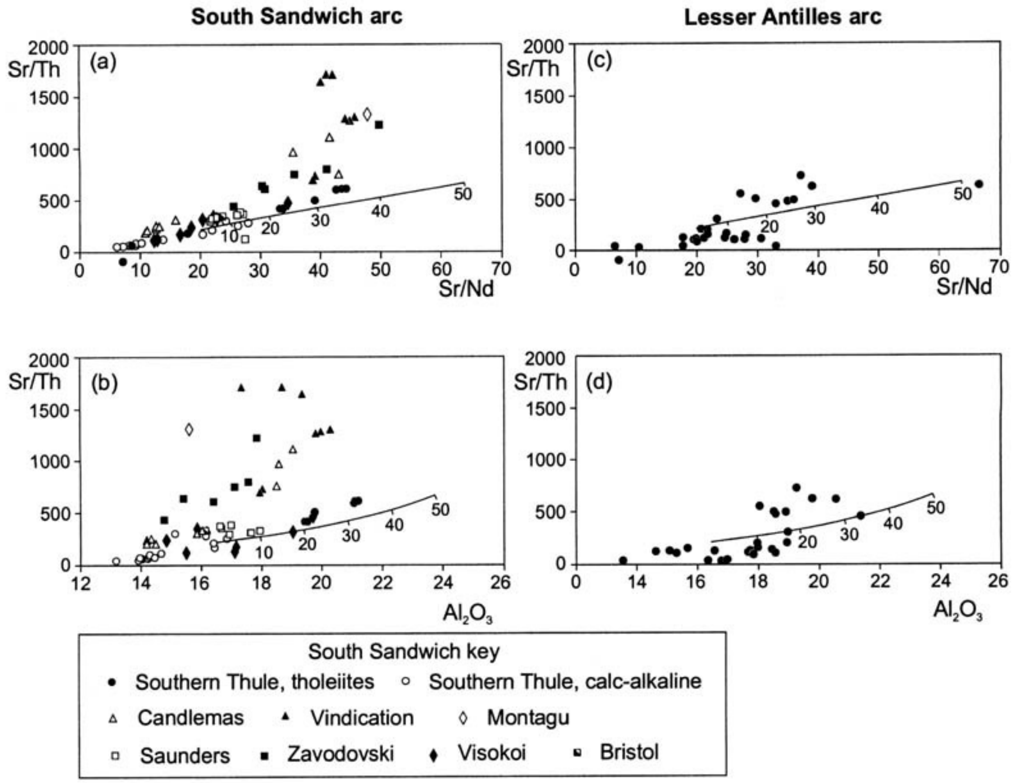

Fig. 12. Plots of Sr/Th v. Sr/Nd and Al_2O_3 for the South Sandwich and Lesser Antilles arcs (data from this study, Pearce *et al.* 1995 and Turner *et al.* 1996). The curves indicate the effects of accumulation of plagioclase to a parental basalt with 16.5 wt% Al_2O_3, 130 ppm Sr, Sr/Th = 220 and Sr/Nd = 20. The plagioclase is assumed to contain 31 wt% Al_2O_3, and have distribution coefficients of 2.4, 0.065 and 0.16 for Sr, Nd and Th, respectively (average of values reported by Dunn & Sen 1994).

with <4 wt% MgO have very low Sr/Nd ratios of 6–18. Figure 10 is strong evidence that Al, Eu and Sr abundances of South Sandwich lavas were controlled largely by plagioclase fractionation.

Limits of plagioclase control on strontium abundances

The control on Sr abundances, and in particular the Sr/Nd ratio, by plagioclase that is evident in Figure 10 raises questions about the extent to which Sr abundances and ratios of Sr v. other incompatible elements are controlled by plagioclase accumulation and removal in arc magmas in general. The issue is pertinent in view of the use of ratios of Sr and other incompatible elements (most commonly Sr/Th and Sr/Nd) to identify various mantle-derived components in arcs by many authors, including Ellam & Hawkesworth (1988), Woodhead & Johnson (1993), Turner *et al.* (1996), Hawkesworth *et al.* (1997) and Woodhead *et al.* (1998). None of these contributions assessed the limits of plagioclase fractionation on the elemental ratios they discussed, and assumed that the ratios correctly reflected those of primary mantle-derived melts. It is also evident from Figure 10 that simply filtering out silicic rocks from data sets removes only low Sr/Nd magma compositions that experienced net plagioclase removal, and does not remove the effects of plagioclase accumulation in basalts.

In Figure 12, the effects of plagioclase accumulation are quantified by modelling the addition of plagioclase to a relatively non-fractionated basalt composition having 16.4 wt% Al_2O_3 and 220 ppm Sr. This is representative of the composition of basalt magmas before any addition of plagioclase took place. Figures 12a, b show data from the South Sandwich Islands.

Samples with Sr/Nd ratios of more than about 20–30 have accumulated plagioclase; samples with Sr/Nd less than about 20 are silicic, and can be modelled by fractional removal of plagioclase. The entire range in Sr/Nd and Al_2O_3 in the rocks can be modelled by plagioclase removal and by up to 40% accumulation of plagioclase. However, the Sr/Th ratio shows additional processes at play. The samples form two groupings. In the first group, the samples have Sr/Th up to about 600, and plot close to the plagioclase accumulation curves, indicating that Al_2O_3 abundances and Sr/Th and Sr/Nd ratios can be modelled by plagioclase accumulation and removal alone. This group includes those from Southern Thule (tholeiitic and calc-alkaline), Saunders, Visokoi and Bristol islands. The second group of rocks, including samples from Vindication, Candlemas, Zavodovski and Montagu have Sr/Th ratios up to 1700, much higher than the plagioclase accumulation curves. While their Sr/Nd ratios and Al_2O_3 abundances can be modelled by plagioclase addition, their Sr/Th ratios cannot. This second group comprises the low-K tholeiite series, which are also the most depleted in having low Nb, Nb/Ta and Zr/Yb ratios (Fig. 6). It has been argued above that these islands have been most affected by a mantle component carried in an aqueous fluid derived from the slab. It is likely that the high Sr/Th in these samples consists of two parts, a part added late in the magmas' evolution amounting to up to Sr/Th = 600 and caused by plagioclase accumulation, and a mantle-derived part imparted during mantle partial melting, and which can be interpreted as resulting from addition of high-Sr, low-Th fluids from the slab to the mantle source (Hawkesworth *et al.* 1997).

Figures 12c, d show comparable data for the Lesser Antilles arc (Turner *et al.* 1996). Like the South Sandwich samples, the Lesser Antilles samples have Sr/Nd ratios and Al_2O_3 abundances that are readily explained in this diagram by accumulation and removal of plagioclase. This agrees with the observations of Macdonald *et al.* (2000) that plagioclase accumulation was widespread in the genesis of tholeiitic and calc-alkaline magmas of the northern and central Lesser Antilles. All of the Lesser Antilles samples have Sr/Th ratios less than 730, and all plot close to the plagioclase accumulation curves (Fig. 12c, d). Any increase in Sr/Th above the effects of plagioclase accumulation in the few Lesser Antilles samples that plot above the plagioclase accumulation curves in Figures 12c, d is too small to be easily resolved.

A contrary view was expressed by Turner *et al.* (1996), who showed an inverse correlation of Sr/Th with $^{87}Sr/^{86}Sr$ in this same Lesser Antilles data set, which they interpreted as a mixing curve between two slab-derived components in the mantle source – aqueous fluid (high Sr/Th) and sediment (high $^{87}Sr/^{86}Sr$). The high Sr/Th samples in the data set of Turner *et al.* (1996) occur in the tholeiitic series from the northern Lesser Antilles. These samples have high Ba/Th and $^{230}Th/^{232}Th$ ratios that clearly indicate that they do, indeed, contain a large contribution from the aqueous fluid component. Moreover, their tholeiitic compositions may have favoured accumulation of plagioclase. The correlation between high Sr/Th and high aqueous fluid components in these samples may therefore only be indirect, as predominance of aqueous fluid component and plagioclase accumulation both tend to occur in depleted tholeiitic magmas. On the other hand, Hawkesworth *et al.* (1997) demonstrated that high Sr/Th ratios are also restricted to low $^{87}Sr/^{86}Sr$ magmas when arc magma compositions are viewed globally. Their group of low $^{87}Sr/^{86}Sr$, incompatible element-depleted arcs (from the Mariana, South Sandwich, Tonga-Kermadec and Vanuatu arcs) have Sr/Th ratios up to 1200. Such Sr/Th ratios are more than likely effects of plagioclase accumulation, and high Sr/Th in these arcs clearly does record the addition of a high Sr/Th component (aqueous fluid) to the mantle source.

Cumulate volumes derived from the fractional crystallization model

A generalized fractional crystallization model can be used to calculate the approximate thicknesses and compositions of cumulate that can be assumed to be present in a vertical section through the South Sandwich crust. We based our model on that proposed by Pearce *et al.* (1995), with the following assumptions.

- The thickness of volcanic arc rocks is 3 km, the approximate height of the volcanic edifices above the surrounding ocean floor.
- The distribution of compositions in the 3 km section of volcanic arc rocks is the same as that currently exposed in the islands, i.e. 47.6% basalts (SiO_2<52%), 30.9% basaltic andesites (SiO_2 = 52–56%) and 21.5% silicic rocks (>56% SiO_2).

There are three fractionation stages in the model (Table 3). Stage 1 models the generation of the most mafic basalts normally erupted at the surface from primitive basalts approximately representing compositions leaving the mantle.

Table 3. *Calculation of cumulate thickness resulting from generation of basaltic, basaltic andesite and silicic volcanic rocks of the South Sandwich Islands by fractional crystallization*

	Stage 1	Stage 2	Stage 3
Cumulate assemblage (%)			
Olivine	31	23	15
Clinopyroxene	55	53	24
Plagioclase	14	24	51
Magnetite	0	0	10
Lithologies	Pyroxenite, wehrlite, dunite, gabbro	Gabbro, pyroxenite, anorthosite	Gabbro, anorthosite, tonalite
Thickness of cumulate (km)			
To form basalt	0.63		
To form basaltic andesite	0.85	0.84	
To form andesite–dactite	0.70	0.69	0.11
F	0.64	0.48	0.84
Density (kg m^{-3})	3200	3000	2700
Total cumulate thickness (km)	2.18	1.53	0.11

The total thickness of volcanic rocks is assumed to be 3 km, with a density 2500 kg m^{-3} and in the proportions <52% SiO_2, 47.6%; 52–56% SiO_2, 30.9%; >56% SiO_2, 21.5%. Stage 1 represents fractionation from primitive basalt (48.7% SiO_2, 11% MgO) to basalt (50% SiO_2, 6% MgO) (Barsdell & Berry 1990). Stage 2 represents fractionation of basalt to basaltic andesite (56% SiO_2), and stage 3 represents fractionation of basaltic andesite to andesite–dacite (63% SiO_2) (Pearce *et al.* 1995). F is the proportion of liquid remaining in each fractionation stage.

This stage was not included in the model of Pearce *et al.* (1995), but was modelled for similar magma compositions from the Vanuatu arc by Barsdell & Berry (1990). The percentage crystallization is assumed to be 36% ($F = 0.64$, where F is the proportion of liquid remaining in each fractionation stage). All erupted magmas are assumed to have gone through this stage. Stage 2 models the generation of basaltic andesite from basalt by 52 wt% fractional crystallization ($F = 0.48$) (Pearce *et al.* 1995). All magmas up to 56% SiO_2 are assumed to have gone through this stage. Stage 3 models the generation of andesite/dacite with 63 wt% SiO_2 by 16% fractional crystallization from basaltic andesite ($F = 0.84$) (Pearce *et al.* 1995).

The results are shown in Table 3. The greatest thickness of cumulate is generated in stage 1 (2.18 km), as all magmas must pass through this stage. As the dominant phenocrysts in this stage are clinopyroxene and olivine, with minor plagioclase, the dominant lithologies are largely ultramafic: pyroxenite, wehrlite and dunite. Stage 2 cumulates are considerably thinner, despite the greater percentage crystallization. This is because only 52% of magmas pass through this stage. The cumulates are dominated by clinopyroxene, with approximately equal amounts of plagioclase and olivine, and are likely to be gabbros, pyroxenites and possibly minor anorthosites. The thickness of stage 3 cumulates is very small (0.11 km), because of the small proportion of silicic eruptives. The cumulates are dominated by plagioclase and are likely to be mainly gabbros, possibly with some plagioclase-rich accumulations forming anorthosites and tonalites.

The thicknesses and lithologies of the modelled cumulates are compared to a simplified section derived from the seismically imaged cross-section (Larter *et al.* 2001) in Figure 13. The rock types assigned to layers of different P-wave velocities in Figure 13a are based on interpretations of seismic velocities in other arcs (Miller & Christensen 1994; Suyehiro *et al.* 1996; Holbrook *et al.* 1999). A model crustal section including the cumulates is shown in Figure 13b. There are assumed to be 2 km of volcanic and hypabyssal rocks, and 3 km of gabbroic rocks derived from the pre-existing ocean plate generated at the back-arc spreading centre. The ultramafic cumulates are assumed to be at the base of the crust, in agreement with the seismic section. We note that such a thick ultramafic keel can only be modelled by assuming that the magma supply to the base of the crust is primitive magma with at least 11 wt% MgO (i.e. by including our stage 1 in the model). The thickness of gabbros and ultramafic cumulate in the model is some 0.85 km less than that of the seismic section. The difference might be a result of errors in the model, but is consistent with

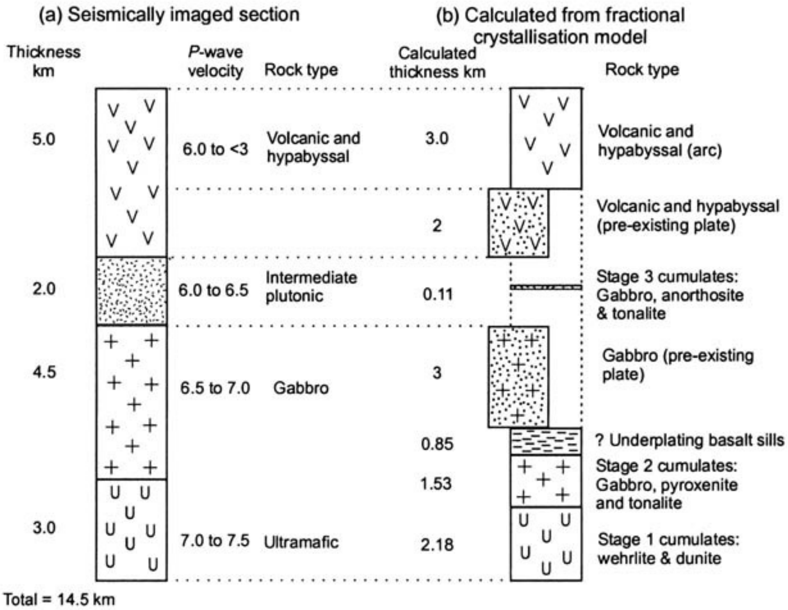

Fig. 13. Vertical sections through the South Sandwich arc crust. The P-wave velocity structure in (**a**) is from the wide-angle section of Larter *et al.* (2001) through Southern Thule, with rock types assigned according to conventional interpretation of seismic velocity structures of arcs (Millar & Christensen 1994; Suyehiro *et al.* 1996; Holbrook *et al.* 1999). The section in (**b**) is calculated from the fractional crystallization model (Table 3). The thicknesses of cumulate in stages 1–3 are calculated assuming that 3.0 km of volcanic rocks, in the observed mafic–silicic ratio, are generated ultimately by fractionation from primitive basalt. The cumulates are positioned according to best fit with the seismic section. There are assumed to be 2 km of volcanic and hypabyssal, and 3 km of gabbroic rocks derived from the pre-existing ocean plate. As the mafic and ultramafic cumulates are 0.85 km less thick in (b) than in (a) this thickness of basalt sills has tentatively been added to (b).

intrusion of mafic magmas within the crust that did not contribute partial fractionate to the volcanic pile. Such intrusions are shown as a 0.85 km-thick layer of underplating basalt sills in Figure 13b. Such sills are anticipated from models of arc magmatism (Petford & Gallagher 2001).

Stage 3 cumulates are placed at the same level as the 6.0–6.5 km s^{-1} seismic layer. Although most of these cumulates must be gabbros, they probably include anorthosites and tonalites with about the correct seismic velocity. It is obvious, however, that even the total thickness of stage 3 cumulates is considerably less than that of the 6.0–6.5 km s^{-1} layer. This is a robust result that cannot be changed even by large variations in the parameters of the fractional crystallization, and there can be no simple explanation for the origin of the seismic layer as intermediate cumulates.

Origin of the silicic magmas

The failure of the fractional crystallization model to explain the origin of the 6.0–6.5 km s^{-1} seismic layer as simple cumulates raises questions about the origin of silicic magmas in the arc. The majority of work on the South Sandwich Islands has argued that the silicic rocks of the arc (andesites, dacites and rhyolites) were derived by fractional crystallization from mafic magmas (Baker 1978; Tomblin 1979; Luff 1982; Pearce *et al.* 1995). This is in accord with both the overall erupted mafic–silicic volume relationships, and most major and trace element variations. A minority view has been that the silicic rocks were generated by partial melting of basaltic crust of the arc (Macdonald *et al.* 1992). The latter view is consistent with recent work on the Kermadec (Smith *et al.* 2003) and Izu–Bonin (Tamura & Tatsumi 2002) arcs, although in the latter case the partially melted source was envisaged as andesite rather than basalt. One of the most powerful tools available to distinguish between these alternative models in continental arcs – Sr, Nd and Pb isotopes – are no help in the South Sandwich Islands because of the lack of variation in these isotopic ratios in the lavas, and the lack of an isotopically distinct crust.

Nevertheless, there is growing evidence that silicic volcanic rocks and granites (s.l.) of continental volcanic margins are dominantly derived by partial fusion of hydrous gabbroic–amphibolitic crust (Atherton & Petford 1993; Millar *et al.* 2001; Petford & Gallagher 2001; Riley *et al.* 2001). This begs the question whether silicic magmas of intra-oceanic island arcs are also dominantly generated by crustal partial fusion.

In continental margin magmatism, the source of the silicic rocks is thought to be mafic amphibolite derived from earlier mafic intrusion (underplate) into the lower crust. Fluid-absent partial melting of such amphibolite starts around 800°C, and reaches 25% at 1000–1050°C (Rushmer 1991; Rapp & Watson 1995). At 1000–1075°C and 8 kbar, melting of volcanic arc basalt compositions produces melts of basaltic andesite–dacite compositions. The required heat is most likely to be transported into the lower crust by mafic magma intrusions. In principle, melting of mafic crust in these conditions is just as likely in an intra-oceanic as in a continental arc, as both the source rocks of the silicic partial melts and the agents of heat input are basaltic intrusions. Supporting evidence comes from intermediate–silicic Tanzawa plutonic complex, Honshu, Japan, which is thought to be the lateral correlative of the *c.* 6 km s^{-1} layer in the Izu–Bonin arc (Suyehiro *et al.* 1996). Geochemical and experimental results suggest that the tonalite was generated by *c.* 59% partial melting of hydrous basalt in the lower crust of the arc (Kawate & Arima 1998; Nakajima & Arima 1998). Modelling shows that incremental intrusion of a 1 km thickness of mafic sills, with magma batches arriving with a periodicity of 20–200 years, can produce silicic melt thicknesses up to 100 m (Petford & Gallagher 2001). This is quite sufficient to generate the amounts of silicic rocks observed in intra-oceanic arcs.

The silicic volcanic rocks on Southern Thule and Candlemas Island are representatives of an association of silicic rocks bimodally related to basalts, which is becoming increasingly recognized as widespread in intra-oceanic island arcs. In many cases, the silicic rocks in such bimodal associations are very closely related to calderas, typically 3–6 km in diameter, such as in the Kermadec (Lloyd *et al.* 1996; Worthington *et al.* 1999; Smith *et al.* 2003), Izu–Bonin (Taylor *et al.* 1990) and Vanuatu (Robin *et al.* 1993; Monzier *et al.* 1994) arcs. The presence of the calderas indicates that relatively large volumes (compared to the size of typical lava flows of associated mafic volcanic series) of silicic magma were present at one time within the upper crust in order to generate the calderas by magma eruption or withdrawal. This implies high rates of production of the silicic magmas, favouring the partial melting model for formation of the silicic rocks.

The partial melting and fractional crystallization models might produce different geochemical relationships between the mafic and silicic rocks. In Figure 14, samples for three basalt–silicic series, the calc-alkaline and tholeiitic series of Southern Thule, and the tholeiitic series of Candlemas Island, are plotted as multi-element variation diagrams. In order to show variation within each series, and hence to provide a test whether the silicic rocks were derived by fractional crystallization from the basalts, the trace element abundances are normalized to a basalt sample belonging to each of the series. There are some non-systematic variations in Cs, K and Rb in a few samples, which probably result from minor mobility of these elements. In all cases, incompatible trace element abundances are higher in dacitic rocks (2.9–8.8 times basalt) than in andesitic rocks (1.8–2.8 times basalt). The elements are ordered along the x-axis of the diagram by increasing incompatibility in an olivine–pyroxene assemblage from right to left (Sun & McDonough 1989; Green 1994). The silicic rocks have greater relative abundances of the more incompatible trace elements than the less incompatible elements, producing curves that overall slope down to the right. Sr, Ti and, to a lesser extent, P have low normalized abundances, consistent with the presence of plagioclase, Fe–Ti oxides and apatite in the fractionating and/or residual assemblages. All these features are consistent with both the fractional crystallization and partial melting models for the origin of the silicic rocks. A distinctive feature of patterns for the Candlemas silicic rocks is the trough at Ta. This is the result of the normalizing basalt having low Nb/Ta. The range of Nb/Ta ratios in the silicic rocks of Candlemas (11.8–13.8) is similar to that of the mafic Candlemas rocks (8.2–12.8), and the Ta troughs are unlikely to be a result of Nb–Ta fractionation during generation of the silicic magmas.

Nevertheless, there is one feature that is questionably consistent with the fractional crystallization model. Zr and Hf have consistently higher normalized abundances than Sm in the silicic rocks, while Zr, Hf and Sm normalized values in the basalts are more or less the same (Fig. 14). The fractional crystallization model would require the bulk distribution coefficient of Sm to be significantly greater than those of Zr and Hf to explain this feature. Published data suggest that Zr, Sm and Hf all have low bulk

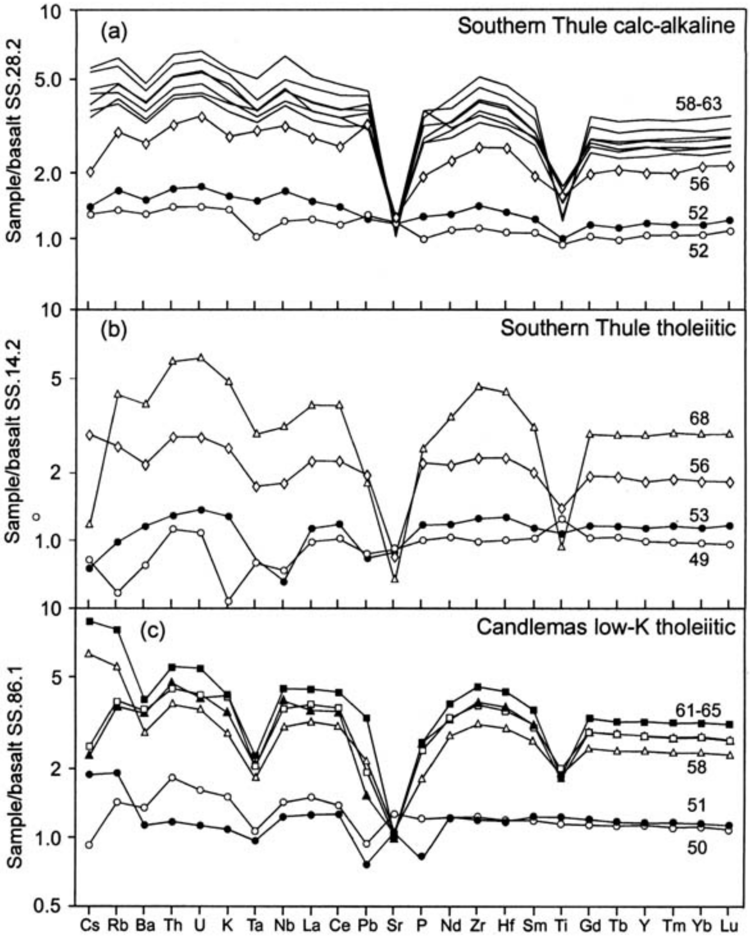

Fig. 14. Basalt-normalized abundances of trace elements in three basalt–silicic series from the South Sandwich Islands. In each part of the diagram, the samples are normalized to a basalt from the same chemical series, in order to illustrate chemical variation within each series. (**A**) The calc-alkaline series of Southern Thule normalized to basalt SS.28.2. (**B**) The tholeiitic series of Southern Thule, normalized to basalt SS.14.2. (**C**) Sample from Candlemas Island, normalized to basalt SS.86.1. Numbers to the right of the diagram are wt% silica.

distribution coefficients in a plagioclase+olivine+clinopyroxene±orthopyroxene assemblage (Hart & Dunn 1993; Rollinson 1993; Dunn & Sen 1994; Green 1994), and fractionation of this assemblage is unlikely to fractionate Sm from Zr and Hf to the extent observed. Addition of magnetite, which sequesters Zr and Hf relative to Sm (Schock 1979; Green 1994) to the fractionating assemblage, renders a significant increase in the Zr/Sm ratio with fractionation highly unlikely. There is, therefore, significant doubt that the observed increase in Zr and Hf relative to Sm in the silicic rocks is a result of fractional crystallization of the observed phenocryst assemblage. However, amphibole probably has distribution coefficients for Sm that are 2–5 times higher than for Zr and Hf (Green 1994; Sisson 1994). Involvement of only 10% amphibole would readily reproduce the high Zr/Sm ratios of the silicic rocks. Amphibole is not known as a phenocryst phase in the South Sandwich Islands (except in calc-alkaline andesite on Leskov Island; Luff 1982), and it is unlikely that it was fractionally crystallized from the main magma series. On the other hand, it is likely that amphibole is present in the mafic plutonic parts of the arc crust that are the potential source for generation of the silicic magmas by partial melting. This feature of the geochemistry significantly favours generation of the silicic magmas by partial melting.

The origin of the 6.0–6.5 km s^{-1} mid-crustal layer

The 2 km-thick, 6.0–6.5 km s^{-1}, mid-crustal layer is interpreted to represent intermediate–silicic composition plutonic rocks (Larter *et al.* 2001). If this interpretation is correct, it has three possible origins.

- It largely consists of intermediate cumulate generated by fractional crystallization of intermediate and silicic magmas. Using the parameters in Table 3, generation of 2 km of such cumulate would generate 67 km of mafic and ultramafic (stages 1 and 2) cumulates. The seismic data clearly rule out this thickness of crust.
- It consists of non-erupted intermediate–silicic, crystallized magma generated by fractional crystallization from mafic magmas. Using the parameters in Table 3, generation of a 2 km-thickness of intermediate–silicic magma by fractional crystallization from mafic magma would generate an additional 11.8 km of mafic, ultramafic and intermediate (stages 1–3) cumulates. The seismic data do not allow this, as the total crustal thickness below the 6.0–6.5 km s^{-1} layer is only 7.5 km (Fig. 13).
- It consists of intermediate–silicic, crystallized magma produced by partial melting of mafic material within the arc. The degree of partial melt required to produce andesitic–dacitic compositions from a basaltic source is probably in the range 20–40% (Rapp & Watson 1995). At 20% partial melting, generation of 2 km of melt would produce about 7.4 km of residue (allowing for density differences). At 40% partial melting, generation of 2 km of melt would produce about 2.7 km of residue. These thicknesses are less than the seismically imaged thickness of the crust, but require that at least a third of the lower crust is residue from partial melting. Most likely potential sources are the underplating basalt sills, and mafic rocks of the pre-existing ocean plate (Fig. 13b).

We conclude that the silicic–intermediate layer was most probably formed by partial melting of mafic lower crust. It should be noted that, in the absence of along-arc wide-angle seismic data, it is impossible to know whether the 6.0–6.5 km s^{-1} layer is a localized feature that concentrated laterally migrating melts, and the volume relationships should therefore be treated with a degree of caution. Nevertheless, both geochemical and volume considerations are in favour of generation of the silicic rocks of the South Sandwich arc by partial melting of mafic crust.

Conclusions

- The mafic magmas of the South Sandwich arc were derived from mantle that had been depleted by a previous melt extraction. All the magmas have subchondritic Nb/Ta and are the most depleted magmas from any island arc. The depletion event probably took place beneath the back-arc East Scotia Ridge.
- No known South Sandwich lavas represent primitive magmas. Instead, all have <8.5 wt% MgO and were significantly fractionated since leaving their mantle sources. This fractionation took place near the base of the crust as the magmas were trapped during their ascent in magma chambers and resulted in high-velocity cumulates that form a significant part of the crustal thickness.
- High-Al basalts are common in the South Sandwich arc, notably in the tholeiite rather than the calc-alkaline series, and are the result of accumulation of plagioclase. Sr abundances and Sr/Nd ratios are largely controlled by plagioclase–liquid fractionation. High Sr/Th ratios in some tholeiites, however, record another process of variable Sr addition to mantle sources, probably in an aqueous phase.
- The tholeiitic series of the South Sandwich arc have a bimodal mafic–silicic distribution in erupted compositions. These silicic magmas were probably generated by partial melting of amphibolitic sources in the arc crust. The partial melting model is supported by the interpretation of a 2 km-thick 6.0–6.5 km s^{-1} layer in the mid-crust as intermediate–silicic plutons. Volume considerations indicate that this layer is most likely to represent partial melts of mafic crust. High (Zr,Hf)/Sm ratios in the silicic rocks support derivation by partial melting of amphibolite.
- The South Sandwich basalts were derived from mantle that was enriched by two subducted components, a sediment component and an aqueous fluid. Addition of the sediment components was independent of the degree of previous depletion of the mantle sources. Addition of an approximately constant amount of the aqueous fluid triggered mantle melting. The degree of mantle depletion and the amount of added sediment

component were the controlling influences in formation of the distinct low-K tholeiitic, tholeiitic and calc-alkaline series. The tholeiitic and calc-alkaline series of Southern Thule were generated by addition of variable amounts of sediment component to a weakly depleted mantle (with the calc-alkaline series having the higher sediment component). The low-K series of Candlemas–Vindication were generated by variable sediment component addition to a strongly depleted mantle source.

We would like to thank the Captains and crews of HMS *Endurance* and RRS *James Clark Ross* for getting us to and (more importantly) retrieving us from the South Sandwich Islands. We are grateful to Terry Plank and Ian Smith for constructive reviews of the paper.

References

ACKERMAND, D., RILEY, T.R., FINKENBERGER, B. & SCHÜMANN, T. 2003. Geology program South Sandwich Islands (Vindication Island). *Berichte für Polarforschung*, in press.

ATHERTON, M.P. & PETFORD, N. 1993. Generation of sodium-rich magmas from newly underplated basaltic crust. *Nature*, **362**, 144–146.

BAKER, P.E. 1968. Comparative volcanology and petrology of the Atlantic island arcs. *Bulletin Volcanologique*, **32,** 189–206.

BAKER, P.E. 1978. *The South Sandwich Islands: III. Petrology of the volcanic rocks*. British Antarctic Survey Scientific Reports, **93**.

BAKER, P.E. 1990. South Sandwich Islands. *In*: LEMASURIER, W.E. & THOMSON, J.W. (eds) *Volcanoes of the Antarctic Plate and Southern Oceans*. Antarctic Research Series, American Geophysical Union, **48**, 361–395.

BAKER, P.E., BUCKLEY, F. & REX, D.C. 1977. Cenozoic volcanism in the Antarctic. *Philosophical Transactions of the Royal Society of London*, Series B, **279**, 131–142.

BARKER, P.F. 1995. Tectonic framework of the East Scotia Sea. *In*: TAYLOR, B. (ed.) *Backarc Basins; Tectonics and Magmatism*. Plenum Press, New York, 281–314.

BARKER, P.F. & HILL, I.A. 1981. Back-arc extension in the Scotia Sea. *Philosophical Transactions of the Royal Society of London*, Series A, **300**, 249–262.

BARREIRO, B. 1983. Lead isotopic compositions of South Sandwich Island volcanic rocks and their bearing on magmagenesis in intra-ocean island arcs. *Geochimica et Cosmochimica Acta*, **47**, 817–822.

BARSDELL, M. & BERRY, R.F. 1990. Origin and evolution of primitive island arc ankramites from western Epi, Vanuatu. *Journal of Petrology*, **31**, 747–777.

BOTTINGA, Y. & WEILL, D. 1970. Densities of liquid silicate systems calculated from partial molar volumes of oxide components. *American Journal of Science*, **269,** 169–182.

BOYNTON, C.H., WESTBROOK, G.K., BOTT, M.H.P. & LONG, R.E. 1979. A seismic refraction investigation of crustal structure beneath the Lesser Antilles island arc. *Geophysical Journal of the Royal Astronomical Society*, **58**, 371–393.

BRUGUIER, N.J & LIVERMORE, R.A. 2001. Enhanced magma supply at the southern East Scotia ridge: evidence for mantle flow around the subducting slab? *Earth and Planetary Science Letters*, **191**, 129–144.

CHRISTENSEN, N.I. & MOONEY, W.D. 1995. Seismic velocity structure and composition of the continental crust: a global view. *Journal of Geophysical Research*, **100**, 9761–9788.

CHROSTON, P.N. & SIMMONS, G. 1989. Seismic velocities from the Kohistan volcanic arc, northern Pakistan. *Journal of the Geological Society, London*, **146**, 971–979.

CLASS, C., MILLER, D.M., GOLDSTEIN, S.L. & LANGMUIR, C.H. 2000. Distinguishing melt and fluid subduction components in Umnak volcanics, Aleutian arc. *Geochemistry Geophysics Geosystems*, **1**, 1999GC000010.

COHEN, R.S. & O'NIONS, R.K. 1982. Identification of recycled continental material in the mantle from Sr, Nd and Pb isotopes. *Earth and Planetary Science Letters*, **61**, 73–84.

CRAWFORD, A.J., FALLOON, T.J. & EGGINS, S. 1987. The origin of island arc high-alumina basalts. *Contributions to Mineralogy and Petrology*, **97**, 417–430.

CRAWFORD, A.J., FALLOON, T.J. & GREEN, D.H. 1989. Classification, petrogenesis and tectonic setting of boninites. *In*: CRAWFORD, A.J. (ed.) *Boninites and Related Rocks*. Unwin Hyman, London, 1–49.

DEBARI, S.M. & SLEEP, N.H. 1991. High-Mg, low-Al bulk composition for the Talkeetna island arc, Alaska: implications for primary magmas and the nature of arc crust. *Geological Society of America Bulletin*, **103**, 37–47.

DUNN, T. & SEN, C. 1994. Mineral/matrix partition coefficients for orthopyroxene, plagioclase, and olivine in basaltic to andesitic systems: a combined analytical and experimental study. *Geochimica et Cosmochimica Acta*, **58**, 717–733.

EGGINS, S.M. 1993. Origin and differentiation of picritic arc magmas, Ambae (Aoba), Vanuatu. *Contributions to Mineralogy and Petrology*, **114,** 79–100.

EGGINS, S.M., WOODHEAD, J.D., KINSLEY, L.P.J, MORTIMER, G.E., SYLVESTER, P. MCCULLOCH, M.T., HERGT, J.M. & HANDLER, M.R. 1997. A simple method for the precise determination of ≥40 trace elements in geological samples by ICPMS using enriched isotope international standardisation. *Chemical Geology*, **134**, 311–326.

ELLAM, R.M. & HAWKESWORTH, C.J. 1988. Elemental and isotopic variations in subducted basalts: evidence for a three component model. *Contributions to Mineralogy and Petrology*, **98**, 72–80.

ELLIOTT, T., PLANK, T., ZINDLER, A., WHITE, W. & BOURDON, B. 1997. Element transport from slab to volcanic front at the Mariana arc. *Journal of Geophysical Research*, **102**, 14 991–15 019.

EWART, A., COLLERSON, K.D., REGELOUS, M., WENDT,

J.I. & NIU, Y. 1998. Geochemical evolution within the Tonga–Kermadec–Lau arc-back-arc systems: the role of varying mantle wedge composition in space and time. *Journal of Petrology*, **39**, 331–368.
FLIEDNER, M.M. & KLEMPERER, S.L. 1999. Structure of an island arc: wide-angle seismic studies in the eastern Aleutian Islands, Alaska. *Journal of Geophysical Research*, **104**, 10 667–10 694.
FORSYTHE, L.M., NIELSEN, R.L. & FISK, M.R. 1994. High-field-strength element partitioning between pyroxene and basaltic to dacitic magmas. *Chemical Geology*, **117**, 107–125.
FRETZDORFF, S., LIVERMORE, R.A., DEVEY, C.W., LEAT, P.T. & STOFFERS, P. 2002. Petrogenesis of the back-arc East Scotia Ridge, South Atlantic Ocean. *Journal of Petrology*, **43**, 1435–1467.
GASS, I.G., HARRIS, P.G. & HOLDGATE, M.W. 1963. Pumice eruption in the area of the South Sandwich Islands. *Geological Magazine*, **100**, 321–330.
GREEN, T.H. 1994. Experimental studies of trace-element partitioning applicable to igneous petrogenesis – Sedona 16 years later. *Chemical Geology*, **117**, 1–36.
GUST, D.A. & PERFIT, M.R. 1987. Phase relations of a high-Mg basalt from the Aleutian Island Arc: implications for primary island arc basalts and high-Al basalts. *Contributions to Mineralogy and Petrology*, **97**, 7–18.
HARRISON, D., LEAT, P.T., BURNARD, P.G., TURNER, C., FRETZDORFF, S. & MILLAR, I.L. 2003. Resolving mantle components in oceanic lavas from segment E2 of the East Scotia back-arc ridge, South Sandwich Islands. *In*: LARTER, R.D. & LEAT, P.T. (eds) *Intra-oceanic Subduction Systems: Tectonic and Magmatic Processes*. Geological Society, London, Special Publications, **219**, 333–344.
HART, S.R. & DUNN, T. 1993. Experimental cpx/melt partitioning of 24 trace elements. *Contributions to Mineralogy and Petrology*, **113**, 1–8.
HAWKESWORTH, C.J., O'NIONS, R.K., PANKHURST, R.J., HAMILTON, P.J. & EVENSEN, N.M. 1977. A geochemical study of island-arc and back-arc tholeiites from the Scotia Sea. *Earth and Planetary Science Letters*, **36**, 253–262.
HAWKESWORTH, C.J., TURNER, S.P., MCDERMOTT, F., PEATE, D.W. & VAN CALSTEREN, P. 1997. U–Th isotopes in arc magmas: implications for element transfer from the subducted crust. *Science*, **276**, 551–555.
HOLBROOK, W.S., LIZARRALDE, D., MCGEARY, S., BANGS, N. & DIEBOLD, J. 1999. Structure and composition of the Aleutian island arc and implications for continental crustal growth. *Geology*, **27**, 31–34.
HOLDGATE, M.W. 1963. Observations in the South Sandwich Islands, 1962. *Polar Record*, **11**, 394–405.
HOLDGATE, M.W. & BAKER, P.E. 1979. *The South Sandwich Islands: I. General description*. British Antarctic Survey Scientific Reports, **91**.
JOHNSON, M.C. & PLANK, T. 1999. Dehydration and melting experiments constrain the fate of subducted sediments. *Geochemistry Geophysics Geosystems*, **1**, 1999GC000014.
JOHNSTON, A.D. 1986. Anhydrous *P–T* phase relations of near-primary high-alumina basalt from the South Sandwich Islands. *Contributions to Mineralogy and Petrology*, **92**, 368–382.
KAWATE, S. & ARIMA, M. 1998. Petrogenesis of the Tanzawa plutonic complex, central Japan: exposed felsic middle crust of the Izu–Bonin–Mariana arc. *The Island Arc*, **7**, 342–358.
KEMP, S.W. & NELSON, A.L. 1931. The South Sandwich Islands. *Discovery Reports*, **3**, 133–198.
KEMPTON, P.D., DOWNES, H. & EMBEY-ISZTIN, A. 1997. Mafic granulite xenoliths in Neogene alkali basalts from the western Pannonian Basin: insights into the lower crust of a collapsed orogen. *Journal of Petrology*, **38**, 941–970.
KURZ, M.D., LE ROEX, A.P. & DICK, H.J.B. 1998. Isotope geochemistry of the oceanic mantle near the Bouvet triple junction. *Geochimica et Cosmochimica Acta*, **62**, 841–852.
LACHLAN-COPE, T., SMELLIE, J.L. & LADKIN, R. 2001. Discovery of a recurrent lava lake on Saunders Island (South Sandwich Islands) using AVHRR imagery. *Journal of Volcanology and Geothermal Research*, **112**, 105–116.
LANGE, R.L. & CARMICHAEL, I.S.E. 1990. Thermodynamic properties of silicate liquids with emphasis on density, thermal expansion and compressibility. *In*: NICHOLLS, J. & RUSSEL, J.K. (eds) *Modern Methods of Igneous Petrology*. Reviews in Mineralogy, Mineralogical Society of America, **24**, 25–64.
LARTER, R.D., BRUGUIER, N.J. & VANNESTE, L.E. 2001. Structure, composition and evolution of the South Sandwich Islands arc: implications for rates of arc magmatic growth and subduction erosion. *Eos, Transactions, American Geophysical Union*, **82**, (47), Fall Meeting Supplement, T32D-10.
LARTER, R.D., KING, E.C., LEAT, P.T., READING, A.M., SMELLIE, J.L. & SMYTH, D.K. 1998. South Sandwich slices reveal much about arc structure, geodynamics, and composition. *Eos, Transactions, American Geophysical Union*, **79**, 281–285.
LARTER, R.D., VANNESTE, L.E., MORRIS, P. & SMYTHE, D.K. 2003. Structure and tectonic evolution of the South Sandwich arc. *In*: LARTER, R.D. & LEAT, P.T. (eds) *Intra-oceanic Subduction Systems: Tectonic and Magmatic Processes*. Geological Society, London, Special Publications, **219**, 255–284.
LEAT, P.T., LIVERMORE, R.A., MILLAR, I.L. & PEARCE, J.A. 2000. Magma supply in back-arc spreading centre segment E2, East Scotia Ridge. *Journal of Petrology*, **41**, 845–866.
LEAT, P.T., RILEY, T.R., WAREHAM, C.D., MILLAR, I.L., KELLEY, S.P. & STOREY, B.C. 2002. Tectonic setting of primitive magmas in volcanic arcs: an example from the Antarctic Peninsula. *Journal of the Geological Society, London*, **159**, 31–44.
LIVERMORE, R.A. 2003. Back-arc spreading and mantle flow in the east Scotia Sea. *In*: LARTER, R.D. & LEAT, P.T. (eds) *Intra-oceanic Subduction Systems: Tectonic and Magmatic Processes*. Geological Society, London, Special Publications, **219**, 315–331.

LIVERMORE, R., CUNNINGHAM, A., VANNESTE, L. & LARTER, R. 1997. Subduction influence on magma supply at the East Scotia Ridge. *Earth and Planetary Science Letters*, **150**, 261–275.

LLOYD, E.F., NATHAN, S., SMITH, I.E.M. & STEWART, R.B. 1996. Volcanic history of Macauley Island, Kermadec Ridge, New Zealand. *New Zealand Journal of Geology and Geophysics*, **39**, 295–308.

LUFF, I.W. 1982. *Petrogenesis of the island arc tholeiite series of the South Sandwich Islands*. PhD thesis, University of Leeds.

MACDONALD, R., HAWKESWORTH, C.J. & HEATH, E. 2000. The Lesser Antilles volcanic chain: a study in arc magmatism. *Earth Science Reviews*, **49**, 1–76.

MACDONALD, R., SMITH, R.L. & THOMAS, J.E. 1992. *Chemistry of the subalkaline silicic obsidians*. US Geological Survey Professional Papers, **1523**.

MILLAR, I.L., WILLAN, R.C.R., WAREHAM, C.D. & BOYCE, A.J. 2001. The role of crustal and mantle sources in the genesis of granitoids of the Antarctic Peninsula and adjacent crustal blocks. *Journal of the Geological Society, London*, **158**, 855–867.

MILLER, D.J. & CHRISTENSEN, N.I. 1994. Seismic signature and geochemistry of an island arc: a multidisciplinary study of the Kohistan accreted terrane, northern Pakistan. *Journal of Geophysical Research*, **99**, 11 623–11 642.

MONZIER, M., ROBIN, C. & EISSEN, J.-P. 1994. Kuwae (≈1425 A.D.): the forgotten caldera. *Journal of Volcanology and Geothermal Research*, **59**, 207–218.

NAKAJIMA, K & ARIMA, M. 1998. Melting experiments on hydrous low-K tholeiite: implications for the genesis of tonolitic crust in the Izu–Bonin–Mariana arc. *The Island Arc*, **7**, 359–373.

NYE, C.J. & REID, M.R. 1986. Geochemistry of primary and least fractionated lavas from Okmok Volcano, central Aleutians – implications for arc magmagenesis. *Journal of Geophysical Research*, **91,** 10 271–10 287.

PANKHURST, R.J. & RAPELA, C.R. 1995. Production of Jurassic rhyolite by anatexis of the lower crust of Patagonia. *Earth and Planetary Science Letters*, **134**, 23–36.

PEARCE, J.A., BAKER, P.E., HARVEY, P.K. & LUFF, I.W. 1995. Geochemical evidence for subduction fluxes, mantle melting and fractional crystallization beneath the South Sandwich arc. *Journal of Petrology*, **36**, 1073–1109.

PEARCE, J.A., BARKER, P.F., EDWARDS, S.J., PARKINSON, I.L. & LEAT, P.T. 2000. Geochemistry and tectonic significance of peridotites from the South Sandwich arc–basin system, South Atlantic. *Contributions to Mineralogy and Petrology*, **139**, 36–53.

PEARCE, J.A., LEAT, P.T., BARKER, P.F. & MILLAR, I.L. 2001. Geochemical tracing of Pacific-to-Atlantic upper-mantle flow through the Drake Passage. *Nature*, **410**, 457–461.

PEARCY, L.G., DEBARI, S.M. & SLEEP, N.H. 1990. Mass balance calculations for two sections of island arc crust and implications for the formation of continents. *Earth and Planetary Science Letters*, **96**, 427–442.

PEATE, D.W. & PEARCE, J.A. 1998. Causes of spatial compositional variations in Mariana arc lavas: trace element evidence. *The Island Arc*, **7**, 479–495.

PELAYO, A.M. & WIENS, D.A. 1989. Seismotectonics and relative plate motions in the Scotia Sea region. *Journal of Geophysical Research*, **94**, 7293–7320.

PETFORD, N. & GALLAGHER, K. 2001. Partial melting of mafic (amphibolitic) lower crust by periodic influx of basaltic magma. *Earth and Planetary Science Letters*, **193**, 483–499.

PICHAVANT, M. & MACDONALD, R. 2003. Mantle genesis and crustal evolution of primitive calc-alkaline basaltic magmas from the Lesser Antilles arc. *In*: LARTER, R.D. & LEAT, P.T. (eds) *Intra-oceanic Subduction Systems: Tectonic and Magmatic Processes*. Geological Society, London, Special Publications, **219**, 239–254.

PLANK, T. & WHITE, W.M. 1995. Nb and Ta in arc and mid-ocean ridge basalts. *Eos, Transactions, American Geophysical Union*, **76**, F655.

RAPP, R.P. & WATSON, E.B. 1995. Dehydration melting of metabasalt at 8–32 kbar: implications for continental growth and crust–mantle recycling. *Journal of Petrology*, **36**, 891–931.

RILEY, T.R., LEAT, P.T., PANKHURST, R.J. & HARRIS, C. 2001. Origins of large volume rhyolitic volcanism in the Antarctic Peninsula and Patagonia by partial melting. *Journal of Petrology*, **42**, 1043–1065.

ROBIN, C., EISSEN, J.-P. & MONZIER, M. 1993. Giant tuff cone and 12 km-wide associated caldera at Ambrym Volcano (Vanuatu, New Hebrides arc). *Journal of Volcanology and Geothermal Research*, **55**, 225–238.

ROLLINSON, H. 1993. *Using Geochemical Data: Evaluation, Presentation, Interpretation*. Longman Scientific and Technical, Harlow.

RUSHMER, T. 1991. Partial melting of two amphibolites: contrasting experimental results under fluid-absent conditions. *Contributions to Mineralogy and Petrology*, **107**, 41–59.

RYAN, J.G., MORRIS, J., TERA, F., LEEMAN, W.P. & TSVETKOV, A. 1995. Cross-arc geochemical variations in the Kurile arc as a function of slab depth. *Science*, **270**, 625–627.

SCHOCK, H.H. 1979. Distribution of rare-earth and other trace elements in magnetites. *Chemical Geology*, **26**, 119–133.

SISSON, T.W. 1994. Hornblende-melt trace-element partitioning measured by ion microprobe. *Chemical Geology*, **117**, 331–344.

SISSON, T.W. & GROVE, T.L. 1993. Temperature and H_2O contents of low-MgO high-alumina basalts. *Contributions to Mineralogy and Petrology*, **113**, 167–184.

SMELLIE, J.L., MORRIS, P., LEAT, P.T., TURNER, D.B. & HOUGHTON, D. 1998. Submarine caldera and other volcanic observations in Southern Thule, South Sandwich Islands. *Antarctic Science*, **10**, 171–172.

SMITH, I.E.M., WORTHINGTON, T.J., PRICE, R.C. & GAMBLE, J.A. 1997. Primitive magmas in arc-type volcanic associations: examples from the southwest Pacific. *The Canadian Mineralogist*, **35**, 257–273.

SMITH, I.E.M., WORTHINGTON, T.J., STEWART, R.B., PRICE, R.C. & GAMBLE, J.A. 2003. Felsic volcanism in the Kermadec arc, SW Pacific: crustal recycling in an oceanic setting. *In*: LARTER, R.D. & LEAT, P.T. (eds) *Intra-oceanic Subduction Systems: Tectonic and Magmatic Processes*. Geological Society, London, Special Publications, **219**, 99–118.

SUN, S.S. & MCDONOUGH, W.F. 1989. Chemical and isotopic systematics of oceanic basalts: implications for mantle composition and processes. *In*: SAUNDERS, A.D. & NORRY, M.J. (eds) *Magmatism in the Ocean Basins*. Geological Society, London, Special Publications, **42**, 313–345.

SUYEHIRO, K., TAKAHASHI, N., ARIIE, Y., YOKOI, Y., HINO, R., SHINOHARA, M., KANAZAWA, T., HIRATA, N., TOKUYAMA, H. & TAIRA, A. 1996. Continental crust, crustal underplating, and low-Q upper mantle beneath an ocean island arc. *Science*, **272**, 390–392.

TAMURA, Y. & TATSUMI, Y. 2002. Remelting of an andesitic crust as a possible origin for rhyolitic magma in oceanic arcs: an example from the Izu–Bonin arc. *Journal of Petrology*, **43**, 1029–1047.

TATSUMI, Y. & EGGINS, S.M. 1995. *Subduction Zone Magmatism*. Blackwell, Cambridge, MA.

TAYLOR, B., BROWN, G., GILL, J.B., HOCHSTAEDTER, A.G., HOTTA, H., LANGMUIR, C.H., LEINEN, M., NISHIMURA, A. & URABE, T. 1990. ALVIN–SeaBeam studies of the Sumisu Rift, Izu–Bonin arc. *Earth and Planetary Science Letters*, **100**, 127–147.

TODT, W., CLIFF, R.A., HANSER, A. & HOFFMANN, A.W. 1984. ^{202}Pb + ^{205}Pb double spike for lead isotope analysis. *Terra Cognita*, **4**, 209.

TOMBLIN, J.F. 1979. *The South Sandwich Islands: II. The Geology of Candlemas Island.* British Antarctic Survey Scientific Reports, **92**.

TURNER, S. & HAWKESWORTH, C. 1997. Constraints on flux rates and mantle dynamics beneath island arcs from Tonga–Kermadec lava geochemistry. *Nature*, **389**, 568–573.

TURNER, S., HAWKESWORTH, C., VAN CALSTEREN, P., HEATH, E., MACDONALD, R. & BLACK, S. 1996. U-series isotopes and destructive plate margin magma genesis in the Lesser Antilles. *Earth and Planetary Science Letters*, **142**, 191–207.

VANNESTE, L. & LARTER, R.D. 2002. Sediment subduction, subduction erosion and strain regime in the northern South Sandwich forearc. *Journal of Geophysical Research*, **107** (B7), EMPS, 1–24, 2149, 10.1029/2001JB000396.

VANNESTE, L.E., LARTER, R.D. & SMYTHE, D.K. 2002. A slice of intraoceanic arc: insights from the first multichannel seismic reflection profile across the South Sandwich arc. *Geology*, **30**, 819–822.

WOODHEAD, J.D. 1988. The origin of geochemical variations in Mariana lavas: a general model for petrogenesis in intraoceanic island arcs? *Journal of Petrology*, **29**, 805–830.

WOODHEAD, J.D. & JOHNSON, R.W. 1993. Isotopic and trace element profiles across the New Britain island arc, Papua New Guinea. *Contributions to Mineralogy and Petrology*, **113**, 479–491.

WOODHEAD, J., EGGINS, S. & GAMBLE, J. 1993. High field strength and transition element systematics in island arc and back-arc basin basalts: evidence for multi-phase melt extraction and a depleted mantle wedge. *Earth and Planetary Science Letters*, **114**, 491–504.

WOODHEAD, J.D., EGGINS, S.M. & JOHNSON, R.W. 1998. Magma genesis in the New Britain island arc: further insights into melting and mass transfer processes. *Journal of Petrology*, **39**, 1641–1668.

WORTHINGTON, T.J., GREGORY, M.R. & BONDARENKO, V. 1999. The Denham caldera on Raoul Volcano: dacitic volcanism in the Tonga–Kermadec arc. *Journal of Volcanology and Geothermal Research*, **90**, 29–48.

This page intentionally left blank

Back-arc spreading and mantle flow in the East Scotia Sea

ROY LIVERMORE
British Antarctic Survey, High Cross, Madingley Road, Cambridge CB3 0ET, UK
(e-mail: ral@bas.ac.uk)

Abstract: The East Scotia Ridge exhibits systematic variations in axial morphology and basalt geochemistry. Central segments have morphology typical of intermediate-rate spreading centres and erupt mainly normal mid-ocean ridge basalt (N-MORB). Segments near the ridge ends exhibit anomalous, inflated, axial morphology and erupt more evolved basalts, influenced by the Bouvet plume in the north. As the end segments lie closer to the volcanic arc, these variations could be caused by coupled flow within the mantle wedge, as inferred from similar studies in the Lau Basin. Three of the four zones of crustal accretion defined from the Lau Basin may be identified in the East Scotia Sea, although there is no counterpart to a zone of diminished magma supply observed at the East Lau Spreading Centre. Superimposed on the pattern of plate-driven flow is a ridge-parallel flow related to inflow of Atlantic mantle into the East Scotia Sea back-arc region at both ends of the South Sandwich slab. The inflow causes enhanced magmatism and propagation of the end segments towards the middle of the back-arc region, and may be related to trench-parallel flow beneath the rapidly retreating slab. Alternatively, it may be driven by buoyancy flux from Atlantic hot spots. There is no evidence that retreat was ever driven by escape flow of Pacific mantle.

Intra-oceanic subduction zones are regions in which mantle flow has a direct influence on topography, geochemistry and chemical fluxes between the geosphere and hydrosphere. In active back-arc regions, the downgoing lithosphere of the subducting slab lies in close proximity to the upward flow associated with back-arc spreading. Mantle upwelling beneath back-arc spreading centres is modified by flow induced in the mantle wedge by the motion of the subducting slab, and by local or regional asthenospheric flows, such as inflow through slab tears or hot-spot-driven flow. Hence, one might expect the mantle-flow pattern in back-arc regions to be complex, as recently shown by seismic shear-wave splitting results in the Lau Basin (Smith *et al.* 2001).

Corner flow is induced in the mantle wedge by viscous coupling with the subducting slab (McKenzie 1969; Sleep & Toksöz 1971; Richter & McKenzie 1978), causing overturn of depleted mantle. The resulting flow is expected to be closely aligned with the motion of the subducting plate (Fischer *et al.* 2000; Hall *et al.* 2000; Winder & Peacock 2001), and may give rise to a simple pattern of morphological and geochemical variations, related to the location of back-arc spreading centre segments with respect to circulation in the mantle wedge (Martinez & Taylor 2002, 2003).

In some back-arc basins, inflow of asthenosphere around slab ends or through gaps is also believed to occur, and may be a direct consequence of slab retreat (Garfunkel *et al.* 1986; Russo & Silver 1994; Livermore *et al.* 1997). In the case of flow around slab ends, mantle flow will tend to be subparallel to the axis of the back-arc spreading centre, and may give rise to variations in morphology and geochemistry, as well as in shear-wave 'fast' directions, along the axis of the ridge. Corner flow and ridge-parallel flow are superimposed on the regional flow in the asthenosphere, driven by global convection, which may also affect ridge characteristics. Back-arc spreading centres are, thus, sensitive indicators of flow-related variations in the fertility, temperature and fluxing of the mantle, particularly where spreading rates are reasonably constant and tectonic complexity minimal.

The only active back-arc spreading in the Atlantic Ocean occurs at the East Scotia Ridge (ESR, Fig. 1), an intermediate-rate spreading centre coupled to the South Sandwich subduction system. This is possibly the simplest and, therefore, best example of back-arc spreading in a purely oceanic setting, opening at intermediate rates (60–70 mm a^{-1}), which make its axial morphology sensitive to small changes in magma supply (Livermore *et al.* 1997). Here, I examine morphological evidence from HAWAII-MR1 (Rognstad 1992) sonar mapping of the ESR, together with geochemical analyses of erupted basalts and a review of evidence from earthquake seismology and plate motion studies, to evaluate the influences of induced flow in the mantle wedge and inflow of South Atlantic

From: LARTER, R.D. & LEAT, P.T. 2003. *Intra-Oceanic Subduction Systems: Tectonic and Magmatic Processes.* Geological Society, London, Special Publications, **219**, 315–331. 0305-8719/03/$15.00

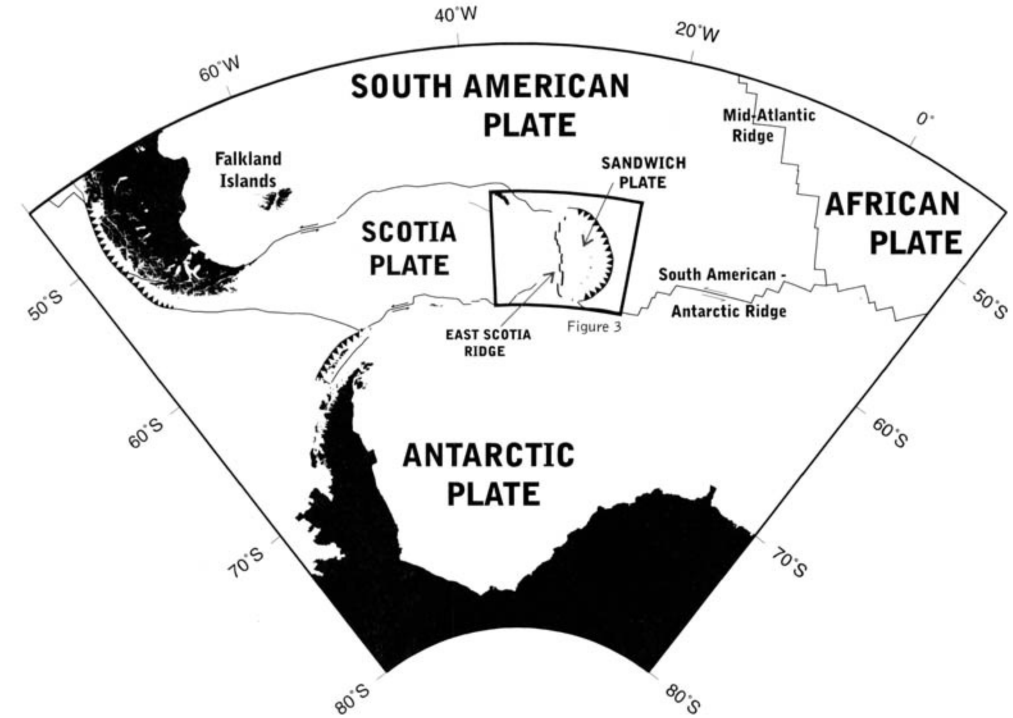

Fig. 1. Location of the South Sandwich arc–East Scotia Sea back-arc system in the South Atlantic.

asthenosphere beneath the South Sandwich back-arc region.

South Sandwich evolution

The modern South Sandwich system, with its W–E-oriented subduction and back-arc opening, probably has its origins in a change in South America–Antarctica (SAM–ANT) motion from WNW–ESE to W–E at approximately 20 Ma (Fig. 2). On the western flank of the ESR, magnetic anomaly C5B is identified with confidence, and C5C tentatively (Larter *et al.* 2003), showing that spreading was underway by 15 Ma. Further anomalies are visible, although not identifiable, to the west of ?C5C, which may indicate that spreading commenced as early as chron C6A (21 Ma). Until that time, oceanic crust formed at the South American–Antarctic Ridge was subducted at a trench forming the northwestern boundary of the Weddell Sea (Barker *et al.* 1984; Livermore & Woollett 1993). Relics of the associated arc now lie at Discovery and Jane banks (Fig. 2), and the Endurance Ridge, which continues westward to the Antarctic Peninsula. This earlier arc was associated with WNW-directed subduction and back-arc opening at Jane Basin. No remnant arc is apparent within the Scotia Sea, although a set of low, irregular topographic highs near 35°W could mark the site of an earlier volcanic line (Livermore *et al.* 1994).

Spreading seems to have been continuous since 15 Ma at least, at accelerating (full) rates of 32–65 mm a^{-1} (Larter *et al.* 2003). Between the time of initial opening and about 6–7 Ma, spreading also occurred at the West Scotia Ridge (Barker & Hill 1981; Livermore *et al.* 1994), and possibly in the central Scotia Sea also (Hill & Barker 1980). After the cessation of spreading at the West Scotia Ridge, spreading rates increased in the East Scotia Sea in partial compensation (Barker 1995). This implies that, within the context of slow SAM–ANT motion, slab roll-back has always been rapid. Spreading on the southernmost segments was initiated much more recently: in the case of the end segment, within the past 1 Ma, reflecting recent ridge–trench interaction (Bruguier & Livermore 2001).

Hypocentres from the ISC catalogue, relocated by Engdahl *et al.* (1998), are shown in Figure 3. The high level of activity at the South Sandwich Trench reflects the rapid motion of the

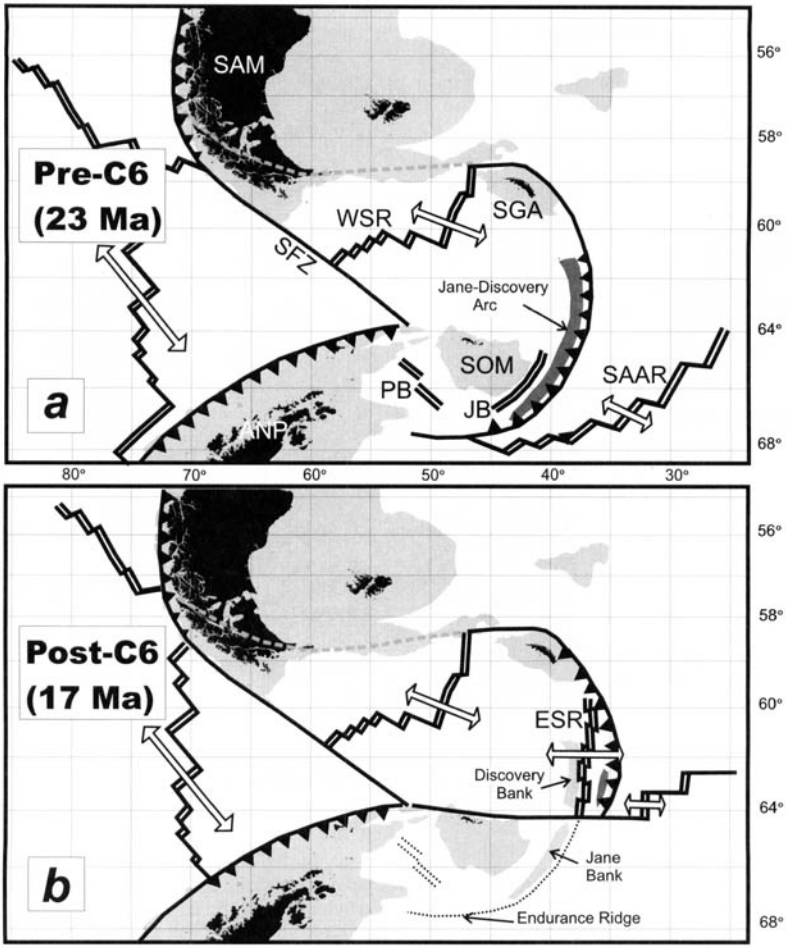

Fig. 2. Plate configuration in the Scotia sea (**a**) prior to and (**b**) following, the proposed reorganization at about C6 (20 Ma), caused by a change in the SAM–ANT Euler pole. Another spreading centre may have existed within the central Scotia Sea, but the age of activity is unknown (Hill & Barker 1981). For the sake of clarity this is omitted, and the central Scotia Sea is regarded as a single plate. ANP, Antarctic Peninsula; ESR, East Scotia Ridge; JB, Jane Basin; PB, Powell Basin; SAAR, South American–Antarctic Ridge; SAM, South America; SFZ, Shackleton Fracture Zone; SGA, South Georgia; SOM, South Orkney Microcontinent; WSR, West Scotia Ridge.

Sandwich (SAN) Plate, which overrides the subducting slab of South American lithosphere. Earthquakes shallower than 100 km tend to follow the curvature of the South Sandwich arc, whereas deeper events (100–350 km) occur mainly within a swath between 26° and 28°W, just west of the arc, suggesting a steepening of slab dip towards the northern and southern extremities. Few deep events occur north of 56°S, the latitude of the tear suggested by Forsyth (1975), which propagates eastward, defining the northern margin of the slab. The deepest events occur at depths of 300–350 km, immediately west of the South Sandwich arc.

The total length of the subducted slab can be estimated from the total opening in the East Scotia Sea, which I estimate to be about 650 km (from *c.* 36°W to *c.* 25°W at 58°S). Assuming a dip of 50° (Brett 1977), this gives an estimated depth of about 500 km for the tip of the slab. This is a minimum figure, inasmuch as it does not take account of slow South America–Scotia (SAM–SCO) plate motion and ignores long-term tectonic erosion of the forearc, and earlier spreading at the West Scotia Ridge (Vanneste & Larter 2002). It gives an average rate of trench rollback of 43 mm a^{-1}, if spreading began at 15 Ma, or 33 mm a^{-1} if it commenced at 20 Ma.

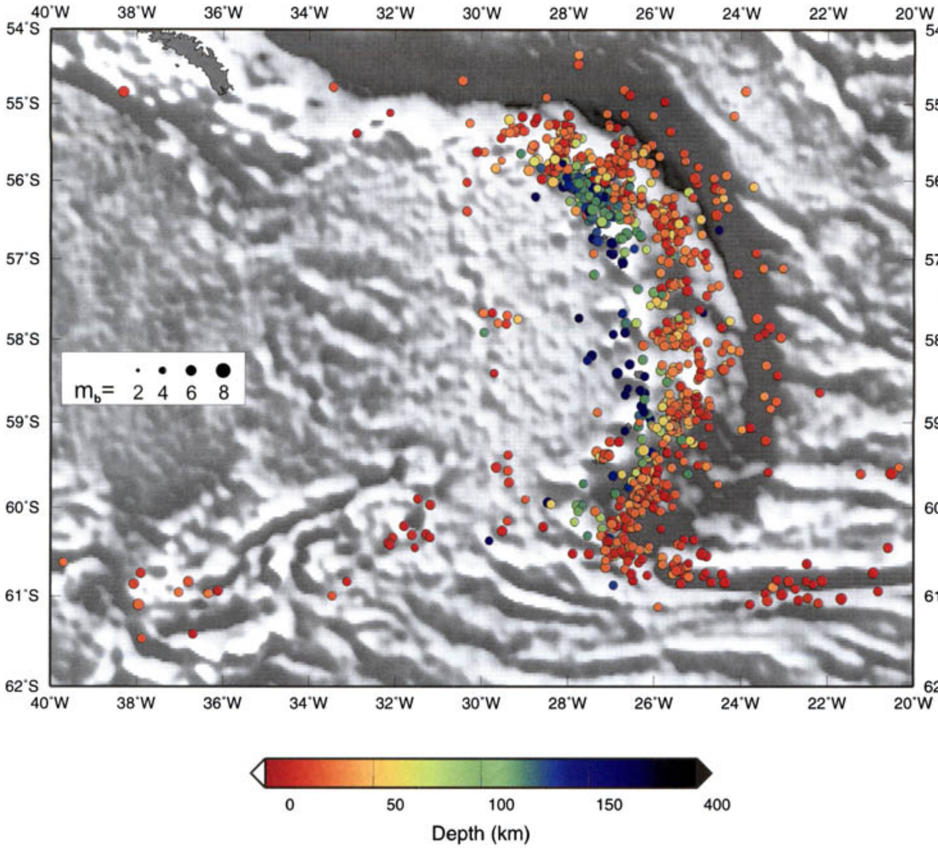

Fig. 3. Earthquake hypocentres for which depth phases have been identified, relocated by Engdahl *et al.* (1998), and superimposed on a satellite-derived free-air gravity map of the East Scotia Sea (Livermore *et al.* 1994). Circle size is proportional to earthquake magnitide (scale shown in inset box), and source depths are colour coded.

Hence, the slab must extend beneath the ESR at a depth of around 350 km, and could penetrate to a depth of over 500 km, close to the mantle transition zone, making it a formidable barrier to flow. This has important consequences for models of trench-parallel flow (see below).

Plate motions

The catalogue of teleseismic events has recently been reviewed by Thomas *et al.* (2003), who used slip vectors, combined with ESR spreading rates, to derive a new model (TLP2003) for the motion of the SCO and SAN plates relative to SAM and ANT. These motions are consistent with the NUVEL-1A global model (DeMets *et al.* 1990, 1994), and predict convergence between SAN and SAM in a direction of *c.* 078° at a rate of 67–80 mm a^{-1}, increasing from north to south (Fig. 4).

Direct measurements of plate motions in the Scotia Arc using Global Positioning System (GPS) and space geodetic methods are now underway, although no reliable results for SAN Plate kinematics, either relative or absolute, have been published yet. However, new estimates have recently been made of ANT Plate motion from GPS measurements made during 1995–1998 (Bouin & Vigny 2000). Combining this motion with TLP2003, I have derived new estimates of the absolute motion of the Scotia Sea plates (Fig. 4). It is important to note that these motions incorporate the assumption of no net rotation of the lithosphere (see Argus & Gordon 1991). The results show that the SAM, ANT and SCO plates are all moving at comparable rates of 5–10 mm a^{-1}, with similar northerly components. The SAN Plate is moving towards 064° at a rapid rate of 69 mm a^{-1} (calculated at 57°5.4′S, 26°44.4′W), with a northerly

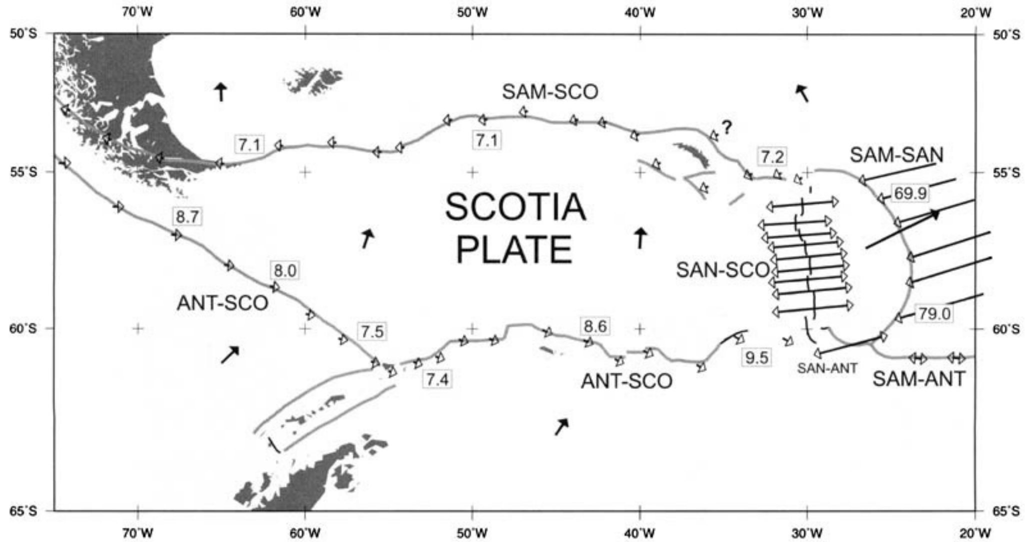

Fig. 4. Motions of the plates within and surrounding the Scotia Sea. Relative motion vectors (open arrow heads) are taken from the study by Thomas *et al.* (2003). Absolute vectors (filled arrow heads) are derived by the addition of these relative motions to the absolute motion (in the ITRF97 frame) of Antarctica from GPS measurements (Bouin & Vigny 2000). Double-headed arrows indicate full spreading rate at the ESR. Numbers in boxes indicate local rate of relative motion of the major plate (SAM or ANT) relative to the smaller plate (SCO or SAN), in mm a^{-1}. All vectors are drawn to scale.

component very similar to SCO, hence the W–E-oriented back-arc opening. Ignoring subduction-erosion of the fore-arc region, which Vanneste & Larter (2002) estimated to have averaged < 5 mm a^{-1}, absolute motion of the upper (SAN) plate may be regarded as a proxy for trench retreat. The direction of SAM Plate absolute motion in the vicinity of the South Sandwich Trench is approximately perpendicular to the absolute motion vector of SAN, and to the convergence direction between SAN and SAM. In this absolute reference frame, the SCO Plate is not retreating, as implied in the model of Chase (1978), but the overriding SAN Plate is advancing. Note that, in the absence of trench rollback, subduction would hardly occur, as the SCO–SAM convergence rate would be only 6–7 mm a^{-1}. Subduction and back-arc opening are therefore maintained by rollback.

The pattern of plate motions in the South Sandwich back-arc region is similar to that observed in the Tonga back-arc region (Hall *et al.* 2000), with rapid convergence between subducting and overriding plates, and predominantly W–E-oriented back-arc spreading. In both cases, trench rollback and back-arc spreading are rapid.

East Scotia Ridge morphology

The ESR system is some 500 km in length, and is divided into nine segments, separated by non-transform offsets. Segments E3–E7 exhibit faulted axial valleys reminiscent of the southern Mid-Atlantic Ridge (Fig. 5A), with maximum relief at E4 and E5. A symmetrical pattern of axial depths is observed (Fig. 5B): segments E2 and E9, close to the ends of the ridge, are anomalously shallow, with minimum depths of 2550–2600 m, compared to 3500–4000 m typical of other segments. The deepest section is between segments E5 and E7, where axial depths exceed 4000 m, although much of E6 lies near 3500 m.

New determinations of Brunhes spreading rates show that ESR opening increases slightly from 63 mm a^{-1} in the north to 69 mm a^{-1} in the south (Fig. 5C). Based on mid-ocean ridge morphology, such rates, in the absence of other factors, would be expected to give rise to axial morphology comparable to the Juan de Fuca or Southeast Indian ridges, characterized by shallow median valleys and non-transform offsets. Within this range, abrupt transitions from 'slow spreading' to 'fast spreading' morphology have been observed (e.g. Ma & Cochran 1996; Shah & Sempere 1998) in response to small changes in magma budget.

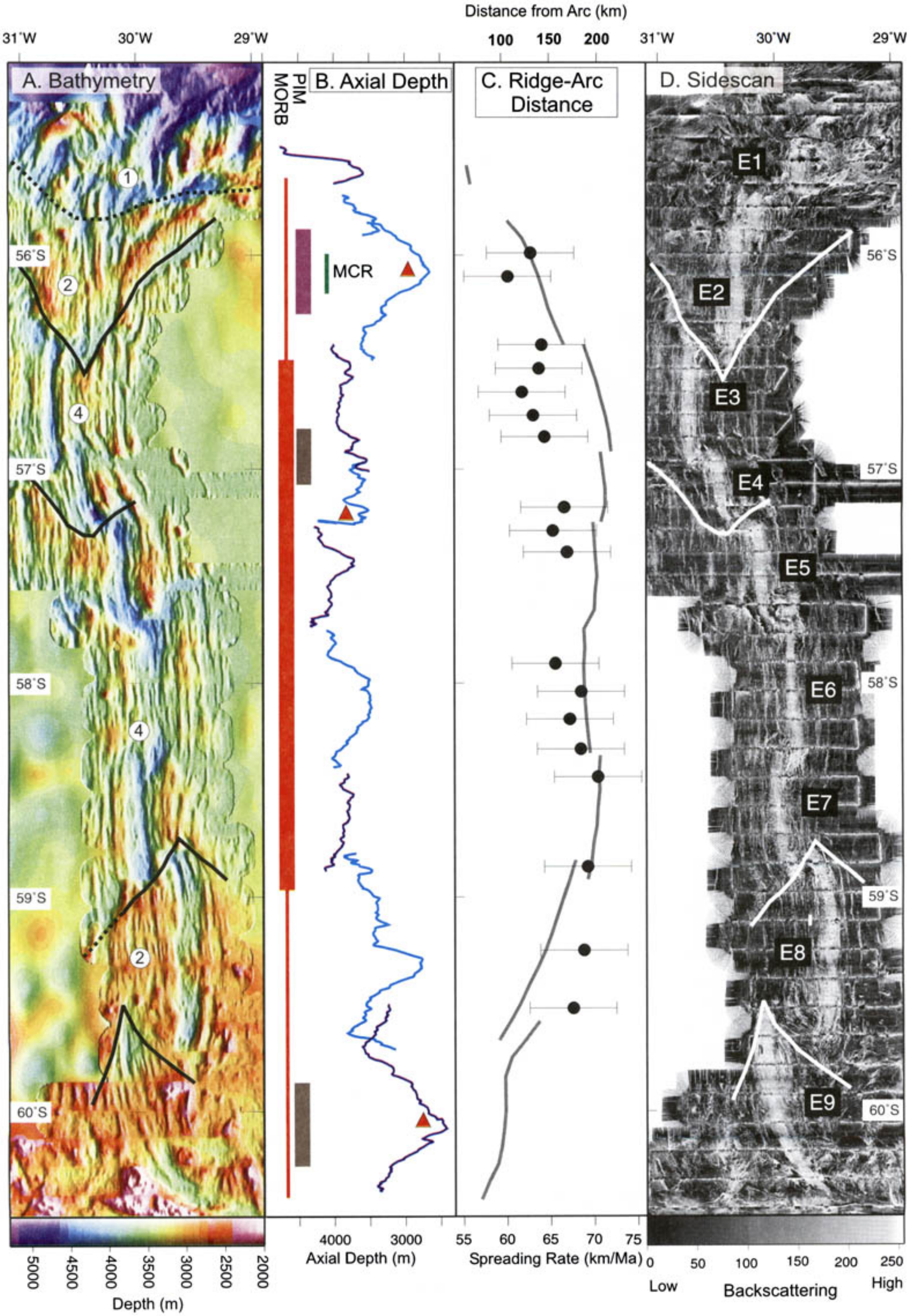

Distance from Arc (km)
100 150 200
31°W 30°W 29°W
31°W 30°W 29°W
A. Bathymetry
B. Axial Depth
C. Ridge-Arc Distance
D. Sidescan
PIM
MORB
MCR
56°S
57°S
58°S
59°S
60°S
E1
E2
E3
E4
E5
E6
E7
E8
E9
5000 4500 4000 3500 3000 2500 2000
Depth (m)
4000 3000
Axial Depth (m)
55 60 65 70 75
Spreading Rate (km/Ma)
0 50 100 150 200 250
Low
Backscattering
High

Segment E1 lies within a trough plunging to depths of 5000 m and greater, on the wall of the northern South Sandwich Trench, and is flanked by chaotic topography, suggestive of distributed extension (Livermore *et al.* 1997). Nevertheless, the HAWAII-MR1 side-scan sonar image of E1 (Fig. 5D) shows that the neovolcanic zone has the same N–S orientation as other ridge segments, and a similar high level of acoustic backscattering, demonstrating that volcanic activity is now focused at the ridge axis.

Segment E2 is highly anomalous, having a narrow, central axial topographic high, surmounted by an apical dome (the 'mermaid's purse'). This feature is associated with a seismic axial magma chamber reflection from a depth of approximately 3 km beneath seafloor (Livermore *et al.* 1997), and probably also with active hydrothermal venting (German *et al.* 2000). High-relief pseudofaults define a southward-pointing 'V', indicating that E2 is propagating southward at approximately 60 mm a^{-1} (Livermore *et al.* 1997). Within this 'V' and flanking E2, the seafloor shows a pattern of closely-spaced, narrow linear ridges and troughs, the former giving rise to bright lineaments in the side-scan image. Also visible in the side-scan image are many small seamounts, both on- and off-axis.

Seismic reflection profiling was also carried out along the axis of segment E3 and across E4 and E5, but found no evidence of magma chamber reflections beneath this section of the ridge. The off-axis topography consists of linear abyssal hills, oriented close to N–S. A NW-trending lineament on the western ridge flank strongly suggests that segment E4 has nucleated and propagated southward within the past 1 Ma. This is supported by the presence of a characteristic deep of over 4400 m near the southern rift tip (Fig. 5A), close to which evidence of hydrothermal activity was detected (German *et al.* 2000).

The only other segment that has been imaged along-axis by seismic reflection profiling is segment E9, where small melt lenses may exist close to the spatial resolution of the seismic data (Bruguier & Livermore 2001). Segment E9 is anomalous in its highly curved plan form, and in the presence of a narrow axial volcanic ridge, shoaling to *c.* 2550 m, complete with collapse caldera (Bruguier & Livermore 2001). Chemical and optical evidence was discovered in the vicinity of this feature for active hydrothermal venting (German *et al.* 2000), while at the northern end (Fig. 5), a sharp 'V'-shaped (in plan view) trough indicates that this segment is extending northwards rapidly at the expense of segment E8.

Off-axis topography flanking both E9 and E8 is anomalously shallow compared with the remaining segments, with several shoals close to the median valley. Those near the southern tip probably relate to the recent rifting history of the southern South Sandwich arc (Bruguier & Livermore 2001), while those near the middle section of E9 seem to represent a particularly robust magma supply to the ridge. Side-scan imagery (Fig. 5D) shows a less well-ordered pattern of seafloor fabric, together with many small circular features, interpreted as recent seamounts.

Segment E8 also has an axial volcanic ridge in its central section (Fig. 5B), and is flanked by shallow topography. The off-axis pattern of side-scan imagery, however, appears well ordered and comparable to those observed to the north. Oblique lineaments suggest that E8 may be propagating northward at a somewhat slower rate than E9.

Seismic anisotropy

Shear-wave splitting occurs when S-waves travel through an anisotropic medium such as the upper mantle or crust. The component of the wave polarized parallel to the 'fast' direction leads the orthogonal component by an amount

Fig. 5. Morphology of the East Scotia Ridge. (**A**) Subsampled HAWAII-MR1 sonar bathymetry of the ridge axis, superimposed on topography predicted from satellite altimetry (Smith & Sandwell 1994). Numbers refer to spreading regimes proposed by Martinez & Taylor (2002), see text. (**B**) Depth of ridge axis from HAWAII-MR1 bathymetry; red triangles denote evidence for hydrothermal activity (German *et al.* 2000); green line indicates extent of axial magma chamber reflection (Livermore *et al.* 1997); red, purple and grey bars show geochemical character of basalts and occurrence of plume-influenced mantle (Fretzdorff *et al.* 2002). Red (MORB = mid-ocean ridge basalt) indicates a mantle source composition close to N-MORB; purple (PIM = plume-influenced mantle) indicates a HIMU Bouvet plume isotopic composition; grey indicates elevated La/Sm and $^{87}Sr/^{86}Sr$, but no Bouvet signature. (**C**) East–west distance between ridge axis and South Sandwich volcanic line; filled circles represent estimates of Brunhes spreading rate from magnetic anomaly profiles. (**D**) HAWAII-MR1 side-scan sonar image of the ridge axis, with segments numbered E1–E9. High acoustic backscattering is represented by light tones: the neovolcanic zones of segments E1–E9 appear as white bands along the crest of the ridge.

depending on the degree of anisotropy. Polarization direction (ϕ) of the fast wave, and delay time (δt) between fast and slow waves, are calculated from the shear-wave phases, to characterize anisotropy within the medium (see Savage 1999 for details). The major cause of splitting of teleseismic shear waves is believed to be the alignment (known as lattice preferred orientation) of anisotropic mantle minerals, chiefly olivine and orthopyroxene, which may be imposed by flow-induced strain or fabric created during the tectonic history of the lithosphere. For large amounts of strain by progressive simple shear, the *a* axes of mantle olivine are expected to be parallel to asthenosphere flow, and this is believed to be the principal contributor to upper mantle anisotropy (Savage 1999). The seismic waves most commonly used in splitting measurements are direct S-phase arrivals at stations above the earthquake source, teleseismic S arrivals at distances of >60°, and SKS phases (doubly-converted phases that traverse the outer core as P-waves).

A major cause of uncertainty in the interpretation of splitting results is the limited vertical resolution of the method. This may be improved by recording events from a number of depths beneath the recording station, or by use of surface waves (e.g. Vuan *et al.* 2000). Depth information is critical in subduction zones, where arrivals may have sampled the mantle above, beneath and within the subducting slab, and where stress and strain may vary over relatively small distances. With inadequate data, it may not be possible to separate anisotropy contributions from the crust, mantle wedge, slab and subslab mantle.

Studies in Pacific back-arc basins show variations in the patterns of anisotropy observed. Beneath the Izu–Bonin and Mariana arcs, fast directions in the mantle wedge appear to parallel the absolute motion vector of the subducting Pacific Plate (Fouch & Fischer 1996, 1998), whereas oblique or trench-parallel directions are observed in the southern Kuril, Aleutian and Hikurangi subduction zones (e.g. Fischer & Yang 1994; Yang *et al.* 1995; Audoine *et al.* 2000).

Experiments in the Tonga back-arc region (Smith *et al.* 2001) show that mantle flow there is more complex than formerly believed, with fast directions parallel to the absolute motion of the down-going Pacific Plate in the west (Fiji platform) and in the southern Tonga arc, but more N–S-oriented directions near the Northern Lau Spreading Centre, and trench-parallel in the eastern mantle wedge beneath the northern Tofua arc. Smith *et al.* (2001) link this complexity to the inflow of Samoan-plume-enriched mantle through the Pacific Plate tear that marks the northern limit of the slab, and which was suggested on the basis of geochemistry (Turner & Hawkesworth 1998).

Preliminary anisotropy measurements have been made in the South Sandwich arc, but station coverage is poor, owing to the logistical difficulties of recording on the rugged and remote South Sandwich Islands. No shear-wave splitting analyses have yet been carried out in the back-arc region, but direct S-wave splitting results from a temporary deployment of seismological receivers on Candlemas Island were obtained from six deep events beneath the arc (Müller 2001). These results are reproduced in Figure 6, which shows the anisotropy bars corresponding to the delay time and azimuth for each event, plotted at its epicentre. For these events, the mantle paths sampled lie along the lines connecting hypocentres with receiver, and occur mainly in the mantle wedge. An average of the fast-wave polarization directions beneath this part of the South Sandwich arc was calculated as 076° (Müller 2001). This is comparable with the direction of SAM–SAN convergence of 077° predicted by model TLP2003 (Thomas *et al.* 2003), suggesting that this anisotropy is caused by shear within the mantle wedge induced by the subducting slab. At the northern end of the arc, however, NW–SE directions are observed (Fig. 6), which may reflect recent flow in the asthenosphere. Preliminary analyses of source-side anisotropy suggest that along-axis flow may occur beneath the slab (C. Müller pers. comm. 2002).

Geochemistry

Segments E2 and E8 both show low Mg and major element compositions that can be modelled by olivine, plagioclase and clinopyroxene fractionation (Fretzdorff *et al.* 2002), with up to about 50% fractionation at E2 (Leat *et al.* 2000). Samples from the shallowest sections of both segments have relatively low $Na_{8.0}$ values (see Klein & Langmuir 1987), indicating a higher degree of melting than elsewhere along the ESR (Fretzdorff *et al.* 2002). Overall, the pattern of $Na_{8.0}$ values along the ridge correlates with axial depth between segments E2 and E8 (see fig. 7 in Fretzdorff *et al.* 2002), while E9 is anomalous in having values close to normal mid-ocean ridge basalt (N-MORB) near its northern end, but higher values (indicating low degrees of melting) in its shallow central and deeper southern sections. Central segments E3, E5, E6, E7, and also segment E9, have $^{230}Th/^{238}U \geq 1$, similar to global MORB, while the range of $^{230}Th/^{232}Th$

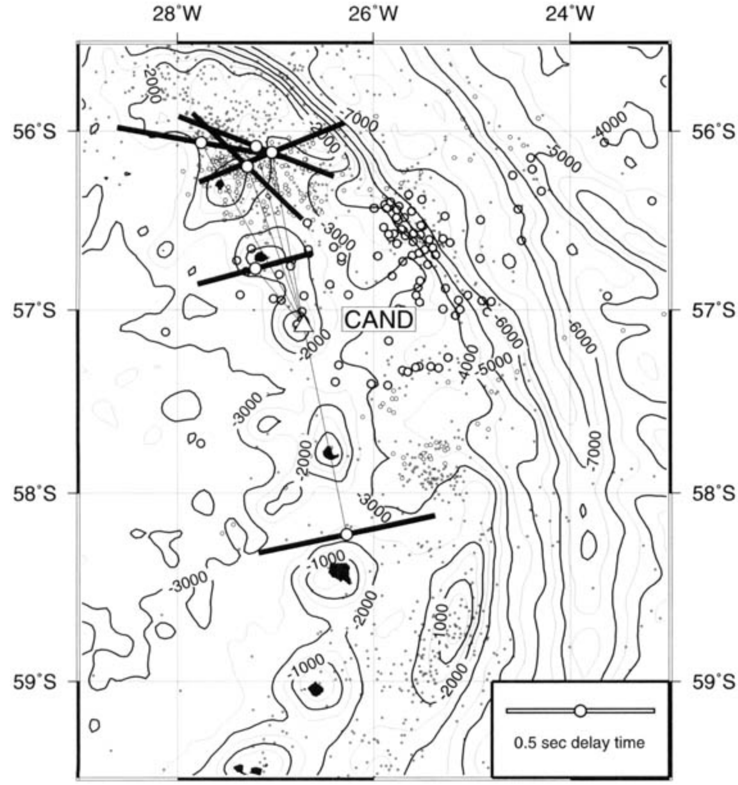

Fig. 6. Seismic anisotropy results from the South Sandwich arc recorded at Candlemas Island (CAND). Results are based on direct S-wave arrivals from six deep events. Bars representing average strength and direction of anisotropy are plotted at epicentres, and result from anisotropy along the path from source to receiver (shown). From the preliminary study by Müller (2001). Reproduced with permission of Blackwell Publishers.

and $^{238}U/^{232}Th$ ratios at the ESR is greater than that reported for any other back-arc region (Fretzdorff *et al.* 2003).

Enrichment factors of subduction-related elements (e.g. Ba, Rb, K, Th) are low (between 0 and 5) in the central segments (see fig. 10 in Fretzdorff *et al.* 2002). Higher values for Ba and Rb (>5) were measured for some samples from segments E2, E8 and the overlapping parts of E3 and E4. The $^{230}Th/^{238}U$ ratios of E4 and E8 lavas are generally ≤1, as frequently found in island arcs, indicating the involvement of slab-derived fluids. $^{143}Nd/^{144}Nd$ and $^{87}Sr/^{86}Sr$ ratios point towards sediment melt at E4, and a hydrous fluid from altered MORB at E8 (Fretzdorff *et al.* 2003).

Strong 'plume' signals were recorded by Nd, Sr and Pb isotope ratios from dredge samples on the flanks of the central topographic high on E2. Elevated $^{206}Pb/^{204}Pb$ ratios for these samples lie close to typical HIMU (high U/Pb) Bouvet Island values (Fretzdorff *et al.* 2002). No analyses have been published of Hf isotopes in these samples, to test the possibility that isotope ratios may have been affected by subduction processes (Pearce *et al.* 1999), but the strong similarity to results from Bouvet Island lends support to the idea of westward-flowing asthenosphere along the SAAR (le Roex *et al.* 1985). On the other hand, samples from E4, E8 and E9 show lower $^{206}Pb/^{204}Pb$ ratios and therefore do not appear to carry a Bouvet signature, although the general chemical similarity of E9 basalts to those erupted at the South American–Antarctic Ridge (Fretzdorff *et al.* 2002) argues for a South Atlantic mantle source.

Mantle flow

Back-arc circulation is a combination of several classes of mantle flow, depending on local conditions. These are summarized in Table 1 for the specific case of the South Sandwich system, and are discussed below, together with results from

Table 1. *Classes of possible mantle flow in the South Sandwich back-arc region*

Class	Type of flow	Flow alignment
I	Upwelling due to back-arc spreading	Vertical
II	Coupled flow induced in mantle wedge	Parallel to plate motions
III	Inflow through tear in subducting plate	Along axis
IV	Ridge migration in absolute frame	Along axis
V	Mantle return flow	Pacific → Atlantic
VI	Hot-spot flow	Following pressure gradient

geochemistry, S-wave splitting and satellite geodesy. Flow types I–III are related to subduction and back-arc spreading, whereas types IV–VI are regarded as regional flow (Winder & Peacock 2001).

Upwelling

Vertical advection beneath back-arc spreading centres (type I) is fundamentally the same as that inferred beneath mid-ocean ridges, but the fertility and temperature of the mantle source, and thus the degree of decompression melting, will be influenced by the nearby slab. Results of numerical modelling led Blackman *et al.* (1996) to conclude that horizontal anisotropy should parallel the base of the plate for passive upwelling, whereas strongly vertical alignment would be expected for buoyant upwelling. The pattern of segmentation of the ESR, with shallow middle sections on most segments, supports a model of three-dimensional passive upwelling beneath the ridge.

Coupled flow

Mechanical coupling between the subducting slab and surrounding mantle results in mantle flow, both above and below the slab, in the direction of subducting plate motion relative to the mesosphere (McKenzie 1969; Sleep & Toksöz 1971). Simple, two-dimensional numerical models of mantle flow in back-arc regions predict flow that is determined primarily by the motion of the subducting and upper (overriding) plates (Fischer *et al.* 2000), in agreement with S-wave splitting directions observed in back-arc mantle of the Marianas and Izu-Bonin subduction zones (e.g. Fouch & Fischer 1996; Fischer *et al.* 1998). Such models could not, however, explain oblique or trench-parallel fast directions observed at some arc systems, such as the Aleutians (Yang *et al.* 1995) and New Zealand (Audoine *et al.* 2000). Three-dimensional, plate-coupled flow was modelled by Hall *et al.* (2000), who concluded that trench-parallel flow in the inner wedge corner could be enhanced by trench-parallel motion of the upper plate, by oblique subduction or by a reduction in slab dip over time. Recent modelling by Winder & Peacock (2001) indicates that the eddy produced by coupled flow is largely unaffected by trench retreat or regional flow.

In the Lau Basin, geochemical variations in back-arc volcanic rocks have been related to distance from the Tofua volcanic arc (Pearce *et al.* 1995*a*; Peate *et al.* 2001), the subduction component being strongest at the Eastern Lau Spreading Centre, close to the arc. Differences in ridge morphology, reflecting variations in magma supply to the back-arc spreading centre, have also been ascribed to arc proximity (Martinez & Taylor 2002, 2003). These geochemical and morphological variations, it is suggested, reflect the pattern of flow in the mantle wedge beneath the arc–back-arc system, involving motion parallel to the subduction direction. Martinez & Taylor (2002) identify four zones of accretion in the Lau Basin, each with a distinctive style of topography and crustal structure, resulting from the position of the spreading centre with respect to the volcanic line and mantle wedge. Ridge segments active near the volcanic line (zones 1 and 2) receive an enhanced magma supply, and show inflated topography and anomalously thick (up to 2 km thicker than normal) crust. Those a little further away (zone 3) tap more depleted mantle, have deeper (by about 1000 m) axes and thinner (by 2000–3500 m) crust, whereas those beyond the arc influence (zone 4) have normal morphology and crustal thickness.

The ESR has a longer history of spreading than other active back-arc basins, and the ridge axis consequently lies further from the arc than is the case for the Lau spreading centres. Nevertheless, there is a striking correlation between axial depth and distance from the arc (Fig. 5B, C). Segments further than 150 km from the arc (E3–E7) exhibit axial depths of 3500–4200 m, together with high relief median valleys, while those within 150 km of the arc (E2, E8 and E9) shoal to 2500–2800 m, and have shallow or absent median valleys. Between segments E2 and E8, the pattern of ridge–arc distances (Fig. 5C) is symmetrical. This reflects arc curvature, and the fact that E9 has a spreading history of <1 Ma (Bruguier & Livermore 2001), before which E8 was presumably the southernmost segment. Likewise, the neovolcanic zone of anomalous segment E1, which lies in a region of distributed extension (Fig. 5D), has probably been established relatively recently.

The configuration of plate boundaries before the initiation of E9 is unknown, but the unstable nature of the SCO–SAN–ANT triple junction region is probably a result of successive interactions between the South American–Antarctic Ridge and the eastern South Scotia Ridge (Hamilton 1989; Bruguier & Livermore 2001), perhaps involving microplate formation and mantle inflow though slab windows. The absence of highly fractionated lavas on E9, and the high $Na_{8.0}$ values found there, seem to conflict with the morphological and seismic evidence for an abundant magma supply (Bruguier & Livermore 2001).

In summary, the ESR, like the Lau spreading centres, has characteristics that are strongly correlated with distance from the arc, and consequently with the position of the spreading centre over the mantle wedge.

Mantle inflow and hot-spot flow

Flow of South Atlantic mantle into the South Sandwich back-arc region, via a tear in the SAM Plate, was suggested by Livermore *et al.* (1997) as an explanation of the anomalous topography, enhanced magma supply and southward propagation of segment E2. This notion was supported by geochemical studies of basaltic glasses from E2 (Leat *et al.* 2000). Further work near the southern end of the ESR (Bruguier & Livermore 2001) indicated that a similar flow may occur around the southern end of the slab, and explain the anomalous topography and evidence for recent volcanism found there.

In the model of Livermore *et al.* (1997), mantle inflow is associated with trench-parallel flow beneath the subducting slab, driven by rapid retreat of the South Sandwich Trench. This assumes that flow underneath the slab tip (i.e. from east to west) is restricted, so that escape flow occurs towards the northern and southern ends of the slab, much as suggested by Russo & Silver (1994) for the Andean subduction zone. The slab is also relatively narrow (i.e. in a N–S direction), having free ends about 500 km apart, which also favours along-axis flow (Dvorkin *et al.* 1993). Laboratory experiments with a viscous fluid (Buttles & Olson 1998) confirmed that rollback is effective in producing a trench-parallel strain orientation, provided that flow underneath the slab tip is prevented. Retrograde motion of subducting slabs implies the displacement of mantle from one side of the slab and inflow of an equal volume on the other (Garfunkel *et al.* 1986). As many slabs have been undergoing retrograde motion for some time (Chase 1978), this redistribution represents an important mass flux associated with plate motion.

Alternatively, the inflow could be driven by pressure difference from the Bouvet plume, without trench-parallel flow. Limited sampling of ocean floor basalts from the Scotia Sea found a Pacific Pb/Nd isotopic signature in rocks in Drake Passage (Pearce *et al.* 2001), while basalt from a dredge site near the western margin of the East Scotia Sea seems to show an Atlantic signature, with elevated radiogenic lead concentrations interpreted as a Bouvet plume influence. The Drake Passage samples come from a fossil spreading centre that ceased spreading at about 6–7 Ma (Barker & Hill 1981; Livermore *et al.* 1994; Maldonado *et al.* 2000). Hence, while spreading on the West Scotia Ridge in Drake Passage was accompanied by inflow of Pacific mantle, the ESR appears to have been fed by Atlantic mantle flowing around the ends of the retreating slab (Fig. 7).

A westward asthenospheric flow away from the Bouvet Island plume was suggested by le Roex *et al.* (1985) to explain the geochemistry of basalts sampled at the South American–Antarctic Ridge. Geochemistry of volcanic rocks recovered from the ESR axis shows evidence of an enriched Bouvet plume-like isotopic signature at E2 (Leat *et al.* 2000; Fretzdorff *et al.* 2002), supporting the notion of inflow. Analysis of dredge samples from the northeastern corner of the East Scotia Sea also supported this notion (Pearce *et al.* 1995*b*). However, the situation for E9 is more complicated. While E9 basalts show some geochemical similarities to those of the South American–Antarctic Ridge, their radiogenic isotope (Nb, Sr, Pb) composition differs from that of Bouvet (see above).

Flow around slab ends has been suggested elsewhere. A tear in the subducting Pacific slab at the Aleutians–Kamchatka boundary has been proposed on the basis of a seismicity gap (Yogodzinski *et al.* 2001). Seismic anisotropy patterns are consistent with flow of asthenospheric mantle around the slab edge, through the slab window (Peyton *et al.* 2001). Warming or

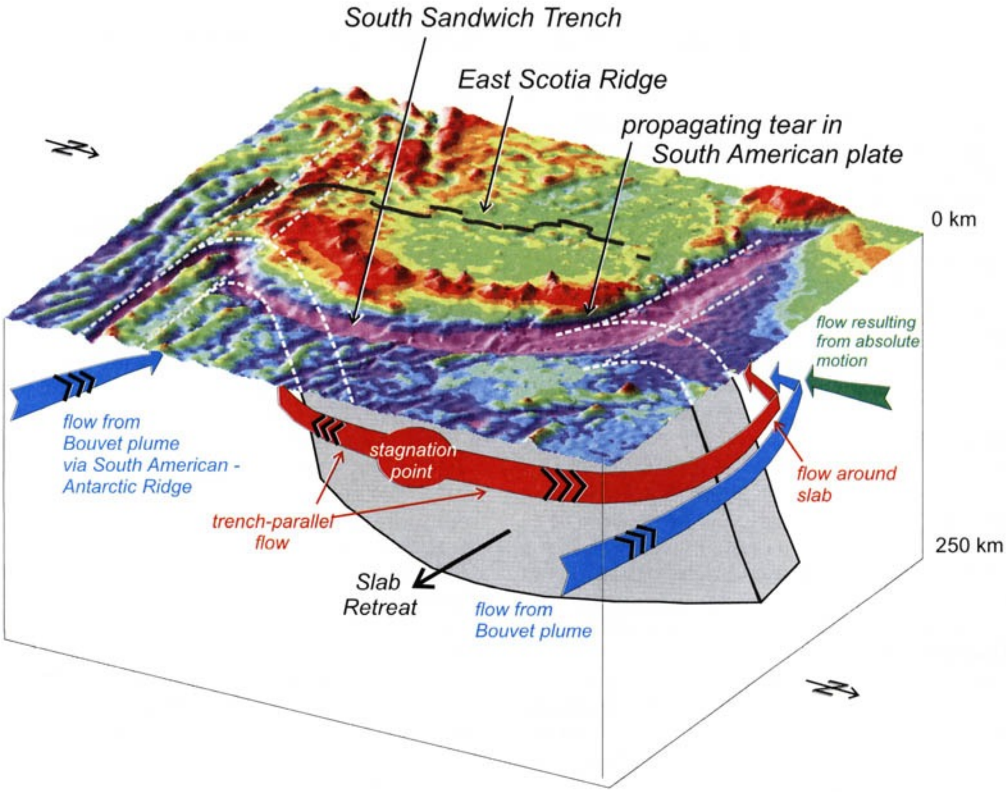

Fig. 7. Schematic diagram of mantle flow beneath the South Sandwich arc and back-arc basin. Predicted topography from Smith & Sandwell (1994) is shown at the surface. Red arrows indicate flow according to the trench-parallel flow–inflow model favoured here. White dotted lines indicate the approximate positions of plate boundaries. Rapid retreat of the subducting slab, together with impeded flow beneath the slab tip and the relatively short slab width, give rise to escape flow, similar to that suggested by Alvarez (1982) and Russo & Silver (1994). Flow extends around the slab ends and into the melting region for the East Scotia Ridge. The blue arrows represent the inflow model of Pearce *et al.* (2001), in which westward flow, driven by pressure differences associated with the Bouvet plume, causes subAtlantic mantle to enter the back-arc region. The green arrow indicates mantle inflow resulting from northward motion of Scotia and Sandwich plates relative to the South American Plate. As a result of the inflow, the magma budgets of the end segments are enhanced, and these segments propagate into the back-arc region. Vertical exaggeration is approximately 2:1 .

ablation of the exposed edge of the slab, it is suggested (Yogodzinski *et al.* 2001), may cause melting, resulting in eruption of a distinctive suite of silicic, calc-alkaline magmas known as adakites. To date, no adakitic rocks have been reported from the South Sandwich arc, although the strong influence of an aqueous fluid in segment E8 could be related to the proximity of the slab end.

Similarly, flow of plume-modified Pacific mantle through a slab window created by the collision of the Cocos Ridge with the Middle America Trench, into the Caribbean, has been proposed (Abratis & Wörner 2001). This flow may have caused melting of the leading edge of the subducted Cocos Ridge, and eruption of Pliocene adakites in southern Costa Rica. Such a flow is supported by variations in basalt geochemistry (Herrstrom *et al.* 1995; Abratis & Wörner 2001) and by shear-wave splitting (Russo & Silver 1996), and has been interpreted as evidence for the Pacific mantle outflow model of Alvarez (1982, 2001).

The two regions most directly comparable with the East Scotia Sea are the back-arc basins of Lau Basin and the Mariana Trough. The Pacific Plate is known to be tearing beneath the northern end of the Tofua arc (Millen & Hamburger 1998). Flow of Pacific asthenosphere into the northern Lau Basin has been suspected for some time, on the basis of Pb, Sr and Nb isotopes in drilled basalts (Hergt & Hawkesworth 1994), and probably occurs through this tear (Pearce *et al.* 1995*a*). Assuming that the tear formed at *c.* 10 Ma, Turner & Hawkesworth (1998) estimated a minimum rate of approximately 40 mm a^{-1} for the southward propagation of the Samoan plume into the Lau Basin.

Ridge migration in an absolute frame

The western flank of the ESR contains subparallel, WNW-trending lineaments seen in satellite free-air gravity maps (Livermore *et al.* 1994). Unfortunately, any similar lineaments on the eastern flank are obscured by thick sediments (Vanneste *et al.* 2002). The HAWAII-MR1 data show that these lineaments are associated with non-transform offsets between ESR segments (Fig. 5), and also with offsets in magnetic anomalies (Larter *et al.* 2003), and seem to record uniform southward propagation of segments E3–E7.

Similar oblique patterns observed on the flanks of the Mid-Atlantic Ridge and East Pacific Rise were interpreted by Schouten *et al.* (1987) as a consequence of subaxial asthenosphere flow caused by migration of the ridge relative to the mesosphere. In the case of the ESR, the spreading centre migrates northward relative to the mesosphere, and hence to the underlying magma supply system. In the model of Schouten *et al.* (1987), the result would be that ridge segments then propagate southward to maintain their position over the melt system. The geometry of these ridges is compatible with such a hypothesis, based on the revised plate motion model (Thomas *et al.* 2003) (Fig. 4). Hence, these lineaments can be explained by vertical flow beneath a spreading centre that is migrating northward relative to the deep mantle.

The greater northward component of SAN motion compared to that of SAM results in the convergence vector being oriented to the north of east (Fig. 4). Hence, the northern part of the back-arc basin will override South Atlantic mantle, causing it to flow into the back-arc region, perhaps becoming entrained with the flow around the slab end. At the southern end of the slab, back-arc mantle will be overridden by the ANT Plate, so that the only flow into the back-arc region will be that displaced by trench retreat. This may explain why a stronger plume signature was found in basalts at the northern end of the ridge. On the other hand, the rapid southward migration of segment E2 (estimated at *c.* 60 mm a^{-1} by Livermore *et al.* 1997), and the northward E8 and E9 propagators, cannot be explained by the ridge migration model, and are more likely to be a consequence of horizontal subaxial inflow from the north (E2) and south (E8 and E9).

Pacific outflow

In his Pacific mantle return flow hypothesis, Alvarez (1982) suggested that eastward flow beneath the Caribbean and Drake Passage oceanic gaps (which are not blocked by continents or subducting slabs) could be responsible for eastward plate motions in these regions, and could drive eastward retreat of the subducting slabs at the Antilles and South Sandwich trenches. In this case, basalts erupted at Scotia Sea spreading centres should carry a Pacific isotopic signature.

Plots of Nd–Pb isotopes from dredged basalts in Drake Passage show that a Pacific influence is discernible at a site on the West Scotia Ridge, which was interpreted as evidence of an eastward mantle flow (Pearce *et al.* 2001). As this site lies close to the ridge axis that became extinct at *c.* 6 Ma (Livermore *et al.* 1994), the implication is that a Pacific outflow existed during at least the earlier part of East Scotia Sea evolution (20–6 Ma). However, a sample from the western part of the East Scotia Sea basin showed an Atlantic isotope signature, suggesting that a Pacific influence never reached this far east, and therefore could not be responsible for retreat of the subducting slab. Geochemical data for the central Scotia Sea are non-existent, so that the location of the Pacific–Atlantic mantle domain boundary cannot be determined at present.

Using a network of temporary, broad-band, seismometers in Patagonia, Helffrich *et al.* (2002) found no evidence for present-day eastward flow in the mantle beneath Drake Passage, and concluded that any such flow must be weak, and countered by a deeper westward flux away from Atlantic hot spots. Müller (2001) used a network of permanent and temporary Antarctic broad-band stations to come to rather different conclusions. Anisotropy polarization directions close to W–E for data recorded in the Falkland Islands, South Georgia and South Orkney are not incompatible with Pacific return flow, although their shallow depths suggest they could be caused by fossil alignment of olivine in the lithosphere. Results of waveform inversion of regional seismograms (Robertson Maurice *et al.* 2003) show that continental lithosphere is relatively thin beneath southern South America, limiting its role as a barrier to flow, while estimates of mantle anisotropy gave very small values for sublithospheric mantle, implying an absence of strong asthenospheric flow.

The revised absolute motions show that the SCO Plate, which floors most of the Scotia Sea west of the ESR, is presently moving slowly northward (Fig. 4), arguing against any significant traction from Pacific to Atlantic mantle escape flow. The suggestion of Alvarez (1982), that a return flow from the shrinking Pacific basin is responsible for the rapid retreat of the South Sandwich trench–arc system, must therefore be incorrect.

Discussion: inflow versus mantle wedge control on accretion

The evidence presented here suggests that first-order variations in axial morphology and basalt geochemistry are related to the distance of the ESR from the volcanic arc, and therefore may be explained by slab-coupled flow in the mantle wedge, causing overturn of depleted mantle, as suggested by Martinez & Taylor (2002) for the Lau Basin.

Segment E1 lies within 100 km of the volcanic arc, and is highly anomalous in its morphology and depth. Topography flanking E1 is disorganized and atypical of seafloor formed at an intermediate-rate ridge. The northernmost region of the East Scotia Sea may, therefore, correlate with zone 1 of Martinez & Taylor (2002), representing rifted and volcanic terrain (Fig. 5, panel A).

Segment E2 is magmatically robust with a strong magma chamber reflection, and is associated with shallow, well-ordered abyssal hills on its flanks, along with many seamounts, indicating a high degree of off-axis volcanism. This is similar to zone 2 of Martinez & Taylor, which they interpreted as seafloor formed when the ridge was close to the volcanic front, and therefore dominated by volcanic extrusion. Most of E2 lies more than 120 km from the volcanic front, however, and its lavas carry a clear Bouvet plume signature. Hence, the anomalous nature of the E2 axis, together with its rapid southward propagation, is attributed to subaxial flow of South Atlantic mantle that has flowed around the torn northern end of the slab. As with the Valu Fa Ridge in the Lau Basin (Martinez & Taylor 2002, 2003), these effects cannot be related to spreading rate as rates at E2 are, if anything, slightly lower than measured over more southerly segments (Fig. 5C).

Near the southern end of the ESR, segments E8 and E9 also display shallow bathymetry relative to segments E3–E7, dotted with many off-axis seamounts. These segments lie at a similar distance from the active arc to E2 (Fig. 5C), and therefore also conform to zone 2 of the Martinez & Taylor (2002) model.

The remaining segments (E3–E7) display shallow median valleys and well-developed linear abyssal hill fabric on their flanks (Fig. 5A). Off-axis depths are greater than for magmatically robust segments, such as E2 and E8, while basalt geochemistry generally lies within the field of normal MORB source (Fretzdorff *et al.* 2002). These are all characteristics of zone 4 in the Martinez & Taylor (2002) model, which they ascribe to melting of undepleted mantle and spreading similar to that of normal mid-ocean ridge spreading centres. The greater depth of these ESR segments compared to normal mid-ocean ridge crust, together with the presence of median valleys (rather than axial highs) despite intermediate spreading rates, suggests that the east Scotia mantle source is perhaps more depleted than that of the northern Lau Basin. Crust corresponding to zone 3 of Martinez & Taylor (2002) is not observed in the East Scotia Sea. In the Lau Basin, this zone (East Lau Spreading Centre) was characterized by greater-than-normal water depths and thin crust with low-relief abyssal hill fabric, interpreted as crust formed by melting of mantle from the depleted wedge corner.

Propagation of end segments into the back-arc region, together with geochemical evidence for mantle inflow, show that along-axis flow is also important, giving rise to more complex patterns of seismic anisotropy than predicted by a coupled flow model alone. This contrasts with results from S-wave splitting studies in the Marianas and Izu–Bonin arcs, showing 'fast' directions subparallel to plate motions, but is comparable to that observed in the Lau Basin (Smith *et al.* 2001).

Both the Lau Basin and the East Scotia Sea appear to experience inflow of plume-enriched mantle, from the Samoan and Bouvet plumes, respectively. Other similarities include well-organized back-arc spreading, rapid southward propagation of the northern segments and rapid trench retreat. On the other hand, the ESR is deeper than the Lau spreading centres, typically by >1000 m, suggesting that crust here is thinner, in turn indicating a cooler and/or less fertile source.

The tendency for arc-parallel flow in the back-arc region, and the occurrence of plume-enriched mantle sources near slab ends, are probably related to rapid trench retreat. Slab migration may give rise to trench-parallel flow beneath the slab, as suggested by Russo & Silver

(1994) for the Andean margin, coupled to flow around the slab ends into the source region for back-arc spreading (Livermore *et al.* 1997) (Fig. 7), producing anomalously robust spreading morphology. Continued horizontal flow then drives propagation of end segments towards the centre of the back-arc basin.

Eastward flow of Pacific mantle is not required by Scotia Sea plate motions or basalt geochemistry, and is not supported by preliminary seismic anisotropy results. Therefore, the eastward retreat of the South Sandwich arc system cannot be driven by outflow from the Pacific region, as suggested by Alvarez (1982). Nevertheless, there is good evidence that the subducting slab does indeed act as a barrier to mantle flow – not of Pacific asthenosphere from the west, but of Atlantic asthenosphere from the east.

The author acknowledges the support of the captain, crew and scientific party of RRS *James Clark Ross* for cruise JR09a, during which the HAWAII-MR1 sonar data illustrated here were acquired. In particular, he thanks the University of Hawaii Mapping Research Group support party for sonar operation and shipboard data processing. Reviews by Brian Taylor and Christian Müller, and careful editing by Rob Larter, have substantially improved the manuscript.

References

ABRATIS, M. & WÖRNER, G. 2001. Ridge collision, slab-window formation, and the flux of Pacific asthenosphere into the Caribbean realm. *Geology*, **29**, 127–130.

ALVAREZ, W. 1982. Geological evidence for the geographical pattern of mantle return flow and the driving mechanism of plate tectonics. *Journal of Geophysical Research*, **87**, 6697–6710.

ALVAREZ, W. 2001. Eastbound sublithosphere mantle flow through the Caribbean gap and its relevance to the continental undertow hypothesis. *Terra Nova*, **13**, 333–337.

ARGUS, D.F. & GORDON, R.G. 1991. No-net-rotation model of current plate velocities incorporating plate motion model NUVEL-1. *Geophysical Research Letters*, **18**, 2039–2042.

AUDOINE, E., SAVAGE, M.K. & GLEDHILL, K. 2000. Seismic anisotropy from local earthquakes in the transition region from a subduction to a strike-slip plate boundary, New Zealand. *Journal of Geophysical Research*, **105**, 8013–8033.

BARKER, P.F. 1995. Tectonic framework of the East Scotia Sea. *In*: TAYLOR, B. (ed.) *Backarc Basins: Tectonics and Magmatism*. Plenum, New York, 281–314.

BARKER, P.F. & HILL, I.A. 1981. Back-arc extension in the Scotia Sea. *Philosophical Transactions of the Royal Society of London*, **A300**, 249–262.

BARKER, P.F., BARBER, P.L. & KING, E.C. 1984. An early Miocene ridge crest–trench collision on the South Scotia Ridge near 36°W. *Tectonophysics*, **102**, 315–332.

BLACKMAN, D.K., KENDALL, J.-M., DAWSON, P.R., WENK, H.-R., BOYCE, D. & PHIPPS MORGAN, J. 1996. Teleseismic imaging of subaxial flow at mid-ocean ridges: traveltime effects of anisotropic mineral texture in the mantle. *Geophysical Journal International*, **127**, 415–426.

BOUIN, M.N. & VIGNY, C. 2000. New constraints on Antarctic Plate motion and deformation from GPS data. *Journal of Geophysical Research*, **105**, 28 279–28 293.

BRETT, C. 1977. Seismicity of the South Sandwich Islands region. *Geophysical Journal of the Royal Astronomical Society*, **51**, 453–464.

BRUGUIER, N.J. & LIVERMORE, R.A. 2001. Enhanced magma supply at the southern East Scotia Ridge: evidence for mantle flow around the subducting slab? *Earth and Planetary Science Letters*, **191**, 129–144.

BUTTLES, J. & OLSON, P. 1998. A laboratory model of subduction zone anisotropy. *Earth and Planetary Science Letters*, **164**, 245–262.

CHASE, C.G. 1978. Plate kinematics: the Americas, East Africa, and the rest of the world. *Earth and Planetary Science Letters*, **37**, 355–368.

DEMETS, C., GORDON, R.G., ARGUS, D.F. & STEIN, S. 1990. Current plate motions. *Geophysical Journal International*, **101**, 425–478.

DEMETS, C., GORDON, R.G., ARGUS, D.F. & STEIN, S. 1994. Effect of recent revisions to the geomagnetic reversal time-scale on estimates of current plate motions. *Geophysical Research Letters*, **21**, 2191–2194.

DVORKIN, J., NUR, A., MAVKO, G. & BEN-AVRAHAM, Z. 1993. Narrow subducting slabs and the origin of backarc basalts. *Tectonophysics*, **227**, 63–79.

ENGDAHL, E.R., VAN DER HILST, R. & BULAND, R. 1998. Global teleseismic earthquake relocation with improved travel times and procedures for depth determination. *Bulletin of the Seismological Society of America*, **88**, 722–743.

FISCHER, K.M. & YANG, X.P. 1994. Anisotropy in Kuril–Kamchatka subduction zone structure. *Geophysical Research Letters*, **21**, 5–8.

FISCHER, K.M., FOUCH, M.J., WIENS, D.A. & BOETTCHER, M.S. 1998. Anisotropy and flow in Pacific subduction zone back-arcs. *Pure and Applied Geophysics*, **151**, 463–475.

FISCHER, K.M., PARMENTIER, E.M., STINE, A.R. & WOLF, E.R. 2000. Modeling anisotropy and plate-driven flow in the Tonga subduction zone back arc. *Journal of Geophysical Research*, **105**, 16 181–16 191.

FORSYTH, D.W. 1975. Fault plane solutions and tectonics of the South Atlantic and Scotia Sea. *Journal of Geophysical Research*, **80**, 1429–1443.

FOUCH, M.J. & FISCHER, K.M. 1996. Mantle anisotropy beneath northwest Pacific subduction zones. *Journal of Geophysical Research*, **101**, 15 987–16 002.

FOUCH, M.J. & FISCHER, K.M. 1998. Shear wave anisotropy in the Mariana subduction zone. *Geophysical Research Letters*, **25**, 1221–1224.

FRETZDORFF, S., LIVERMORE, R.A., DEVEY, C.W., LEAT, P.T. & STOFFERS, P. 2002. Petrogenesis of the back-arc East Scotia Ridge, South Atlantic Ocean. *Journal of Petrology*, **43**, 1435–1467.

FRETZDORFF, S., HAASE, K.M., LEAT, P.T., LIVERMORE, R.A., GARBE-SCHÖNBERG, C.-D., FIETZKE, J. & STOFFERS, P. 2003. ^{230}Th–^{238}U disequilibrium in East Scotia back-arc basalts: implications for slab contributions. *Geology*, in press.

GARFUNKEL, Z., ANDERSON, C.A. & SCHUBERT, G. 1986. Mantle circulation and the lateral migration of subducted slabs. *Journal of Geophysical Research*, **91**, 7205–7223.

GERMAN, C.R., LIVERMORE, R.A., BAKER, E.T., BRUGUIER, N.I., CONNELLY, D.P., CUNNINGHAM, A.P., MORRIS, P., ROUSE, I.P., STATHAM, P.J. & TYLER, P.A. 2000. Hydrothermal plumes above the East Scotia Ridge: an isolated high-latitude back-arc spreading centre. *Earth and Planetary Science Letters*, **184**, 241–250.

HALL, C.E., FISCHER, K.M., PARMENTIER, E.M. & BLACKMAN, D.K. 2000. The influence of plate motions on three-dimensional back arc mantle flow and shear wave splitting. *Journal of Geophysical Research*, **105**, 28 009–28 033.

HAMILTON, I.W. 1989. *Geophysical investigations of subduction-related processes in the Scotia Sea*. PhD Thesis, University of Birmingham, UK.

HELFFRICH, G., WIENS, D.A., VERA, E., BARRIENTOS, S., SHORE, P., ROBERTSON, S. & ADAROS, R. 2002. A teleseismic shear-wave splitting study to investigate mantle flow around South America and implications for plate-driving forces. *Geophysical Journal International*, **149**, F1–F7.

HERGT, J.M. & HAWKESWORTH, C.J. 1994. Pb-, Sr-, and Nd-isotopic evolution of the Lau Basin: Implications for mantle dynamics during backarc opening. *In*: HAWKINS, J.W., PARSON, L.M., ALLAN, J.F. *et al. Proceedings of the Ocean Drilling Program, Scientific Results*, **135**, 505–517.

HERRSTROM, E.A., REAGAN, M.K. & MORRIS, J.D. 1995. Variations in lava composition associated with flow of asthenosphere beneath southern Central America. *Geology*, **23**, 617–620.

HILL, I.A. & BARKER, P.F. 1980. Evidence for Miocene back-arc spreading in the central Scotia Sea. *Geophysical Journal of the Royal Astronomical Society*, **63**, 427–440.

KLEIN, E.M. & LANGMUIR, C.H. 1987. Global correlations of ocean ridge basalt chemistry with axial depth and crustal thickness. *Journal of Geophysical Research*, **92**, 8089–8115.

LARTER, R.D., VANNESTE, L.E., MORRIS, P. & SMYTHE, D.K. 2003. Structure and tectonic evolution of the South Sandwich arc. *In*: LARTER, R.D. & LEAT, P.T. (eds) *Intra-oceanic Subduction Systems: Tectonic and Magmatic Processes*. Geological Society, London, Special Publications, **219**, 255–284.

LEAT, P.T., LIVERMORE, R.A., MILLAR, I.L. & PEARCE, J.A. 2000. Magma supply in back-arc spreading centre segment E2, East Scotia Ridge. *Journal of Petrology*, **41**, 845–866.

LE ROEX, A.P., DICK, H.J.B., REID, A.M., FREY, F.A., ERLANK, A.J. & HART, S.R. 1985. Petrology and geochemistry of basalts from the American–Antarctic Ridge, Southern Ocean: implications for the westward influence of the Bouvet mantle plume. *Contributions to Mineralogy and Petrology*, **90**, 367–380.

LIVERMORE, R., CUNNINGHAM, A., VANNESTE, L. & LARTER, R. 1997. Subduction influence on magma supply at the East Scotia Ridge. *Earth and Planetary Science Letters*, **150**, 261–275.

LIVERMORE, R., MCADOO, D. & MARKS, K. 1994. Scotia sea tectonics from high-resolution satellite gravity. *Earth and Planetary Science Letters*, **123**, 255–268.

LIVERMORE, R.A. & WOOLLETT, R.W. 1993. Sea-floor spreading in the Weddell Sea and southwest Atlantic since the Late Cretaceous. *Earth and Planetary Science Letters*, **117**, 475–495.

MA, Y. & COCHRAN, J.R. 1996. Transitions in axial morphology along the Southeast Indian Ridge. *Journal of Geophysical Research*, **101**, 15 849–15 866.

MALDONADO, A., BALANYA, J.C., BARNOLAS, A., GALINDO-ZALDIVAR, J., HERNANDEZ, J., JABALOY, A., LIVERMORE, R., MARTINEZ-MARTINEZ, J.M., RODRIGUEZ-FERNANDEZ, J., DE GALDEANO, C.S., SOMOZA, L., SURINACH, E. & VISERAS, C. 2000. Tectonics of an extinct ridge–transform intersection, Drake Passage (Antarctica). *Marine Geophysical Researches*, **21**, 43–68.

MARTINEZ, F. & TAYLOR, B. 2002. Mantle wedge control on back-arc crustal accretion. *Nature*, **416**, 417–420.

MARTINEZ, F. & TAYLOR, B. 2003. Controls on back-arc crustal accretion: Insights from the Lau, Manus and Mariana basins. *In*: LARTER, R.D. & LEAT, P.T. (eds) *Intra-oceanic Subduction Systems: Tectonic and Magmatic Processes*. Geological Society, London, Special Publications, **219**, 19–54.

MCKENZIE D.P. 1969. Speculations on the consequences and causes of plate motions. *Geophysical Journal of the Royal Astronomical Society*, **18**, 1–32.

MILLEN, D.W. & HAMBURGER, M.W. 1998. Seismological evidence for tearing of the Pacific Plate at the northern termination of the Tonga subduction zone. *Geology*, **26**, 659–662.

MÜLLER, C. 2001. Upper mantle seismic anisotropy beneath Antarctica and the Scotia Sea region. *Geophysical Journal International*, **147**, 105–122.

PEARCE, J.A., ERNEWEIN, M., BLOOMER, S.H., PARSON, L.M., MURTON, B.J. & JOHNSON, L.E. 1995*a*. Geochemistry of Lau Basin volcanic rocks: influence of ridge segmentation and arc proximity. *In*: SMELLIE, J.L. (ed.) *Volcanism Associated with Extension at Consuming Plate Margins*. Geological Society, London, Special Publications, **81**, 53–75.

PEARCE, J.A., KEMPTON, P.D., NOWELL, G.M. & NOBLE, S.R. 1999. Hf-Nd element and isotope perspective on the nature and provenance of mantle and subduction components in Western Pacific arc-basin systems. *Journal of Petrology*, **40**, 1579–1611.

PEARCE, J.A., LEAT, P.T., BARKER, P.F. & MILLAR, I.L.

1995*b*. Geochemical evidence for mantle dynamics and mantle melting beneath the Scotia Sea and surrounding region. *Eos, Transactions, American Geophysical Union*, **76**(46), Fall Meeting Supplement, F542.

PEARCE, J.A., LEAT, P.T., BARKER, P.F. & MILLAR, I.L. 2001. Geochemical tracing of Pacific-to-Atlantic upper-mantle flow through the Drake passage. *Nature*, **410**, 457–461.

PEATE, D.W., KOKFELT, T.F., HAWKESWORTH, C.J., VAN CALSTEREN, P.W., HERGT, J.M. & PEARCE, J.A. 2001. U-series isotope data on Lau Basin glasses: the role of subduction-related fluids during melt generation in back-arc basins. *Journal of Petrology*, **42**, 1449–1470.

PEYTON, V., LEVIN, V., PARK, J., BRANDON, M., LEES, J., GORDEEV, E. & OZEROV, A. 2001. Mantle flow at a slab edge: Seismic anisotropy in the Kamchatka region. *Geophysical Research Letters*, **28**, 379–382.

RICHTER, F. & MCKENZIE, D.P. 1978. Simple plate models of mantle convection. *Journal of Geophysics*, **44**, 441–471.

ROBERTSON MAURICE, S.D., WIENS, D.A., KOPER, K.D. & VERA, E. 2003. Crustal and upper mantle structure of southernmost South America inferred from regional waveform inversion. *Journal of Geophysical Research*, **108**(B1), ESE15-1–ESE15-10, 2038, 10.1029/2002JB001828.

ROGNSTAD, M. 1992. HAWAII-MR1: a new underwater mapping tool. *In*: *International Conference on Signal Processing and Technology*. DSP Associates, Newton, MA, 900–905. World Wide Web address: http://www.soest.hawaii.edu/HMRG/MR1/index.html

RUSSO, R.M. & SILVER, P.G. 1994. Trench-parallel flow beneath the Nazca Plate from seismic anisotropy. *Science*, **263**, 1105–1111.

RUSSO, R.M. & SILVER, P.G. 1996. Cordillera formation, mantle dynamics, and the Wilson cycle. *Geology*, **24**, 511–514.

SAVAGE, M.K. 1999. Seismic anisotropy and mantle deformation: what have we learned from shear wave splitting? *Reviews of Geophysics*, **37**, 65–106.

SCHOUTEN, H., DICK, H.J.B. & KLITGORD, K.D. 1987. Migration of mid-ocean-ridge volcanic segments. *Nature*, **326**, 835–839.

SHAH, A.K. & SEMPERE, J.C. 1998. Morphology of the transition from an axial high to a rift valley at the Southeast Indian Ridge and the relation to variations in mantle temperature. *Journal of Geophysical Research*, **103**, 5203–5223.

SLEEP, N. & TOKSÖZ, M.N. 1971. Evolution of marginal basins. *Nature*, **233**, 548–550.

SMITH, G.P., WIENS, D.A., FISCHER, K.M., DORMAN, L.M., WEBB, S.C. & HILDEBRAND, J.A. 2001. A complex pattern of mantle flow in the Lau backarc. *Science*, **292**, 713–716.

SMITH, W.H.F. & SANDWELL, D.T. 1994. Bathymetric prediction from dense satellite altimetry and sparse shipboard bathymetry. *Journal of Geophysical Research*, **99**, 21 803–21 824.

THOMAS, C., LIVERMORE, R.A. & POLLITZ, F. 2003. Motion of the Scotia Sea plates. *Geophysical Journal International*, in press.

TURNER, S. & HAWKESWORTH, C. 1998. Using geochemistry to map mantle flow beneath the Lau Basin. *Geology*, **26**, 1019–1022.

VANNESTE, L.E. & LARTER, R.D. 2002. Sediment subduction, subduction erosion, and strain regime in the northern South Sandwich forearc. *Journal of Geophysical Research*, **107**(B7), EPM5-1–EPM5-24, 2149, 10.1029/2001JB000396.

VANNESTE, L.E., LARTER, R.D. & SMYTHE, D.K. 2002. Slice of intraoceanic arc: Insights from the first multichannel seismic reflection profile across the South Sandwich island arc. *Geology*, **30**, 819–822.

VUAN, A., RUSSI, M. & PANZA, G.F. 2000. Group velocity tomography in the subantarctic Scotia Sea region. *Pure and Applied Geophysics*, **157**, 1337–1357.

WINDER, R.O. & PEACOCK, S.M. 2001. Viscous forces acting on subducting lithosphere. *Journal of Geophysical Research*, **106**, 21 937–21 951.

YANG, X.P., FISCHER, K.M. & ABERS, G.A. 1995. Seismic anisotropy beneath the Shumagin Islands segment of the Aleutian-Alaska subduction zone. *Journal of Geophysical Research*, **100**, 18 165–18 177.

YOGODZINSKI, G.M., LEES, J.M., CHURIKOVA, T.G., DORENDORF, F., WÖERNER, G. & VOLYNETS, O.N. 2001. Geochemical evidence for the melting of subducting oceanic lithosphere at plate edges. *Nature*, **409**, 500–504.

This page intentionally left blank

Resolving mantle components in oceanic lavas from segment E2 of the East Scotia back-arc ridge, South Sandwich Islands

D. HARRISON[1,2], P.T. LEAT[3], P.G. BURNARD[1,4], G. TURNER[1], S. FRETZDORFF[5] & I.L. MILLAR[6]

[1]*Geochemistry and Cosmochemistry Group, Department of Earth Sciences, University of Manchester, Manchester M13 9PL, UK*

[2]*Current address: Isotopengeologie, ETH Zentrum, NO C 61.2, Sonneggstrasse 5, CH-8092, Zurich, Switzerland (e-mail: harrison@erdw.ethz.ch)*

[3]*British Antarctic Survey, Madingley Road, High Cross, Cambridge CB3 0ET, UK*

[4]*Current address: Department of Earth and Space Sciences, University of California, Los Angeles, CA 90095–1567, USA*

[5]*Institut für Geowissenschaften, Christian-Albrechts-Universität zu Kiel, Olshausenstrasse 40, 24118 Kiel, Germany*

[6]*British Antarctic Survey, c/o NERC Isotope Geoscience Laboratory, Kingsley Dunham Centre, Keyworth, Nottingham NG12 5GG, UK*

Abstract: The East Scotia Ridge, situated in the South Atlantic, is the back-arc spreading centre to the intra-oceanic South Sandwich arc. Samples from the ridge show a wide diversity in erupted magma compositions. Segment E2, in the northern part of the ridge, has an axial topographic high, which contrasts with the rift-like topography common to most of the ridge. Lava compositions in the segment have been modelled by mixing of magmas derived from normal mid-ocean ridge basalt (N-MORB)-like mantle, a mantle plume component similar in composition to that sampled by Bouvet Island and mantle modified by addition of components from the subducting slab. The 'Bouvet'-like plume signature has higher $^{87}Sr/^{86}Sr$, $^{206}Pb/^{204}Pb$, Nb/Yb, and lower $^{143}Nd/^{144}Nd$ and $^{4}He/^{3}He$, than the local upper mantle. It can be traced geochemically from the Bouvet Island hot spot to segment E2, via the South American–Antarctic Ridge, which connects the Bouvet triple junction to the South Sandwich subduction system.

Four samples dredged from segment E2 have $^{4}He/^{3}He$ ratios of 85 000–90 200 (8.5–8.0 R/R_A, where)R/R_A is the $^{4}He/^{3}He$ ratio normalized to air) and three wax core samples taken from the segment axis have values of 104 300, 101 560 and 176 620 (6.9, 7.1 and 4.1 R/R_A). These latter data are similar to values from the South American–Antarctic Ridge which have no discernable plume input. Whilst the dredge samples have a measurably lower $^{4}He/^{3}He$ ratio than the South American–Antarctic Ridge and samples from the segment axis, these He isotope data contrast with a dominant plume signature recorded by other petrogenetic tracers. This is interpreted to be due to re-melting of an entrained plume component, with an inherent low He concentration, incorporated into the E2 mantle. Helium depletion from the plume component can be seen to be a consequence of mantle processing and does not imply shallow-level degassing prior to entrainment within the upper-mantle-melting zone. As a consequence, He is characterized in the back-arc by values more similar to the upper mantle, whereas lithophile tracers are more influenced by the plume component.

Helium isotope studies of mantle-derived rocks have demonstrated that some ocean islands and seamount chains sample a more primitive region of the mantle than the majority of basalts that erupt at mid-ocean ridge spreading centres. The data currently available require the existence of isolated reservoirs, within sections of the mantle, that have different time-integrated parent/noble gas, daughter ratios (e.g. (U+Th)/He) and that have remained isolated for long periods. Mid-ocean ridge basalts (MORB) are thought to be sourced within the shallow upper mantle and have a gross global $^{4}He/^{3}He$ ratio of *c.* 90 000 (*c.* 8R/R_A, where R/R_A is the $^{3}He/^{4}He$ ratio normalized to air) (Allègre *et al.* 1983; Staudacher *et al.* 1989; Moreira *et al.* 1998). Ocean islands such as Hawaii and Iceland have ratios down to *c.* 21 000 (*c.* 34R/R_A) (Kaneoka *et al.* 1983; Kurz

From: LARTER, R.D. & LEAT, P.T. 2003. *Intra-Oceanic Subduction Systems: Tectonic and Magmatic Processes.* Geological Society, London, Special Publications, **219**, 333–344. 0305-8719/03/$15.00

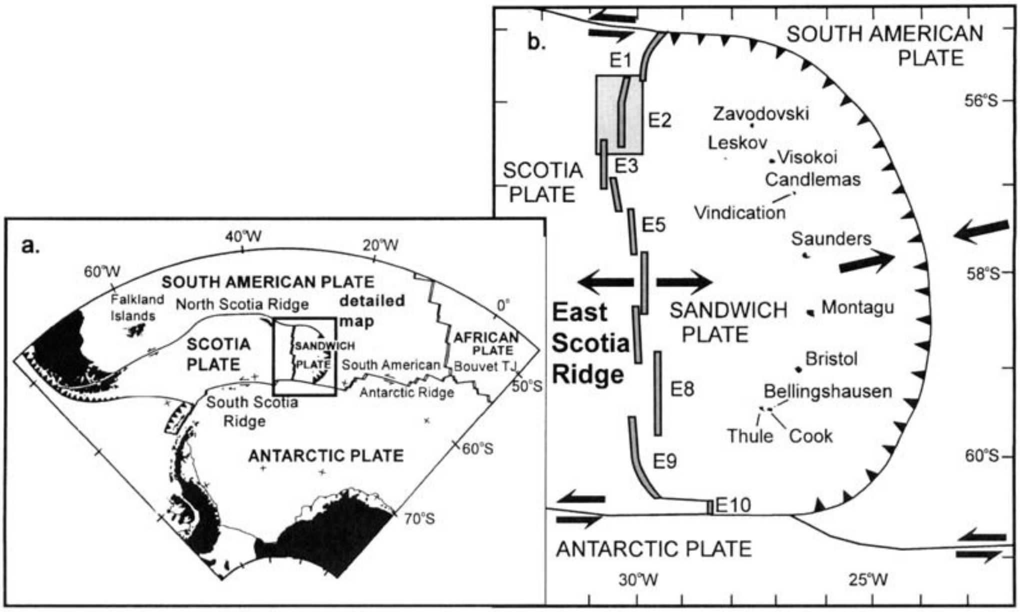

Fig. 1. (**a**) Tectonic setting of the East Scotia Ridge in the South Atlantic region. The oceanic Sandwich Plate is situated between the South American, Antarctic and Scotia plates. The North and South Scotia ridges are largely amagmatic transform fault boundaries. The South American–Antarctic Ridge spreading centre connects the southern boundary of the Sandwich Plate to the Bouvet Triple Junction. (**b**) Sketch map of the Sandwich Plate and the East Scotia Ridge. The ridge consists of 10 segments, from north to south, E1–E10. The South American Plate is subducting beneath the Sandwich Plate at the South Sandwich Trench. The South Sandwich Islands are the volcanic arc associated with this subduction. The dredge samples DR.157 and DR.158 are from segment E2.

et al. 1983; Rison & Craig 1983; Sarda *et al.* 1988; Hiyagon *et al.* 1992; Valbracht *et al.* 1997) and *c.* 19 500 (*c.* $37R/R_A$) (Hilton *et al.* 1999), respectively, and are thought to be the product of a plume (hot spot) derived from a more primitive region situated in the deeper mantle, be it the lower mantle or elsewhere.

The clear difference between the He isotope signatures of MORB and ocean island basalts (OIB) can therefore provide a powerful tool in constraining mantle sources for volcanic samples. Nevertheless, the spatial characteristics of plume He signatures, compared to those of lithophile tracers (i.e. Pb, Nd and Sr) are complex. The spatial extent (effective geographic limit of detection) of plume He relative to other plume tracers in 'hot spot-ridge' systems can be smaller or greater depending on the locality. A plume He signature (^{3}He excess) is present up to 1700 km south along the Mid-Atlantic Ridge from Iceland, whereas an Icelandic Pb signature appears to be present up to only around 1200 km (Taylor *et al.* 1997). By contrast, along the East Pacific Rise between 13 and 23°S the plume ^{3}He excess is more spatially restricted than lithophile tracers (Niedermann *et al.* 1997; Kurz *et al.* 1999). This complicates the use of He as a tracer for plume-derived contamination of the shallow mantle.

The data reported in this paper represent new major, trace and isotope analyses of dredge samples from segment E2 of the East Scotia Ridge along with supplementary He isotope data of three wax core samples from the summit axis region of the segment; analysed in order to clarify the He structure of the local upper mantle.

Geological background

There are three major tectonic plates enclosing the East Scotia Sea, the Antarctic, the South American and the Scotia plates (Fig. 1a); all are moving at a rate of <22 km Ma^{-1} relative to the global hot-spot reference frame (Barker 1995). The north and south edges of the Scotia Plate are defined by the North Scotia and South Scotia ridges, respectively, and are essentially amagmatic strike-slip faults. Within this framework of slow-moving plates, the small Sandwich Plate (Fig. 1b) is overriding the South American Plate at a rate of 70–85 km Ma^{-1} (Pelayo & Wiens 1989). The South American Plate is subducting beneath the Sandwich Plate at an angle of 45–55° to the west, and is being wrenched from the non-subducting portion of the South American Plate in a scissor-like motion (Brett 1977). The South American–Antarctic Ridge consists of long transform faults interspersed with short spreading segments (Barker & Lawver 1988) and connects, at its eastern end, with the Mid-Atlantic and Southwest Indian ridges at the Bouvet triple junction (Fig. 1a). There are two documented hot spots within the vicinity of the Bouvet triple junction, the Bouvet hot spot underlying Bouvet Island, situated near the Southwest Indian Ridge (le Roex *et al.* 1985; Kurz *et al.* 1998) and the Shona hot spot, a ridge-centred plume on the southern Mid-Atlantic Ridge (Douglass *et al.* 1995; Moreira *et al.* 1995). Geochemical analyses of dredge samples from the South American–Antarctic Ridge have been previously used to suggest that mantle from one of these hot spots (or both) is migrating westward towards the Sandwich Plate (le Roex *et al.* 1985).

The South Sandwich Islands are the subaerial volcanic portion of the intra-oceanic arc related to the subduction of the South American Plate beneath the Sandwich Plate. The islands consist of dominantly basalt and basaltic andesite volcanics, with minor andesites and dacites. Magnetic data indicate that the islands are built on oceanic crust that formed at the East Scotia Ridge up to 10 Ma ago (Barker & Hill 1981; Larter *et al.* 2003).

The East Scotia Ridge back-arc spreading centre consists of 10 segments: E1 (north)–E10 (south) (Fig. 1b). Segment E1 has a wide trough-like morphology that increases in depth from 4.2 km in the south to 5.5 km in the north. Segments E3–E8 are characterized by axial rifts with rift floors at *c.* 4 km depth and are considered to be typical of slow-spreading ocean ridges. Segments E2 and E9, however, have inflated axial highs rising to *c.* 2.5 km water depth, more characteristic of fast spreading ocean ridges. The spreading rate along the whole ridge is essentially constant at 65–70 km Ma^{-1}, therefore implying that excess magma production in segments E2 and E9 is the result of a relatively more fertile mantle component underlying these segments (Livermore *et al.* 1997).

Segment E2, discussed here, is approximately 70 km long and is expanding southward at the expense of E3 (Livermore *et al.* 1997). The segment decreases in depth from 3.5 km at the segment tips to 2.6 km at the axial high summit. A constructive volcanic edifice ('Mermaid's Purse') in the north-central part of the segment forms an area of positive topography at less than 3.1 km depth and stands 500 m high with a 2 km-wide summit graben. Geophysical surveys report that the floor of the axial graben is the site of the most recent eruptions and also that the 'Mermaid's Purse' edifice is underlain by a melt lens running 20 km N–S, *c.* 1 km wide and about 3 km deep below seafloor (Livermore *et al.* 1997).

There have been a number of geochemical studies on the East Scotia Ridge (Hawkesworth *et al.* 1977; Saunders & Tarney 1979; Cohen & O'Nions 1982; Pearce *et al.* 1995*b*, 2001; Eiler *et al.* 2000*a*; Fretzdorff *et al.* 2002). These studies conclude that the lavas of the East Scotia Ridge represent weak and variable contamination of the local ambient upper-mantle MORB source by fluids and/or sediments derived from the subducting slab (i.e. elevated large ion lithophile element (LILE) signatures). However it is also recognized that some lavas along the ridge were enriched in light rare earth elements (REE)/heavy REE relative to both MORB and the South Sandwich Islands (Hawkesworth *et al.* 1977; Saunders & Tarney 1979). Enrichments in ratios such as Nb/Yb up to 12 in segment E2, relative to 0.7 in normal MORB (N-MORB), which are unlikely to be affected by fluids from the slab, led to the suggestion that an enriched plume mantle component is present in the back-arc (Pearce *et al.* 1995*b*).

Samples described in this paper were collected in 1996 and 1999 from segment E2 by RRS *James Clark Ross*. Lavas along the axis of the segment were sampled at 30 localities using a rock chipping (wax coring) technique. Wax core samples WX.42, 43 and 44 were taken from 56° 06.03′S, 30° 19.51′W, 56° 09.40′S, 30° 18.51′W and 56° 02.01′S, 30° 19.51′W, respectively, and from depths between 2758 and 2885 m. The steep (>20°) lateral flanks of the summit were also sampled by two dredges: DR.157 and DR.158. Dredge DR.157 was on the east flank of the summit (56° 06.83′S, 30° 16.66′W) and dredge DR.158 was on the west flank (56° 06.93′S, 30° 21.01′W). Both dredges were within the depth range 2581–2960 m. The dredge hauls consisted mostly of vesicular mafic lava, many having pillowed and ropy surfaces.

Analytical techniques

For noble gas analysis, splits of fresh, unaltered glassy rinds from the samples were broken down to a size between 2 and 5 mm and ultrasonically cleaned with 20% HNO_3, de-ionized water and, finally, acetone. The dried samples were hand-picked under a binocular microscope and loaded into a screw-type crusher system (Stuart & Turner 1992). The crusher and neighbouring sections of the stainless steel extraction line were baked at ≤150°C under vacuum for 12 h.

Helium determinations were performed using a MAP 215 noble gas mass spectrometer at the University of Manchester, UK. Gases extracted by crushing were exposed to a SAES Zr–Al getter operating at 250°C to clean up and remove any active gases (i.e. N_2, O_2 and CO_2) released during sample crushing. After purification, the gases were condensed on to an activated charcoal finger held at liquid nitrogen temperature (–196°C). The non-condensable species, including He, Ne and H_2, were then exposed to another SAES Zr–Al getter, operating at room temperature to reduce any H_2 prior to introduction into the mass spectrometer. A second charcoal finger (held at –196°C), adjacent to the source inlet valve, was used to minimize and stabilize the background levels of any residual Ar, CO_2 and H_2O during the He analysis.

After He analysis, the condensable gases were released off the charcoal finger and, prior to expansion into the mass spectrometer for Ar analysis, were exposed to a room temperature SAES Zr–Al getter for secondary clean up.

^4He and $^{36,40}Ar$ isotopes were measured using a Faraday collector, whilst ^3He was measured using an electron multiplier in digital pulse-counting mode. A resolution of 650 on the electron multiplier at 5% of the peak height allows for the complete separation of the $^3He^+$ beam from any interference by the H_3–HD^+ doublet. Noble gas abundances were calculated by peak height comparison to a known pressure of calibration gas.

Analytical banks were determined prior to crushing steps: ^3He and ^4He blanks were undetectable (i.e. ^4He blank $<1 \times 10^{-9}$ ml at standard temperature and pressure (STP)). ^{40}Ar blanks were in the range 1.55×10^{-10}–1.22×10^{-9} ml STP.

Major element determinations of samples DR.157.1 and DR.157.2 were by standard X-ray diffraction analysis (XRF) procedures at Keele University, UK. The major element concentrations of samples DR.157.4, DR.157.7, DR.157.9a, DR.157.9b and DR.158.24b were analysed with a Cameca SX50 electron microprobe at Geomar Kiel, Germany. All trace element data were determined by inductively coupled plasma-mass spectroscopy (ICP-MS) Plasmaquad at Durham University (following the procedures of Pearce *et al.* 1995*a*). Sr, Nd and Pb isotopes were analysed on a Finnigan MAT 262 mass spectrometer at the NERC Isotope Geoscience Laboratories, Keyworth, UK using previously described methods (Leat *et al.* 2000).

Results and discussion

Compositional variations in the dredge samples

Samples from segment E2 are chemically varied. None has lower Nb/Yb ratios than N-MORB, implying that depleted subarc mantle is not present beneath the segment. Samples from the segment tips have compositions closest to N-MORB. Lavas overlying the imaged melt lens are the most evolved in the segment (SiO_2 >53.5 wt%), consistent with magma storage and fractionation having occurred in the melt lens. Many of the summit lavas have low $Na_{8.0}$ values relative to the rest of the segment, consistent with locally, higher degree partial melting of mantle below the summit. Because these low $Na_{8.0}$ samples have high Ba/Nb ratios, the high degree of partial melting is thought to have been caused by influx of Ba-bearing, slab-derived, aqueous fluids into their source (Leat *et al.* 2000). Dredge samples DR.157 and DR.158 contain compositions not observed in the samples from the segment axis, and have Pb isotope and incompatible trace element ratios comparable to those of mantle plume-derived mafic rocks from Bouvet Island, as we shall detail below. Wax core samples WX.42, WX.43 and WX.44 collected from the summit are relatively evolved (SiO_2 values between 52.7 and 53.4) and do not belong to the low $Na_{8.0}$ group, instead they have $Na_{8.0}$ values of 2.8–3.0 (Fretzdorff *et al.* 2002) similar to samples described previously (Leat *et al.* 2000).

New major, trace element and Sr, Nd and Pb isotopic data for seven samples from dredges DR.157 and DR.158 are presented in Table 1. Data for an additional five samples from the same two dredge sites have previously been reported (Leat *et al.* 2000). The 12 samples from two dredges are compositionally varied requiring three distinct mantle enrichment events (Figs 2–4):

- Ba-enriched and Nb-depleted samples (i.e. high Ba/Yb, Ba/Nb and Th/Nb ratios, and low Nb/Yb ratios), found only in DR.158, which are interpreted to record a dominant addition of a sediment component to the mantle source (Figs 2, 3).

Table 1. *Analyses of dredge and wax core samples from segment E2, East Scotia Ridge*

Sample	DR.157.1	DR.157.2	DR.157.4	DR.157.9a	DR.157.9b	DR.157.7	DR.158.24B
Major elements							
Method	xrf	xrf	probe	probe	probe	probe	probe
N			8	10	15	9	14
SiO_2	49.98	50.36	48.24	49.00	49.96	53.54	54.52
TiO_2	1.63	1.59	1.81	1.83	1.80	1.51	1.91
Al_2O_3	15.32	15.24	15.34	15.42	15.62	16.75	16.25
FeO	8.61	8.39	8.88	9.04	9.12	8.57	9.58
MgO	7.46	7.53	6.58	6.55	6.55	4.54	3.58
MnO	0.16	0.15	0.19	0.18	0.19	0.20	0.22
CaO	11.89	11.51	11.46	11.46	11.55	8.38	7.32
Na_2O	2.83	2.73	2.91	2.94	2.90	3.61	3.96
K_2O	0.68	0.65	0.75	0.71	0.74	0.80	0.73
P_2O_5	0.26	0.27	0.41	0.42	0.44	0.51	0.49
LOI	0.19	0.22	–	–	–	–	–
Total	99.01	98.64	96.60	97.55	98.88	98.41	98.56
Trace elements by ICP-MS							
Sc	35.1	34.7	34.6	35.0	33.5	27.3	24.3
V	267	267	304	305	296	289	345
Cr	259	260	308	311	321	24	5
Co	37.6	38.0	39.5	40.5	39.9	24.3	25.4
Ni	92	89	92	96	153	25	5
Cu	67	59	59	59	57	54	36
Zn	90	89	82	78	77	84	96
Ga	16.3	16.4	16.9	16.6	16.1	18.5	19.2
Rb	15.9	16.4	16.3	16.1	15.9	16.8	14.6
Sr	296	296	290	291	281	273	231
Y	24	24	24	24	23	37	39
Zr	125.0	124.6	125.2	125.4	122.0	126.0	148.2
Nb	24.73	24.74	24.96	25.12	24.38	9.42	12.10
Cs	0.16	0.17	0.17	0.16	0.17	0.27	0.26
Ba	196	194	193	189	191	216	176
La	16.15	16.27	15.98	15.69	15.83	10.75	11.44
Ce	34.74	34.62	33.71	33.09	33.40	26.28	27.44
Pr	4.33	4.36	4.39	4.30	4.31	3.82	3.95
Nd	18.07	18.23	17.99	17.56	17.60	17.96	18.16
Sm	4.14	4.17	4.37	4.34	4.36	5.33	5.38
Eu	1.38	1.39	1.43	1.40	1.41	1.69	1.73
Gd	4.43	4.44	4.45	4.42	4.36	6.06	6.19
Tb	0.68	0.69	0.71	0.69	0.71	1.00	1.05
Dy	4.21	4.17	4.17	4.15	4.18	6.15	6.47
Ho	0.83	0.84	0.84	0.84	0.83	1.29	1.37
Er	2.31	2.30	2.30	2.28	2.29	3.58	3.87
Tm	0.353	0.353	0.342	0.337	0.343	0.541	0.591
Yb	2.17	2.17	2.11	2.10	2.08	3.39	3.70
Lu	0.34	0.33	0.33	0.32	0.33	0.54	0.58
Hf	2.96	3.01	3.04	3.07	3.00	3.21	3.71
Ta	1.52	1.52	1.53	1.50	1.52	0.59	0.72
Pb	3.07	1.91	1.47	1.05	1.06	1.40	1.88
Th	1.87	1.86	1.80	1.78	1.77	1.28	1.33
U	0.55	0.54	0.53	0.51	0.52	0.34	0.37

Sample	DR.157.1	DR.157.4	DR.157.9a	DR.157.9b	WX.42	WX.43	WX.44
Radiogenic isotopes							
$^{87}Sr/^{86}Sr$	0.703444	0.703453	0.703454	0.703440	–	–	–
$^{143}Nd/^{144}Nd$	0.512975	0.512977	0.512999	0.512969	–	–	–
$^{206}Pb/^{204}Pb$	19.3156	19.1941	19.3208	19.3462	–	–	–
$^{207}Pb/^{204}Pb$	15.5868	15.5833	15.6212	15.6422	–	–	–
$^{208}Pb/^{204}Pb$	38.9295	38.8289	39.0284	39.1027	–	–	–
$^{4}He/^{3}He$	85 320	88 500	90 210	85 010	104 300	101 560	176 620
1 σ error	1950	1740	2120	1500	1640	1200	13770
$^{3}He/^{4}He$ (R/R_A)	8.4	8.1	8.0	8.5	6.9	7.1	4.1
^{4}He ml STP	1.95×10^{-8}	7.21×10^{-9}	2.71×10^{-9}	1.11×10^{-8}	1.18×10^{-7}	1.47×10^{-7}	7.07×10^{-10}
$^{40}Ar/^{36}Ar$	301.8	302.5	281.5	301.7	–	–	–
1 σ error	0.3	1.6	12.5	4.2	–	–	–
Weight* (g)	0.278	0.405	0.494	0.397	0.216	0.045	0.124

N = number of probed points averaged to reported value.
* Weight for noble gas analysis.

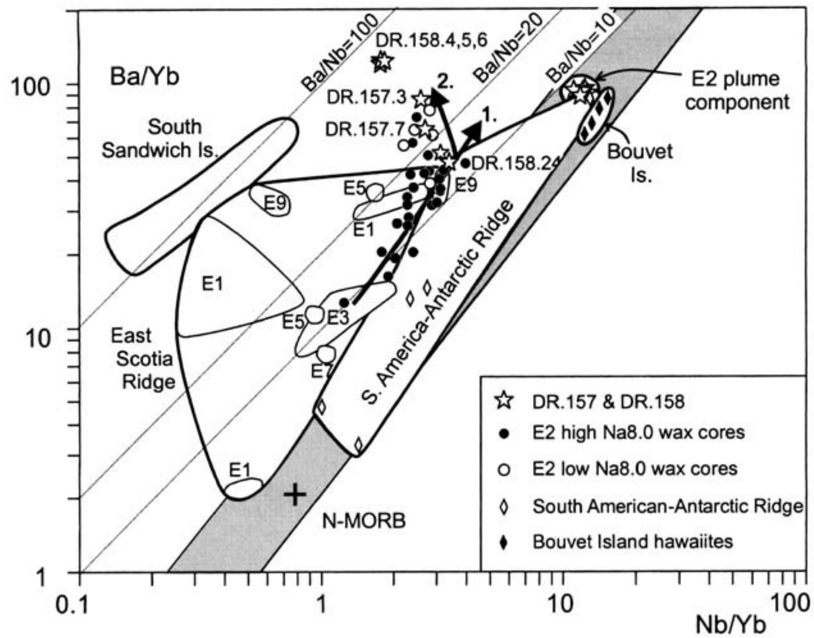

Fig. 2. Ba/Yb v. Nb/Yb. A comparison of DR.157 samples with others from Segment E2 and the East Scotia Ridge (Leat *et al.* 2000 and references therein) and placing data within a regional context. The shaded field defines the regional upper mantle where it is unaffected by the Sandwich subduction system and includes average N-MORB (Sun & Mcdonough 1989), dredge samples from the South American–Antarctic Ridge (le Roex *et al.* 1985) and Hawaiites from Bouvet Island (le Roex & Erlank 1982). The upper mantle beneath the South American–Antarctic Ridge appears to be variably contaminated by mantle from the Bouvet plume, which has flowed westward relative to the plume, the ridge system and the South Sandwich Islands. Trend 1 indicates increasing Nb/Yb and Ba/Yb in the E2 wax core samples resulting from addition of a mantle plume component to ambient MORB-source mantle. Trend 2 indicates addition of the subduction components.

- Samples that form a trend of strongly increasing Ba/Yb, Ba/Nb and Ba/Th ratios with slightly decreasing Nb/Yb ratios and slightly increasing Th/Nb ratios, found in both DR.157 and DR.158, which are interpreted to record addition of slab-derived aqueous fluid to the mantle source (Figs 2, 3). Note that the compositional trends in Figure 3 unambiguously differentiate slab-derived compositions dominated by addition of aqueous fluid to the mantle sources from those dominated by addition of sediment.
- Five samples are Ba enriched but not Nb depleted (i.e. with high Ba/Yb and Nb/Yb ratios, and low Ba/Nb, Ba/Th and Th/Nb ratios): these are found only in one dredge, DR.157. These samples have identical inter-incompatible trace element ratios to OIB from Bouvet Island. They have $^{206}Pb/^{204}Pb$ ratios that are higher than those of any other known rocks from the East Scotia Sea and South Sandwich Islands, but which are similar to Bouvet OIB (Fig. 4).

The five samples of this ‘plume-derived’ group are basalts (medium-K series), having >6.5 wt% MgO (Table 1), and are therefore moderately fractionated from mantle-derived melts. The samples have the highest La_N/Yb_N ratios (*c.* 5.0) and Nb/Yb ratios (11.4–12.0) in segment E2. The five samples are similar to one another in most elemental abundances, notably the incompatible elements (Table 1). However, there are differences among the five samples that are significantly greater than analytical errors, for some trace elements, including Cr, Ni and Pb, and for $^{143}Nd/^{144}Nd$, $^{206}Pb/^{204}Pb$, $^{207}Pb/^{206}Pb$ and $^{208}Pb/^{204}Pb$. Variations in $^{87}Sr/^{86}Sr$ are slightly greater than analytical errors. The samples are therefore interpreted to represent either a group of chemically similar lava flows, or fragments from one chemically heterogeneous flow. The five samples have significantly different Sr, Nd and Pb isotope compositions from the rest of the samples from segment E2, which rules out derivation of the magma type by dynamic melting processes from

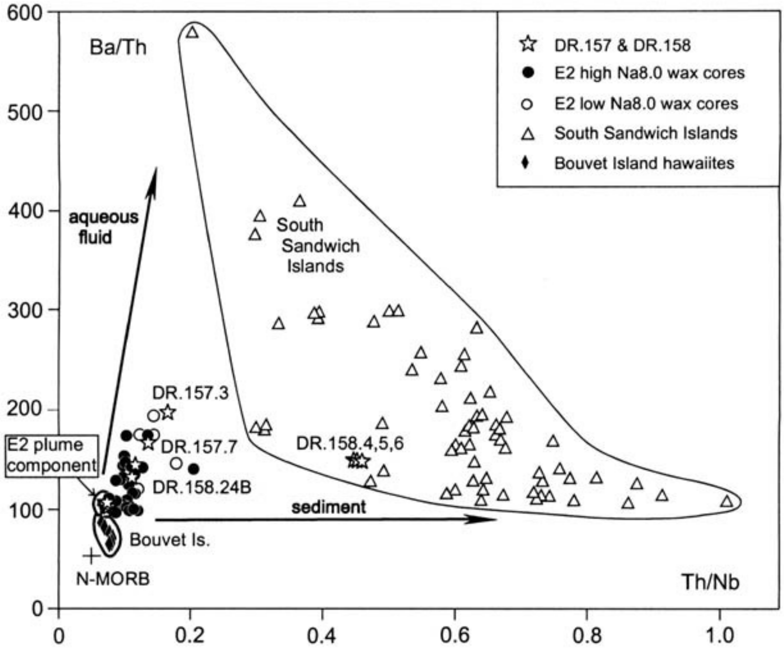

Fig. 3. Ba/Th v. Th/Nb. Data sources as in Fig. 2. Trends highlighted are enrichments caused by fluid addition and sediment addition from the subducting slab.

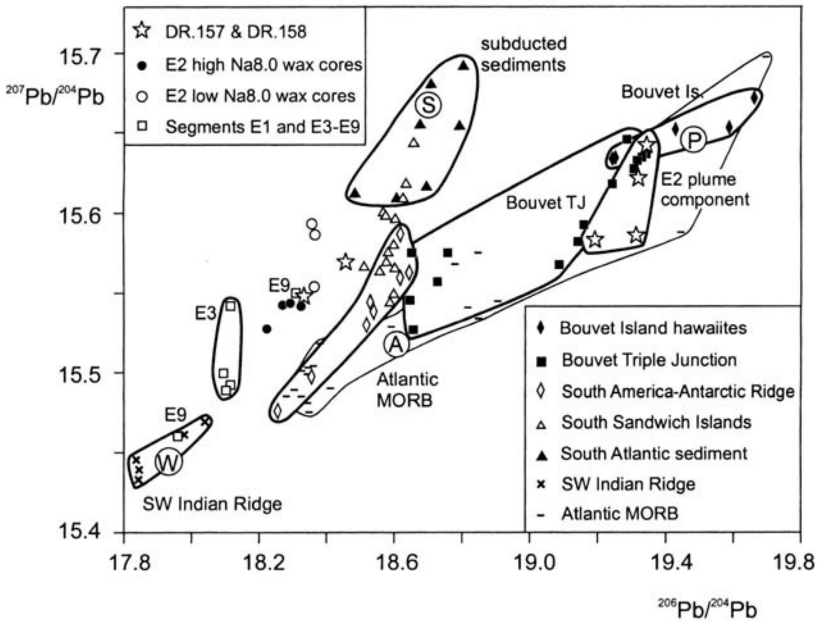

Fig. 4. $^{207}Pb/^{204}Pb$ v. $^{206}Pb/^{204}Pb$. Data sources as in Fig. 2, and Bouvet Island (Sun 1980; Kurz *et al.* 1998), Bouvet Triple Junction (Kurz *et al.* 1998), Atlantic MORB (Ito *et al.* 1987), Southwest Indian Ridge and Central Indian Ridge (Mahoney *et al.* 1989), South Atlantic sediments subducting at the sandwich Trench (Barreiro 1983) and East Scotia Ridge (Cohen & O'Nions 1982). W, A, S and P are the approximate positions of putative end-members mantle wedge, subducted sediment, altered basaltic subducting slab and mantle plume, respectively (Pearce *et al.* 1995*a*; Leat *et al.* 2000).

the same mantle sources that dominate the rest of the segment.

We recognize that enriched MORB-like (E-MORB) chemical heterogeneities similar to those present in segment E2 are also present along other mid-ocean ridges that appear not to be dynamically related to any nearby hot spot (Graham *et al.* 1996). Such anomalies may take the form of a passive heterogeneity that resembles those caused by the interaction of ridges with hot spots. The most important premise behind recognizing such heterogeneities is that their source be geochemically dissimilar to nearby plumes (Michael *et al.* 1994). By way of contrast, the DR.157 samples from segment E2 are similar geochemically to the Bouvet mantle plume (Figs 2–4). The length scale of any proposed (transient?) mantle flow connection from Bouvet to the East Scotia Ridge via the South American–Antarctic Ridge also appears to be high (approximately 1500 km) when compared to scaling models of plume–ridge interactions (Schilling *et al.* 1985; Kincaid *et al.* 1996). However, we feel that the geochemical (le Roex *et al.* 1985; Leat *et al.* 2000) and geophysical evidence (Livermore *et al.* 1997) support such a hypothesis. Our preferred interpretation is, therefore, that the DR.157 group of samples are melts sampling a plume component (entrained blob) that has migrated into the back-arc basin around the north edge of the South Sandwich subducting slab. The most likely source of this plume material, based on geochemical and geophysical evidence (Livermore *et al.* 1997), is the Bouvet hot spot (Fig. 1).

Resolving mantle plume components using the helium isotope system

The measured $^4He/^3He$ ratios for samples DR.157.1, DR.157.4, DR.157.9a and DR.157.9b, (Table 1) are in the range 85 000–90 200 (8.5–8.0R/R_A). These data are indistinguishable from the oft-quoted global MORB value, 90 000 ± 11 250 (Allègre *et al.* 1983; Staudacher *et al.* 1989; Moreira *et al.* 1998), and similar to other back-arc basin basalts that have no discernible plume or slab-derived input, i.e. the Lau Basin (Honda *et al.* 1993). Argon isotope ratios are all atmospheric-like: compared to oceanic samples erupted at greater depths, the preferential atmospheric contamination of the heavy noble gases is likely to have occurred during residence within shallow magma reservoirs and relatively shallow-level eruption (Burnard 1999; Harrison *et al.* 2003).

At face value, these He data are consistent with an origin within MORB-source mantle. However, they contrast with other petrogenetic tracers discussed above that indicate a plume component is present in these samples (Figs 2–4). The premise that the MORB-source region (upper mantle) is completely homogenous and has a constant He isotope structure is an oversimplification. In fact, there is a bias within the reported noble gas record for the shallow mantle towards Atlantic sample collections, and several recent publications have highlighted significant small-scale chemical differences from within different ocean basins (Graham *et al.* 1999, 2001; Kurz *et al.* 1999). For example, variations in He isotope ratios, which have localized correlations with Sr, Nd and Pb isotopes (across individual ridge segments), are found in MORB samples from the following ocean basins: Mid-Atlantic Ridge near 26°S (n = 13) (Graham *et al.* 1996); and southern East Pacific Rise (n = 16) (Kurz *et al.* 1998). Small variations, outside of analytical error, appear within the He data reported here. These also correlate with those described for Sr, Nd and Pb isotopes (Table 1). Heterogeneity in the isotopic structure along spreading centres and between basins can be attributed to recycling of crustal material into the local shallow mantle (Eiler *et al.* 2000*b*). It is also possible that fine-scale He isotope heterogeneities within the shallow mantle source are related to recycling of high (U+Th)/He material (sedimentary material?) into the mantle melting zone. Preferential He extraction (fractionated from U+Th) during decompression melting and degassing processes will enhance the (U+Th)/He ratio of any melt residue and may, therefore, lead to variably high, time-integrated $^4He/^3He$ values in the source reservoir. The assumption that the $^4He/^3He$ value for the MORB source is 90 000 is, therefore, overly simplistic for modelling geochemical processes within individual tectonic settings and a more precise value for each setting is required.

It has also been noted that higher (more radiogenic) $^4He/^3He$ values than the global average value are found within samples from the South American–Antarctic Ridge; a $^4He/^3He$ value *c.* 97 200 has been estimated to best represent the upper mantle source in this area (Kurz *et al.* 1998). These data are geographically the nearest available to E2 for 'normal' MORB but such values appear to be common for slow spreading ridges. The wax core samples, taken from the summit axis of E2, were analysed in order to clarify the He isotope structure of the local upper mantle; these data are similar to the South American–Antarctic Ridge values (Table 1). The observed variation in He isotopes between the dredge and wax core samples cannot be explained due to shallow-level degassing and

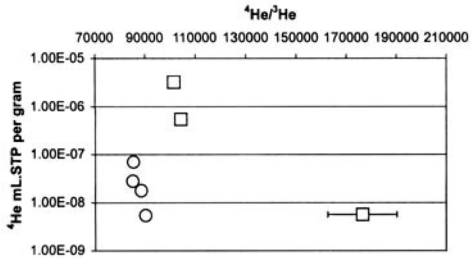

Fig. 5. ^4He ml STP per g v. $^4He/^3He$. Dredge samples circles, wax core samples squares. No correlation between isotope ratio and concentration exists between the sample groups. If the wax core samples were evolved from the dredge samples then a correlation between concentration and isotope ratio would be observed.

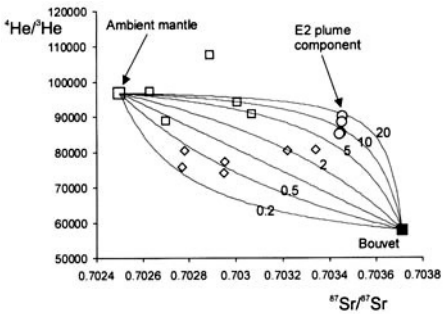

Fig. 6. $^4He/^3He$ v. $^{87}Sr/^{86}Sr$. A comparison of data from Bouvet Island, plume-influenced South American–Antarctic Ridge at approximately 6°W (diamonds) and ambient mantle at *c.* 16°W (squares) (Kurz *et al.* 1998) with E2 plume component (circles). Mixing lines are defined by $(He/Sr)_{MORB}/(He/Sr)_{PLUME}$. The E2 data can be explained by mixing between ambient upper mantle and a He-depleted plume source, isotopically similar to the Bouvet hot spot.

subsequent ingrowth of radiogenic ^4He, as detailed below.

Figure 5 is a plot of He isotope ratios against He concentration. If the variations were related to degassing and subsequent ingrowth of radiogenic ^4He, then a correlation of increasing $^4He/^3He$ with decreasing concentration would be evident. Whilst such a correlation can be seen within the wax core samples, there is no correlation between the two sample groups; indicating that the dredge and wax core samples are not related to each other by such a dynamic process. In fact DR.157.9a and WX.44 have almost identical He concentrations, but WX.44 has the highest $^4He/^3He$ value of all the samples, 176 620 (4.1 R/R_A), indicating extensive shallow-level magmatic volatile degassing (during magma storage) prior to eruption coupled with radiogenic ingrowth of ^4He. These two sample groups appear, therefore, not to be related to each other. The wax core samples have similar He isotope values to those found on the South American–Antarctic Ridge, whereas the dredge samples have lower $^4He/^3He$ values. This variation therefore requires further explanation.

He–Sr systematics of the DR157 samples and He depletion from the plume mantle

The He–Sr compositions reported here can be explained by mixing between a Bouvet-like plume source and local shallow mantle (as measured in the South American–Antarctic Ridge and clarified by the wax core analyses; Fig. 6 and Table 1). The curvature of the mixing lines passing through these data (r *c.* 8–20, where $r = [He/Sr]_{MORB}/[He/Sr]_{PLUME}$) requires that He was variably depleted from the plume component in the E2 segment prior to incorporation into the E2 mantle. Modelling the same data with the MORB end-member $^4He/^3He$ value of 90 000 (Atlantic MORB average) does not alter the above hypothesis (that He has been preferentially extracted from the 'plume' component in the E2 segment), but merely increases the curvature of the mixing lines passing through the E2 data and therefore infers a greater degree of He loss from the plume component. Assuming a MORB end-member similar to that estimated for the South American–Antarctic Ridge, we estimate the proportion of the plume component required to generate these data to be approximately 80%. A binary mixing system, 80% Bouvet plume and 20% South American–Antarctic Ridge MORB material, would give a $^4He/^3He$ value of approximately 63 000. This, again, highlights that He was removed from the plume component prior to mixing with the E2 mantle.

As already discussed, the preferential extraction of He from the shallow mantle during MORB genesis may lead to small-scale variations in (U+Th)/He and, therefore, $^4He/^3He$. Similarly, the above hypothesis infers preferential extraction/depletion of He, fractionation from the lithophile elements *within* deep plume mantle.

Experimental and theoretical studies show that He probably behaves as a highly incompatible element under normal mantle conditions (Kaneoka *et al.* 1983; Marty & Lussiez 1993; Carroll & Draper 1994). The bulk partition coefficient of He (KD_{He}) is unlikely to be greater or smaller than one order of magnitude from that of Sr (*c.* 0.01) (Marty & Lussiez 1993). It is therefore very difficult to envisage decoupling of He from Sr during equilibrium partial melting unless the degree of melting was very small (perhaps <1%) and the actual KD_{He} was, in fact, smaller than the KD_{Sr}. The required difference in the bulk partition coefficients of He and Sr can be estimated by the modelled mixing curves in Figure 6: KD_{He} would have to be in the order of >20 times lower than the KD_{Sr} for He and Sr to efficiently separate during equilibrium melting. This is similar to reported data from the Galapagos Archipelago (Kurz & Geist 1999), certain ridge segments on the East Pacific Rise (Poreda *et al.* 1993; Niedermann *et al.* 1997) and along parts of the Southeast Indian Ridge (Graham *et al.* 1999).

As seems likely, He extraction/fractionation from Sr is occurring at depths greater than the decompression–melting zone. A spatial and/or temporal separation of He from Sr (and therefore Nd and Pb) may occur when a volatile-rich (CO_2) melt phase (into which noble gases will preferential partition) separates from the plume mantle during incipient thermal melting (Kurz *et al.* 1999). He–Sr fractionation under this regime could be further enhanced due to the higher diffusivity of He compared to Sr (Kurz *et al.* 1987). Accumulation and channelling of small melt aggregates (with high plume-sourced He/Sr) into the local asthenosphere would deplete the plume mantle residue leading to low He/Sr (as seen in the E2 samples). Conversely, subsequent partial melting of any shallow mantle containing channelled melt aggregates from a plume source (i.e. with enhanced He/Sr) and ambient local MORB mantle would be expected to generate mixing lines in He–Sr isotope space with *r* values <1 (as opposed to *r* values >1 for the E2 data). Analyses from the South American–Antarctic Ridge at approximately 6°W (Kurz *et al.* 1998) have *r* values as low as 0.2, supporting this hypothesis (Fig. 6).

Nevertheless, irrespective of the exact mechanism required to separate He from the lithophile elements, the DR.157 data require that He depletion occurred within the plume mantle (assumed to be the Bouvet plume). Subsequently, a sample of 'He-depleted' residual plume component was detached and channelled into the South American–Antarctic Ridge and then on to the Scotia Plate.

Interestingly, He depletion from mantle plumes and channelling of this material into the athenosphere is consistent with mantle models that describe mass transfer between the deeper and shallow mantle reservoirs; i.e. 'steady-state' degassing models (Allègre *et al.* 1983; Kellogg & Wasserburg 1990; Porcelli & Wasserburg 1995; O'Nions & Tolstikhin 1996; Harrison *et al.* 1999). Such models envisage that noble gases in the upper-mantle source region of MORB arise from three sources: a radiogenic/nucleogenic component arising from *in situ* radiogenic decay of U, Th and K, and accumulated within the upper mantle over a residence time of approximately 1.4 Ga; a subducted atmospheric component, possibly restricted to the heavy noble gases; and a primitive component, introduced by bulk transfer from the deeper mantle via plumes. These data, tentatively, support mantle models that require transfer/replenishment of primitive noble gases (i.e. plume-like He) into the MORB source region via deeper mantle plumes.

Summary

Migration of plume-derived mantle from the Bouvet hot spot is proposed in support of previous hypotheses, on the basis of trace elements and radiogenic isotope systematics, to account for the enriched nature of some E2 lavas (le Roex *et al.* 1985; Leat *et al.* 2000). The E2 plume component, based on tectonic constraints (Livermore *et al.* 1997), is believed to have flowed along the South American–Antarctic Ridge, then around the northern edge of the South Sandwich subduction system. Similarly, flow of plume mantle into a back-arc around a lateral slab edge is also believed to be occurring at the north end of the Lau Basin (Turner & Hawkesworth 1998). Helium isotope values for these enriched lavas within the E2 segment are similar to the average Atlantic MORB value of *c.* 90 000 but lower than local ambient mantle values. The apparent disparity between helium and the other mantle source tracers within these enriched E2 segment samples can be explained by mixing of a MORB component with a He-depleted plume component. Depletion of noble gases from plume mantle is an inherent property of mantle models that describe mass transfer of volatiles from the deeper mantle into the MORB source region.

D. Harrison would like to thank D. Blagburn and B. Clementson in the Manchester Noble Gas Laboratory for technical support. Also thanks to the people at the British Antarctic Survey for support and supply of samples. D. Harrison was funded by NERC grant GR3/11637.

References

ALLÈGRE, C.J., STAUDACHER, T., SARDA, P. & KURZ, M.D. 1983. Constraints on evolution of Earth's mantle from rare gas systematics. *Nature*, **303**, 762–766.

BARKER, P.F. 1995. Tectonic framework of the East Scotia Sea. *In*: TAYLOR, B. (ed.) *Backarc Basins: Tectonics and Magmatism.* Plenum Press, New York, 281–314.

BARKER, P.F. & HILL, I.A. 1981. Back-arc extension in the Scotia Sea. *Philosophical Transactions of the Royal Society of London, Series A*, **300**, 249–262.

BARKER, P.F. & LAWVER, L.A. 1988. South American–Antarctic plate motion over the past 50 Ma, and the evolution of the South American–Antarctic Ridge. *Geophysical Journal of the Royal Astronomical Society*, **94**, 377–386.

BARRIERO, B. 1983. Lead isotopic compositions of South Sandwich Island volcanic rocks and their bearing on magmagenesis in intra-oceanic island arcs. *Geochimica et Cosmochimica Acta*, **47**, 817–822.

BRETT, C.P. 1977. Seismicity of the South Sandwich Islands region. *Geophysical Journal of the Royal Astronomical Society*, **51**, 453–464.

BURNARD, P.G. 1999. Comment on 'Argon–Lead Isotopic Correlation in Mid-Ocean Ridge Basalts' by Sarda, Moreira & Staudacher. *Science*, **286**, 871a.

CARROLL, M.R. & DRAPER, D.S. 1994. Noble gases as trace elements in magmatic processes. *Chemical Geology*, **117**, 37–59.

COHEN, R.S. & O'NIONS, R.K. 1982. Identification of recycled continental material in the mantle from Sr, Nd and Pb isotope investigations. *Earth and Planetary Science Letters*, **61**, 73–84.

DOUGLASS, J., SCHILLING, J.G., KINGSLEY, R.H. & SMALL, C. 1995. Influence of the Discovery and Shona mantle plumes on the Mid-Atlantic Ridge: rare earth evidence. *Geophysical Research Letters*, **22**, 2893–2896.

EILER, J.M., CRAWFORD, A., ELLIOTT, T., FARLEY, K.A., VALLEY, J.W. & STOLPER, E.M. 2000*a*. Oxygen isotope geochemistry of oceanic-arc lavas. *Journal of Petrology*, **41**, 229–256.

EILER, J.M., SCHIANO, P., KITCHEN, N. & STOLPER, E.M. 2000*b*. Oxygen-isotope evidence for recycled crust in the sources of mid-ocean ridge basalts. *Nature*, **403**, 530–534.

FRETZDORFF, S., LIVERMORE, R.A., DEVEY, C.W., LEAT, P.T. & STOFFERS, P. 2002. Petrogenesis of the back-arc East Scotia Ridge, South Atlantic Ocean. *Journal of Petrology*, **43**, 1435–1467.

GRAHAM, D.W., CASTILLO, P.R., LUPTON, J.E. & BATIZA, R. 1996. Correlated He and Sr isotope ratios in the South Atlantic near-ridge seamounts and implications for mantle dynamics. *Earth and Planetary Science Letters*, **144**, 491–503.

GRAHAM, D.W., JOHNSON, K.T.M., DOUGLAS, L.M. & LUPTON, J.E. 1999. Hotspot–ridge interaction along the Southeast Indian Ridge near Amsterdam and St Paul islands: helium isotope evidence. *Earth and Planetary Science Letters*, **167**, 297–310.

GRAHAM, D.W., LUPTON, J.E., SPERA, F.J. & CHRISTIE, D.M. 2001. Upper-mantle dynamics revealed by helium isotope variations along the Southeast Indian Ridge. *Nature*, **409**, 701–703.

HARRISON, D., BURNARD, P.G. & TURNER, G. 1999. Noble gas behaviour and composition in the mantle: constraints from the Iceland Plume. *Earth and Planetary Science Letters*, **171**, 199–207.

HARRISON, D., BURNARD, P.G., TRIELOFF, M. & TURNER, G. 2003. Resolving atmospheric contaminants in mantle noble gas analyses. *Geophysics, Geochemistry, Geosystems*, 4(3) 2002GC000325.

HAWKESWORTH, C.J., O'NIONS, R.K., PANKHURST, R.J., HAMILTON, P.J. & EVENSON, N.M. 1977. A geochemical study of island arc and back-arc tholeiites from the Scotia Sea. *Earth and Planetary Science Letters*, **36**, 253–262.

HILTON, D.R., GRONVOLD, K., MACPHERSON, C.G. & CASTILLO, P.R. 1999. Helium isotope investigations of source mixing in the Icelandic mantle. *In*: *Ninth Annual V.M. Goldschmidt Conference*, LPI Contribution, **971**, 125.

HIYAGON, H., OZIMA, M., MARTY, B., ZASHU, S. & SAKAI, H. 1992. Noble gases in submarine glasses from mid-oceanic ridges and Loihi Seamount; constraints on early history of the Earth. *Geochimica et Cosmochimica Acta*, **56**, 1301–1316.

HONDA, M., PATTERSON, D.B., MCDOUGALL, I. & FALLOON, T. 1993. Noble gases in submarine pillow basalt glasses from the Lau Basin: detection of a solar component in back-arc basin basalts. *Earth and Planetary Science Letters*, **120**, 135–148.

ITO, E., WHITE, W. & GÖPEL, C. 1987. The O, Sr, Nd and Pb isotope geochemistry of MORB. *Chemical Geology*, **62**, 157–176.

KANEOKA, I., TAKAOKA, N. & CLAGUE, D.A. 1983. Noble gas systematics for co-existing glass and olivine crystals in basalts and dunite xenoliths from Loihi Seamount. *Earth and Planetary Science Letters*, **66**, 427–437.

KELLOGG, L.H. & WASSERBURG, G.J. 1990. The role of plumes in mantle He fluxes. *Earth and Planetary Science Letters*, **99**, 276–789.

KINCAID, C., SCHILLING, J.G. & GABLE, C. 1996. The dynamics of off-axis plume–ridge interaction in the uppermost mantle. *Earth and Planetary Science Letters*, **137**, 29–43.

KURZ, M.D. & GEIST, D. 1999. Dynamics of the Galapagos hotspot from helium isotope geochemistry. *Geochimica et Cosmochimica Acta*, **63**, 4139–4156.

KURZ, M.D., GARCIA, M.O., FREY, F.A. & O'BRIEN, P.A. 1987. Temporal helium isotopic variations within Hawaiian volcanoes: basalts from Mauna Loa and Haleakala. *Geochimica et Cosmochimica Acta*, **51**, 2905–2914.

KURZ, M.D., JENKINS, W.J., HART, S.R. & CLAGUE, D. 1983. Helium isotopic variations in volcanic rocks from Loihi Seamount and the island of Hawaii. *Earth and Planetary Science Letters*, **66**, 388–399.

KURZ, M.D., LE ROEX, A.P. & DICK, H.J.B. 1998. Isotope geochemistry of the oceanic mantle near the Bouvet triple junction. *Geochimica et Cosmochimica Acta*, **62**, 841–852.

KURZ, M.D., MOREIRA, M., CURTICE, J., MAHONEY, J. & SINTON, J. 1999. The Neon isotope anomaly in the mantle beneath the superfast spreading East Pacific Rise. *Eos, Transactions, American Geophysical Union, 1999 Fall Meeting*, V11E-09.

LARTER, R.D., VANNESTE, L.E., MORRIS, P. & SMYTHE, D.K. 2003. Tectonic evolution and structure of the South Sandwich arc. *In*: LARTER, R.D.

& LEAT, P.T. (eds) *Intra-oceanic Subduction Systems: Tectonic and Magmatic Processes*. Geological Society, London, Special Publications, **219**, 255–284.

LEAT, P.T., LIVERMORE, R.A., MILLAR, I.L. & PEARCE, J.A. 2000. Magma supply in back-arc spreading segment E2, East Scotia Ridge. *Journal of Petrology*, **41**, 845–866.

LE ROEX, A.P. & ERLANK, A.J. 1982. Quantitative evaluation of fractional crystallisation in Bouvet Island lavas. *Journal of Volcanology and Geothermal Research*, **13**, 309–338.

LE ROEX, A.P., DICK, H.J.B., REID, A.M., FREY, F.A., ERLANK, A.J. & HART, S.R. 1985. Petrology and geochemistry of basalts from the American–Antarctic Ridge, Southern Ocean: implications for the westward influence of the Bouvet mantle plume. *Contributions to Mineralogy and Petrology*, **90**, 367–380.

LIVERMORE, R., CUNNINGHAM, A., VANNESTE, L. & LARTER, R. 1997. Subduction influence on magma supply at the East Scotia Ridge. *Earth and Planetary Science Letters*, **150**, 261–275.

MAHONEY, J.J., NATLAND, J.H., WHITE, W.M., POREDA, R., BLOOMER, S.H., FISHER, R.L. & BAXTER, A.N. 1989. Isotopic and geochemical provinces of the western Indian Ocean spreading centres. *Geophysical Research Letters*, **94**, 4033–4052.

MARTY, B. & LUSSIEZ, P. 1993. Constraints on rare gas partition coefficients from analysis of olivine-glass from a picritic mid-ocean ridge basalt. *Chemical Geology*, **106**, 1–7.

MICHAEL, P.J., FORSYTH, D.W., BLACKMAN, D.K., FOX, P.J., HANAN, B.B., HARDING, A.J., MACDONALD, K.C., NEUMANN, G.A., ORCUTT, J.A., TOLSTOY, M. & WEILAND, C.M. 1994. Mantle control of a dynamically evolving spreading center: Mid-Atlantic Ridge 31–34°S. *Earth and Planetary Science Letters*, **121**, 451–468.

MOREIRA, M., KUNZ, J. & ALLÈGRE, C. 1998. Rare gas systematics in Popping Rock: isotopic and elemental compositions in the upper mantle. *Science*, **279**, 1178–1181.

MOREIRA, M., STAUDACHER, T., SARDA, P., SCHILLING, J.G. & ALLÈGRE, C.J. 1995. A primitive plume neon component in MORB: the Shona Ridge anomaly, South Atlantic (51–52°S). *Earth and Planetary Science Letters*, **133**, 367–377.

NIEDERMANN, S., BACH, W. & ERZINGER, J. 1997. Noble gas evidence for a lower mantle component in MORBs from the southern East Pacific Rise: decoupling of helium and neon isotope systematics. *Geochimica et Cosmochimica Acta*, **61**, 2697–2715.

O'NIONS, R.K. & TOLSTIKHIN, I.N. 1996. Limits on the mass flux between lower and upper mantle and stability of layering. *Earth and Planetary Science Letters*, **139**, 213–222.

PEARCE, J.A., BAKER, P.E., HARVEY, P.K. & LUFF, I.W. 1995*a*. Geochemical evidence for subduction fluxes, mantle melting and fractional crystallization beneath the South Sandwich Island Arc. *Journal of Petrology*, **36**, 1073–1109.

PEARCE, J.A., LEAT, P.T., BARKER, P.F. & MILLAR, I.L. 1995*b*. Geochemical evidence for mantle dynamics and mantle melting beneath the Scotia Sea and surrounding region. *Eos, Transactions, American Geophysical Union*, **76**(46), Fall Meeting Supplement, F542.

PEARCE, J.A., LEAT, P.T., BARKER, P.F. & MILLAR, I.L. 2001. Geochemical tracing of Pacific-to-Atlantic upper mantle flow through the Drake passage. *Nature*, **410**, 457–461.

PELAYO, A.R. & WIENS, D.A. 1989. Seismotectonics and relative plate motions in the Scotia Sea region. *Journal of Geophysical Research*, **94**, 7293–7320.

PORCELLI, D. & WASSERBURG, G.J. 1995. Mass transfer of helium, neon, argon and xenon through a steady-state upper mantle. *Geochimica et Cosmochimica Acta*, **59**, 4921–4937.

POREDA, R.J., SCHILLING, J.G. & CRAIG, H. 1993. Helium isotopes in Easter microplate basalts. *Earth and Planetary Science Letters*, **119**, 319–329.

RISON, W. & CRAIG, H. 1983. Helium isotopes and mantle volatiles in Loihi seamount and Hawaiian basalts and xenoliths. *Earth and Planetary Science Letters*, **66**, 407–426.

SARDA, P., STAUDACHER, T. & ALLÈGRE, C. 1988. Neon isotopes in submarine basalts. *Earth and Planetary Science Letters*, **91**, 73–88.

SAUNDERS, A.D. & TARNEY, J. 1979. The geochemistry of basalts from a back-arc spreading centre in the east Scotia Sea. *Geochimica et Cosmochimica Acta*, **43**, 555–572.

SCHILLING, J.G., THOMPSON, G., KINGSLEY, R. & HUMPHRIS, S. 1985. Hotspot–migrating ridge interaction in the South Atlantic. *Nature*, **313**, 187–191.

STAUDACHER, T., SARDA, P., RICHARDSON, S.H., ALLÈGRE, C., SAGNA, I. & DIMITRIEV, L.V. 1989. Noble gases in basalt glasses from a Mid-Atlantic Ridge topographic high at 14°N: geodynamic consequences. *Earth and Planetary Science Letters*, **96**, 119–133.

STUART, F.M. & TURNER, G. 1992. The abundance and isotopic composition of the noble gases in ancient fluids. *Chemical Geology*, **101**, 97–109.

SUN, S.S. 1980. Lead isotopic study of young volcanic rocks from mid-ocean ridges, ocean islands and island arcs. *Philosophical Transactions of the Royal Society of London, Series A*, **297**, 409–445.

SUN, S.S. & MCDONOUGH, W.F. 1989. Chemical and isotopic systematics of oceanic basalts: implications for mantle compositions and processes. *In*: SAUNDERS, A.D. & NORRY, M.J. (eds) *Magmatism in the Ocean Basins*. Geological Society, London, Special Publications, **42**, 313–345.

TAYLOR, R.N., THIRLWALL, M.F., MURTON, B.J., HILTON, D.R. & GEE, M.A.M. 1997. Isotopic constraints on the influence of the Icelandic plume. *Earth and Planetary Science Letters*, **148**, 1–8.

TURNER, S. & HAWKESWORTH, C. 1998. Using geochemistry to map mantle flow beneath the Lau Basin. *Geology*, **26**, 1019–1022.

VALBRACHT, P.J., STAUDACHER, T., MALAHOFF, A. & ALLÈGRE, C.J. 1997. Noble gas systematics of deep riftzone glasses from Loihi Seamount, Hawaii. *Earth and Planetary Science Letters*, **150**, 399–411.

Index

Page numbers in *italic*, refer to figures and those in **bold** refer to entries in tables.